ELECTROCRYSTALLISATION STUDIES ON CADMIUM

BY

STEPHEN JOHN CHURCHOUSE Bsc Msc, (SOUTHAMPTON)

THESIS SUBMITTED FOR THE DEGREE OF DOCTOR OF PHILOSOPHY IN THE FACULTY OF SCIENCE,

UNIVERSITY OF NEWCASTLE UPON TYNE.

ELECTROCHEMISTRY RESEARCH LABORATORIES,

DEPARTMENT OF PHYSICAL CHEMISTRY,

UNIVERSITY OF NEWCASTLE UPON TYNE,

NEWCASTLE UPON TYNE, NE1 7RU.

DECEMBER 1984

To my parents; Freda & Ernest Churchouse

ABSTRACT

An investigation into the electrocrystallisation deposition of cadmium has been carried out. The work presented here was followed with the aim of increasing the understanding of cadmium electrodeposition processes, with relevance to general metal deposition. In particular the cadmium deposition behaviour that leads to dendritic growth has been studied. This is particularly relevant in the nickel/cadmium battery industry, where cadmium dendritic growth is a frequently attributed cause for cell failure.

The investigative approach has been from both the theoretical and direct experimental sides. The main experimental techniques involved, a.c. impedance, electron microscopy, rotating disc and potentiostatic studies. The usage of a.c. impedance to study double layer capacity changes, proved to be a very accurate method of detecting dendritic growth (through surface area changes). From a more theoretical angle, extensive use has been made of computer simulation, in order to follow the initial stages of deposition of hexagonal close-packed atoms.

Experiments involving cadmium dissolved as the species $Cd(OH)_4^{2-}$, in 10.00M KOH (saturation limit 0.00035M), have revealed that only grainy cadmium is deposited at timescales of <20 Hours (-400mV overpotential). Continued deposition in 10.00M KOH + 0.00028M Cd(II) at -300mV overpotential, has revealed dendrites of length 30μm can be grown after 6 days. This deposition behaviour remains largely unaffected by changes in surface roughness, electrode pretreatment and the presence of oxygen. However, cadmium deposition behaviour is highly

dependent on the presence of small quantities of cadmium salts in suspension. As little as 1 x 10^{-6}M of $Cd(OH)_2$ in suspension will dramatically lower the time required for dendrite deposition (25μm dendrites can be grown within 6 hours). This finding is of importance to the battery industry, since the negative plate in the nickel cadmium cell, consists of powdered $Cd(OH)_2$ contained within a nickel-plated steel support.

In the absence of suspension, cadmium dendritic growth was found to follow along conventional lines, such that the growth time required for a particular dendrite is given by;

$$\Delta t = \frac{\ln[h/h_o]\rho r\delta}{MDC_o}$$

Observed dendritic growth times quite closely fitted the calculated values. Studies involving deposition from acidic cadmium sulphate (0.001 - 0.1M) solutions, revealed a similar agreement with the calculated dendritic growth times. However, these times are considerably lower than for the alkaline solutions, primarily due to the concentration increase in Cd(II). In 0.1M $CdSO_4$ + 0.5M H_2SO_4 the growth time for a 25μm dendrite is reduced to ~60 s.

Applying an adapted 'Monte Carlo' method, computer simulation of multilayer electrodeposition onto perfect hexagonal close-packed surfaces has been simulated. It is shown that under diffusion-independent conditions the shape of the computer-generated current/time curve is dependent on the size of the lattice used and the 'trueness' of the random site selection. When diffusion is allowed to become important in the simulation, the deposit shows a dramatic change in morphology, with some clear parallels to observed deposits of cadmium. It

is shown that even in the absence of surface defects and impurities, grainy microcrystallites can be simulated under the linear diffusion conditions. This implies that, contrary to the established belief, surface abnormalities are not necessary precursors for dendritic growth.

CONTENTS

CHAPTER 3 DEPOSITION FROM 10.00M KOH CONTAINING DISSOLVED CADMIUM

CHAPTER 4 DEPOSITION FROM 10.00M KOH + $Cd(OH)_2$ SUSPENSION

CH 1 INTRODUCTION

1.1 BACKGROUND

This project was part of a continuing investigation into the properties and function of nickel-cadmium cells, in relation to their performance in the working battery. This was carried out in cooperation with the Ever Ready battery division. It was decided to investigate one believed failure mode in operation, namely dendritic shorting.

Dendritic shorting has long been blamed in the battery industry for failure of nickel-cadmium cells, however it is difficult to detect in failed batteries due to the problems of taking the cells apart, and finding dendritic shorts which may at best be 0.5 mm long. At the time of commencement no work on the subject of dendritic growth of cadmium had been reported, despite its obvious importance to the battery industry. To date the author knows of no other work on this specific subject, although some commercial institutions have looked at dendrite growth as one of the possible failure modes. By contrast a relatively large amount of material is available on dendritic growth of zinc, although this probably reflects the increased ease with which dendrites can be formed in the zinc system, due to the higher concentration of aqueous zinc species obtainable in the zinc cell. Thus the work presented here is an investigation into the more fundamental aspects of electrocrystallisation in specific relation to the nickel cadmium cell.

Evidence for dendritic failure in Ni/Cd cells is largely

circumstantial in nature. Abrupt failure of a complete cell or specific plates of a cell by a sudden loss of charge retention capacity, is associated with dendritic shorting, rather than the more gradual loss of the charge retention capacity normally associated with other ageing failure modes. This abrupt failure has been observed in cells under test[1]. These 'overnight' failures of cells can be explained by a few mechanisms of which dendritic shorting seems the most likely. Other evidence has been found on 'autopsy' of failed cells, whereupon examination has revealed small burn marks on the plates (largely confined to the nickel supports). These are taken as indicators of where dendritic shorting has occurred[2]. Burn marks could be anticipated since most dendrites would not be expected to survive the shorting, due to the large current they would have to carry. Thus causing considerable local thermal heating (cadmium having a melting point of 321^{o}C). As far as the author knows no dendritic connections have actualy been observed, but the evidence for their existence is fairly (but not entirely) conclusive. It is important within this context to realise the physical constraints of the Ni/Cd battery [see CH 1.2.1], which usually have an intended separation of somewhat less than 0.5 mm between the positive and negative plates. This could be reduced considerably if damage occurs or if the manufacture is less than perfect. Hence dendrite growth only has to bridge a small gap to cause loss of charge carrying capacity. However, due to the local heating effects, growth of a single dendrite would be unlikely to cause failure of a cell in itself, it is more likely that cell failure would require several such dendrites appearing at the expected short site.

Initially it was considered that growth of dendrites proceeded via an aqueous species (principally as $Cd(OH)_4^{2-}$ in 5-10 molar KOH[3-15]) during charging of the cell, whereby cadmium dendrites would grow out from the negative plate. It was considered that any dendrites growing out from the actual negative material would be very unlikely to cause failure due to oxidation on contact with the positive plate material. However, dendrites growing out from the nickel support of the negative plate would be likely to contact the nickel support of the positive plate, and thus cause failure. A second possible mechanism of dendritic shorting has also been postulated[16], where the presence of aqueous cadmium species during cell discharge might cause dendritic growth onto the nickel support of the positive plate. In this case outward growth of the dendrite could not be halted via oxidation since it would contact only the negative plate material. Dendrite growth caused during cell charging would reasonably be expected to be reduced during normal cell usage as the cadmium is consumed, however some dendritic growth could be expected to continue during any overcharging period. Each cycle of the cell can be expected to leave a residual deposit of cadmium at any site where the thickness of the deposit is above normal, due to incomplete oxidation. Thus after several cycles a buildup of dendritic cadmium could be expected, unless total discharge of the cell could be achieved. Growth of dendrites out from the positive plate support during cell usage was originally considered [16] to be a more likely cause of failure than dendrites from the negative plate due to the non-reduction of the cadmium thus formed during normal cell cycling.

It was with these factors in mind that an investigation into the more fundamental aspects of the electrocrystallisation of cadmium in relation to the nickel cadmium cell has been carried out. Originally more detailed information on actual cell failure was to have been obtained in cooperation with Ever Ready, but this could not be obtained due to circumstances beyond the author's control (Ever Ready were taken over by Hanson trust who proceeded to cut most of their research effort). In addition to these aspects concerned with the Ni/Cd system, it was hoped that the project would provide a more general knowledge of crystal growth that might be applicable to other areas of electrochemistry.

1.2 THE NICKEL-CADMIUM CELL

1.2.1 DESIGN AND CONSTRUCTION

Nickel cadmium cells are available from a number of manufacturers in numerous different shapes and sizes for a wide range of uses. Despite this the cell designs can basically be divided into two main types, containing either sintered plate or porous pocket plate electrodes. Both types can be either sealed or vented in design, vented batteries (usually high capacity) have a valve outlet to the air to enable any gas buildup to be avoided. Whilst sealed cells (usually lower capacity or specialised usage batteries), have a modified electrode electrochemistry to enable any gas produced to be recombined without causing any appreciable buildup of pressure.

1.2.1.1 SINTERED PLATE CELLS

Fig 1.1 shows the design of a typical low capacity sintered plate nickel cadmium cell of cylindrical construction. Most of the smaller cells are of this design since they are largely for uses where maintenance is difficult or impossible to carry out. The cell consists of a positive electrode, separator, negative electrode, the electrolyte and the container. The sintered nickel supports for the electrodes are prepared by applying a nickel powder on top of a nickel mesh support and sintering (fusing the metal by high temperature treatment). This provides a porous matrix of nickel into which the active material can be impregnated. Usually this is achieved by applying a hard vacuum treatment to maximise the filling of the support. This provides a good electrical contact to the active material when in use. Both the positive and negative electrodes are prepared in this way. The two electrodes are separated by using a 'porous non-woven organic material' (ie a matted fibre of some description), this is to ensure that no direct electrical shorting occurs but that ionic conduction is unimpeded. The sandwich of the three basic components is in the design shown, wound round into a tight coil and placed in a nickel plated steel container. The negative plate is connected to the main body of the cell and the positive connected to the cap (as is conventional in most simple cells). With the electrolyte in the cell the container is sealed leaving a safety vent in the cap, to ensure that in the event of pressure buildup due to cell failure, an explosion is avoided. This safety feature is not used in some cells of cheap manufacture or where it is not

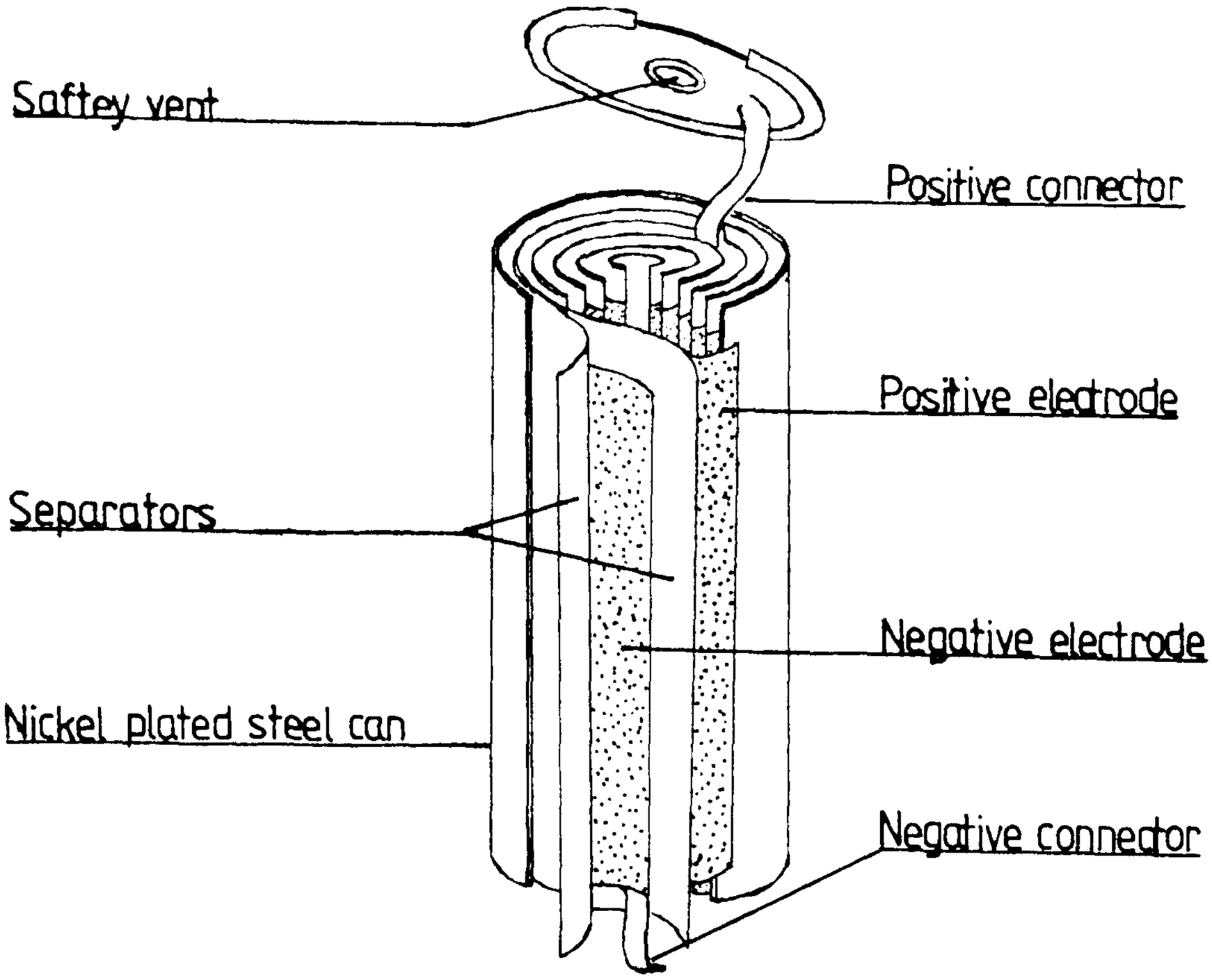

Fig 1.1 Typical sintered cylindrical nickel/cadmium cell.

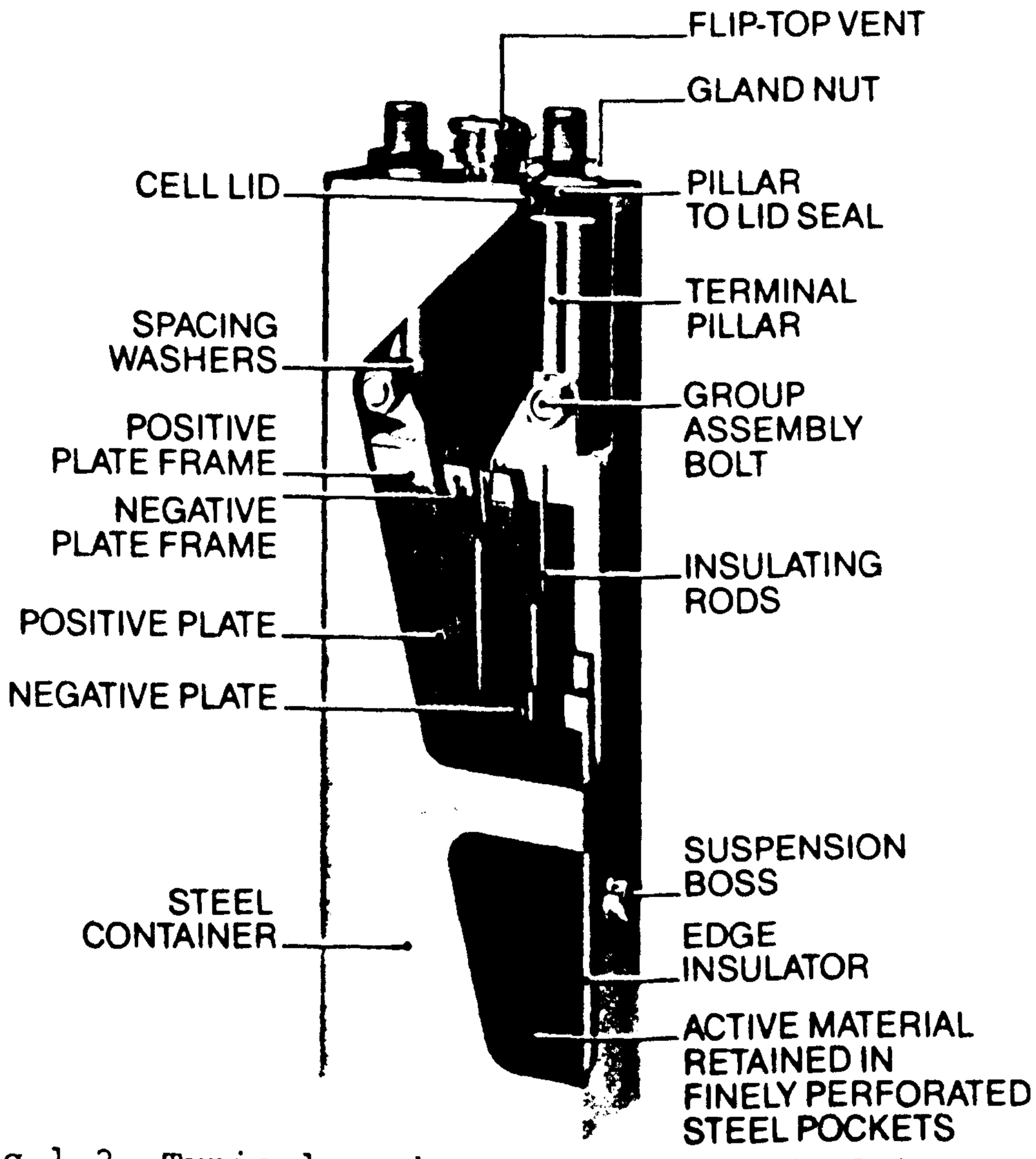

Fig 1.2 Typical pocket plate nickel/cadmium cell.

considered necessary in the cell's proposed usage. Generally several cells are used together in series to form a battery providing a suitable output voltage and current supply for the intended usage (at approximately 1.2 V per cell).

1.2.1.2 POCKET PLATE CELLS

The pocket plate (or mass plate) design of cell is an alternative method of construction to sintered plate cells. Fig 1.2 shows a diagram of a typical heavy duty cell of this type. The essential difference between this and the sintered plate cell is the way the active material is held. The active material is held between perforated strips of nickel plated steel, which are crimped closed at the edges to give discrete strips containing the active material (usually ~1 cm wide). These are then fitted together either single or double thickness and welded to the supporting plate and electrical connector. Alternate positive and negative electrodes are stacked together with plastic rod separators and bolted (with nickel plated bolts) to the appropriate terminal. The electrode assembly is attached to the container (either nickel plated steel or plastic) and immersed in the electrolyte solution. Several cells are connected in the appropriate way to give a battery suitable for the intended usage. Each cell will usually have a vent to allow gases to escape or in the case of sealed cells a safety valve. Pocket plate cells have a very robust construction and with proper maintenance they will last a long time, in some cases > 40 years (for vented cells)[17].

Both types of cell have advantages, the pocket plate design

is cheaper, more robust and has a greater stability towards temperatures. However, they have a lower electrical efficiency than the sintered plate cells (approximately 72% compared with 84%) and hence are heavier per Watt hour of charge. Additionally they require more maintenance than the sintered type. Sintered electrodes also have a longer life in normal usage than pocket plate cells, by up to 60%[18,19] although this is highly dependent on conditions of usage [see CH 1.3.2.1].

1.2.1.3 ACTIVE MATERIALS

The first nickel/cadmium battery using an alkaline electrolyte, is attributed to Waldemar Junger, a Swedish scientist working in the 1890´s. At around this time Edison invented a nickel/iron battery and proceeded to patent similar designs, using both cadmium and iron as the negative active material. It is to Edison that we owe much of the present day design and construction of these cells. To this day many of the minor components found in the cells can be attributed to components that Edison originally used in some of his cell designs, despite the fact that often their value to the cell performance is unknown. For example the inclusion of cobalt hydroxide and carbon to the positive active material or lithium hydroxide to the electrolyte. The main reason for their continued incorporation into the batteries, is because manufacturers do not want to risk a long term failure of their cells. Which could be caused by the lack of a component that whilst not apparently improving cell performance, does not degrade it. These original ´active´ ingredients were largely

included as a result of empirical judgements based on the somewhat inaccurate data available at the turn of the century. Generally despite the age of the system, commercial manufacturers still like to keep the exact details of their additives secret. Although there seems to be little difference in the claimed performance between manufacturers.

The chemicals used in construction are generally of a high degree of purity although this may not necessarily improve performance. Essentially the positive active material consists of nickel hydrate (NiOOH or $Ni(OH)_2$ depending on the state of charge) with added quantities of cobalt hydroxide and graphite. In sealed cells the positive active material has some $Cd(OH)_2$ incorporated to recombine any oxygen evolved [see CH 1.3.1]. The negative active material consists of cadmium hydroxide ($Cd(OH)_2$ or cadmium dependent on the state of charge), with varying amounts of iron hydroxide added. The electrolyte, although not consumed in the electrochemical reaction, is considered to be important in the cell function and is usually 4-7 molar KOH with some LiOH added (up to 5% by weight). Some manufacturers use more diluted electrolyte in their sealed cells with no apparent detrimental effect. The influence of the many additional additives to the cells is often poorly understood and may indeed have no beneficial result on electrode performance.

1.2.2 ELECTROCHEMISTRY OF CELL OPERATION

Normal Ni/Cd cells involve the following two half reactions (on discharge);

Positive electrode:-

$$2NiOOH + 2H_2O + 2e^- \rightleftharpoons 2OH^- + 2Ni(OH)_2 \quad \{1.1\}$$

Negative electrode:-

$$Cd + 2OH^- \rightleftharpoons Cd(OH)_2 + 2e^- \quad \{1.2\}$$

combining this gives us an overall reaction of;

$$2NiOOH + Cd + 2H_2O \rightleftharpoons 2Ni(OH)_2 + Cd(OH)_2 \quad \{1.3\}$$

$$E_{cell} = 1.25\ V$$

Thus on charging or discharging, the cell reaction does not substantially alter the electrolyte (although the consumed or generated water will cause a slight change in concentration and volume during cell usage). Upon charging in a conventional cell, a point is reached where all the active material has been converted, when futher charging will result in the reduction of water and hence oxygen being evolved from the positive and hydrogen from the negative plates. This is a potentially highly explosive mixture and to avoid this an excess of the negative active material is provided, such that only oxygen is evolved. This will not however, prevent a possible buildup of pressure and thus the cell requires a suitable vent. Thus in a conventional cell the electrolyte will be gradually consumed and require topping up at regular intervals (although intervals of up to 5 years are claimed for some cells). In the case of sealed cells this would severely limit their use, hence to combat this a modified positive active material is used. This modified design of cell avoids any buildup of gas pressure by

limiting evolution to oxygen and allowing it to be recombined on the other electrode during any overcharge or overdischarge period. This process is illustrated in fig 1.3. Essentially the negative plate contains an excess of negative active material, thus on overcharge hydrogen is not evolved due to the following two reactions occurring instead;

$$O_2 + 2Cd + 2H_2O \rightleftharpoons 2Cd(OH)_2 \quad \{1.4\}$$

$$Cd(OH)_2 + 2e^- \rightleftharpoons Cd + 2OH^- \quad \{1.5\}$$

giving an overall reaction of:-

$$O_2 + 2H_2O + 4e^- \rightleftharpoons 4OH^- \quad \{1.6\}$$

This is reliant on there being a transferance of oxygen evolved at the positive electrode to the negative electrode, thus a small partial pressure of oxygen will exist during overcharge, but this should soon reach a steady state. The reaction at the positive electrode is thus;

$$4OH^- \rightleftharpoons O_2 + H_2O + 2e^- \quad \{1.7\}$$

Hence no net consumption of the electrolyte occurs on overcharge. During overdischarge evolution of gas is suppressed via a similar mechanism, whereby oxygen evolved from the negative electrode is recombined at the positive electrode. This is achieved by incorporating a small amount of the negative active material in the positive electrode material. Thus on overdischarge, reactions {1.4} and {1.5} will take place on the positive electrode and again no net consumption of the electrolyte will take place. This addition of around 5% negative active material to the positive electrode does not seem to substantially effect the normal working of the cell[3,20].

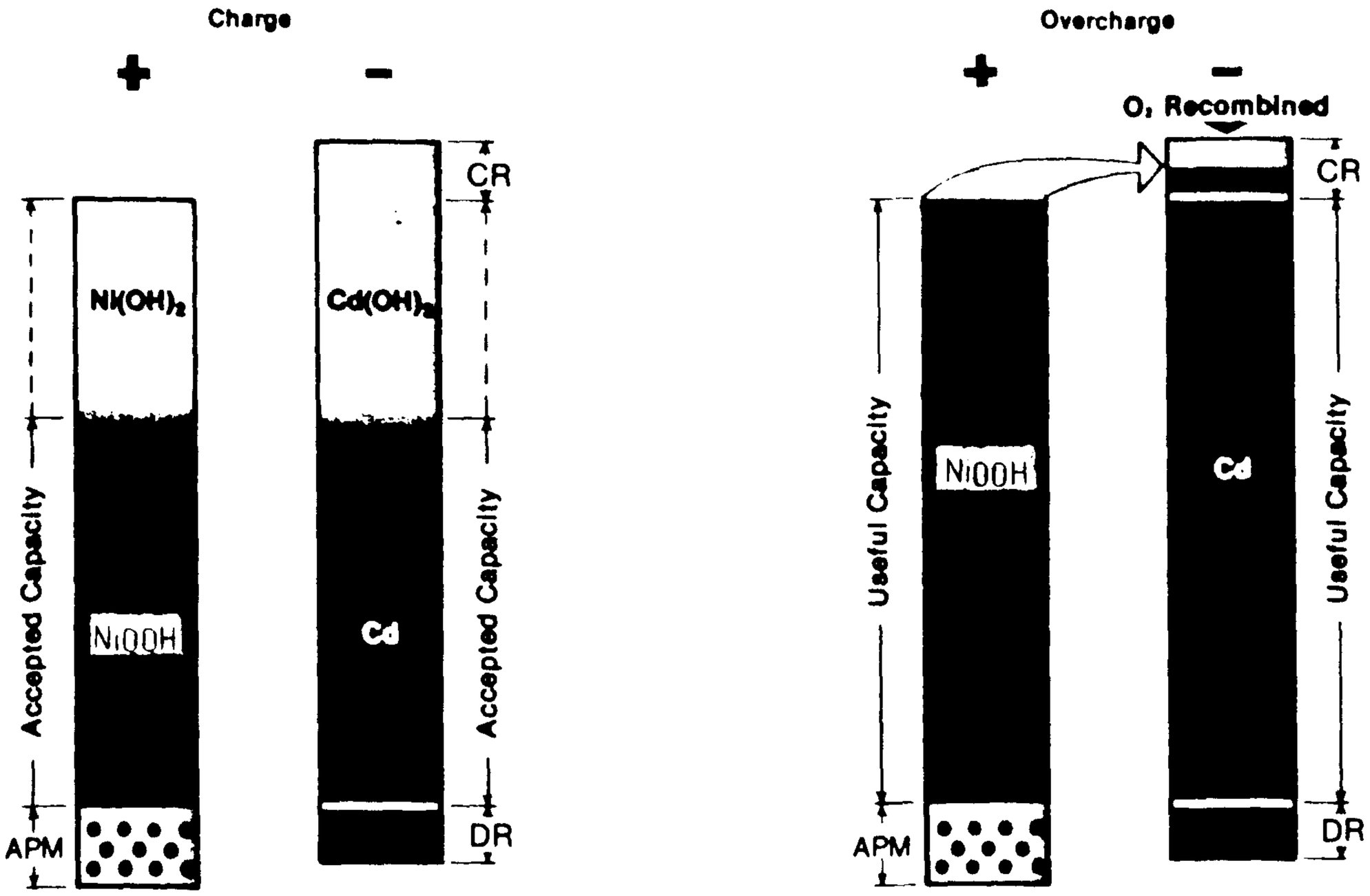

Charge on the positive electrode produces: Nickel (III) Hydroxide NIOOH
Charge on the negative electrode produces: Metalized cadmium - Cd

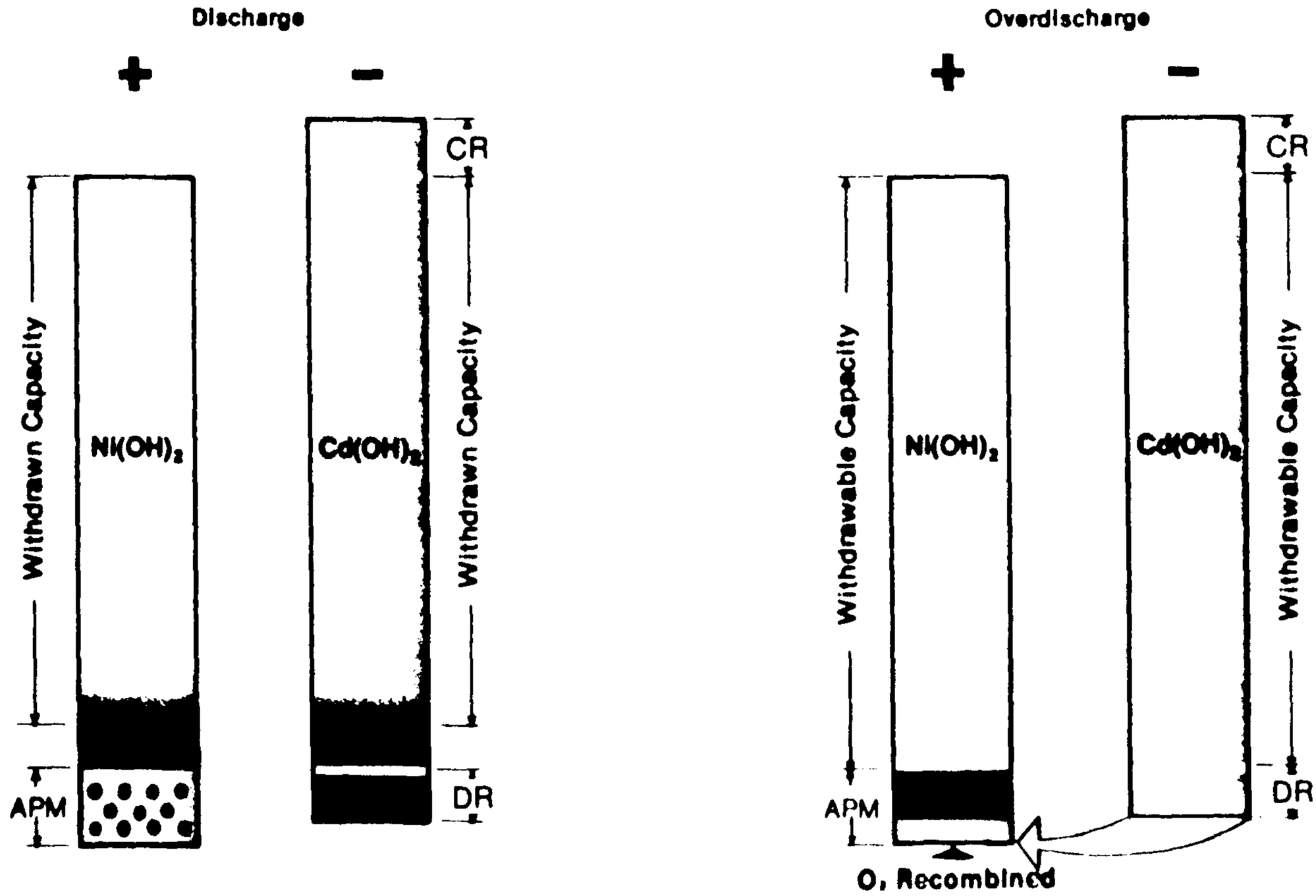

Fig 1.3 The electrochemical process in sealed nickel/cadmium cells.

1.3 PREVIOUS WORK

Discussion here is limited to planar cadmium electrochemistry (in alkaline solution), dendrite growth and computer simulation. No aspects of the positive plate of the cell were investigated, although much work has been published in this area[3,20].

1.3.1 THE ELECTROCHEMISTRY OF CADMIUM IN ALKALINE SOLUTION

1.3.1.1 SOLUBLE AQUEOUS SPECIES

There have been many investigations into the nature of the soluble cadmium species formed in alkaline solution[3-15,22-48], but little new work has been forthcoming on this subject, since the review article by Armstrong et al[6].

In alkaline solution the species Cd^{2+} has a sufficiently low equilibrium concentration for it to be ignored. This follows from the data of Latimer[49] for the solubility product of $Cd(OH)_2$ (2×10^{-14}), as interpreted by Lake and Goodings[11]. This was obtained using polarographic techniques. In alkaline media, virtually all the dissolved cadmium is believed to be in complexed form, but the exact nature of the aqueous species is highly dependent on the concentration of the alkaline ions. In the battery electrolyte the only significant cations are OH^- and CO_3^{2-}, with the concentration of CO_3^{2-} largely dependent on the electrolyte exposure to air. A minima in the solubility of $Cd(OH)_2$ with increasing pH has been observed by several researchers[7,8,11,22,25,26,50]. This dependence has resulted in workers

proposing the existence of various different species, dependent on their interpretation of the data available. Pourbaix[21] determined the equilibrium potential - pH diagram for cadmium and proposed in agreement with Piater[51], that the sole aqueous species above pH 10 in hydroxide based solutions was CdO_2. Sholder[52] however, showed that in NaOH, the salt $Na_2Cd(OH)_4$ could be formed. This was interpreted by Pourbaix as marginal evidence for the existence of the complex CdO_2^{2-}. Lake, using both KOH and K_2CO_3 solutions, proposed the species $Cd(OH)_4^{2-}$ and $Cd(CO)_3^{4-}$, in their respective electrolytes, with the hydroxide species predominating in mixed solutions. Milner and Thomas[3], in their review of the nickel cadmium battery, report that $Cd(OH)_2$ may dissolve as a neutral species to the extent of 3×10^{-6}M. They suggest the principal ionic species is CdO_2H^- or $Cd(OH)_3^-$ [30] and conclude the predominant aqueous species will be $Cd(OH)_4^{2-}$. Suggestions for $Cd(OH)_3^-$ were limited to high OH^- concentrations. This is in agreement with several other workers[5,7,13 ,24,48], although considerable doubt has been expressed on the data interpretation justifying this conclusion[6]. Since the work of Visco and Sonner[24], most of the studies of this system have concluded the species $Cd(OH)_4^{2-}$ is going to predominate at the concentrations of alkali present in the Ni/Cd cell[4-6,8-10 ,12,15,]. Armstrong et al[8], using impedance techniques, showed that $Cd(OH)_4^{2-}$ was reversibly produced during dissolution of cadmium amalgams in alkaline solution. In reviewing the information on this subject, Armstrong et al, conclude the evidence is only consistent with the existence of $Cd(OH)_4^{2-}$ as the predominant species for alkaline systems of pH > 12. At lower concentrations of

hydroxide, the presence of the species $CdOH^+$ has been postulated[7,25].

Several studies of the solubility of $Cd(OH)_2$ have been carried out, whereby the solubility dependence on KOH concentration has been determined[6,50]. There is a broad measure of agreement between these studies, with a value for the solubility of $Cd(OH)_2$ in 10.00M KOH of 0.00035M obtained by Lake and Goodings[11]. This solubility value for $Cd(OH)_2$, is used throughout this thesis.

1.3.1.2 CADMIUM ANODIC FLIMS

i) FORMATION

Considerable argument has been expressed over the mechanism of formation of anodic films and associated passivating layers on cadmium. Two main mechanisms of formation have been proposed; 1) solid phase and, 2) dissolution precipitation. Barnard[4] in his review, considers that the underlying passivating film of $Cd(OH)_2$ or CdO, forms by a solid phase mechanism. Armstrong and West[10], using rotating ring-disc experiments, observed that upon linear sweeping, a small fraction of the disc current is due to formation of soluble cadmium species (this being detected by reduction on the ring). This agreed with earlier work by Okinaka[26], proposing a dissolution precipitation mechanism. However, the apparent independence of this current upon rotation rate, was taken to be strong evidence that a solid state mechanism of formation of the passive anodic layer, must be operating. After the initial

period of anodic film formation, a steady state is reached where the anodic film maintains constant thickness[6]. The steady state current being dependent on rotation rate, consistent with the outer surface of the film dissolving as $Cd(OH)_4^{2-}$ [10]. The possibility of a very fast dissolution precipitation mechanism was proposed by Oshe et al[53,54]. Using rotating ring-disc techniques they compared theoretical and actual ring collection currents. The apparent discrepancy was explained by precipitation upon the insulator between the two working electrodes. This mechanism could be investigated by the usage of high rotation rates and microscopy, but as yet, no work has been published.

Within the Ni/Cd battery, the importance of the solid phase mechanism is reduced, since cell operation rarely extends into the passive region[3,13]. Hence the dissolution precipitation mechanism is of considerably increased importance, in determining the recrystallisation of the $Cd(OH)_2$ within the negative plate. Barnard considers that in the Ni/Cd cell, both mechanisms must be operating.

Some evidence exists for the production of O_2^- and O_3^{2-}, involving production of CdO_2 within a supposed micro-layer of CdO[26,35, 37-9,55]. The existence of peroxides in the passive film[42], has been confirmed by Casey and Gardner[13] using electron spin resonance (ESR) studies. The paramagnetic ions O_2- and O_3^{2-}, were detected in the electrolyte around an electrode operating in the oxygen evolution range. Peroxide was found to be favoured at low temperatures. However, production of any such peroxides and ozonides, is only likely to occur with overdischarge or cell reversal.

ii) STRUCTURE AND COMPOSITION

Five compounds are generally accepted to be present in anodic films[4,6], α, β, and $\gamma Cd(OH)_2$, CdO and CdO_2. The α form of $Cd(OH)_2$, is of poorly defined structure (forming relatively small crystallites[4]), and is unstable in strong alkaline solution, where transition occurs to β $Cd(OH)_2$ [55]. The instability of this α phase has not enabled a good elucidation of its structure. It is known that both the α and β phases have the Brucite strcture (hexagonal close packed C6 type[56]). The α phase is probably able to accept a greater hydration number than the β [4], which would explain some of the variability in the structure (lattice parameters, a = 3.496, c = 4.702 Angstroms). The interlayer spacing of the α phase is somewhat variable, giving rise to a number of secondary structures of different properties[57]. The γ phase has a monoclinic structure (a = 5.67, b = 10.25 and c = 3.41 Angstroms), and has been found to be more stable than the other phases at low and room temperatures[32, 33,58].

iii) REDUCTION

As with mechanisms for anodic film formation, the reduction mechanism for anodic films is believed to take place via a combination of both solid phase and soluble intermediate mechanisms. Evidence for the solid phase reduction has been found by several workers[27-33], by employing rotating disc and linear sweep techniques. The cyclic voltammograms change

little with change in the rotation rate. Evidence for soluble intermediate reduction (presumably via $Cd(OH)_4^{2-}$), has been found[6,13, 26,34]. In particular, Okinaka[26], found an increasing effect as the reduction proceeded. The soluble intermediate mechanism is likely to be of greatest importance in unstirred electrolytes and where the anodic film is particularly thick. These conditions are found within the Ni/Cd battery, where the active material is an amorphous powder. It is thus unlikely to reduce via a pure solid state mechanism, due to the physical separation of particles from the electrode (support) surface.

There is good evidence, that under certain conditions, solution intermediate deposition could occur directly onto conducting $Cd(OH)_2$ or CdO. Evidence for this has been found from SEM observations[4], and with cyclic voltammetric studies[10,13, 38-41,42]. This cadmium deposition onto conducting surface films allows some $Cd(OH)_2$ to become trapped in the unreduced form, thus leading to inefficiency in the battery. Deposition of this kind, requires the underlying film to have a reasonable electronic conductivity. β $Cd(OH)_2$ has a low conductivity but CdO and to some extent γ $Cd(OH)_2$ are known to have some conductivity. CdO is known to have semiconducting properties, and a conductivity of 800 Ω/cm has been reported at 300K[59]. γ $Cd(OH)_2$ is likely to have a measure of conductivity and some evidence for the solid state mechanism has been found[60]. Semiconducting hydroxides can be formed from phases having defective crystal structures, where a stiochometric excess of cadmium exists in the lattice, thus allowing the solid state mechanism to operate.

iv) HYDROGEN EVOLUTION

The influence of hydrogen evolution on planar cadmium in the alkaline systems, has not been extensively studied, despite its obvious importance to the battery industry. This is not the case for hydrogen evolution on nickel where a number of different studies have been carried out[61]. Studies in various alkaline media[62], have indicated that a slow direct reduction of the water is involved, with no evidence for any intermediary step in KOH electrolytes. The Tafel slope (taken over 4 decades of current with $\alpha = 0.5$), of 118mV/decade, is in agreement with theoretical considerations.

1.3.2 THE NEGATIVE PLATE

1.3.2.1 EFFICIENCY AND CAPACITY LOSS

Nearly all the changes in the cycling efficiency and other properties of the negative plate, can be attributed to changes in the morphology of the active materials. Both the charged and discharged negative active materials, being subject to such changes. The factors influencing these morphological changes are numerous and somewhat convoluted. The main factors include, temperature, ageing, rate of charge/discharge, depth of discharge, number of previous cycles, additives, pore size and degree of plate impregnation. This complication has lead to most publications concentrating on one aspect in particular. It is difficult if not impossible at this stage, to say exactly what factor is most important in any individual working cell.

i) TEMPERATURE

The influence of cell storage and ageing at different temperatures, has been studied by a few workers, with the effects compared to room temperature performance (usually 20^{o}C). The subject is somewhat complicated by the heating effects encountered during normal cell charge and discharge, which can elevate cell temperature by >50^{o}C. Ageing effects are encountered at all temperatures, but the electrodes are relatively stable at 20^{o}C, showing little change after 5 years in the discharged state[63]. The deterioration noted is largely confined to morphological changes, the $Cd(OH)_2$ crystallite size is seen to increase with cycling, as does the cadmium crystallite size on charging[64]. At elevated temperatures, this process is considerably more rapid, and studies of similar cadmium electrodes in Ag/Cd cells[65], has revealed a 10-100x increase in cadmium crystallite size after only 6 months storage at 50^{o}C. $Cd(OH)_2$ crystallites also increased in size by a factor of x10 over a 12 month period. Other studies have however, shown smaller changes[66]. Porous plate studies of cells aged at 70^{o}C, have shown an increased loss of efficiency, but that this can, to some extent, be reversed with low temperature (-20^{o}C) cycling[63]. The greatest problems occur in cells operated at one temperature, when previously used or formed at a different temperature. Cells formed at -20^{o}C, show a marked increase in the cadmium nucleation overpotential. Thus decreasing the cell efficiency by causing evolution of hydrogen at the start of the

charging[63]. Part of the problem at the lower cell operating temperatures, is probably due to the decreased solubility of the hydroxide species, thus further increasing the importance of other solution and solid state processes. Another temperature related phenomenon, is the 'memory effect' sometimes observed when cells are trickle charged at a high temperature, then operated at a lower temperature. The effect is revealed as a 120mV voltage step in the discharge curve[67,68]. It is believed to be associated with the production of a nickel/cadmium alloy layer (probably Ni_5Cd_{21})[4], although other proposals have been previously forwarded[68]. The effect is removed by a fast complete cycle of the cell.

ii) RATE OF CHARGE

Both the rate of charge and discharge effect the cell efficiency and ageing, thus understanding of their involvement is based upon experiments holding either the charge or discharge at a constant rate. With a high (C/1) discharge rate, Barnard et al[69-71], have found most capacity loss to be associated with incomplete conversion of the cadmium metal. After 100 cycles the efficiency is still ~80%. However, at the C/8 charge rate this drops to 55%, and is still worse at the C/50 rate. This general trend has been observed by other workers[37,70]. Observation of surface area changes confirm the lower the charge rate the lower the surface area of cadmium. SEM observations correlate this with increasing cadmium crystallite size. Similar effects have also been observed for $Cd(OH)_2$[37], where at low discharge rates the $Cd(OH)_2$

crystallites increase in size, decreasing efficiency (where a high charge rate is used). The discharge rate is however, less of an influence on cell performance than the charge rate[69]. The influence of the discharge is also dependent on the depth of discharge[72], a greater depth of discharge causing increased capacity loss.

iii) ADDITIVES

In addition to the 'normal' active constituents of Cd, $Cd(OH)_2$, NiOOH, $Ni(OH)_2$ and KOH, the cells contain a number of other components, most contain LiOH, $Co(OH)_2$, iron oxides and carbon. These latter ingredients are incorporated largely for the benefit of the positive plate[3]. Additives to the negative plate are generally aimed at reducing the morphological changes of Cd or $Cd(OH)_2$, that lead to inefficiency. Many additives such as $Ni(OH)_2$, antimony[41], oxalic acid[19], cellulose[4], starch[4], carboxymethylcellulose[73], quaternary ammonium salts[74], surfactants[76] and even sunflower oil[75], have been investigated. All of these are said to increase efficiency by reducing the extent of morphological change in the active material. Exact details of the quantities and effects of the additives actually used, is difficult to obtain due to commercial secrecy.

iv) ALLOY FORMATION

The formation of nickel/cadmium alloys within operating cells has been observed[4], and has some influence on cell

performance. Alloy formation can reduce the efficiency of the cell by reducing the quantity of active material available and more importantly, by altering the operating potential of the cell. Artifical inclusion of 20% $Ni(OH)_2$ to the negative plate has been observed to convert to alloy after 1000 hours of cell operation at 75^oC[77]. Alloys are believed to be formed when $Ni(OH)_2$ and $Cd(OH)_2$ are in contact for prolonged periods of time, particularly at raised cell temperatures. The appearance of $Ni(OH)_2$ in the negative plate, is either as a recrystallisation inhibitor or as a corrosion/oxidation product of the support material.

Studies of alloys formed by heating of mixtures of the metals at 300 - 400^oC, has confirmed the appearance of three alloys, Ni_5Cd_{21}, Ni_2Cd_5 and NiCd[78,79]. At this temperature the Ni_5Cd_{21} is the least stable. However, electrochemical reduction of Ni/Cd hydroxide mixtures only produces Ni_5Cd_{21}[80]. Cyclic voltammetry of Cd/Ni_5Cd_{21} mixtures produces an alloy peak at $\backsimeq$120mV more anodic than the Cd peak, at around $\bar{}$0.820V (versus Hg/HgO at 25^oC)[79,81]. This value fits in with the alloy formation explanation of the memory effect, which produces a step of 120mV in the cell output voltage[67,68]. The oxidation of the Ni_2Cd_5 phase is believed to take place at -0.75V (Hg/HgO)[81], but has not been detected in working cells.

1.3.3 DENDRITIC GROWTH

Previous work on dendritic growth is conveniently divided into two distinct areas, 1) dendritic growth produced by cooling from melts and 2) dendritic growth of metals by

electrodeposition from solution. Other forms of dendritic deposit can be found, depending on the interpretation of what is a dendrite. Strictly speaking, anything tree-like in form can be regarded as dendritic (dendroid - having the form of a tree). Hence deposits formed from vapours (eg snowflakes), resublimation (eg iodine) and the crystals of some salts formed by evaporation, could also be taken as examples of dendrites. However, they are of little relevance to the work within this thesis. Dendritic deposition from melts is analogous to electrodeposition, the driving forces for the two processes being solution undercooling and overpotential respectively. One mechanism depending on heat transfer, the other on mass transfer. The laws concerning melt dendrites have been extensively studied[82,83], but are of little direct relevance.

Work on the growth of electrodeposited dendritic systems is largely confined to the practical problems of dendrites in battery systems, although a few mechanistic and theoretical studies have been carried out. The available material on metal dendrites covers the following elements, lead[84-87], copper[85,88,89], silver[85-87,90-92], cadmium[85,88,93,94], tin[85], gold[86,87], aluminium[86,87] and zinc[98-113]. By far the greatest volume of material being for zinc, both in alkaline zincate[98-109] (ZnO battery), and acidic electrolytes ($ZnCl_2$ battery)[108-113]. This probably reflects the size of the problem for the zinc system, where high aqueous zinc concentrations are experienced. Nearly all the studies have been on aqueous electrolytes, but with some notable exceptions carried out on molten salts[90,92]. At present

the only substantial work on cadmium dendrites in alkaline solution, is that by the author and R.D.Armstrong[94] and by Barnard et al[95-97] carried out at Ever Ready research laboratories, in cooperation with this project. A couple of studies are available for cadmium deposition from acidic solutions[88,93], this probably reflecting their relative ease of growth, due to the higher concentrations obtainable in the acidic system.

The first notable work on electrocyrstallisation of dendrites was by Wranglen[85], who in 1960 studied current densities in relation to the rate of deposition. He related the minimum current density required for dendritic growth to an activation overpotential. Wranglen was also the first to describe dendrites as single crystals and observe morphological dependence by x-ray techniques. He observed conventional twinning phenomena, as have many other workers in other systems[86,87,91], although evidence for twinned cadmium dendritic deposits is scant[16]. His description of dendrites as single crystals is contradicted by the discovery by Faust and Johns[86,87], of grain boundaries in dendrites growing in the (211) and (110) directions for all the metals they studied, although no boundaries were found in the (100) direction. Barton and Bockris[90], in their study of silver dendrites from $AgNO_3$/ KNO_3 + $NaNO_3$ melts, gave the first systematic insights into dendritic deposition and related theory. They introduced the concepts of critical overpotential, critical current density and induction time. The main conclusions of their work were; 1) that the critical current density is proportional to C_b. 2) once initiated, dendritic

growth proceeds at a constant velocity. 3) a maximum in the dendritic growth velocity occurs at some value of overpotential, above which the morphology of growth is substantially altered (this they describe as the appearance of multiple dendrites at the original dendrite tip). 4) decreasing of the deposition overpotential below that required for continued dendritic growth, is accompanied by a change in deposition morphology towards a more granular deposit. These conclusions were confirmed by other workers, both in melts[92] and aqueous electrolytes[116]. Subsequent work by Bockris et al[100,102] on alkaline zincate solutions, lead to them producing a model for deposition, whereby dendrites are initiated from pyramidal growth at screw dislocations. This occurs under bulk diffusion control, until the deposit morphology changes sufficiently to allow spherical diffusion control to set in. However, Despic et al[116] have shown that even in the absence of spherical diffusion conditions, deposition at the dendrite tip is greatly enhanced. Further work by Bockris et al[102] on zinc dendrite precursors, showed that the dendrite growth rate remained constant whilst the dendrite was within the diffusion layer, confirming results found in melts. Observations that the radius of curvature of a precursor tip increases in proportion to its height (ie angle of deposit is constant), have been made by several workers[116]. This is in agreement with the Barton - Bockris theory, but is only true whilst diffusion conditons are constant at the tip. Hamilton[117] investigated the change in the diffusion conditions caused by the transition from linear to spherical diffusion, and found that the conditions for dendrite propagation, can be attained with differing tip radius

of curvature and growth rates. This result was expounded by other workers[100,102,116] showing the maximum growth rate for any dendrite corresponds to some optimum tip radius under the conditions prevalent. This being the result of a compromise between the optimum spherical diffusion conditions (requiring $r \rightarrow 0$), and the increasing surface energy contribution required as the tip radius decreases[102,116]. This Kelvin surface tension (or curvature overpotential) effect is given by;

$$\eta_r = (2V\gamma/nFr)$$

Barton and Bockris derived an equation for the optimum tip radius given by;

$$r_{opt} = \frac{1 \pm [1 + DC_b F^2 \eta / 2\gamma V i_o]^{1/2}}{F\eta / 2\gamma V}$$

Despic et al[100] derived equations for the initiation current and tip current density dependence on tip radius at various overpotentials. This giving rise to a value for the limiting tip current density for dendritic growth of;

$$i_c = i_o[f_c(\eta) - f_a(\eta)] \geq i_L$$

with a critical overpotential of;

$$-\eta_c = RT \ln(i_L/i_o)/\beta F$$

They illustrate the importance of the tip radius by comparing the silver and zinc systems, far fewer silver dendrites are found per unit area electrode than for zinc, but growth rates for silver dendrites are higher than that for zinc. Silver dendrites have been grown at rates of 1.2mm/min[116]. This difference is attributed to the higher likelihood of the zinc precursors having the required tip radius for growth.

Amplification of surface irregularities, is regarded as a separate phenomenon from dendrite initiation according to Despic

and Popov[116], who distinguish the two effects for two main reasons, a) the existence of a critical overpotential for dendritic growth and b) the well defined crystal structure of dendritic deposits. However, evidence presented in this thesis suggests that the two processes are interlinked, with dendritic growth appearing from amplified surface irregularities under the right conditions.

Despic and Popov describe the critical overpotential required for dendritic growth largely in terms of the change in crystal structure accompanying dendritic growth, rather than the overpotential of rotation of screw dislocation favoured by Bockris[102]. Despic and Popov regard the initiation time as an independent effect from the critical overpotential, due to the great variability that is found for different metals. They contrast silver and zinc. Bockris et al[102] derived the growth time for dendritic growth as;

$$T_d = -h_o nF/i_c V$$

Moshtev and Zlatilova[101] re-defined the initiation time for dendritic growth in terms of the time required for a precursor to grow through the diffusion layer, hence their definition of;

$$t_i = \delta/v_d + [\delta r/VDC_o]$$

Despic and Popov in their comprehensive treatment of metal deposition and dissolution[116], interpreted the induction time for dendritic growth, as the period required for the exponental growth of a protrusion to cause piercing the hydrodynamic layer, and thus become 'visible'. They derive the induction time as;

$$t_i = \frac{\delta r[\ln(\delta/h_o) - 1]}{MDC_o[1-(2\gamma V/r)f_a(\eta)/f_c(\eta)]}$$

Here they consider the critical dendrite height is reached when $h = \delta$.

Popov et al[88], have extended the work of Barton and Bockris and Despic et al, to investigate the mechanism of powdery deposit formation. They identify a second critical overpotential in addition to the critical overpotential for dendritic growth (η_c), that of powder formation (η_p). Both are associated with deposit morphological change. They define the critical potential for powder formation as the maximum overpotential at which powdery deposition occurs. ie they identify three morphologically defined regions;

powdery deposition only $\leqslant \eta_c$

mixed $\geqslant \eta_c \leqslant \eta_p$

dendritic deposition only $\geqslant \eta_p$

Thus at overpotentials $\geqslant \eta_p$ the initiation time for dendritic growth tends to zero. Despic and Purenovic[114], determined values for η_c and η_p from plots of η versus $1/t_i$. Their values for t_i were obtained by extrapolation of the linear phase of dendrite growth back to zero time. The height of a protrusion within the diffusion layer being given by[116,118];

$$h_t = h_o \exp(VDC_o t/\delta^2) \qquad \{1.1\}$$

Hence they define a critical height h_i, where the current densities at the tip of a dendritic and non dendritic protrusion are equal. This point is taken as the initiation time of dendritic growth t_i. they derive equations for η_c and η_p given by;

$$\eta_p = 2.3\eta_o \log\left[\frac{nFDC_o}{i_o h_o}\right] + \eta_r \qquad \{1.2\}$$

and;

$$\eta_c = 2.3\eta_o \log\left[\frac{4nFDC_o}{i_o \delta}\right] + \eta_r \qquad \{1.3\}$$

η_r being the Kelvin surface overpotential.

From their results for cadmium and copper deposition in acidic solution, Despic and Purenovic obtained experimental values for of 110 and 660 mV respectively. The values obtained for η_t were 27 and 260 mV. They compare these values with those calculated for copper from equations {1.2} and {1.3} of η_c = 242 and η_p = 550 mV[89]. They claim good correlation with the results obtained by Barton and Bockris for silver[90]. Studies of the critical dendritic overpotential for zinc in ZnCl acidic systems, have produced values of 11 - 14 mV[110,114], compared with values of 60 - 80 mV from alkaline zincate solutions[102,114]. Despic and Purenovic[114] suggest the thermodynamic dendritic critical overpotential should be < 10 mV for the alkaline system. However, the value for zinc critical overpotential in acidic solution with hydrogen evolution has been determined at 173 mV by Popov et al[89,111].

Studies of the factors influencing deposit morphology have been made by a number of workers[84,103-109,112,113,115], with the aim of controlling or modifying dendritic growth. This is of particular importance in both electroplating and battery operation. It has been known for some time, that the addition of additives to plating baths can hinder dendritic growth[119]. Some adsorbed additives reverse the effect of surface amplification[116], by preferential adsorption onto higher features of the surface. Thus deposition is relatively

enhanced on the lower relief of the surface by inhibition of deposition at the raised areas. The effect of additives on zinc deposition has been reasonably well studied[103-105,107-109], and the addition of lead ions to alkaline zincate solutions has been seen to cause modification of dendritic growth towards a smaller more branched deposit[103,105,107]. Mansfield and Gilman[103], indicate this is due to blocking of the active sites for deposition, with deposition preferentialy nucleated from microscopic defects. The same authors[104] studied the addition of tin ions with similar results to that for lead. The only other significant dendrite inhibitors that have been investigated are organics, although electrolyte purity has been studied, with the role of common contaminants such as silicates being discounted[107] (for alkaline systems). However, successful dendrite inhibitors have been reported including a variety of quaternary ammonium compounds, benzylacetone, n-decylamine and commercial preparations[105,107,108,114]. Concentrations as low as 10^{-8} Molar in the case of n-decylamine have been found sufficient to inhibit pyramidal growth[120]. Bressan and Wiart[108,109] have investigated the effects of impurities on the kinetics of deposition by way of a.c impedance techniques. They found a shift in the i/V curves towards more cathodic values and a decrease in current efficiency. This they associate with increased cation and hydrogen adsorption, which has an important influence at kink sites.

1.3.4 COMPUTER SIMULATION

Computer simulation and related techniques have been used for a number of years for the elucidation of theoretical problems, where an analytical solution is either difficult or impossible to achieve. Many workers have used computers to study two-dimensional nucleation and growth on a layer by layer basis, and their work can largely be divided into three main approaches:

1) numerical integration (integral method)[121-124];

2) computer simulation by a semi- Monte Carlo or "hybrid" method[125-130];

3) true Monte Carlo computer simulation[131-154].

The integral method has been investigated using the Kolmogoroff[155] - Avrami[156] relationship, whereby calculations are based on the growth at constant rate of nuclei where:

$$S = 1 - \exp(-S_{ex}) \qquad \{1.4\}$$

This gives the current due to growth of a single layer of circular patches as[157]:

$$i = q_{mon} 3\beta t^2 \exp(\beta t^3) \qquad \{1.5\}$$

and for subsequent layers[121]:

$$i_{n+1}(t) = q_{mon} \int_0^t 3\beta(t-u)^2 \exp[-\beta(t-u)^3]\, i_n(u)\, du \qquad \{1.6\}$$

Armstrong and Metcalfe[122] used numeric integration of:

$$i_n(t) = q_{mon} \sum_{u=0}^{t} f_{n-1}(u) f_1(t-u) \Delta u \qquad \{1.7\}$$

to give an accurate current-time curve incorporating contributions from the first 50 layers. However, unlike direct simulation, the integral method is not quantised, and the contribution of the nucleation process to the overall current is assumed to be zero. The current-time curve produced [see CH

6.4.2], is an accurate reflection of the initial i/t transient found by Budevski et al[162], for low overpotential potentiostatic deposition onto perfect crystal faces.

Computer simulation of two-dimensional growth by the hybrid method is not a true Monte Carlo simulation since growth and nucleation occur as separate processes. The Monte Carlo procedure[158,159] is used in deposition of the nuclei, but growth is achieved by periodically advancing the edge of each growing centre. Current-time curves produced by this method are far inferior to those found by the integral method. This can be explained by several factors, the main one applying to true Monte Carlo simulations as well, is that the process of time averaging the 'random' simulation to achieve a satisfactory result, requires a vast amount of computer time. Thus most of the older studies had to employ quite severe restrictions on the model, just to enable the simulation to be carried out on any reasonable timescale. However, continued advances in computer hardware now allow sufficient accuracy to be achieved. Some previous work[126,127] using the hybrid method, resulted in current-time curves sufficiently removed from the integral case, that inadequacies in the programming/model may be to blame. The importance of 'true' random numbers for simulation, cannot be underestimated[154] [see CH 6.4.5], and may be a cause of error.

The true Monte Carlo simulation procedure for modelling of two-dimensional layer by layer, growth has been followed by a number of workers, notably Gilmer[144-148] et al[134,136,138, 140,143,160]. In this simulation of crystal growth, no distinction is made between the nucleation and growth stages.

Growth like nucleation occurs at randomly chosen sites.

Gilmer´s work is largely confined to studies of specific factors in crystal deposition, using the same simulation model. His model for the simulation is based upon the Ising (lattice gas - vapour deposition) model[163]. The model uses a fixed array of lattice sites (usually 60 by 60 although one model used 20 by 60), represented as a square array of integers indicating columns of atoms up from the base layer. Thus vacancies and overhangs are not allowed, somewhat limiting the validity of his results compared with real systems. These restrictions would not allow simulation of ´true´ crystal formation, since only deposition in the base plane allows nucleation and unrestricted growth. However, this simplification greatly reduces the computational requirements, both in memory and time. Most of Gilmer´s studies concern fcc lattices, with atoms adherence being determined by the sum of the energies from bond formation with nearest neighbours. Edges are avoided by using reflection, ie neighbours of one edge site are found at the opposite edge, thus giving a tordial system as used within this thesis [see CH 6.2]. A curious twisted tordial model is used by Gilmer et al[138,142], whereby edge atoms are found at the opposite edge ±1 row. This is probably a computational restriction imposed by the usage of a high speed shift register within a special purpose computer. The simulation is carried out with both deposition and evaporation processes, with surface migration incorporated in some models. In Gilmer´s model, atoms impinge at a rate given by;

$$k^{+} = \nu \exp(\beta\mu) \qquad \{1.8\}$$

and evaporate at a rate dependent on coordination given by;

$$k_n^- = \nu \exp(-\beta n \varphi) \qquad \{1.9\}$$

with equilibrium achieved when;

$$\mu = -z\varphi/2$$

The deposition rate/time (= current/time) transients are varied by adjusting β, the Boltzmann temperature term (= deposition probability). Using this model Gilmer et al, have studied surface diffusion[134], step progression[131,140], spiral growth[145-148], impurities[145,146] and the growth and evaporation of a crystal surface containing a hole[145]. In most cases the morphology is depicted. However, much of Gilmer's work is overlapping and no description or flow diagram of the computer simulation programs is given in any of the papers. Additionally, with the exception of the special purpose computer[138,142], no description is given of the computer used. It is also not clear whether the programs were written by the authors.

Bertocci[131] has investigated 2D nucleation and growth from an electrochemical viewpoint, employing a similar model to Gilmer. Bertocci used lattices up to 180 by 180 atoms, his results indicating some model size dependence, but this was not investigated. This point is important with regard to some studies on a restricted model size, which can be as low as 10 by 10 atoms. The work within this thesis indicates a considerable size influence might be expected, thus questioning the use of such small models. Van der Eerden et al[142], used the special purpose computer[138] to simulate a lattice size of 20 by 20. However, the notable feature of this work is the apparent speed of calculation which was claimed to be 200x

faster than an IBM 370/55 mainframe computer. This was achieved using a shift register operating in parallel. However, no subsequent work using this computer has been reported to date, probably due to its inflexibility.

Cherepanova et al[150] have simulated ionic lattice deposition using the Ising model. In this model the atoms are essentially of two kinds (positive and negative), such that an additional charge component has to be considered during deposition. They found that at high supersaturations the regularity of the crystal phase diminished, due to the formation of small internally regular domains. Franke and Lacmann[152,153] studied two dimensional dendritic growth from the melt by a Monte Carlo simulation. The model, based upon that of Bennema and Gilmer[134,136], used a two-dimensional cubic lattice with nearest neighbour interaction (with 1- 3 neighbours at the interface). Overhanging configurations were allowed in the model, without which the authors could not simulate any true dendritic growth. Into the model was incorporated either a linear or radial temperature gradient normal to the interface (thus also modelling a two dimensional linear diffusion layer). Their results show that at low melting entropies the interface remains stable, but at higher entropies the interface becomes unstable and dendrites develop. They claim good agreement with experiments using ammonium chloride.

Other studies have been carried out using high nucleation rates where the concept of two-dimensional nucleation becomes more inappropriate, especially if the surface becomes very rough. In this case a more elaborate examination of the interaction between atoms can be achieved using the mean field

model[161] or the pair approximation[143,164].

1.4 ELECTROCHEMICAL THEORY

This section on electrochemical theory is not intended as a complete treatise on electrochemistry, rather it is aimed principally at just the relevant areas to the project. For a more comprehensive treatment of electrochemistry and electrochemical techniques the reader should consult a general electrochemical handbook such as those by Bard and Faulkner[165], or Bockris and Reddy[166].

1.4.1 REFERENCE ELECTRODES AND CONVENTIONS

Electrochemical potentials are generally referenced to an arbitrary zero point, determined by the standard hydrogen electrode (SHE):- $Pt/H_2/H^+$ at unit activity. The SHE operates with a continuous stream of hydrogen passing the platinum surface in HCl solution. This reference electrode is of little use as a experimental reference electrode due to its inconvenience in use. Hence a number of other reference electrodes are used in electrochemical measurements, their potentials versus the SHE being accurately known. The criteria for selection of a reference electrode is the stability of its rest potential with regard to the system it is to be used in (eg pH stability). The commonly used reference electrodes are given below with their rest potentials versus SHE at 25^oC:

Electrode	Potential	Uses
Ag/AgCl/1M HCl	0.222 V	:small temperature coefficient
Ag/Ag^+ (0.01M in CH_3CN)	-0.020 V	:non aqueous
Hg/Hg_2Cl_2/sat KCl	0.2424 V	:general for most systems
Hg/Hg_2Cl_2/3.8M KCl		
Hg/Hg_2Cl_2/1.0M KCl	0.2800 V	
Hg/HgO	0.098 V	:high alkaline stability
$Hg/HgSO_4/K_2SO_4$ sat	0.6158 V	:no Cl^-

Thus systems with standard potentials versus SHE > 0 V will oxidise hydrogen and those with potentials < 0 V will reduce protons.

1.4.2 POTENTIALS

In electrochemical systems we are generally concerned with the measurement of an absolute (or inner) electrode/electrolyte potential difference at an interface. This potential is sometimes referred to as the Galvani potential difference ($\Delta\Phi$). Although in real electrochemical cells two such interfaces will exist, we can theoretically consider each in isolation. Considering a model of an electrochemical metal electrolyte interface (fig 1.4), we find an inner surface layer (of thickness 1 - 2 atoms or around 2 - 3 Angstroms), containing adsorbed charged ions (same charge as metal) and surface solvent molecules. In this region (the inner Helmholtz plane), charge transfer can occur between adsorbed species and the electrode. Moving into solution, it becomes clear that a charged metal

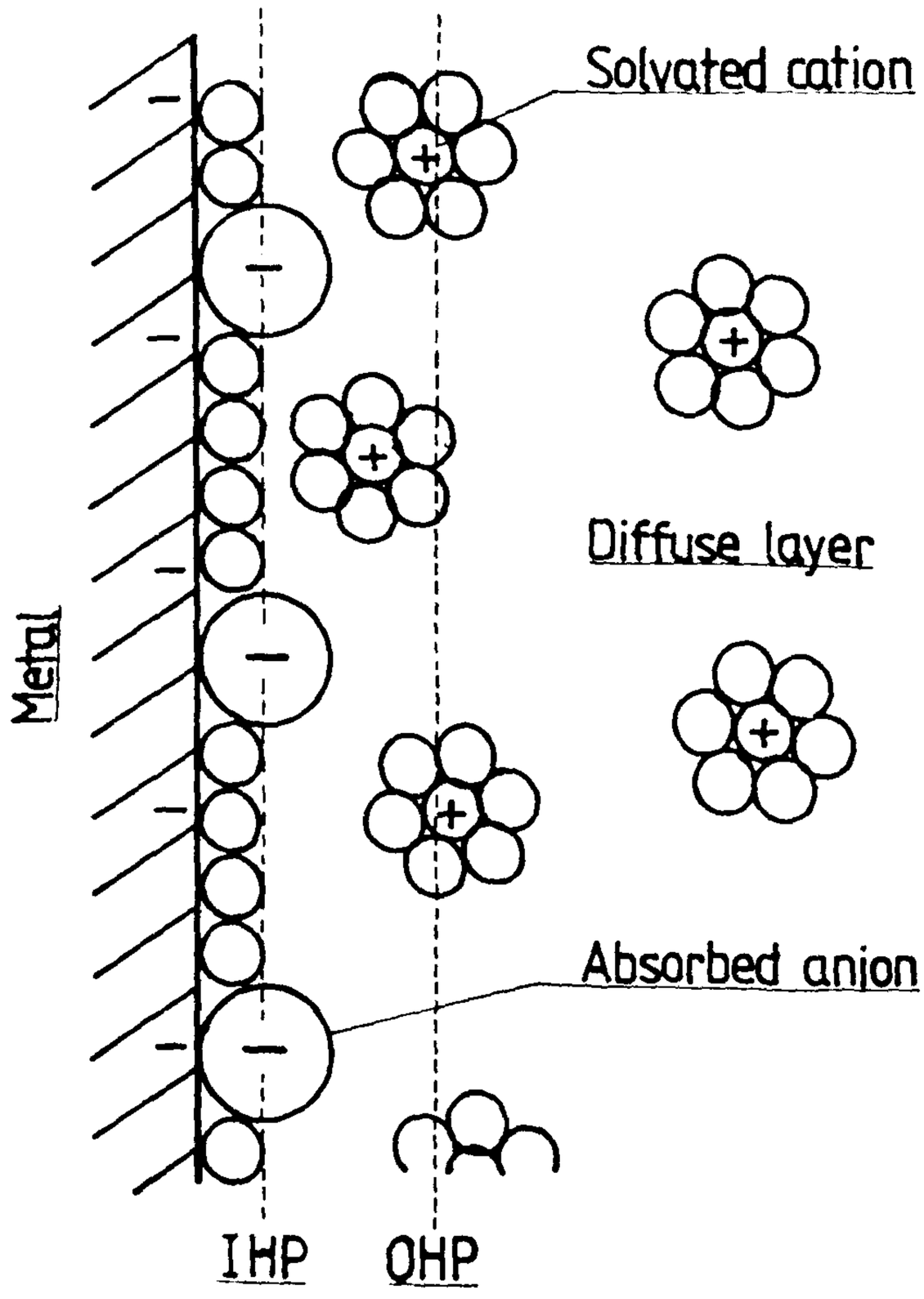

Fig 1.4 Electrochemical model of the charged metal-solution interface (the electrochemical double layer) showing the inner and outer Helmholtz planes (IHP or OHP).

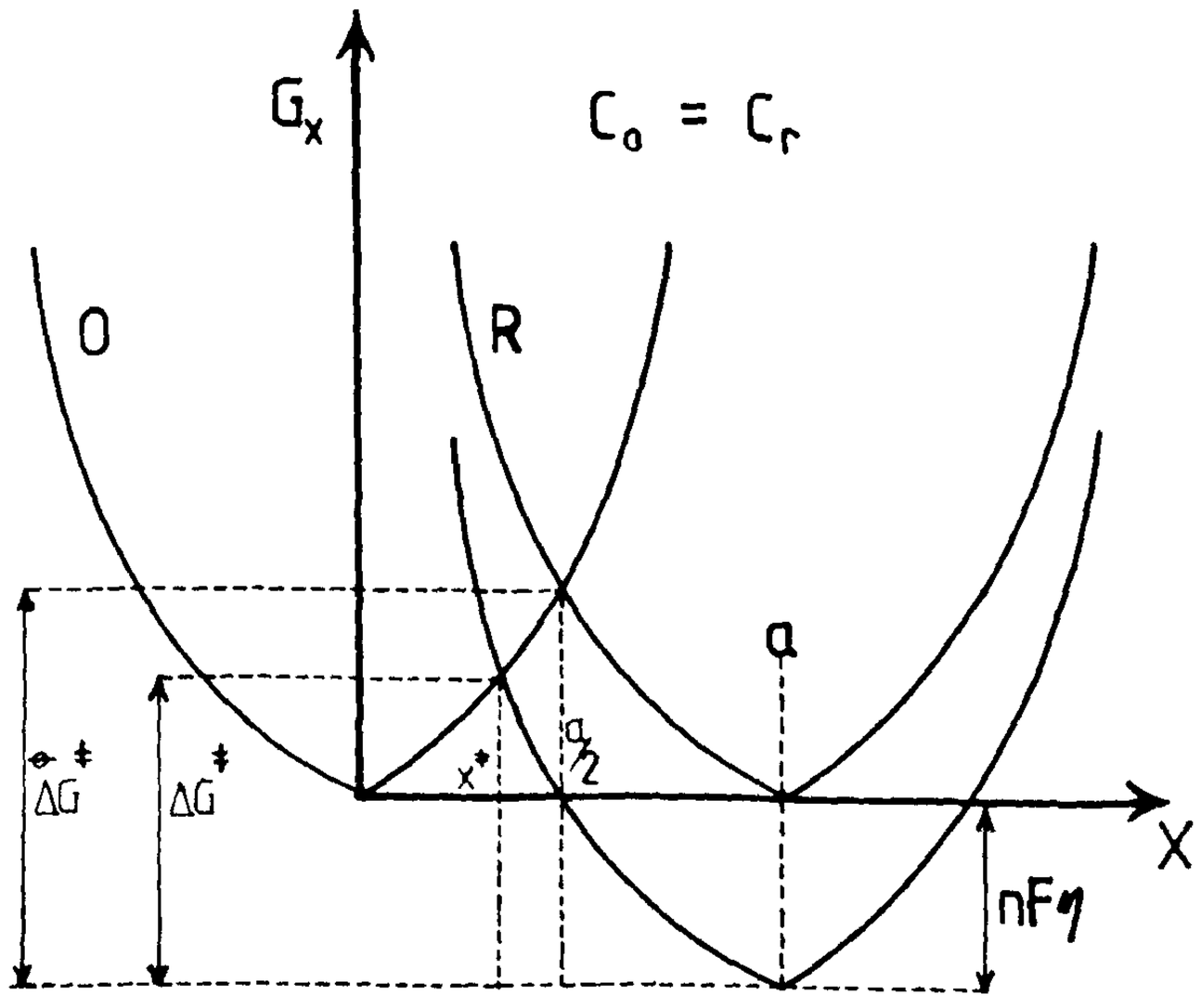

Fig 1.5 Free energy versus reaction coordinate for the reaction $O + e^- \rightleftharpoons R$, under the application of an overpotential η. The initial concentrations of both species are the same.

surface will attract opposite charged ions to the surface layer. Their closest point of approach whilst remaining in solution, defines the outer Helmholtz plane. The charge will also cause orientation of any solvent dipoles at the surface. Thus a diffuse charged layer is formed out from the electrode. Moving away from the electrode, we find the presence of a first diffuse charged layer can be expected to cause a second (and subsequent), diffuse charged layer to be attracted to the first layer. Thus the interface can be conceved of as a series of very diffuse dipole/ion layers out from the metal surface. This interface is called the electrical double layer. However, the subsequent diffuse charged layers can generally be ignored, since molecular motion makes their contribution insignificant. The electrical double layer can be thought of as a simple combination of electrical components;

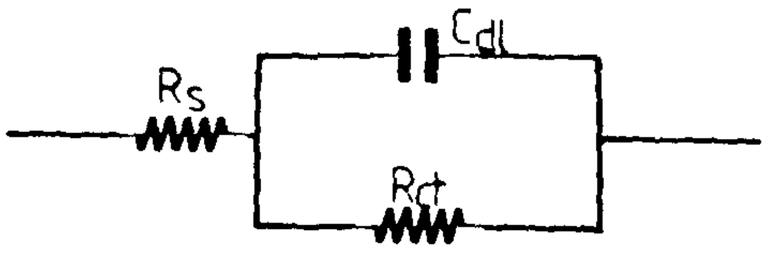

where R_{ct} is the resistance to transfer of charge at the interface (the charge transfer or Faradaic resistance), and C_{dl} is the Faradaic capacity arising from the presence of the charged surface layers (the double layer capacity).

The Galvani potential at the interface, arises as the sum of two potential contributions at such that;

$$\Delta\Phi = \Delta\Psi + \Delta\chi = (\text{Volta}) + (\text{dipole}) \qquad \{1.10\}$$

where the Volta potential difference is the potential required to bring a charged species from the bulk solution (effectively infinite distance) to the dipole layer at the surface. The dipole potential difference is the potential required to transport the charged species accross the orientated dipole

layer at the metal-solution interface. The Galvani potential difference cannot be directly measured for a single interface, since any electrochemical system will require at least two such interfaces. However, we are generally concerned with potentials due to the sum from both interfaces in a system, rather than their separate contributions.

The electrochemical potential ($\bar{\mu}_i$) of a species i, is defined as;

$$\bar{\mu}_i^{\alpha} = \mu_i^{\alpha} + zF\Phi_{\alpha} \qquad (\text{phase } \alpha) \qquad \{1.11\}$$

Where the work done to bring a mole of the species from infinity to the bulk of an uncharged material phase, is the chemical potential (μ_i^{α}), with $nF\Phi_{\alpha}$ being the electrical work required to bring a mole of the species into the material phase (taking into account only the dipole and charge contributions). Thus the electrochemical potential can be defined in terms of the electrochemical free energy ($\bar{G}$), as;

$$\bar{\mu}_i^{\alpha} = \left(\frac{\partial G}{\partial n_i}\right)^{\alpha}_{\mu_j,T,P} + zF\Phi_{\alpha} = \left(\frac{\partial \bar{G}}{\partial n_i}\right)_{\mu_j,T,P} \qquad \{1.12\}$$

With the free energy change associated with an electrochemical reaction being given by;

$$\Delta G = -nFE_{cell} \qquad \{1.13\}$$

1.4.3 DERIVATION OF THE NERNST EQUATION

For a simple electrochemical system at equilibrium, eg;

$$Cd^{2+} + 2e^{-} \rightleftharpoons Cd_s$$

we can write;

$$\bar{\mu}_{Cd} = \bar{\mu}_{Cd^{2+}} + 2\bar{\mu}_e$$

where;

$$\bar{\mu}_{Cd} = \mu^{\ominus}_{Cd}$$

$$\bar{\mu}_{Cd^{2+}} = \mu_{Cd^{2+}} + 2F\Phi_s$$

$$\bar{\mu}_e = \mu_e - F\Phi_m$$

therefore;

$$\Delta\Phi_{ms} = \frac{1}{2F}\left(\mu_{Cd^{2+}} - \mu^{\ominus}_{Cd} + 2\mu_e\right) \qquad \{1.14\}$$

From thermodynamics, we can express the chemical potential as;

$$\mu_i = \mu_i^{\ominus} + RT\ln(a_i) \qquad \{1.15\}$$

hence combining {1.14} and {1.15};

$$\Delta\Phi_{ms} = \frac{1}{2F}\left(\mu^{\ominus}_{Cd^{2+}} - \mu^{\ominus}_{Cd} + 2\mu_e\right) + \frac{RT}{2F}\ln\left(a_{Cd^{2+}}\right)$$

or in more general terms;

$$E_{cell} = E^{\ominus} + \frac{RT}{zF}\ln\left(\frac{a_{ox}}{a_{red}}\right) \qquad \{1.16\}$$

Equation {1.16} being the Nernst equation.

1.4.4 ELECTRON EXCHANGE AT AN ELECTRODE

Consider a simple redox reaction;

$$O + ne^- \underset{k_b}{\overset{k_f}{\rightleftharpoons}} R$$

At the standard potential ($E^{\ominus}$) the concentrations of the reduced and oxidised species will be equal (ie $C_0 = C_r$), and the rate of the forward and backward reactions will be the same ($k_f = k_b$). However, if we shift the system from equilibrium by the application of an overpotential η ($\eta = E_{cell} - E^{\ominus}$), the rate of forward and backward reactions will be different ($k_f \neq k_b$). The free energy is thus changed by an amount $nF\eta$ ($Jmol^{-1}$) and the activation energy ($\Delta G^{\ddagger}$), changes by some smaller amount (see fig 1.5). Considering a cathodic reaction with n = 1, the

reaction coordinate (x) of O is zero and that of R is some value a. If we assume both species have the same force constant (q) and a parabolic function of energy with reaction coordinate about their centres, then at equilibrium;

$$\Delta G_f^{\ddagger} = \Delta G_b^{\ddagger} = qx^2 \qquad \{1.17\}$$

The value for the free energy of both species at any reaction coordiate is given by;

$$\bar{G}_o(x) = \bar{G}_{o,min} + qx^2$$

and;

$$\bar{G}_r(x) = \bar{G}_{r,min} + q(x - a)^2$$

the reaction coordinate of the activated species is given by;

$$x^{\ddagger} = a/2 \qquad [\text{ie } qx^2 = q(x - a)^2]$$

thus the equilibrium value for the activation energy is;

$$\ominus_{\Delta G^{\ddagger}} = qa^2/4 \qquad \{1.18\}$$

Applying a cathodic overpotential, the free energy of the reduced species is changed by $F\eta$, ie;

$$\bar{G}_r(x) = \bar{G}_{r,min} + q(x - a)^2 - F\eta$$

thus the new reaction coordinate becomes;

$$x^{\ddagger} = \frac{qa^2 - F\eta}{2qa} \qquad \{1.19\}$$

and the new activation energy for the forward reaction is given by {1.17} and {1.19};

$$\Delta G_f^{\ddagger} = q\left[\frac{q^2a^4 + F^2\eta^2 - 2qa^2F\eta}{4q^2a^2}\right]$$

The change in the forward activation energy is thus;

$$\Delta(\Delta G_f^{\ddagger}) = \frac{F^2\eta^2}{4qa^2} - \frac{F\eta}{2}$$

combining with {1.18};

$$\Delta(\Delta G_f^{\ddagger}) = \frac{F^2\eta^2}{16\ominus_{\Delta G^{\ddagger}}} - \frac{F\eta}{2} \qquad \{1.20\}$$

From transition state theory it can be shown that;

$$k_f = \beta \exp(-\Delta G_f^{\ddagger}/RT) \quad ; \quad \beta = k_B T/h$$

hence the rate constant for the forward reaction is given by;

$$k_f = \beta \exp\left[\frac{-\Delta G_f^{\ddagger}}{RT}\right] \exp\left[\frac{1}{RT}\left[\frac{F^2\eta^2}{16\,{}^{\ominus}\Delta G^{\ddagger}} - \frac{F\eta}{2}\right]\right] \qquad \{1.21\}$$

since;

$$k^{\ominus} = \exp(-{}^{\ominus}\Delta G^{\ddagger}/RT)$$

and defining the catodic transfer coefficient α;

$$\alpha = \frac{1}{2} - \frac{F\eta}{16\,{}^{\ominus}\Delta G^{\ddagger}} \qquad \{1.22\}$$

we can re-write {1.21} for the general reaction at equilibrium as;

$$k_f = k^{\ominus} \exp\left[\frac{-\alpha n F \eta}{RT}\right] \qquad \{1.23\}$$

similarly;

$$k_b = k^{\ominus} \exp\left[\frac{(1-\alpha) n F \eta}{RT}\right] \qquad \{1.24\}$$

For the case at equilibrium, where the concentrations of the oxidised and reduced species are not the same the electrochemical free energy of the more stable species will be decreased by $-nF(E_{cell} - E^{O})$ (from {1.13}). This value is given by the Nernst relationship {1.16}. The forward and reverse activation energies (ignoring activity coefficients), are given by;

$$\Delta G_f^{\ddagger} = {}^{\ominus}\Delta G^{\ddagger} + \alpha RT \ln(C_o/C_r)$$

and;

$$\Delta G_b^{\ddagger} = {}^{\ominus}\Delta G^{\ddagger} + (1-\alpha) RT \ln(C_o/C_r)$$

Upon application of an overpotential, the forward and reverse activation energies are changed by $+\alpha n F \eta$ and $-(1-\alpha) n F \eta$

respectively, such that the in the cathodic direction the forward activation energy becomes;

$$\Delta G_f^{\ddagger} = {}^{\ominus}\Delta G^{\ddagger} + \alpha RT\ln(C_o/C_r) + \alpha nF\eta \qquad \{1.25\}$$

The resultant cathodic current at an electrode area A, is given by;

$$i_c = nFAk_fC_o^s \qquad \{1.26\}$$

with k_f being given by;

$$k_f = \beta\exp(-\Delta G_f^{\ddagger}/RT) \qquad \{1.27\}$$

Thus in a heterogenous system with;

$$k_f^h = \beta C_o^s/C_o \qquad \{1.28\}$$

the cathodic current can be obtained by combining {1.25} - {1.28};

$$i_c = nFAk_f^hC_o\exp\left[\frac{-{}^{\ominus}\Delta G^{\ddagger} - \alpha RT\ln(C_o/C_r) - \alpha nF\eta}{RT}\right] \qquad \{1.29\}$$

with;

$$k_h^{\ominus} = k_f^h\exp(-{}^{\ominus}\Delta G^{\ddagger}/RT)$$

{1.29} becomes;

$$i_c = nFAk_h^{\ominus}C_o^{(1-\alpha)}C_r^{\alpha}\exp\left[\frac{-\alpha nF\eta}{RT}\right] \qquad \{1.30\}$$

Similarly for the anodic current;

$$i_a = nFAk_h^{\ominus}C_o^{(1-\alpha)}C_r^{\alpha}\exp\left[\frac{(1-\alpha)nF\eta}{RT}\right] \qquad \{1.31\}$$

Thus at equilbrium ($\eta = 0$) when the net current is zero, the cathodic and anodic currents become equal in magnitude. This equilibrium current magnitude is called the exchange current (i_o) and is given by;

$$i_o = |i_a| = |i_c| = nFAk_h^{\ominus}C_o^{(1-\alpha)}C_r^{\alpha} \qquad \{1.32\}$$

The overall current ($i = i_c - i_a$) is therefore given by;

$$i = i_o\left\{\exp\left[\frac{-\alpha nF\eta}{RT}\right] - \exp\left[\frac{(1-\alpha)nF\eta}{RT}\right]\right\} \qquad \{1.33\}$$

This expression is the Butler - Volmer equation[167].

Figure 1.6a gives the resultant current/overpotential dependence predicted. At low overpotentials, the Butler - Volmer expression can be linearised (since at low values of x, $e^x \longrightarrow 1 + x$), giving;

$$i = i_o nF\eta/RT \qquad \{1.34\}$$

or;

$$\eta/i = RT/nFi_o = R_{ct} \qquad \{1.35\}$$

The ratio η/i is called the charge transfer or Faradaic resistance. At high overpotentials the Butler - Volmer relationship reduces to the form observed by Tafel[168], where the cathodic and anodic currents become;

$$i_c = i_o \exp\left[\frac{-\alpha nF\eta}{RT}\right]$$

$$i_a = i_o \exp\left[\frac{(1-\alpha)nF\eta}{RT}\right]$$

or;

$$\eta = \frac{2.303RT}{\alpha nF}\left[\log(i_o) - \log(i_c)\right] \qquad \{1.36\}$$

and;

$$\eta = \frac{2.303RT}{(1-\alpha)nF}\left[\log(i_o) - \log(i_a)\right] \qquad \{1.37\}$$

{1.36} and {1.37} have the form;

$$\eta = a + b\log(i)$$

as described by Tafel. These give the characteristic Tafel plots as shown in fig 1.6b.

For a system, where at equilibrium the reduced species has zero concentration, eg;

$$Cd^{2+} + 2e^- \rightleftharpoons Cd_s$$

we can write {1.32} as;

$$i_o = nFAk_h^{\ominus}C_o$$

combining with {1.35}, we get an expression for the heterogenous

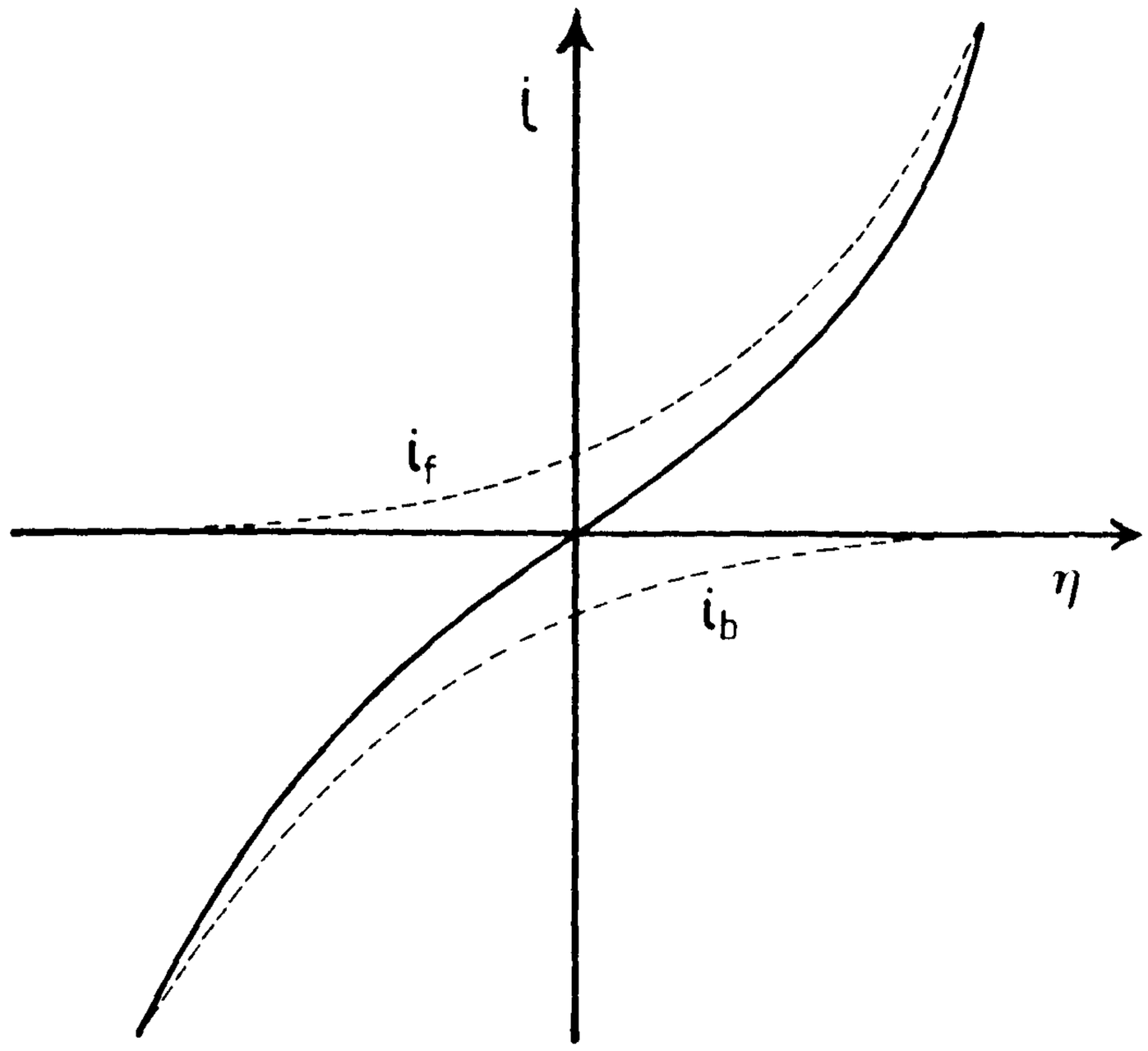

Fig 1.6a Plot of the Butler - Volmer equation for a reversible reaction.

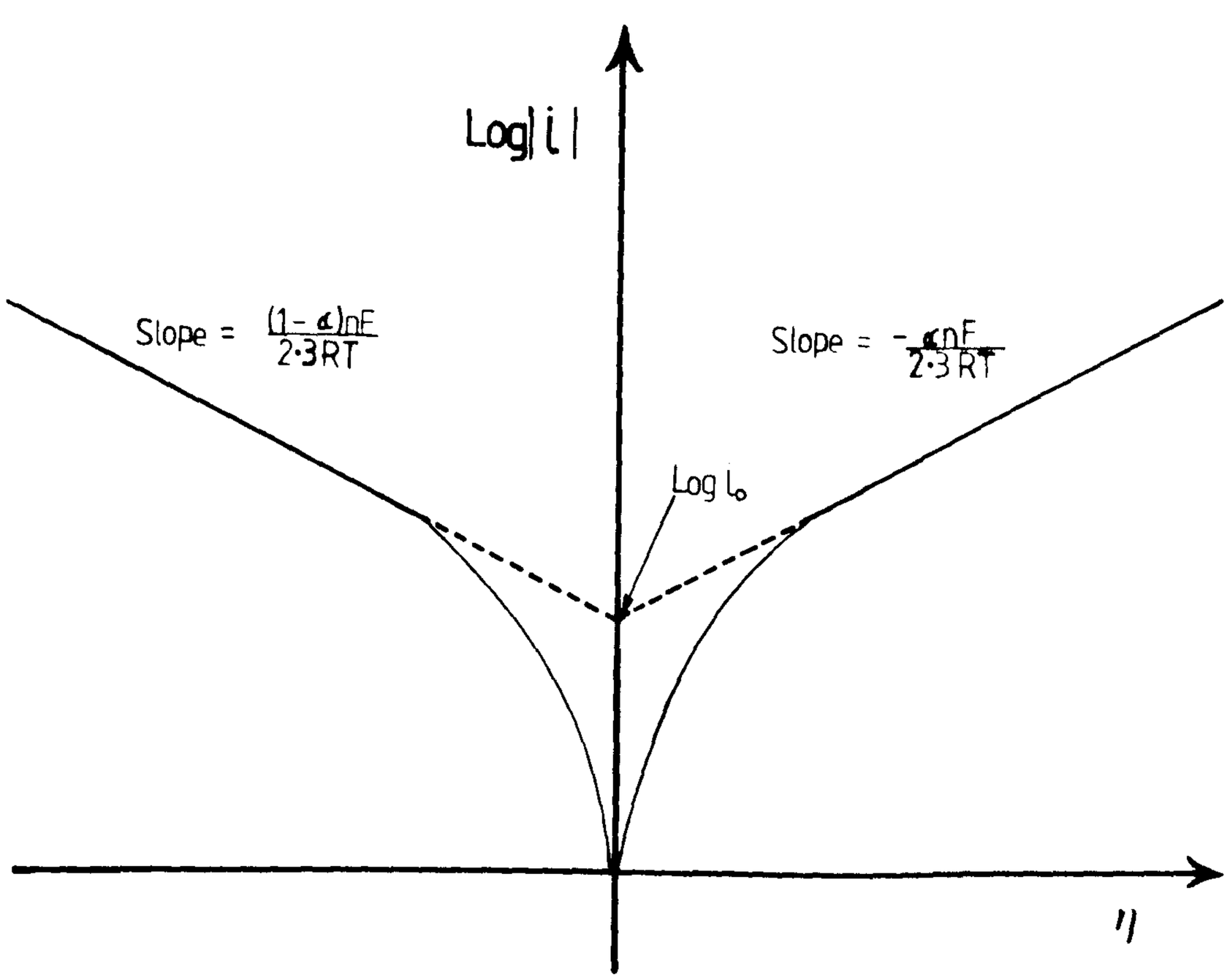

Fig 1.6b Tafel plot of an idealised reversible reaction.

rate constant in terms of measureable quantities, given by;

$$k_h^{\ominus} = \frac{RT}{n^2F^2C_oR_{ct}} \qquad \{1.38\}$$

1.4.5 CYCLIC VOLTAMMETRY

Considerations of the fairly complex boundary value problems associated with both, reversible and irreversible reactions under the influence of a potential changing at at constant rate, have been carried out by a number of workers[169-172] most notably by Nicholson[172]. It can be shown that for a reversible reaction, the peak potential is independent of sweep rate and the peak current is given by;

$$i_p = 2.69 \times 10^5 n^{3/2} D_o^{1/2} C_o v^{1/2} \qquad \{1.39\}$$

For the irreversible case the peak potential is dependent on the sweep rate and is given by;

$$E_p = E^{\ominus} - \frac{RT}{nF\alpha}\left[0.780 + \frac{1}{2}\ln\left(\frac{\alpha n D_o F v}{RT}\right) - \ln(k_o^{\ominus})\right] \qquad \{1.40\}$$

and the peak current for the irreversible case is;

$$i_p = 2.99 \times 10^5 n(\alpha n)^{1/2} D_o^{1/2} C_o v^{1/2} \qquad \{1.41\}$$

Thus linear sweep techniques allow determination of α, n and k .

1.4.6 ROTATING DISC DYNAMICS

If we consider a stationary electrode with a simple redox reaction occurring (see fig 1.7), it is clear that two processes are involved in determining the rate of product formation, a) mass transfer of the substrate to the surface and b) charge transfer at the electrode. At low overpotentials the process is

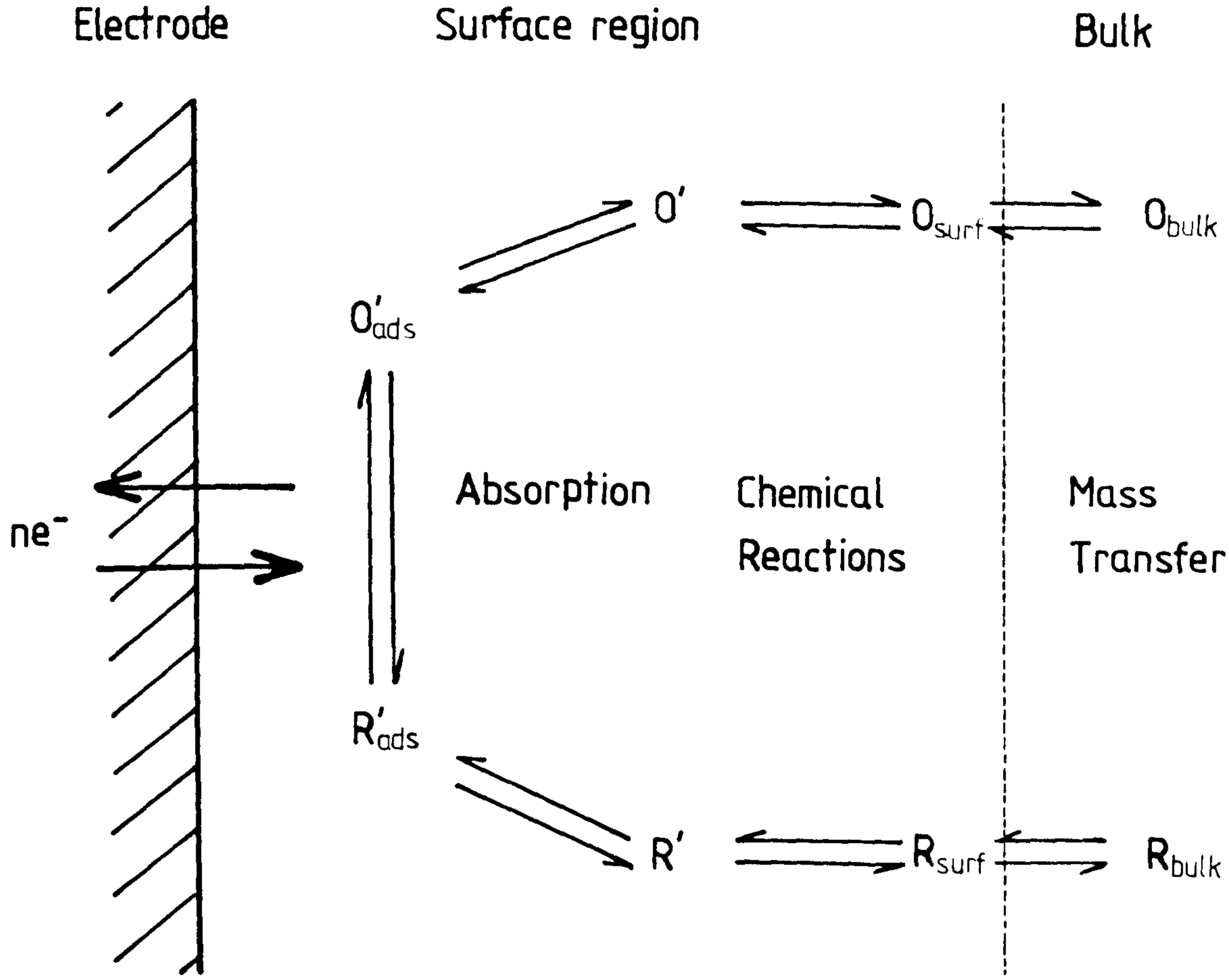

Fig 1.7 Electrode processes involved for a simple reaction $O + e \rightleftharpoons R$, involving mass transport.

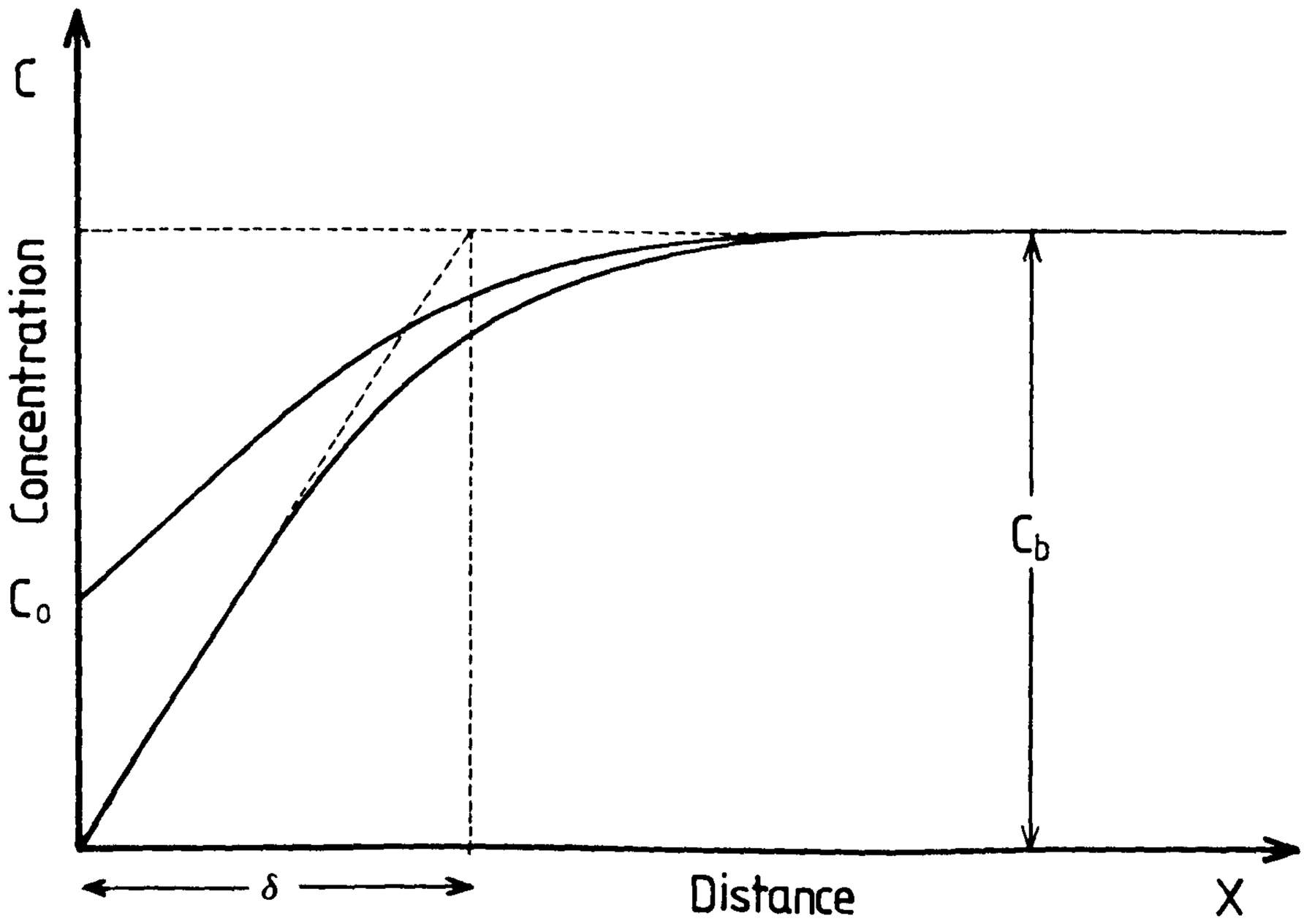

Fig 1.8 Concentration profiles for the substrate O for the reaction $O + e \rightleftharpoons R$, bulk concentration C_b. Lower curve is under diffusion control, giving rise to a linear Nernst diffusion layer of thickness δ. The upper curve shows a typical profile under mixed control, giving rise to a surface concentration C_o^s.

charge transfer (activation) controlled, and at high overpotentials mass transfer controlled. This gives rise to characteristic concentration profiles as shown in fig 1.8. Under steady-state conditions, the initial portion of the substrate concentration profile will be linear. If this linear portion is extended to the bulk substrate concentration, we obtain the Nernst diffusion layer thickness. Thus we can simplify the real concentration profile to two regions, a) the bulk where convection occurs, keeping the substrate concentration constant and b) the Nernst diffusion region, where mass transfer of substrate is determined soley by diffusion. Assuming linear diffusion, the flux of substrate O at the electrode surface is given by Fick´s laws of diffusion. The first law gives the rate of mass transfer at a location x, time t as;

$$-J_O(x,t) = D_O \frac{\partial C_O(x,t)}{\partial x} \qquad \{1.42\}$$

The second law gives the change in substrate concentration with time as;

$$\frac{\partial C_O(x,t)}{\partial t} = D_O \frac{\partial^2 C_O(x,t)}{\partial x^2} \qquad \{1.43\}$$

In the absence of convection, the Nernst diffusion layer at an electrode grows out at a rate (from statistical analysis[165]), approximately given by;

$$\bar{\Delta} = \sqrt{2Dt} \qquad \{1.44\}$$

However, in the real system the diffusion layer soon reaches a steady-state thickness, determined by the convective conditions encountered. With stationary electrodes convection conditions cannot be accurately defined, but with a rotating disc electrode

the convective hydrodynamics can be solved to a reasonable degree of accuracy. Under these conditions Levich[173] has shown that the diffusion layer thickness is given by;

$$\delta_o = 1.61\, D_o^{1/3} \omega^{-1/2} \nu^{1/6} \qquad \{1.45\}$$

The current being determined by;

$$i = \frac{nF(k_f C_o - k_b C_r)}{1 + 1.61 \nu^{1/6}(k_f D_o^{-2/3} + k_b D_r^{-2/3})\omega^{-1/2}} \qquad \{1.46\}$$

and if the back reaction can be ignored, the current flowing is;

$$i = \frac{nFAk_f C_o}{1 + 1.61 k_f D_o^{-2/3} \nu^{1/6} \omega^{-1/2}} \qquad \{1.47\}$$

At high η and k_f (diffusion control region), this becomes;

$$i = 0.621\ nFD_o^{2/3} \nu^{-1/6} \omega^{1/2} C_o \qquad \{1.48\}$$

and at low k_f (charge transfer control), {1.45} becomes;

$$i = nFk_f C_o \qquad \{1.49\}$$

Therefore an electrode operating in the diffusion controlled region, will have a current flowing dependent on the root of rotation rate. Whilst if in the charge transfer controlled region, current will be independent of rotation rate. Thus rotating disc techniques can allow determination of D_o, k_f and k_b.

1.4.7 A.C. IMPEDANCE

The application of a small amplitude sinusoidal perturbation ($E_o \sin\omega t$) to an electrochemical system, causes a variation in the current response dependent on the electrode processes occurring. The current response is given by $I_o \sin(\omega t + \theta)$, and has the vector properties of magnitude (E_o/I_o) and direction (the phase angle θ). The overall impedance can be conveniently represented in terms of complex plane impedances,

with an in phase component Z′ and an out of phase component Z′′. This can be represented as a complex plane plot with Z′ and Z′′ plotted along the x and y axes (real and imaginary), respectively. Since most impedance measurements are dependent on the frequency of the sinusoidal signal applied, it is usual to present impedance data in the form of an a.c. impedance spectrum. This consists of a series of impedance measurements made at different frequencies and diplayed in a complex plane plot.

The analysis of a.c. impedance data is simplified by considerations of equivalent circuits. A pure resistance R, gives a pure in phase response Z′ = R, Z′′ = 0. A pure capacitance C, only has an out of phase response ($\theta = 90^{\circ}$) Z′′ = $-j/\omega C$, Z′ = 0. Impedances can mathematically be treated in circuit analysis as are pure resistances, ie in series;

$$Z = Z_1 + Z_2$$

and in parallel;

$$\frac{1}{Z} = \frac{1}{Z_1} + \frac{1}{Z_2}$$

Hence a simple network consisting of a resistance and capacitance in series;

has an impedance given by;

$$Z = R - j/\omega C \qquad \{1.50\}$$

For a parallel network of a resistance and a capacitance;

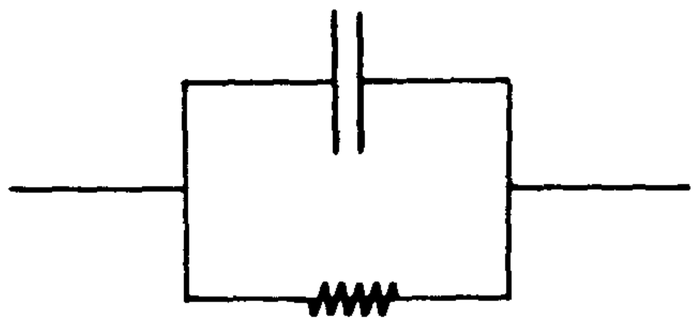

the impedance is more complex and is given by;

$$\frac{1}{Z} = \frac{1}{R} + \frac{1}{-j/\omega C}$$

ie

$$Z = [1/R + j\omega C]^{-1} \qquad \{1.51\}$$

Figure 1.9 shows the a.c. impedance spectra found for these simple equivalent circuits. Thus analysis of a.c. impedance spectra can be made by comparison to the appropriate equivalent circuit.

For an electrode, where the reaction;

$$O + e^{-} \rightleftharpoons R$$

is occurring, the a.c. impedance can be thought of as the sum of contributions from four equivalent components. It will have a pure resistive component, due to the solution resistance (R_s), a pure capacitive component due to the double layer capacity (C_{dl}), a second pure resistive component due to the charge transfer resistance (R_{ct}), and an impedance due to mass transfer dependence, called the Warburg impedance (W). This can be represented as;

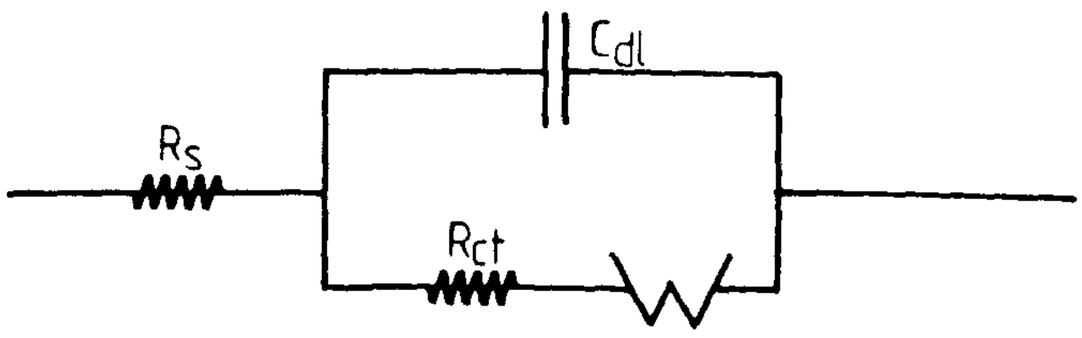

Under charge transfer control, diffusional effects are unimportant, hence the Warburg impedance contribution can be neglected. Under mixed or diffusion control the Warburg impedance becomes important and cannot be ignored. By setting

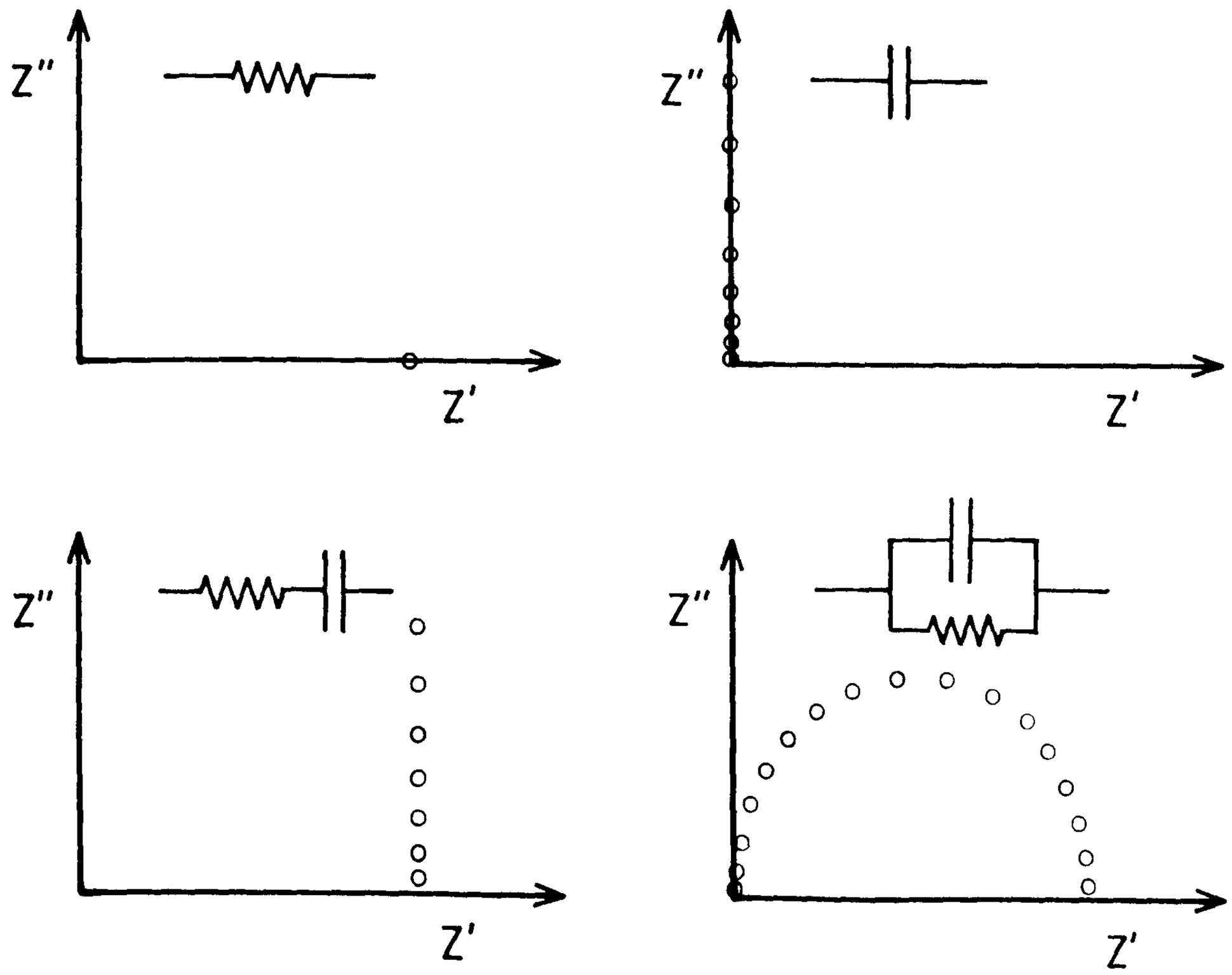

Figs 1.9 &1.10 A.c. impedance spectra associated with some simple electrical circuits (top), and that for the idealised equivalent circuit for an operating electrode (bottom).

the appropriate boundary values, a solution to Fick's laws of diffusion, leads to the derivation of the Warburg impedance. For the simple electrochemical system considered, the Warburg impedance is given by;

$$W = \sigma\omega^{-1/2} - j\sigma\omega^{-1/2} \qquad \{1.52\}$$

where the Warburg coefficient is defined by;

$$\sigma = \frac{RT}{n^2F^2\sqrt{2}}\left[\frac{1}{C_o^s D_o^{1/2}} + \frac{1}{C_r^s D_r^{1/2}}\right] \qquad \{1.53\}$$

Thus for the equivalent circuit above, the total impedance is given by;

$$Z = R_s + \frac{1}{j\,C_{dl} + [R_{ct} + \sigma\omega^{-1/2} - j\sigma\omega^{-1/2}]^{-1}}$$

or;

$$Z = R_s + \frac{R_{ct} + \sigma\omega^{-1/2} - j\sigma\omega^{-1/2}}{1 + \omega C_{dl}\sigma\omega^{-1/2} + j\omega C_{dl}(R_{ct} + \sigma\omega^{-1/2})}$$

which gives;

$$Z = R_s + \frac{R_{ct} + \sigma\omega^{-1/2} - j[\omega R_{ct}^2 C_{dl} + 2\sigma\omega^{1/2} R_{ct} C_{dl} + 2\sigma^2 C_{dl} + \sigma\omega^{-1/2}]}{1 + \omega^2 R_{ct}^2 C_{dl}^2 + 2\sigma\omega^{1/2} C_{dl} + 2\sigma^2\omega C_{dl}^2 + 2\sigma\omega^{3/2} R_{ct} C_{dl}^2}$$

separating into the real and imaginary components;

$$Z' = R_s + \frac{R_{ct} + \sigma\omega^{-1/2}}{(\sigma\omega^{1/2}C_{dl} + 1)^2 + \omega^2 C_{dl}^2 (R_{ct} + \sigma\omega^{-1/2})^2} \qquad \{1.54\}$$

and;

$$Z'' = -j\left[\frac{\omega C_{dl}(R_{ct} + \sigma\omega^{-1/2})^2 + \sigma\omega^{-1/2}(\sigma\omega^{1/2}C_{dl} + 1)}{(\sigma\omega^{1/2}C_{dl} + 1)^2 + \omega^2 C_{dl}^2 (R_{ct} + \sigma\omega^{-1/2})^2}\right] \qquad \{1.55\}$$

At low frequencies where the process is diffusion controlled, $\omega \rightarrow 0$, thus the impedance is given by;

$$Z' = R_s + R_{ct} + \sigma\omega^{-1/2}$$

$$Z'' = \sigma\omega^{-1/2} + 2\sigma^2 C_{dl}$$

combining (as in the complex plane plot of Z' versus Z'') we

get;

$$Z' = R_s + R_{ct} + Z'' - 2\sigma^2 C_{dl} \qquad \{1.56\}$$

which is the equation of a straight line of unity slope, intercept $(R_s + R_{ct} - 2\sigma^2 C_{dl})$. At high frequencies where charge transfer is rate limiting, $\omega^{-1/2} \longrightarrow 0$, hence {1.54} and {1.55} reduce to;

$$Z' = R_s + \frac{R_{ct}}{1 + \omega^2 C_{dl}^2 R_{ct}^2}$$

$$Z'' = \frac{\omega C_{dl} R_{ct}^2}{1 + \omega^2 C_{dl}^2 R_{ct}^2}$$

combining in the complex plane;

$$(Z'')^2 = (R_{ct}/2)^2 - (Z' - R_s - R_{ct}/2)^2 \qquad \{1.57\}$$

which is the equation of a circle, with maximum Z'' at a frequency given by;

$$\omega_{max} = \frac{1}{C_{dl} R_{ct}} \qquad \{1.58\}$$

Hence, in a system with mixed control, the characteristic impedance spectrum (see fig 1.10), tends towards a semicircle at higher frequencies and a straight line, slope 1, at lower frequencies.

Thus a.c. impedance measurements can be used to obtain values for R_s, R_{ct} (and thus i_o and k_o), σ and C_{dl}.

CH 2 EXPERIMENTAL

2.1 ROTATING DISC CELL FOR A.C. IMPEDANCE

This cell design (fig 2.1) was used for the majority of the short term (<14 hours) experimental work, and was constructed specifically for the rotating disc electrodes and assembly described in CH 2.2 and CH 2.4.1. It was constructed along conventional lines with a reference electrode compartment connected to the main body of the cell via a Luggin probe with a Teflon/glass tap. Two secondary electrodes were provided, one in the main body, consisting of 2.5 cm^2 of platinum foil positioned $\simeq$1 cm below the Luggin tip. Thus providing a symmetrical arrangement for the a.c. impedance work. The other secondary electrode (platinum 1.5 cm^2) is in a separate compartment connected to the main body via a grade 2 glass fritt. This allowed experiments to be carried out whereby products from the secondary electrode (principally oxygen) could escape to the air. Thus avoiding any contamination of the bulk of the electrolyte in the main body of the cell, hence keeping the working electrodes free from the influence of oxygen. Provision for deoxygenation was included by incorporating a nitrogen gas inlet into the main cell base. When assembled [CH 2,8,2], all glass joints required a Teflon sleeve to avoid any possibility of KOH/glass welding.

2.1.2 LONG TERM CELL

This cell was essentially a modified rotating disc cell

without the separate secondary electrode compartment. An identical Luggin probe connection is used with a similar main platinum foil secondary electrode. The cell was connected up as described in CH 2.8.3, using Teflon sleeves at all glass joints.

2.2 ELECTRODES

2.2.1 REFERENCE ELECTRODES

2.2.1.1 MERCURY/MERCURIC OXIDE

All experiments in alkaline solution used mercury/mercuric oxide reference electrodes in 10.00M KOH stock solution. The electrodes were constructed as shown in fig 2.1 Electrodes were made up by placing doubly distilled mercury in the bottom of the reference compartment, sufficient to cover the platinum wire contact. A small quantity of 10.00M KOH then being added, followed by a quantity of yellow mercuric oxide (HgO), providing a complete covering of the mercury. The electrode is then topped up with 10.00M KOH and placed in a 4 way electrode holder, containing 10.00M KOH. Three such electrodes were made up in this way and allowed to settle down overnight before being used (allowing a ´amalgam´ of Hg/HgO to be formed). One electrode was kept as a reference for the other two. All three electrodes were initially within 0.2 mV of each other. After a period of one week the agreement was improved to ±0.02 mV of each other. Over a year of usage no electrode deterioration was seen (maximum difference ≐0.4 mV). This stability is dependent on the provision of Teflon sleeves, to ensure no glass welding

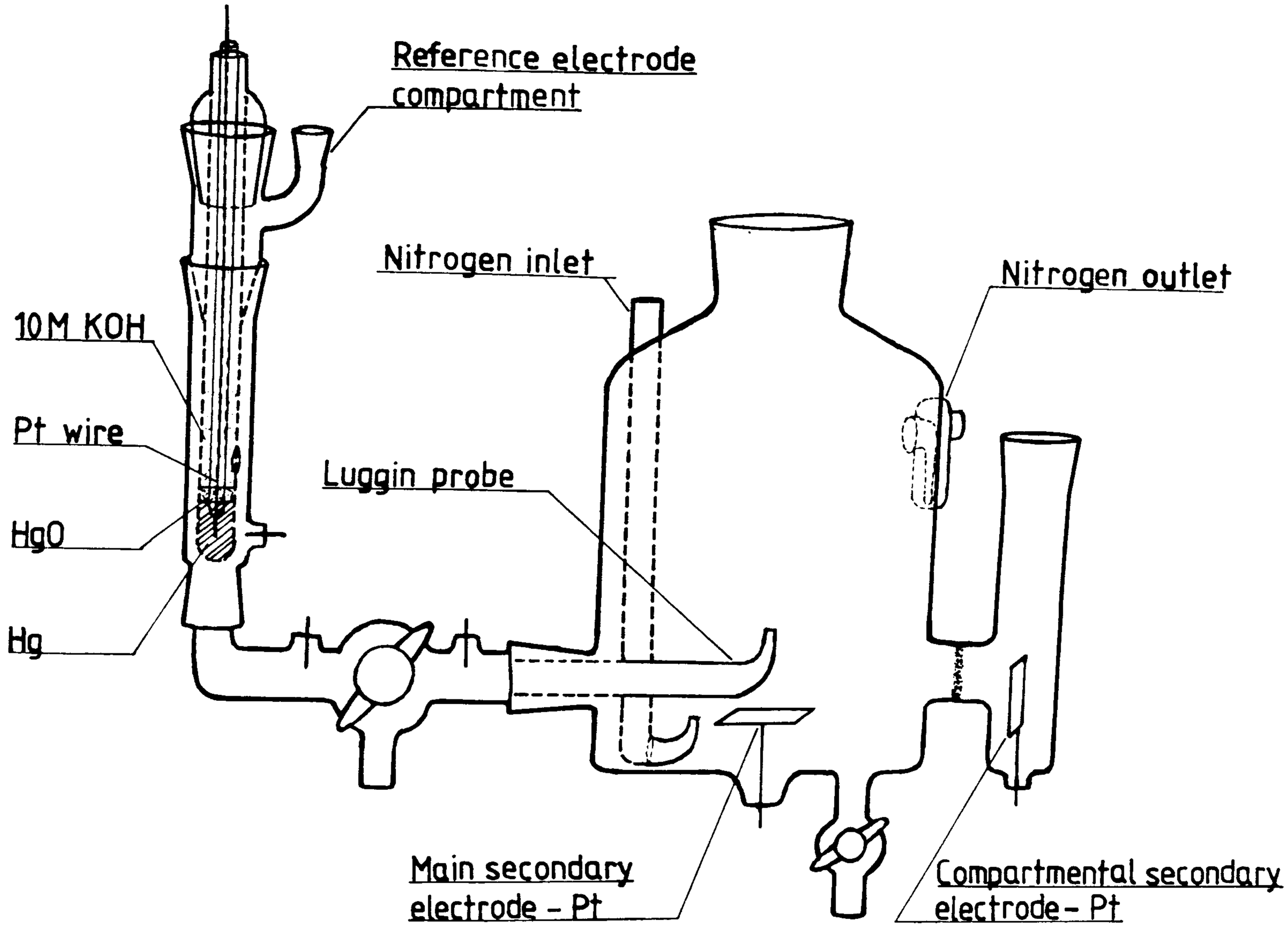

Fig 2.1 Main rotating disc cell used for shorter term experiments, and the Hg/HgO reference electrode used for all alkali experiments.

occurs and that KCO_3 formation is kept to a minimum. In addition care had to be exercised in use since a direct blow could cause mercuric oxide to contaminate the main reference electrode compartment of the cell.

2.2.1.2 MERCURY/MERCUROUS CHLORIDE - CALOMEL

These electrodes were intended for use in acidic solutions of cadmium sulphate and were prepared using a similar reference design as for the Hg/HgO system, with the addition of a glass fritt to the side outlet of the electrode. Doubly distilled mercury was placed in the bottom of the compartment followed by a previously prepared mercury/mercurous chloride paste. This was covered with a mercurous chloride top layer and was topped up with saturated potassium chloride solution. Three such electrodes were prepared and kept in a 4 way reference holder when not in use. Rest potentials were not in such good agreement as with the Hg/HgO reference electrodes and showed some instability upon movement, despite allowance for a settling down period. The agreement was ±1.5 mV.

2.2.1.3 $Cd/Cd^{2+}/0.1M\ CdSO_4 + 0.5M\ H_2SO_4$

A simple reference electrode system was used for most acidic solutions, consisting of a cadmium wire (99.9999% purity) placed into 0.100M $CdSO_4$/0.5M H_2SO_4 solution in the reference electrode compartment. The electrode showed reasonable stability for the short term (< 3 hour) experiments, of ±2mV versus the working electrode (99.999% Cd) in the same solution,

with both exposed to the air. However if left open for any period of time, a deterioration in the cadmium reference was noted with some evidence of dissolution (timescale > 1 week). This effect was not considered significant for experiments in 0.1M $CdSO_4$/0.5M H_2SO_4 solutions, but posed some difficulties in lower concentration solutions due to 1) junction potentials between reference and main cell solution and 2) leakage of Cd^{2+} across the tap and out of the Luggin probe causing changes in the effective bulk concentration. Thus the 0.1M Cd^{2+}/Cd reference electrode could only be reliably used for experiments in Cd/0.001M $CdSO_4$ solutions over short periods (<20 mimutes). For longer periods a calomel reference was used. Experiments using 0.001M $CdSO_4$ as the reference electrolyte were unsucsessful due to the instability of the rest potential (due to a low exchange current).

2.2.2 COUNTER ELECTRODES

All counter electrodes used in experimental work (see fig 2.1), were constructed of 0.125 mm thick platinum foil (99.99+ %) welded to 0.25 or 0.5 mm platinum wire (99.99+ %). The platinum wire first being heat sealed into the glass cell, then additional Epoxy resin being used on the outside of the cell/wire junction to ensure no leakage of the electrolyte out. A perfect platinum/glass seal is difficult to achieve, hence usage of the Epoxy resin.

2.2.3 NICKEL ROTATING DISC ELECTRODES

The nickel disc electrodes (fig 2.2) were constructed to fit the cell [see CH 2.1] and rotating disc assembly as described in CH 2.2. Each consisted of a Teflon holder with a tapered working electrode space. The working electrodes were made up from 5 mm nickel rod (99.98+ %), several being machine tapered down to a 4 mm diameter working electrode surface, each pellet being 5 or 8 mm in length. The angle of taper was slightly less than that of the holder, to ensure a good tight fit. Two versions of the nickel rotating disc electrode were used, either; a) using 8 mm long nickel pellets kept in place by pressure from the electrical contact spring, or; b) using 5 mm long pellets sealed into place using Epoxy resin [quick set Epoxy adhesive from Radio Spares limited]. This latter design gives improved leakage resistance after prolonged immersion in the electrolyte. It should be noted that Epoxy resin only bonds well to the nickel, and thus some leakage is possible between the Epoxy and Teflon. This will not effect results, provided the leakage electrolyte does not make electrical contact with the nickel.

The electrodes screw fit onto the rotating disc electrode assembly (fig 2.3), with electrical contact being achieved via the spring connector. When in place the working electrode surface is $\simeq$8 mm above the tip of the Luggin probe and $\simeq$2 cm above the main secondary electrode.

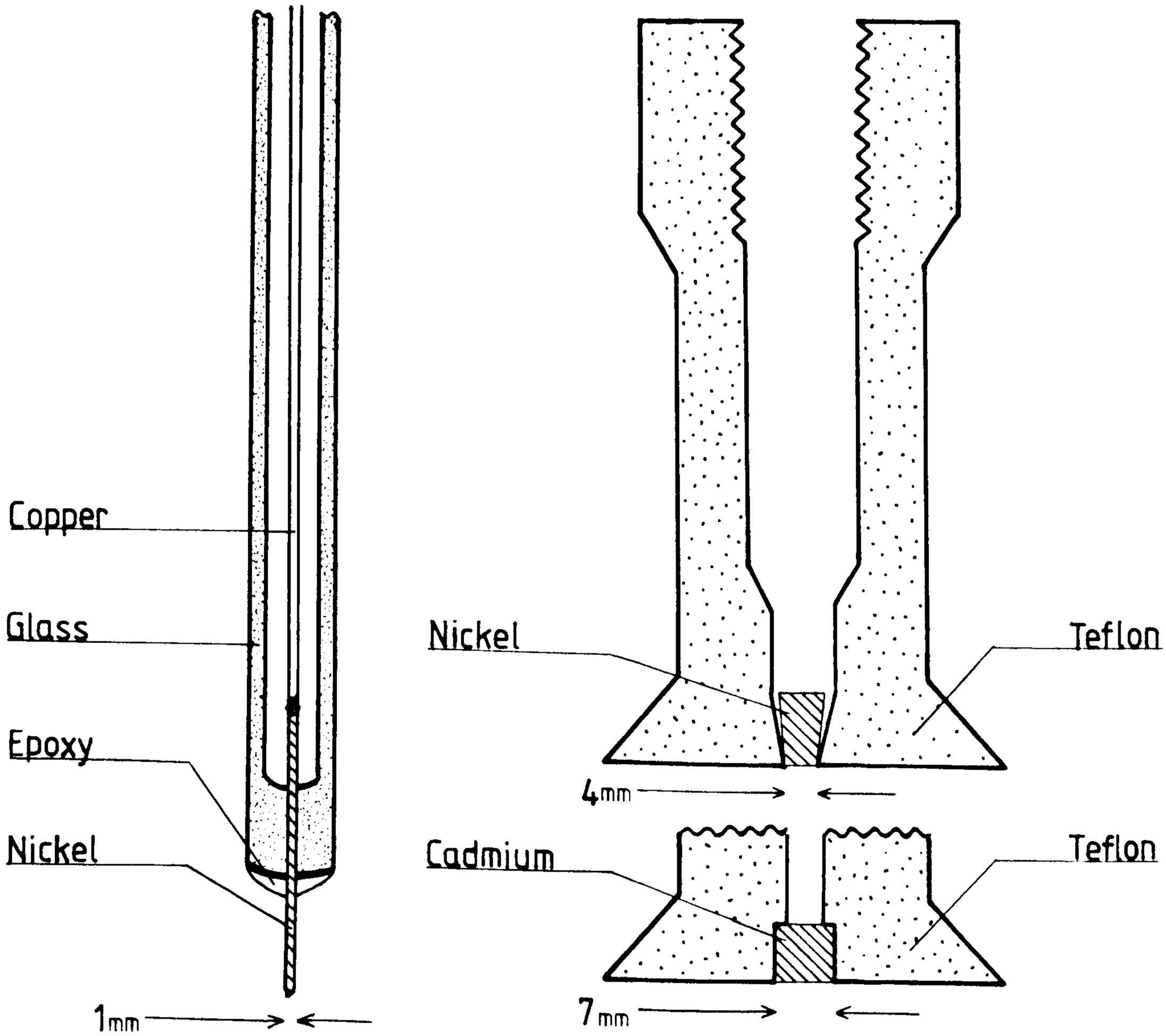

Fig 2.2 Design of main working electrodes used; left:- nickel wire (long term deposition); right:- rotating disc (top - nickel; bottom - cadmium).

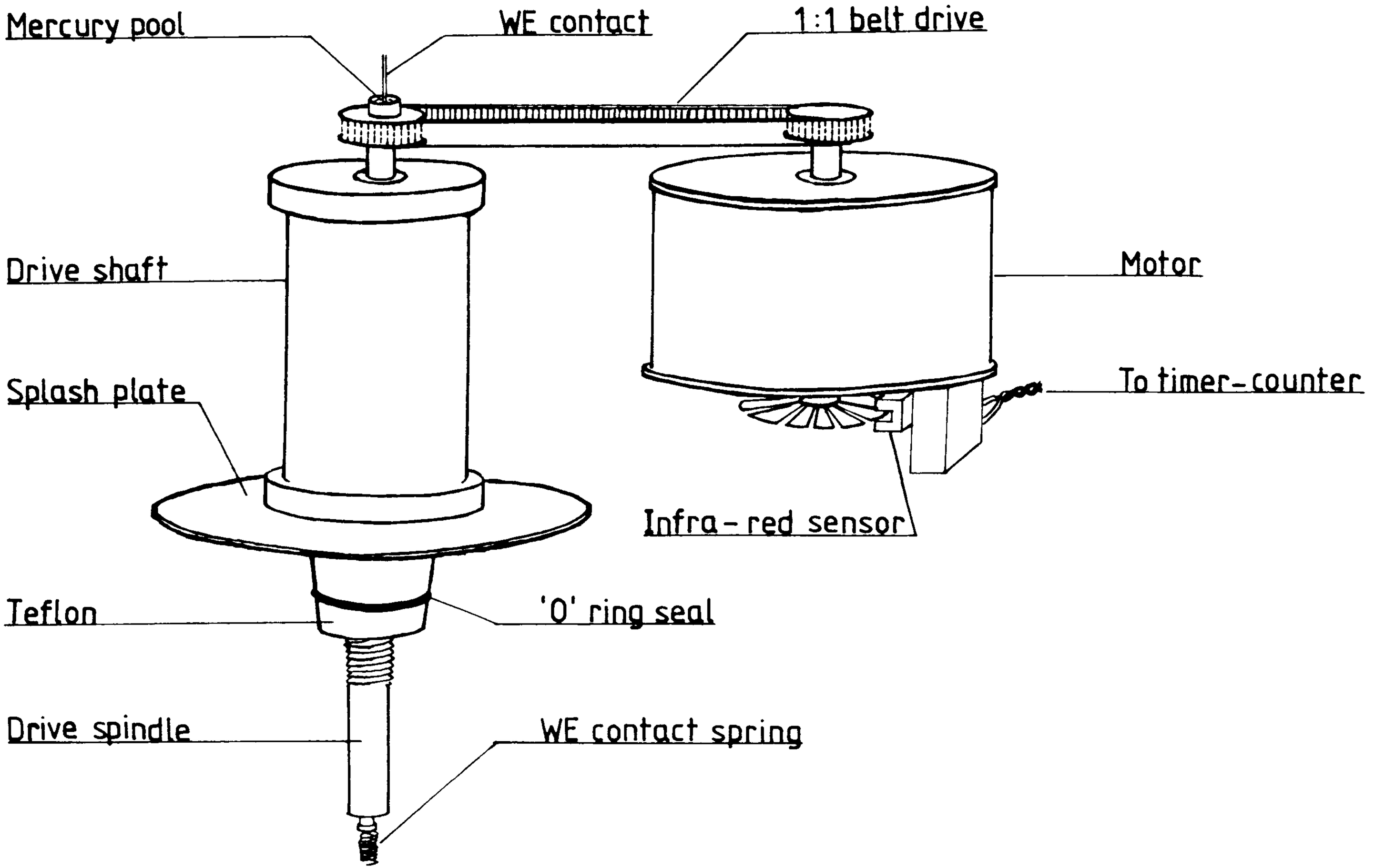

Fig 2.3 Rotating disc electrode assembly.

2.2.4 NICKEL WIRE ELECTRODES

For long term deposition experiments (≐6 days deposition) nickel wire electrodes were produced (fig 2.2). These were prepared by welding copper wire electrical connectors to 3 cm sections of 1 mm nickel wire (99.99+ %), then heat sealing the nickel into 6 mm Pyrex glass tubing, leaving 1.5 cm nickel exposed. Due to the difficulty of heat sealing nickel effectively into glass (nickel catalises bubble formation in glass at high temperatures), each electrode was sealed at the exposed nickel/glass junction with Epoxy resin (after electrode preparation as described in CH 2.2.6.2). Each experiment required a fresh electrode, since the wire had to be cut for viewing in the scanning electron microscope. The electrodes were held in place in the cell via a B29/6 mm glass tube stopper, this enabled the wire tip to be positioned 2-3 mm from the Luggin tip.

2.2.5 CADMIUM ROTATING DISC ELECTRODES

Cadmium disc electrodes used (see fig 2.2) were of similar design to the nickel electrodes, the only real difference being the cadmium pellets and associated Teflon holder were not tapered, since upon polishing, the soft cadmium metal soon wears down, making a good fit impossible to achieve. The cadmium discs were machined down to 7 mm diameter from 8 mm cadmium rod (99.999 %). Some difficulty was found in producing an evenly finished surface due to the pores found in the cadmium rod (presumably caused by gassing of the metal during casting from

melt). Teflon holders were designed to provide a tight fit for the discs and after fitting, the working surface of both holder and disc were machined to give an even finish. To improve leakage resistance the electrodes were sealed in to the holders using Epoxy resin. Electrical contact was achieved via the spring connector onto the rotating disc assembly as for the nickel rotating disc electrodes.

2.2.6 PREPARATION OF WORKING ELECTRODES

2.2.6.1 NICKEL ROTATING DISC ELECTRODES

Each nickel disc was prepared using the following sequence;

1) removal from holder (if mounted).

2) rough cleaning of the surface with 240 grit Emery paper and rinsing with distilled water.

3) rotary polishing using a Struers Dp 10 rotating wheel polisher, with Hyprez Spray diamond lapping compound used on Hyprocel Pellon adhesive discs, in conjunction with the appropriate lubricating fluid. Diamond spray of grades 25μm and 6μm being used successively (cleaning the electrode surface with distilled water and wiping on a clean filter paper before changing grades). Other grades were experimented with but the aforementioned grades were considered optimum. Smaller grades could be used but diamond crystals tended to be incorporated into the electrode surface (see plate 2.1).

4) polishing using Sevyt cloth and 1μm polishing alumina, rinsing with 3x distilled water then further polishing with 0.05μm alumina. The electrode was given a final rinsing with 3x

Plate 2.1 Polished nickel electrode showing incorporation of 6μm diamonds from the diamond polishing spray.

Plate 2.2 Nickel electrode surface after polishing down to the 0.05μm alumina. The horizontal lines are not scratches, but were due to filament problems in the electron microscope.

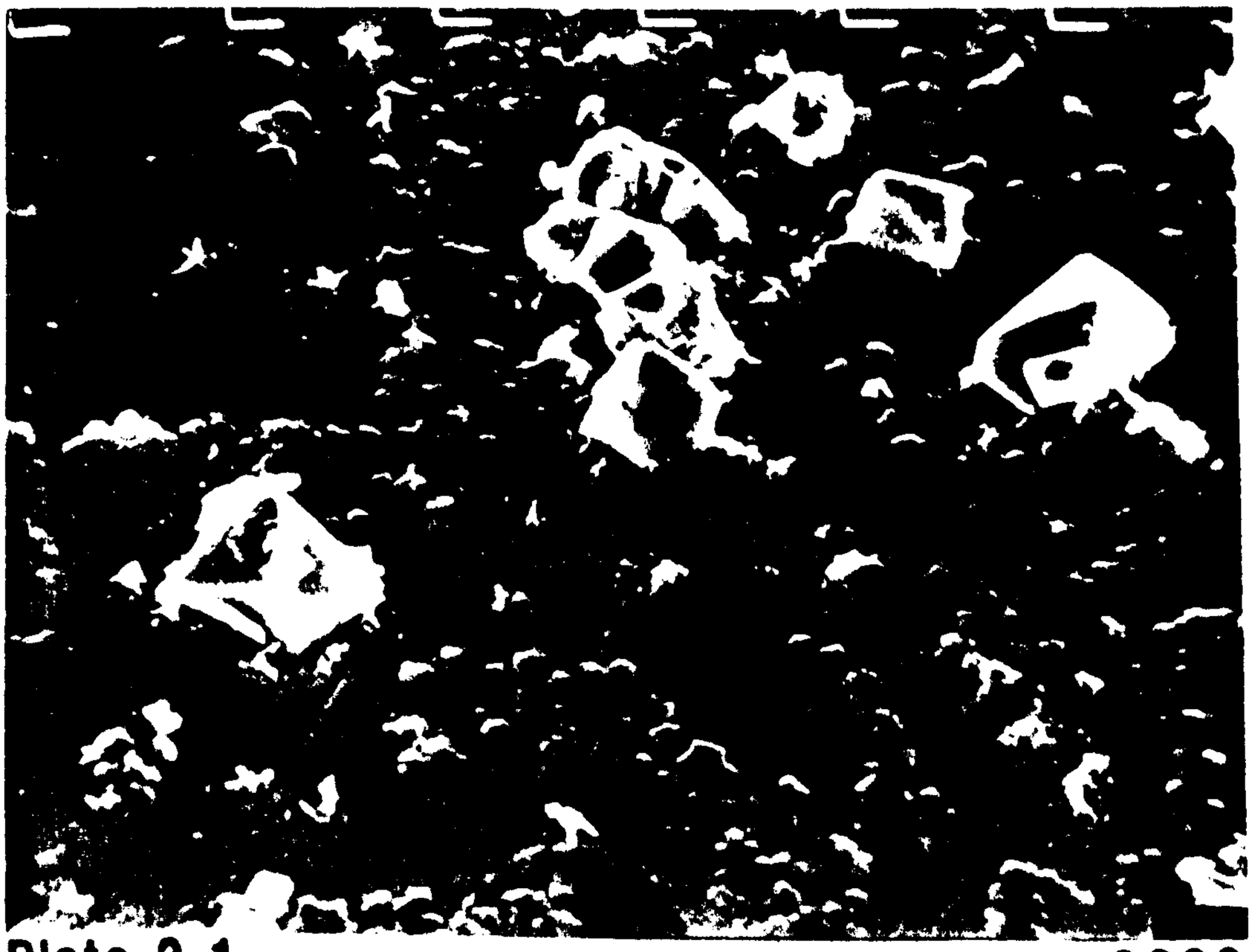

Plate 2.1 x2000

Plate 2.2 x10000

distilled water then carefully wiped on a clean Sevyt cloth. The resulting surfaces have a mirror finish with very few scratches observable with a 25x optical surface microscope. This optical inspection frequently revealed sufficient electrode marking, to require the electrode to be re-polished. Re-polishing usually only required going back to the 1μm alumina stage. Each nickel disc was then mounted into its Teflon holder as shown in fig 2.2. Where Epoxy resin was used, the electrode edge was given a small coating of the resin and force fitted into the holder, ensuring no gaps were left open to the electrolyte. This required the electrode and holder to be polished at the alumina stage, to remove traces of Epoxy resin from the working surface. Plate 2.2 shows a scanning electron microscope picture of the electrode surface.

2.2.6.2 NICKEL WIRE ELECTRODES

Roughened wire surfaces were used to ensure that the surface of the wire was free from any surface oxides produced during the heat sealing process. This also avoids the difficulty of polishing the wires, which was considered impractical (CH 3.4.3.1 investigates the influence of surface roughness). Wire electrodes were used as described in CH 2.2.4. Wire electrodes were abraded with 240 grit Emery paper and then the cut end abraded to give a chisel shaped tip. After optical inspection under the 25x surface microscope, the wire glass junction was sealed with Epoxy resin, exposing $\doteq$1 cm of wire (approximate geometric surface area 0.30 cm^2). Each electrode was rinsed with 3x distilled water and wiped on a clean Selvyt cloth to

remove any traces of carborundum from the Emery paper, although this is believed to be inactive in alkaline solution.

2.2.6.3 CADMIUM ROTATING DISC ELECTRODES

Due to the softness of cadmium electrodes, different polishing procedures were used from that for nickel electrodes. The polishing was carried out as follows;

1) removal from holder (if mounted).

2) rough polishing with grade 240 grit Emery paper to give an even surface (this was only required when a substantial deposit of cadmium had been formed) this stage being necessary due to the ductility of the deposited cadmium, which merges into the surface upon direct alumina polishing.

3) polishing using 45μm alumina on a Selvyt cloth, rinsing with 3x distilled water. Visual inspection was then carried out to ensure no traces of deposit remained.

4) polishing with 1μm alumina and rinsing with 3x distilled water and wiping on a clean Selvyt cloth. No improvement in surface finish could be obtained using finer grades of alumina, due to the incorporation of the polishing material into the surface layer. The discs were then mounted and re-polished with 1μm alumina if required, giving a reasonable mirror finish. Chemical polishing of the surface was achieved (where necessary), by exposing the electrode to $\simeq$ 0.1M nitric acid for 10 seconds. This has the effect of etching away the amorphous surface layer of cadmium, leaving a lightly etched surface with individual crystalline domains visible to the naked eye.

2.3 SOLUTION PREPARATION

2.3.1 ALKALINE SOLUTIONS

10.00M KOH stock solution was prepared from triply distilled water and 'AristaR' grade potassium hydroxide (minimium purity 85 %, the rest being water and 1 % carbonate). Storage was in tightly stoppered volumetric flasks with Teflon sleeves. Care has to be exercised to minimise formation of potassium carbonate, which occurs on exposure to atmospheric carbon dioxide).

Cadmium (II) solutions were produced by adding excess 'AnalaR' cadmium oxide ($\simeq 0.5 g/dm^3$), to the stock 10.00M KOH solution and stirring the solution for a minimum of 4 hours at room temperature ($22^{o}C$) to obtain a saturated solution of 3.5x 10^{-4}M cadmium (II) in 10.00M KOH (principally as the aqueous species $Cd(OH)_2^{2-}$ (6,50)). The solution was then filtered with a grade 4 glass sinter to give a suspension free solution. Solutions of 2.8x 10^{-4}M Cd(II) in 10.00M KOH (80 % of saturation level), were produced by dilution of the saturated solution with stock 10.00M KOH, thus ensuring no micro-precipitation of cadmium hydroxide could occur, due to variations in temperature.

2.3.2. ALKALINE SUSPENSIONS

All alkaline suspensions were prepared from the Cd(II) saturated solution [see CH 2.3.1], with the addition of a known quantity of cadmium oxide powder. Four suspension

concentrations were prepared, initially containing the following cadmium oxide suspension concentrations; 1.00, 0.200, 0.040 and 0.0005 g/dm^3 CdO. The lower concentration suspensions were prepared by quick dilution of the stirred 1.0g/dm^3 suspension solution. This gave suspensions whose concentrations were dependent on agitation. After rapid stirring, approximately 80 % of the suspension was observed to settle out within 15 minutes. This figure was estimated by sampling the solution at intervals, and observing particle concentrations under a transmission optical microscope (100-600x). In use in the rotating disc system, an equilibrium suspension concentration is achieved. This gave approximate true suspension concentrations in use of; 0.2, 0.04, 0.008 and 0.0001 g/dm^3, in equivalent CdO mass. However, in 10.00M KOH, CdO is largely converted to $Cd(OH)_2$ over a 3 hour period. Particle size was observed to be very variable within the solutions, average observed size was 5μm, with most particles in the range 1 - 10μm. However, since these observations were for the highest concentration suspension, it seems reasonable to predict that the lower concentration suspensions will have a considerably reduced average particle size.

2.3.3 ACIDIC SOLUTIONS

Solutions of cadmium sulphate in 0.50 M sulphuric acid were prepared using triply distilled water with the addition of a known weight of AristaR grade H_2SO_4 (minimum purity 98%). to give a final concentration of 0.50 M (the exact concentration of acid was not considered critical). AnalaR grade $CdSO_4$

.$3H_2O$ (minimum purity 98%) was added to give solutions of 0.100 and 0.001 M $CdSO_4$ in 0.50 M sulphuric acid. The lower concentration solution being prepared by appropriate dilution of the 0.100 M solution.

2.4 INSTRUMENTATION

2.4.1 THE ROTATING DISC ASSEMBLY

Fig 2.3 shows the rotating disc assembly used for the work contained in this thesis, it consists of a 16 pole d.c motor driving the working electrode via a belt connection. Speed monitoring consisted of a timer/counter to observe the number of revolutions a second. The observed speed accuracy allowed a 2% drift, over 10 hours of operation at low rotation rates (< 10 Hz). Maximum rotation rate used being $\simeq$50 Hz. Electrical contact to the working electrode is achieved via a mercury pool contact at the top of the spindle. This is connected to the working electrode by a spring. When assembled with the cell in place, an 'O' ring seal is achieved to isolate the cell from the air.

2.4.2 WAVEFORM GENERATOR

The waveform generator used for this work was constructed by the Physical Chemistry department workshop facility, and could be used at sweep rates of up to 1000 Vs^{-1} over a linear range of up to $\pm$3V.

2.4.3 POTENTIOSTATS

A Chemical electronics potentiostat (model 120), was used for all the short term and rotating disc experiments. It can maintain potentials of ± 3V versus the reference electrode, with provision for the addition of external signals. Current measurements were made by measuring the potential drop accross a standard resistor. For long term experiments a Chemical electronics T70/2A type potentiostat was used.

2.4.4. FREQUENCY RESPONSE ANALYSER

Two Solartron frequency response analysers were used (model numbers 1170/2 and 1170/4), as automatic phase sensitive detectors, allowing rapid measurement of impedances to be made. The F.R.A. incorporates a programmable waveform generator (frequency range 0.0001 - 1000000 Hz from the 1170/4 or 0.0001 - 10000 Hz from the 1170/2). This provides a small amplitude sinusoidal signal of programmable amplitude and waveform. The F.R.A. has a phase sensitive detection system, to give the real and imaginary components of the complex plane impedance of the cell response to the applied a.c. signal. The impedance can also be expressed in polar coordinates; as a phase angle and modulus (log(r) + theta or a,b and theta) if required. For all the work here the impedance was interpreted in the form of a complex plane plot (or Argand diagram), where the real and imaginary components are given the symbols Z′ and Z′′ respectively. The 1170 series of F.R.A.s can be programmed to take impedance measurements in a variety of ways. It is

possible to set upper and lower limits for the frequency and sweep between the two, either linearly or logarithmically, taking a variable (1-99) number of results per decade frequency change. The results are displayed digitally on the front panel, and can be output via a data transfer unit, to give both punched tape and/or a hard copy of the output. Direct real time graphical plotting could be obtained on a Bryans A3 x-y recorder. The experimental procedure is as described in CH 2.8.2. Data output was usually via the North Star Horizon microcomputer and Hewlett Packard digital plotter described in CH 2.5.1 and 2.5.3 respectively, using the programs described in CH 2.6. The first usage of the 1170 F.R.A. system was described by Armstrong and Metcalfe[175].

Latter work involved the usage and development of an integrated computerised impedance measuring system, incorporating a Solartron 1183c interface unit with Solartron IEEE 488 computer interface. This was coupled to an Apple II (48K) microcomputer with complete data handling and analysis facilities via program control. The complex programs were developed in conjunction with Gary P. Evans (PhD thesis, department of Physical Chemistry, Newcastle university 1984/5) and are described in CH 2.7. A full listing of most of the jointly written programs can be found in Gary Evans's thesis.

2.4.5 RECORDING DEVICES

For cyclic voltammetry (linear sweep) and a.c. impedance experiments, Bryans A3/A4 x-y recorders were used. Potentiostatic current/time transients were recorded on a

Chartwell strip chart recorder. Digital readings of currents and voltages were taken using a Solartron mutimeter (accuracy 0.01 mV) or Sinclair multimeter (accuracy 0.1 mV). For a.c. impedance data, a teletype attached to the 1170/2 F.R.A. was used to provide punched tape output of the data. This could be entered via a tape reader to the North Star Horizon microcomputer, and thence onto magnetic floppy discs. Most experimental data was stored on floppy discs for convenience of access and data manipulation.

2.5 COMPUTER SYSTEMS AND PERIPHERALS

2.5.1 THE NORTH STAR HORIZON MICROCOMPUTER

This is a 48 kilobyte (K; 1K= 1024 bytes of 8 bit information), 4 MHz Z80A microprocessor based microcomputer with twin 180 K disc drives (5.25 inch single sided double density). An IEEE 488, bit parallel, byte serial communications interface (Hewlett Packard HPIB type), is fitted enabling communication with other talking devices like the HP plotter. The IEEE 488 has 8 signal, 8 data transmition, 3 handshake and 5 BUS management lines, with this up to 14 devices can be communicated to simultaneously. With this is an asynchronous serial Tuart RS 232 communications interface, transmitting at 10-9600 baud rate (1 baud = 1 bit per second transferred). This enables communication with peripherals (such as an Anadex bi-directional dot matrix printer of 112 characters per second capability or a paper tape reader). Keyboard input is via an Adds Consul 980 terminal at 900 baud rate, giving 24 lines at 80 characters per

line of text. The North Star Horizon was run under North Star D.O.S (Disc Operating System) using North Star Basic (Beginners All Purpose Symbolic Instruction Code) language for most application programs. The Basic language required 14 K of memory leaving ≐32 K RAM (Random Access Memory) available to the user (the rest being allocated to the DOS).

2.5.2 THE APPLE II MICROCOMPUTER

This is a 64K 1MHz, 6502 microprocessor based microcomputer with built in keyboard, and separate twin 140K, 5.25 inch, single sided double density disc drives. The computer has a high resolution graphics capability, normally displayed on a green 12 inch monitor. Most programs used Applesoft/Apple monitor system, with some usage of Pascal structured language for minor tasks. With normal Basic, the display consisted of 23 lines of 40 characters per line of upper case text. Graphics display consisted of two regions of memory (8K each) lying in successive regions, which were interpreted as a graphic representation of 280 by 192 pixels (one pixel is a single graphics dot on the screen). Each pixel is represented in memory as a single bit, '1' signifying on. Although the computer has a colour display capability, this could not be used and thus all graphics work used monochrome representation. The computer could be connected up to a number of peripheral devices, via both an RS 232 serial port (connecting to other devices such as the North Star Horizon) and an IEEE 488 parallel interface. This enabled intelligent communications with either the 1183c/1170(4) Solartron a.c. impedance system or to the

Hewlett Packard 7225a digital plotter. In addition an Epson communication card enabled an Epson MX80(II) dot matrix printer to operate, giving hard copy output of both textual and graphical information.

2.5.3 THE HEWLETT PACKARD DIGITAL PLOTTER

High quality graphical output could be obtained from a Hewlett Packard A4 7225a digital plotter. It has a resolution of 11400 by 8900 pixels. A full character set of the normal Ascii characters is available, enabling printing of three characters per second (at normal character size). It is communicated with by any standard IEEE 488 parallel interfaced computer, and has its own plotting language, comprising of 38 different instructions. Typically an average graph could be plotted in about 2 minutes.

2.5.4 THE EPSON DOT MATRIX PRINTER

Hard copy output from the Apple microcomputer could be obtained via an Epson MX80(II) dot matrix printer. This printer is a 9 wire bidirectional machine, enabling characters to be printed at a rate of up to 120 per second, in any of several different print formats. A direct 'dump' of on screen graphics, via the special commands from the Epson/Apple communication card, enabled graphical data to be printed within approximately two minutes (for a full sized plot). The reproduction on the MX80(II) is scaled 1:1 in the x and y directions (this is not true for the other Epson models available at the time of

writing). It is also possible to use a bit image facility, whereby the print head wires can be directly addressed, to enable any user defined image to be printed.

2.6 COMPUTER PROGRAMS FOR DATA OUTPUT

2.6.1 MISCELLANEOUS PROGRAMS

Several programs were written to manipulate and output data using the North Star Horizon + Hewlett Packard digital plotter. All were written in Basic to facilitate standardisation of the data format. The main programs written enabled; 1) processing of double layer capacity data either from paper tape, keyboard or disc sources to give d.l.c. versus time plots. 2) current dependence on rotation rate and overpotential could be plotted. 3) a.c. impedance data could be plotted via a program originally developed by D.P Sellick (PhD thesis department of Physical Chemistry, University of Newcastle Upon Tyne 1980) and subsequently modified to plot data collected from the 1170/2 F.R.A. This enabled plotting of complex plane impedance data from paper tape or disc. 4) Genplot programs; these three programs written for the North Star Horizon/HP 7225 in conjunction with G.P. Evans [see CH 2.7]. They were designed to plot any form of data from keyboard or disc, giving automatically scaled axes. Several graph enhancing features were incorporated to give multiple plots, non-zero, negative or coloured graphs. Many of the diagrams contained within this thesis were drawn up using this system. They were designed to be used by non-computer programmers, and thus contained help

commands for the inexperienced user.

2.7 THE COMPUTERISED IMPEDANCE SYSTEM

Using the 1174 FRA + 1183c linked via the IEEE 488 parallel interface, to a double disc drive Apple II microcomputer (see fig 2.4), it was decided to develop a fully comprehensive a.c. impedance measuring and data handling system. The system was developed jointly with G.P. Evans (PhD thesis department of Physical Chemistry, University of Newcastle Upon Tyne 1984/5) along commercial lines, to give a measuring system of great flexibility. Many advanced features were incorporated into the programs, to enable the operator the maximum experimental freedom, whilst retaining ease of usage. The system consists of six programs written in Applesoft/machine code, with separately accessible analysis and plotting programs. Using this system, the program operator first enters an information file on the experimental conditions, containing details of date, sample number etc. This information file is saved with any data collected. The program automatically checks the disc to ensure the file names used are new, and that there is enough space on the disc for the data. All the program options are then selected, these include;

1) Adding new data to an old file.

2) Setting the 1174 in one of three ways, either; local operation (by front panel controls rather than by the computer), normal computer operation or lastly via the conditions used for a previous experiment (all data files contain the information necessary to repeat the experiment). This last option still

Fig 2.4 The computerised impedance system; from left to right Hewlett-Packard 7225a digital plotter, Epson MX82 F/T dot-matrix printer, Apple II europlus computer (48K), Solartron 1186 electrochemical interface (top) and the Solartron 1174 frequency response analyser (bottom).

enables the operator to alter any of the loaded conditions for the new experiment.

3) Altering of any parameter once set, via a review facility (eg measurement delay, integration time, display mode etc).

4) Setting of the generator functions, frequency sweep or single frequency. This involves entering frequency limits and sinusoidal amplitude. This section also requires the direction of sweep (up or down in frequency), the number of data points taken and the choice of logarithmic or linear change in frequency.

5) Mode of display; four choices here, either Z´ versus Z´´ (normal complex plane impedance plot) or for the single frequency measurements a display of Z´,Z´´ or C_{dl} versus time.

6) Choice of multiple run delay. For frequency sweeps, this involves a timed wait between each of several frequency sweeps, thus allowing a whole series of automatic experiments to be carried out over a period of time. For the single frequency measurements, the operator can set a delay between each measurement of from 1s to 3 hours. The maximum number of results for the single frequency experiments is 600 data points. For single frequency experiments the data is stored in the form Z´, Z´´ and time. Where timing is required, it is achieved by usage of a calibrated machine code timing subroutine.

The main features of the system include;

a) real time plotting of data on screen, using auto scaling and re-scaling of axes to fit all data. Decade changes in frequency are marked by symbols. The numeric values of the data can be displayed at any time during the data collection, by a

simple keyboard option, enabling switching between numerical and graphical representation.

b) Single frequency measurements, including real time plotting, of either real, imaginary or double layer capacity (C_{dl}) versus time. Measurements being taken at an interval set by the user, from 1 second upwards.

c) Multiple run facility for frequency sweeps, allowing pre-programming of a series of runs, with a time interval between each run and the next, again set by the user.

d) Data output (plots and numerical data) onto an Epson printer, giving semicircle maxima and all the relevant information for the run. This section of the program system can be used separately from the main system, and allows several sets of data to be displayed on the screen at one time. The analysis programs also include many additional features such as, labeling options, decade marking and user controlled re-plotting. Further advanced features such as digitisation, expansion, editing and linear regression of the data are incorporated in the second section of the analysis program.

e) Data output to the HP 7225 plotter with facility for several plots per page and/or several sets of data on one set of axes. Linear regression lines can also be incorporated.

f) Full facility to review and change parameters before commencing a run.

g) Parameters can be set via local or program control or from a previous data file.

h) Facility for interrupting a run and either ending it, or continuing after altering the current measure resistor value. During a run, it is possible to alter most of the front panel

switches of the 1174, with the program taking into account the new values.

i) Data is converted before storage, to absolute values using the current measure resistor value (if in the a, b mode).

j) 500+ point data array capacity.

k) Storage space on the discs is maximised, using machine code data saving routines. This gives a capacity of (for instance) 50, 100 point data files per disc, including a full description file for each data file. 12) Full error trapping to ensure even the most inexperienced user can correct any mistakes.

Fig 2.5 shows typical data output from these programs from the Epson printer.

2.8 EXPERIMENTAL PROCEDURES

2.8.1 ROTATING DISC EXPERIMENTS

The cell and electrodes described in CH 2.1 and 2.2, were set up and filled with the electrolyte. All glass joints used glass sleeves with leakage minimised by attaching springs across the joint. With the working electrode in place attached to the rotating disc assembly, the cell was degassed using 'white spot' nitrogen, for a minimum of 15 minutes. During this period the electrode was rotated at 5 rev/s. A 2μF capacitor was attached across the reference electrode tap to minimise any high frequency oscillations that might arise. Care had to be exercised in case the tap dried out, causing the potentiostat to go to its maximum output voltage of ±70V. For the nickel

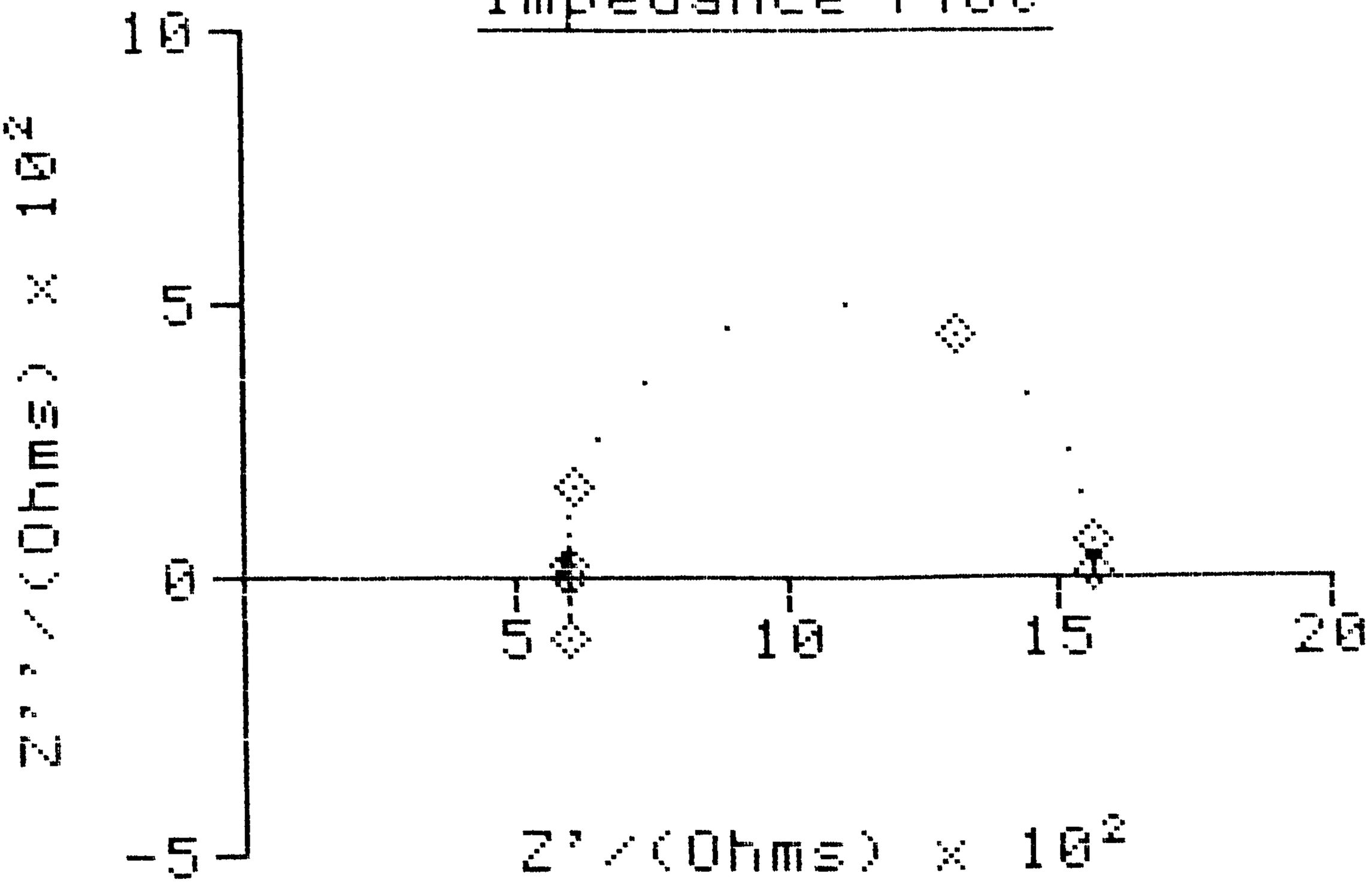

FREQUENCY	Z'/ (OHMS)	Z''/(OHMS)
9.999E+05	6.02E+02	-1.09E+02
6.298E+05	6.01E+02	-6.72E+01
3.971E+05	6.01E+02	-4.48E+01
2.504E+05	6.00E+02	-2.72E+01
1.578E+05	6.00E+02	-1.75E+01
9.980E+04	5.99E+02	-9.58E+00
6.298E+04	5.98E+02	-6.38E+00
3.971E+04	5.98E+02	-1.58E+00
2.504E+04	5.98E+02	1.59E+00
1.578E+04	5.97E+02	7.98E+00
9.980E+03	5.98E+02	1.59E+01
6.298E+03	5.97E+02	2.71E+01
3.971E+03	5.98E+02	3.99E+01
2.504E+03	5.99E+02	6.56E+01
1.578E+03	6.03E+02	1.01E+02
9.980E+02	6.18E+02	1.60E+02
6.298E+02	6.56E+02	2.45E+02
3.971E+02	7.42E+02	3.53E+02
2.504E+02	8.97E+02	4.56E+02
1.578E+02	1.11E+03	4.92E+02
9.980E+01	1.32E+03	4.41E+02
6.298E+01	1.45E+03	3.28E+02
3.971E+01	1.52E+03	2.22E+02
2.504E+01	1.55E+03	1.48E+02
1.578E+01	1.56E+03	9.49E+01
9.980E+00	1.57E+03	5.92E+01
6.298E+00	1.57E+03	4.11E+01
3.971E+00	1.57E+03	2.57E+01
2.504E+00	1.57E+03	1.54E+01
1.578E+00	1.57E+03	1.28E+01
1.000E+00	1.57E+03	7.72E+00

Operator : STEVE
Filename : DUMMY CELL1
Date : 10TH DEC 1984
Temperature : 25 C
Pressure : 1027 MB
Membrane No : NONE
Surface Area: 1 cm2
Solution 1 : HELIUM OXIDE
Solution 2 : HELIUM OXIDE
Electrodes : CALIFORNIUM
C.M.R : 1000 Ohms
Freq Max : 999900 Hz
Freq Min : 1 Hz
Semi Max : 157.8 Hz

DUMMY CELL
570 OHMS PLUS 1000 OHMS IN PARALLEL
WITH 1 MICROFARAD

Fig 2.5 Typical program output from the computerised impedance system via the Epson dot-matrix printer.

rotating disc electrodes a pretreatment of several hours evolution of hydrogen was often used. This was continued until the i/t curve reached a steady state. The aim of this is to decrease the purported effect of nickel surface oxides [see CH 3.3]. The solution is then changed to the appropriate cadmium containing electrolyte, and deposition started by switching in the potentiostat at the required overpotential. The current is measured by following the potential drop across a known value resistance in series with the secondary electrode. The usual value for the current measure resistor was 1000 Ohms. The current was followed using a Chartwell strip chart recorder. The potentiostat voltage was checked using an external digital volt meter (DVM), attached across the working and reference electrodes. Most rotating disc experiments used a background rotation rate of 5 rev/s unless otherwise stated. A constant slow bubbling of nitrogen was maintained, to ensure the electrolyte remained free from the influence of oxygen.

Rotational spectra were taken by rapidly adjusting the rotation rate to a new value, allowing sufficient time for the current to stabilise at the new rotation rate. The current was then measured and the rotation rate changed to the next value required. The typical rotation rates used were; 5, 10, 15, 25, 35 and 50 rev/s. Under these conditions, a time of approximately 2 minutes was required for the whole spectra to be taken.

2.8.2 A.C. IMPEDANCE

Using the experimental procedure described in CH 2.8.1, for

the rotating disc experiments, a.c. impedance / double layer capacity measurements were carried out. This required the 1174/2 FRA to be programmed to produce a small sinusoidal perturbation (of amplitude ±10 mV peak-peak), which was then superimposed on the d.c. signal from the potentiostat. The amplitude of the a.c. signal has to be big enough to avoid noise problems, but small enough to have negligible effect on the electrode behaviour. This signal is fed back directly to the FRA for the input reference signal, so that no noise was encountered from the cell. However, for the high frequency impedance measurements in low conductivity electrolytes, the reference signal was taken directly back from the reference/working electrodes, thus eliminating the phase angle shift due to the time delay in the potentiostat. For both a.c. impedance in alkaline and acidic solution, the frequency range used was normally 0.01 - 10000 Hz. The double layer capacity versus time transients, were obtained by using a single frequency response (normally at 1000 Hz in alkaline solution). This gave a series of measurements over an extended time-period. In most cases, the data from the FRA was plotted in real time as a complex plane impedance plot, using either the computer screen or a Bryans A3 plotter. The results were for the most part collected on paper tape for later computer analysis (using the North Star Horison system described in CH 2.5.1). Later experiments were carried out using the fully automated computerised impedance system described in CH 2.7.

Using the 1172/4 FRA, impedance measurements could be taken automatically once the FRA had been programmed. This is achieved either by using the computerised impedance system,

described in CH 2.7 or by local control from the front panel keys of the FRA. The FRA can be programmed to carry out a number of different tasks, the settings more usually altered by the user, are the following;

1) Frequency range: From 0.0001 to 9999 Hz (999900 Hz for the 1174)

2) Points per decade: From 0 (repetitive single frequency) to 99 points per decade change in frequency, whilst in the logarithmic mode. In the linear mode, this represents the constant frequency increment.

3) Output voltage: This is the root mean square (RMS) of the amplitude of the output signal. The range is 0.01 - 10V, but for this work it is always attenuated by a factor of 1/100; giving an effective output range of 0.0001 - 0.1V.

4) Display mode: This option allows the output of data either as real versus imaginary components (a,b or Z´,Z´´), to give an Argand diagram, or in polar coordinates (r,θ or log(r)θ). All work presented here used the a,b mode.

5) Sweep type: Either logarithmic, taking a set number of points per decade change in frequency, or linear, taking results at set frequency increments.

6) Sweep direction: The sweep can be run from either high to low or low to high frequency.

7) Integration time: This corresponds to the number of waveform cycles the response is averaged over. The user has the option of minimum, x10, x100 and x1000 integration, allowing increased accuracy at the expense of speed.

8) Measurement delay: The user has the option of allowing a settling down period between each measurement of 0.1 (the

minimum), 1, 10 or 100s.

Typically for an a.c. impedance spectrum, the frequency range was 0.01 - 9999 Hz, using the minimum settings of integration and delay times. The sweep was generally from high to low frequency for alkaline electrolytes and low to high for acidic electrolytes. The frequency sweep was usually carried out logarithmically at 10 points per decade. Since the time of measurement depends on the frequency range and integration time used, the time for a spectrum is very variable. Typical spectra, using the settings given above required ≐40 minutes.

Single frequency measurements for repetitive evaluation of the double layer capacity of an electrode, could be achieved by setting both the maxima and minima to the required frequency. Sweeping with a setting of 0 points per decade, at x100 integration and 100s delay, resulted in measurements being obtained at intervals of 121s. These settings at 1000 Hz were the values used for nearly all the double layer capacity versus time measurements taken.

2.8.3 LONG TERM DEPOSITION

Using the cell described previously [CH 2.1.2], with a prepared nickel wire electrode [CH 2.2.4 and 2.2.6.2], the working cell was assembled with Teflon sleeves at all glass joints. The cell was the filled with the 2.8×10^{-4}M Cd(II) in 10.00M KOH electrolyte. With the working electrode in place 3 mm above the Luggin tip, the solution was degassed, using 'white spot' nitrogen for a minimum of 15 minutes. After this period the potentiostat was switched in at the required

overpotential. The initial current/time curve was followed for 10+ hours, using a Chartwell strip chart recorder, to give a record of the settling down period of the electrode. A slow constant bubbling of nitrogen kept the electrolyte degassed during the experiment. The standard period used for the long term deposition experiments was 140 hours (6 days).

2.8.4 ELECTRON MICROSCOPY

Most of the electron micrographs of electrode surfaces, were obtained using a JEOL JSM T20 scanning electron microscope, set at 20 KV. This gave a maximum resolution of $\pm$30 nm, corresponding to a maximum magnification of x30000. Some higher resolution work was carried out using a JEOL JSM T35 microscope, where the maximum magnification obtainable is x180000. However, the resolution is greatly affected by sample preparation and imperfections of the microscope (eg the state of the filament, vibration resistance etc), such that this resolution was not achieved.

It was anticipated that some sample damage might occur, due to heating of the cadmium deposit (mp 321^{o}C) by the electron beam (which can attain >100^{o}C). However, throughout all the electron microscopic observations, no evidence of electron beam sample damage was observed.

2.8.4.1 ELECTRON MICROSCOPY - SAMPLE PREPARATION

Disc electrodes were prepared by first carefully rinsing the electrode free of the electrolyte, using 3x distilled water.

Then removing them from their Teflon holders (for tapered holders where Epoxy sealing was used, this could cause some damage by scratching, of a small section of the surface). After removal, any remaining traces of Epoxy resin on the outside of the electrode were removed and the electrode rinsed in 3x distilled water. The electrode was then placed in a sample tube under a flow of nitrogen until dry, when the tube was sealed. This process was designed to minimise the possibility of contamination. Wire electrodes were prepared by rinsing with 3x distilled water and cutting the tip, to give ≃1 cm of undamaged wire surface (care taken to avoid wire tip). This was then rinsed in 3x distilled water, and dried under nitrogen and placed in a sample tube. Coating of the samples was not necessary, and samples could be directly attached to scanning electron microscope studds using conducting cement.

2.8.5 EDAX ELEMENTAL ANALYSIS

EDAX (Energy Dispersive Analysis of X-rays) was carried out with a cambridge stereoscan mkII scanning electron microscope, giving a maximum resolution of x20000. Emission lines for elements over the atomic weight of 17, could be detected with this system (detection of lower weight elements is limited by the usage of a berillium x-ray window). Samples were prepared as described in CH 2.8.4.1.

CH 3 DEPOSITION FROM 10.00M KOH CONTAINING DISSOLVED CADMIUM

3.1 THEORY OF DENDRITE GROWTH

In the absence of suspension dendrite growth can be expected to follow existing theory[114]. If we consider a protrusion of height h on a flat surface (see fig 3.1), a linear diffusion gradient will exist on the flat surface. However, at the dendrite tip, we can approximate to a spherical diffusion layer. For the case where we have diffusion control on the flat surface, but mixed control at the tip, the tip and flat deposition currents are given by;

$$i_f = \frac{nF D_o C_o}{\delta} \qquad \{3.1\}$$

where D_o/δ is sometimes called the mass transfer coefficient. At the tip the current is given by;

$$i_t = nFk_r C_o^s = nFD_o(C_o^x - C_o^s)/r \qquad \{3.2\}$$

k_r being the rate constant for deposition onto the dendrite tip, related to the deposition current on the flat (k_o) by;

$$k_r = k_o \exp(-2\gamma V/RTr) \qquad \{3.3\}$$

where $2\gamma V/r$ is the Kelvin term, relating to the effect the radius of curvature has on the free energy of the reaction [see CH 1.3.3]. From {3.2};

$$C_o^s = \frac{i_t}{nFk_r} \qquad \{3.4\}$$

Hence with {3.2} we get;

$$i_t = \frac{nFD_o}{r}\left[\frac{C_o h}{\delta} - \frac{i_t}{nFk_r}\right] \qquad \{3.5\}$$

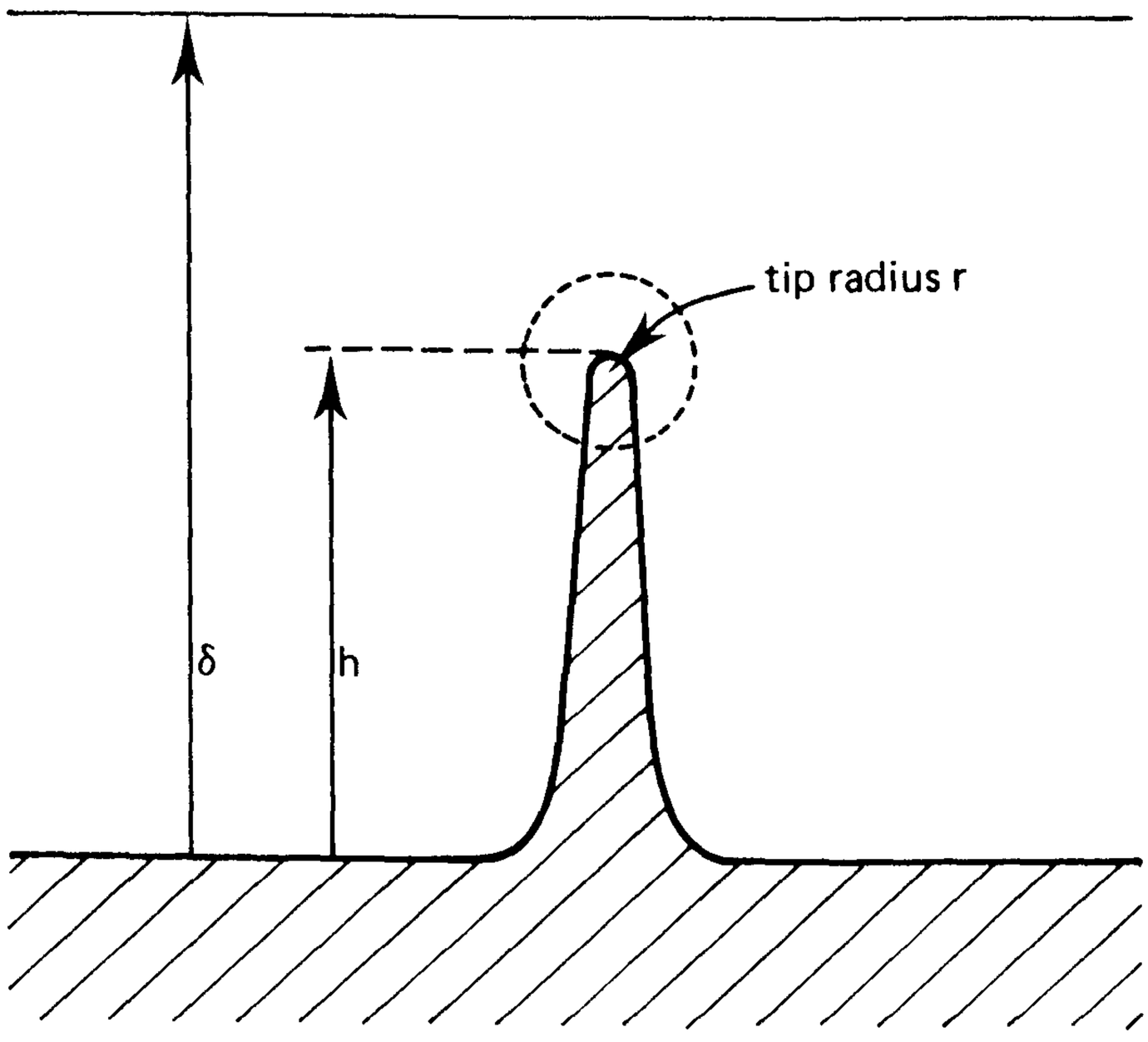

Fig 3.1 Schematic diagram of a dendrite.

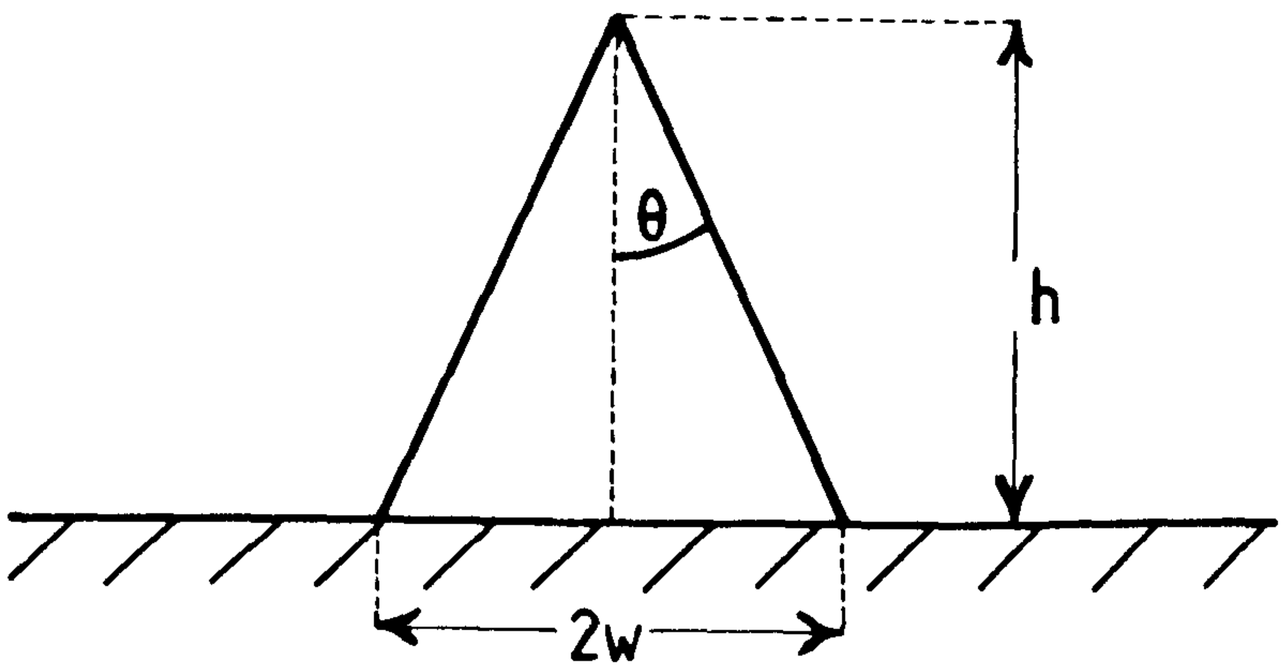

Fig 3.2 Cone model of dendrite growth.

($C_x = C_o h/\delta$, ie the concentration at height x).

Rearranging;

$$i_t = \frac{nFD_oC_oh}{r\delta} - \frac{D_o i_t}{r\kappa_r}$$

or;

$$i_t\left[1 + \frac{D_o}{rk_r}\right] = \frac{nFC_o hD_o}{r\delta}$$

therefore;

$$i_t = \frac{nFC_o hD_o}{r\delta}\left[\frac{\kappa_r r}{D_o + r\kappa_r}\right] \qquad \{3.6\}$$

or;

$$i_t = \frac{nFC_o hD_o k_o \exp(-2\gamma V/RTr)r}{r\delta[\, D_o + r\kappa_o \exp(-2\gamma V/RTr)\,]} \qquad \{3.7\}$$

combining {3.1} and {3.7};

$$\frac{i_t}{i_f} = \frac{hk_r}{D_o + r\kappa_r} \qquad \{3.8\}$$

or;

$$\frac{i_t}{i_f} = \frac{hk_o \exp(-2\gamma V/RTr)}{(D_o + r\kappa_r)} \qquad \{3.9\}$$

Hence at the limit of high overpotential where $r\kappa_r >> D_o$, the ratio $i_t/i_f = h/r$. This corresponds to the case of diffusion control at both the flat surface and the tip.

Equation {3.8} can be integrated with respect to time;

$$dh = \frac{M}{\rho nF} i_t \, dt$$

or;

$$i_t = \frac{dh\rho nF}{Mdt} \qquad \{3.10\}$$

combining {3.9} and {3.10};

$$\frac{dh\rho nF}{M\,dt\,i_f} = \frac{hK_r}{(D_o + rk_r)}$$

therefore;

$$\frac{dh}{h} = \frac{hk_r}{(D_o + rK_r)} \cdot \frac{Mi_f}{\rho nF}\,dt \qquad \{3.11\}$$

integrating with respect to time;

$$\int_{h_o}^{h} \frac{1}{h}\,dh = \frac{k_r}{(D_o + rk_r)} \cdot \frac{M\,i_f}{\rho nF} \int_{t=0}^{t} dt$$

therefore;

$$\ln[h/h_o] = \frac{k_r i_f M\,\Delta t}{nF(D_o + rK_r)\rho} \qquad \{3.12\}$$

combining {3.1} with {3.12};

$$\ln[h/h_o] = \frac{MD_oC_ok_r\,\Delta t}{\rho\delta(D_o + rk_r)}$$

at high η where $rk_r >> D_o$ we get;

$$\ln[h/h_o] = \frac{MD_oC_o\,\Delta t}{\rho\delta\,r}$$

or;

$$\Delta t = \frac{\ln[h/h_o]\rho r\delta}{MD_oC_o} \qquad \{3.13\}$$

Thus we have a relationship giving the time of growth for any dendrite where linear diffusion exists at the surface and spherical diffusion at the tip. However, the point at which spherical diffusion starts is thought to correspond to the induction time for dendritic growth (t_i), such that the total time for growth of a dendrite from the start of deposition on a planar surface is given by;

$$t_g = t_i + \Delta t \qquad \{3.14\}$$

If the shape of a protrusion is approximated to that of a cone (fig 3.2) of angle 2θ, base radius 2w and height h. The critical induction time will come when the height reaches some proportion of the Nernst diffusion layer thickness, where the tip can be said to experience spherical diffusion. No attempt is made to calculate this value at this point, as its value is by definition going to be somewhat arbitrary. The proportion is later estimated by experimental observation of electrode surfaces. Hence, as the volume of a cone = $\pi r^2 h/3$, we can write the volume of a dendrite cone as;

$$V_c = \pi w^2 h/3 \qquad \text{where } h = w/\text{Tan}\,\theta$$

hence;

$$V_c = \frac{\pi w^3}{\tan(\theta)\times 3} \qquad \{3.15\}$$

therefore on a surface with q dendrite cones, the number of moles of deposited metal is given by;

$$V_t = \frac{q\,\pi\, w^3}{3AV\tan\theta} \qquad \{3.16\}$$

Now under diffusion limited conditions for a planar electrode, the current (at high overpotential), is given by {3.1}.

Integrating this gives the charge passed as;

$$C_t = \int_{t=0}^{t_i} \frac{nFD_oC_o}{\delta}\, dt = \frac{nFD_oC_ot_i}{\delta}$$

hence the number of moles deposited is given by;

$$V_t = \frac{D_oC_ot_i}{\delta} \qquad \{3.17\}$$

combining {3.16} and {3.17};

$$\frac{D_oC_ot_i}{\delta} = \frac{q\pi w^3}{3AV\tan\theta}$$

or;

$$t_i = \frac{q\pi w^3 \delta}{3D_o C_o AV\tan\theta} \qquad \{3.18\}$$

Thus from {3.13} and {3.18}, we can obtain an expression relating the total time for such dendrite initiation and growth, given by;

$$t_g = \frac{q\pi w^3 \delta}{3D_o C_o AV\tan\theta} + \frac{\ln[h/h_o]\rho r\delta}{MD_o C_o}$$

or;

$$t_g = \frac{\delta}{D_o C_o V}\left[\frac{q\pi w^3}{3A\tan\theta} + \ln[h/h_o]\, r\right] \qquad \{3.19\}$$

The usage of this relationship is however, somewhat restricted by the approximations involved regarding the initiation time. The estimation of the critical height into the Nernst diffusion layer, where spherical diffusion is said to start, is somewhat arbitrary. In real dendritic systems this transition would be gradual, rather than abrupt as assumed by this model. The growth time for a dendrite as given by {3.13}, assumes spherical diffusion during all growth and is not constrained by this limitation, providing one accepts the further approximation that the initiation time is zero.

3.2 DETERMINATION OF THE CADMIUM - CADMIUM HYDROXIDE REVERSIBLE POTENTIAL

The reversible potential of the reaction;

$$Cd + 2OH^- \rightleftharpoons Cd(OH)_2 + 2e^-$$

in 10.00M KOH was determined relative to the Hg/HgO reference electrode described in CH 2.2.1.1. The experimental procedure

required preparation of a cadmium rod electrode from 8mm diameter cast cadmium (99.9999% as used for subsequent cadmium disc experiments [see CH 3.5, 4.2 and 5]). Before use the cadmium rod was cleaned by brief immersion in dilute nitric acid to remove any possible traces of contaminants. An adapted polyethylene stopper was used to hold the electrode in place in the rotating disc cell [as described in CH 2.1.1]. This allowed the rod to be immersed in pre-degassed 10.00M KOH electrolyte [prepared as in CH 2.3]. The cell and electrodes were degassed for 30 minutes. The observed rest potential for the clean electrode in 10.00M KOH at 24^{o}C was -0.896 $\pm$ 0.008 V versus the Hg/HgO reference. This value was established by observing the current changeover point, but was subject to some short term drift. To ensure measurement of the $Cd/Cd(OH)_2$ couple, the electrode was polarised at a potential of -0.800V for a period of 10 minutes, to establish a surface layer of $Cd(OH)_2$ over the electrode. This also ensured the electrolyte was saturated in Cd(II) species. After this period, the electrode was raised to allow only the lower 3cm of the electrode to be immersed in the electrolyte. Thus the peculiarities of the previous electrolyte solution interface, and any resultant incomplete $Cd(OH)_2$ covering of the electrode could not affect the rest potential. The rest potential was observed to stabilise towards a value of -0.9023 $\pm$ 0.004 V (Hg/HgO) at 24^{o}C. This stabilisation took 1 hour. This value compares with the calculated thermodynamic equilibrium potential[3] of;

$$-0.906 + RT\ln[a_{H_2O}] \text{ V at } 25^{o}C$$

Corresponding to a value of -0.899V in 30% KOH (5.35M) as used

by Edmondson[50].

The usage of an anodic polarising potential of -0.800V, causes a not insignificant evolution of oxygen. Thus it is possible that the surface layer of the electrode contains CdO, which has a reversible potential of -0.863V[176] for the reaction;

$$Cd + 2OH^- \rightleftharpoons CdO + H_2O + 2e^-$$

However, after equilibration at the reversible potential, it is unlikely that any CdO would remain. The observed cathodic increase in the rest potential during equilibration, is most likely due to conversion of CdO formed to $Cd(OH)_2$. Observed electrode morphology showed no evidence of CdO, only an even deposit of greyish $Cd(OH)_2$. It is observed that if CdO is added to 10.00M KOH, an immediate change in the surface appearance occurs on the oxide. There is a transition from the brown CdO to white $Cd(OH)_2$, although the larger particles are somewhat impervious to this change due to the low solubility of $Cd(OH)_2$. Work at low overpotentials by Armstrong et al[6,9], has shown the presence of $\beta Cd(OH)_2$ and some $\gamma Cd(OH)_2$, but no CdO, in agreement with other workers[13,27]. Barnard, in his review of cadmium in alkaline solution[4], concludes that CdO will only be formed at high anodic overpotentials of > 0.200V greater than the $Cd/Cd(OH)_2$ couple.

3.2.1 CYCLIC VOLTAMMETRY

To characterise the cadmium electrode used in the determination of the rest potential, a series of linear sweep

experiments were carried out. Fig 3.3 shows the resultant cyclic voltammogram obtained, sweeping between -0.700V and -1.000V (Hg/HgO) at 1 mV/s. It shows a single anodic peak attributed to $Cd(OH)_2$ formation and overlapping H_2 evolution. A peak current of 10 $mAcm^{-2}$ is observed. Passivation of the electrode surface (presumably by formation of CdO), occurs at about -0.860 V. This agrees with previous work[3,50]. Repetitive cycling between -0.800V and -1.100V, showed a slight shift in the peak positions and current. This indicated a change in the electrode morphology consistent with the appearance of a more spongy cadmium surface layer.

For the purposes of the thesis, the rest potential for the $Cd/Cd(OH)_2$ couple was taken as -0.900V (Hg, HgO). Any overpotentials expressed, are relative to this value, unless otherwise indicated. All absolute potentials for the alkaine system are relative to the Hg/HgO reference electrode in 10.00M KOH.

3.3 NICKEL ELECTRODE PRETREATMENT

Due to the possible influence of surface oxides on the nickel electrodes[16], most electrode surfaces were pretreated before usage by cathodic evolution of hydrogen in cadmium-free, degassed 10.00M KOH. Evolution being maintained until a steady state current was obtained. The hydrogen evolution current is believed to reflect the electrode oxide state, in that hydrogen evolution should result in reduction of any surface oxides present.

X ray photoelectron spectroscopy has shown[177], that the

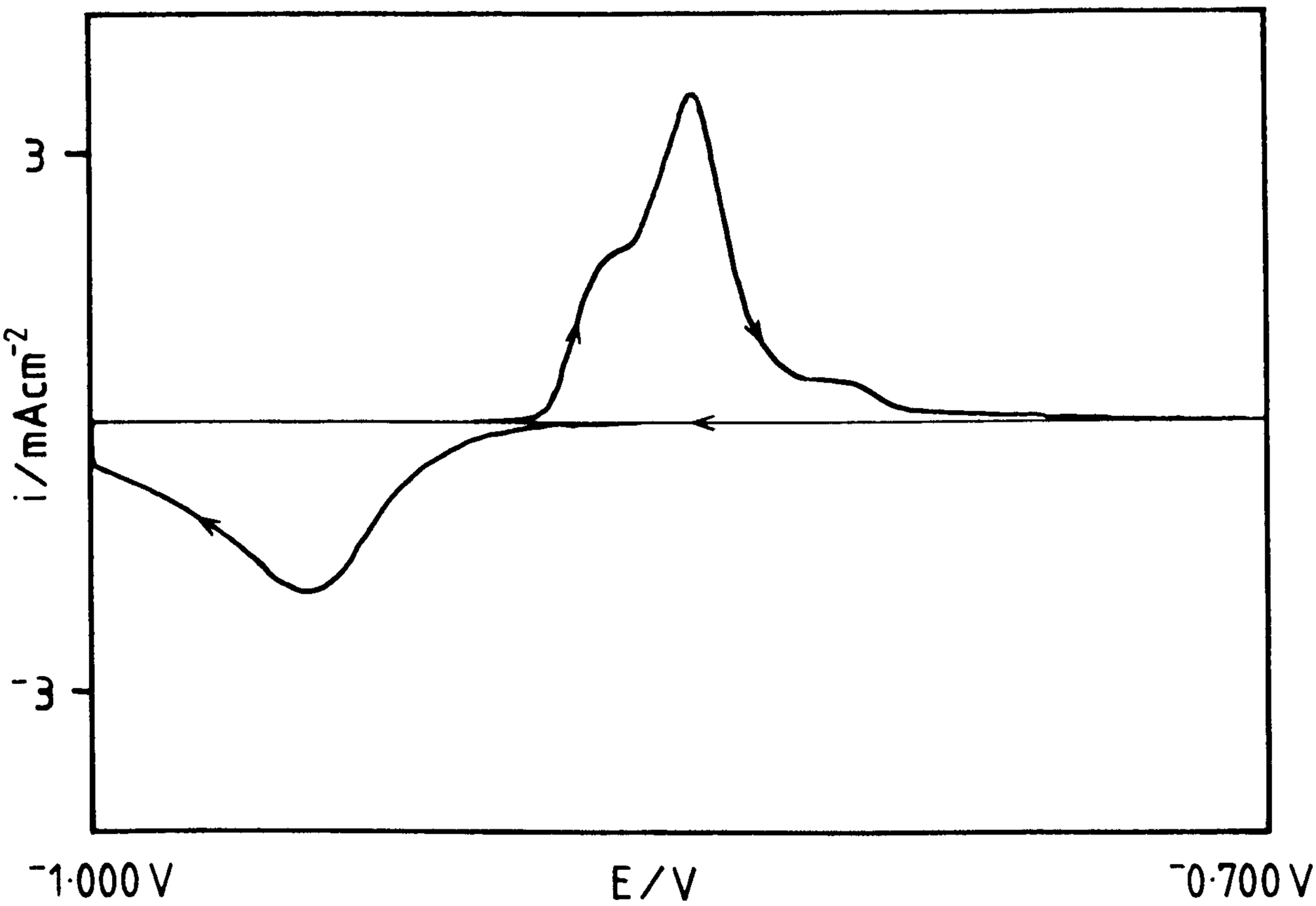

Fig 3.3 Single cyclic voltammogram obtained sweeping on a fresh cadmium electrode in 10.00M KOH. The limits were -1.000V to -0.700V (versus Hg/HgO), and the sweep rate was 1mV/s.

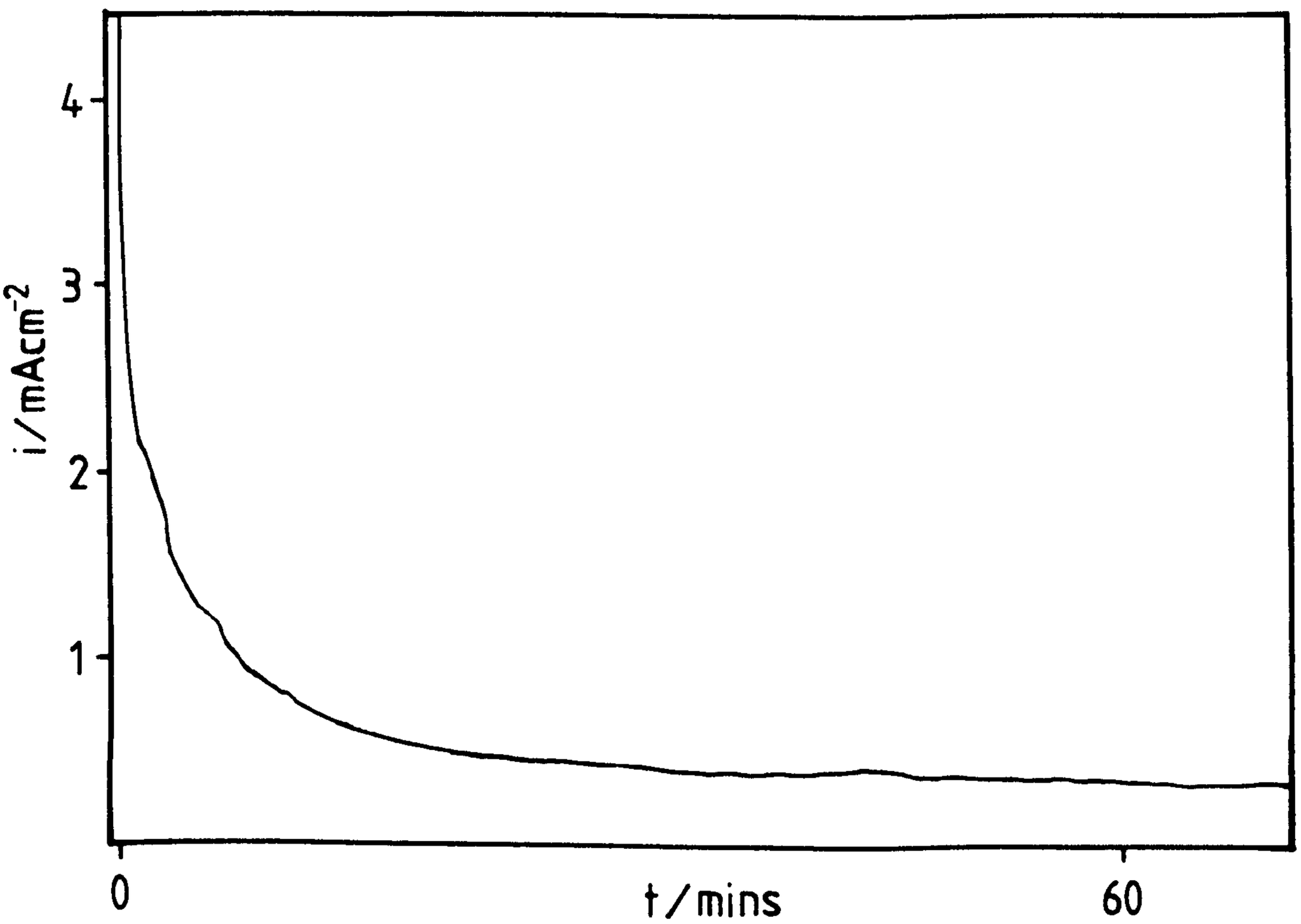

Fig 3.4 Current/time transient during hydrogen evolution on a rotating nickel electrode (5 rev/s), at -1.100V (versus Hg/HgO).

surface films present on nickel can include, NiO, Ni_2O_3 , NiO_{ads} and $Ni(OH)_2$. The additional adsorbed species, O_2^-, O_2^{2-} , O^- and H_2O can also be detected in the nickel oxide layer. However, under normal conditions, NiO is the only stable oxide formed in air or oxygen[178]. In NaOH, strong anodic oxidation of Nickel resulting in forced surface oxide formation has been found to be reversed upon cathodic polarisation[61]. Studies on nickel in both acidic[179] and alkaline[61] media, have shown similar surface film properties, consistent with the appearance of a NiO film. Observations of capacitive films on nickel sinters in alkali, gave estimated film thickness of 5 - 11 Angstroms, this is to be compared with values of 10 - 20 Angstroms, found for planar electrodes[50].

The influence of surface pretreatment and its absence on cadmium deposition, is discussed in CH 3.4.3.2.

3.3.1 EXPERIMENTAL

Using the rotating disc cell and assembly described in CH 2.1.1 and 2.4.1, with the nickel rotating disc electrodes prepared as in CH 2.2.6.1, it was possible to pretreat electrodes under different conditions. The two pretreatment methods employed (where used), were 1) overnight (16 + hour) evolution of hydrogen at -1.100V, followed by 3 hours at -1.300V or, 2) 3 hours evolution at -1.300V. In both cases the electrolyte was degassed cadmium-free 10.00M KOH. After pretreatment, the electrolyte was quickly drained and the cell re-filled with the pre-degassed working solution. This change took $\simeq$ 2 minutes and necessitated some exposure of the wet

electrode surface to air.

3.3.2 DISCUSSION

As can be seen from figure 3.4, the current/time transient during the hydrogen evolution takes some time to settle to the steady state value at -1.100V (on a rotating electrode). The time required being dependent on both the potential applied and the degree of convection in solution, although the presence of oxygen would doubtless have some influence. This time to steady state, decreases with increasing potential and was found to be independent of the state of polish of the electrode. The hydrogen evolution current is sensitive to any electrode disturbance, switching the electrode to its rest potential for 2 minutes (corresponding to the time required for solution exchange), required an additional 15 minutes of evolution at -1.100V to return the current levels to steady state. This effect is in part, likely to be due to the removal and re-establishment of hydrogen bubbles at the surface.

The production of OH^- at the electrode surface during evolution, will alter the boundary layer conditions during hydrogen evolution, but was considered to be negligible in the 10.00M KOH system. This might however, be of some importance in any low alkali concentration electrolyte.

3.4 DEPOSITION FROM 10.00M KOH + 0.00035M Cd(II) ONTO NICKEL DISCS

With the rotating disc cell and assembly described in CH

2.1.1 and 2.4.1, and the electrolytes prepared as in CH 2.3, a series of experiments were carried out to determine the deposition characteristics of 10.00M KOH saturated in Cd(II). The most likely dissolved species for all the 10.00M KOH systems is $Cd(OH)_4^{2-}$ [see CH 1.3.1.1]. The solubility of $Cd(OH)_2$ has been studied by a number of workers[4-6, 8-10,12,15] and a solubility of 0.00035M for $Cd(OH)_2$ in 10.00M KOH at 25°C, has been assumed for the work presented within this thesis. This value corresponds to that obtained by both Lake and Goodings[11] and Armstrong et al[8].

3.4.1 CYCLIC VOLTAMMETRY

3.4.1.1 EXPERIMENTAL

Using a polished nickel electrode prepared as in CH 2.2.6.1, an electrode was pretreated by cathodic evolution of hydrogen for 16 hours at -1.100V. This was followed by a further 3 hours at -0.950V on a stationary electrode. The hydrogen evolution current stabilised at the lower potential within 20 minutes. After stabilisation the electrolyte was exchanged to allow deposition at η= -50mV in 10.00M KOH + 0.00035M Cd(II). A standard rotation rate of 5 rev/s was employed.

3.4.1.2 RESULTS AND DISCUSSION

Figure 3.5 shows the current/time response during deposition at η= -50mV. As expected, the hydrogen evolution current on nickel is small at this overpotential. However, on solution

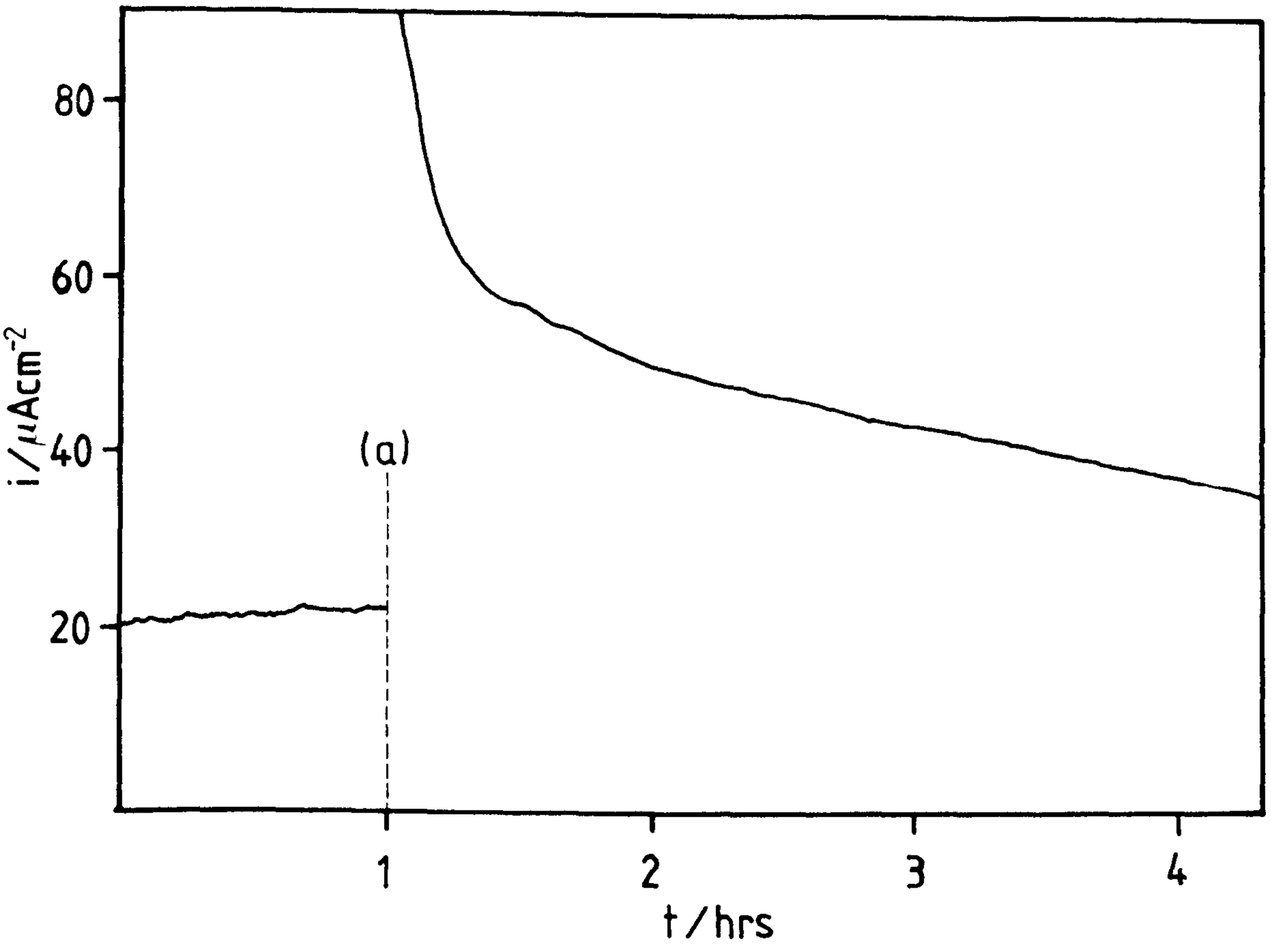

Fig 3.5 Current/time transient obtained at -0.950V (versus Hg/HgO) in 10.00M KOH, changing from cadmium-free to 0.00035M Cd(II) saturated 10.00M KOH electrolyte at (a).

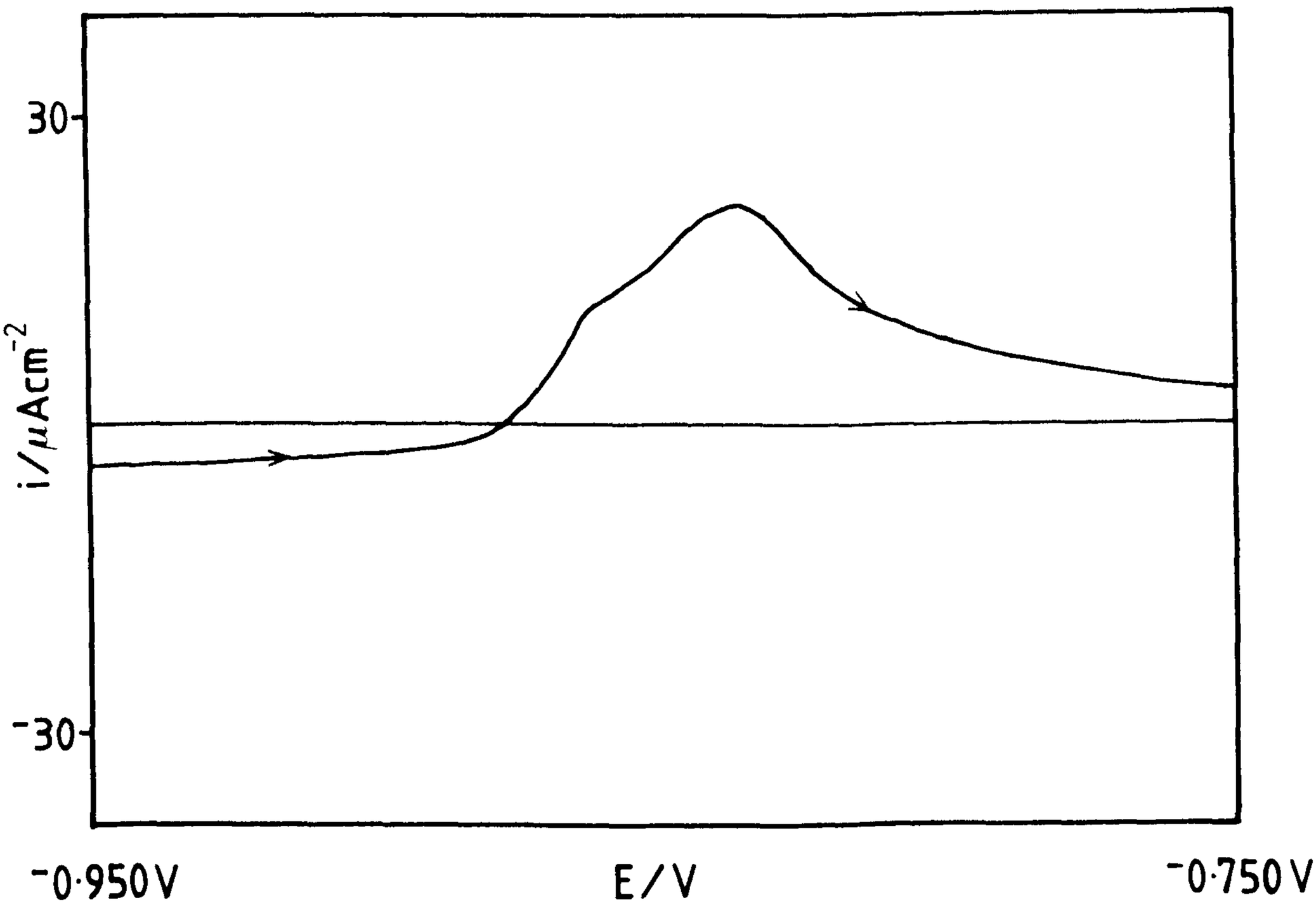

Fig 3.6 Anodic linear sweep performed on a nickel electrode after 5 hours deposition at -0.950V (versus Hg/HgO). Sweep limits were from -0.950V to -0.750V at a sweep rate of 0.3mV/s.

change from cadmium-free to cadmium-saturated 10.00M KOH, we see an increase in the current due to cadmium deposition coupled with a decreasing hydrogen evolution current due to the surface changing from nickel to cadmium, the cadmium depositon current is of the order 30 - 50 μFcm^{-2}. Oscillations observed in the i/t transient are due to bubble formation.

After 5 hours of deposition, a linear sweep in the anodic direction from the rest potential, was performed at a sweep rate of 0.3mV/s (see fig 3.6). This showed two probable cadmium dissolution peaks at -0.861 and -0.838V, presumably due to oxidation of two different crystalline forms of cadmium. Dendritic and other complex crystals, would be expected to have a lower stability compared with more uniform deposits of cadmium. Increasing the deposition time, increases the dissolution peak at -0.861V consistent with a change in morphology. However, it is possible that the peak at -0.838V, corresponds to oxidation of an alloyed layer of nickel/cadmium of unknown structure. Since it is inevitable that an alloy layer will be produced during deposition. This alloy layer is unlikely to be of any appreciable thickness, since subsequent double layer capacity studies show transition from nickel to cadmium occurs rapidly, typically within 500s [see CH 4.1]. The possibility of alloy formation between the $Cd(OH)_2$ and $Ni(OH)_2$ during charging, was noted by Levina and Rozentsveg[180]. This was later confirmed by Barnard et al[37,80]. At normal cell operating temperatures, the alloy detected is Ni_5Cd_{21} [76,77], although heat treatment of mixtures of nickel and cadmium at 300 - 400^{o}C, has resulted in the identification of Ni_5Cd_{21}, Ni_2Cd_5 and NiCd[76]. The formation of alloy requires

the inclusion of $Ni(OH)_2$ into the negative plate, presumably via corrosion of the nickel support sinter[4]. Thus it seems unlikely that any detectable alloy formation could occur during such short time-periods as used here. Additionally, the discharge region for Ni_5Cd_{21} is in the range -0.74 to -0.78V (in 10.00M KOH)[77,181], some 60 - 100 mV more anodic than detected here.

The total charge passed during dissolution = 0.0096 Coulombs, hence assuming all the cadmium is removed, this will correspond to deposition of 5.62×10^{-6}g of cadmium. This is provided that production of CdO does not occur and thus no passivation of the electrode surface interferes with dissolution. If evenly deposited, this quantity would produce a film of thickness 0.052 μm. Subsequent examination of the electrode surface under a 25x binocular optical microscope, showed the mirror finish to be retained, if slightly tarnished.

3.4.2 A.C. IMPEDANCE

Employing the frequency response analyser and associated equipment described in CH 2.4.4, coupled with the data processing system described in CH 2.6.1, it was possible to make a.c. impedance measurements. Rotating disc electrodes attached to the rotating disc cell and assembly [see CH 2.1.1 and 2.4.1], were used under a number of differing conditions.

Figure 3.7, shows a typical spectrum taken on a rotating electrode (5 revs/s). This was with steady state hydrogen evolution at -1.300V on a polished nickel disc electrode (prepared as in CH 2.2.6.1), in cadmium-free 10.00M KOH. In

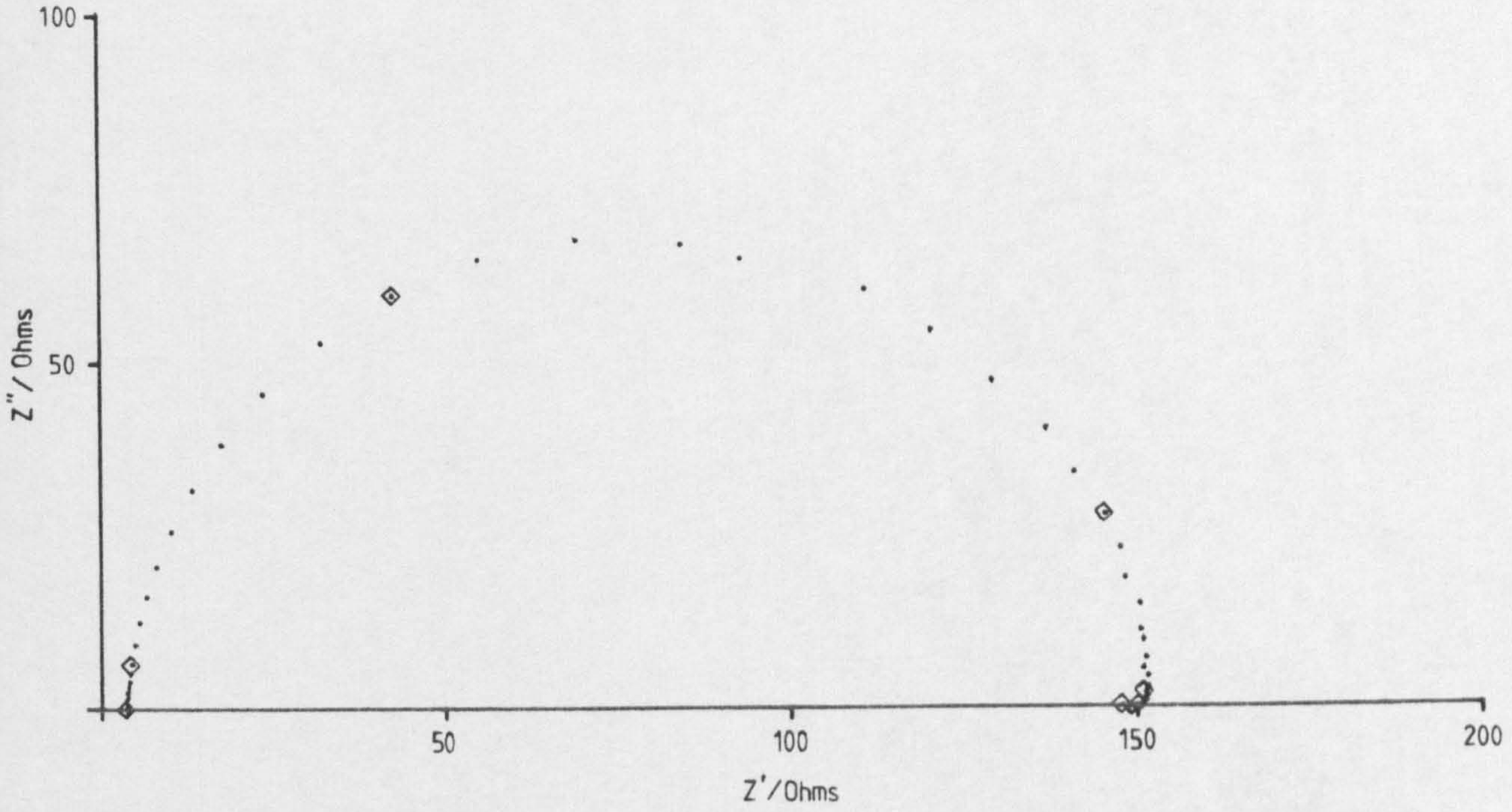

Fig 3.7 A.c. impedance spectra taken on a polished rotating nickel electrode (5 rev/s), in 10.00M KOH under steady-state hydrogen evolution at -1.300V (versus Hg/HgO). Frequency limits were 10kHz to 0.1Hz.

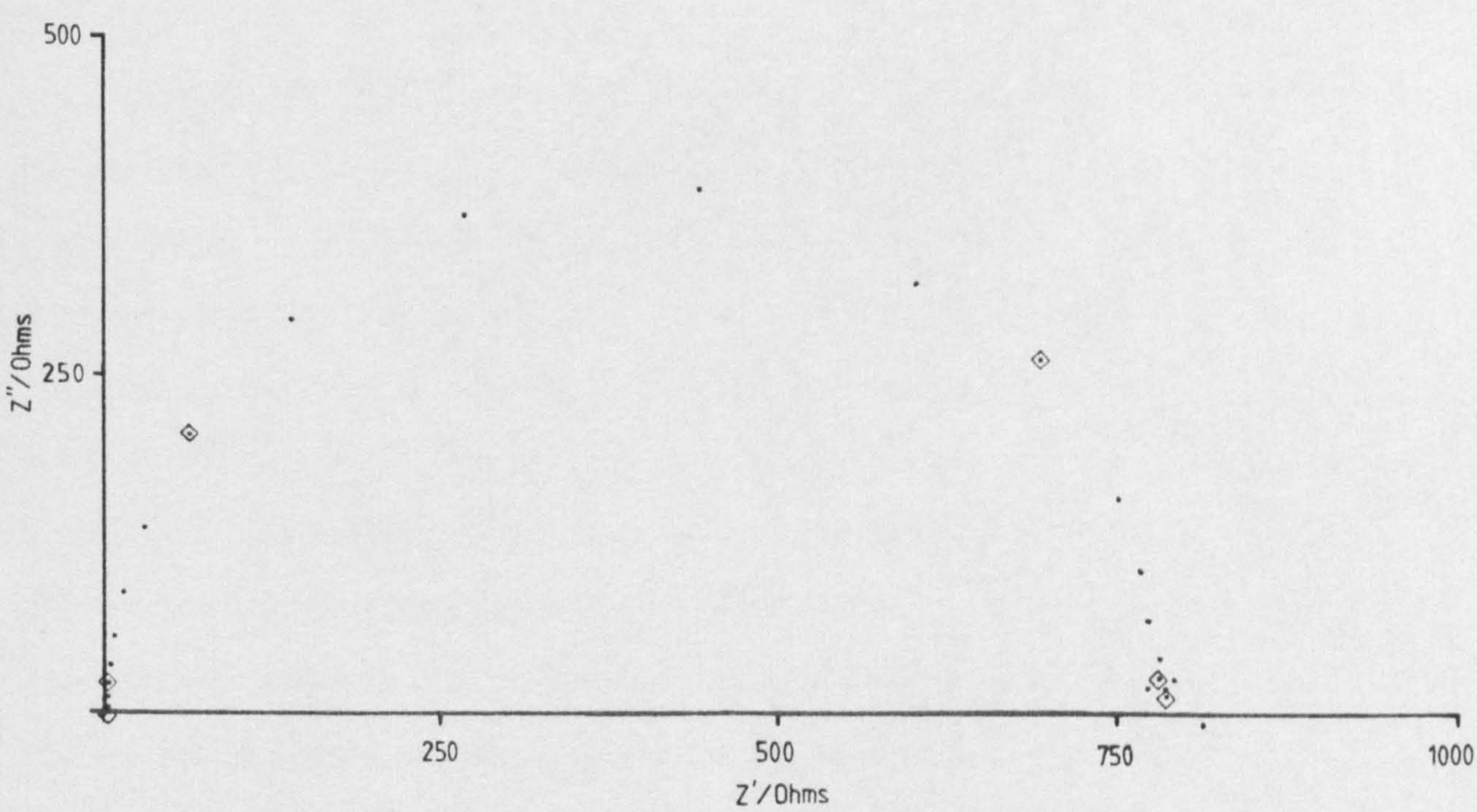

Fig 3.8 A.c. impedance spectra taken on a polished rotating nickel electrode (5 rev/s), after 70 minutes deposition at -1.300V (versus Hg/HgO) in 10.00M KOH containing 0.00035M Cd(II). Frequency limits were 10kHz to 0.1Hz.

degassed KOH, hydrogen evolution should be the only reaction occurring viz,

$$2HOH + 2e^- \rightleftharpoons H_2\,[g] + 2OH^-\,[aq]$$

via;

$$HOH + M(e^-) \rightleftharpoons MH + OH^-$$

$$MH + MH \rightleftharpoons 2M + H_2$$

At -1.300V the electrode is operating in the active controlled region, ie the hydrogen evolution current is diffusion independent [see CH 3.4.4.2], and thus no Warburg impedance is observed. From the semicircle, the charge transfer resistance is $1200\,\Omega\,/cm^2$. Since;

$$i_o = \frac{RT}{nFR_{ct}}$$

a value for the hydrogen evolution exchange current density of $\log i_o = -4.7\ Acm^{-1}$, is obtained for the nickel electrode at -1.300V. This reduces to $\log i_o = -5.4\ Acm^{-1}$, after 70 mins of deposition (see fig 3.8). At -0.950V after 4 hours of deposition, a value of $\log i_o = -6.85\ Acm^{-1}$ is found. These compare with values of $\log i_o$ for nickel and cadmium metals of, -5.2 and $-10.8\ Acm^{-1}$ respectively, at equilibrium in 1M H_2SO_4 (166). Observation of a.c. impedance spectra taken at times during deposition, showed an increase in charge transfer resistance and a corresponding decrease in i_o. Clearly this reflects a change in surface composition from the relatively noble nickel to cadmium, cadmium having a considerably smaller hydrogen evolution exchange current density. The slow changeover from nickel to cadmium, probably indicates the incomplete coverage of the nickel by the grainy cadmium deposit, rather than alloy formation. At low overpotentials the two

competing reactions (hydrogen evolution and cadmium deposition), give rise to spectra where the real axis is not reached. The a.c. impedance spectra being influenced by the diffusion dependent cadmium deposition reaction, presumably;

$$Cd(OH)_4^{2-} + 2\ e^- \rightleftharpoons Cd_s + 4OH^-$$

At higher overpotentials (> 50 mV), the cadmium deposition current becomes diffusion controlled, whereas the hydrogen evolution current is dependent on overpotential, ie;

$$i = i_{Cd} + i_H$$

Hence at increased overpotentials, the a.c. impedance spectra should reflect a change from i_{Cd} being dominant (diffusion dependent), to i_H dominance (diffusion independent), any diffusional effects are thus reduced.

Observation of the double layer capacity behaviour by a.c. impedance during deposition, should indicate changes in the electrode moprphology, since it is influenced by both the surface/solution composition and the surface area of the electrode. Other influences that affect double layer capacity of a diffuse double layer, are electrolyte concentration and potential. These factors are largely constant for the systems encountered, hence it is possible to interpret double layer capacity (d.l.c.) changes in terms of surface morphological changes. Since dendritic growth has a very large surface area compared to flat or grainy deposits, an upturn in d.l.c. can be expected upon the onset of dendritic growth. For high overpotential systems, it is possible to estimate the d.l.c. values from the a.c. impedance semicircle maximum (ie Z'' max), where $C_{dl} = 1/R_{ct}\omega$. But at lower overpotentials, where the real axis is not reached, the d.l.c. is more conveniently obtained

from the high frequency approximation for the imaginary component of the complex plane impedance [see CH 1.4.7], given by;

$$Z = R_s + \frac{R_{ct}}{1 + \omega^2 C_{dl} R_{ct}^2} - \frac{j\omega C_{dl} R_{ct}^2}{1 + \omega^2 C_{dl}^2 R_{ct}^2}$$

where;

$$Z'' = \frac{\omega C_{dl} R_{ct}^2}{1 + \omega^2 C_{dl}^2 R_{ct}^2}$$

hence at high frequencies; where $\omega^2 C_{dl}{}^2 R_{ct}{}^2 >> 1$;

$$Z'' = 1/\omega C_{dl}$$

For the 10.00M KOH electrolytes used, a frequency of 1000Hz was employed at which the impedance is almost purely capacitive.

For deposition at η= -50mV, the values for d.l.c. decreased from 78 to 58 μFcm^{-2}, over 5 hours of deposition (78μFcm^{-2} representing the pure nickel value). At this overpotential, deposit morphology should be fairly uniform and approximately constant in surface area. Thus the reduction in d.l.c. found is almost certainly due to the change in properties of the surface from nickel to cadmium. At higher overpotentials, initial d.l.c. values appeared to be reproducible (after 500s settle down period). A figure of 35.5 μFcm^{-2} being obtained at η = -400mV, using the standard nickel electrode preparation as described in CH 2.2.6.1. This value, although highly dependent on the state of electrode polish, is comparable to a value of 40 μFcm^{-2} obtained by Edmondson[50] at η = -100mV.

3.4.3 POTENTIOSTATIC STUDIES

Utilising the rotating disc and electrode system described previously, a series of experiments were carried out to determine the deposition characteristics of cadmium onto polished nickel discs in the 10.00M KOH + 0.00035M Cd(II) electrolyte. In order to determine the factors influencing dendritic growth, several possible contributory factors were investigated. Except where otherwise indicated, the procedure used for the potentiostatic experiments, required usage of the compartmented secondary electrode and standard rotation rate of 5 revs/s. Polished, Epoxy sealed electrodes were employed with an initial pretreatment of 100 minutes hydrogen evolution at -1.300V. Double layer capacity measurements were all evaluated using the high frequency approximation at 1000Hz, with a 0.005V RMS ($\pm$ 0.007V peak-peak) amplitude signal. This amplitude is considered small enough to avoid background noise problems.

Deposition for 12 hours at η = -400mV under the conditions decribed above, gave rise to the current/time and d.l.c./time transients shown in figs 3.9 and 3.10. As can be seen from these, no indication of any increase in surface area is found. Additionally, the flat i/t curve, shows that cadmium deposition rate is approximately constant. At η = -300mV the d.l.c./time transient shows a similar form (fig 3.11). The usage of force fitted nickel electrodes gave the same result, indicating the inertness of the Epoxy used. From these results, one can conclude the deposit is flat, with no dendritic growth. Optical observation of the electrode revealed a shiny greyish appearance, consistent with an even deposit. Plates 3.1a/b

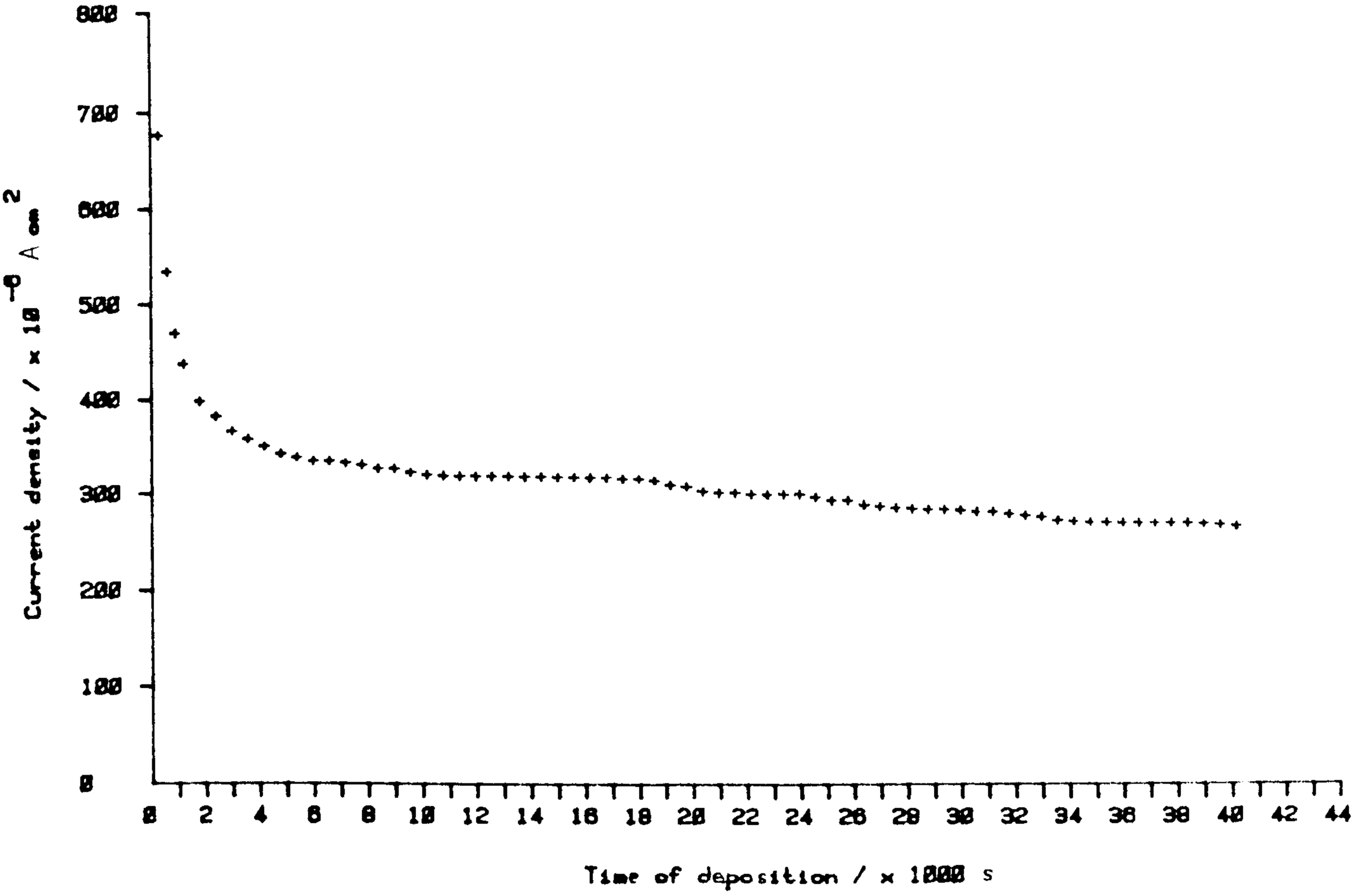

Fig 3.9 Current/time transient found during deposition onto a polished rotating nickel electrode (5 rev/s), at -400mV overpotential in 10.00M KOH containing 0.00035M Cd(II).

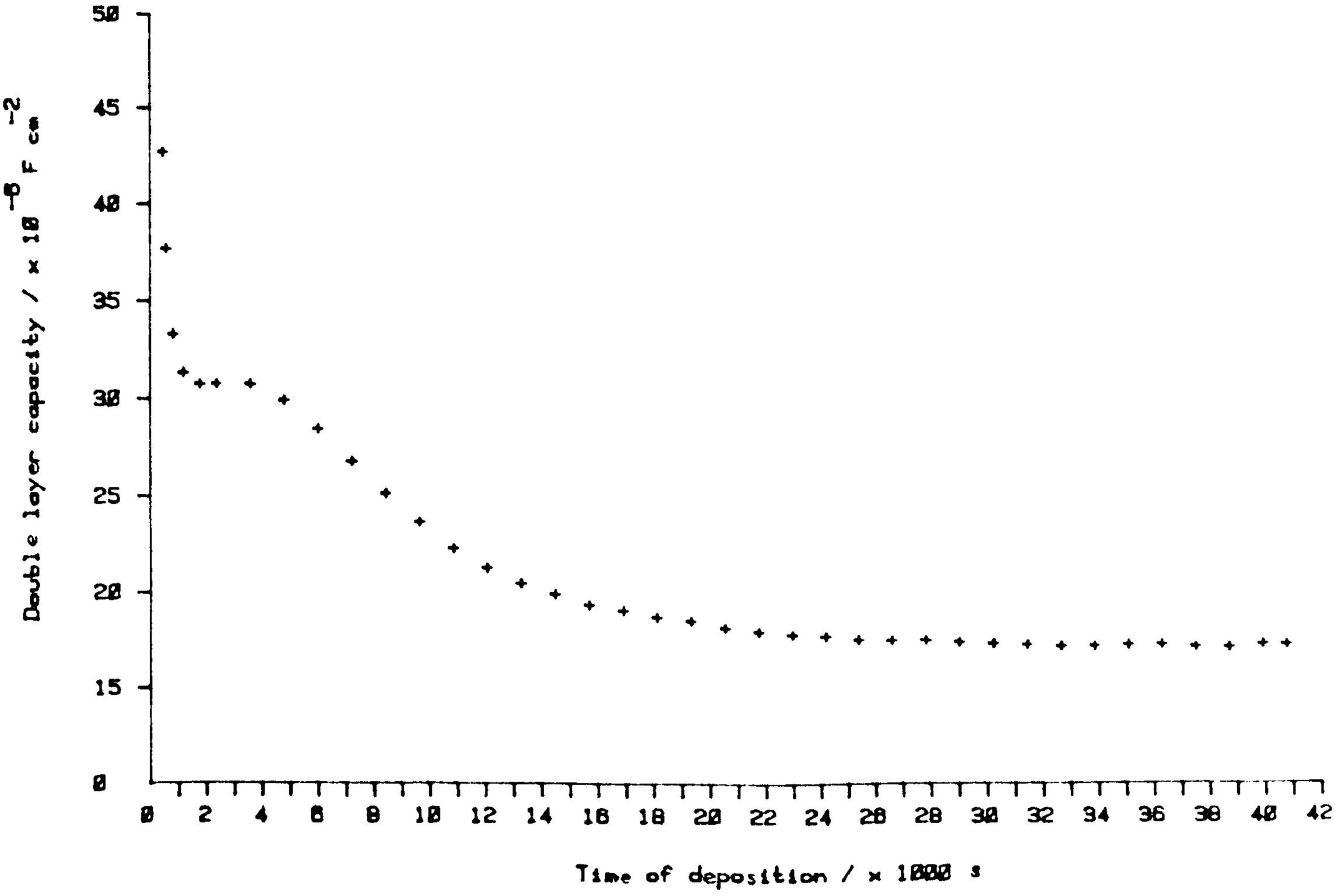

Fig 3.10 Double layer capacity/time transient for the electrode as in fig 3.9

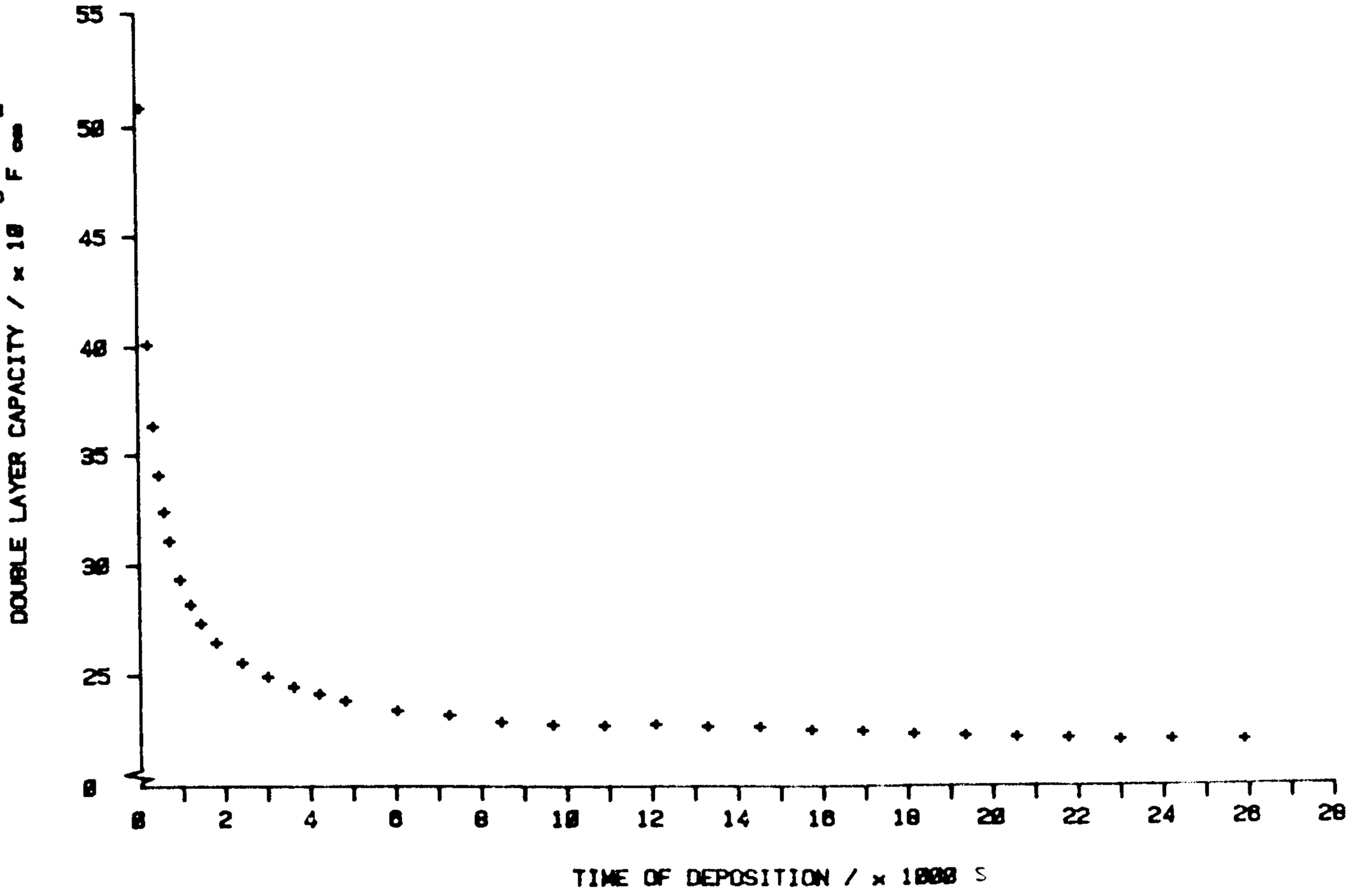

Fig 3.11 Double layer capacity/time transient found during deposition onto a polished rotating nickel electrode (5 rev/s), at -300mV overpotential in 10.00M KOH containing 0.00035M Cd(II).

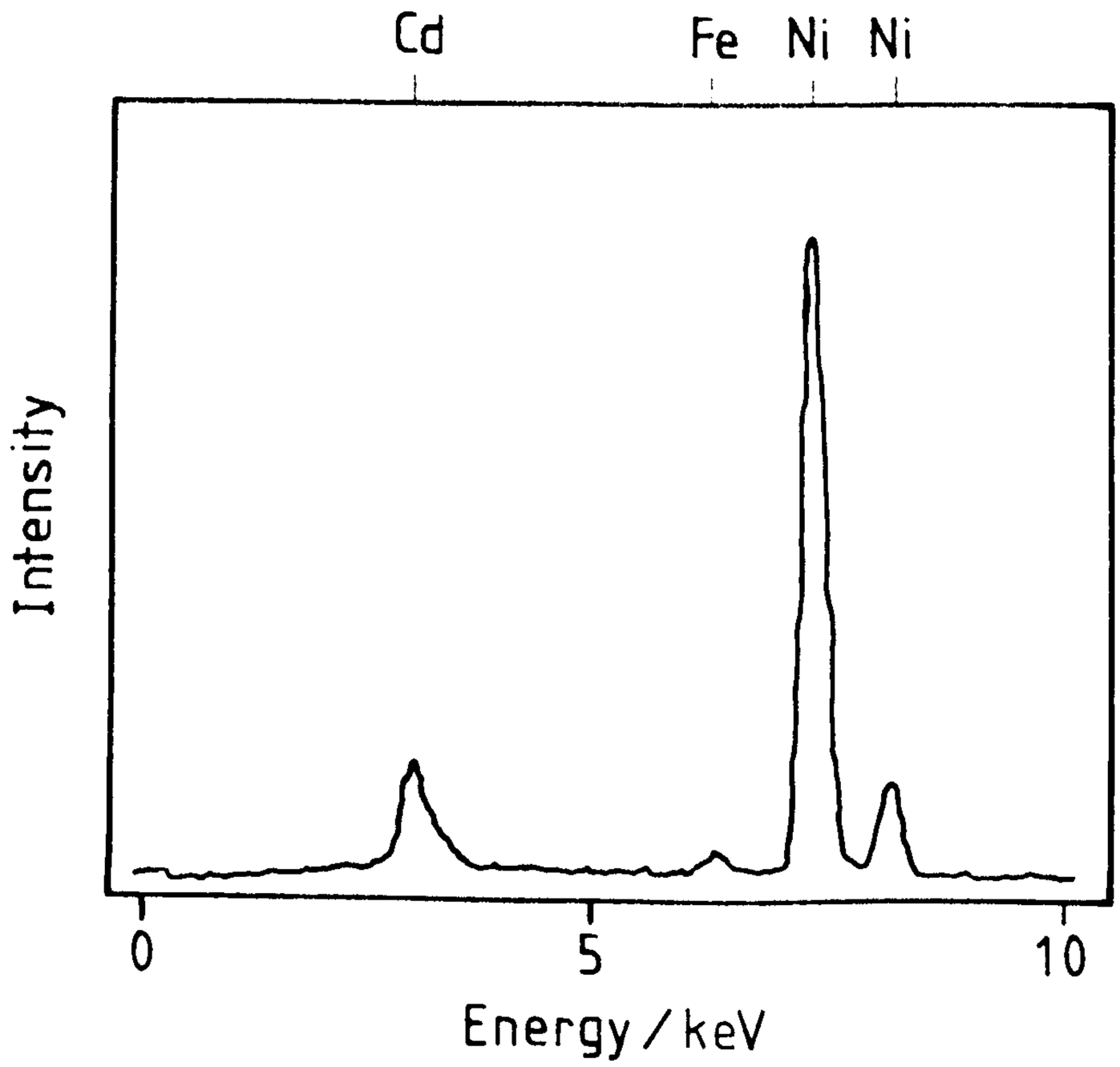

Fig 3.12 EDAX elemental analysis of a nickel electrode surface after 6 hours deposition at -400mV overpotential in 10.00M KOH containing 0.00035M Cd(II).

Plate 3.1 Polished nickel electrode surface after 12 hours deposition at -400mV overpotential, in 10.00M KOH + 0.00035M Cd(II).

Plate 3.1a x500

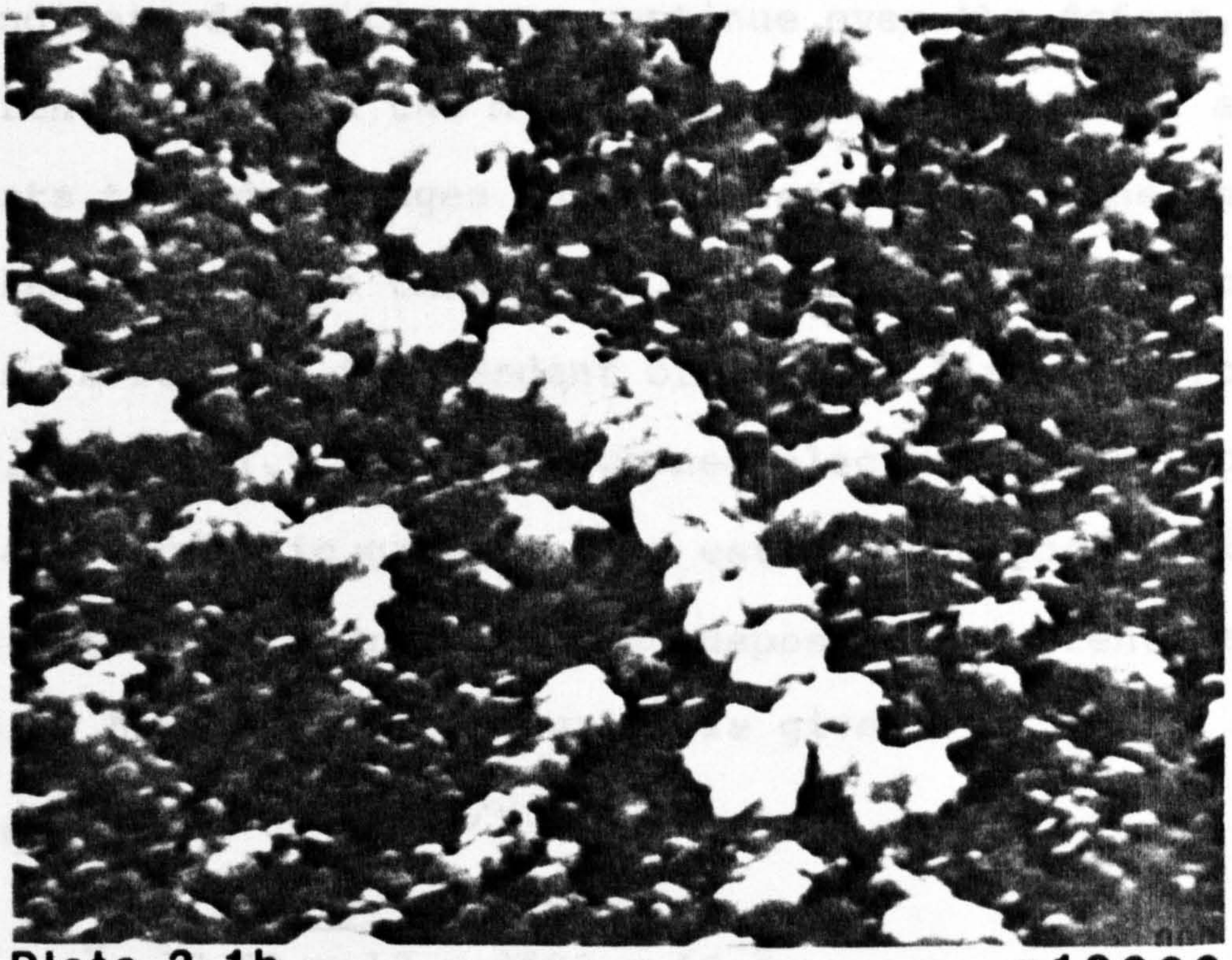

Plate 3.1b x10000

show scanning electron micrographs of the electrode surface after deposition. Comparison with the polished surfaces, found before deposition (plate 2.1b), shows deposition morphology is essentially flat. The deposit appears to comprise of 200 - 600nm grains of cadmium, approximately hexagonal in shape with an estimated thickness 50nm. From plate 3.1b, it is clear that deposition has highlighted any original flaws in the polished surface of the nickel. Presumably this is achieved by the cadmium grains being orientated differently along the line of the surface features (mainly scratches), thus enhancing their visibility (in the electron microscope, the contrast sometimes exaggarates any the appearance of surface prominences). It is possible that there is a simple increase in deposition along the scratches, as has been found in other systems[114].

However, close examination of the surface shows such deposition along scratch lines to be discontinuous. Gaps (as seen in plate 3.1b), indicate deposition can continue over the defect, without any apparent change in the morphology from nearby flat areas. This points towards changes in the orientation of the deposit, rather than changes in thickness. Further evidence that deposit thickness is roughly independent of surface flaws, is found in CH 3.4.3.1 and 4.1.2, where roughened electrodes were not found to initiate dendritic growth. The estimated deposit thickness is 500nm, thus the average cadmium deposition current required over the 12 hour deposition period is given by;

$$i_{Cd} = 5 \times 10^{-7} \times nF/Vt$$

$$= \frac{2 \times 96487 \times 5 \times 10^{-11}}{12.99 \times 12 \times 3600 \times 10^{-6}}$$

$$= 1.7 \times 10^{-5} \text{ Acm}^{-2}$$

This is in good agreement with the value of 18μAcm^{-2}, found from the rotating disc spectra discussed in CH 3.4.4, thus indicating the uniformity of the deposit observed. This uniformity of deposit at high overpotentials and relatively long periods of time, is contrary to some previous observations[16].

Elemental analysis via EDAX (Electron Dispersive X-ray Analysis) of nickel surfaces, was carried out after deposition at η = -400mV for 6 hours. This only showed the presence of nickel and cadmium in the sample (see fig 3.12). The high nickel peak observed, is due to the penetration depth of the electron beam being some 2μm. Hence the 0.5μm cadmium film will not mask the underlying nickel surface completely. Observed Fe and Cu peaks were found to be due to other sources, caused by the EDAX facility itself.

3.4.3.1 SURFACE ROUGHNESS

To investigate the role that surface roughness has on deposition morphology, polished nickel disc electrodes were prepared as in CH 2.2.6.1 and roughened with 45 μm diamond polish. The electrodes were then cleaned in triply distilled water, revealing a visibly scratched electrode finish. From optical microscope observations, the scratches were uniformly produced and of depth 5 - 20 μm. After pretreatment for 100 minutes at -1.300V (rotation rate at the standard 5 rev/s), deposition was carried out at η = -400 mV over a period of 9 hours. The d.l.c./time transient is shown in fig 3.13. The initial value for the d.l.c., (initial in this context is taken to be at the earliest time-period where the surface composition

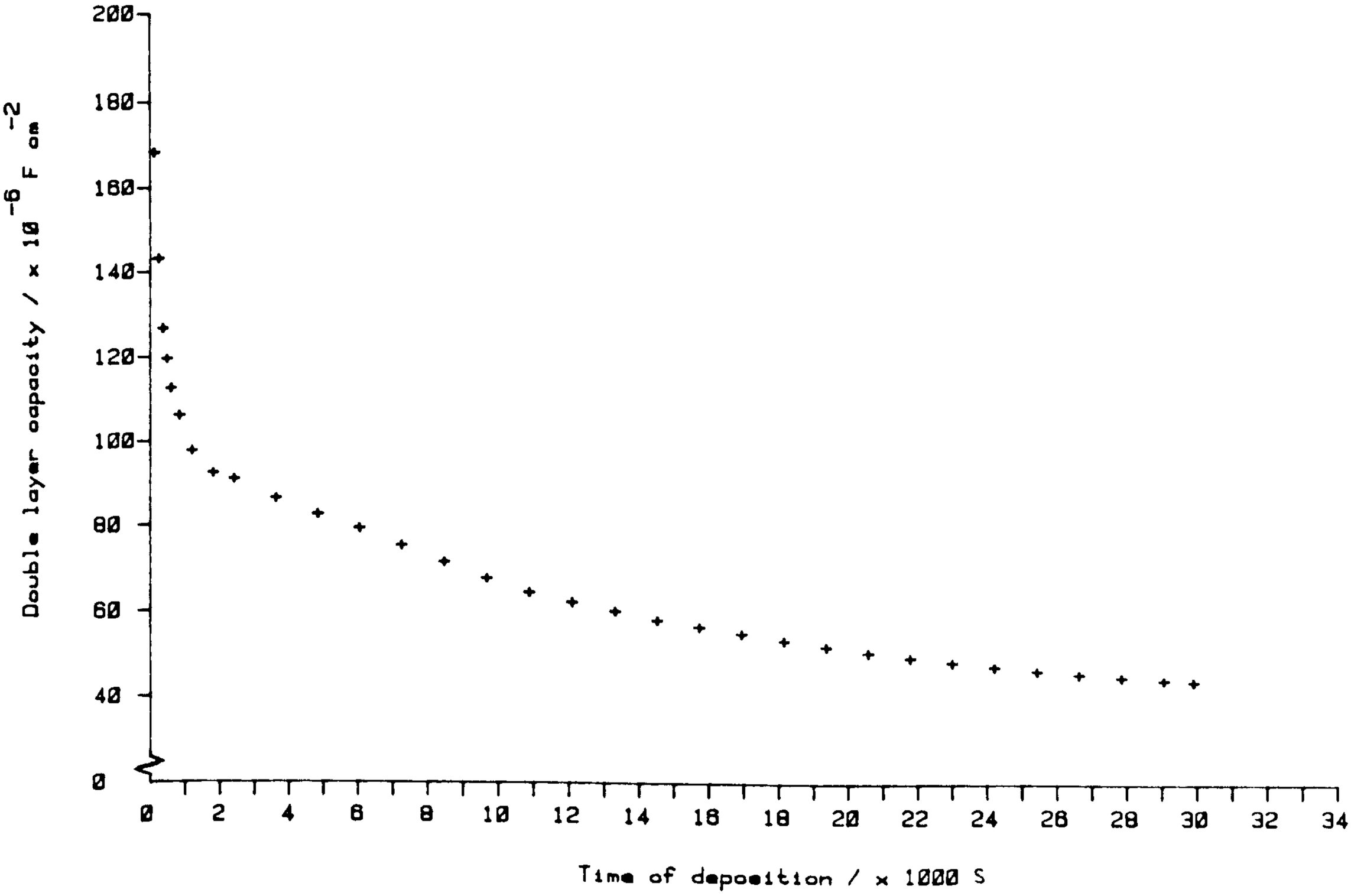

Fig 3.13 Double layer capacity/time transient found during deposition onto a roughened (45 micron diamond polish), rotating nickel electrode (5 rev/s), at -400mV over-potential in 10.00M KOH containing 0.00035M Cd(II).

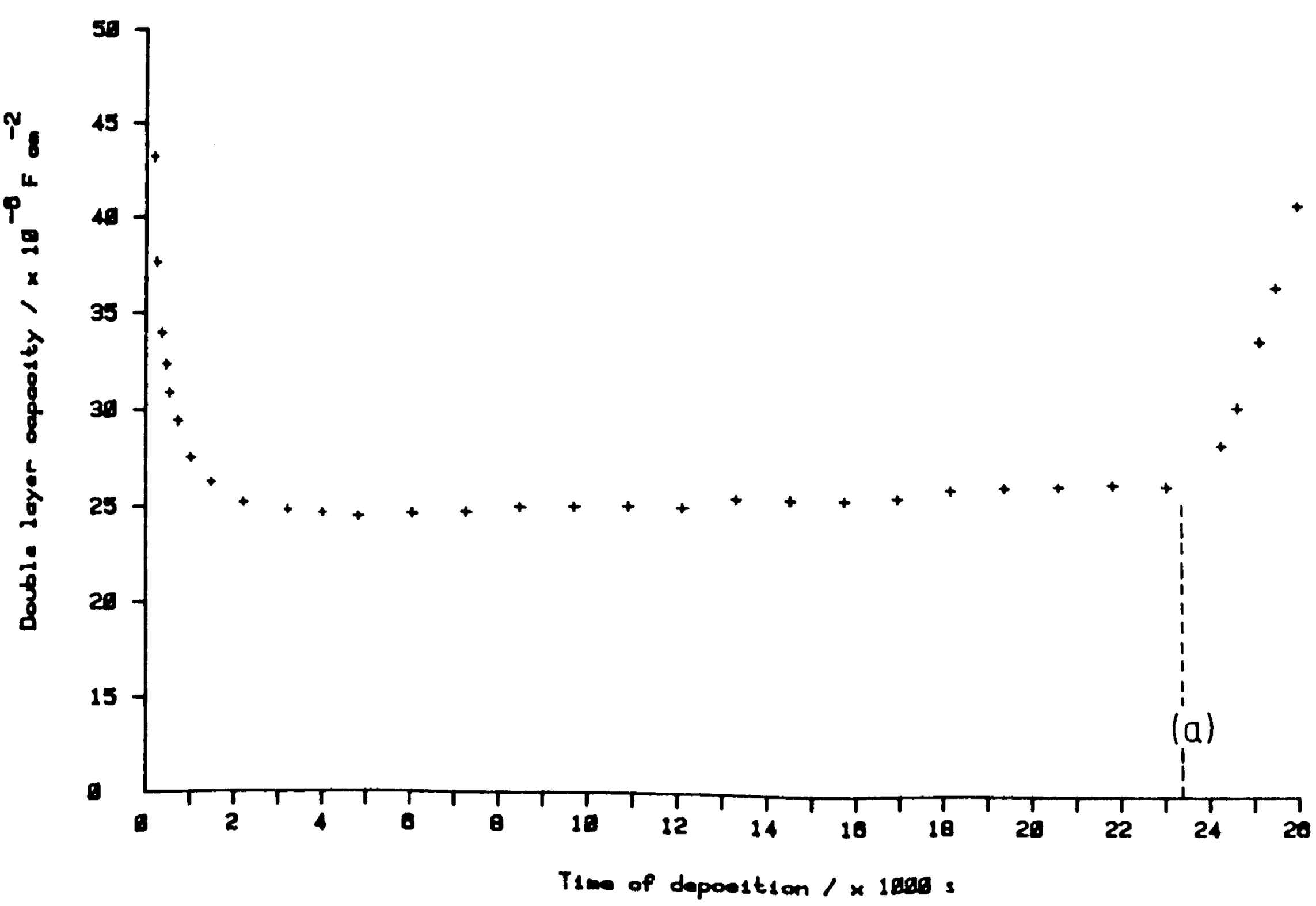

Fig 3.14 Double layer capacity/time transient found during deposition onto polished rotating nickel electrodes (5 rev/s), in 10.00M KOH containing 0.00035M Cd(II) at -400mV overpotential. 0.1g CdO powder was added to the cell electrolyte at (a).

is constant, ie cadmium, at around 2000s) of 93 μFcm^{-2}, compares with an average value of 37 μFcm^{-2}, for the polished electrodes. Thus indicating a roughness factor of x2.7. No evidence of dendritic growth is to be seen from this transient. The value of the d.l.c. after 30000s is 44 μFcm^{-2}, compared with an average value of 17μFcm^{-2}, found for the polished electrode surface at the same time-period (see fig 3.10). These final values of d.l.c. give a relative roughness factor of x2.6 (initially rough versus polished), again indicative of the uniform nature of the deposit. The constant surface roughness factor is to be expected in the absence of dendritic growth, since a deposit thickness of 0.5 μm is considerably smaller than the average scratch depth. Optical examination of the surface revealed no dendrites.

Theories of surface amplification of irregularities[116], indicate that dendritic growth should be enhanced at any roughened surface. Thus, further electrodes were prepared and roughened with Emery paper (240 grit), to give a surface with scratches of 10 - 100 μm depth. The initial d.l.c. of 225 μFcm^{-2} indicated a surface roughness factor of x6.4. However, deposition did not cause any significant change in d.l.c. after 6 hours of deposition at η = -400 mV. Hence it is clear that under these conditions, deposition morphology is uniform and independent of the initial surface irregularities (ie, at timescales of up to 12 hours deposition at η = -400 mV in 10.00M KOH + 0.00035M Cd(II) onto nickel).

3.4.3.2 PRETREATMENT AND DISSOLVED OXYGEN

To examine the influence that the pretreatment of nickel electrode surfaces has on deposition behaviour, a series of deposition experiments were carried out, which varied the pretreatment.

No difference in deposition behaviour was discernible between electrodes pretreated in 10.00M KOH for 16 hours at -1.100V (stationary), followed by 3 Hours at -1.300V (5 rev/s), and those where only 30 minutes of hydrogen evolution at -1.300V was used. Indeed usage of electrodes without any pretreatment, seemed to have no effect on the cadmium deposition behaviour, although initial hydrogen evolution currents were higher. The involvement of oxygen was investigated, due to its importance in the nickel oxide surface film formation. It is possible for some small quantity of dissolved oxygen to diffuse through the fritt from the secondary electrode compartment, despite the usage of degassed electrolytes and constant slow bubbling of nitrogen. The deposition experiment was repeated, using the second secondary electrode within the main cell compartment [see CH 2.1.1]. No noticeable change in deposition behaviour was found under the same conditions. Thus it can be assumed that the deposition behaviour is not influenced by the relatively low concentrations of oxygen normally present. The exposure of the electrode to air during solution change was also investigated, with only a slightly increased hydrogen evolution current (10%) found after 10 minutes of exposure (normal solution change requires 2 minutes).

3.4.3.3 CADMIUM SALTS IN SUSPENSION

Previous work[1,2], has indicated that cadmium dendrites do occur in cells and have caused cell failure. Dendrites can be grown in alkaline electrolytes under controlled conditions[16]. In order to explain the lack of apparent dendritic growth for solutions of 10.00M KOH saturated in $Cd(OH)_4^{2-}$, experiments into the role of suspended cadmium salts during deposition, were carried out. It seems probable that in operating Ni/Cd cells, some of the negative plate active material would find its way into suspension. Hence a second mechanism of cadmium deposition via suspension, rather than solution soluble species, could be involved.

Using the cell and electrodes described previously, polished nickel discs were pretreated at -1.300V for 100 minutes. The electrolyte was then changed to Cd(II) saturated 10.00M KOH, allowing deposition to be carried out for a period of 8 hours at η = -400mV. After 6 hours of deposition, a quantity of CdO powder (0.1g/ 100ml), was added to the cell. Fig 3.14 shows the d.l.c./time transient observed. The response is seen to be almost flat, until the addition of the CdO to the system, whereupon an immediate rising trend in the d.l.c. values was found. Examination of the electrode after deposition, showed a dull grey deposit over the surface. Optical microscope observations, revealed the surface to have a dendritic deposit of cadmium. Scanning electron microscopy (SEM), revealed the fine structure of the deposit. Plates 3.2a/b, are micrographs of the surface, showing the nature of the deposit morphology to consist of a grainy background, with numbers of small 'fern-

Plate 3.2 Polished nickel electrode surface after 8 hours deposition at -400mV overpotential, in 10.00M KOH + 0.00035M Cd(II), with the addition of 0.1g/dm^3 CdO powder after 6 hours of deposition.

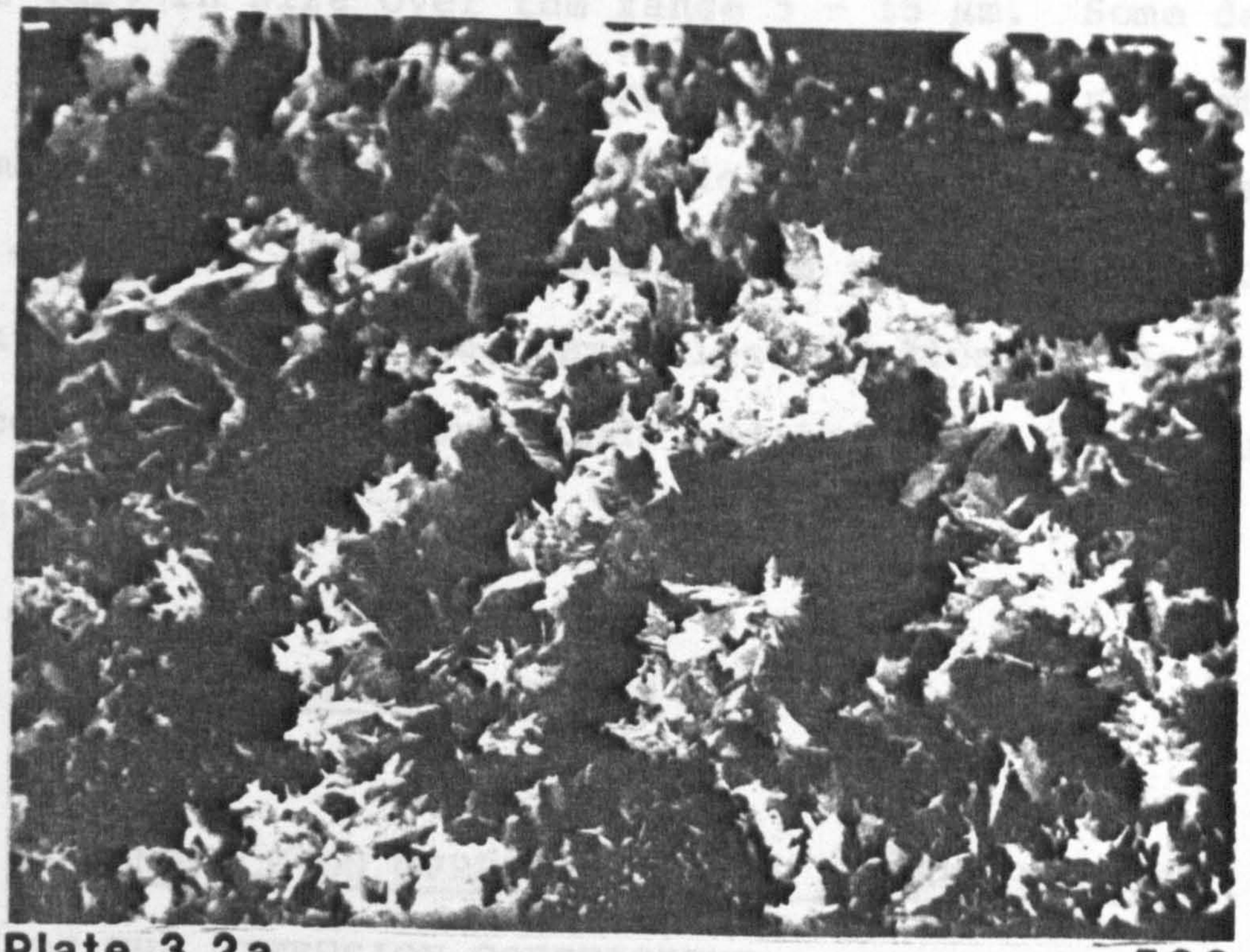

Plate 3.2a

x500

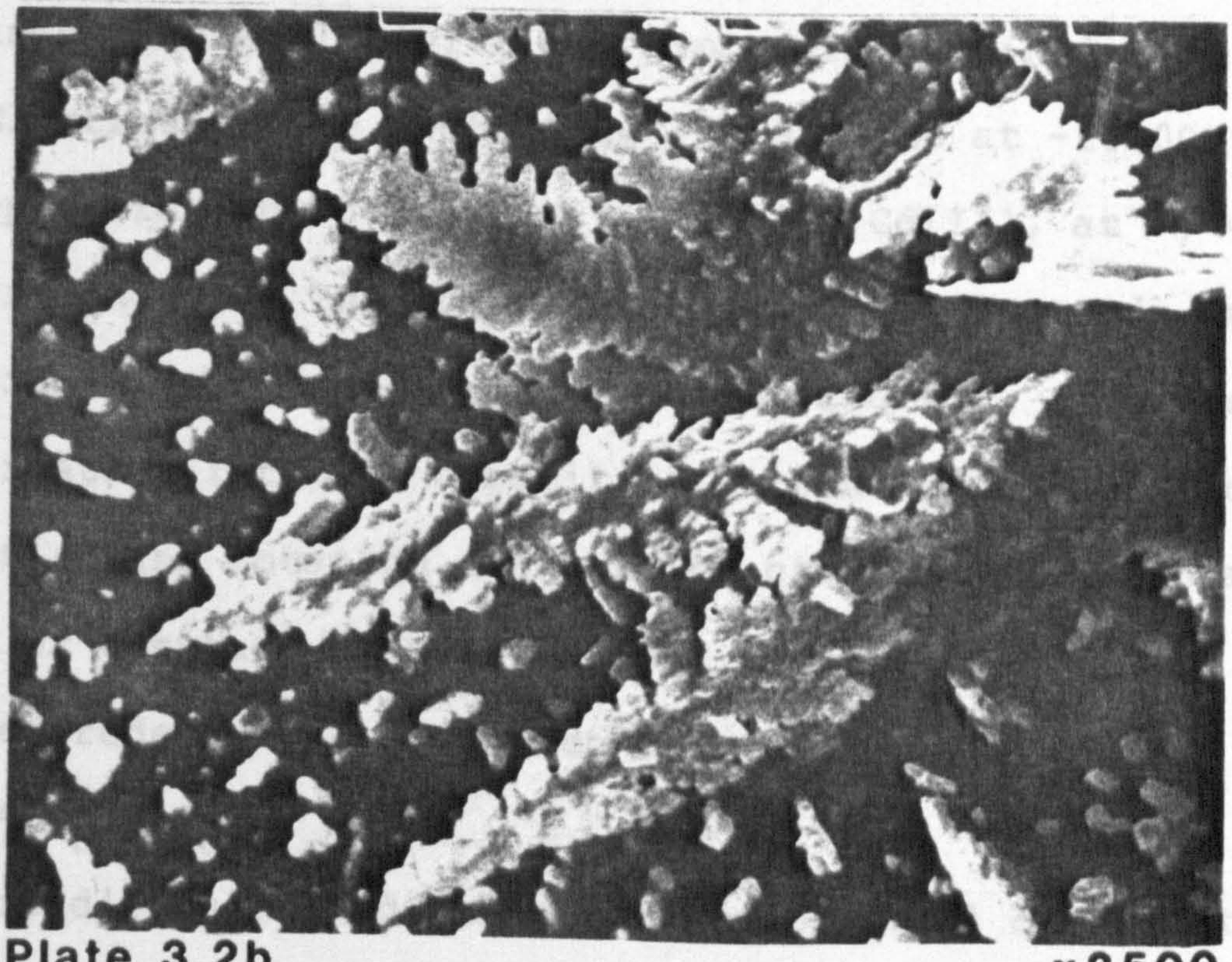

Plate 3.2b

x3500

like´ dendrites scattered liberally across the electrode. The dendrites vary in size over the range 5 - 15 μm. Some dendrites are seen to clump together, in apparently random orientations. This dramatic change in the deposition behaviour with the addition of < $1gdm^{-3}$ CdO, (corresponding to < 0.001M CdO after settling of the larger particles), indicates the importance of any supension found, and is investigated further in CH 4.

3.4.4 ROTATION RATE DEPENDENCE

3.4.4.1 DEPENDENCE ON OVERPOTENTIAL - DETERMINATION OF THE DIFFUSION COEFFICIENT

The rotating disc apparatus and polished nickel electrodes were as used previously, with the procedures as indicated in CH 2.8.1. Electrodes were pretreated for 3 hours at -1.300V, before deposition in 10.00M KOH + 0.00035M Cd(II), at η = -400mV for 2 hours. This preparation gave an electrode surface, covered with a uniform deposit of grainy cadmium. This enabled an investigation into the deposition current dependence, on overpotential and rotation rate, to be carried out, with an electrode of constant composition and surface area.

The electrode current is given by;

$$i = i_H + i_{Cd}$$

where i_H is diffusion independent (overpotential dependent), and i_{Cd} is diffusion controlled (overpotential independent). This total current arises from the two competing reactions;

$$2H_2O + 2e^- \rightleftharpoons H_2 + 2OH^-$$

$$Cd(OH)_4^{2-} + 2e^- \rightleftharpoons Cd_s + 4OH^-$$

Diffusion dependent reactions on rotating disc electrodes should give rise to a current dependence given by the Levich[173] equation;

$$i = 0.621 nFC_o D_o^{2/3} \nu^{-1/6} \omega^{1/2} \qquad \{3.20\}$$

Hence the total current should be given by;

$$i = i_H + 0.621 nFC_o D_o^{2/3} \nu^{-1/6} \omega^{1/2}$$

Such that a plot of current versus root rotation rate, should be a straight line, intercept i_H, slope $0.621 nFC_o D_o^{2/3} \nu^{-1/6}$

Figure 3.15, shows the dependence of current upon rotation rate, over a series of overpotentials from -50 to -400mV. A clear straight line relationship is found, with the slope approximately independent of overpotential above η = -50mV. Thus the current deposition reaction is diffusion controlled over η= -50mV. For overpotentials of > -100mV, an average slope of 245 $\pm$ 30μAm^{-2}(rad/s)$^{-1/2}$ was found over three experiments performed under the same conditions. Hence using {3.20};

$$0.621 nFC_o D_o^{2/3} \nu^{-1/6} = 2.45 \times 10^{-6} \text{ Acm}^{-2}(\text{rad/s})^{-1/2}$$

$$0.621 \times 2 \times 96487 \times 3.5 \times 10^{-7} \times D^{2/3} \times 1.82 = 2.45 \times 10^{-6}$$

(using ν; kinematic viscosity; of 2.8 x 10^{-6}m^2/s, calculated from data for water and adjusted for the increased viscosity of 10.00M KOH)

therefore;

$$D^{2/3} = 3.23 \times 10^{-5}$$

$$D_o = 1.84 \pm 0.4 \times 10^{-7} \text{ cm}^2/\text{s}$$

This value is somewhat lower than the value of 5.32 x 10^{-7}cm^2/s, obtained by Armstrong et al[9].

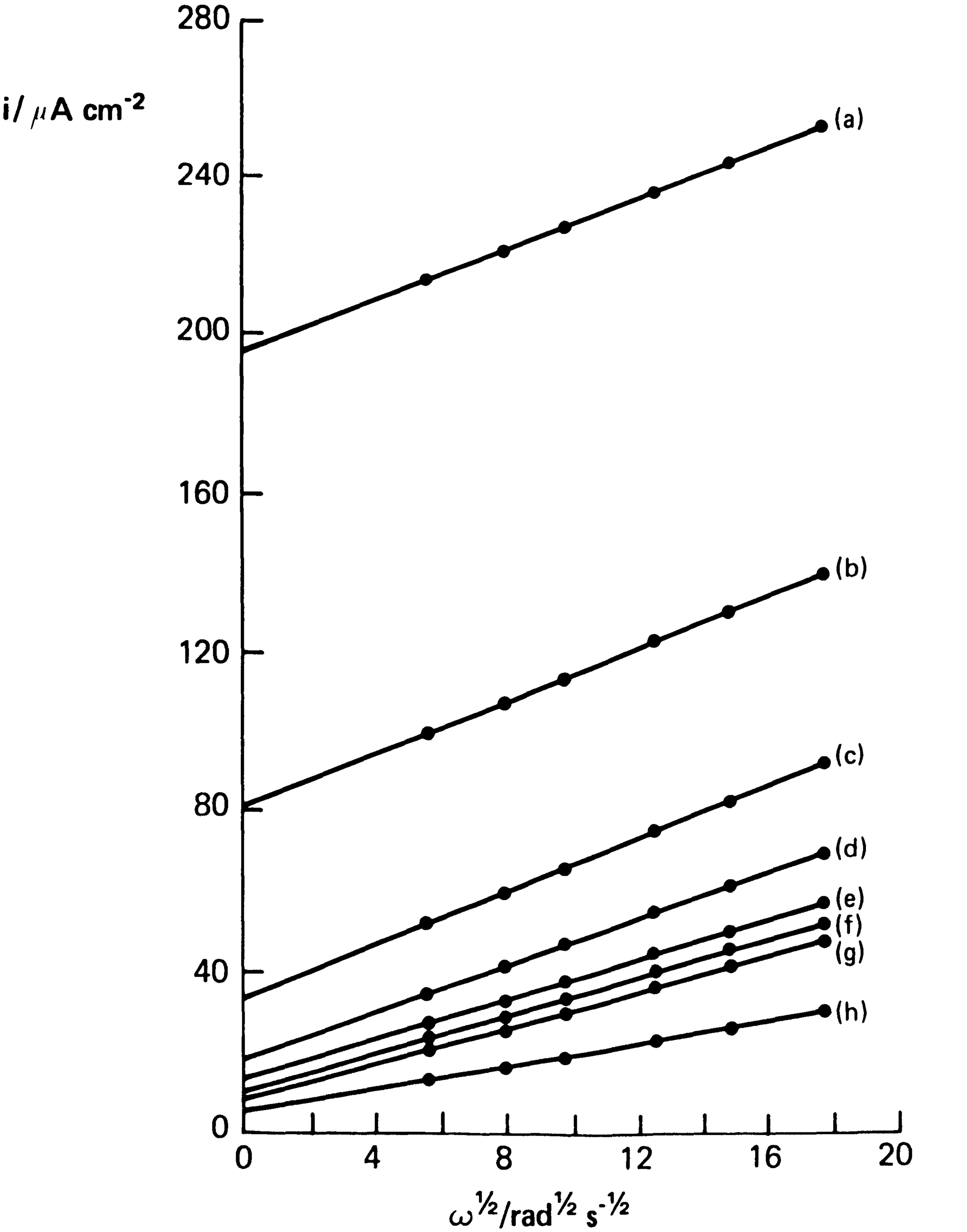

Fig 3.15 Dependence of current upon rotation rate and overpotential for deposition from 10.00M KOH containing 0.00035M Cd(II) on nickel discs with a uniform deposit of cadmium. (a) -400mV; (b) -350mV; (c) -300mV; (d) -250mV; (e) -200mV; (f) -150mV; (g) -100mV; (h) -50mV.

3.4.4.2 DEPENDENCE OF HYDROGEN EVOLUTION CURRENT ON OVERPOTENTIAL

From extrapolation to the intercept, values for the hydrogen evolution current can be obtained for each of the overpotentials used in the rotating disc experiments [described in CH 3.4.4.1]. In the absence of mass transfer effects (ie surface concentration of species $\triangleq$ bulk concentration), the Tafel limits of the Butler - Volmer equation[165] can be applied [see CH 1.4.4];

$$i = i_o[\exp(-\alpha nF\eta/RT) - \exp((1-\alpha)nF\eta/RT)]$$

which can be re-written;

$$i = i_o\exp(-\alpha nF\eta/RT)[1 - \exp(nF\eta/RT)]$$

therefore;

$$\log\left[\frac{i}{1 - \exp(nF\eta/RT)}\right] = \log(i_o) - \frac{\alpha nF\eta}{2.3RT}$$

hence if $1 >> \exp(nF\eta/RT)$ (at $\eta = -0.1V$, $\exp(nF\eta/RT) = 0.00036$);

$$\log(i) = \log(i_o) - \frac{\alpha nF\eta}{2.3RT}$$

or;

$$\eta = \frac{2.3RT}{\alpha nF}\log(i_o) - \frac{2.3RT}{\alpha nF}\log(i) \qquad \{3.21\}$$

corresponding to the Tafel relationship[166];

$$\eta = a + b\log(i)$$

Thus from {3.21}, a plot of log(i) versus η, should have slope $nF/(2.303RT) = 1/0.116$, ie b = 116mV/decade change in current at 20^{o} C, with intercept $\log(i_o)$. Figure 3.16, gives a plot of $\log(i_H)$ versus η, giving a slope of 215mV/decade, over the

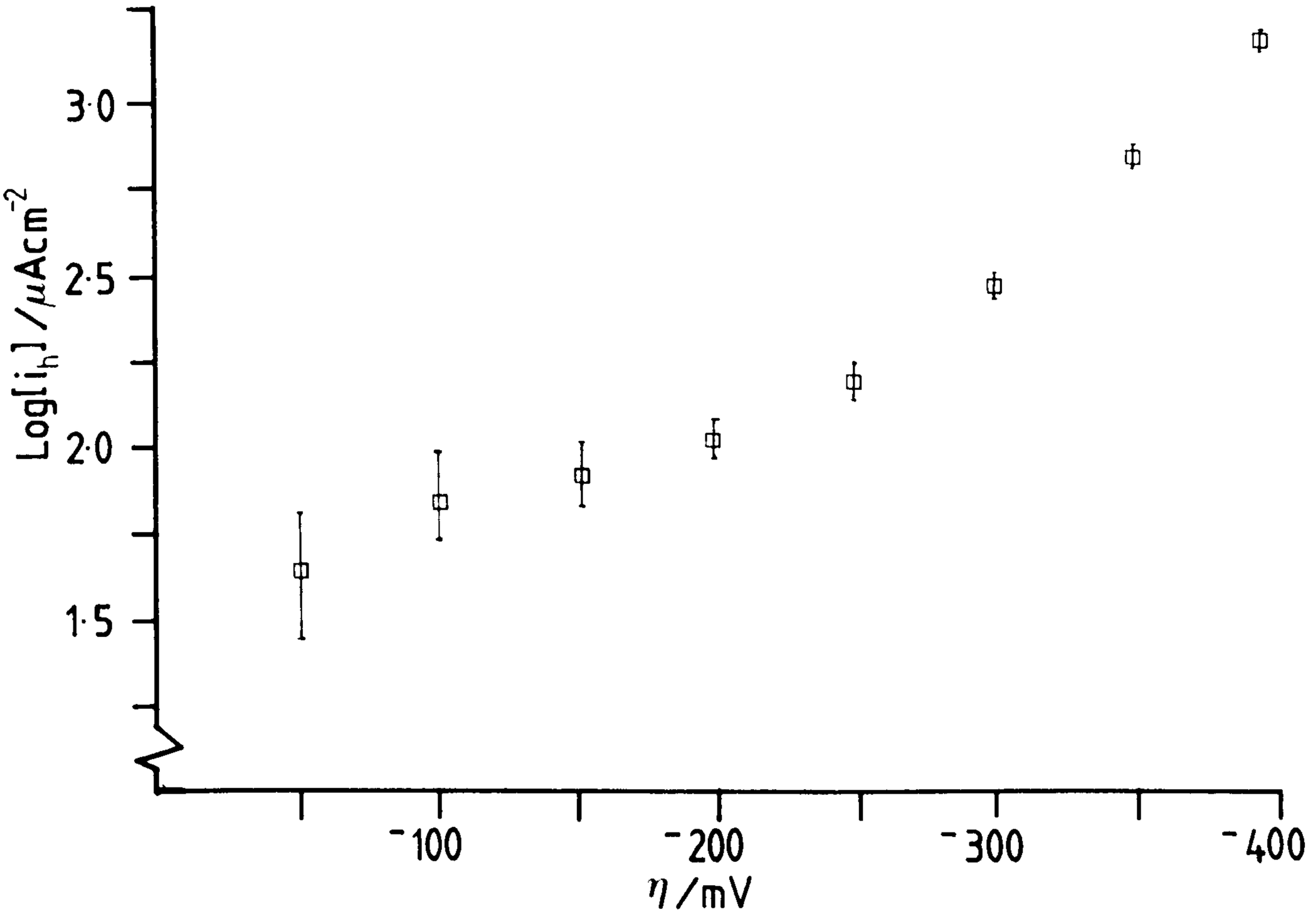

Fig 3.16 Dependence of hydrogen evolution current upon overpotential for deposition from 10.00M KOH containing 0.00035M Cd(II) on nickel discs with a uniform deposit of cadmium.

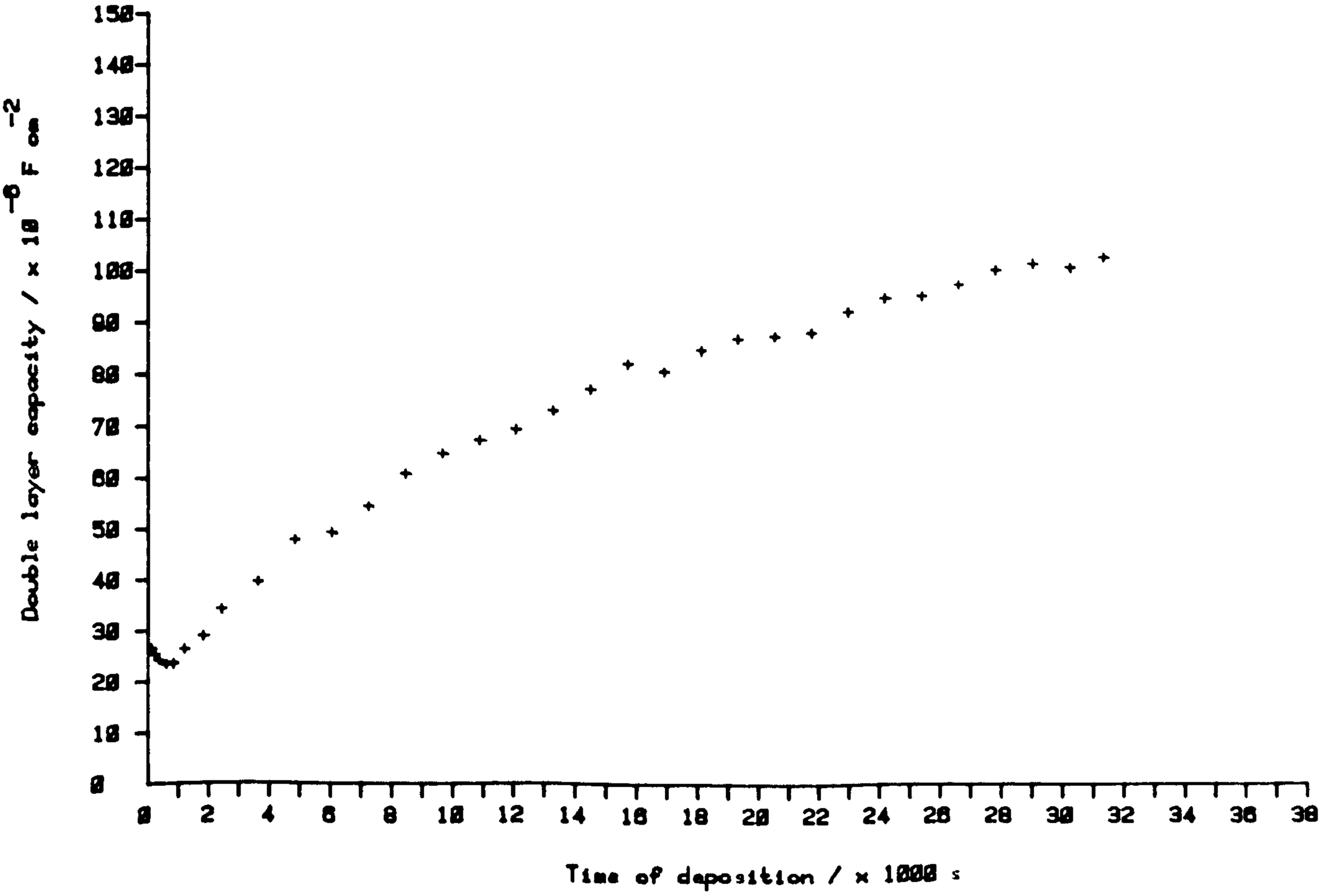

Fig 3.17 Double layer capacity/time transient found during deposition onto an alumina polished rotating cadmium electrode (5 rev/s), at -400mV overpotential in 10.00M KOH containing 0.00035M Cd(II).

range η = -100 to -400mV. However, this discrepancy is less if the slope over η = -200 to -400mV is calculated, giving a value of 140mV/decade. This value is somewhat higher than the value of 118mV/decade previously found by other workers, for currents obtained over 4 decades[62]. The errors in both extrapolation and experimental technique, are inevitably going to be large, especially at lower overpotentials. Errorbars on fig 3.16 refer only to the estimation of intercept values. The intercept for fig 3.16, gives a value for the exchange current of 3.4×10^{-6} Acm^{-2} ($\log(i_o) = -5.47$), which compares to a value of 1.4×10^{-4} Acm^{-2}, obtained by a.c. impedance at η = -50mV ($\log(i_o) = -3.85$).

3.5 DEPOSITION FROM 10.00M KOH + 0.00035M Cd(II) ONTO CADMIUM DISC ELECTRODES

Using cadmium rotating disc electrodes prepared as described in CH 2.2.5, and the rotating disc system as used elsewhere in this chapter, it was possible to investigate deposition onto both mechanically and chemically polished electrodes. The electrode preparation procedures are as described in CH 2.2.6.3.

3.5.1 DEPOSITION ONTO MECHANICALLY POLISHED ELECTRODES

Cadmium rotating disc electrodes employed were mechanically polished down to 1μm alumina (giving a dull grey, moderately reflective surface). These were rotated at 5 revs/s for 30 minutes, whilst degassing with nitrogen. Deposition was then carried out at η = -400mV in the degassed 10.00M KOH + 0.00035M

Cd(II) electrolyte.

Figures 3.17 and 3.18, show the d.l.c./time and current/time transients observed during deposition over a 9 hour time-period. A gradually rising d.l.c. curve is found, tending towards a limiting value of $\doteq 110 \mu F cm^{-2}$. The d.l.c. increases from a value of 23 to $100 \mu F cm^{-2}$, after 6 hours of deposition. This indicates an increase in surface roughness (or area) of $\doteq$ x 4, provided the surface composition remains constant. However, optical examination of the electrode after deposition, revealed a dull grey surface, with no evidence of dendritic growth. Further examination, using scanning electron microscopy, revealed the surface to be relatively uniform in nature (plate 3.3a). Two different surface features are to be seen (plate 3.3b). EDAX elemental analysis (fig 3.19), of the electrode, showed the presence of cadmium as the major consitituent, but the probable presence of 1 - 2 % aluminium, offers some explanation of the deposit found. It seems likely that 1μm alumina particles are embedded into the surface, causing the initial surface area to be partially blocked, thus changing the surface morphology. Thus a low value for the initial d.l.c. is recorded. This value would increase, as the deposition of cadmium caused coverage of this surface with fresh cadmium.

Due to the ductility of cadmium metal and friction during polishing, the surface layer of mechanically polished cadmium is likely to form an amorphous layer, incorporating quantities of polishing materials. The deposition characteristics of more crystalline cadmium, can thus only be studied after removal of this layer (conveniently by chemical dissolution).

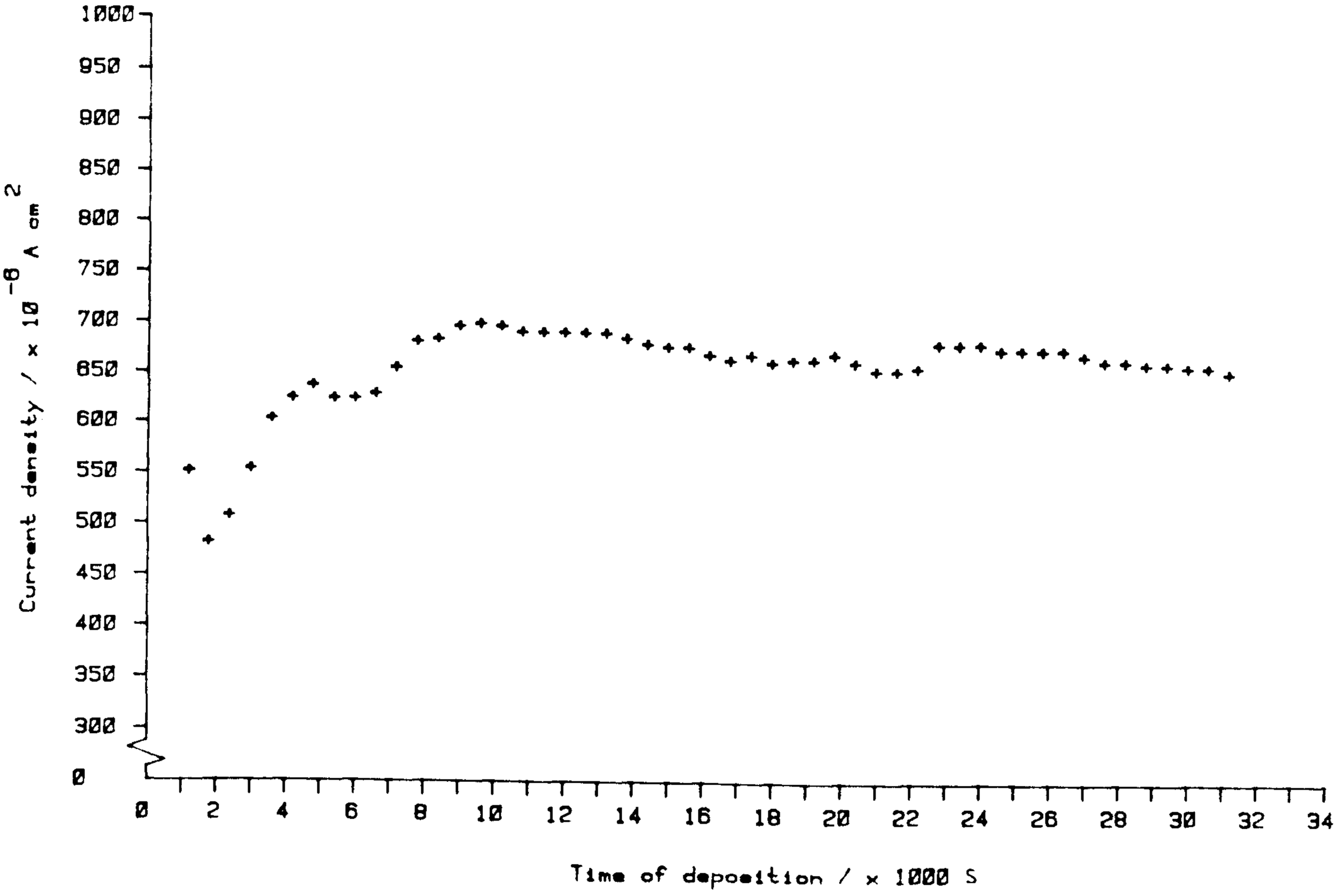

Fig 3.18 Current/time transient for the electrode as in fig 3.17.

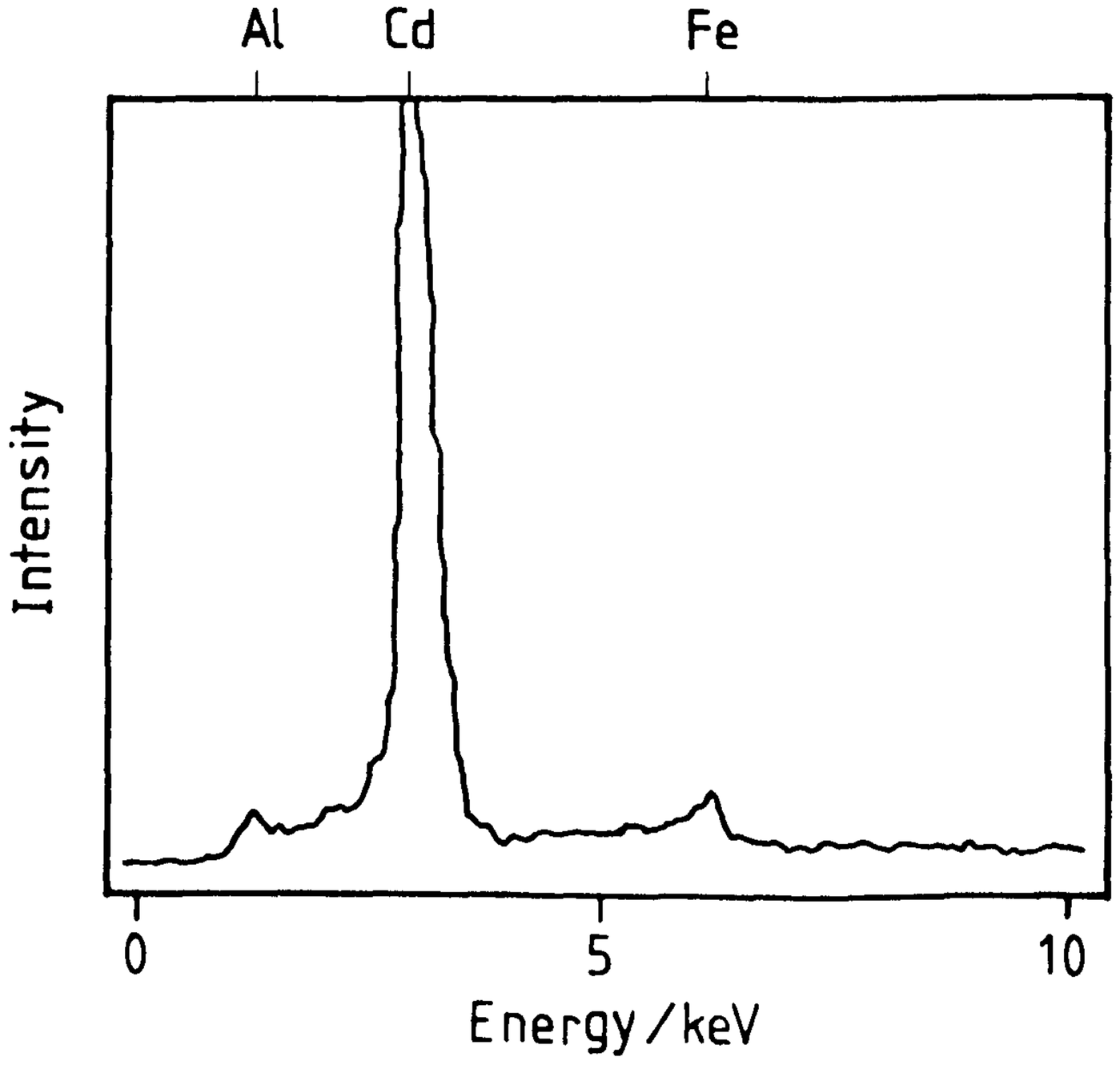

Fig 3.19 EDAX elemental analysis of the an alumina polished rotating cadmium electrode surface after 6 hours deposition at -400mV overpotential in 10.00M KOH containing 0.00035M Cd(II) (see figs 3.17 and 3.18).

Plate 3.3 Mechanically polished cadmium electrode surface after 9 hours deposition at -400mV overpotential, in 10.00M KOH + 0.00035M Cd(II).

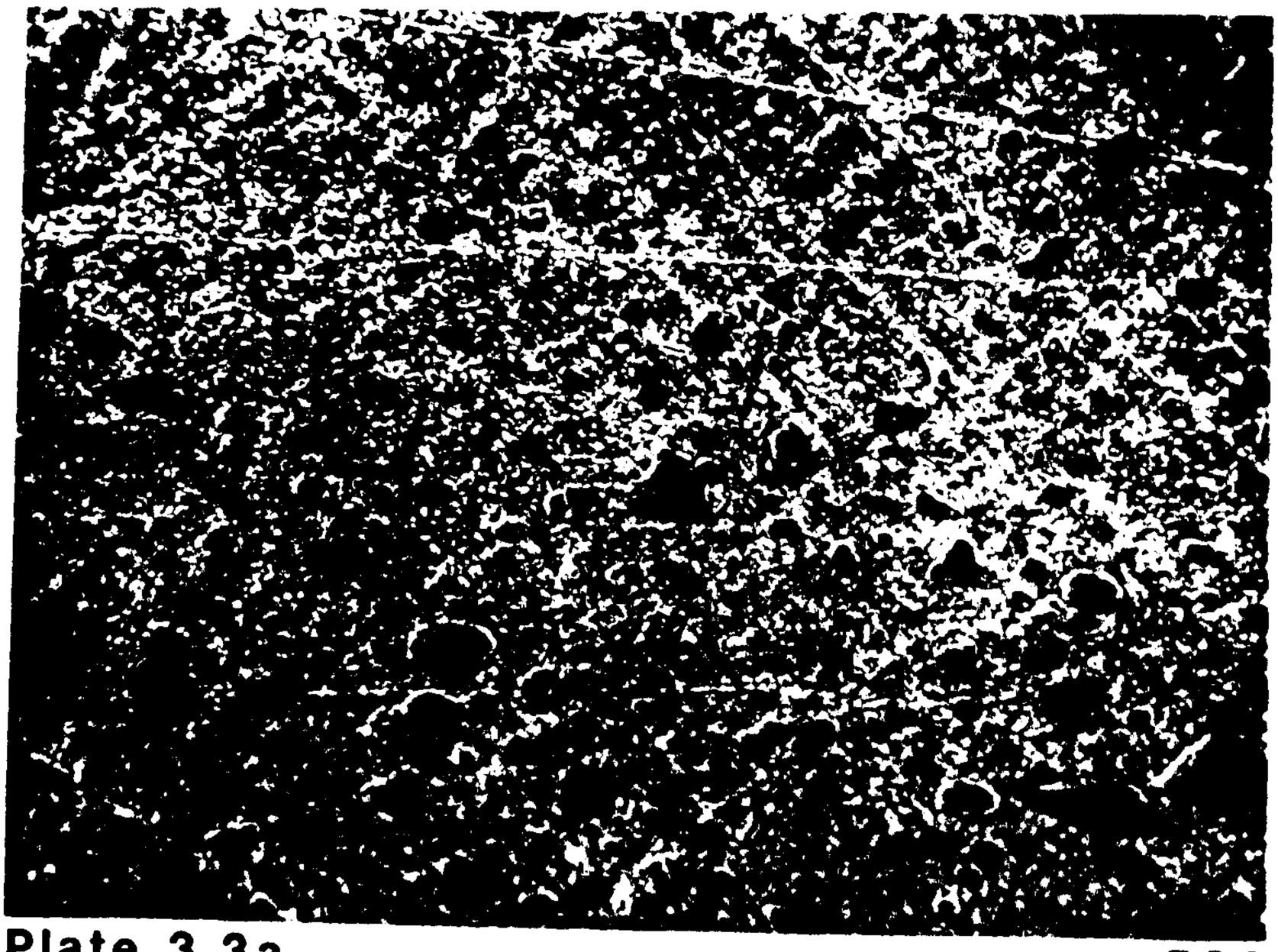

Plate 3.3a

x500

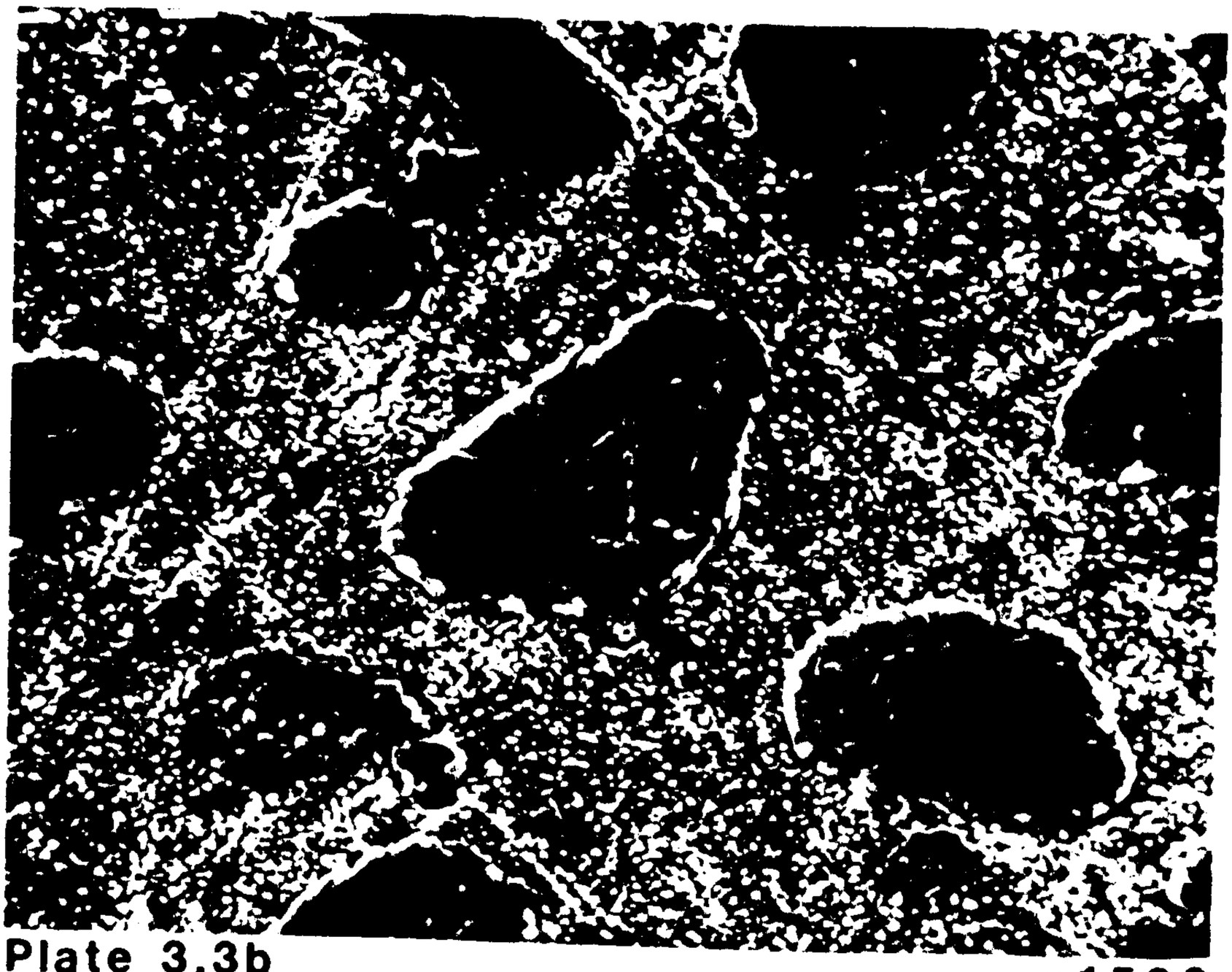

Plate 3.3b

x1500

3.5.2 DEPOSITION ONTO ETCHED CADMIUM ELECTRODES

With the experimental system as described and used in CH 3.5.1, deposition was followed using etched cadmium electrodes (preparation as in CH 2.2.6.3). The etched electrode surface was produced by treatment of mechanically polished electrodes with dilute nitric acid. Examination by SEM and optical microscopy, revealed the etched surface to be composed of flat crystalline domains, 30 - 500μm across.

Figures 3.20 and 3.21, show the d.l.c./t and i/t transients observed during deposition onto the electrode at η = -400mV (5 revs/s in degassed 10.00M KOH + 0.00035M Cd(II)). A marked rise is observed in both the transients, reflecting a change in surface morphology. The initial d.l.c. value is 38μFcm^{-2}, rising to 300μFcm^{-2} after 6 hours of deposition, thus indicating an increase in surface roughness of $\simeq$x 8. SEM of the electrode surface (plates 3.4a/b), shows a considerably changed morphology, whereby an aligned grainy deposit is found. This is not considered to be a truly dendritic form, but an alignment of hexagonal 'platelets', caused by the favourable orientational constraints of the underlying etched surface. Plate 3.4a, clearly shows how the deposited cadmium is aligned within areas of the same size as observed crystalline domains [see CH 5 and plate 5.1]. The size of observed cadmium hexagonal platelets is 0.3 - 0.8μm and is of the same order of size as observed in CH 3.4.3. EDAX elemental analysis of these electrodes only indicated the presence of cadmium, with no other contaminants. A parallel experiment, using nitric acid treated nickel electrodes (nickel being largely unaffected by nitric acid),

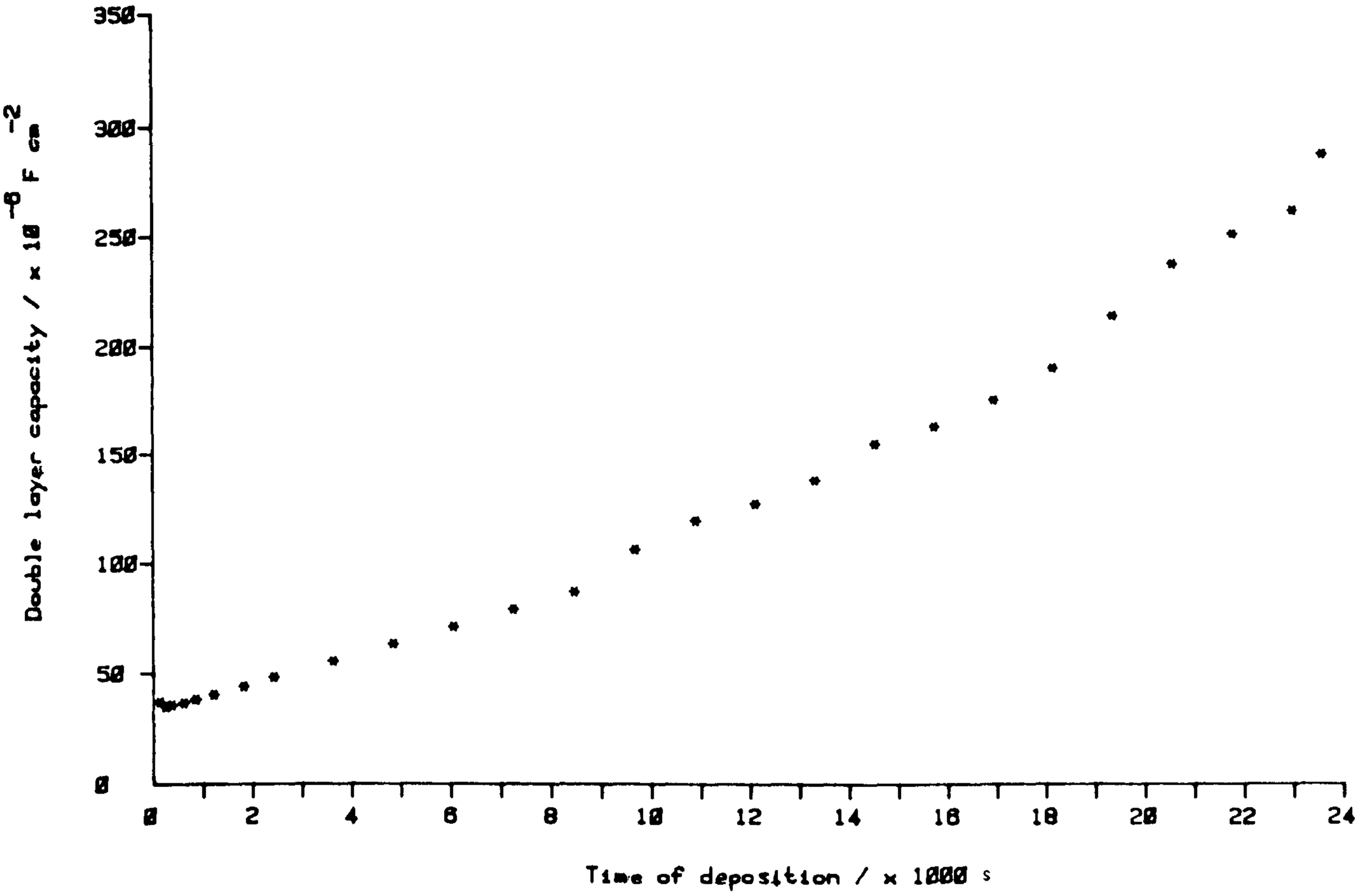

Fig 3.20 Double layer capacity/time transient found during deposition onto an etched rotating cadmium electrode (5 rev/s), at -400mV overpotential in 10.00M KOH containing 0.00035M Cd(II).

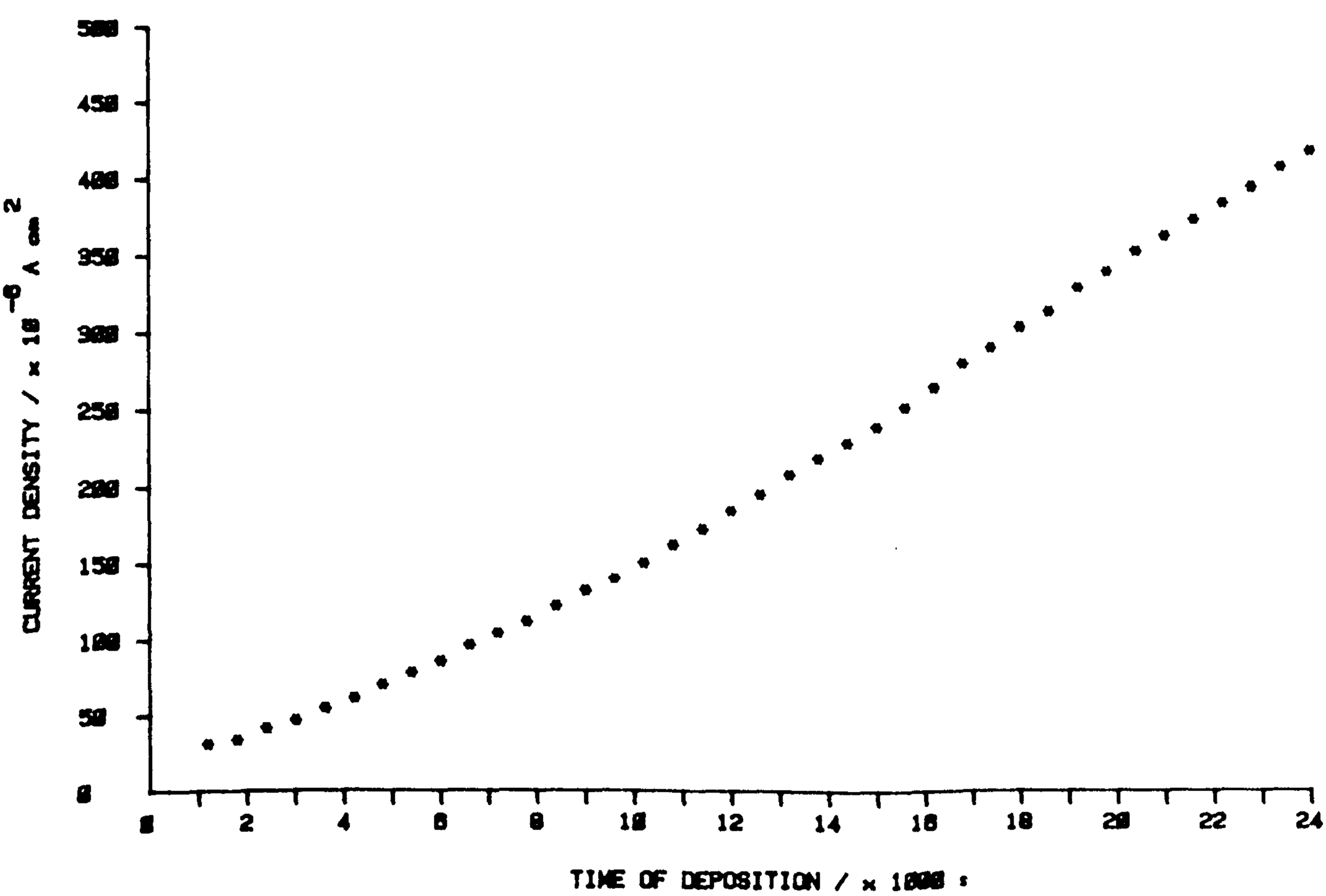

Fig 3.21 Current/time transient for the electrode as in fig 3.20

Plate 3.4 Etched (previously mechanically polished), cadmium electrode surface after 6 hours deposition at -400mV overpotential, in 10.00M KOH + 0.00035M Cd(II).

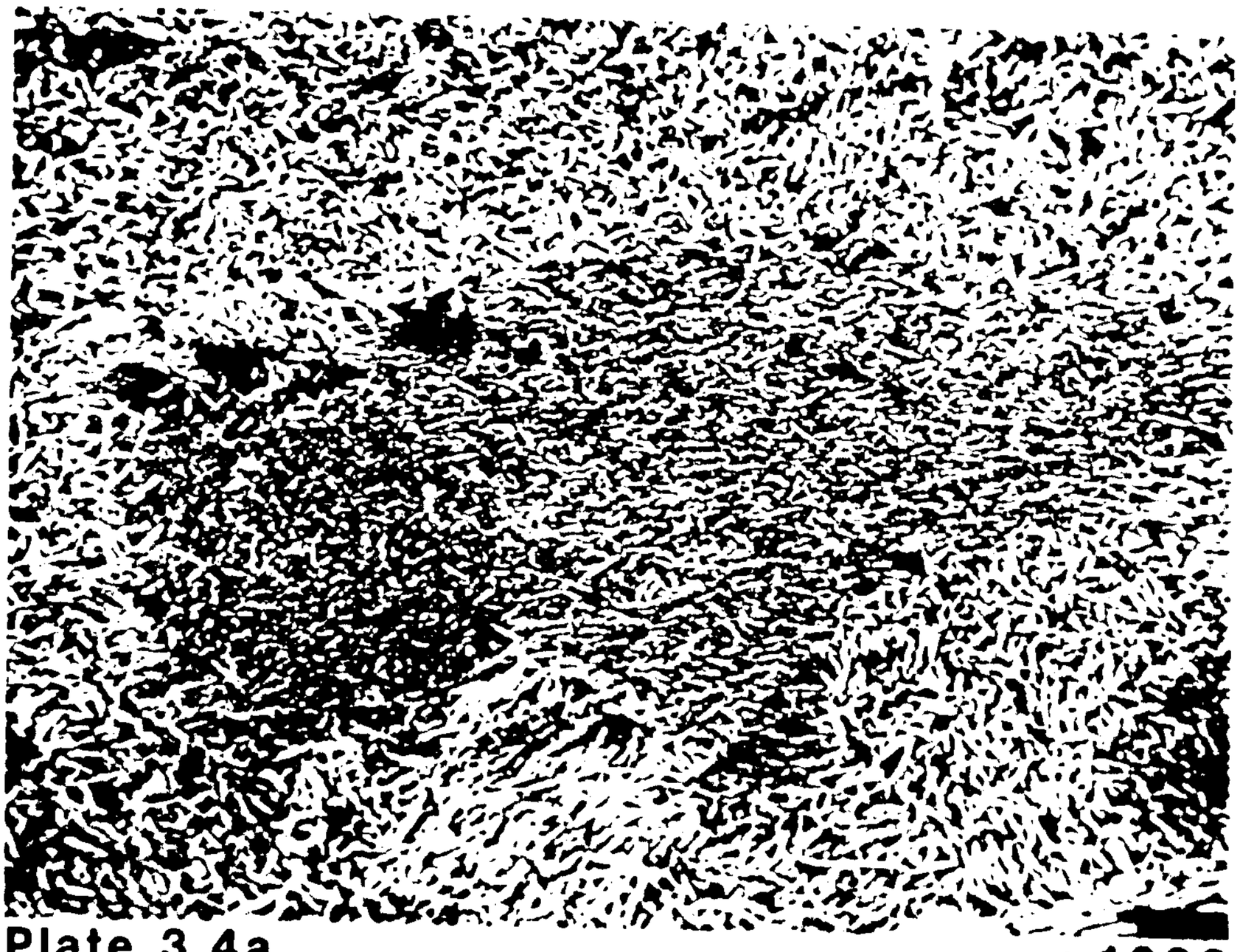

Plate 3.4a

x1000

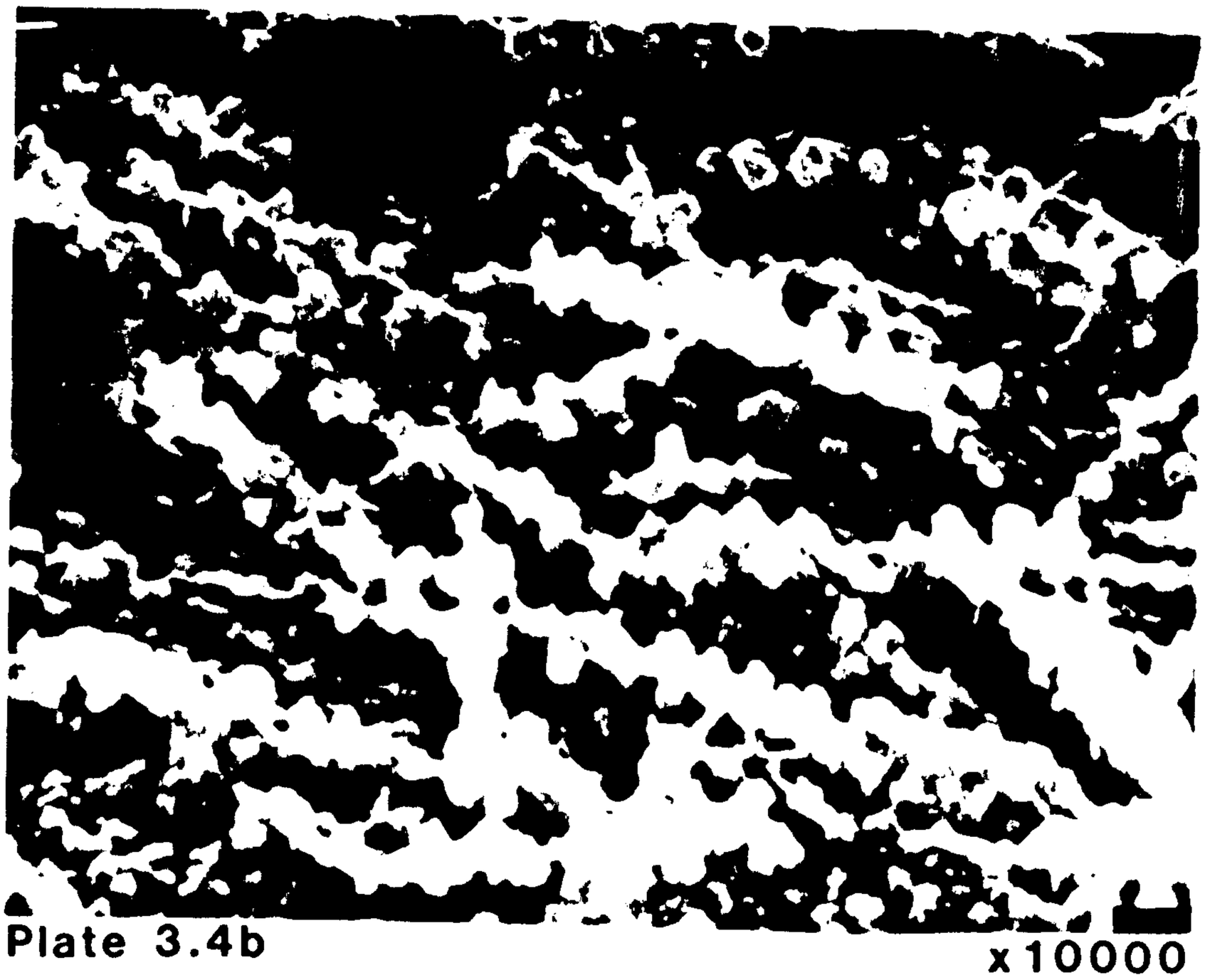

Plate 3.4b

x10000

revealed no connection between deposit morphology and any chemical influence the etching process might have.

3.6 DEPOSITION FROM 10.00M KOH + 0.00028M Cd(II) ONTO NICKEL WIRE ELECTRODES

Rough nickel wire electrodes (1mm dia), prepared as in CH 2.2.6.2, were placed into the cell described in CH 2.1.2. The cell was then filled with 80% Cd(II) saturated 10.00M KOH (0.00028M Cd(II)), and deposition observed on the stationary electrodes in degassed electrolyte [see CH 2.3.1]. Electrode pretreatment was considered unnecessary for this system. The usage of 80% saturated electrolyte prevents any possibility of suspended cadmium salts influencing deposition, by avoiding possible precipitation caused by changes in the saturation level (principally temperature fluctuations).

3.6.1 DEPOSITION MORPHOLOGY DEPENDENCE ON OVERPOTENTIAL

A series of long term deposition experiments at η = -300, -250, -200 and -100mV, were carried out over a deposition time-period of 140 hours. This enabled the deposition morphology dependence on overpotential to be observed, in the absence of cadmium salts in suspension. Current/time transients (where observed), were found to reach a steady state value after about 3 hours and gave no indication of surface changes, and are not presented here. Due to the timescale, it was additionally not possible to record d.l.c./time transients. After deposition the electrodes were examined by scanning electron microscopy.

Plates 3.5 to 3.9, show typical deposit morphology found for deposition at the various overpotentials used. The morphological trends are summarised as follows;

a) η = -100mV; plates 3.5a/b. An uneven grainy deposit of hexagonal cadmium platelets (0.5 - 1μm), is found over the entire surface. The original scratch marks on the wire are clearly visible, indicating the deposit to be relatively thin. No increased deposition was found at the wire tip.

b) η = -200mV; plates 3.6a-c. Over most of the surface, an even grainy deposit is to be seen (plate 3.6c), with $\sim$1μm cadmium grains forming a mosaic. At the wire tip, a $\sim$25μm spongy deposit is found (plate 3.6b), comprising of irregular cadmium crystallites 0.5 - 3μm in diameter.

c) η = -250mV; plates 3.7a-c. Again over most of the surface (away from the tip), a grainy deposit is found with occasional protruding spongy deposits, up to 5μm in height. Examination of the wire tip reveals a quite considerable deposit of 40 - 80μm thickness, with a morphology somewhat between the spongy and dendritic forms. Areas can be seen where the deposit is more clearly spongy or dendritic, but generally the intermediate morphology is to be found. Some small dendrites of up to 10μm length are to be seen.

d) η = -300mV; plates 3.8a-c and 3.9a/b. The entire surface is covered with small dendritic deposits against a grainy background (plate 3.8a-c). Towards the tip, clearly defined dendrites of up to 30μm are found (plates 3.9a/b). These appear to be comprised of stacked hexagonal platelets. Other areas of the deposit (plate 3.8c), are somewhat more spongy in character. At the tip, the total deposit thickness reaches 50 - 100μm.

Plate 3.5 Nickel wire electrode surface after 140 hours deposition at -100mV overpotential in 10.00M KOH + 0.00028M Cd(II).

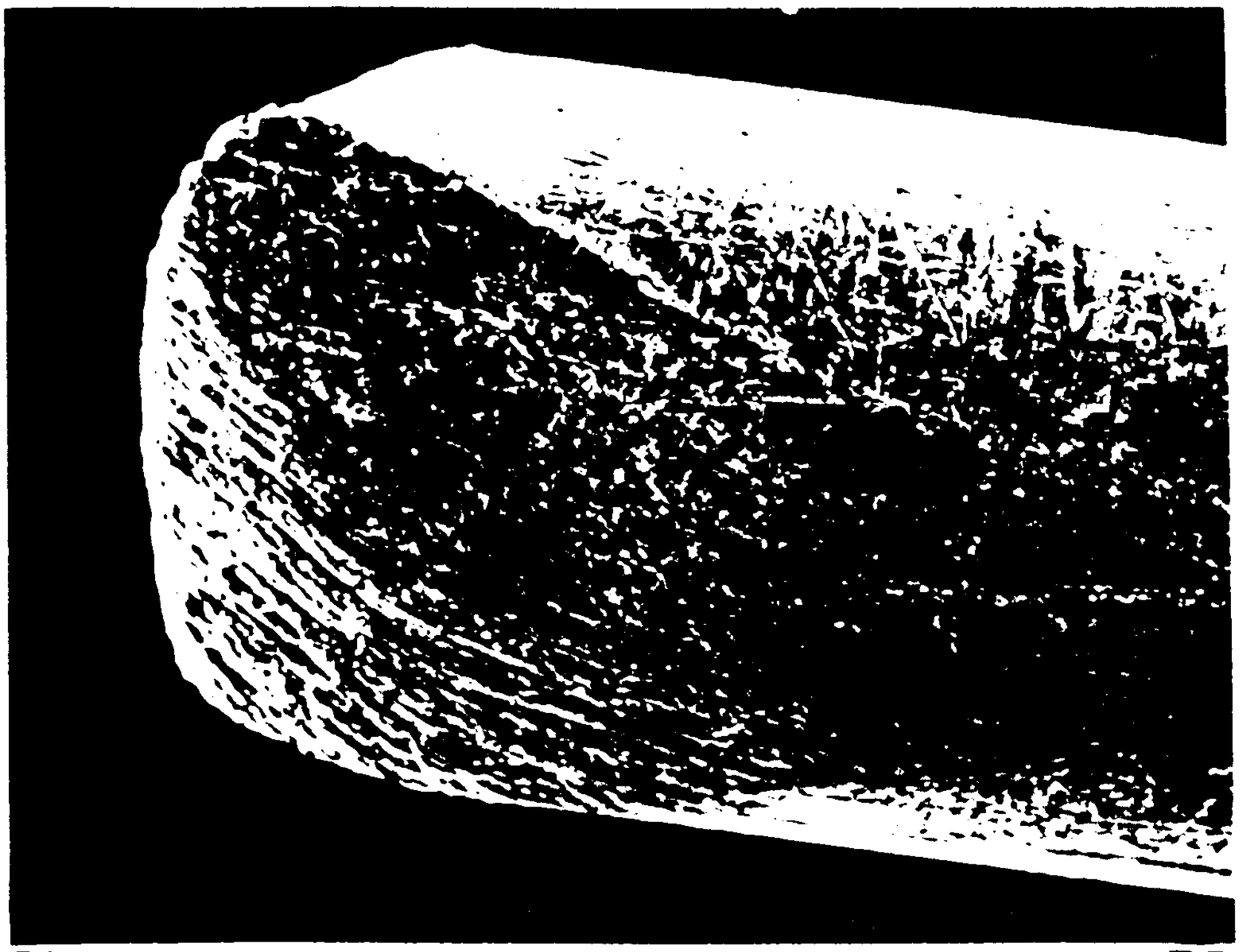

Plate 3.5a x75

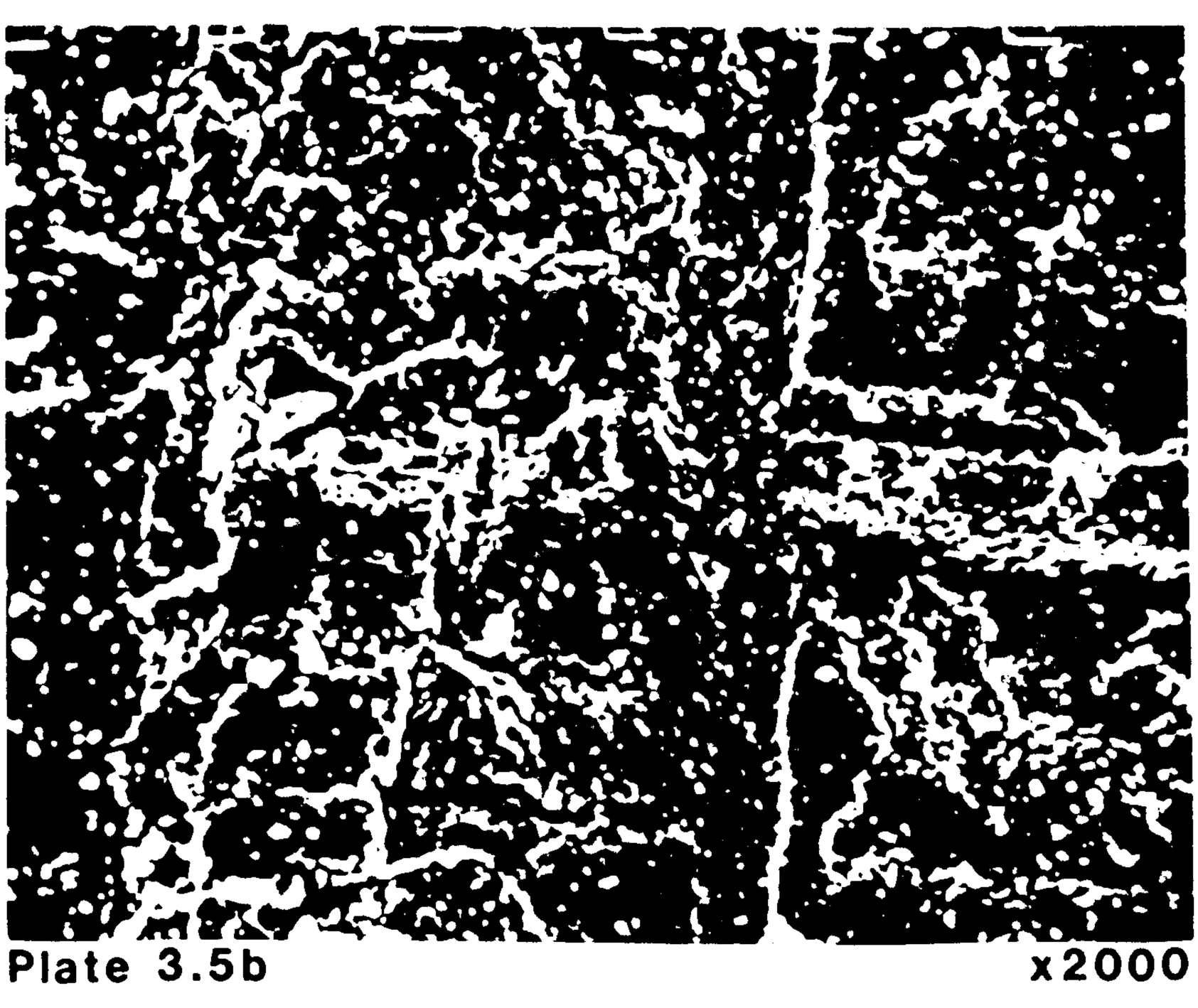

Plate 3.5b x2000

Plate 3.6 Nickel wire electrode surface after 140 hours deposition at -200mV overpotential in 10.00M KOH + 0.00028M Cd(II).

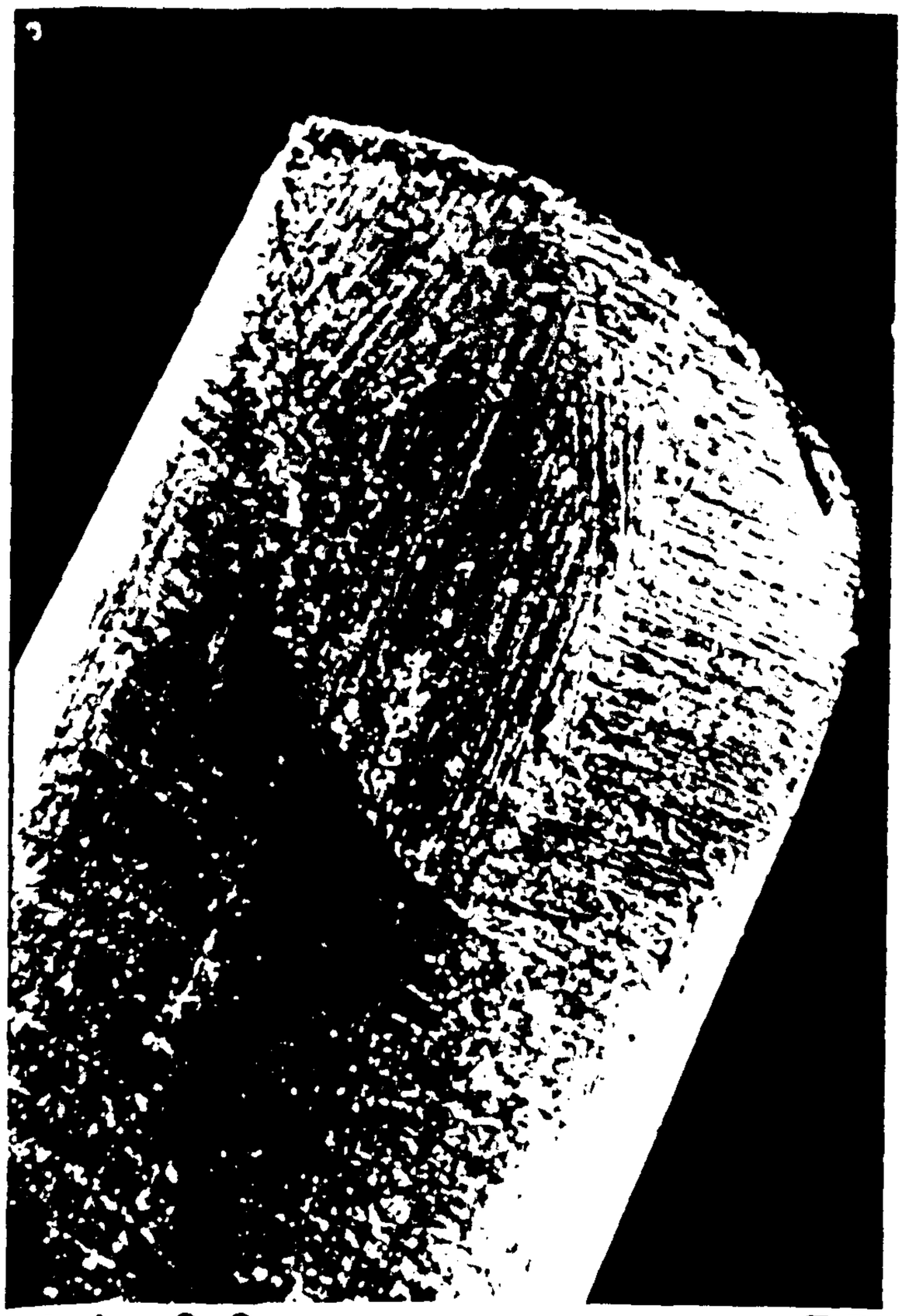

Plate 3.6a x75

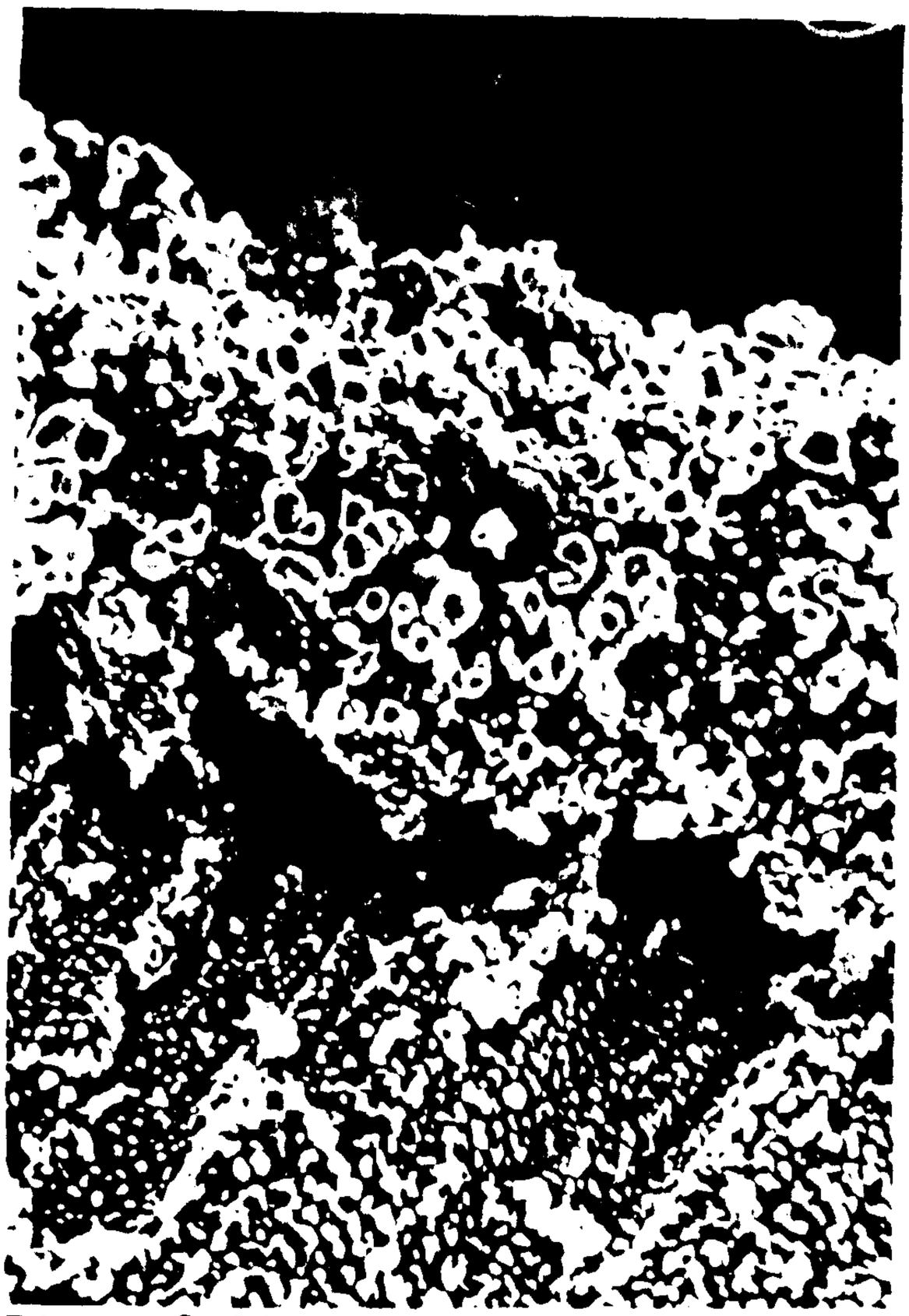

Plate 3.6b x2000

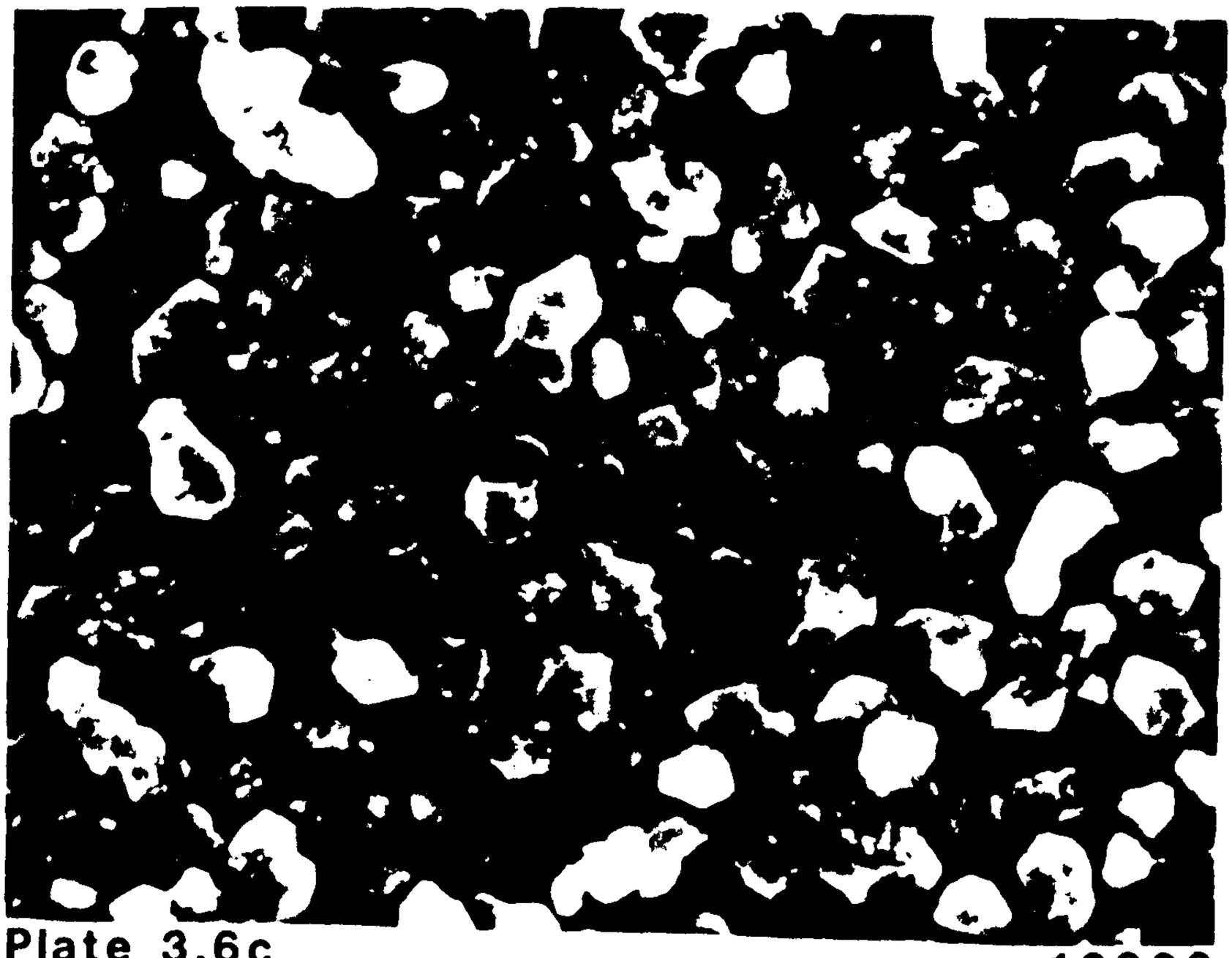

Plate 3.6c x10000

Plate 3.7 Nickel wire electrode surface after 140 hours deposition at -250mV overpotential in 10.00M KOH + 0.00028M Cd(II).

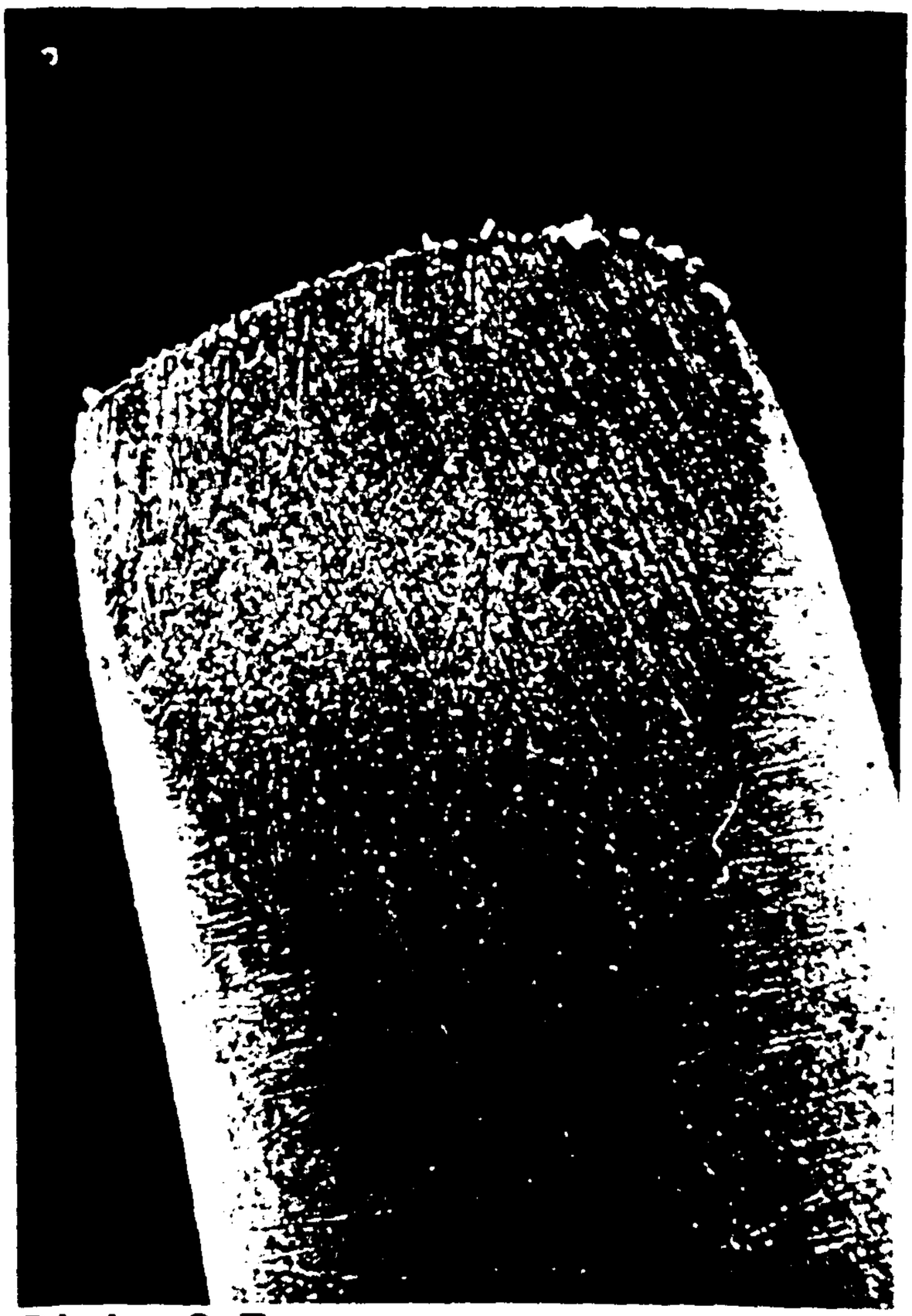

Plate 3.7a x75

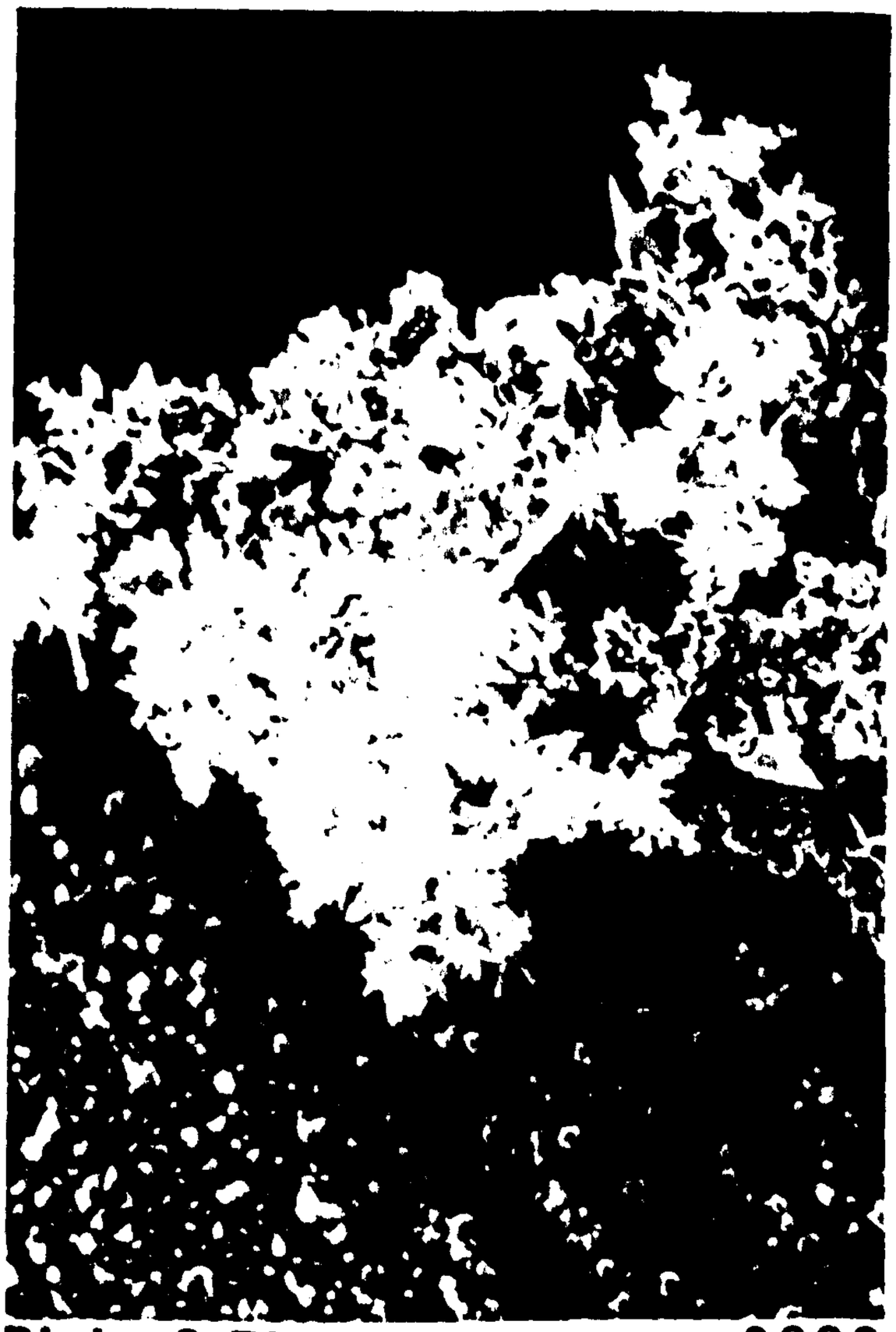

Plate 3.7b x2000

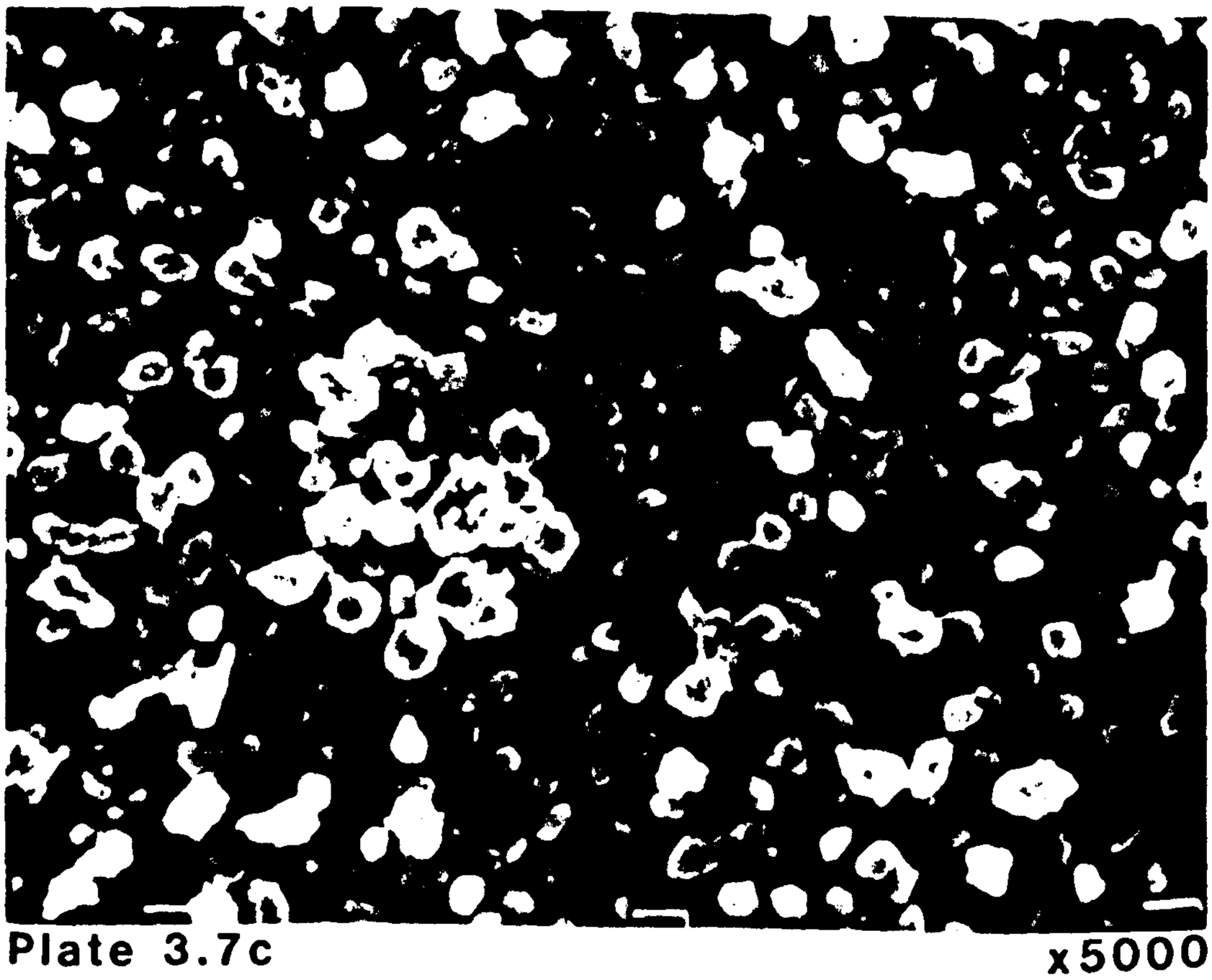

Plate 3.7c x5000

Plate 3.8 Nickel wire electrode surface after 140 hours deposition at -300mV overpotential in 10.00M KOH + 0.00028M Cd(II).

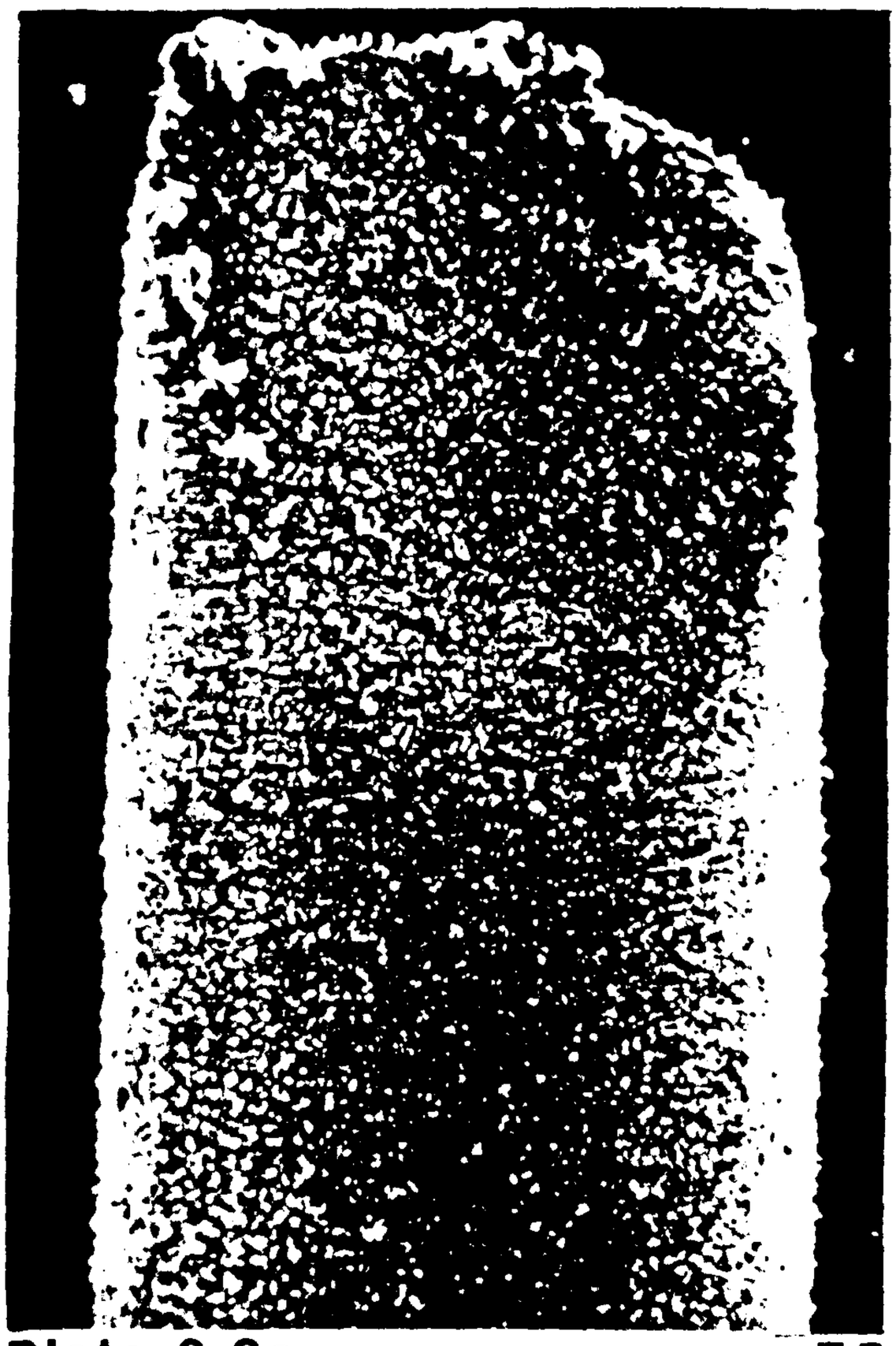

Plate 3.8a x75

Plate 3.8b x1000

Plate 3.8c x3500

Plate 3.9 Dendrites found on a nickel wire electrode after 140 hours deposition at -300mV overpotential, in 10.00M KOH + 0.00028M Cd(II) (see plate 3.8).

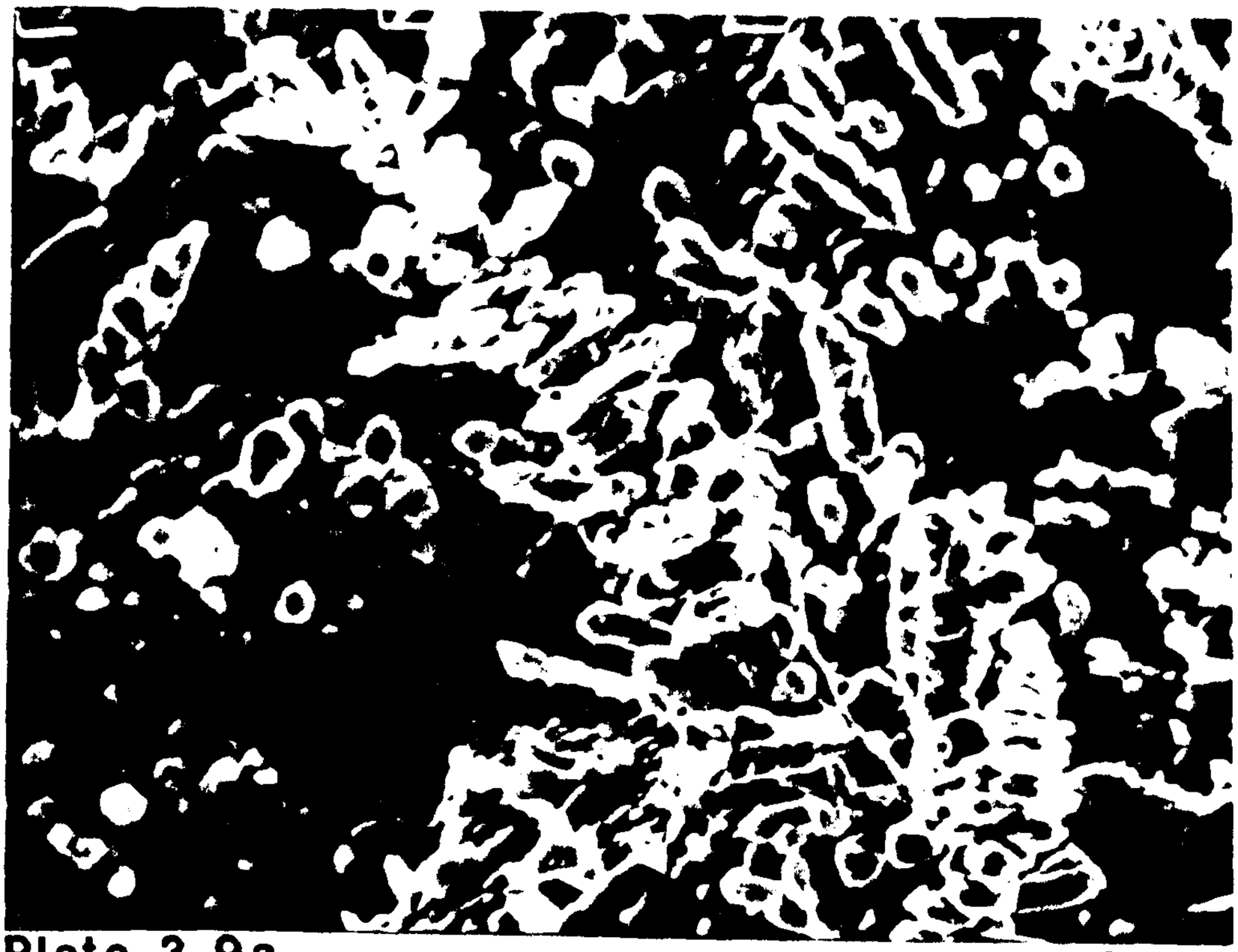

Plate 3.9a x3500

Plate 3.9b x7500

These observations indicate a critical overpotential for cadmium dendritic growth of η_c = -230 $\pm$ 20 mV, although the transition in the morphology is somewhat gradual over the range η = -200 to -300mV. Some dependence on the underlying surface is indicated by the enhanced deposit at the wire tip. It is noticeable that all observed (individual) dendrites are to be found growing at approximately 90^{o} to the surface. This is in contrast to the deposition found when suspended cadmium salts are present. In the suspensions, nearly all the dendrites subtend to angles of < 60^{o} to the surface. If growth in both systems proceeds via staged deposition of hexagonal platelets. It would seem likely that suspended particles at the surface provide a local concentration gradient of $Cd(OH)_4^{2-}$, towards (or into) which dendrites will grow, hence favouring growth along the surface towards the local Cd(II) source. Whereas in the absence of suspension, development of a linear diffusion layer perpendicular to the surface is the dominant factor, figure 3.22 illustrates this possible mechanism.

3.6.2 FIT OF EXPERIMENTAL TO THEORY

Observation of dendrites found at η = -300mV, allow estimation of both induction and growth times. The induction time is given by;

$$t_i = \frac{q\pi w^3 \delta}{3D_o C_o AV\tan\theta}$$

from SEM observations (plates 3.5 - 3.9), a critical protrusion height of 5μm (2μm width) appears to be the transition point for

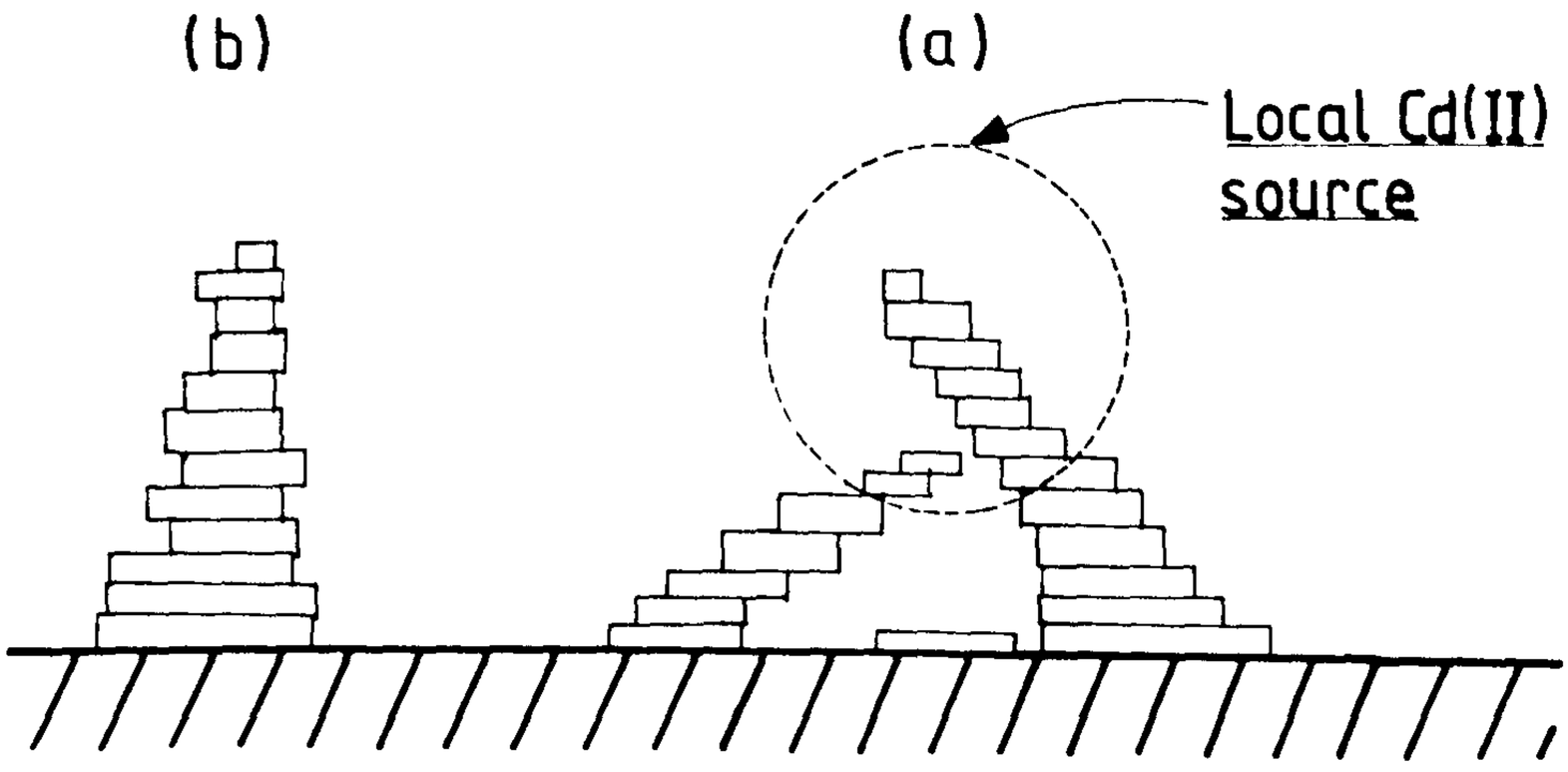

Fig 3.22 Model for cadmium deposition in the presence (a), and absence of cadmium salts in suspension (b).

dendritic growth. If we take this as the critical height at which spherical diffusion becomes dominant at the tip, then the growth time for the protrusion corresponds to the induction time for dendritic growth within this system. Thus with;

$q/A = 2 \times 10^{6}$ cm^{-2} (nucleation site density)

$w = 1 \times 10^{-4}$ cm

$\theta = 10^{o}$

$D_o = 1.8 \times 10^{-7}$ cm^2/s

$V = 12.99$ cm^3/mol

$C_o = 2.8 \times 10^{-7}$ molcm^{-3}

$\delta = 0.01$ cm

we can estimate t_i;

$$t_i = \frac{2 \times 10^{6} \times \pi \times 1 \times 10^{-12} \times 0.01}{1.8 \times 10^{-7} \times 2.8 \times 10^{-7} \times 12.99 \times 3 \times 0.2}$$

$t_i \doteq 180000$s

$\doteq 50$ hours

If the values above correspond to the critical dendrite height then an induction time of ~50 hours is indicated. The growth times for observed dendrites (once spherical diffusion has been established), can be estimated from;

$$\Delta t = \frac{\ln[h/h_o]r\delta}{D_o V C_o}$$

Using the dendrite shown in plate 3.9a (the largest single dendrite seen), the following values are estimated;

$h_o = 5 \times 10^{-4}$ cm

$h = 2.8 \times 10^{-3}$ cm

$r = 2 \times 10^{-5}$ cm

Other values remaining were as used for the calculations above, hence;

$$\Delta t = \frac{\ln(28/5) \times 2 \times 10^{-5} \times 0.01}{12.99 \times 1.8 \times 10^{-7} \times 2.8 \times 10^{-7}}$$

$\Delta t \simeq 530000s$

$\Delta t \simeq 145$ hours

Hence from these values the total dendrite growth time (t_g) is approximately 195 hours. These values agree quite well with the deposition time-period of 140 hours, considering the approximations involved. The value for the initiation time t_i cannot be checked, since surface morphological changes were not correlated with time. However, with the rotating disc experiments, it is apparent that t_i > 12 hours since no dendrites were observed within that time [see CH 3.4.3]. The agreement is sufficiently good, to give some tentative support to the theoretical model proposed in CH 3.1. However, it is accepted that with a different set of experimental data values for the same system, a considerable error range is indicated. The evaluation of this error, with such estimates, cannot sensibly be made.

CH 4 DEPOSITION FROM 10.00M KOH + CADMIUM SALTS IN SUSPENSION

Reference to work in suspension-free electrolytes [see CH 3], has shown that in the absence of suspension, cadmium dendrites are somewhat difficult to grow. At -300mV overpotential in 80% Cd(II)-saturated 10.00M KOH, a dendrite of 28μm length takes ~140 hours of deposition to grow [CH 3.6]. Under these conditions, obtaining a sufficient thickness of deposit to cause cell failure, would require somewhere in the region of 200 hours at η = -300mV. This assumes cells where the separator thickness is a minimum of 0.2 - 1 mm. Thus for a normal cell, where recharge/discharge cycles are performed, it would be almost inconceivable for such a thickness deposit to build up. Additionally, usage of trickle charging for cells would be very unlikely to cause sufficient deposit, due to the lower overpotentials involved in charging. Thus in the light of invesigations into the factors influencing dendrite growth [CH 3.4], the effect of cadmium salts in suspension becomes of great significance. In particular, when one considers the likelihood of negative plate active material escaping from the porous negative support, the formation of some form of suspension seems a likely occurrence. This might be expected during any agitation in usage (eg vigorous hydrogen evolution). Hence further investigations into the influence of this aspect on dendrite growth.

With the rotating disc cell, assembly and electrodes described previously [CH 2.1.1 and 2.4.1], a series of experiments investigating cadmium deposition from suspensions of

$Cd(OH)_4^{2-}$ in 10.00M KOH (prepared as in CH 2.3.2), were carried out.

4.1 DEPOSITION ONTO NICKEL DISC ELECTRODES

Polished nickel rotating disc electrodes, prepared as in CH 2.2.6.1, were pretreated by hydrogen evolution at -1.300V in degassed, cadmium-free 10.00M KOH. The solution was then switched to that to be investigated. This procedure, carried out at a standard rotation rate of 5 revs/s, was used for all the experiments in this chapter.

4.1.1 DEPENDENCE ON SUSPENSION CONCENTRATION

Suspensions of $CdO/Cd(OH)_2$ in Cd(II)-saturated 10.00M KOH were prepared as described in CH 2.3.2, to give suspended concentrations of 0.2, 0.04, 0.008 and 0.0001 g/dm^3 CdO (estimated equivalent at 5 revs/s within the cell). These concentrations are equivalent to 1.6, 0.31, 0.062, and 0.001 x 10^{-3} Mdm^{-3} of cadmium salts in suspension. Initially the observed particle sizes for the 0.2 gdm^{-3} suspension, were in the range 1 - 10μm. However, the average size would undoubtedly be smaller for lower concentration suspensions. Detection of smaller particle sizes was limited by the resolution of the optical microscopes employed.

Deposition for 5 hours at η = -400mV, in the 0.2 gdm^{-3} suspension, resulted in the d.l.c./time and current/time transients shown in fig 4.1 and 4.2. An almost exponential increase in surface area is indicated, the d.l.c. increases from

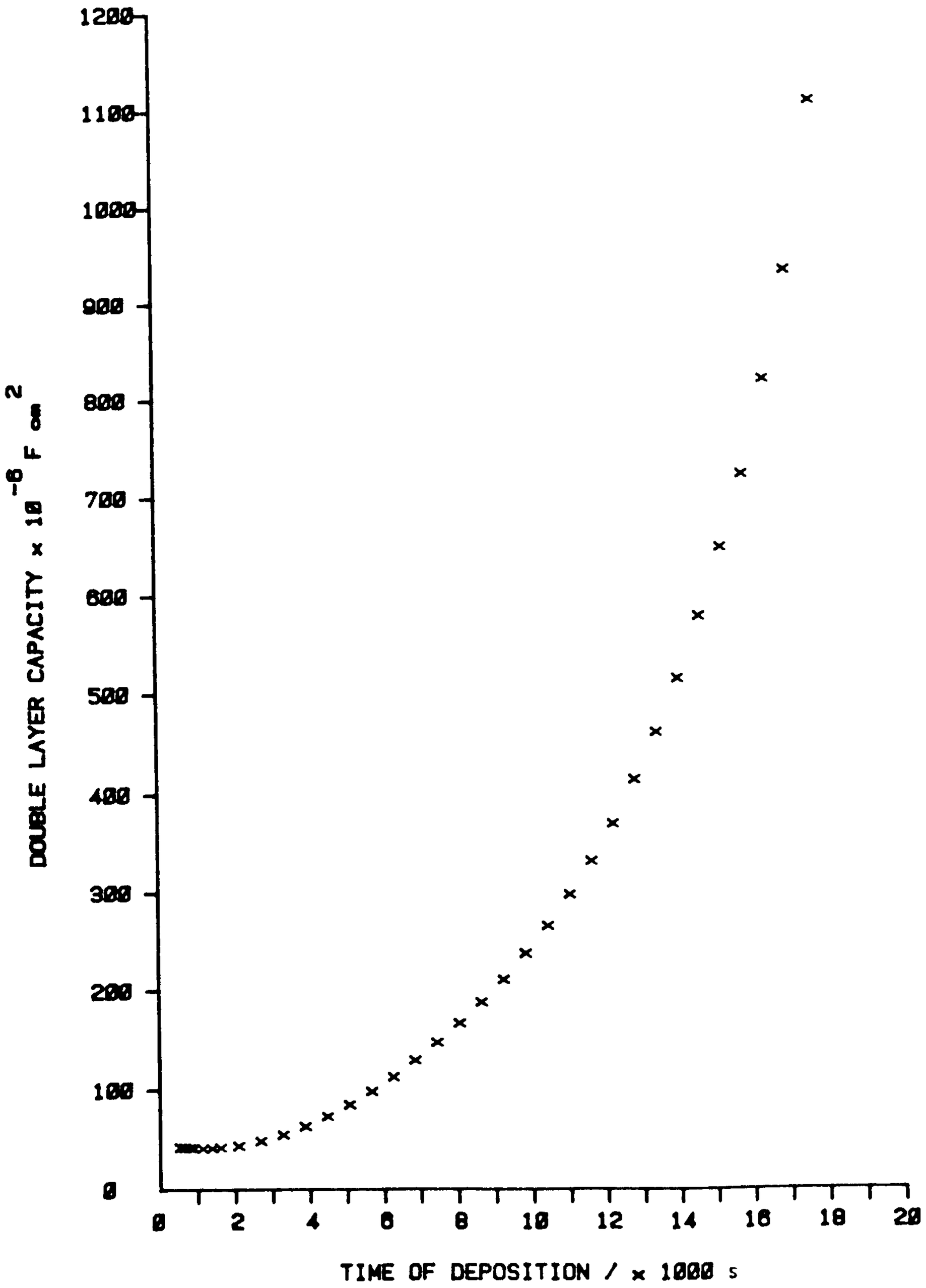

Fig 4.1 Double layer capacity/time transient found during deposition at -400mV overpotential, onto a polished nickel disc electrode in 10.00M KOH, containing $0.2g/dm^3$ $Cd(OH)_2$ suspension.

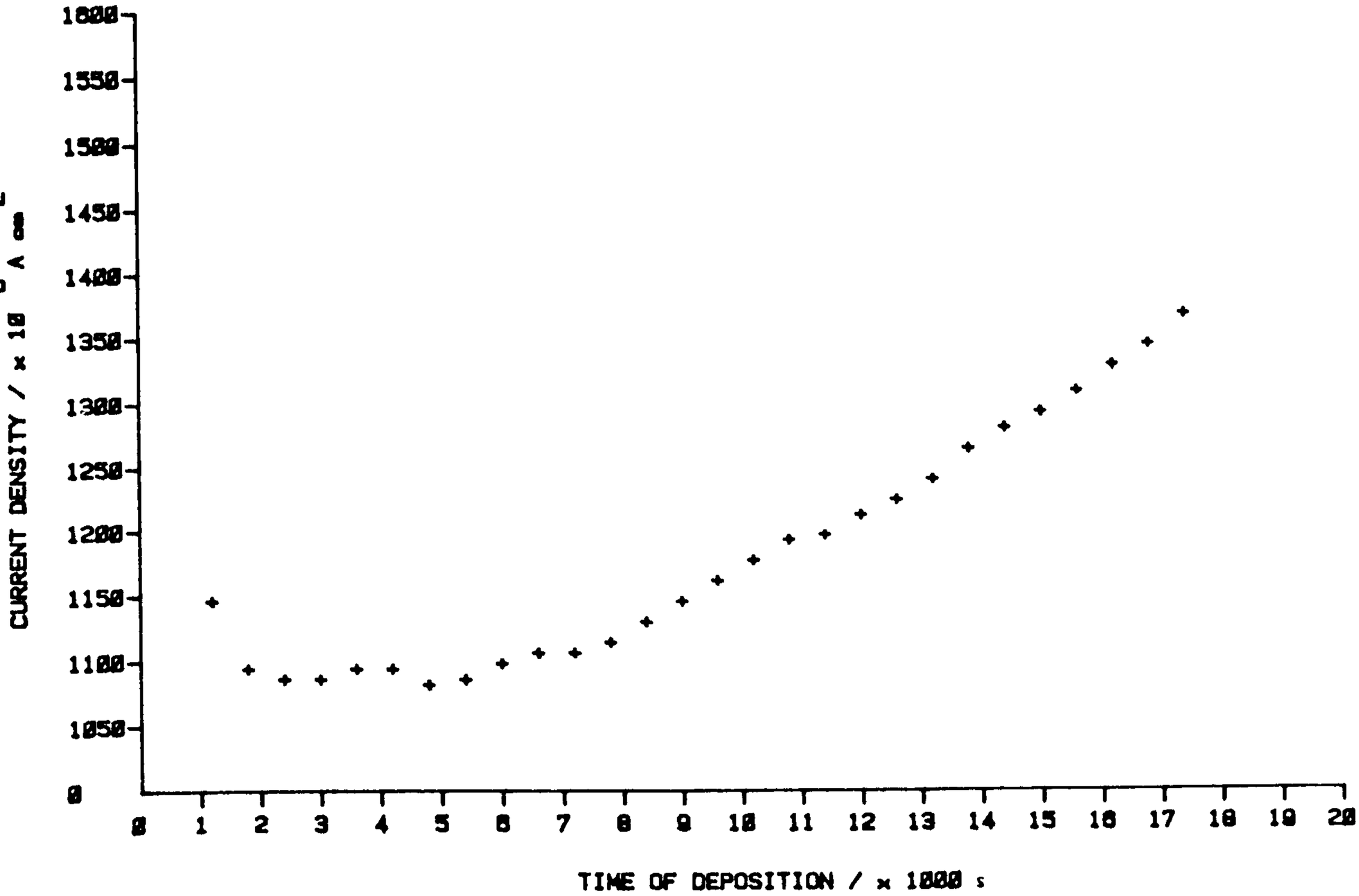

Fig 4.2 Current/time transient for the electrode as in fig 4.1.

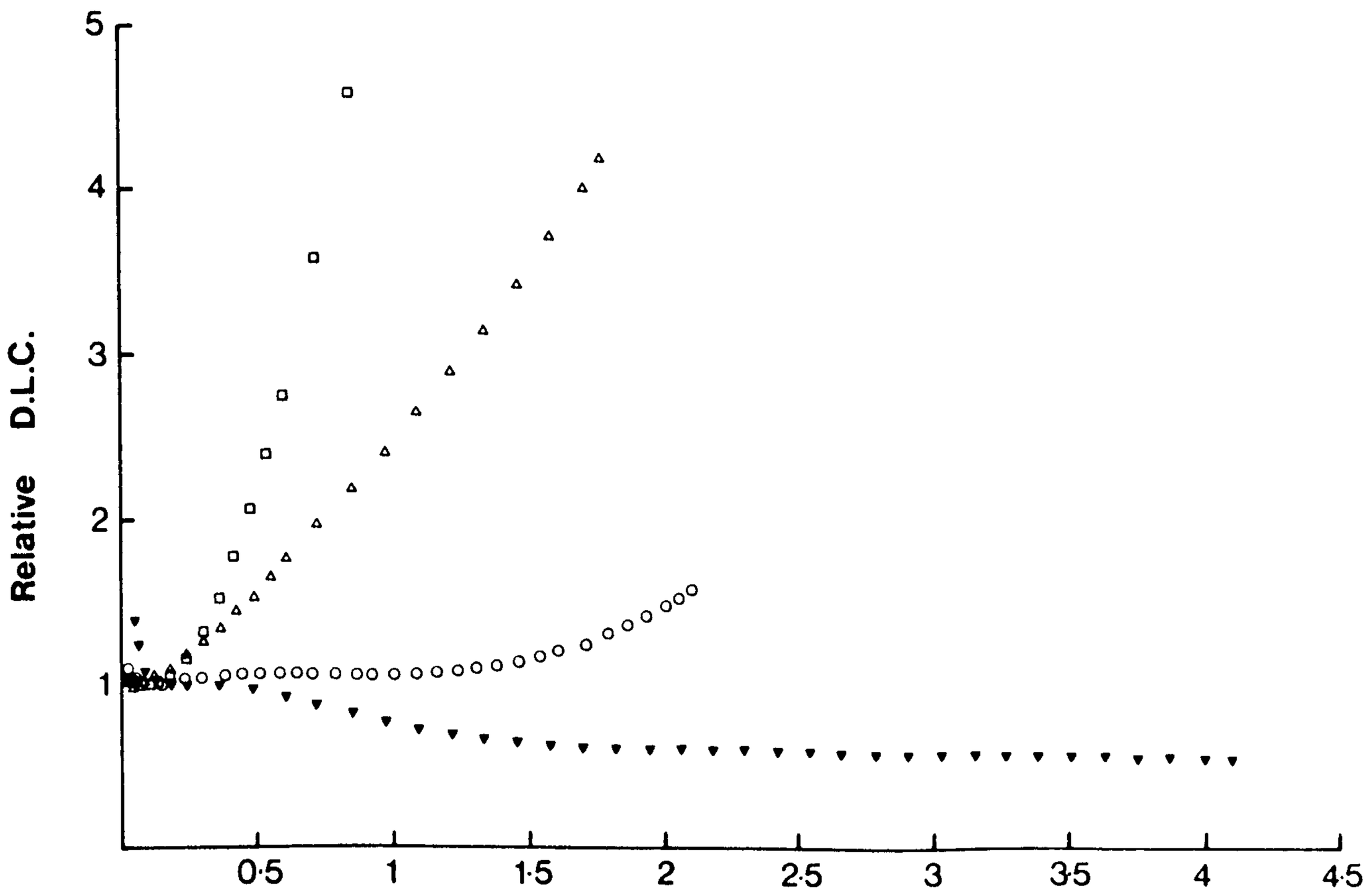

Fig 4.3 Dependence of relative double layer capacity on time for deposition in 10.00M KOH with different suspension concentrations at -400mV overpotential. (□) 0.2g/dm^3; (△) 0.01g/dm^3; (○) 0.0001g/dm^3; (▼) no suspension. Values for $Cd(OH)_2$ concentration.

an initial value of 40 to 1200μFcm^{-2}. This gives a surface area increase of ~x 30. This is considerably greater than for deliberately roughened electrodes, and can only be caused by a dramatic change in electrode surface morphology. Similar time-period depositions with 0.04 and 0.008 gdm^{-3} suspensions, also gave rapidly rising d.l.c. curves. Fig 4.3 compares three d.l.c./t transients with that found in Cd(II)-saturated, suspension-free 10.00M KOH. Reference to fig 4.4, confirms the approximate exponential rise in d.l.c. found for the higher suspension concentration. This would be expected, if 1) the deposition rate was dependent on the surface area of the cadmium exposed to the electrolyte and 2) the surface area increase was linearly proportional to the amount of cadmium deposited (ie the deposited cadmium has a well defined crystal structure, with a constant volume to area ratio). Hence, if one considers these factors over small time increments, the initial area A_o would increase by a factor b in time t, ie

$$A_{(1)} = bA_o$$

therefore after a second time increment;

$$A_{(2)} = bA_{(1)} = bbA_o$$

and after a third time increment;

$$A_{(3)} = bbbA_o$$

hence at time t; the surface area is given by

$$A_{(t)} = b^tA_o \qquad \{4.1\}$$

or;

$$\log[A_{(t)}] = t\log(b) + \log(A_o)$$

$$\log[A_{(t)}/A_o] = t\log(b)$$

If the double layer capacity is proportional to $A_{(t)}$;

$$\log[C_{dl\ (t)}/C_{dl\ (o)}] = t\log b = tb' \qquad \{4.2\}$$

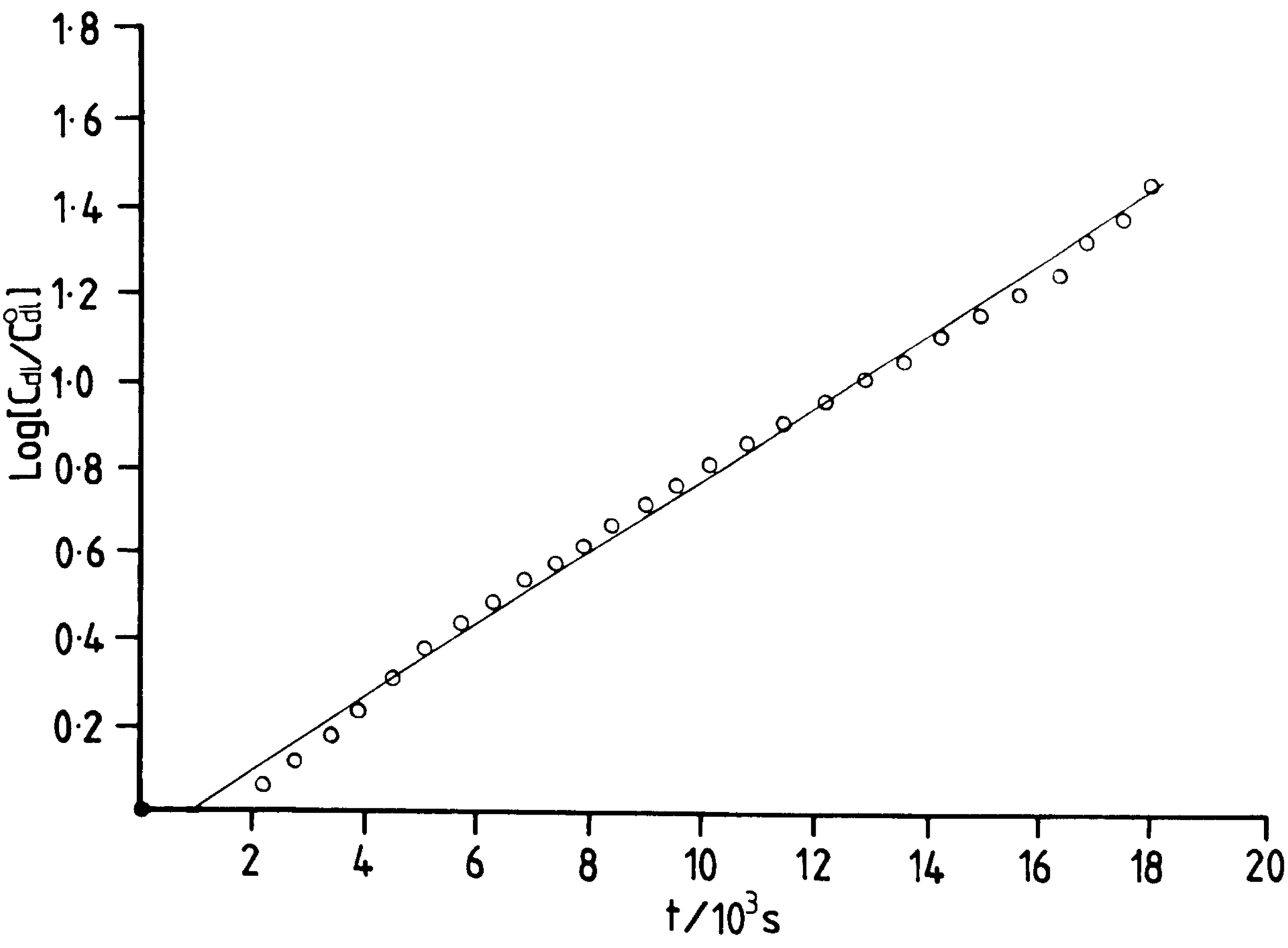

Fig 4.4 Plot of log[d.l.c.] versus time for the electrode d.l.c-/time transient as in fig 4.1, (deposition at η = -400mV in 10.00M KOH containing 0.2g/dm^3 suspension).

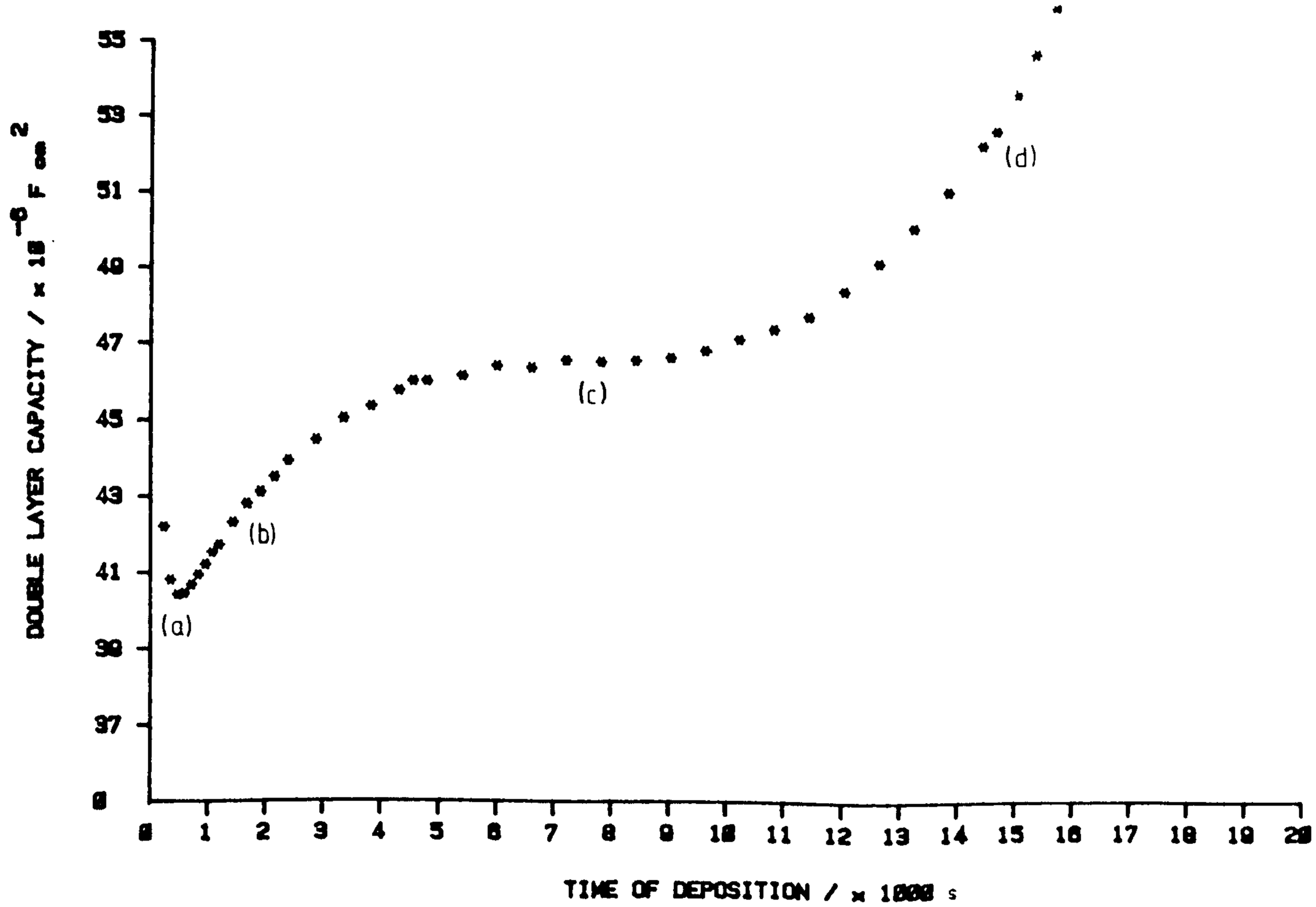

Fig 4.5 Double layer capacity/time transient found during deposition at -400mV overpotential, onto a polished nickel disc electrode in 10.00M KOH, containing 0.0001g/dm^3 $Cd(OH)_2$ suspension.

From fig 4.4 we can see this relationship for deposition from the higher concentration suspension , but only after a certain time-period, presumably corresponding to the induction time t_i for dendritic growth. Hence deposition for $t < t_i$ can be expected to follow a different deposition mechanism. The slope b´ of the $\log[C_{dl}/C_{dl(o)}]$/time plots (fig 4.4), appears to increase approximately linearly with total cadmium concentration, although insufficient data is present to confirm this. It is clear, however, that the presence of suspension causes a dramatic reduction in the initiation time for dendrite growth. An estimated induction time of 50 hours for η = -300mV deposition in suspension-free 10.00M KOH, is reduced to ~3 hours, with 0.0001 gdm^{-3} CdO, and further reduced to ~25 minutes for suspension concentrations of > 0.01 gdm^{-3}. The most likely mechanism to explain this, is that some particles of cadmium salts in suspension passing the electrode surface ´stick´, thus providing a greatly increased localised concentration of Cd(II) (see fig 3.22). Growth could then proceed via two possible mechanisms, 1) gradual dissolution of the particle as $Cd(OH)_4^{-2}$ and subsequent local reduction, or 2) direct growth of dendrites into the particle and a mixture of solid state and aqueous reduction. Case 2 seems the more likely mechanism, since direct reduction of cadmium metal from the particle as it passes the surface is more likely to cause adherence, than the chance trapping of a particle via surface defects. Thus such increased localised Cd(II) concentration, would more quickly establish the spherical diffusion conditions necessary for true dendritic growth, than would be the case in the absence of suspension. Additionally, any mechanism whereby

particles adhere to the surface, would be expected to give rise to a deposit where dendritic growth is not uniformly distributed over the surface, but concentrated around particular areas. This appears to be the case observed.

Examination of electrode surfaces for depositions carried out in suspensions of > 0.01 gdm^{-3} CdO, revealed a dull grey deposit. Optical microscope observations, showed the electrode surface to be covered in a dendritic deposit of cadmium. SEM observations showed the fine structure of this deposit, plates 4.1a/b, give micrographs of that found for the 0.2 gdm^{-3} suspension. The deposit consists of a mass of small (5 - 25μm) dendrites, clumped together in apparently random orientations, giving a deposit of maximum thickness 80μm. The variability of this dendritic surface coverage is doubtless due to 1) the suspension particles randomly adhering to the surface, and 2) nucleation of hydrogen bubbles at preferred sites, thus reducing deposition by blockage. At lower suspension concentrations, dendrite 'clumps' are not so dense, but individual dendrites are of the same size (10 - 20μm). Their randomness in orientation also supports the view that suspension particles adhere to the surface, since dendritic growth in the absence of suspension is predominantly at 90^{o} to the surface [see CH 3.6].

In plates 4.1b and 4.2a, we can see the typical 'fern-leaf' structure found for individual dendrites, each dendrite having average dimensions 15 x 6 x 0.5μm. This dendritic deposit appears to be built up of overlapped hexagonal crystallites of diameter 0.5 - 1μm. This feature of the deposit is found for all the deposition experiments in alkaline solution [see CH 3.4 and 3.6]. Higher resolution electron microscopy, for deposits

Plate 4.1 Polished nickel electrode surface after 5 hours deposition at -400mV overpotential, in 10.00M KOH + 0.2g/dm^3 CdO suspension (Cd(II) saturated).

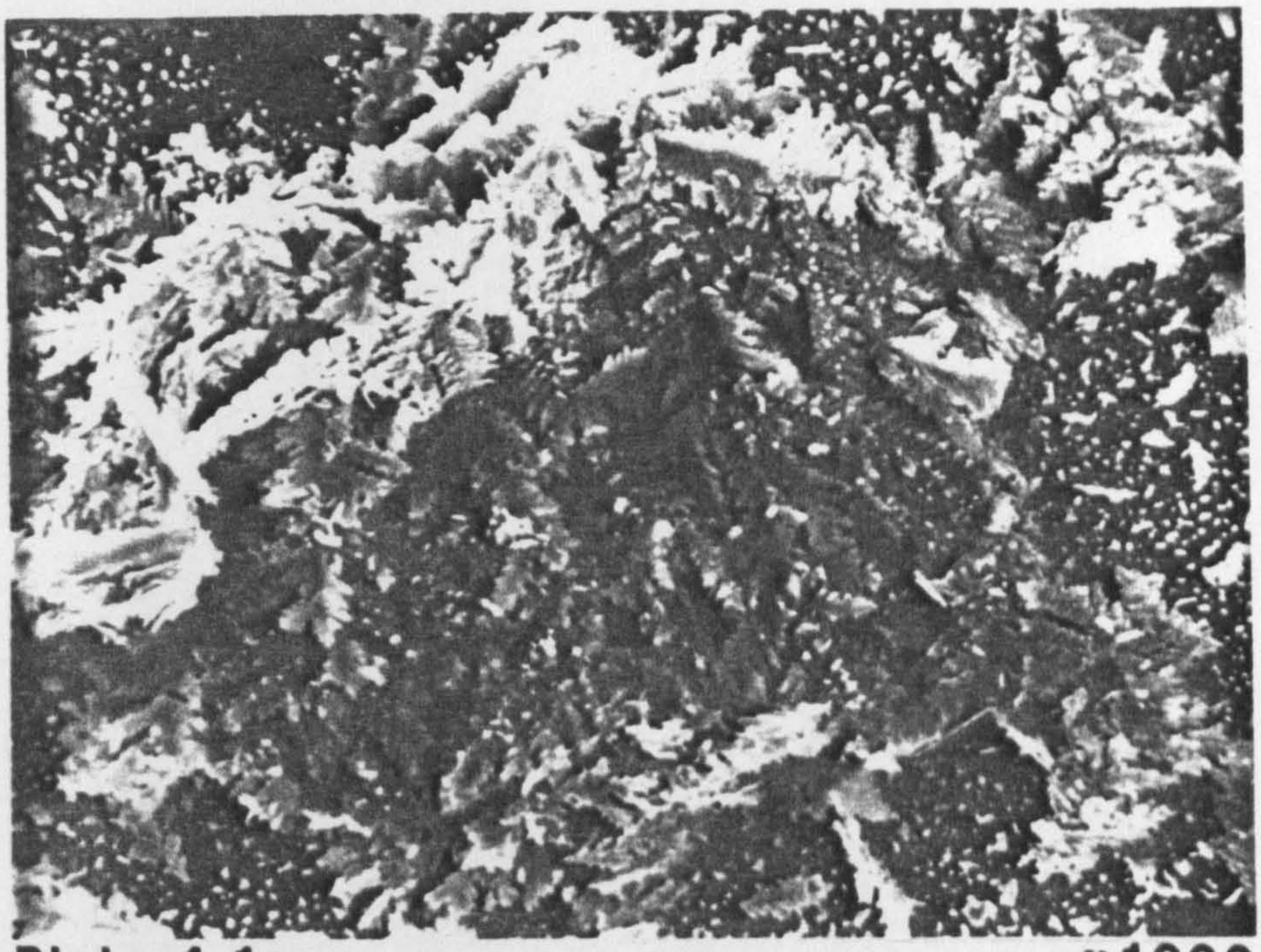

Plate 4.1a x1000

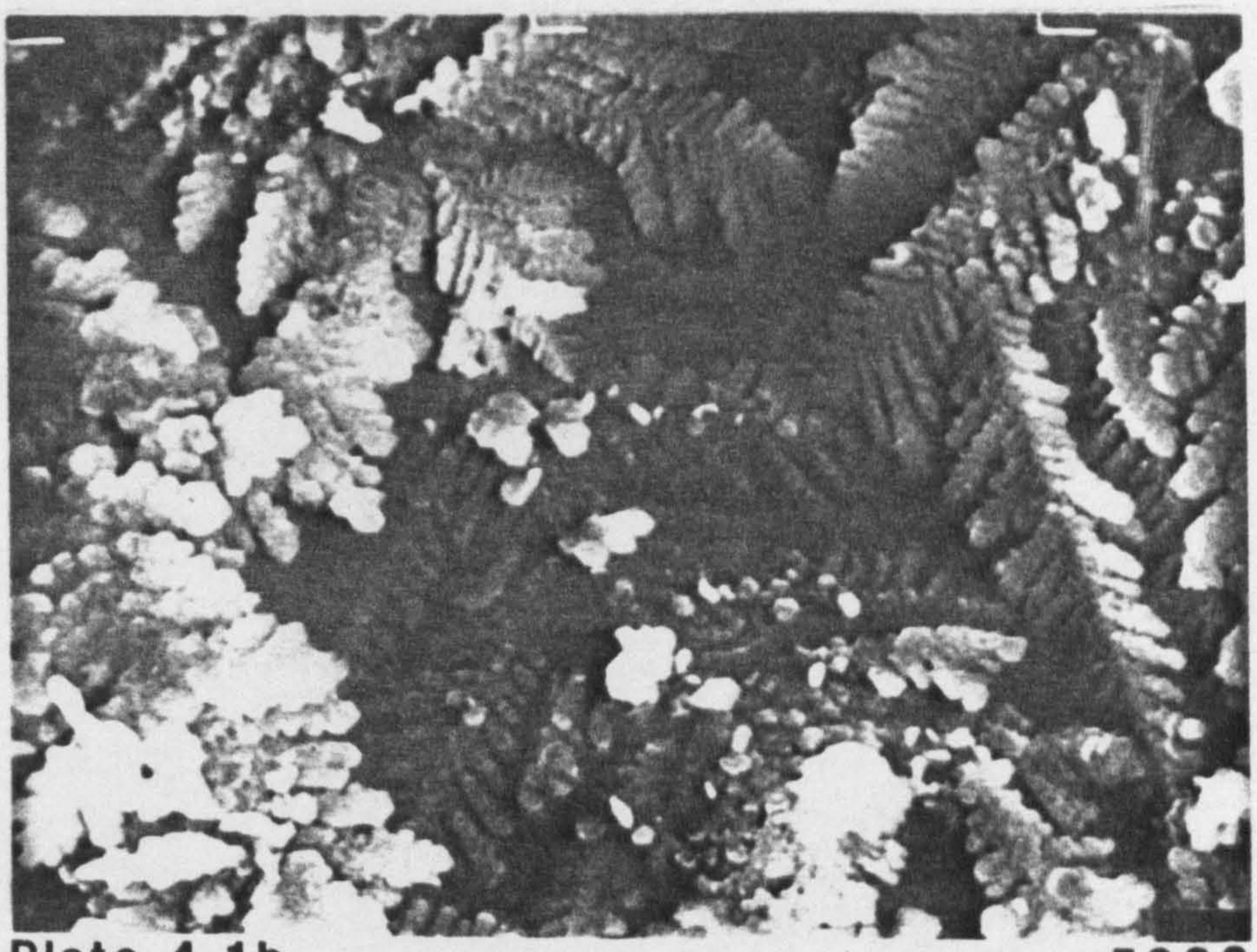

Plate 4.1b x5000

Plate 4.2 Fine structure of cadmium dendrites grown after 5 hours depositon at -400mV overpotential, onto a polished nickel electrode in 10.00M KOH + 0.2g/dm³ suspension (Cd(II) saturated).

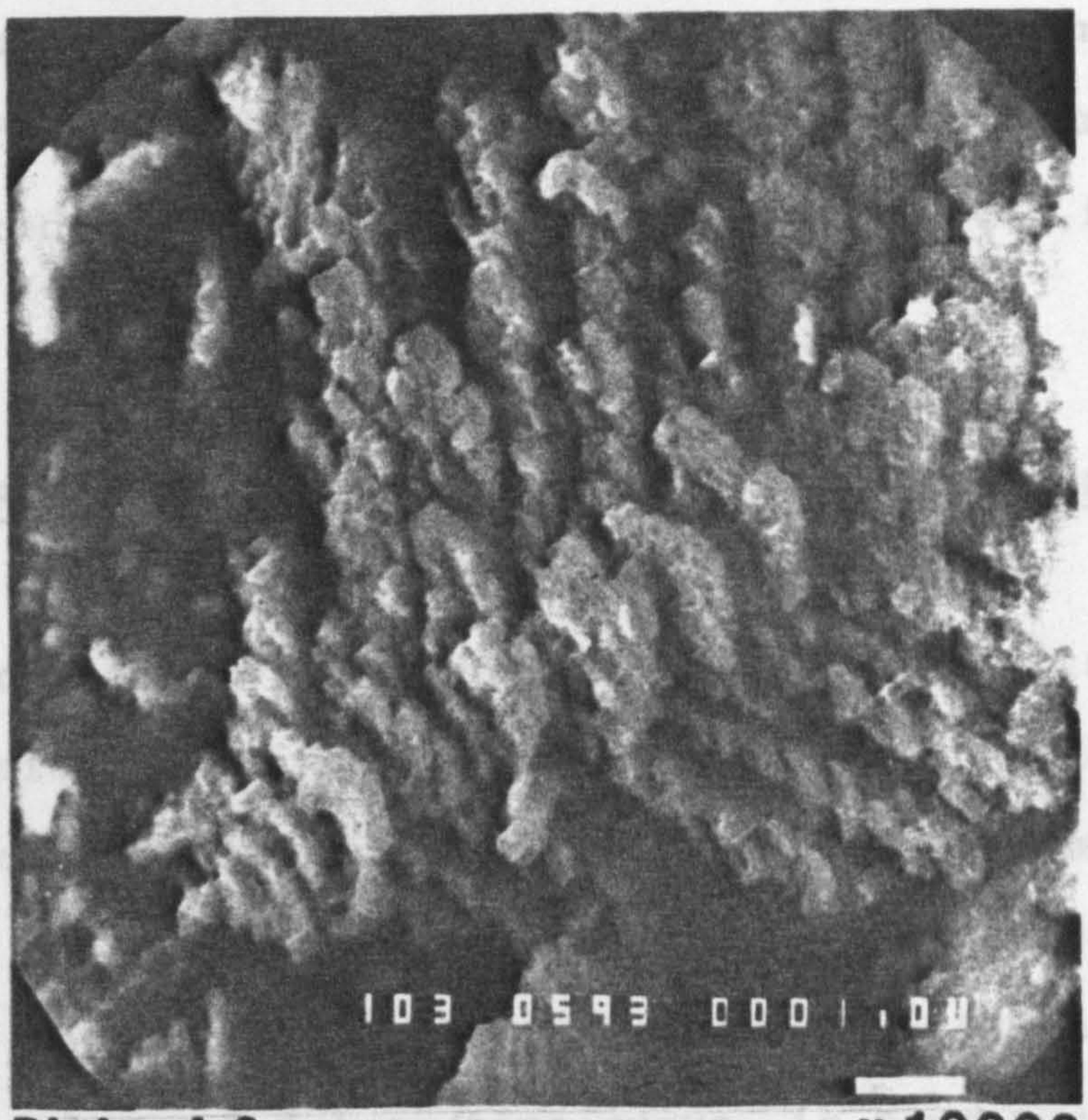

Plate 4.2a **x 10000**

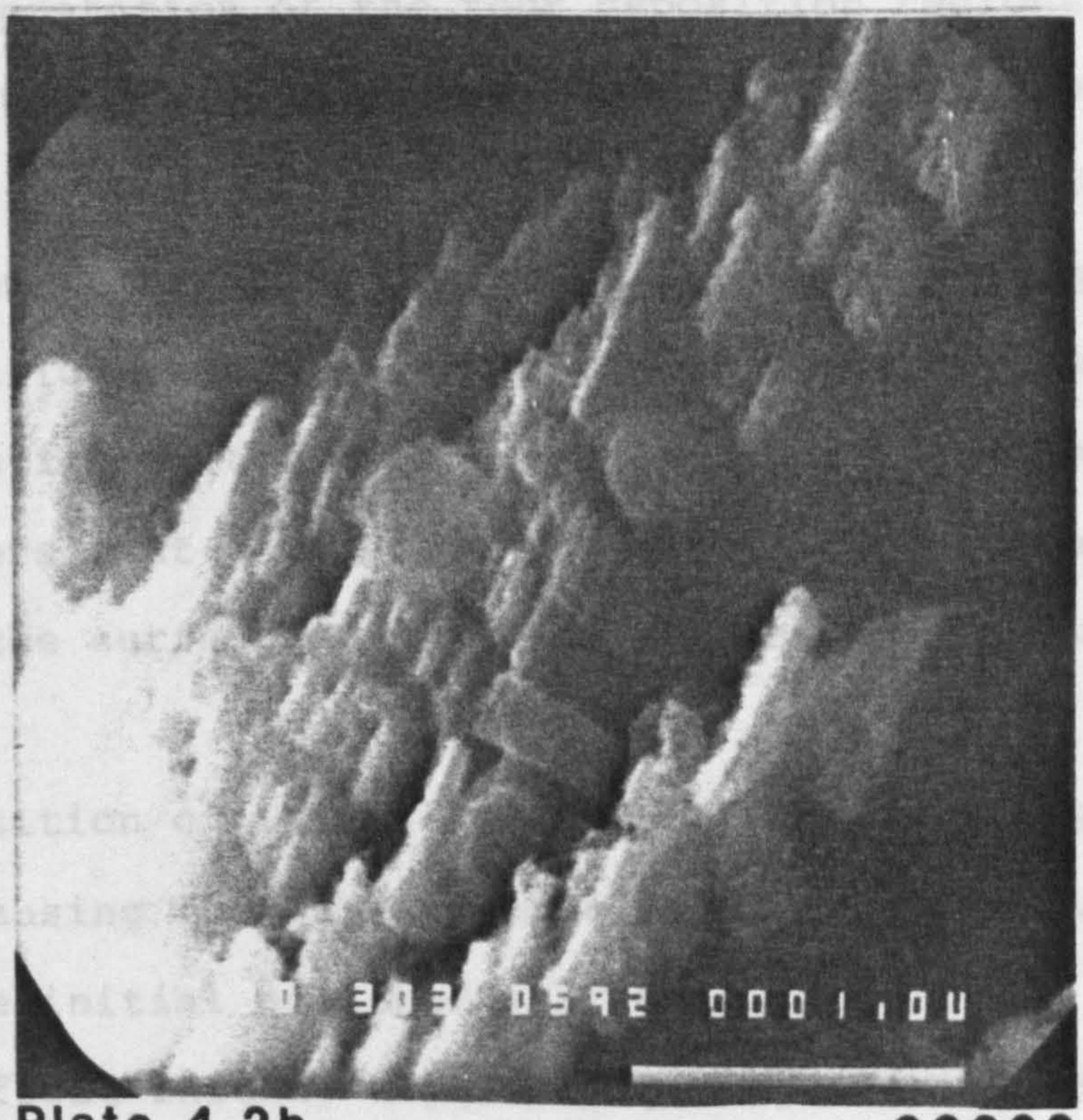

Plate 4.2b **x30000**

from both the suspension and suspension-free electrolytes, confirms this observation (plates 4.2a/b). It appears that deposition of hexagonal 'platelets' occurs in the direction of the anticipated concentration gradient (as depicted in fig 3.22).

4.1.1.1 SURFACE AMPLIFICATION AT LOW SUSPENSION CONCENTRATION

Deposition from Cd(II)-saturated, 10.00M KOH + 0.0001 gdm^{-3} suspension, at η = -400mV, was carried out under the same conditions as used in CH 4.1.1. The d.l.c./time transient shown in fig 4.5 corresponds to deposition over 6 hours, the current/time response being approximately flat during this period. This form of d.l.c./time curve, is reproducibly found for very low suspension concentrations.

The interpretation of the four deposition regions (a - d in fig 4.5), found during the experiment, is based on electron microscopy of the electrode surfaces taken at different stages of deposition. This interpretation is unavoidably qualitative in nature (illustrated in fig 4.6), but is as follows;

a) Formation on the microscale of alloy layers and initial cadmium layers. At this stage the double layer capacity rapidly changes as the surface composition changes from nickel to cadmium.

b) Deposition of initial grainy cadmium as hexagonal platelets causing the surface area to increase gradually over that for the initial polished surface.

c) The first initial layers of grainy cadmium have been deposited at this stage and further deposition of grainy cadmium

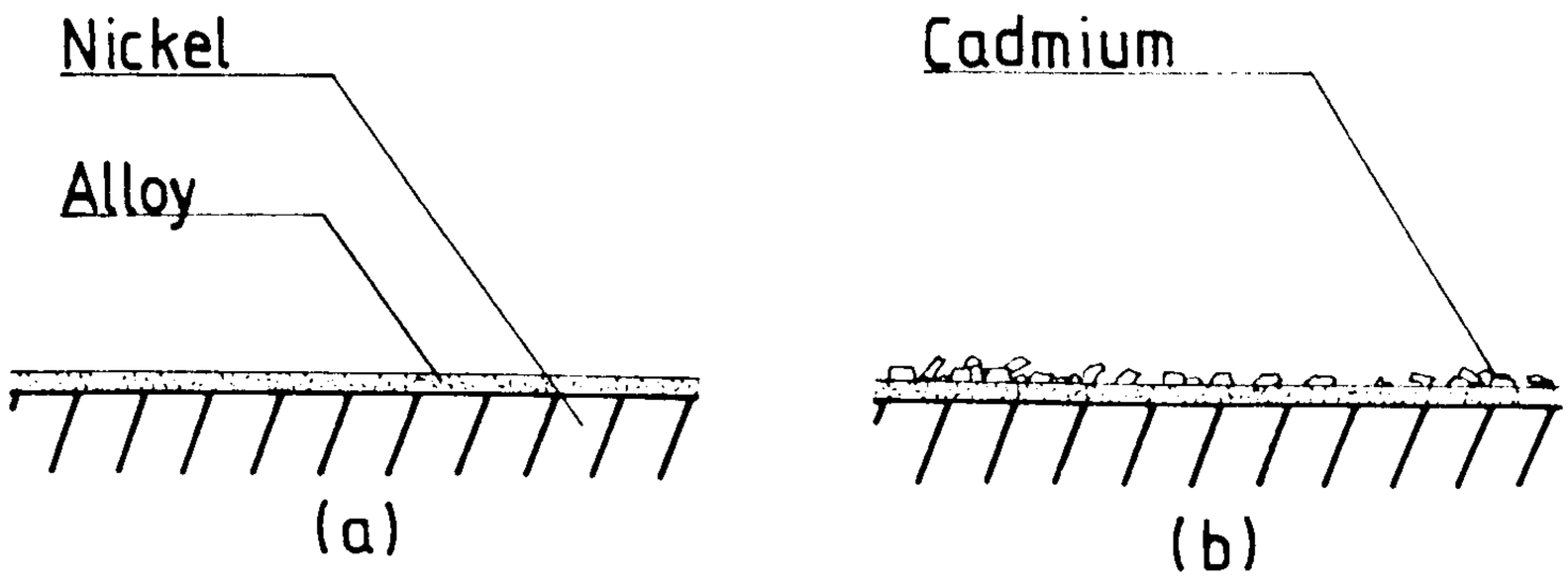

Fig 4.6 Interpretation of the electrode surface morphology associated with the regions (a) - (d) in fig 4.5. (a) surface changes form nickel to cadmium; (b) initial deposition of grainy cadmium onto the flat surface; (c) grainy cadmium deposition onto grainy surface; (d) runaway dendritic growth from surface amplified features.

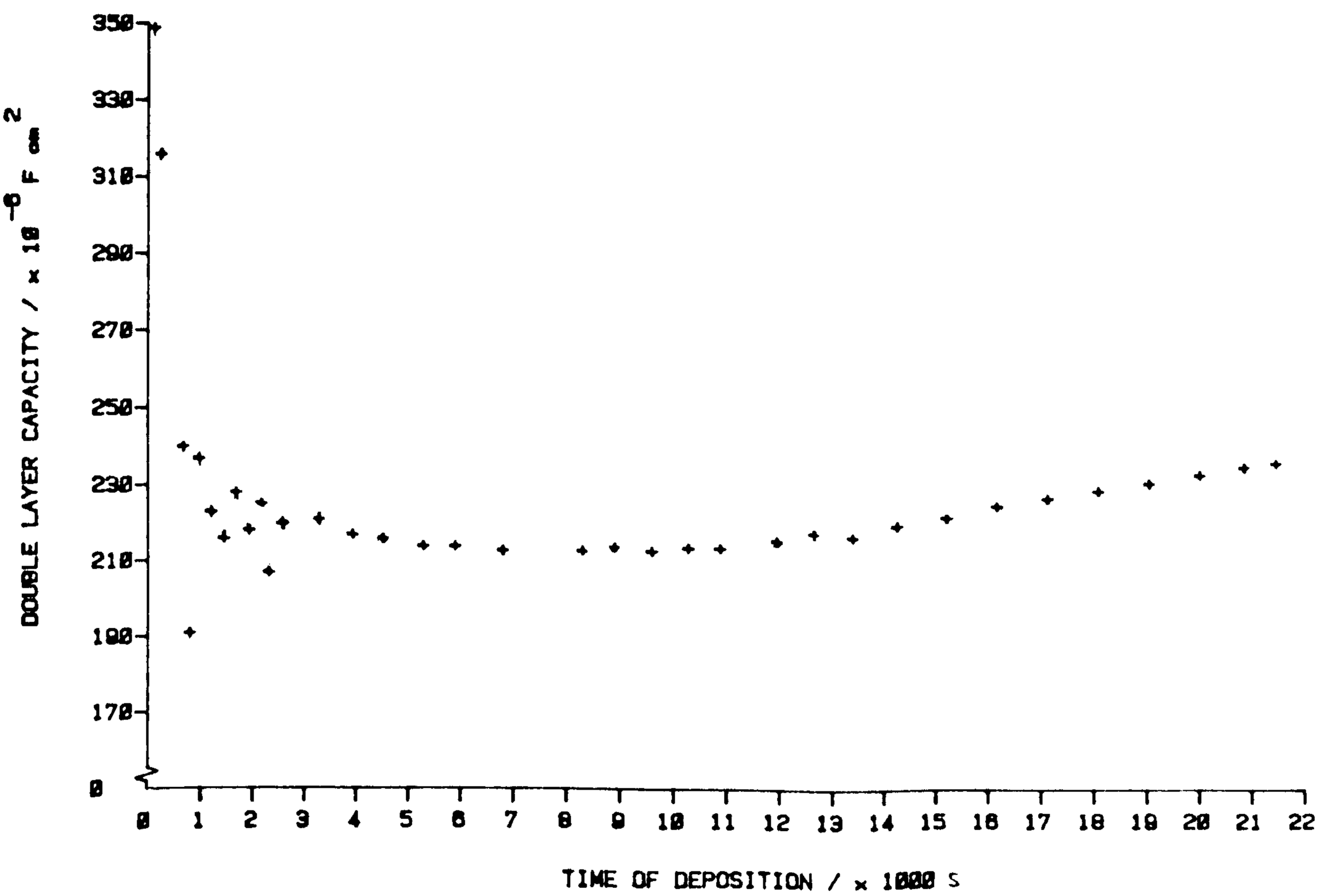

Fig 4.7 Double layer capacity/time transient found during deposition onto an emery roughened nickel disc electrode in 10.00M KOH, containing 0.0001g/dm^3 $Cd(OH)_2$ suspension at -400mV overpotential.

maintains a roughly constant surface area. Any underlying features are exaggerated by amplification of irregularities.

d) Surface amplification continues until runaway dendritic growth ensues at favoured sites. Thus surface area rapidly increases.

Plates 4.3a/b, illustrate the electrode taken at stage d) and clearly show surface features associated with amplification of irregularities. Raised features found are of greater prominence than found on polished electrode surfaces. Most of the raised areas show some form of dendritic growth and are consistent with an indicated initiation time of ~3 hours. Dendrites observed, do not have as clearly defined fern-like appearance as with higher suspension concentrations (cf, Plates 4.1 and 4.2).

4.1.2 SURFACE ROUGHNESS

Using a polished nickel rotating disc electrode, a roughened electrode surface was prepared by abrasion with 240 grit Emery paper, to provide an evenly roughened electrode. The initial d.l.c. of 212μFcm^{-2}, indicates a roughness factor of ~x 5.5 over the normal polished electrode. After initial pretreatment by hydrogen evolution at -1.300V for 100 minutes (in Cd-free 10.00M KOH), deposition was followed in the 0.0001 gdm^{-3} suspension. The d.l.c./time transient observed is given in fig 4.7. Initial values of d.l.c. are erratic due to blockage of the electrode by hydrogen bubbles, but the hydrogen evolution reduces as the surface composition changes to cadmium and this is reflected in the increasing stability of the d.l.c./time transient with time. From the d.l.c. transient it is clear that

Plate 4.3 Examples of surface amplification of irregularities found after deposition for 6 hours at -400mV over-potential, onto a polished nickel electrode in 10.00M KOH + 0.0001g/dm^3 CdO (Cd(II) saturated). Light patches are raised areas of dendrites.

Plate 4.3a x100

Plate 4.3b x500

surface roughness is not an important factor in dendritic growth from suspension. An initiation time of ~3 hours, is consistent with deposition experiments under identical conditions onto polished electrodes [see CH 4.1]. The final rising d.l.c. curve of ~3μFcm^{-2}/1000s, compares with typical values of 1 - 2 μFcm^{-2}/1000s for polished electrodes. This value is somewhat lower than anticipated and indicates that dendritic growth from suspension is not solely dependent on surface area. The probable cause of lower than anticipated dendritic growth, is that suspension particles are less likely to adhere to surfaces inside scratches on the electrode, adherence being more dependent on geometric surface area.

Examination of the electrode after deposition, shows some dendritic growth over the surface, but not apparently orientated in relation to the scratch marks observed. The electrode observed did not show any substantial surface amplification, in contrast to that found in CH 4.1.1.1; the reasons for this are not clear.

4.1.3 ROTATION RATE DEPENDENCE DURING DEPOSITION

Polished nickel disc electrodes for deposition experiments, were prepared as elsewhere in CH 4.1 by pretreatment for 100 minutes hydrogen evolution at -1.300V in Cd-free 10.00M KOH. Deposition was followed at η = -50 and -400mV, in the 0.0001 gdm^{-3} suspension, employing a standard background rotation rate of 5 revs/s. Rotation spectra were taken at various time intervals during the deposition, using the procedure as in CH 2.8.1. The changing rotational dependence for both

overpotentials with time is shown in figs 4.8 and 4.9 respectively.

For deposition at η = -50 and -400mV, the current follows the form;

$$i = i_{Cd} + i_{H}$$

where i_{Cd} is given by the Levich equation, as used previously in CH 3.4.4. At η = -400mV, the cadmium deposition current (given by the slope of the i versus $\omega^{1/2}$ plot), increases slowly until after the onset of dendritic growth. Initially at 5 revs/s, i_{Cd} ~10μAcm^{-2}, increasing to ~40μAcm^{-2}, after 220 minutes of deposition. By contrast, the hydrogen evolution current, shows a smaller increase, from 560μAcm^{-2} to ~700μAcm^{-2}, presumably due to the surface area changes. At η = -50mV, a different dependence with time is seen (fig 4.8), initially the cadmium deposition current is large at ~40μAcm^{-2} after 5 minutes deposition, but this drops to ~10μAcm^{-2} after 2 hours. The hydrogen evolution current remains approximately constant at 25μAcm^{-2}. This behaviour is probably associated with the change in surface composition from nickel to cadmium at short timescales. With the current indicated, the cadmium deposit thickness (if evenly distributed), would be < 100nm after 2 hours deposition. From double layer capacity measurements [see CH 4.1.1], the surface appears to be covered with cadmium after ~1000s (initial settle down period), corresponding to a deposit of ~250 Angstroms, or about 100 atoms thick.

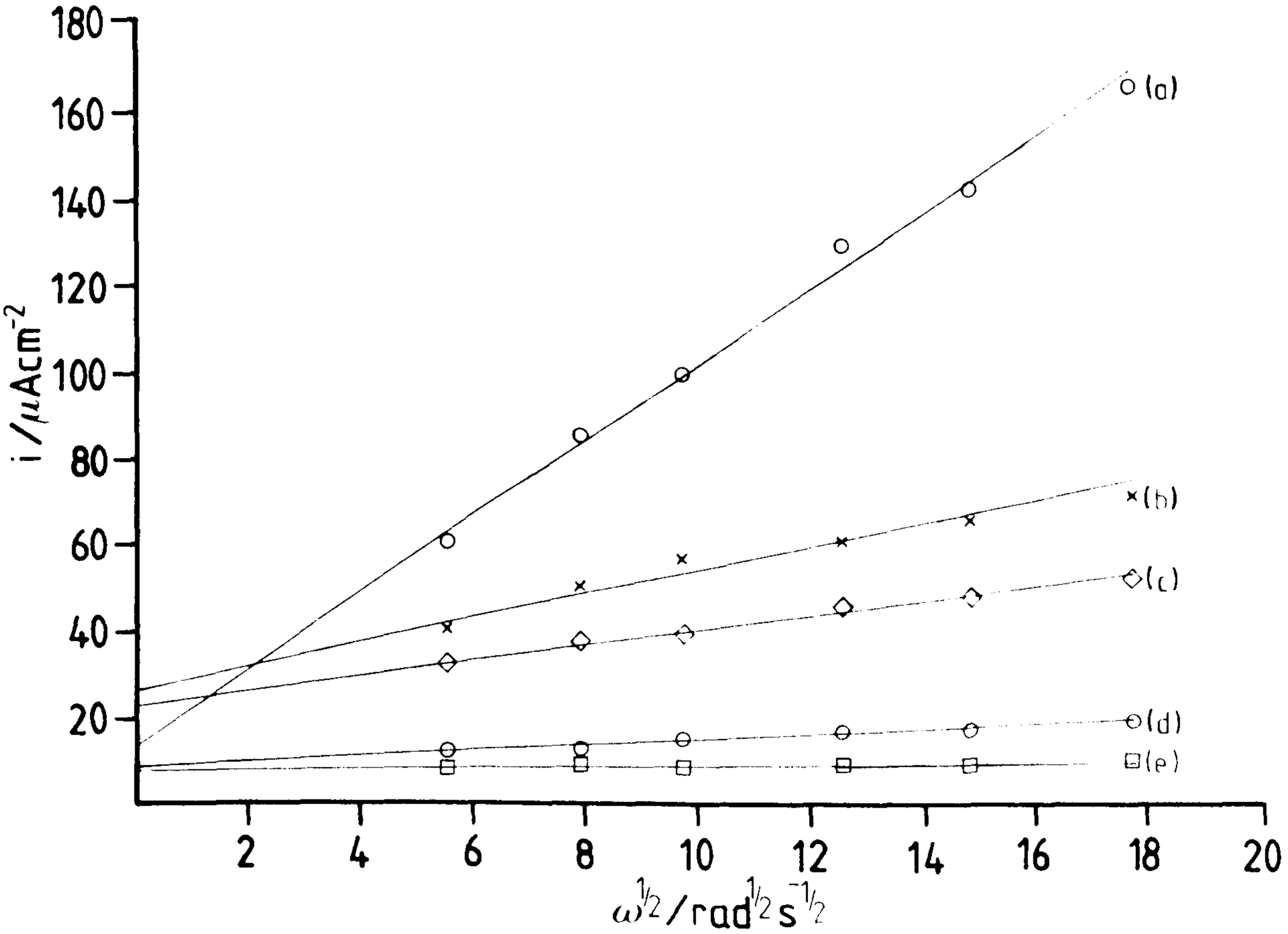

Fig 4.8 Rotation rate dependence during deposition of cadmium at -50mV overpotential. (a) after 300s of deposition; (b) after 7200s of deposition; (c) after 10800s of deposition; (d) before deposition in cadmium-free 10.00M KOH; (e) after deposition in cadmium-free 10.00M KOH (a - c in 10.00M KOH containing 0.00035M Cd(II)).

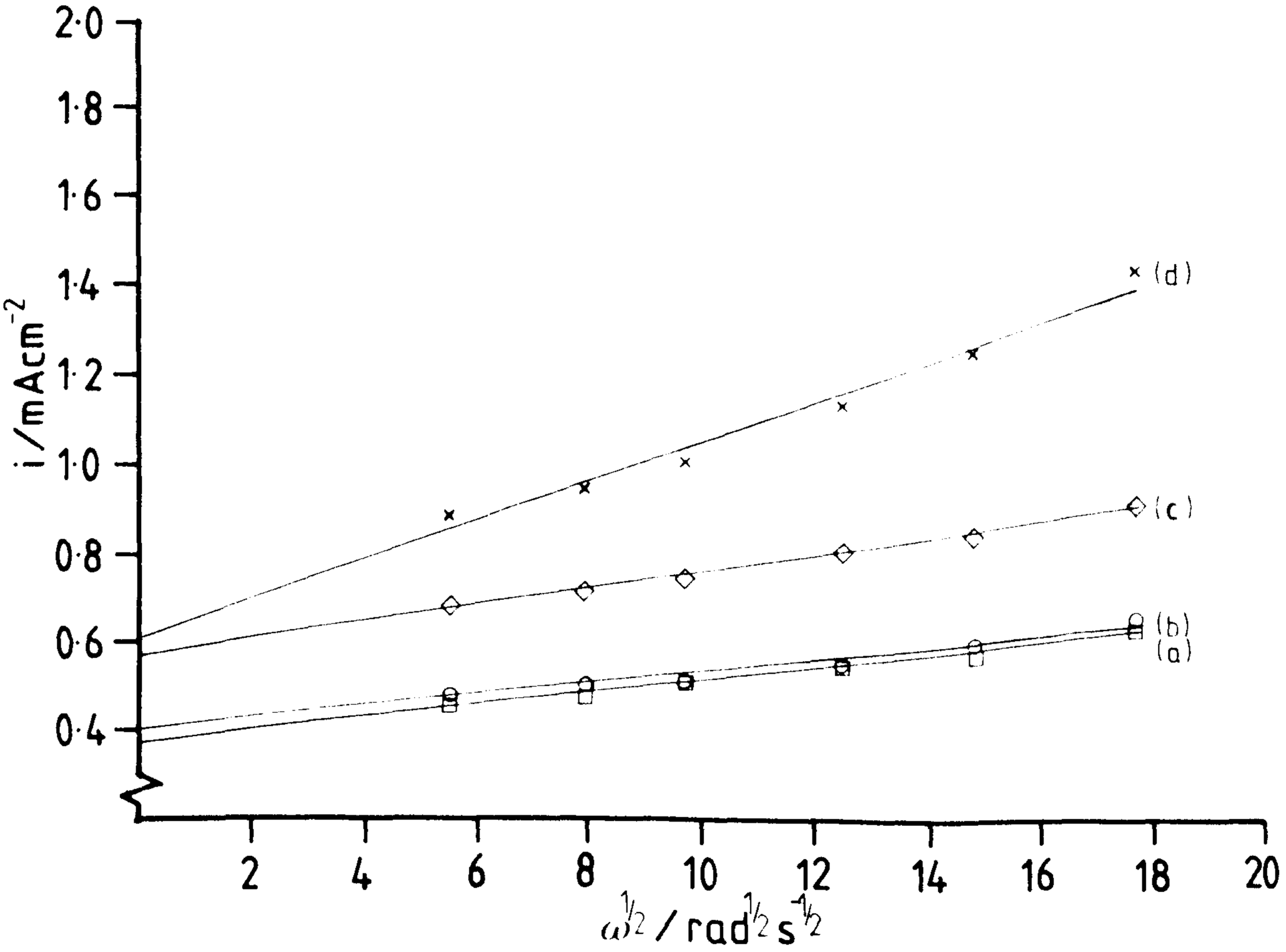

Fig 4.9 Rotation rate dependence during deposition of cadmium at -400mV overpotential. (a) after 600s of deposition; (b) after 4700s of deposition; (c) after 7800s of deposition; (d) after 13200s of deposition in 10.00M KOH containing 0.00035M Cd(II).

4.1.4 DEPOSITION MORPHOLOGY DEPENDENCE ON OVERPOTENTIAL

Polished nickel disc electrodes were prepared as elsewhere in CH 4.1, and pretreament was by hydrogen evolution at -1.100V in Cd-free 10.00M KOH for 16 hours [see CH 2.8.2]. Pretreatment was then continued at the deposition potential for a period of 2 - 3 hours, allowing the electrode to re-equilibrate at this value, before solution change to the 0.008 gdm^{-3} suspension. Deposition was then followed for periods of 3 - 5 hours, at the following overpotentials, -50, -100, -200, -300 and -400mV. The morphological changes observed are as follows;

a) 200 minutes at η = -50mV, plate 4.4a. Deposition at this potential gives a grainy background deposit (0.3 - 1μm), corresponding to that found in suspension-free solutions. Double layer capacity values are observed to slowly decrease during deposition.

b) 210 minutes at η = -100mV, plate 4.4b. At this overpotential, a uniform deposit of grainy cadmium is found, each crystallite being more hexagonal in nature than at η = -50mV, and of more regular size (0.3 - 0.6μm diameter). No evidence of dendritic growth is found. The d.l.c. values remain approximately constant during deposition.

c) 240 minutes at η = -200mV. Deposition is largely grainy in nature, but patches of poorly defined semi-dendritic growth were found.

d) 280 minutes at η = -300mV, plate 4.4c. Clumps of dendritic cadmium are to be found over the surface, against an uneven grainy background deposit. Dendrites deposited have a more poorly defined structure than at higher overpotentials.

Plate 4.4 Deposition morphology found for polished nickel electrodes after ≐4 hours deposition, in 10.00M KOH + 0.008g/dm^3 CdO (Cd(II) saturated). (a) -50mV; (b) -100mV; (c) -300mV overpotential.

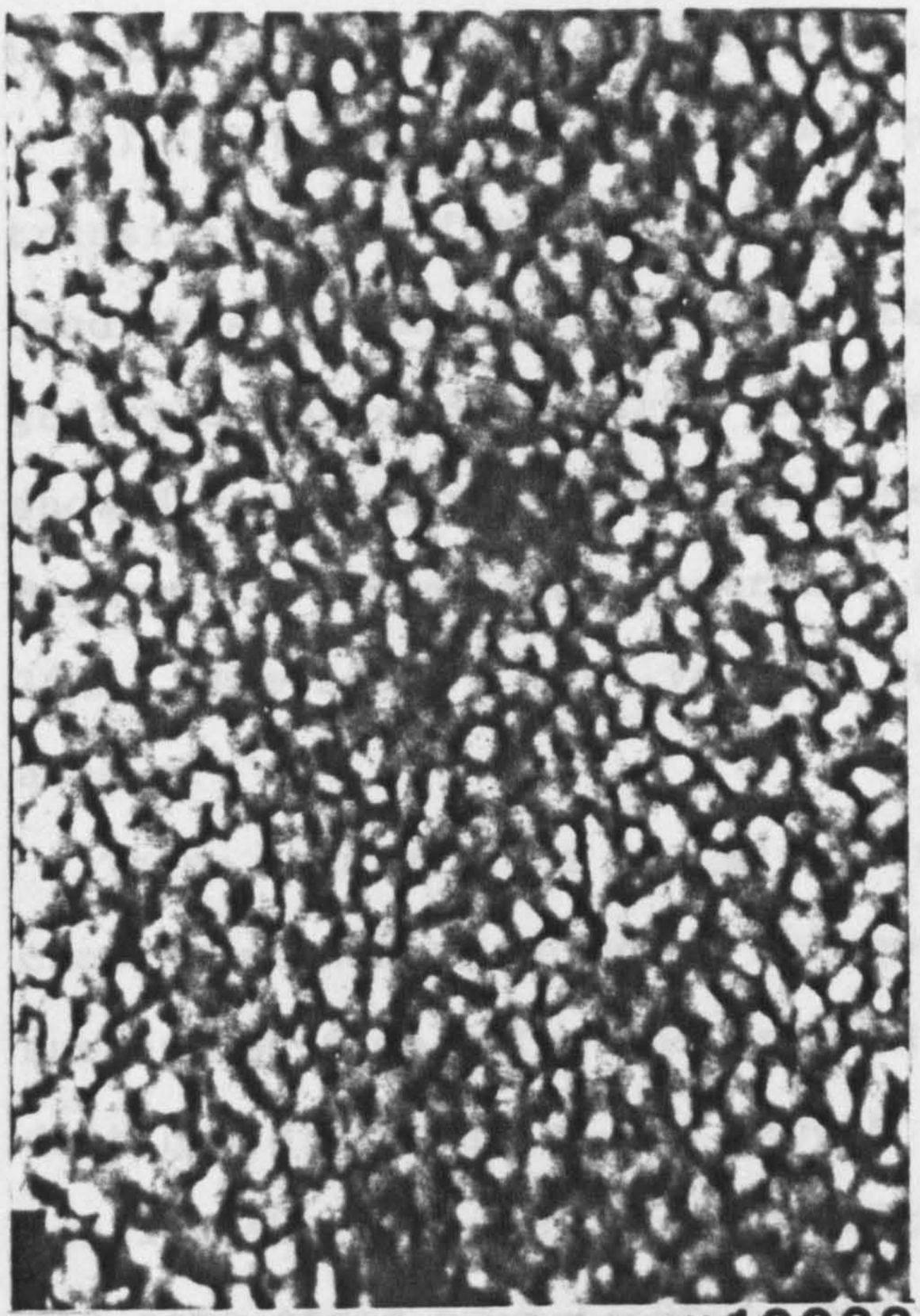

Plate 4.4a x10000

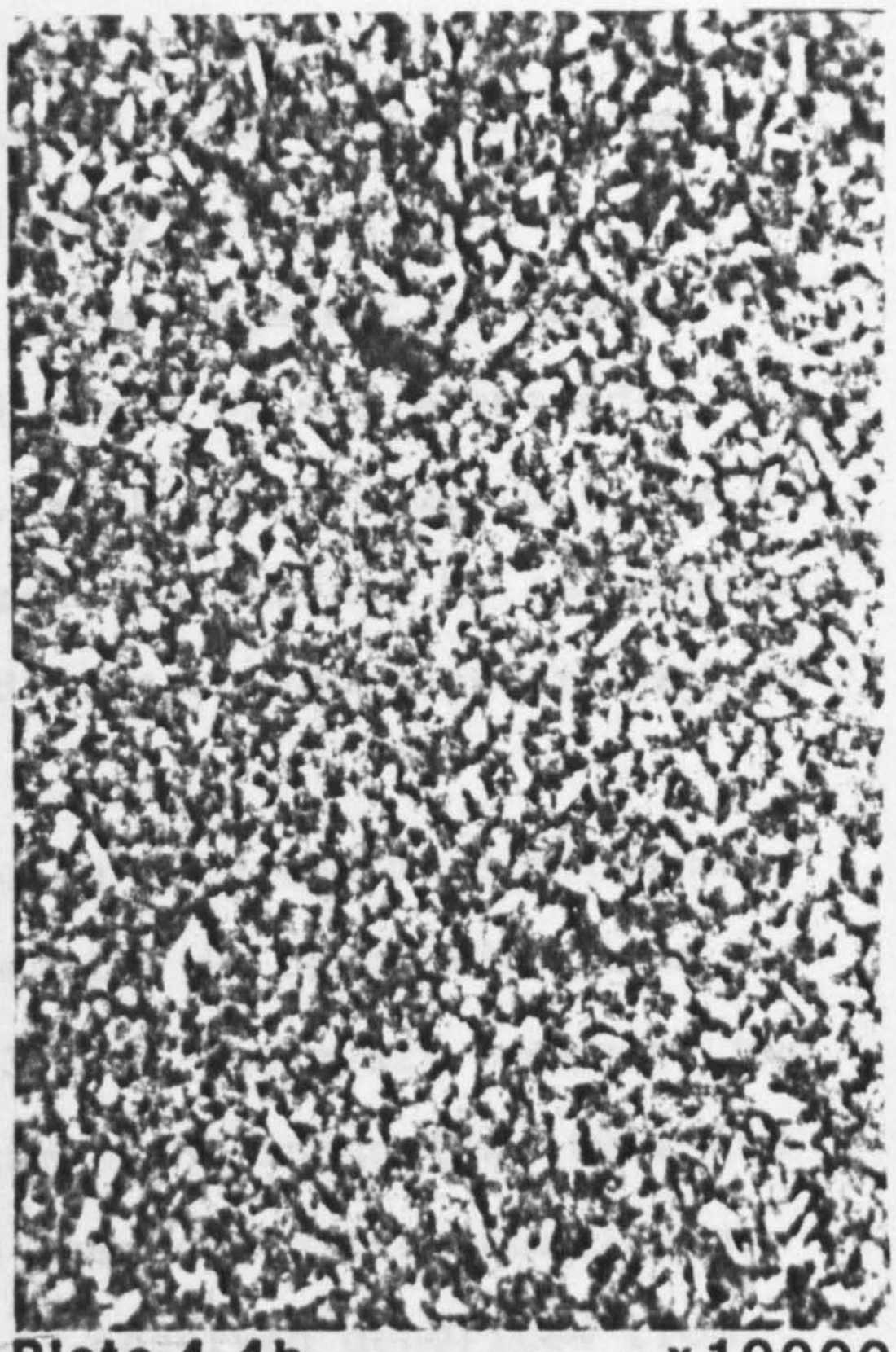

Plate 4.4b x10000

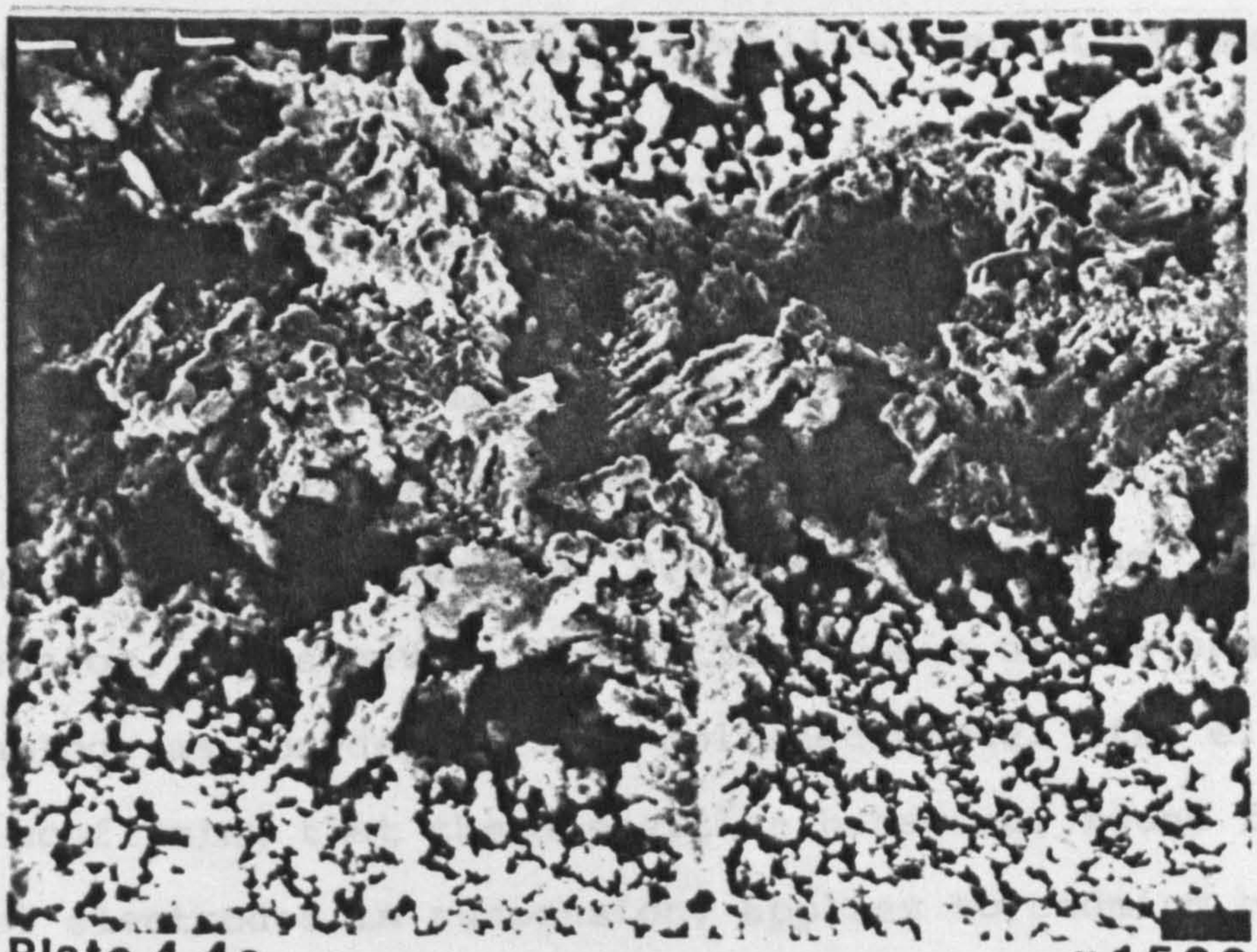

Plate 4.4c x1500

Double layer capacity measurements clearly indicate the increase in surface area during deposition.

e) 220 minutes at η = -400mV, plates 4.5a/b, d.l.c./time transient as in fig 4.10. Here, clearly defined single dendrites of length up to 25μm are found, against an uneven grainy background deposit. Several areas of the electrode showed conglomeration of dendrites, with patches up to 0.1mm in diameter. These areas protruded from the surface by as much as 30μm. The final d.l.c. values, indicate an increase in surface area of ~x 4.

These observations largely coincide with the morphological changes seen with changing overpotential in deposition from suspension-free solutions [see CH 3.6]. There are however, two distinct differences; 1) growth times and induction times are considerably reduced compared with suspension-free conditions (in some cases by x 1/50th), and 2) observed dendrites from suspensions appear in clumps and have more random orientation. This is consistent with particulate cadmium salts adhering to the surface, causing increased localised dendritic growth.

4.2 DEPOSITION ONTO CADMIUM DISC ELECTRODES

Deposition was carried out onto mechanically polished cadmium rotating disc electrodes (prepared as in CH 2.2.6.3), at η = -400mV, in Cd(II)-saturated 10.00M KOH + 0.01 gdm^{-3} CdO suspension. This gave a dendritic deposit of the same morphology as for deposits on polished nickel disc electrodes. Thus confirming that the deposition behaviour found for polished nickel electrodes in suspension, applies to cadmium electrodes.

Plate 4.5 Deposition morphology found for polished nickel electrodes after ≏4 hours deposition at -400mV overpotential, in 10.00M KOH + 0.008g/dm^3 CdO (Cd(II) saturated).

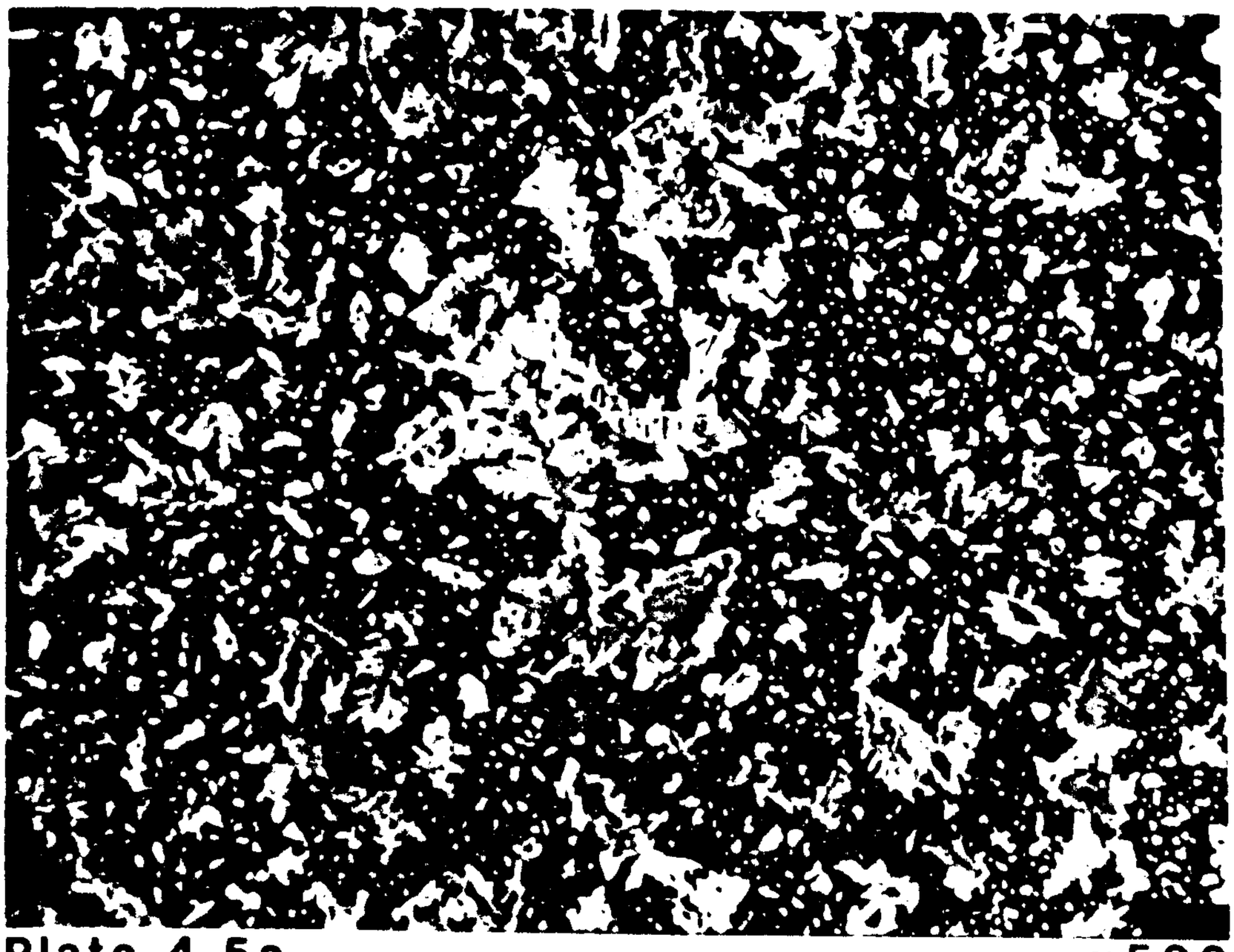

Plate 4.5a x500

Plate 4.5b x5000

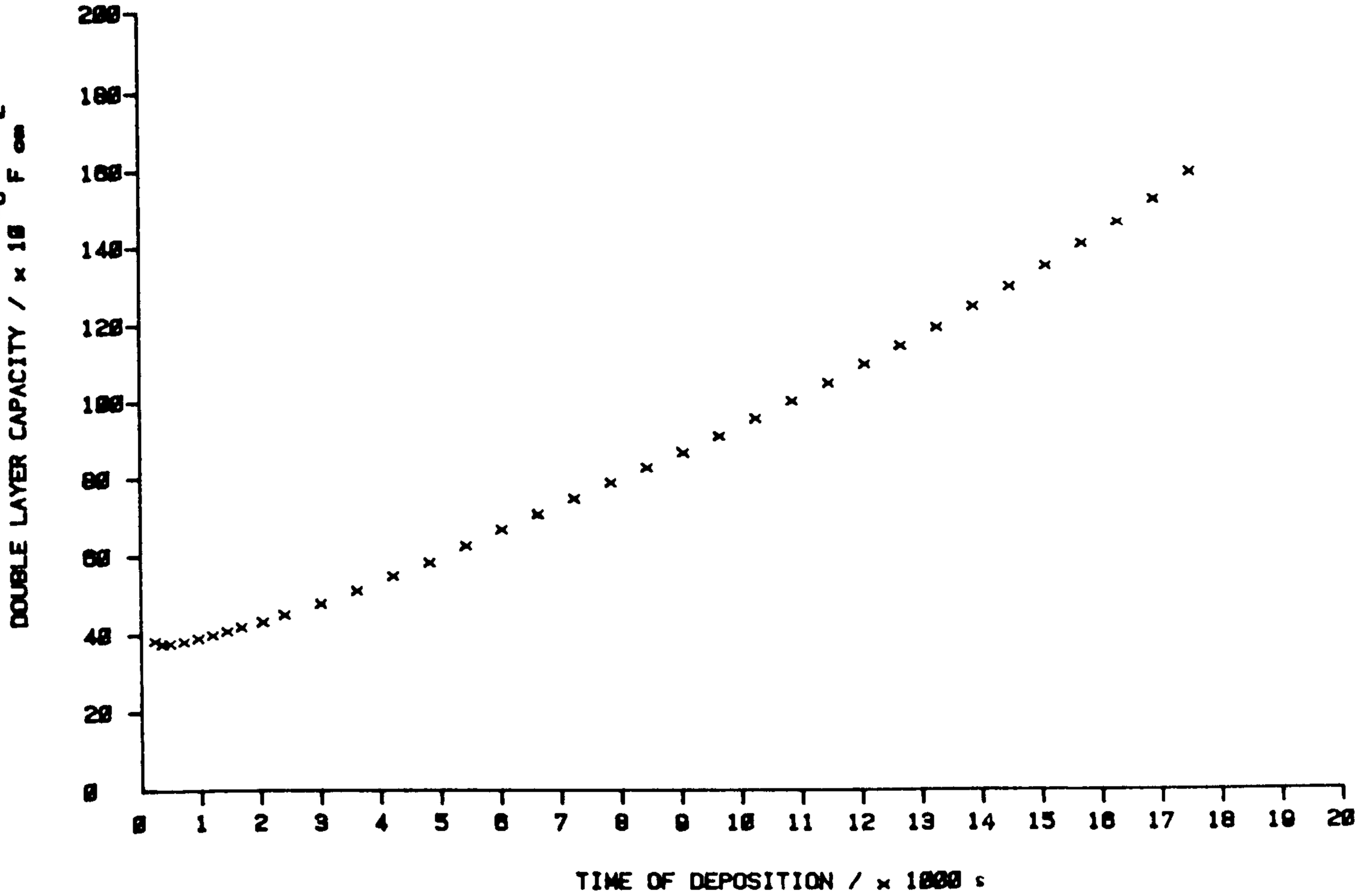

Fig 4.10 Double layer capacity/time transient found during deposition at -400mV overpotential, onto a polished nickel disc electrode in 10.00M KOH, containing 0.008g/dm^3 $Cd(OH)_2$ suspension.

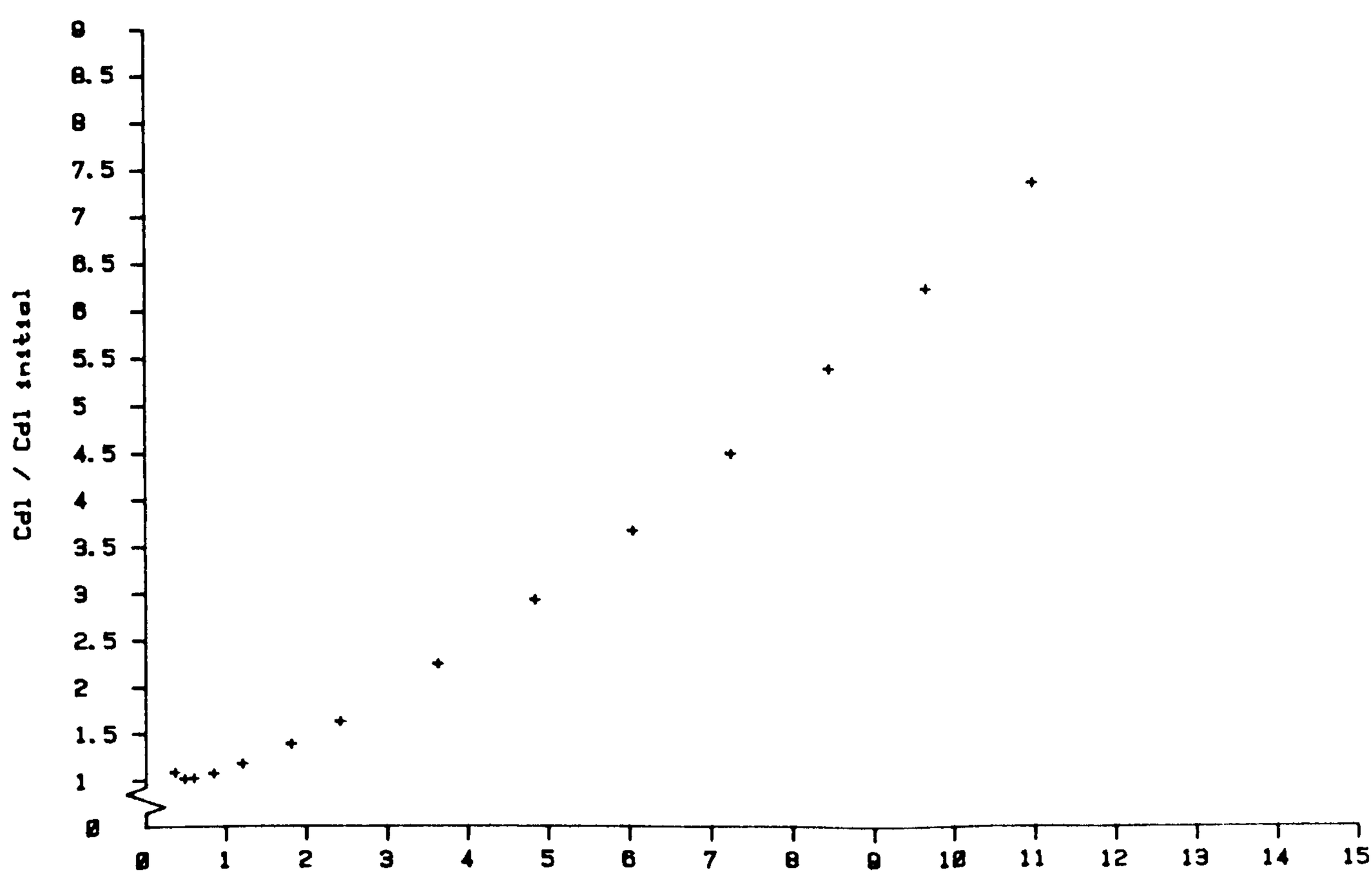

Fig 4.11 Double layer capacity/time transient found during dendritic electrode preparation, depositing at -400mV overpotential, for 3 hours in 10.00M KOH, containing 0.2g/dm^3 $Cd(OH)_2$ suspension.

However, deposition from suspension onto polished cadmium discs was not studied in any great detail and results are somewhat qualitative.

4.3 DEPOSITION ONTO DENDRITIC ELECTRODE SURFACES FROM SUSPENSION-FREE SOLUTION

To establish the changes found in morphology of the deposit, between suspension and suspension-free solutions, a series of experiments were carried out, depositing from suspension-free solutions onto dendritic electrode surfaces.

4.3.1 PREPARATION OF DENDRITIC ELECTRODE SURFACES

Dendritic electrode surfaces were prepared from polished nickel rotating disc electrodes, with the standard rotating disc cell and assembly described in CH 2.1.1 and 2.4.1. The experimental procedure was as follows;

a) Pretreatment of polished nickel electrode surfaces for 100 minutes at -1.300V, in cadmium-free 10.00M KOH (at 5 revs/s).

b) Solution change to a pre-deoxygenated suspension of 0.2 gdm^{-3} CdO, in Cd(II)-saturated 10.00M KOH. Rotation was then continued at 5 revs/s for 20 minutes, to allow establishment of a reproducible equilibrium level of suspension in the cell. Deposition was then carried out at η = -400mV for a period of 3 hours, monitoring the d.l.c./time transient.

c) Solution change to pre-deoxygenated 10.00M KOH + 0.00035M Cd(II) (after rinsing the cell with Cd-free 10.00M KOH).

A typical d.l.c./time transient observed during dendritic electrode preparation, is shown in fig 4.11. SEM microscopy of the electrode revealed a uniform covering of dendrites, with the same morphology as that previously observed (plates 4.1 and 4.5). The average surface area increase over 10 such electrode preparations was x 4.6, and varied over a range of x 3.6 - 5.8 greater than the initial surface area. This gave dendritic electrodes with values of double layer capacity around 200μFcm^{-2}. Variability in the dendritic electrode state, is caused by the difficulty of both initial mechanical polishing of electrodes to a reproducible finish, and maintaining a constant level of suspension for several experiments. Electrodes thus produced, were dull grey in appearance and observations by SEM, confirmed the presence of a dendritic deposit of cadmium covering much of the surface (average thickness of ~15μm).

4.3.2 DEPOSITION DEPENDENCE UPON OVERPOTENTIAL

Having established a suitable dendritic electrode surface, deposition was followed in the Cd(II)-saturated suspension-free 10.00M KOH for a further 6 hours. Four overpotentials were investigated, -100, -200, -300 and -400mV. The d.l.c./time transients associated with each are shown in figure 4.12, which compares the four transients when the initial double layer capacity values for the starting dendritic surface have been normalised. Fig 4.13 shows the i/t behaviour for η = -400mV. Other i/t transients are not shown, due to the large difference in the hydrogen evolution current encountered upon switching deposition potential from that used in dendritic electrode

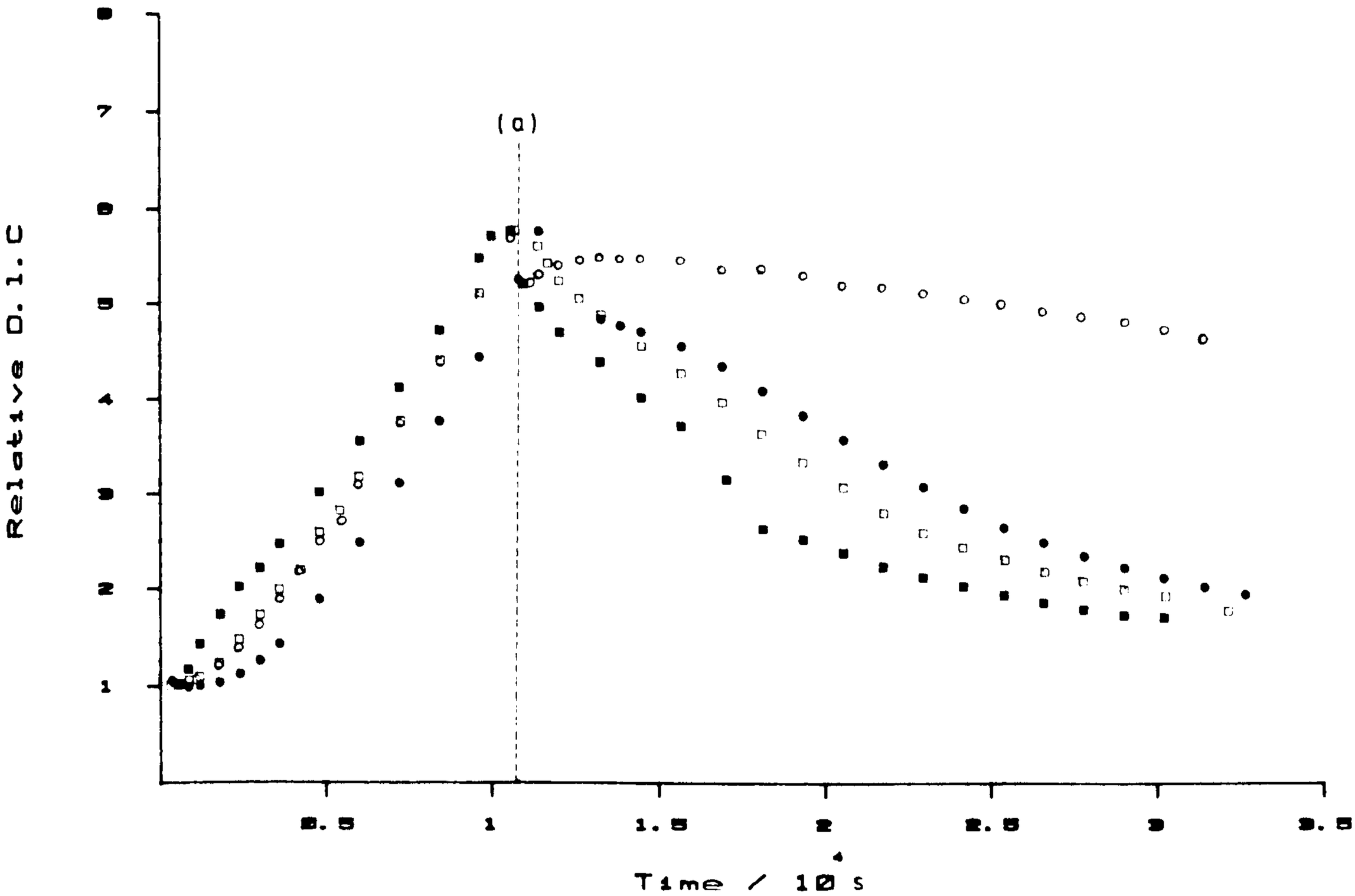

Fig 4.12 Dependence of relative double layer capacity on time, changing the electrolyte from 10.00M KOH + 0.2g/dm³ suspension to suspension-free 10.00M KOH + 0.00035M Cd(II). (○) -400mV; (●) -300mV; (□) -200mV; (■) -100mV.

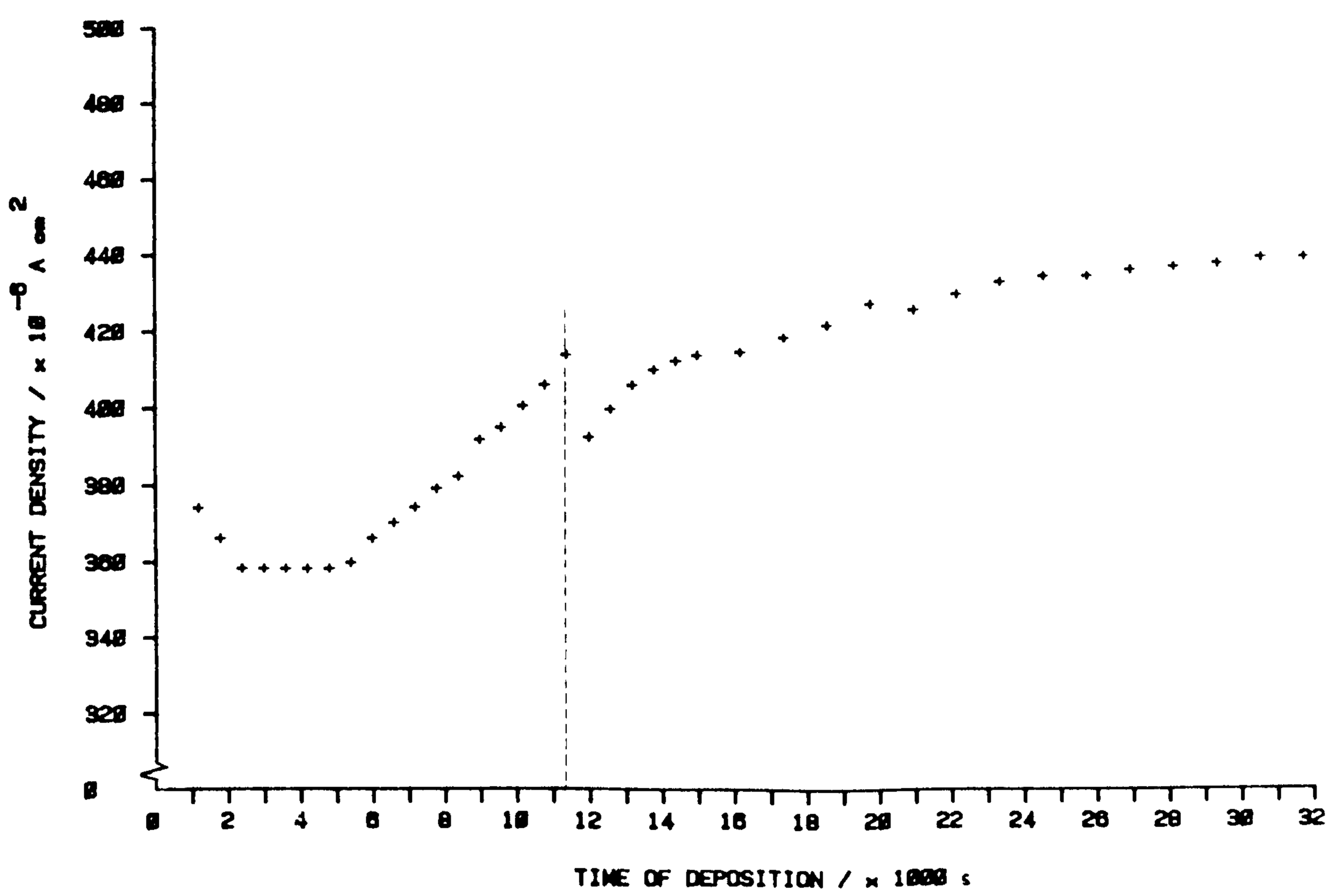

Fig 4.13 Current/time transient associated with the -400mV over-potential deposition as in fig 4.12.

preparation, thus masking any changes due to morphological effects.

Examination of the transient shown, reveals that deposition is not continued in the same way as in suspension. For η < -400mV, the decreasing d.l.c./time transients after solution change indicate an abrupt change in morphology. For η = -400mV, the d.l.c. values after solution change are approximately constant. This would be anticipated if either the deposition rate is dramatically reduced or some slight morphology change is encountered. Reference to fig 4.13, reveals the i/t response found at η = -400mV, and shows a continuing rising current after solution change, but at a lower rate of increase. At low overpotential and deposition rates, a decreasing d.l.c./time transient can be expected, if a transition from dendritic to grainy cadmium occurs. Thus dendrites would become more rounded in appearance and effective surface area is decreased. An additional factor that may effect d.l.c. values, on changing to lower overpotential, could be the dependence of hydrogen evolution bubble size. Since a change in coverage from small bubbles to large or vice versa, could effect the degree of wetting of the surface. Thus changing the d.l.c. values measured to some extent.

SEM of the resultant electrode surfaces, showed all surfaces to have dendritic growth of some form, with changes in morphology from that more normally found for dendritic deposits in suspension, particularly prevalent at the lower overpotentials. Comparisons of the deposits found with that before solution change (plates 4.1, 4.2 and 4.5), are summarised as follows;

a) η = -400mV, plates 4.6a/b. The form of the original dendritic deposit is clearly retained, but comparison with other dendrites grown entirely from suspensions, shows a changeover in morphology. Towards the extremities of the dendrites, the growth is seen to be considerably more branched, losing some of the original fern-like form. Depositon is clearly favoured at sites further out from the surface, indicating the increased importance of the linear diffusion layer in the absence of suspension.

b) η = -300mV. This electrode exhibits the observed changes in morphology found at η = -400mV, but to a lesser extent, presumably due to the deposit being more evenly distributed.

c) η = -200mV, plates 4.7a/b. A clear change of deposit morphology is found, with a gainy covering of cadmium found on most surface features. Plate 4.7b, shows a typical example of a dendrite losing its original fern-like structure under a more grainy deposit.

d) η = -100mV. Deposit morphology here is entirely grainy cadmium and is found over all surface features. Considerable rounding of dendrites can be seen.

These observations indicate;

1) Some form of dendrite growth is continued above η = -300mV, but at a considerably reduced rate.

2) A morphological change towards a more grainy deposit is found upon deposition at $\eta < -200$mV, consistent with a critical overpotential for dendrite growth of $\eta = -230 \pm 20$ mV.

Plate 4.6 Deposition morphology found after continued deposition at -400mV overpotential, in suspension-free 10.00M KOH + 0.00035M Cd(II) onto a previously prepared dendritic electrode surface (CH 4.3.1).

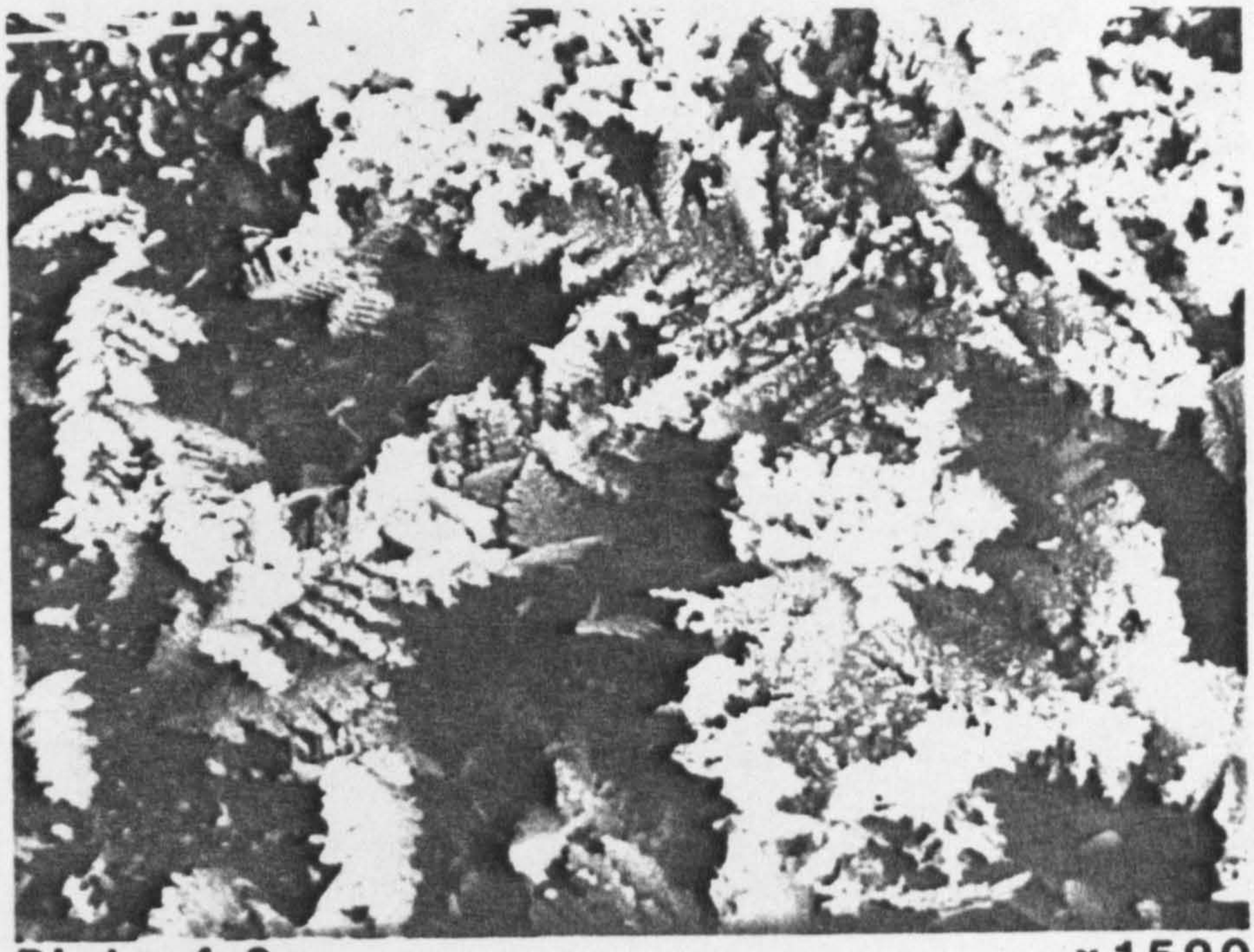

Plate 4.6a x1590

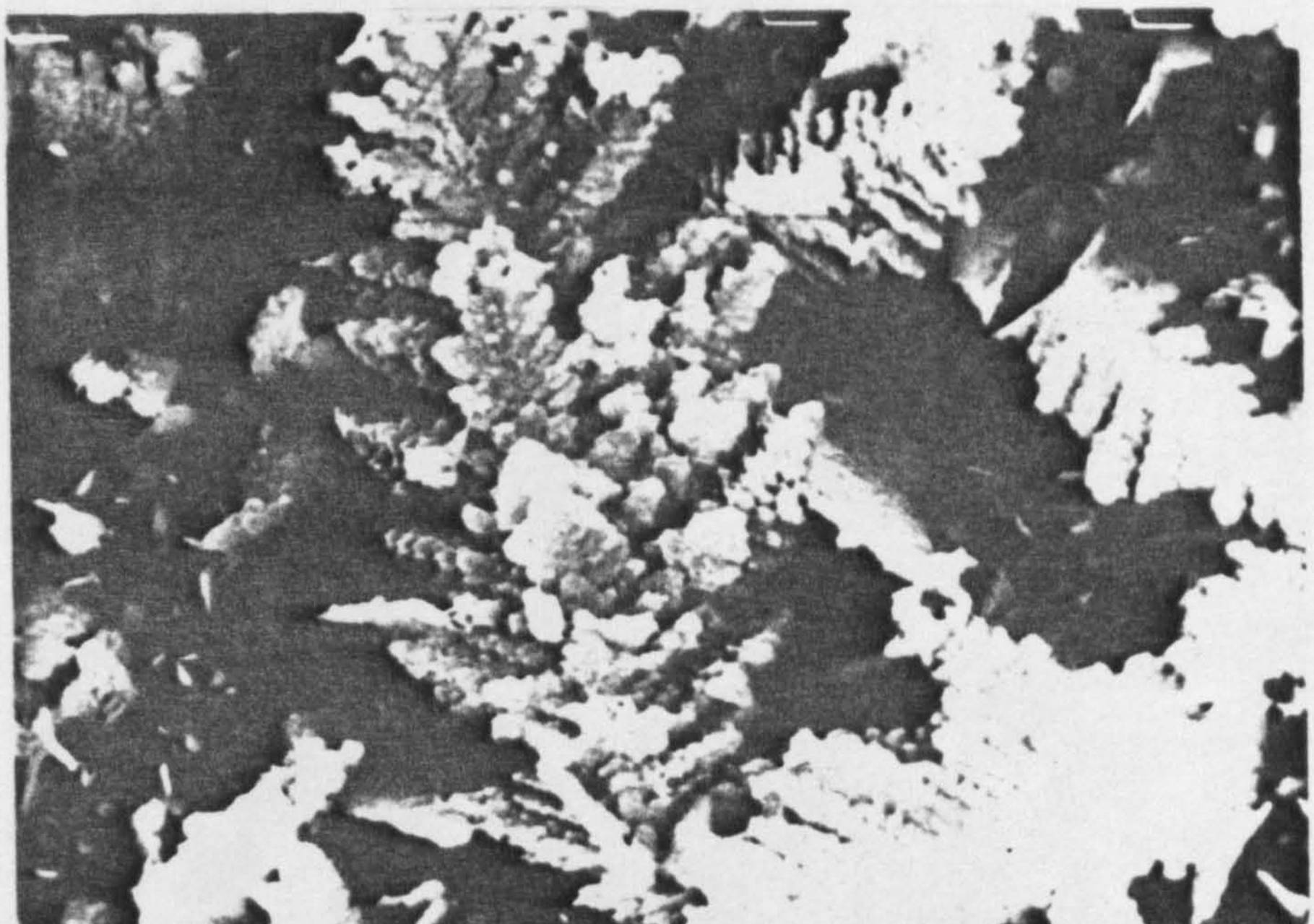

Plate 4.6b x3710

Plate 4.7 Deposition morphology found after continued deposition at -200mV overpotential, in suspension-free 10.00M KOH + 0.00035M Cd(II) onto a previously prepared dendritic electrode surface (CH 4.3.1).

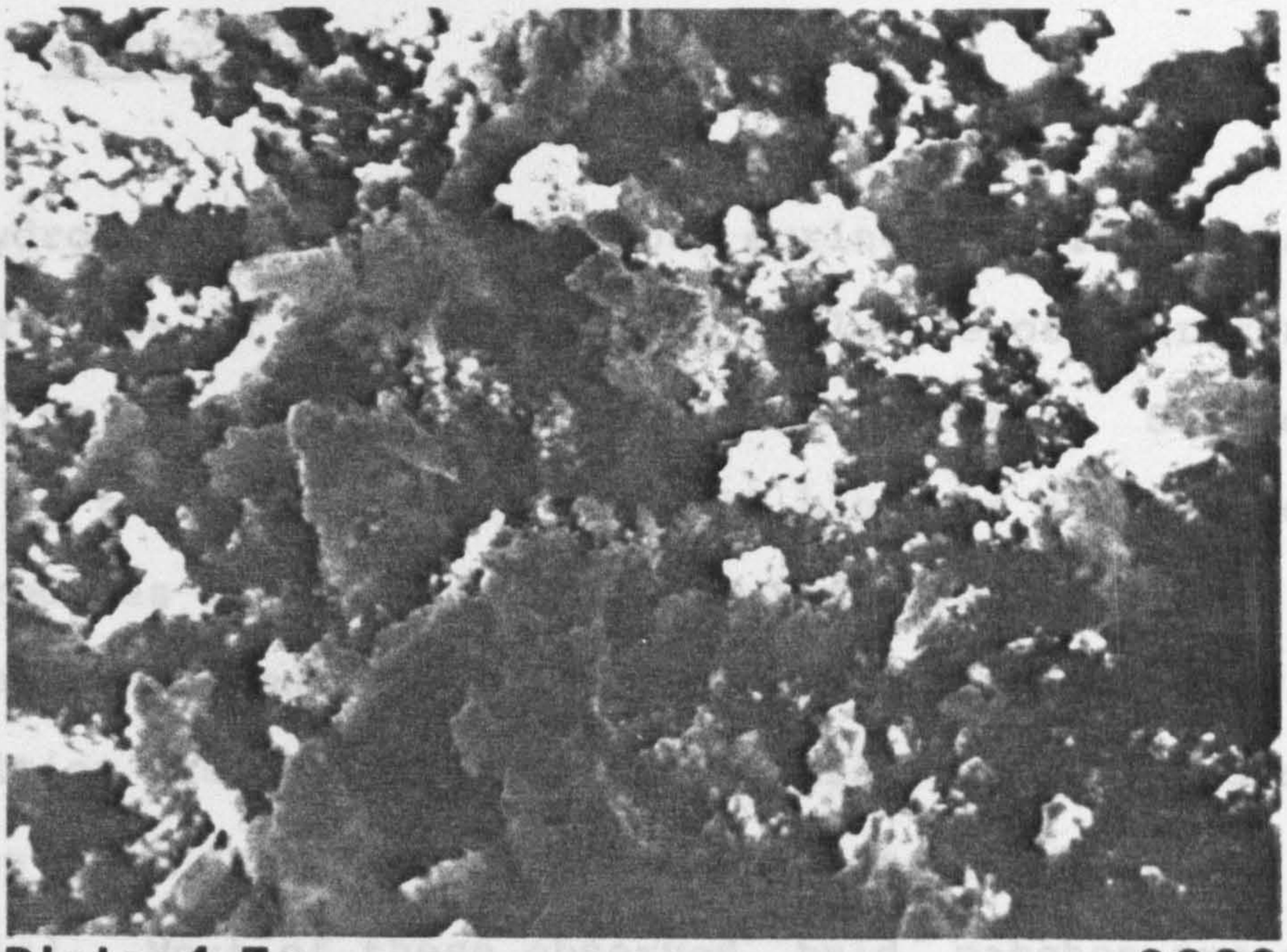

Plate 4.7a x2000

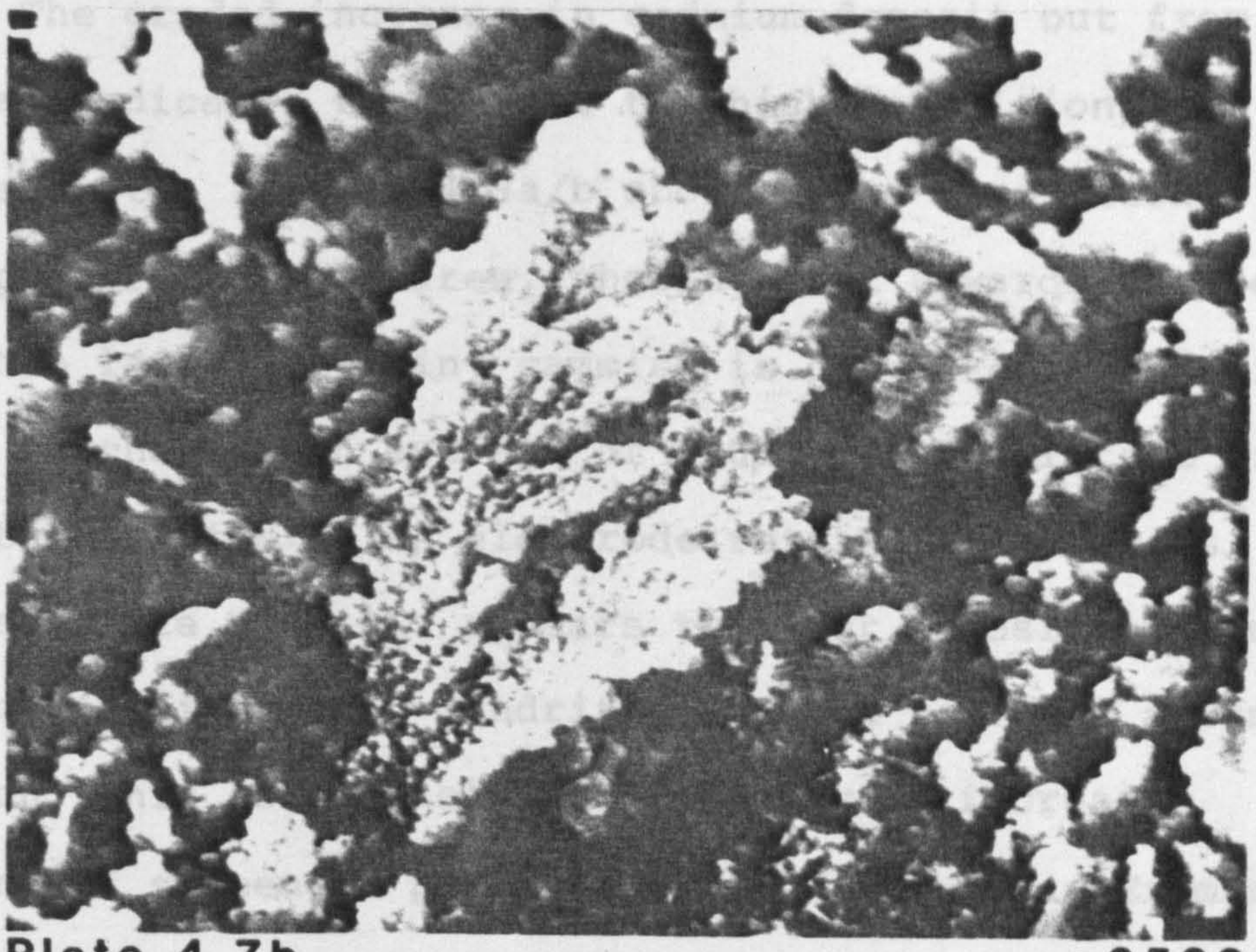

Plate 4.7b x3500

4.4 INFLUENCE OF HYDROGEN EVOLUTION ON DEPOSITION MORPHOLOGY

The hydrogen evolution behaviour during deposition has been investigated in CH 3.4.4.2, but the influence of hydrogen evolution on deposition is difficult to estimate. Some clear evidence is to be found that physical blockage by hydrogen bubbles reduces cadmium deposition. Referring to plates 4.8a/b, we can see that dendritic electrodes show 'bald' patches, where no deposition has occurred. This feature is also found on electrodes after deposition from suspension-free solution (see plate 3.1a). Most of these observed 'bald' patches are centred around a surface defect, which presumably exposes part of the underlying nickel, thus enhancing hydrogen bubble nucleation and growth. The graded increase in cadmium deposit out from these bald areas indicates the extent to which deposition is interfered with. Plates 4.9a/b show higher resolution micrographs of the bald area, showing that towards the centre, only a thin layer of grainy cadmium is deposited. The size of the bald patches at an average of 100μm, is consistent with the average bubble size on an electrode rotated at 5 revs/s. Looking at plate 4.8b, it appears that for deposition from suspension, an increased dendritic deposit is found around each bald patch, this is probably associated with increased entrapment of suspended particles by the bubbles. Examination of plates 4.8a/b, clearly show that the shape of the bald areas is elongated and determined by the characteristic flow lines for a rotating disc electrode[174]. This is shown in fig 4.14 for the 2mm section of the electrode in plate 4.8a.

Plate 4.8 Morphology found after 4 hours deposition at -400mV overpotential in 10.00M KOH + 0.008g/dm^3 (Cd(II) saturated), showing 'bald' areas. These are often seen to be associated with surface defects, and believed due to hydrogen evolution catalised from the underlying nickel (see fig 4.14).

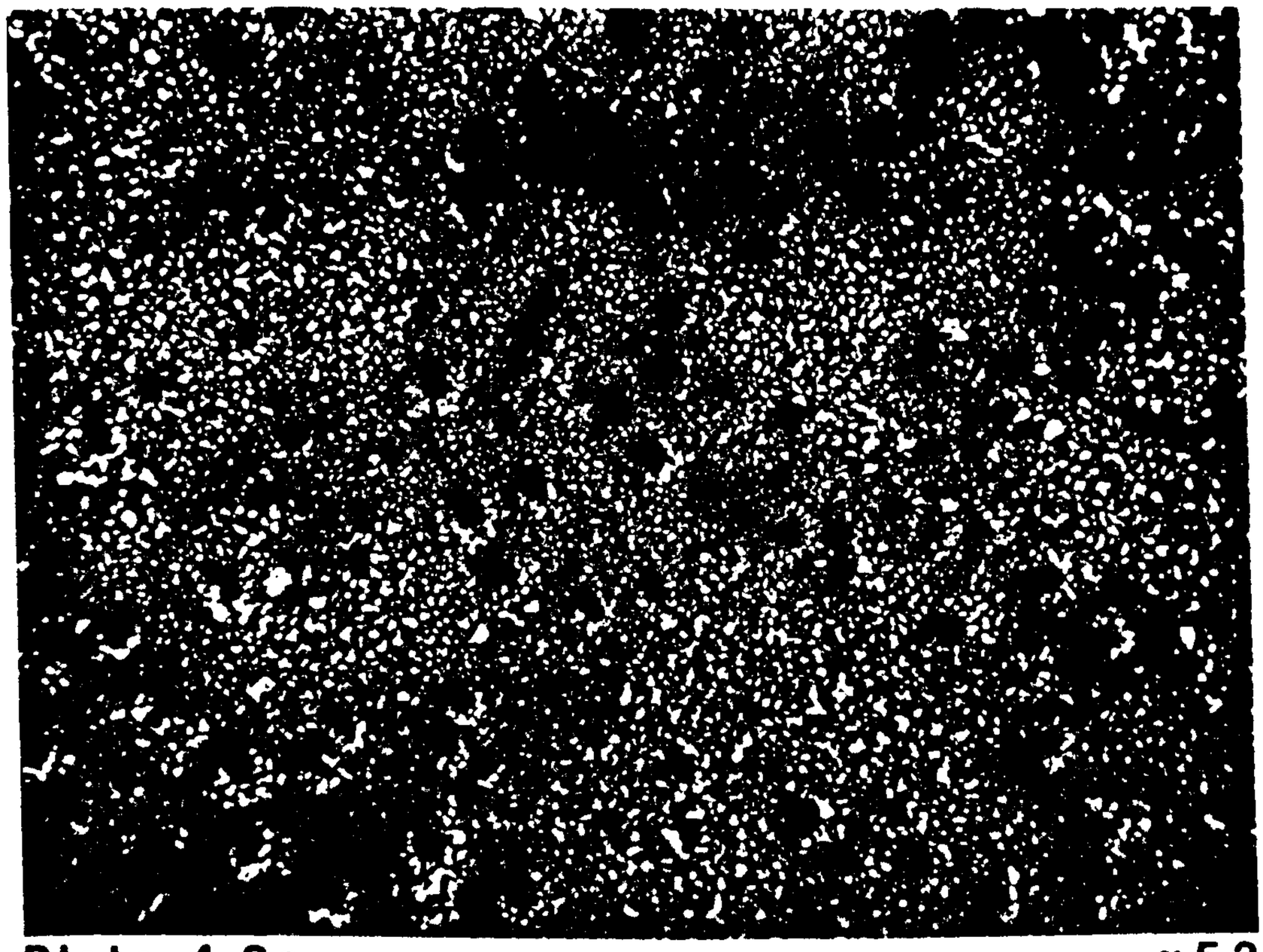

Plate 4.8a x53

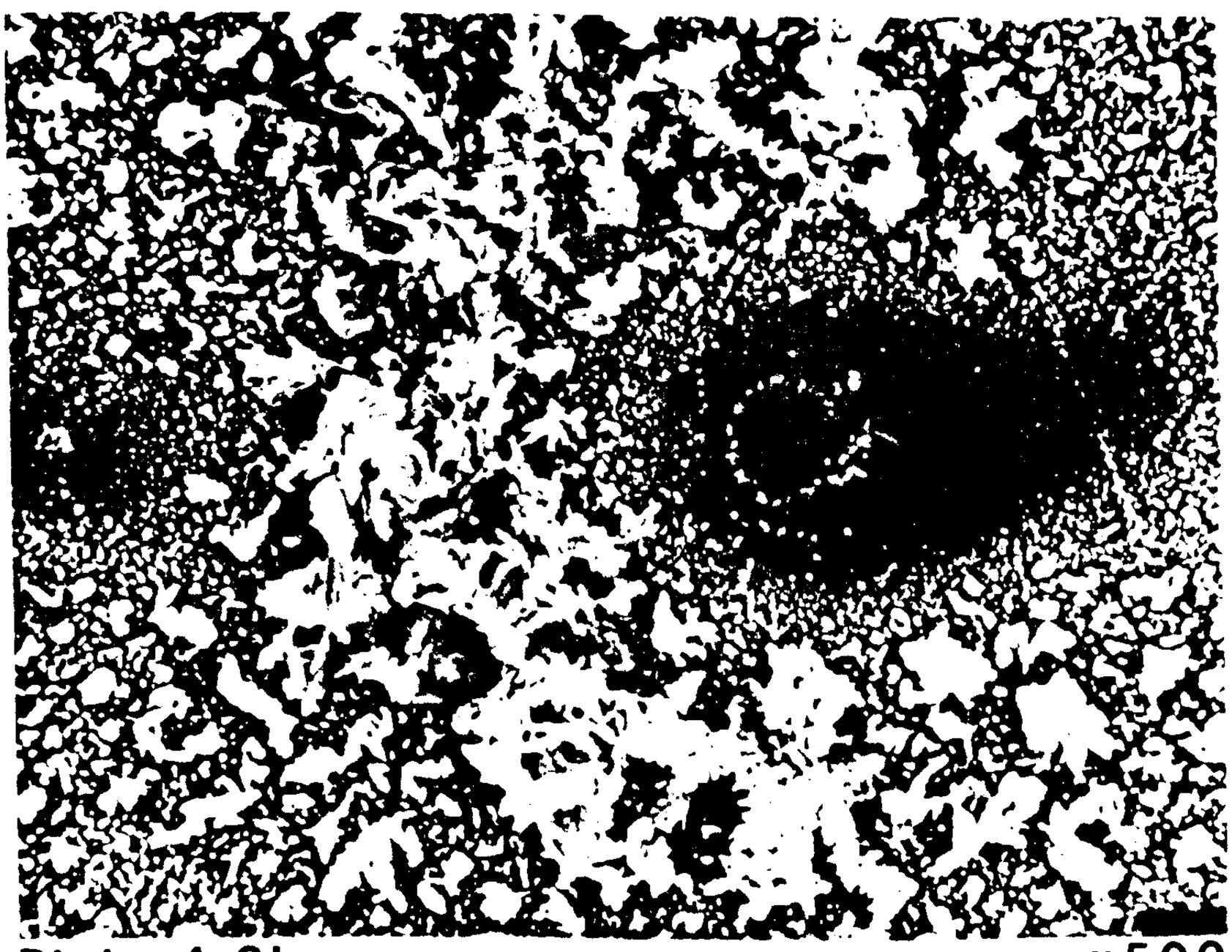

Plate 4.8b x500

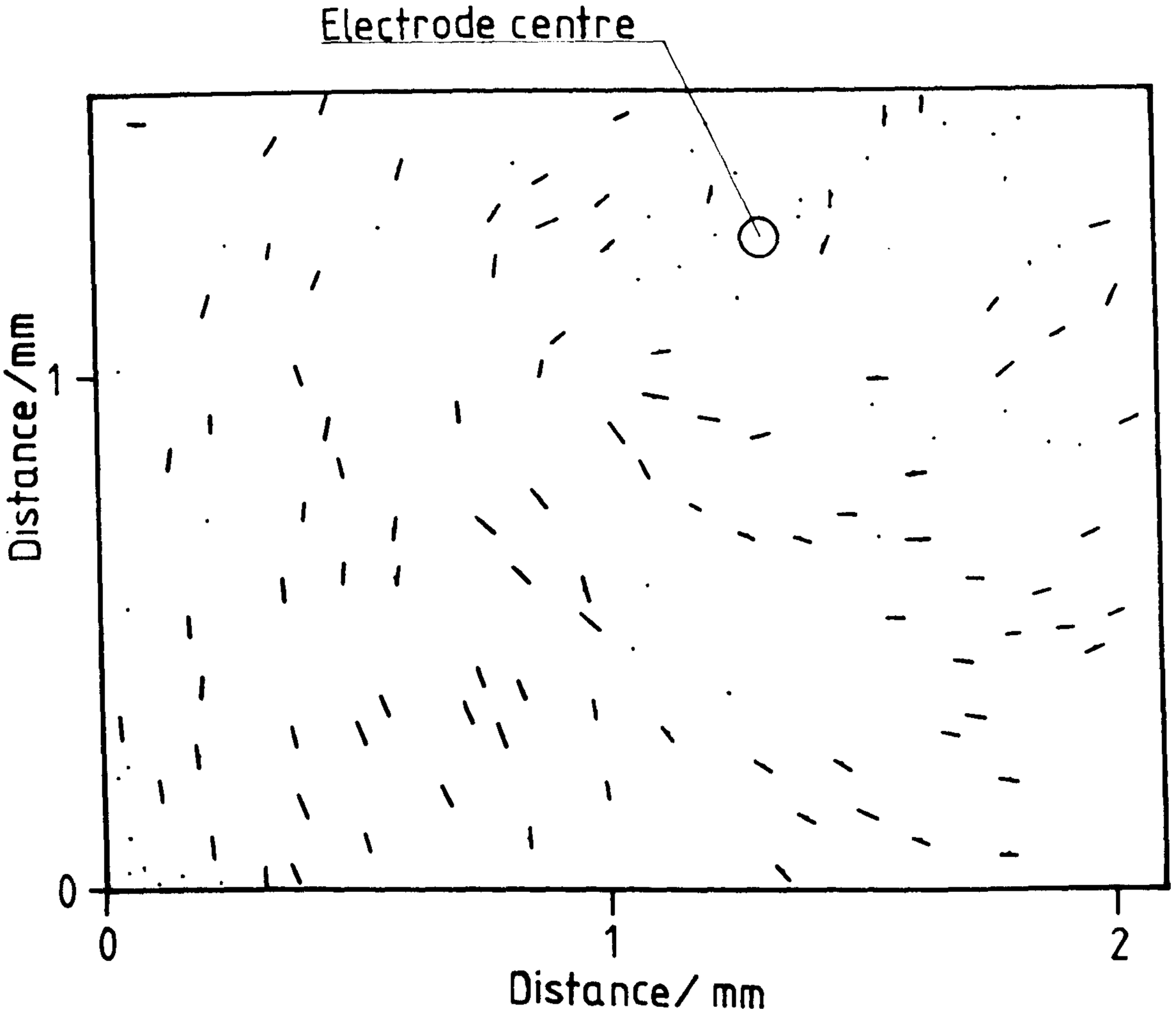

Fig 4.14 Alignment found for the elongated 'bald' patches over the 2mm section of electrode shown in plate 4.8a.

Plate 4.9 Higher resolution micrographs of the morphology found within the ´bald´ areas shown in plate 4.8.

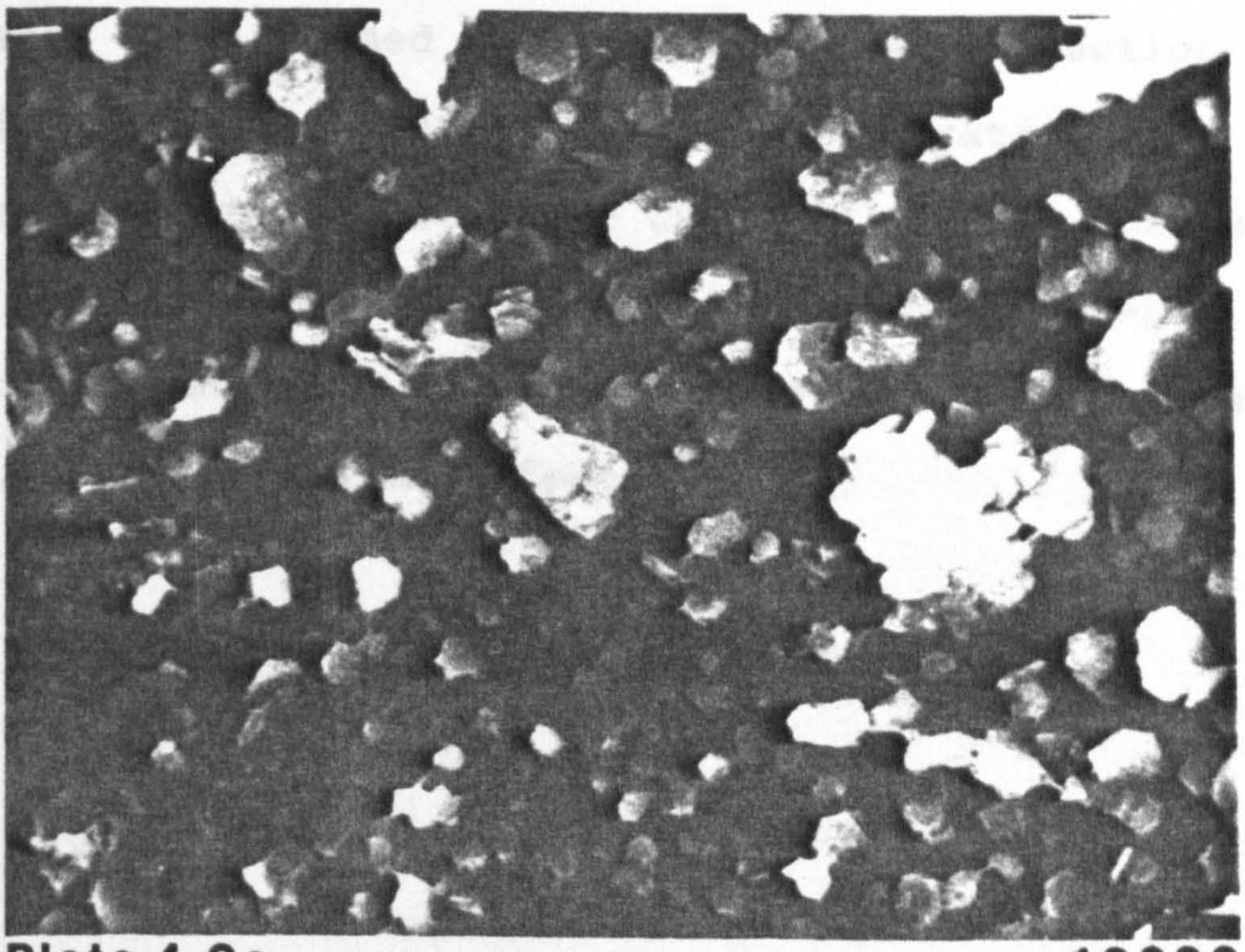

Plate 4.9a x10600

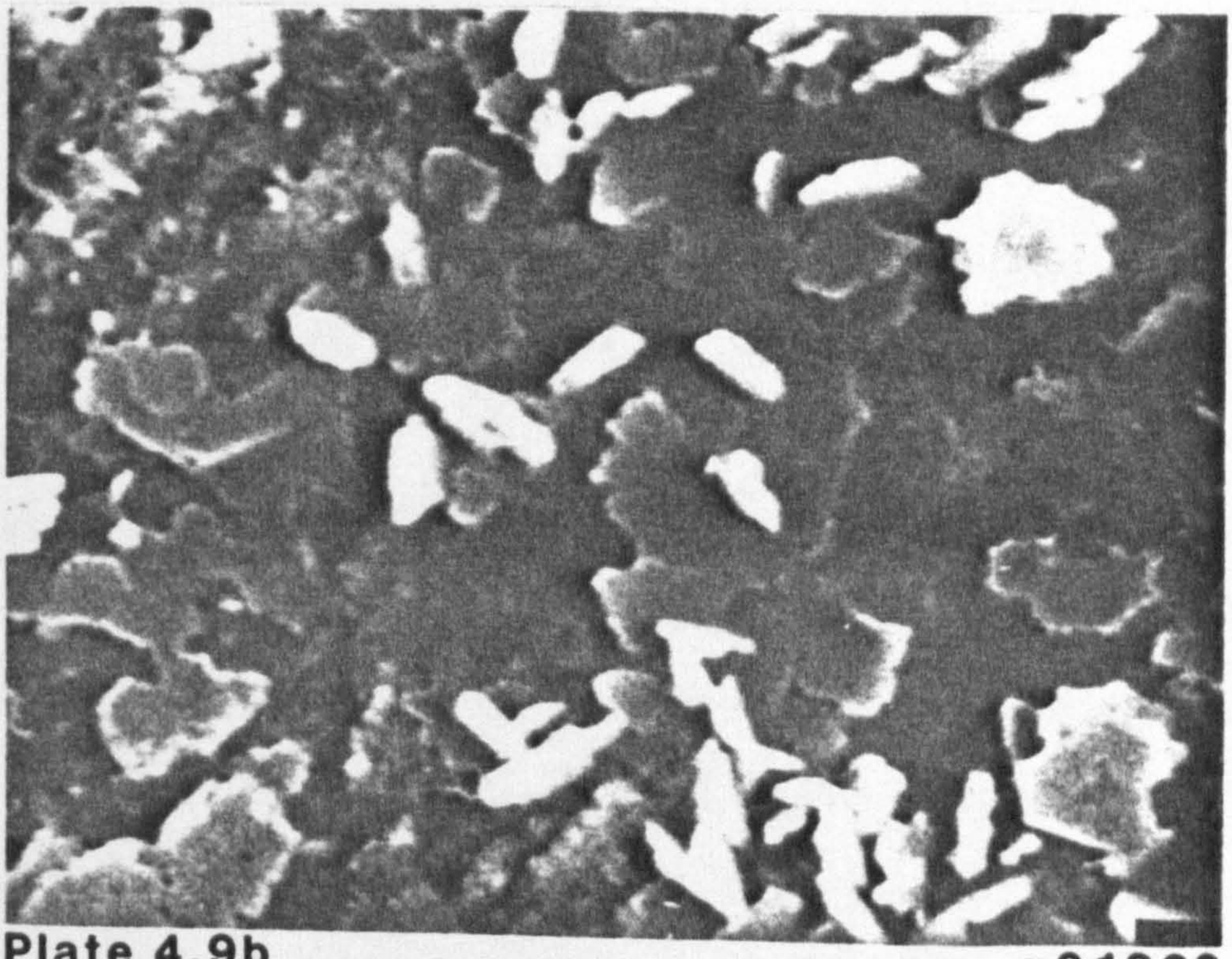

Plate 4.9b x31800

The possible influence of hydrogen bubbles upon d.l.c. measurements is minimised by both the forced convection at the surface (by rotation), and by the long integration time used for d.l.c. measurements of 100s [see CH 2.8.2]. Some influence may still be exerted on d.l.c. values if, on changing deposition overpotential, the size of the hydrogen bubbles is changed, thus altering the surface area affected.

CH 5 DEPOSITION FROM ACIDIC SOLUTIONS OF CADMIUM SULPHATE

Studies of cadmium deposition in alkaline electrolytes are somewhat limited by the solubility of the cadmium salts, requiring deposition times that are necessarily long. In KOH solutions, this solubility increases with concentration and temperature, with a solubility for cadmium hydroxide of 3.5 x 10^{-4}M in 10.00M KOH[6]. However, there is no such limitation with $CdSO_4$ solutions (saturation point at 25^{o}C is 0.38M[182]), enabling deposition studies of more macroscopic dendrite growth at considerably shorter timescales. Deposition from acidic solution enables a further estimation of the real and theoretical growth (and induction) times, thus comparisons with the alkaline morphology can be made.

5.1 EXPERIMENTAL

All experiments in this chapter, used the standard rotating disc cell and assembly described in CH 2.1.1 and 2.4.1, with polished or etched cadmium rotating disc electrodes. Electrode preparation was as in CH 2.2.6.3. For the a.c. impedance work presented in this chapter, electrodes were pre-subjected to a 0.01Hz,±5mV peak-peak a.c. signal from the frequency response analyser [see CH 2.4.4]. This low frequency signal was to electropolish the electrode and was applied for ~1 hour, before the electrode was used. The effect of the signal is to subject the electrode to alternate low overpotential dissolution and deposition. During this period the a.c. impedance at this frequency was monitored, the values decreasing towards a steady

state value after about 1 hour. Without this electropolishing, the a.c. impedance spectra were subject to considerable drift in both the real and imaginary values at low frequencies (< ~0.2Hz). Optically, the electrode retains a lightly etched appearance after the electropolishing. To observe the effect low frequency cycling has on electrodes, a series of experiments were carried out on both unpolished and mechanically polished electrodes. An extended period of low frequency cycling of 2 - 3 hours, resulted in the mechanically polished electrodes taking on the appearance of the lightly etched electrodes. This surface change is presumably caused by the removal or redistribution of any amorphous surface layer on the electrode [see CH 3.5]. Chemical etching is seen to increase the stability of the electrode to low frequency cycling and to thus reduce the electropolishing time required. It should be noted that although cadmium has a low dissolution rate in sulphuric acid (0.5M), an extended period (24+ hours) of exposure will result in a mechanically polished electrode taking on a lightly etched appearance. Care has also to be exercised, with the cadmium wire reference electrodes [see CH 2.2.1.3], to ensure that any additional cadmium dissolution in the reference electrode compartment, does not change the concentrations in the main cell body.

Electrolyte solutions were prepared as in CH 2.3.3. A.c. impedance experiments were carried out at a standard rotation rate of 5 revs/s, unless otherwise stated.

5.2 DEPOSITION FROM 0.1M CADMIUM SULPHATE IN 0.5M SULPHURIC ACID

5.2.1 DEPENDENCE ON OVERPOTENTIAL

Deposition was observed in degassed 0.1M $CdSO_4$ + 0.5M H_2SO_4 at η = -30, -50, -80 and -100mV, with respect to the reversible potential for;

$$Cd \rightleftharpoons Cd^{2+} + 2e^-$$

The reference electrode was a cadmium wire in the same electrolyte [see CH 2.3.3]. Three current/time transients are shown in fig 5.1. D.l.c./time transients are not shown, owing to the difficulty of observing such a fast reaction on a stationary electrode by a.c. impedance. Observation of fig 5.1, shows that at high potentials (η > -50mV), the current rises rapidly, indicating rapid dendritic growth; whereas lower potentials (η = -30mV), show a flat i/t response, indicating a relatively flat deposit. From the i/t transients, one can predict approximate induction times for dendrite growth of 150s at η = -100mV and 400s at η = -80mV. This compares to induction times of the order 1000 x larger for the alkaline systems in the absence of suspension [see CH 3.6]. The indicated induction times obtained from the i/t curves are in good agreement with optical observations of the electrode state during deposition. Dendritic growth rapidly becomes visible to the naked eye within a couple of minutes at η = -100mV. This points towards a value of η_c = -65 ± 15mV, for the critical overpotential for dendrite growth onto polished electrodes in this system. However, deposition using roughened electrodes (prepared by abrasion with

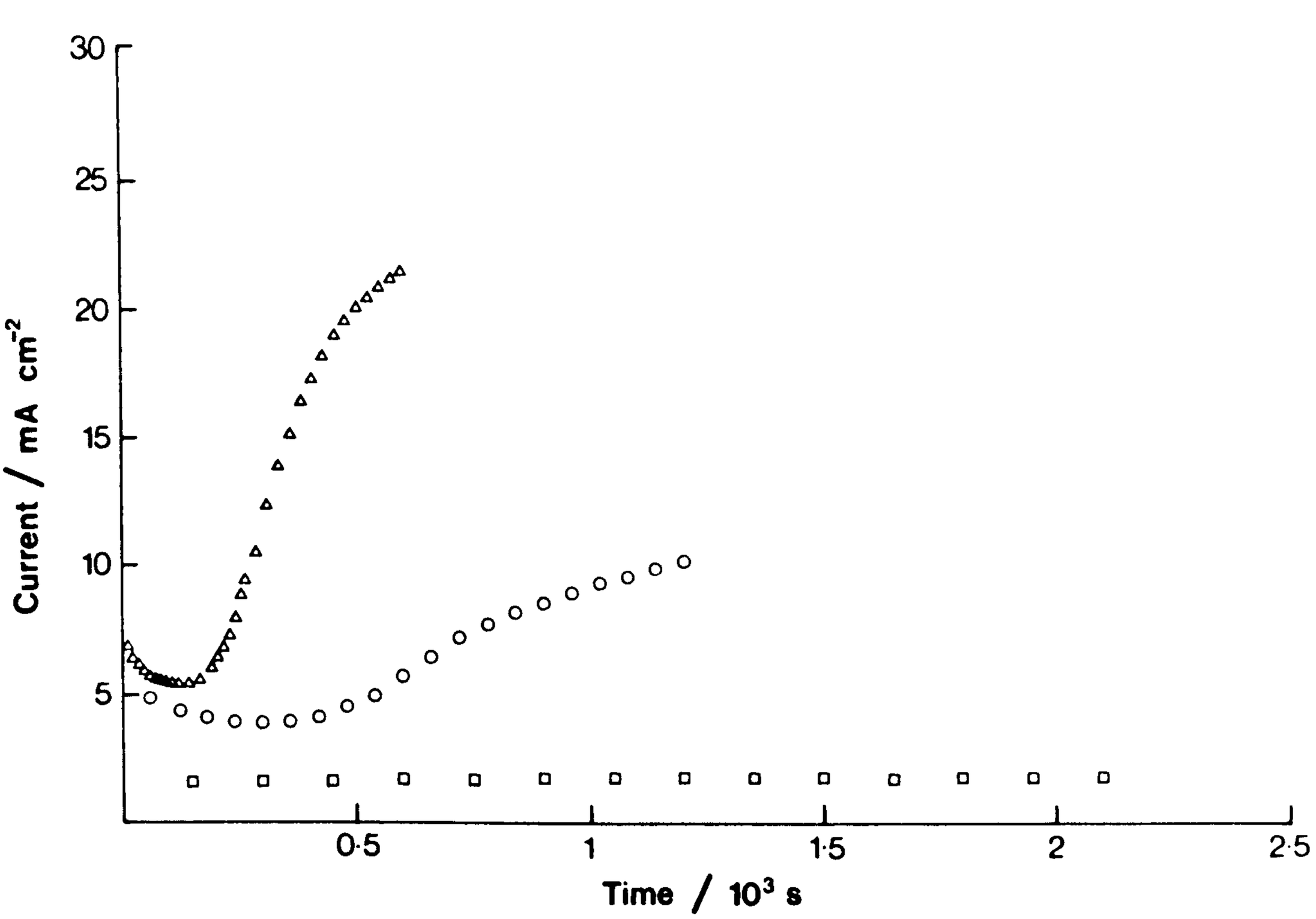

Fig 5.1 Dependence of current on time for deposition from 0.5M H_2SO_4 + 0.1M $CdSO_4$ onto polished cadmium discs. (△) -100mV; (○) -80mV; (□) -30mV overpotentials.

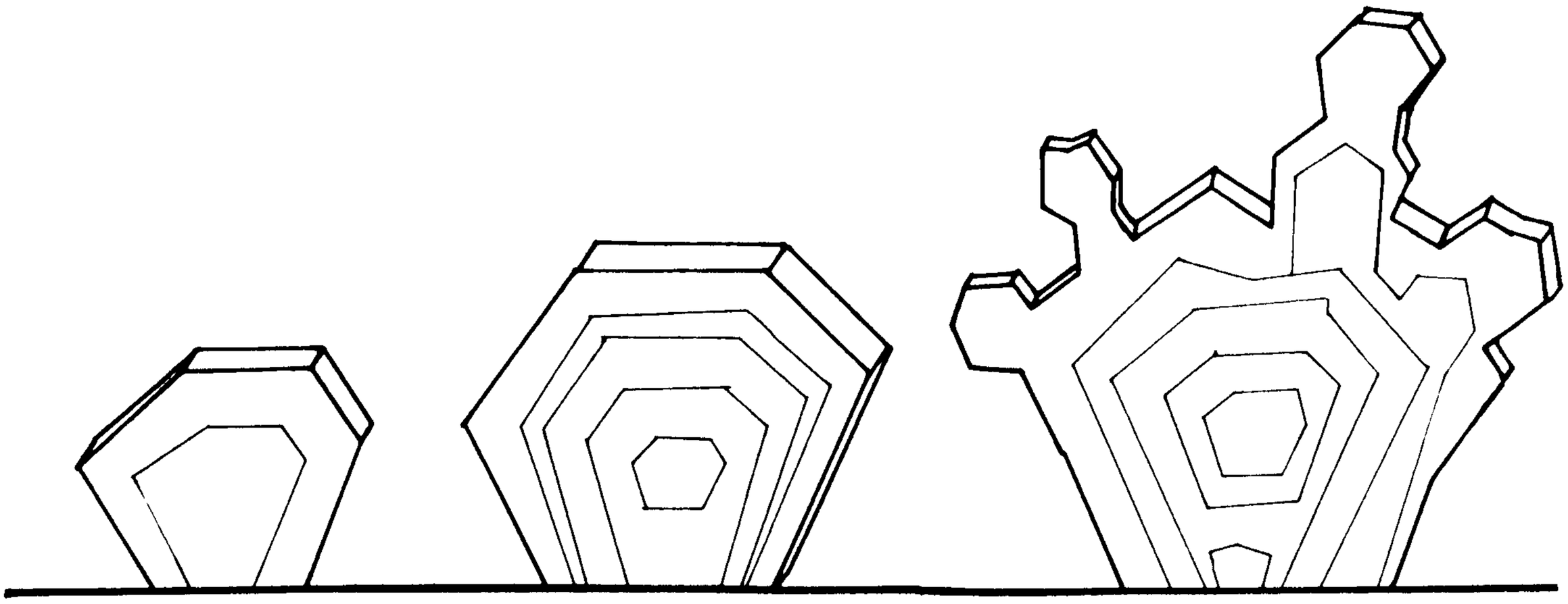

Fig 5.2 Pictorial mechanism of the initial stages of dendritic growth out from a favourably orientated surface crystallite.

240 grit Emery paper), has shown dendrite growth can be initiated from surface abnormalities at η = -50 and -30mV. Additionally, dendrites grown at η = -80mV, continue to grow at η = -30mV. These factors point towards a true critical potential of η < -30mV for rough electrodes, and indicate that the dendrite initiation time is highly dependent on the electrode state, with initiation times being dramatically reduced for roughened electrodes. This is in direct contrast to the apparent independence observed in alkaline systems [see CH 3.4.3.1].

Examination of polished electrode surfaces after deposition showed substantial dendritic growth at both η = -100 and -80mV, but at lower overpotentials, no evidence was seen under optical observation. At η = -100mV, dendrites 1 x 8 mm long can be grown after 1 hour of deposition. Deposition is favoured towards the edge of the stationary electrodes, due to the limitation of the linear diffusion region. This effect becomes greater as the dendrites grow further out from the electrode, but is not found on rotating electrodes, due to the forced convection.

Scanning electron microscopy of electrodes taken after different deposition times, revealed details of the deposition morphology at different stages of the deposition. The morphology found at η = -30, -50, -80 and -100mV, is as follows;

a) η = -30mV. Deposition in the absence of surface irregularities is largely grainy in nature, though giving an incomplete coverage of the surface (contrast with the alkaline deposition case in CH 3.6). Grain size is very variable (see plate 5.1a), and is dependent on the time of deposition. Grain

Plate 5.1 Deposition morphology found on etched cadmium electrodes at -30mV overpotential, in 0.1M $CdSO_4$ + 0.5M H_2SO_4. (a) 40 minutes deposition; (b) 5 minutes deposition (edge of electrode).

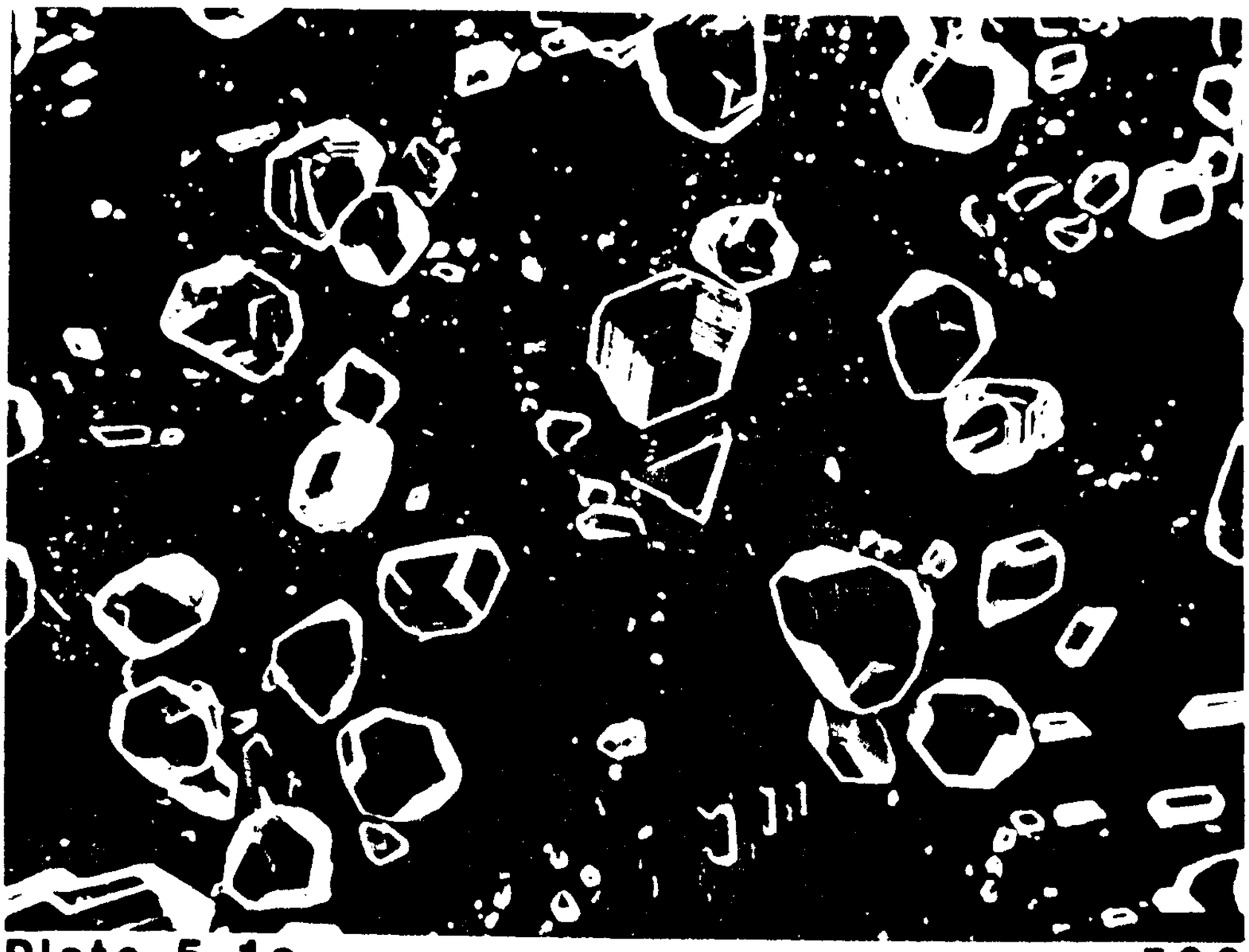

Plate 5.1a x500

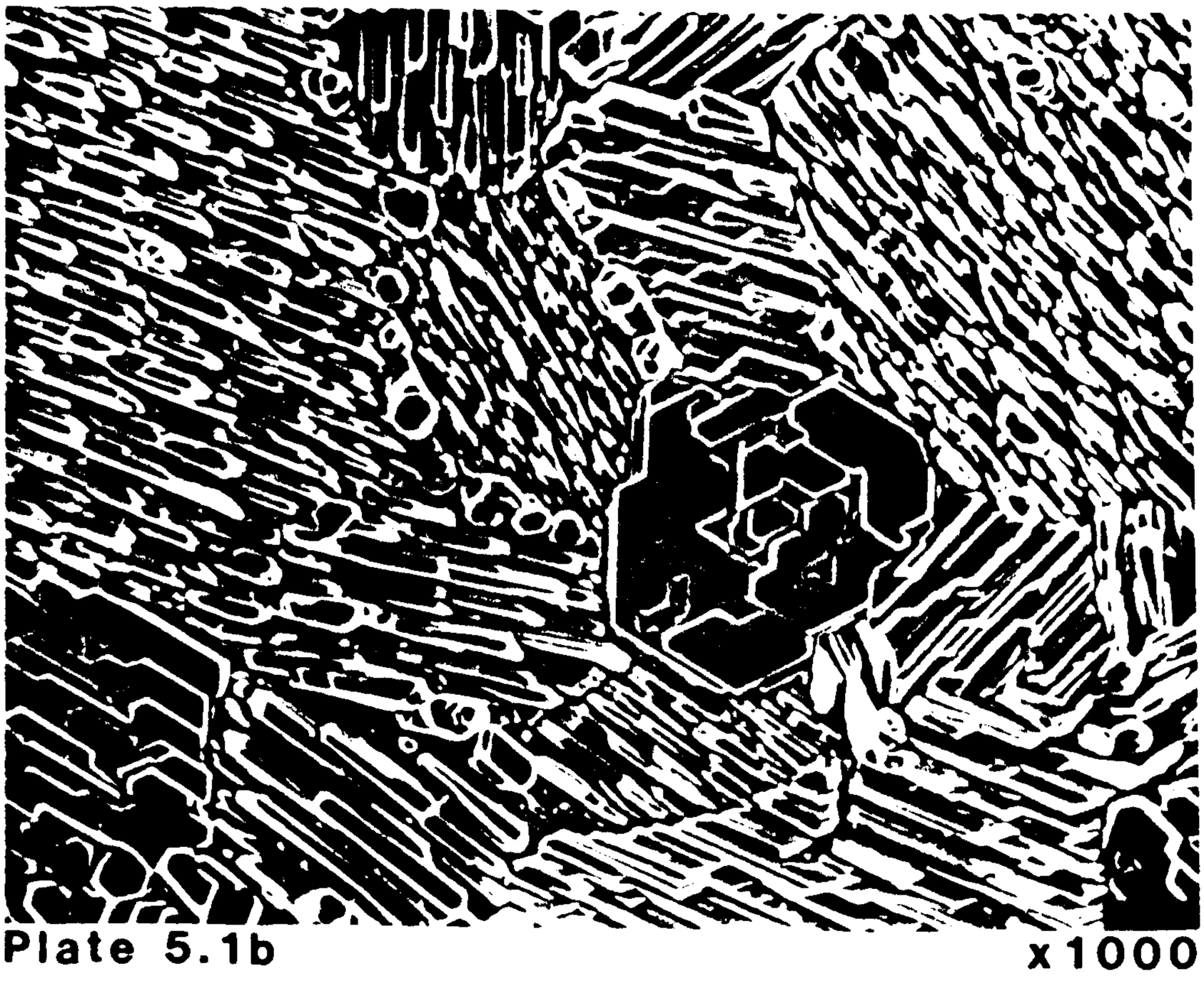

Plate 5.1b x1000

size ranges from 1 - 40μm after 10 minutes of deposition. Over shorter timescales, the deposit is aligned with the underlying crystalline domains, as shown in plate 5.1b.

b) η = -50mV. Deposit morphology is similar to that at η = -30mV, but more rapid. Plate 5.2a, shows a grainy deposit partially aligned with the underlying crystalline domains. Plate 5.2b, shows the surface of a roughened electrode after deposition for 10 minutes at η = -50mV. Here, dendritic growth is found against a largely grainy background deposit. The average grain size is 6μm.

c) η = -80mV. At this potential, deposition is grainy with dendrites developing after ~250s, giving a morphology exactly as for η = -100mV, except for the longer timescales.

d) η = -100mV. Deposition is initially grainy with dendrites developing within 60s. After 1 minute of deposition (see plates 5.3a/b), the surface deposit largely consists of grainy cadmium (grain size average 4μm), with the same small fern-shaped dendrites found at differing stages of development (up to 25μm long). It is clear from this, that dendritic growth in this system is initiated from favourably orientated crystallites. The pictorial mechanism of initiation is shown in fig 5.2. After 10 minutes of deposition, dendrites of up to 600μm in length are to be found (plates 5.4a/c). These dendrites show a change in morphology away from the fine structure as found in plates 5.3 and 5.4b, to a considerably thickened dendritic deposit. This is doubtless due to flat deposition occurring onto the large dendrite side surfaces, due to the establishment of a linear diffusion layer out from this surface. In this case, the dendrite dimensions are considerably larger than the

Plate 5.2 Deposition morphology found on etched cadmium electrodes at -50mV overpotential, in 0.1M $CdSO_4$ + 0.5M H_2SO_4. Plate (a) 10 minutes deposition; (b) 5 minutes deposition onto a roughened electrode surface.

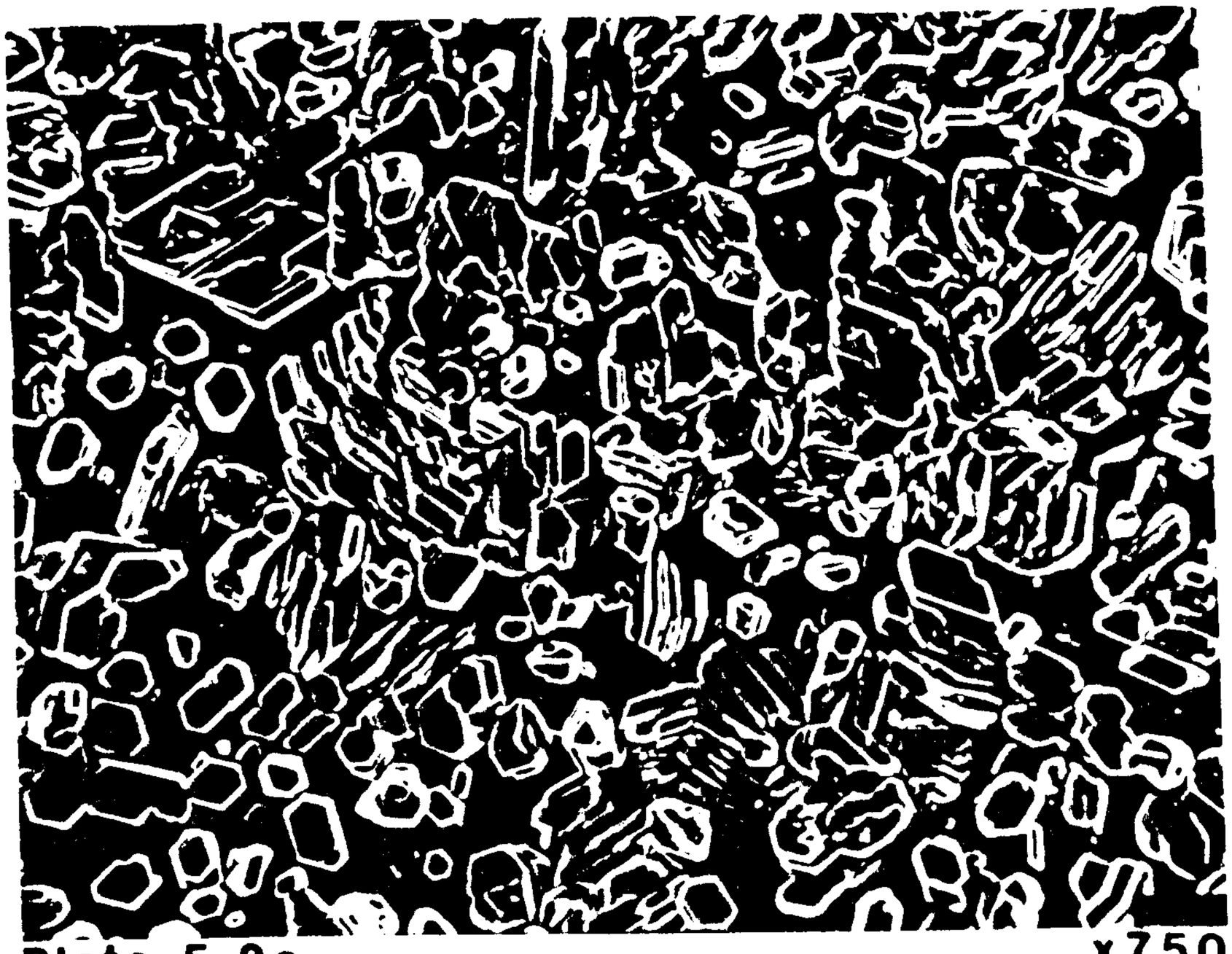

Plate 5.2a x750

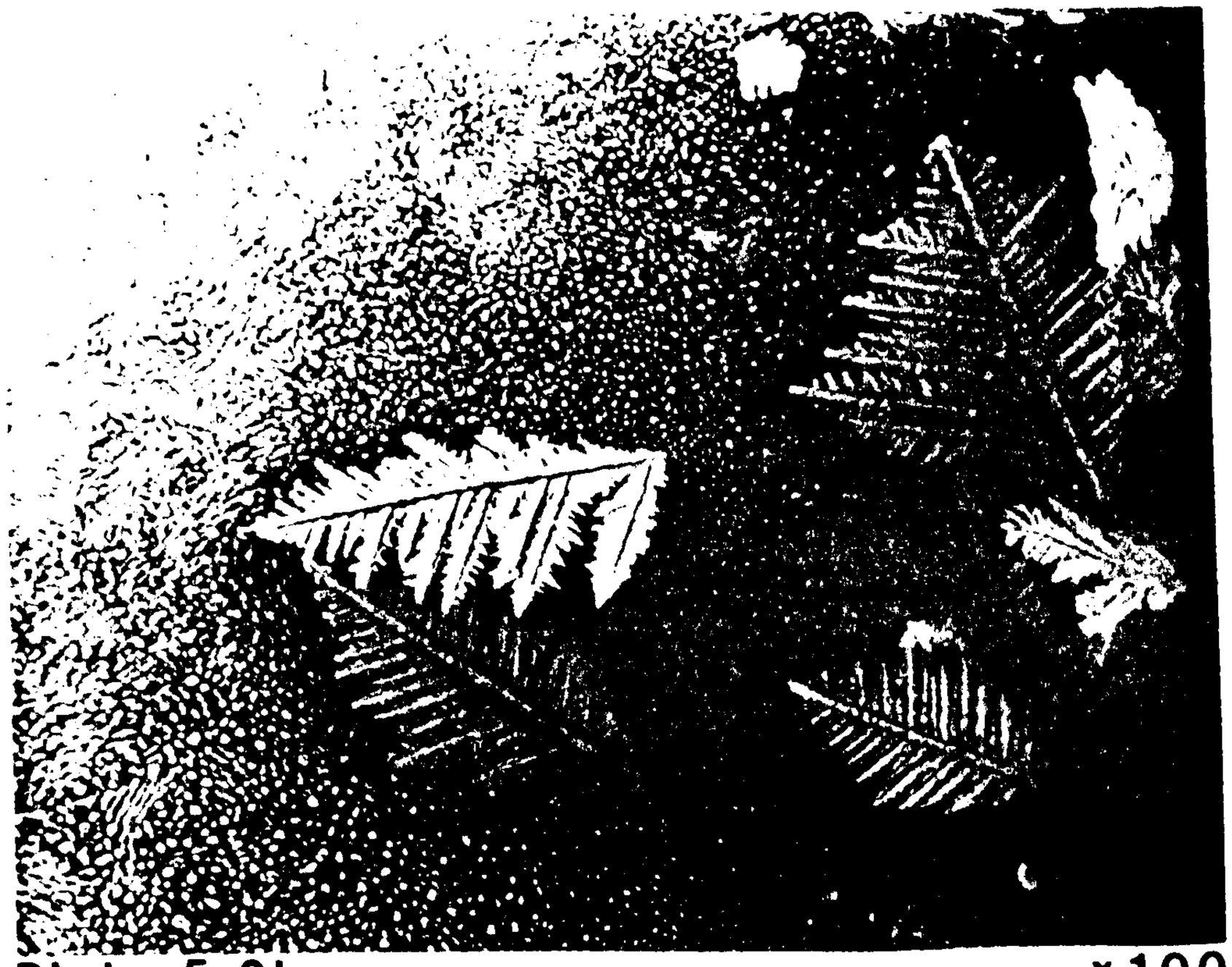

Plate 5.2b x100

Plate 5.3 Deposition morphology found on etched cadmium electrodes after 1 minute at -100mV overpotential, in 0.1M $CdSO_4$ + 0.5M H_2SO_4.

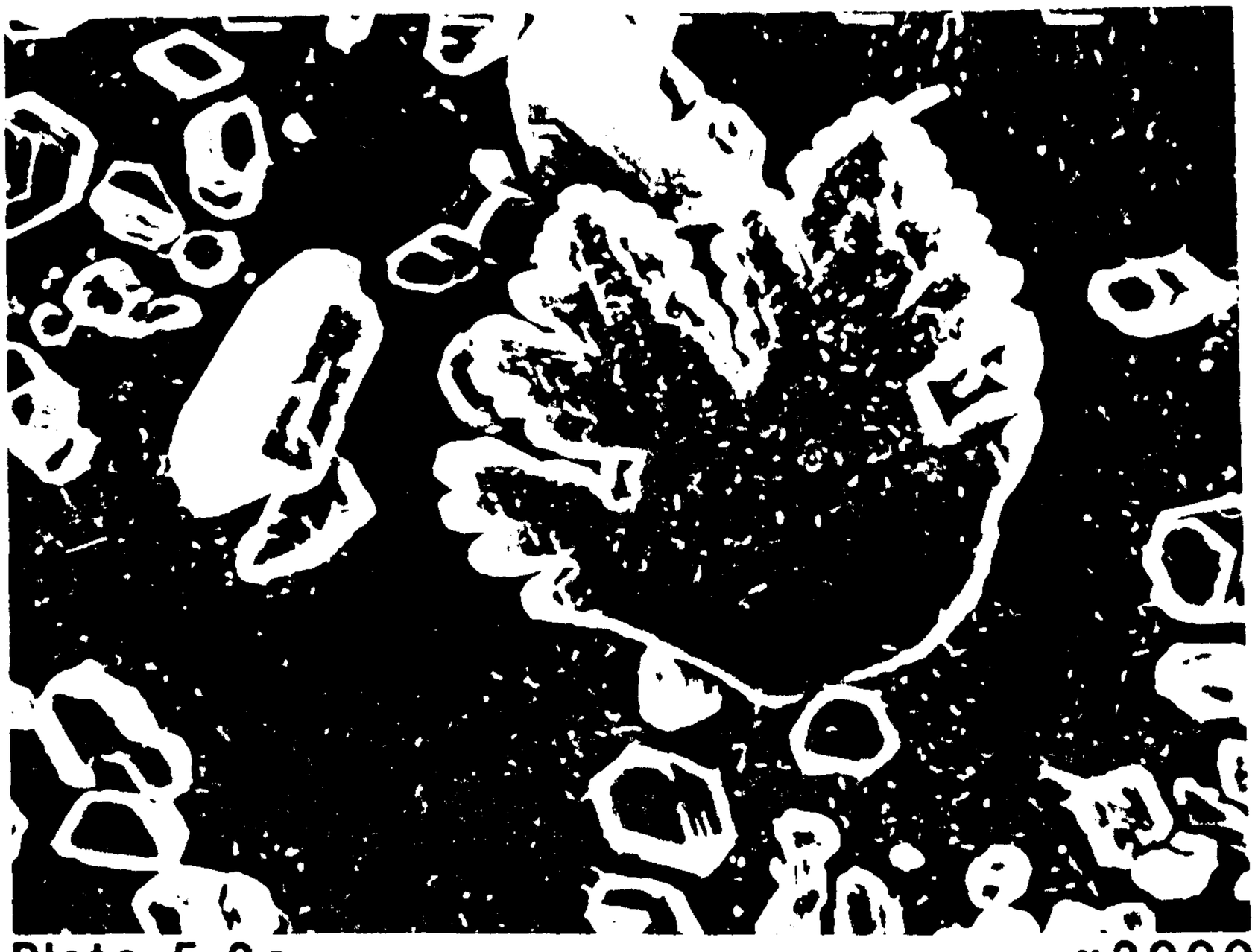

Plate 5.3a x2000

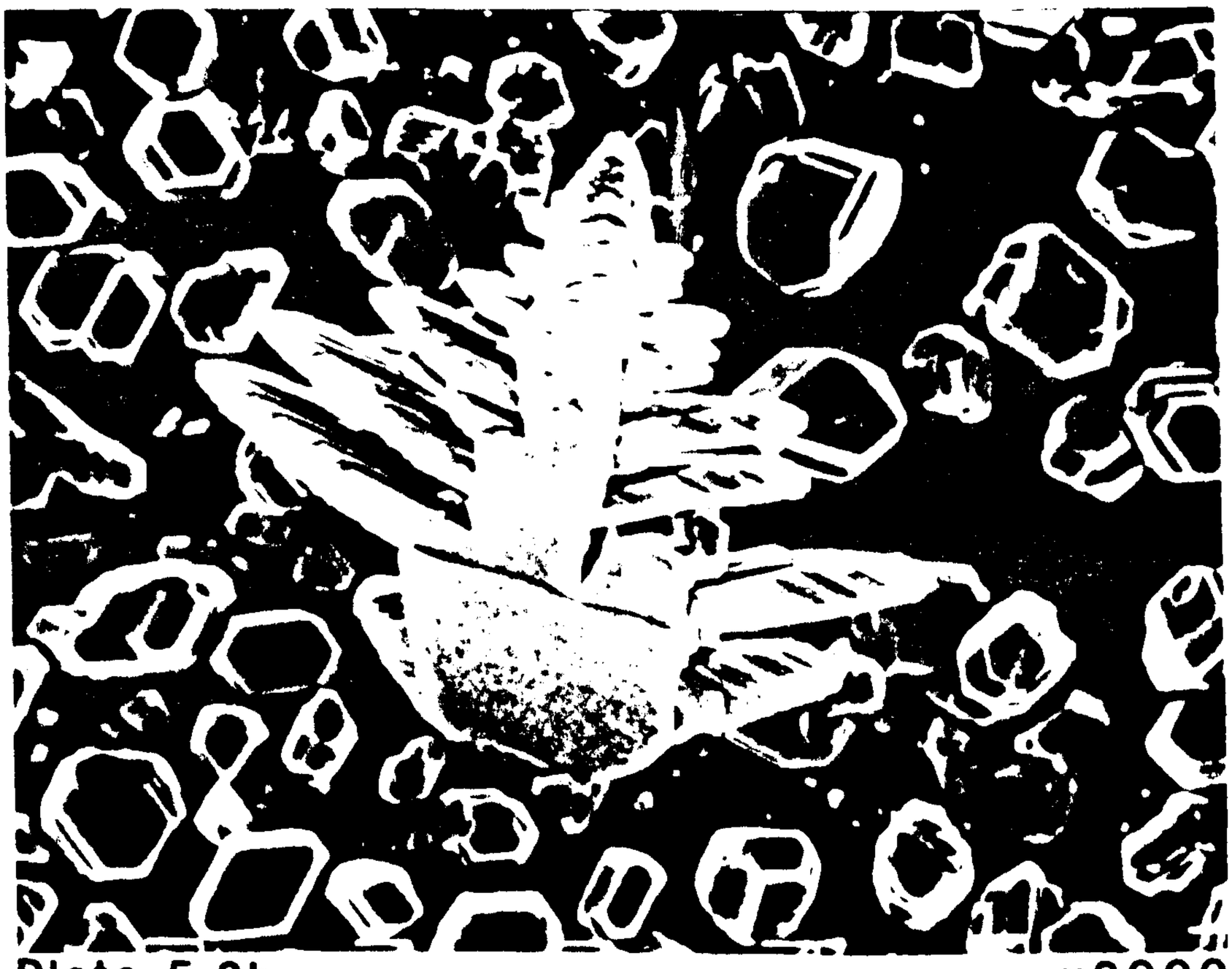

Plate 5.3b x2000

Plate 5.4 Deposition morphology found on etched cadmium electrodes after 10 minutes at -100mV overpotential, in 0.1M $CdSO_4$ + 0.5M H_2SO_4.

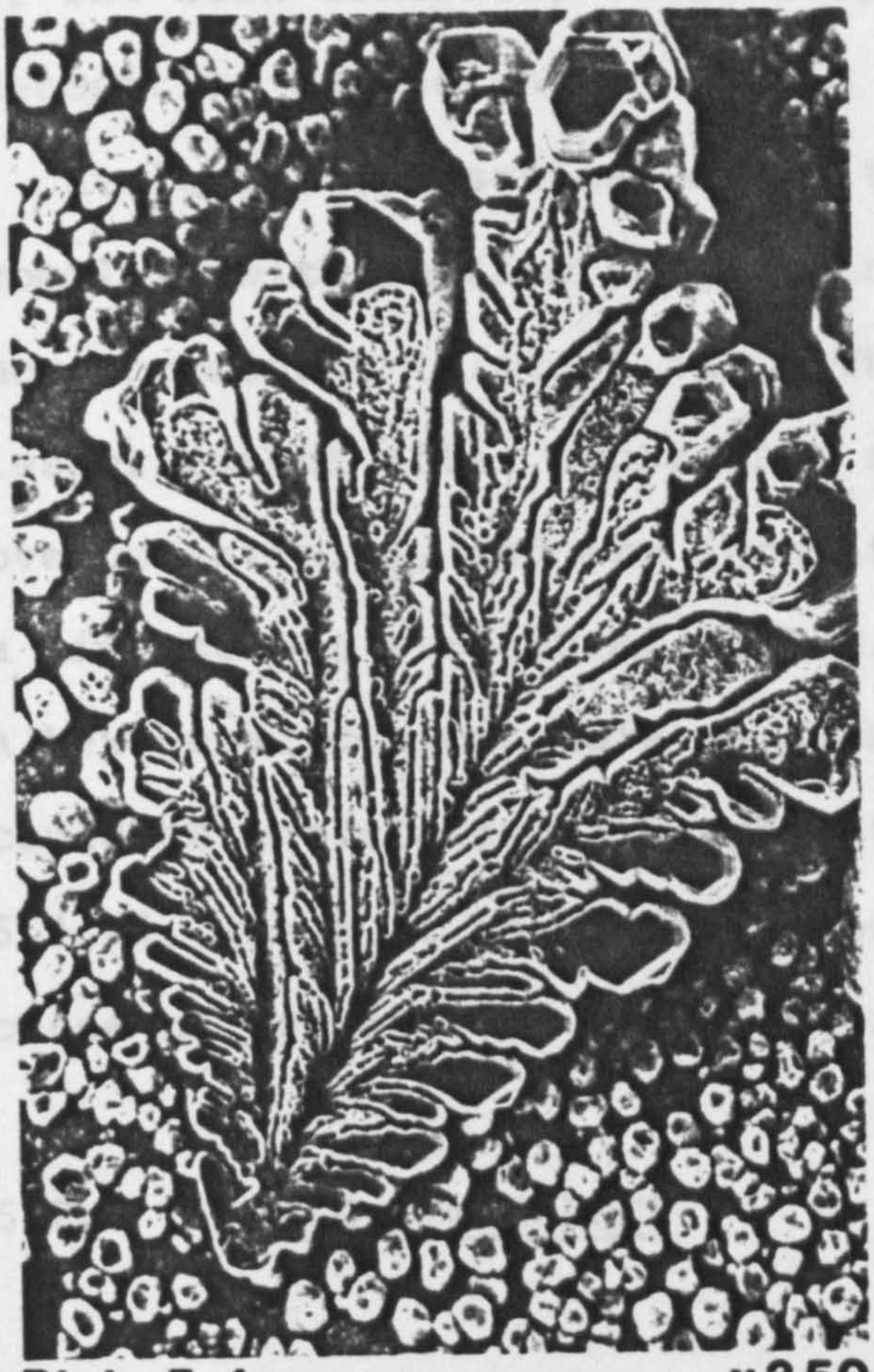

Plate 5.4a x350

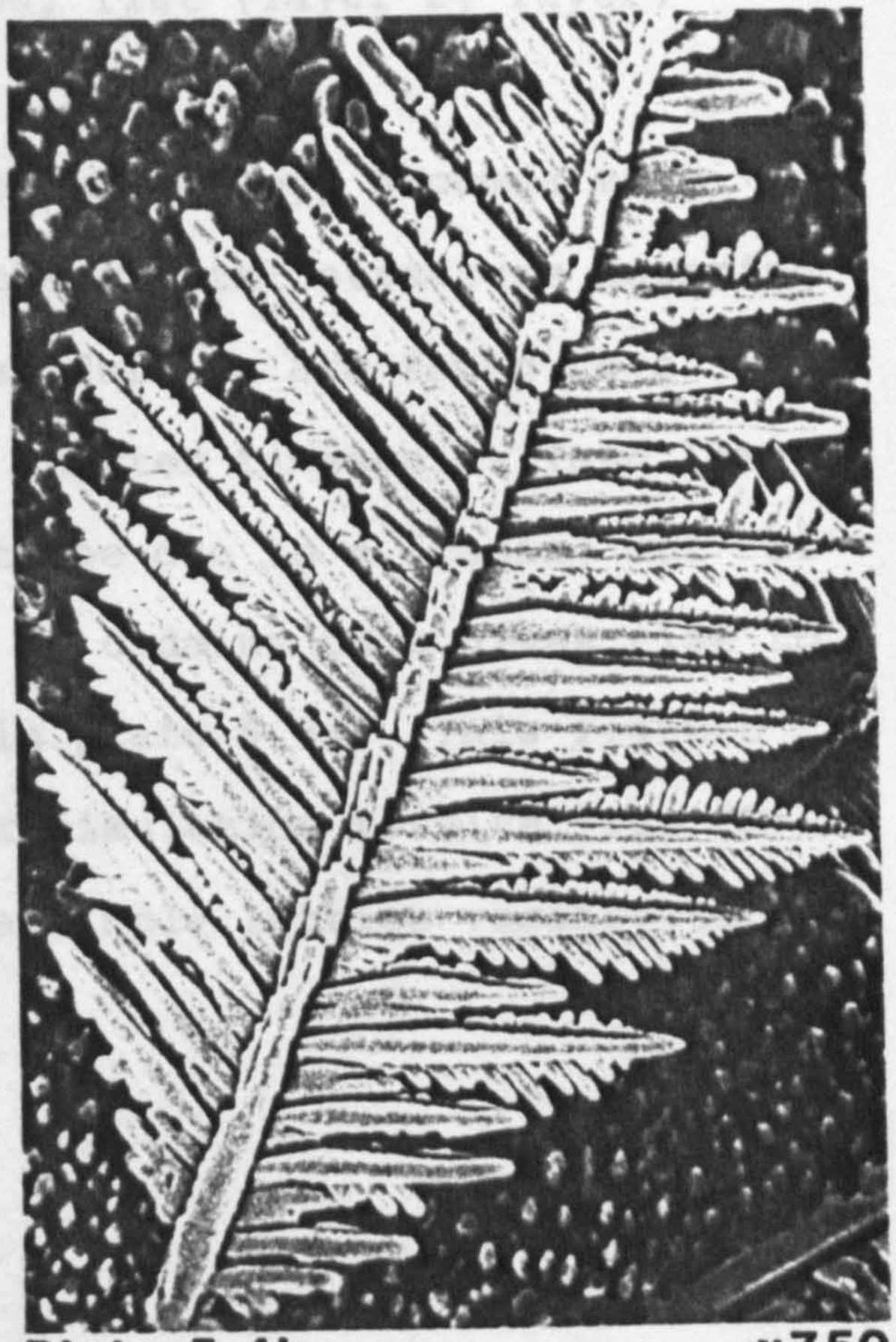

Plate 5.4b x750

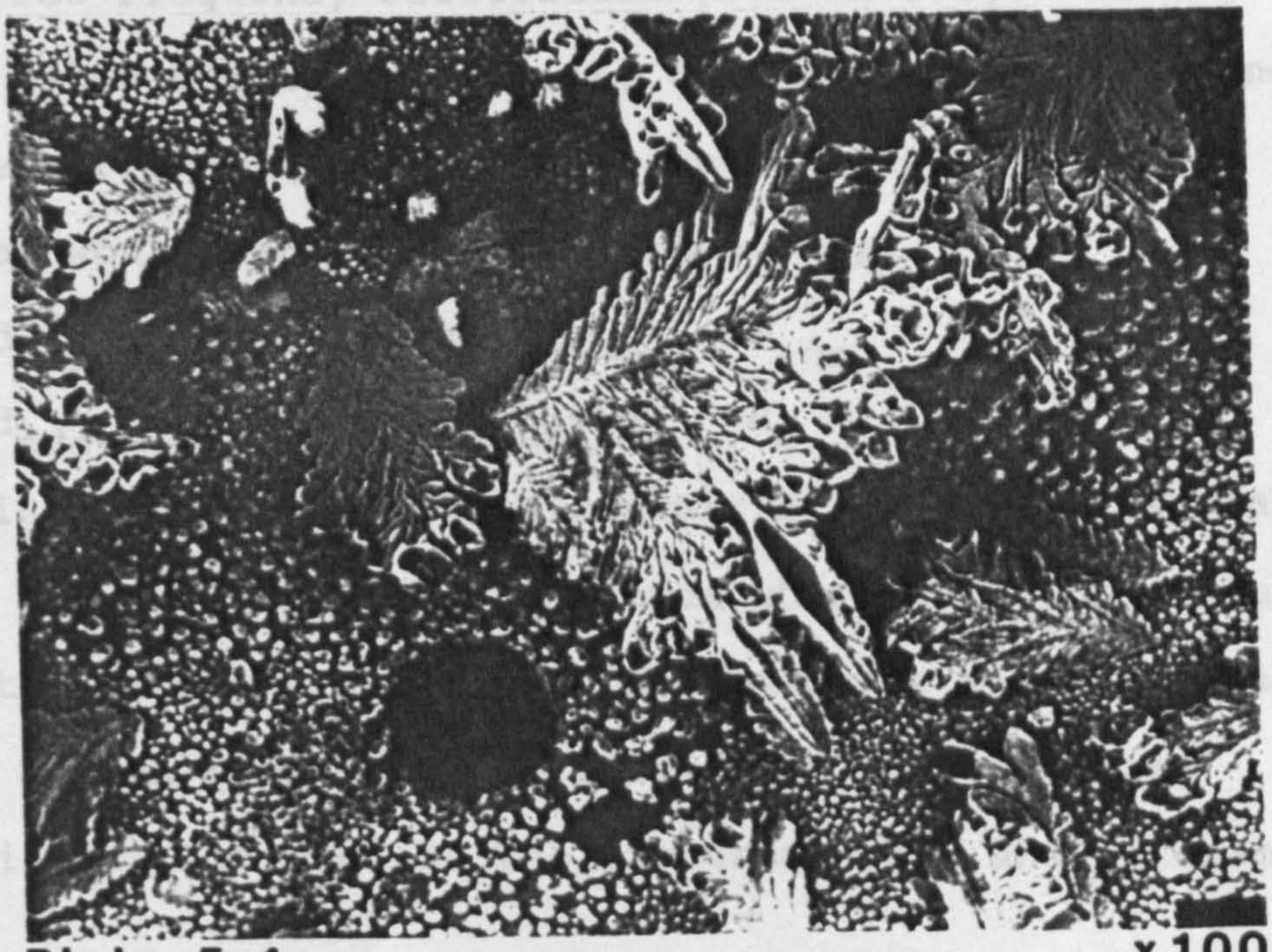

Plate 5.4c x100

Nernst diffusion layer thickness. Plate 5.5b, displays the tip of one such dendrite, where stepped, flat (layer by layer) deposition can be seen.

At longer timescales, deposition morphology becomes very complex, with surface defects in the crystal structure becoming more prominent (plate 5.5a). These defects are found to a lesser extent after deposition at shorter timescales (and lower overpotentials), and are thought to be due to a 'coning out' of a microscopic structural defect. In cadmium this gives rise to a hexagonal conical hole as seen in plate 5.5a. This feature could be anticipated from computer simulation results [see CH 6.4.6], where it is possible for a simple lattice vacancy to cause hexagonal cone propagation.

5.2.2 A.C. IMPEDANCE

A.c. impedance measurements for this system were taken at the equilibrium rest potential, after stabilisation of the electrode state by low frequency oscillation [see CH 5.1]. Measurements were not taken during deposition, due to the rapidly changing electrode surface morphology. In the acidic system the deposition would be expected to proceed by;

$$Cd^{2+}_{aq} \xrightarrow{\text{charge transfer}} Cd_{ads}$$

$$Cd_{ads} \xrightarrow{\text{surface diffusion}} Cd_{s}$$

giving rise to the equivalent circuit for the a.c. impedance shown in fig 5.3. Thus for the case where solution diffusion is important, one might anticipate an impedance spectrum where there is a high frequency deviation from this adsorbed intermediate. The rest of the spectrum would show a response

Plate 5.5 Close-up of dendrite morphology shown in plate 5.4. (a) hexagonal cone defects in the crystal structure; (b) dendrite tip showing stepped deposition (and hexagonal defects).

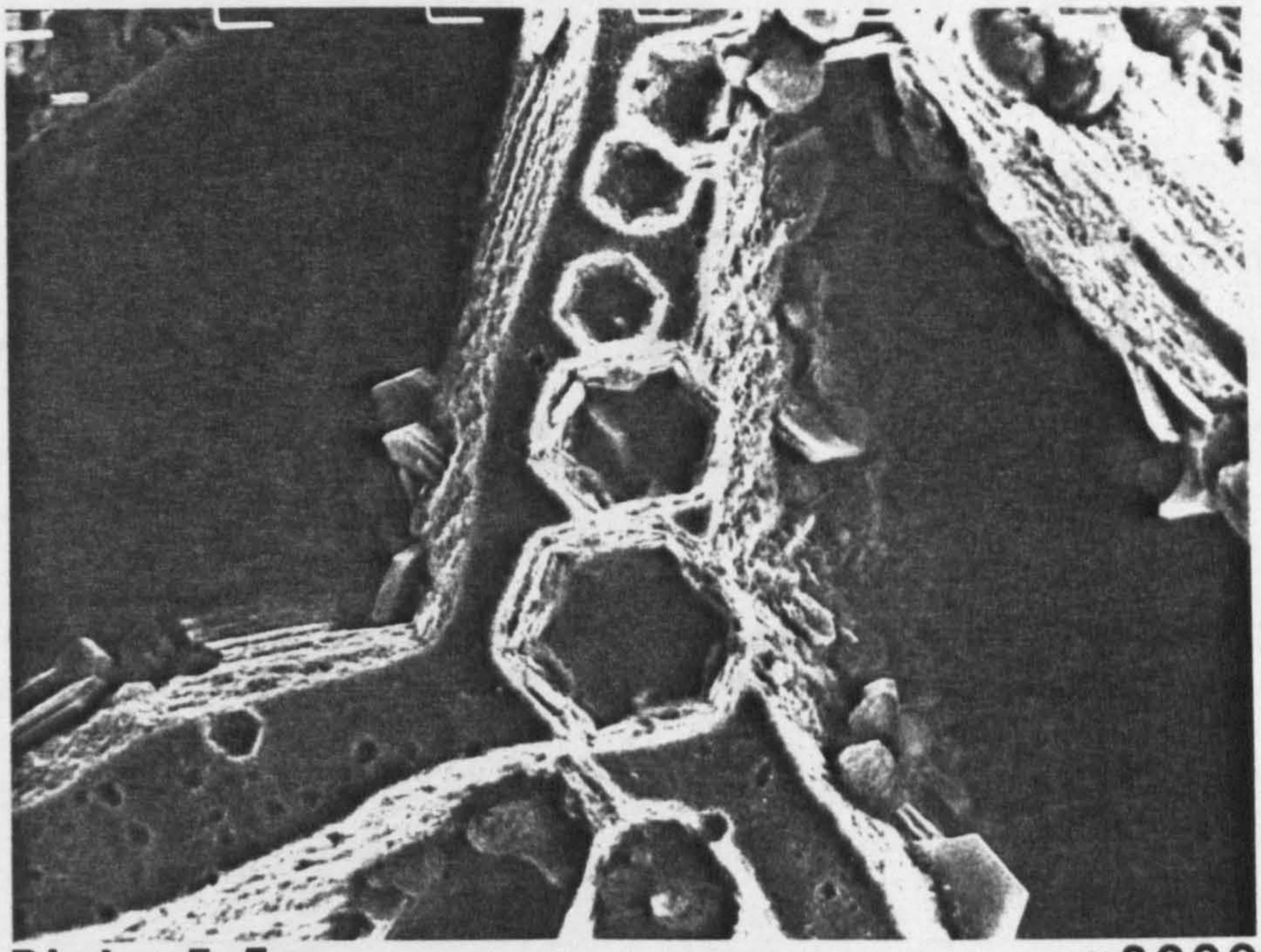

Plate 5.5a x2000

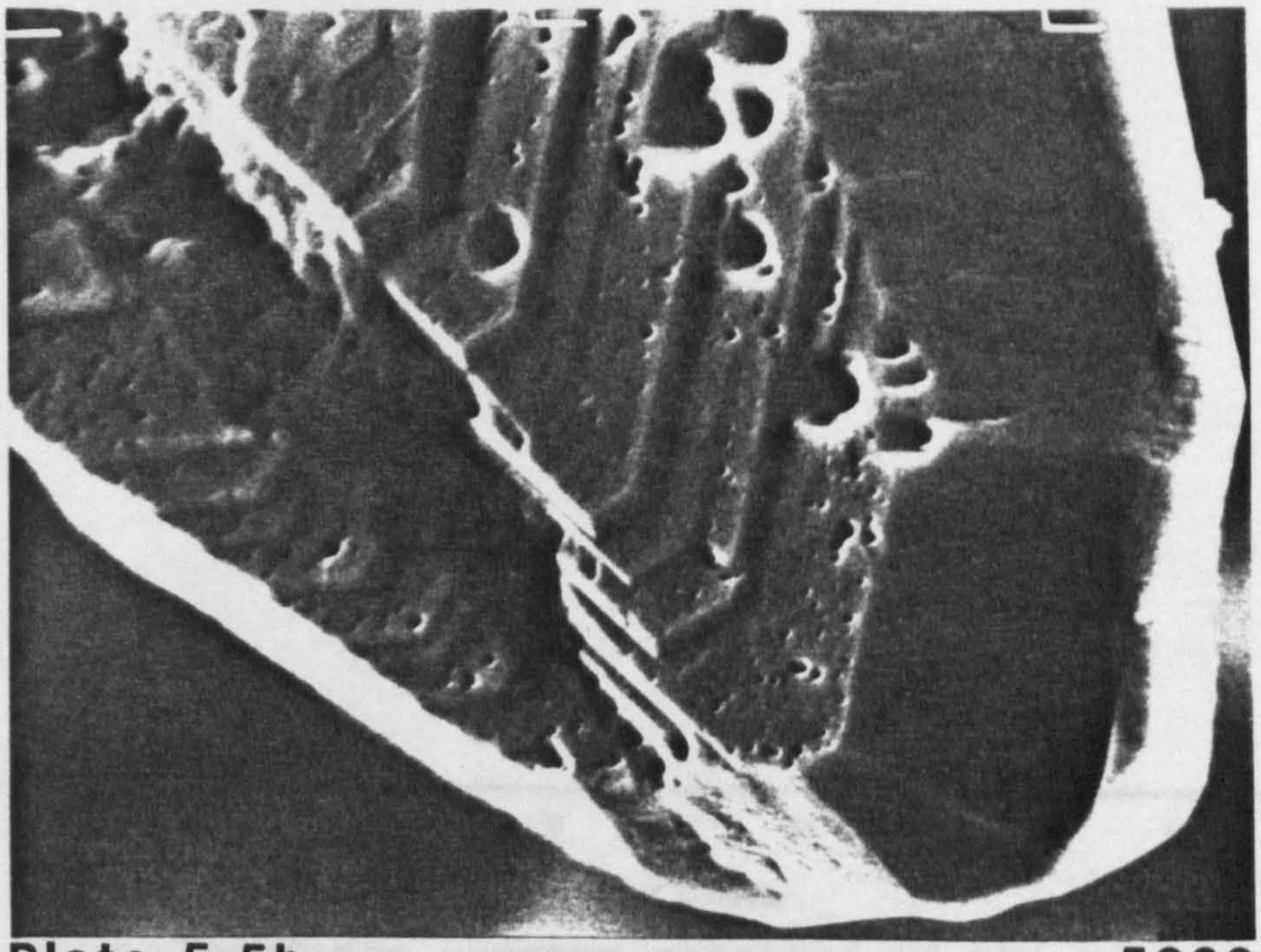

Plate 5.5b x5000

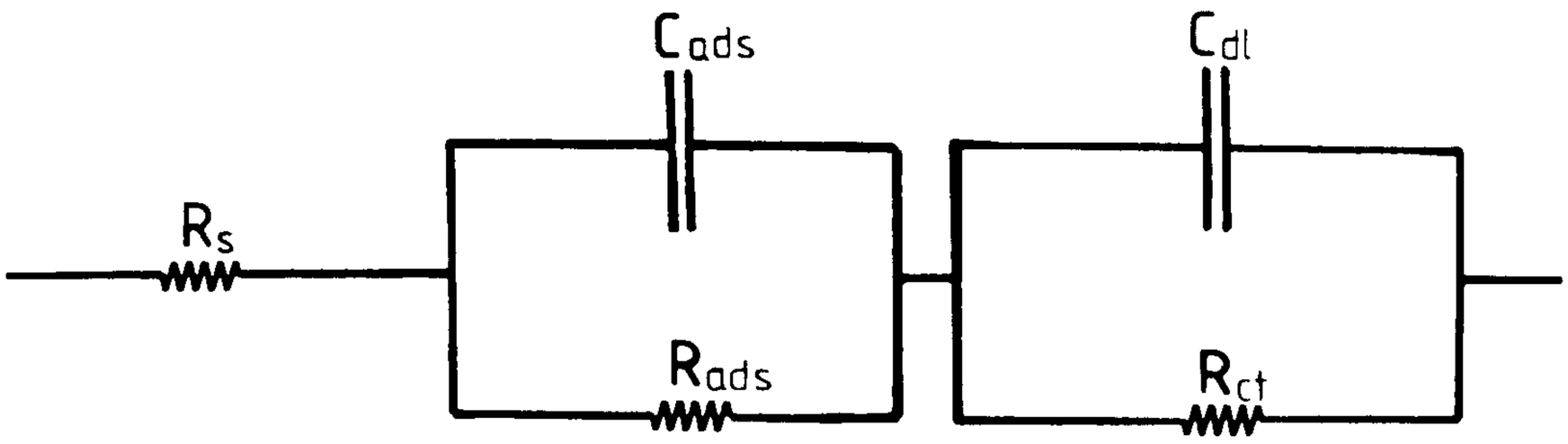

Fig 5.3 Equivalent circuit for a simple electrochemical process involving a surface adsorbed stage.

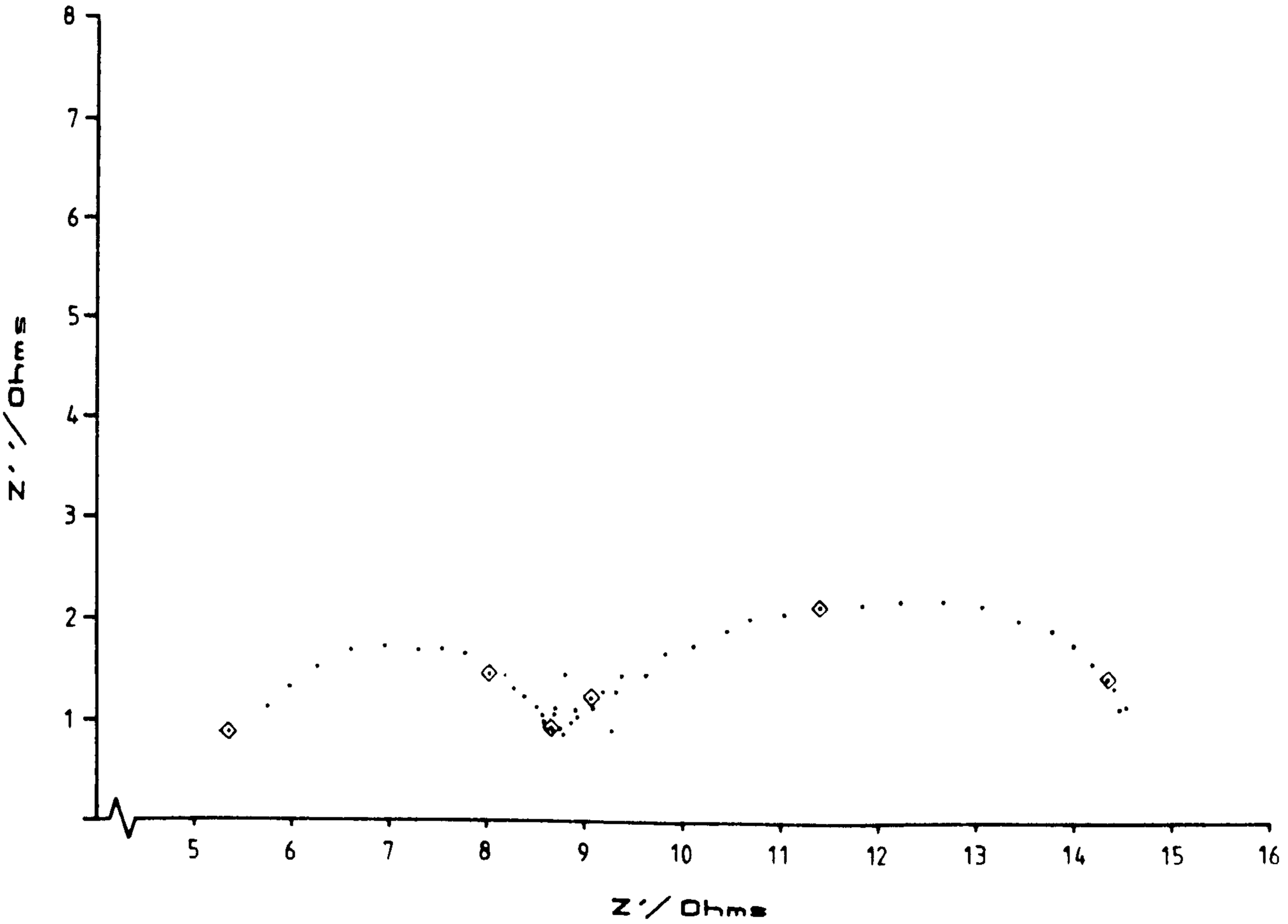

Fig 5.4 A.c. impedance spectra obtained at the rest potential on an etched, rotating (5 rev/s) cadmium disc electrode, in 0.5M H_2SO_4 + 0.1M $CdSO_4$. The frequency sweep was from 10kHz to 0.05Hz.

due to a charge transfer resistance, and a low frequency Warburg impedance dependent on mass transfer [see CH 1.4.7]. Fig 5.4, shows the a.c. impedance spectrum taken at the rest potential (at 5 revs/s), this indicates a charge transfer resistance of $1.4 \pm 0.2\ \Omega cm^2$, with a solution resistance of ~5.2Ω in the cell. From the semicircle maximum for the charge transfer resistance of 3160Hz, the double layer capacity is given by;

$$C_{dl} = 1/R_{ct}\omega = 1/(1.4 \times 3160 \times 2 \times \pi)$$

$$C_{dl} = 36\mu Fcm^{-2}$$

The Warburg impedance at low frequencies can be separated from the charge transfer resistance by its dependence on mass transfer, since at low frequencies;

$$Z_{\omega \to o} \simeq R_{dc} = \frac{\sigma\delta}{\sqrt{D_o/2}} \qquad \text{[see CH 1.4.7]}$$

Thus the impedance is dependent on δ, the Nernst diffusion layer thickness, given by {5.1} for a rotating disc electrode;

$$\delta = 1.61 D_o^{1/3} \nu^{1/6} \omega^{-1/2} \qquad \{5.1\}$$

Hence at low frequencies, the a.c. impedance on a rotating disc electrode is given by;

$$Z = \frac{1.61 D_o^{1/3} \sigma\ \nu^{1/6} \omega^{-1/2}}{\sqrt{D_o/2}} = 2.28 D_o^{-1/6} \sigma\ \nu^{1/6} \omega^{-1/2} \qquad \{5.2\}$$

Figure 5.5, shows how the a.c. impedance changes with different rotation rates for settled electrodes at the rest potential. From these, the Warburg coefficient σ, has been estimated at ~4 $\Omega\ s^{-1/2}$ at 5Hz.

Since;

$$R_{ct} = RT/nFi_o \qquad \{5.3\}$$

we can obtain a value for the exchange current density of $9.0 \times 10^{-3}\mu Acm^{-2}$ for the deposition reaction in 0.1M $CdSO_4$ + 0.5M H_2SO_4.

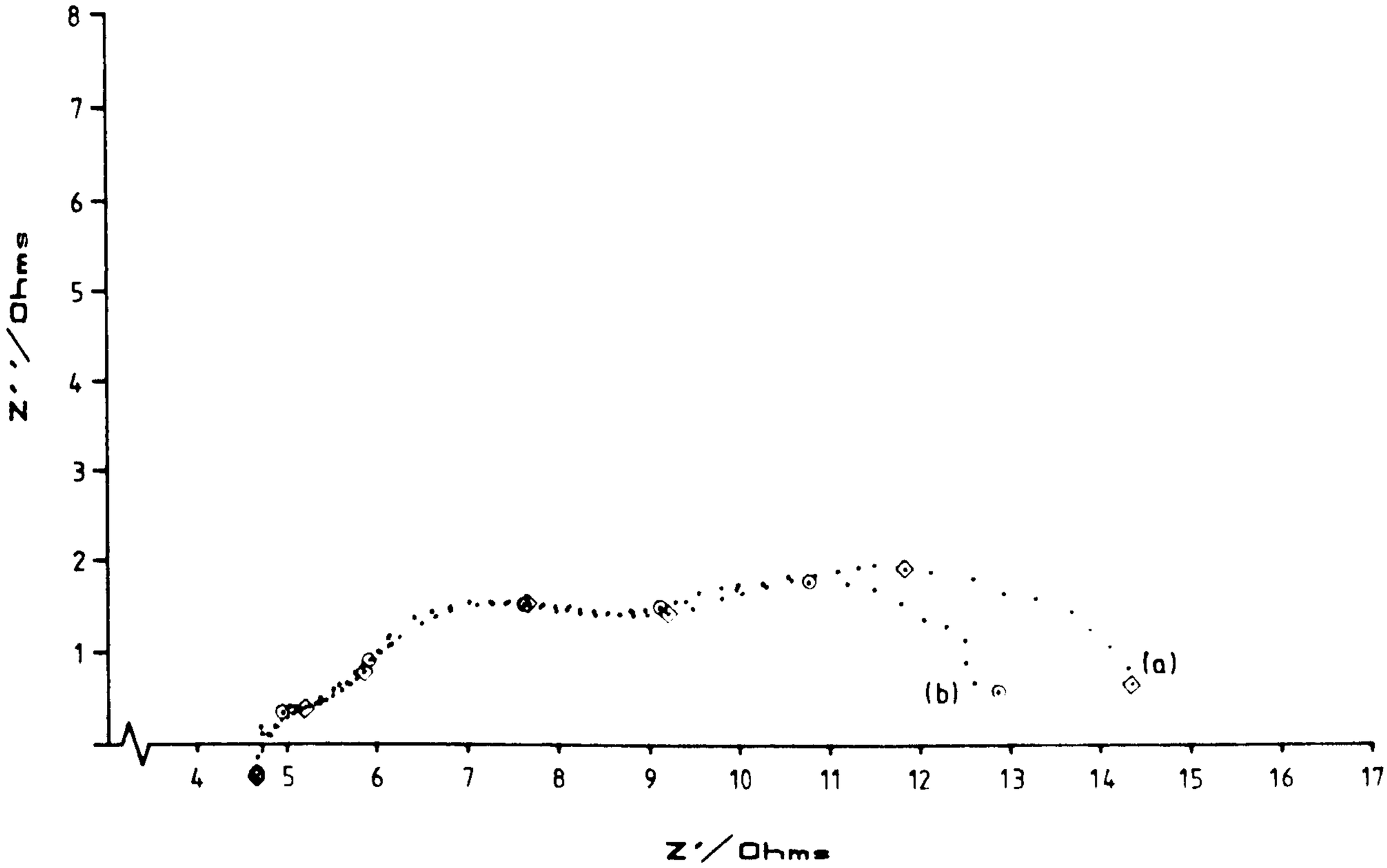

Fig 5.5 A.c. impedance spectra obtained at the rest potential on an etched cadmium disc electrode, in 0.5M H_2SO_4 + 0.1M $CdSO_4$. (a) 2 rev/s rotation rate; (b) 20 rev/s rotation rate. In both spectra the frequency range was 10kHz to 0.01Hz.

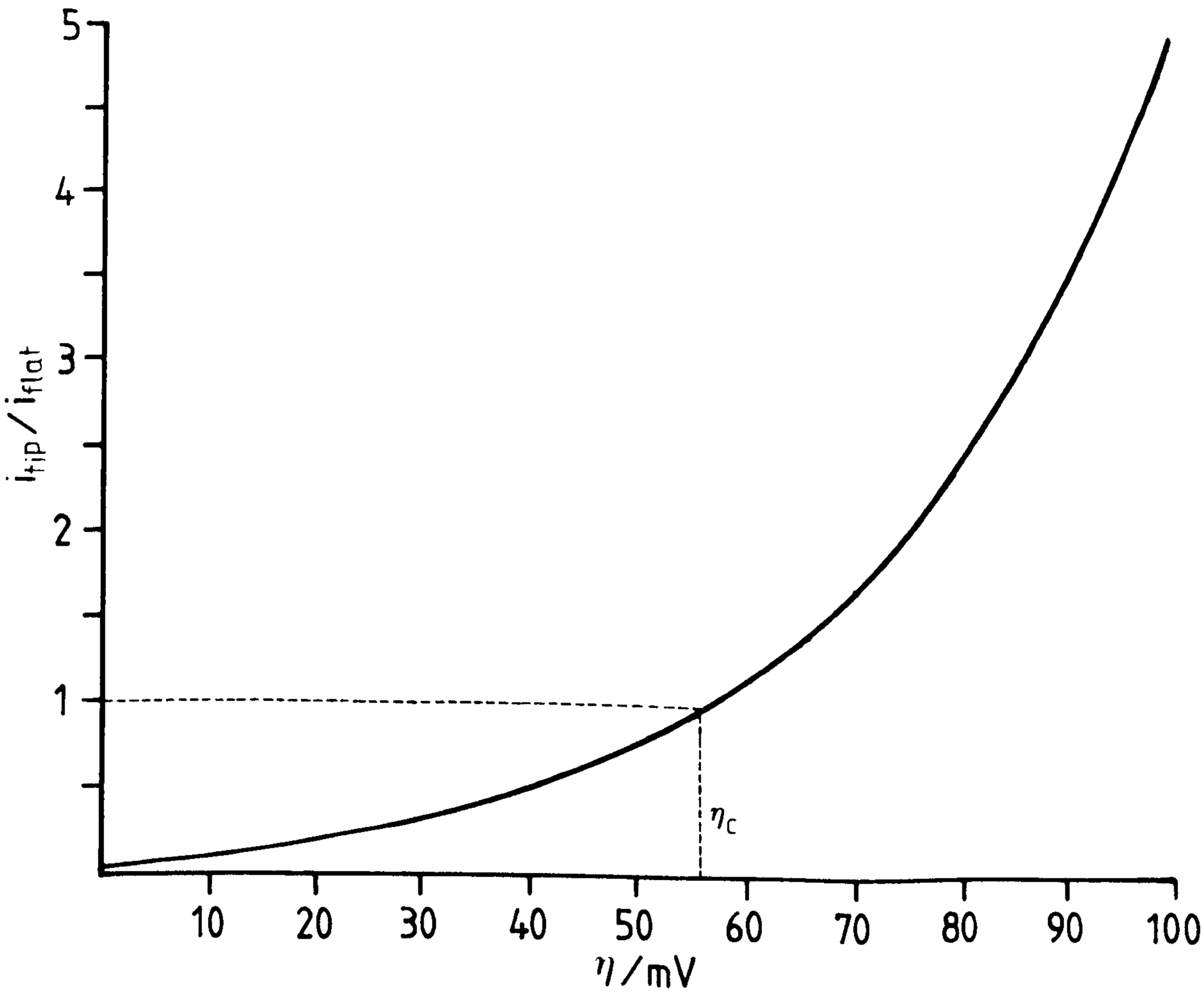

Fig 5.6 Theoretical dependence of the tip/flat current ratio on overpotential for dendritic growth in 0.5M H_2SO_4 + 0.1M $CdSO_4$ onto cadmium, using k_o = 4.7 x 10 cm/s.

At equilibrium ($\eta = 0$), the exchange current density is given by;

$$i_o = nFk_oC_o \qquad \{5.4\}$$

Hence combining {5.3} and {5.4};

$$k_o = \frac{RT}{n^2F^2C_oR_{ct}} \qquad \{5.5\}$$

Thus for this system, the rate constant for deposition onto a flat surface (k_o), is given by;

$$k_o = \frac{8.314 \times 293}{4 \times 96487^2 \times 1.4 \times 10^{-4}}$$

$$k_o = 4.7 \pm 1 \times 10^{-4} \text{ cm/s}$$

The deposition rate constant onto a dendrite tip, where spherical diffusion is established, is given by {3.2};

$$k_r = k_o\exp[-2\gamma V/RTr]$$

Thus an estimate of the current ratio i_{tip}/i_{flat}, can be obtained by using {3.8};

$$\frac{i_t}{i_f} = \frac{hk_o\exp(-2\gamma V/RTr)}{[D_o + rk_o\exp(-2\gamma V/RT)]}$$

The Kelvin term, $\exp[-2\gamma V/RTr]$ [see CH 1.3.3], is dependent on the surface tension γ, and the radius of curvature of the dendrite tip r. The surface tension for cadmium is calculated to be 1.13×10^{-4} Jcm^{-2}. This is obtained from the energy of vapourisation of cadmium metal[182] and compares with values of 0.5 and 1.5×10^{-4} Jcm^{-2} for mercury and zinc respectively[114].

Hence for observed dendrite radii of 1×10^{-4} cm, the Kelvin term is $\doteq 1$ and can be ignored. Thus {3.8} becomes;

$$\frac{i_t}{i_f} = \frac{hk_o}{(D_o + rk_o)} \qquad \{5.6\}$$

From scanning electron microscopy of a typical initial dendrite, $h = 0.0025$cm, $r = 0.0001$cm and $D = 1 \times 10^{-5}$ cm^2s^{-1}, therefore

at $\eta = 0$, we have;

$$\frac{i_t}{i_f} = \frac{2.5 \times 10^{-3} \times 4.7 \times 10^{-4}}{(1 \times 10^{-5} + (1 \times 10^{-4} \times 4.7 \times 10^{-4})}$$

$$\frac{i_t}{i_f} = 0.12$$

Hence, as would be anticipated, dendritic growth is highly unfavourable at the reversible potental. At higher overpotentials, the back reaction;

$$Cd_s \rightleftharpoons Cd^{2+}_{aq} + 2e^-$$

can be ignored, and the deposition rate constant becomes k_f.

From the Butler-Volmer equation [see CH 1.4.4];

$$k_f = k_o \exp[-\alpha n F \eta / RT] \qquad \{5.7\}$$

and substituting k_f for k_o, an expression relating the current ratio i_t/i_f to the overpotential can be given;

$$\frac{i_t}{i_f} = \frac{h k_o \exp(-\alpha n F \eta / RT)}{[D_o + r k_o \exp(-\alpha n F \eta / RT)]} \qquad \{5.8\}$$

Figure 5.6, shows the tip/flat current ratio dependence on overpotential for this system, using $k_o = 4.7 \times 10^{-4}$ cms^{-1}. The critical potential for dendritic growth can be expected at the point where $i_t/i_f = 1$. From fig 5.6, a critical overpotential of 55 $\pm$ 6mV is anticipated. This value is in good agreement with experimental observations on polished surfaces, which gave a value of 65 $\pm$ 10mV for the critical overpotential. Equation {3.8}, can be re-written in terms of the critical overpotential η_c (when $i_t/i_f = 1$), as;

$$\eta_c = \frac{-RT}{\alpha n F} \ln\left[\frac{D_o}{k_o(h - r)}\right] \qquad \{5.9\}$$

Thus giving a relationship for the critical overpotential in terms of measureable parameters.

5.3 DEPOSITION FROM 0.001M CADMIUM SULPHATE IN 0.5M SULPHURIC ACID

With the same experimental conditions and apparatus used in CH 5.2, deposition could be studied with 0.001M $CdSO_4$ + 0.5M H_2SO_4, and contrasted with that found in 0.1M $CdSO_4$ + 0.5M H_2SO_4. The only experimental difference was that it was possible to follow the d.l.c./time behaviour with the frequency response analyser [see CH 2.4.4].

5.3.1 DEPENDENCE ON OVERPOTENTIAL

Deposition was observed at η = -30, -50, -80 and -100mV, for time-periods of up to 4 hours. This gave the d.l.c./time transients shown in fig 5.7. The current/time behaviour is essentially a flat response for the lower overpotentials, but a slight rising trend is observed at η = -100mV (see fig 5.8). Comparing the d.l.c./t and i/t transients (fig 5.7 and 5.8), it is clear that d.l.c. observations are considerably more sensitive to electrode morphological changes. However, d.l.c./t transients on stationary electrodes are not entirely reproducible due to the production of hydrogen bubbles. These occasionally cause some form of blockage of the electrode surface, as is seen in fig 5.7, whereupon removal of bubbles causes an immediate rise in the d.l.c.. Observation of the d.l.c./t transients at η = -80 and -100mV, clearly show that dendritic growth occurs, whereas at η = -50mV, a slight rising trend indicates a more moderate increase in surface area. At

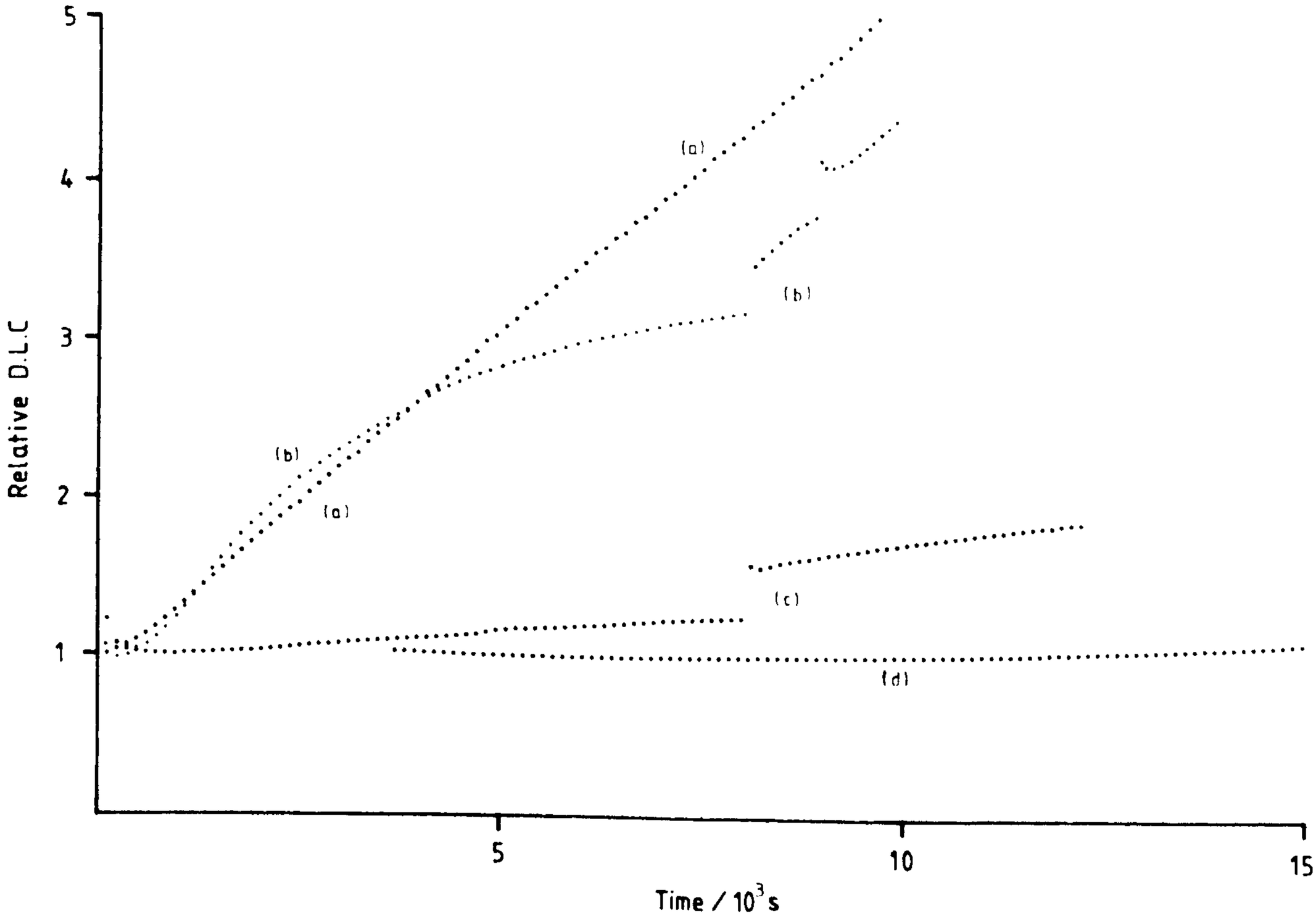

Fig 5.7 Double layer capacity/time transients found for deposition from 0.5M H_2SO_4 + 0.001M $CdSO_4$ onto stationary etched cadmium disc electrodes. (a) -100mV; (b) -80mV; (c) -50mV; (d) -30mV overpotentials.

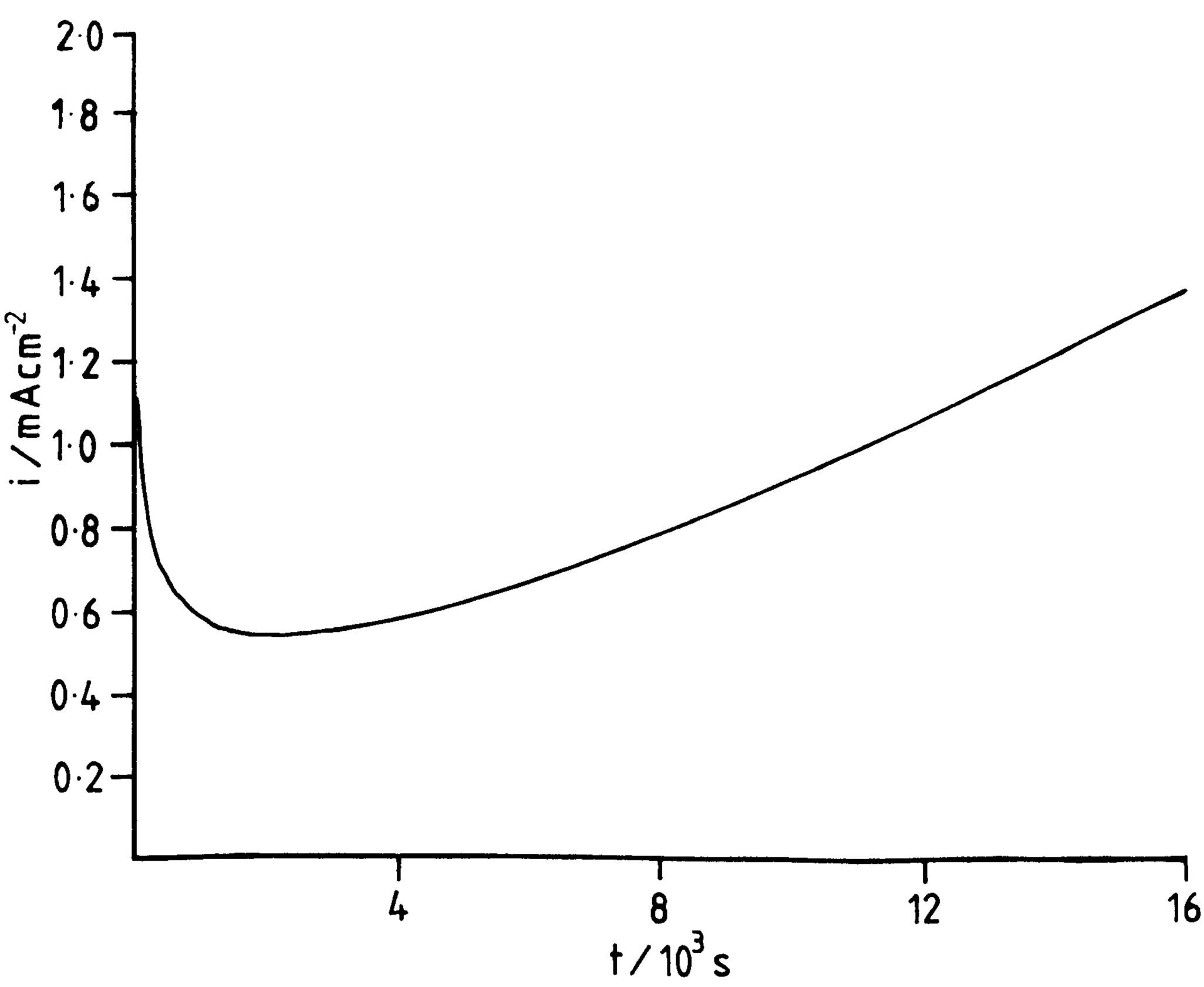

Fig 5.8 Current/time transient found for deposition at -100mV overpotential in 0.5M H_2SO_4 + 0.001M $CdSO_4$ onto a stationary cadmium disc electrode, corresponding to the -100mV d.l.c/time transient in fig 5.7.

η= -30mV, no dendritic growth is indicated. With deposition at η= -100mV, an induction time for dendritic growth of < 100s is found, which increases to 250s at η = -80mV.

These values are consistent with observations in 0.1M $CdSO_4$ solutions and indicate that the critical overpotential for polished electrodes, and the short induction times encountered, are reasonably independent of Cd^{2+} concentration.

SEM of the electrode surfaces, revealed a very different deposition morphology from that found in the 0.1M $CdSO_4$ electrolyte. At η = -100mV after 3 hours of deposition, three distinct types of dendritic growth could be observed against a largely flat, etched electrode surface. The background surface shows no evidence of grainy growth, although some form of spongy deposit can be found around favourably orientated areas of the etched surface (see plate 5.6a/b). Several pits in the electrode could be detected (as in plate 5.6a); these were observed before deposition and are presumed to be due to gassing during casting of the original cadmium rod used for the electrodes [see CH 2.2.6.3]. These pits did not appear to catalyse dendritic growth to any extent. The three types of dendritic deposit found, can be divided into three morphologies;

a) plate 5.7a. A needle-like dendritic deposit, where side branching occurs frequently, but main stem thickening does not seem to occur. Growth appears to be initiated by some edge condition of the electrode and in this case has resulted in a dendritic mass 1mm in width. The apparent alignment of the dendrites towards the electrode centre, could be due to a flattening of the delicate deposit during electrode removal and preparation for SEM.

Plate 5.6 Deposition morphology found on etched cadmium electrodes after 3 hours at -100mV overpotential, in 0.001M $CdSO_4$ + 0.5M H_2SO_4. (a) spongy deposit near a surface defect; (b) transition deposit between spongy and true dendritic growth.

Plate 5.6a x1500

Plate 5.6b x750

Plate 5.7 Deposition morphology found on etched cadmium electrodes after 3 hours at -100mV overpotential, in 0.001M $CdSO_4$ + 0.5M H_2SO_4. (a) true dendritic deposit found at the electrode edge; (b) disc like dendrites.

Plate 5.7a x500

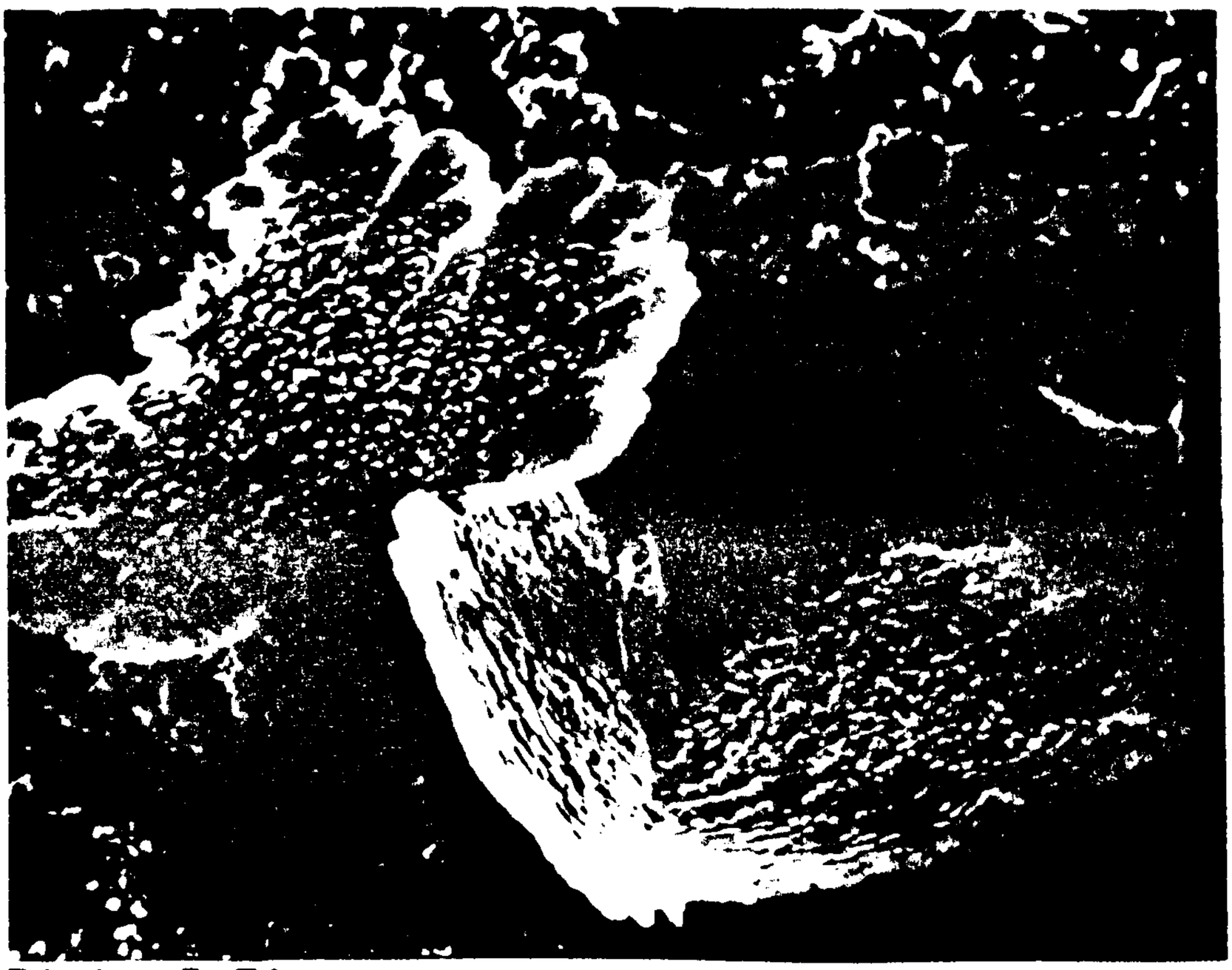

Plate 5.7b x1000

b) plate 5.6a/b. Spongy or grainy dendritic growth can be found, particularly away from the electrode edge. These are blunt dendrites, similar in many respects to the morphology found for spongy zinc deposits[110]. Reference to plate 5.6b, shows how with larger spongy dendrites (100μm long), the definition of the crystal structure improves as they grow. Observation of several dendrites, indicates a change towards the morphology found in case a).

c) plate 5.7b. Flat disc shaped dendritic deposits are to be seen at high angles relative to the surface. Growth is clearly propagated outwards from the edges of the disc, resulting in a dendrite of approximate dimensions 60 x 40μm, and thickness 0.5 - 3μm. A possible mechanism for this form of growth, could involve the formation of secondary diffusion layer gradients out from the surface of the dendrite at 90^{o} to the primary electrode diffusion layer. Such dendrites are large enough with respect to the Nernst diffusion layer, for this effect to have some influence on deposition. If a comparison is made with secondary diffusion layers around cylindrical and flattened protrusions, it becomes clear that any flattened protrusion will have increased deposition at the edge. Edge sites will have almost spherical diffusion conditions, whereas side sites will experience a linear diffusion gradient out from the electrode surface. Hence, once a dendrite deviates from the circular towards a more ovoid cross-section, one can expect increasing favouring of the edge sites and thus consequential flattening out of the dendritic form.

5.3.2 A.C. IMPEDANCE

Experimental conditions were as described previously [see CH 5.2], except using the 0.001M $CdSO_4$ electrolyte solution.

A.c impedance spectra show considerable dependence on the state of the electrode finish, even for etched electrode surfaces. Fig 5.9, shows the spectra observed for a fresh electrode, the lower frequency measurements show a decreasing real component, indicating the electrode surface morphology is changing, probably due to the influence of the a.c. signal. The a.c. signals used for impedance work, had 5mV RMS amplitude (±7mV peak - peak); this value is an attempt at a compromise between a big signal with low noise that influences the electrode state, and a small signal resulting in high noise but little effect on the electrode. Clearly in this case, the signal has an effect on the electrode condition, as noted in CH 5.2. Usage of a low frequency signal to settle the electrode [see CH 5.1], results in increased low frequency stability. The effect of low overpotential deposition upon a.c. impedance is illustrated in fig 5.10. Transient a), represents the spectra taken after 1 hour of low frequency (0.01Hz 5mV RMS) oscillation, comparison with fig 5.9 (taken before the settling down period), shows how the spectra has stabilised. A charge-transfer resistance of 17Ω cm^{-2} is indicated. Transient b) gives the a.c. spectra observed at η = -30mV after 1 minute of deposition. Considerable low frequency drift is observed. Reducing the overpotential to -15mV (transient c)), shows a flattening out of the spectra, allowing an estimate of the charge-transfer resistance at 30Ωcm^{-2}. Fig 5.11 illustrates the change in

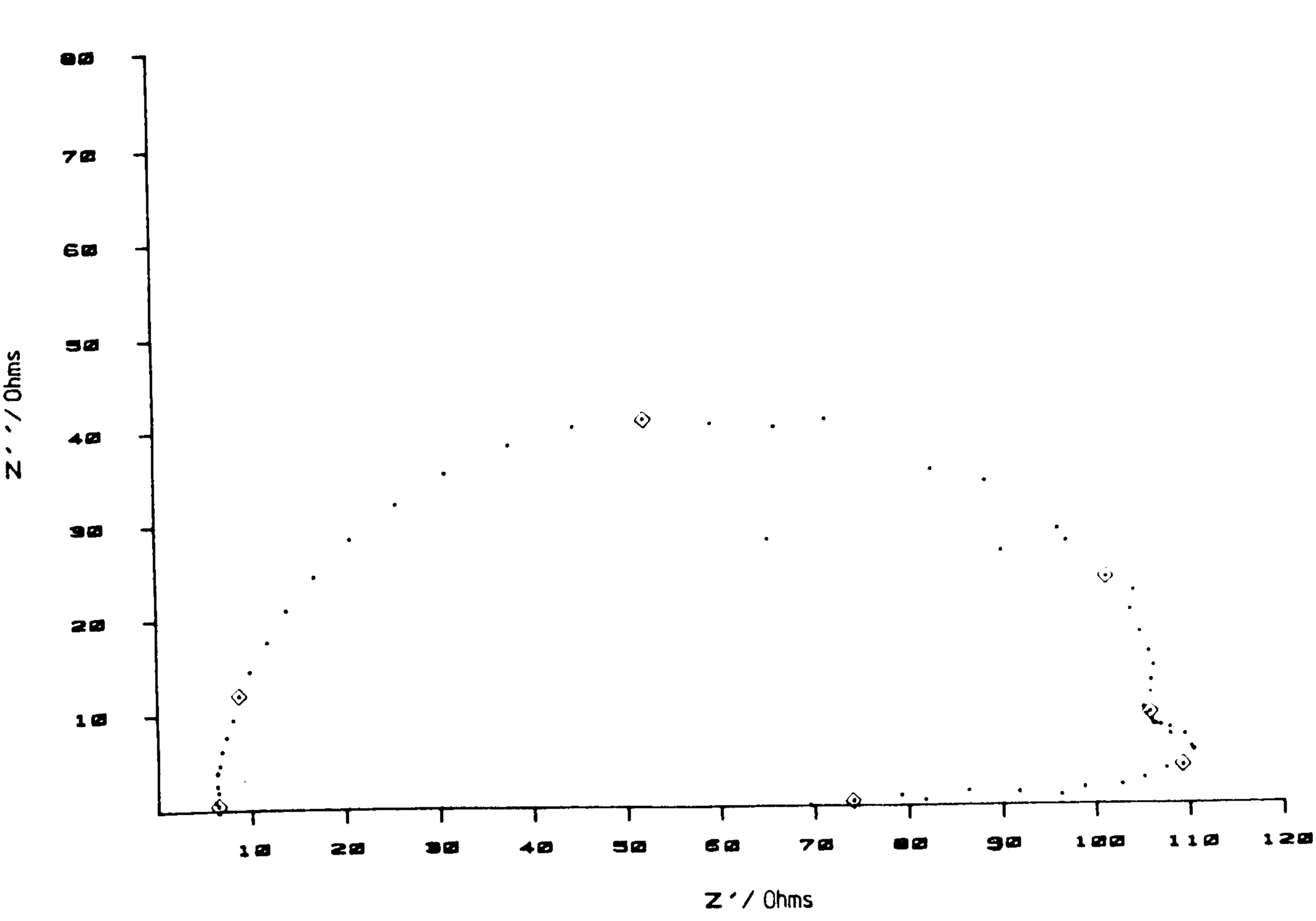

Fig 5.9 A.c. impedance spectra obtained at the rest potential on a freshly polished rotating cadmium disc electrode (5 rev/s), in 0.5M H_2SO_4 + 0.001M $CdSO_4$. Frequency range 10kHz to 0.01Hz.

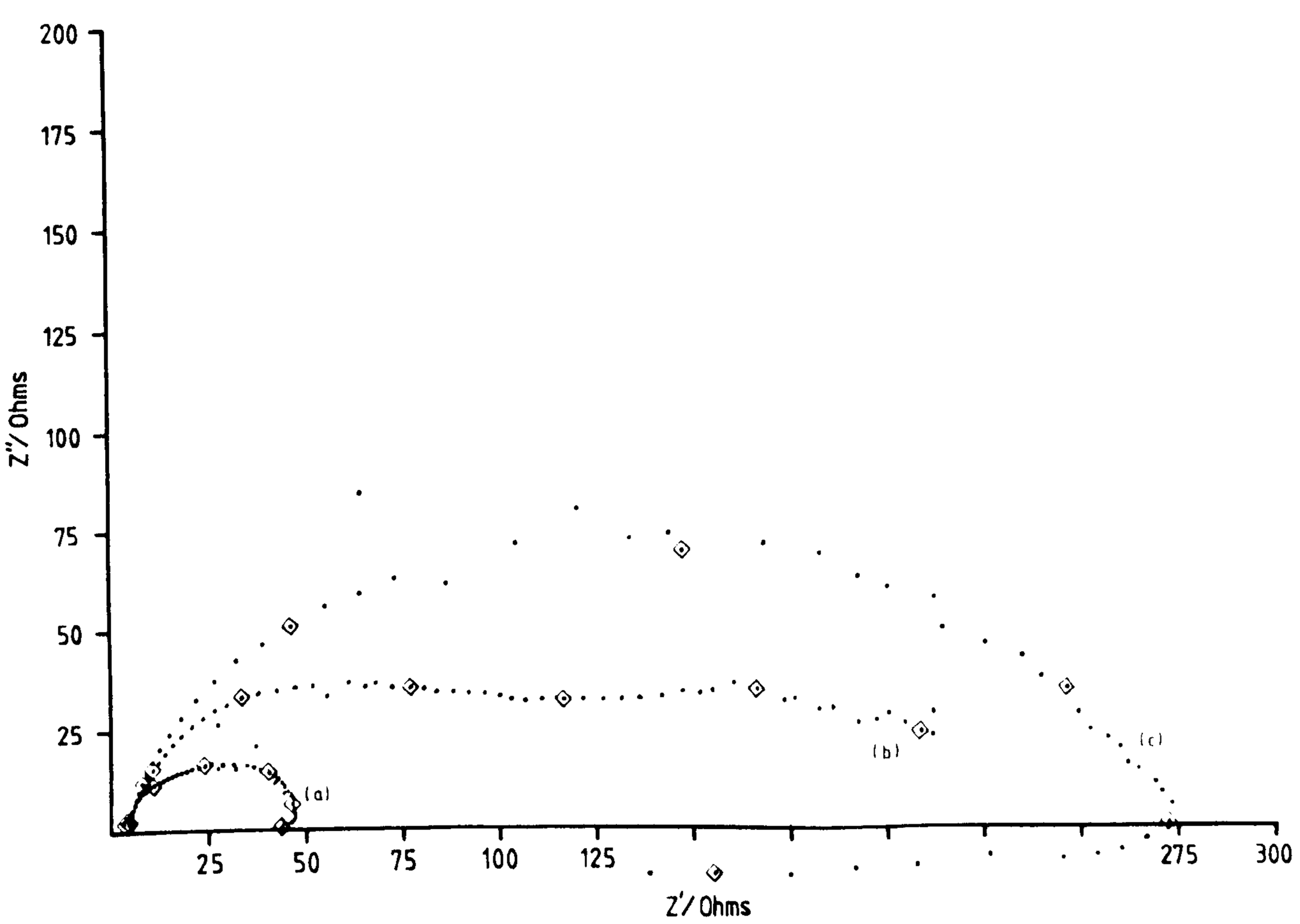

Fig 5.10 A.c. impedance spectra obtained on an etched, equilibrated rotating cadmium disc electrode (5 rev/s), in 0.5M H_2SO_4 + 0.001M $CdSO_4$. Frequency ranges for all curves, 10kHz to 0.01Hz. (a) 0.0mV; (b) -15mV; (c) -30mV overpotentials.

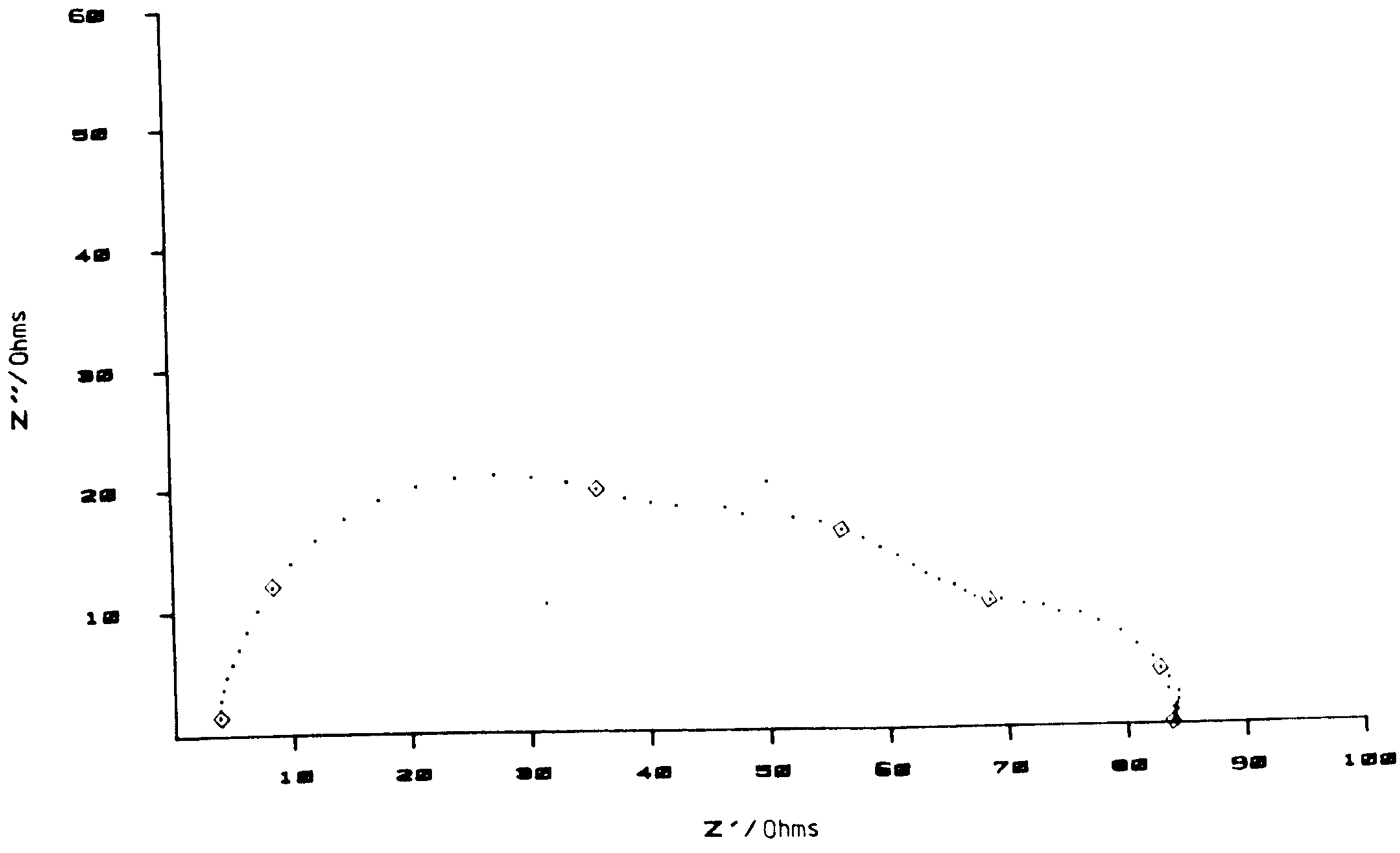

Fig 5.11 A.c. impedance spectra obtained at the rest potential on an etched, equilibrated rotating cadmium disc electrode (5 rev/s), after being left at the rest potential for 16 hours in the electrolyte; 0.5M H_2SO_4 + 0.001M $CdSO_4$. Frequency range 10kHz to 0.01Hz.

the a.c. impedance spectra found on leaving the etched electrode in solution (at the rest potential), for a period of 16 hours. Since no leakage of electrolyte around the electrode edge is observed, the difference can only be attributed to a change in the surface morphology. However, optical observations of the electrode surface showed no apparent change. Due to this high instability of the a.c. impedance spectra, it is not possible to obtain conclusive results. However, an average value of ~20 Ωcm^{-2} for the charge-transfer resistance (5 electrodes), gives a value for the deposition rate constant onto a flat surface of;

$$k_o = \frac{8.314 \times 293}{4 \times 96487^2 \times 0.001 \times 10^{-3} \times 20} = 3{\cdot}3 \times 10^{-3} cms^{-2}$$

5.4 FIT OF EXPERIMENTAL OBSERVATIONS TO THEORY

Theoretical dendrite growth in a suspension-free solution, has been investigated in CH 3.1, whereby the total growth time for dendrite growth is given by;

$$t_g = t_i + \Delta t$$

t_i is the induction time required for a cone-shaped dendrite of constant base width, to grow until spherical diffusion is established at the tip; t_i is given by {3.18};

$$t_i = \frac{q \pi w^3 \delta}{3 Tan\theta DC_o AV}$$

The growth time Δt for the dendrite, relates to the growth of a dendrite through the diffusion layer, from an initial height h_o to a final height h. During this period, spherical diffusion is assumed at the tip, such that diffusion control is found on the flat surface, but mixed control at the tip. Δt is given by

{3.13};

$$\Delta t = \frac{\ln[h/h_o]r}{D_o V C_o}$$

Deposition at η = -100mV in 0.1M $CdSO_4$ + 0.5M H_2SO_4, results in very rapid dendritic growth, against a grainy background deposit. The critical size for cadmium crystallites before dendritic growth sets in, appears to be ~10μm (see plates 5.3a/b). The nucleation site density is ~1.5 x 10^6 sites/cm^2, and appears to be approximately constant, in that this value is found after 1 or 10 minutes of deposition. Thus with the following values;

$q/A = 1.5 \times 10^6$ sites/cm^2

$w = 3 \times 10^{-4}$ cm

$\theta = 26^o$ ($Tan\theta = 0.3$)

$D_o = 1 \times 10^{-5}$ cm^2/s

$V = 12.99$ cm^3/mol

$C_o = 1 \times 10^{-4}$ mol/cm^3

$\delta = 0.01$ cm

we get;

$$t_i = \frac{1.5 \times 10^6 \times \pi \times 27 \times 10^{-12} \times 0.01}{1 \times 10^{-5} \times 1 \times 10^{-4} \times 12.99 \times 3 \times 0.3}$$

$$t_i = 108s$$

This value is however, very dependent on the approximations involved, especially in that dendritic growth is assumed to be conical in shape during the initiation period. Referring to plates 5.3a/b, we can see this approximation is not particularly valid in this case, giving rise to values for w of 1 - 5 x 10^{-4} cm. Thus the error in the initiation time is large, ie for this range of w, t_i lies in the region 12 - 300s.

For the observed dendrites in plates 5.3b and 5.4b , values for Δt were estimated using the following parameters;

plate 5.3b	plate 5.4b
h = 30 mm	h = 400μm
h_o = 10μm	h_o = 10μm
r = 1μm	r = 4μm

and;

δ = 0.01 cm

$D = 1 \times 10^{-5}$ cm^2/s

$C_o = 1 \times 10^{-4}$ mol/cm^3

Thus for the initial dendrite in plate 5.3b;

$$\Delta t = \frac{\ln[3/1] \times 1 \times 10^{-4} \times 0.01}{1 \times 10^{-5} \times 1 \times 10^{-4} \times 12.99}$$

Δt = 85s

and for the dendrite in plate 5.4b;

$$\Delta t = \frac{\ln[40/1] \times 4 \times 10^{-4} \times 0.01}{1 \times 10^{-5} \times 1 \times 10^{-4} \times 12.99}$$

Δt = 1135s

Thus we arrive at rough values of t_g of 190 and 1200s for the two dendrites observed. This compares to the actual deposition times of 60 and 600s respectively. The agreement is quite good considering the approximations involved.

Dendritic growth found in 0.001M $CdSO_4$ + 0.5M H_2SO_4 , is observed in several morphologies [see CH 5.3], and no distinct transition can be seen from granular to dendritic growth. It is therefore difficult to calculate the dendritic induction time. However, it is assumed that the grainy dendrites seen in plates 5.6a/b, are the result of deposition before the onset of spherical diffusion conditions, hence for these dendrites,

$\Delta t = 0$, and $t_g = t_i$. From plate 5.6a, it appears that the transition from grainy to 'normal' dendritic growth, occurs at a critical length of around 50μm. Thus the growth times for dendrites observed in plates 5.6a/b, are less than the induction time for true dendritic growth. For the dendrite observed in plate 5.6b, the following parameters were used;

$h = 100\mu m$

$h_o = 50\mu m$

$w = 3\mu m$

$\theta = 3{\cdot}4^{\circ}$ ($\mathrm{Tan}\,\theta = 0.06$)

$r = 1\mu m$

$q/A = 100000$ sites/cm^2

$C_o = 1 \times 10^{-6}$ mol/cm^3

$\delta = 0.01$ cm

$D_o = 1 \times 10^{-5}$ cm^2/s

Thus a value for the induction time for dendritic growth is given by;

$$t_i = \frac{100000 \times \pi \times 27 \times 10^{-12} \times 0.01}{1 \times 10^{-5}\ 1 \times 10^{-6} \times 12.99 \times 3 \times 0.06}$$

$$t_i = 3600s$$

The growth times for the above dendrites using {3.13} are given by;

$$t_g = 3600 + \Delta t$$

and;

$$t_g = 3600 + \frac{\ln[2] \times 1 \times 10^{-4} \times 0.01}{1 \times 10^{-5} \times 1 \times 10^{-6} \times 12.99}$$

$$t_g = 3600 + 5340$$

therefore we arrive at;

$$t_g = 8900s$$

This compares well with the actual deposition time of 10600s,

although as with other measurements, it is very dependent on the estimations involved. Table 5.1, compares parameters and calculated values for induction and growth times, for both the alkaline and acidic systems. It is clear that there is a good measure of agreement between calculated and observed values.

TABLE 5.1

System	η /mV	Cd(II) /mol dm^{-3}	D /cm^2 s^{-1}	h_o /μm	h /μm	r /μm	Δt/s theoretical	observed
10.00 M KOH + 2.8×10^{-4} M Cd(II)	-300	2.8×10^{-4}	1.8×10^{-7}	0.5	28	0.2	5.3×10^{5}	5.0×10^{5}
0.5 M H_2SO_4 + 0.1 M Cd(II)	-100	0.1	1×10^{-5}	4	400	4	1400	600
0.5 M H_2SO_4 + 0.1 M Cd(II)	-100	0.1	1×10^{-5}	4	20	1	120	60
0.5 M H_2SO_4 + 0.001 M Cd(II)	-100	1×10^{-3}	1×10^{-5}	0.7	45	0.7	2.2×10^{4}	1.1×10^{4}

Table 5.1 Comparison of calculated and observed dendritic growth times for acidic and alkaline electrolytes.

CH 6 COMPUTER SIMULATION OF ELECTROCRYSTALLISATION

6.1 INTRODUCTION

In order to obtain a greater understanding of the initial stages of deposition that occur before the onset of dendritic growth, it was decided to investigate theoretical electrochemical deposition by computer simulation. Originally the aim was to produce a realistic model for the deposition characteristics of cadmium. Many aspects of the electrodeposition process can be studied by this method, but work here is limited to deposition onto an initially perfect crystalline surface (ie modelling the cadmium 0001 plane). Computer simulation has been used extensively to model crystal growth and deposition; CH 1.3.4 covers much of the relevant work to date. Little of the work covers the specific field of electrodeposition, although much of it is of relevance to this work by covering analogous aspects.

6.2 THE SIMULATION

Using the microcomputer systems described in CH 2.5, a number of computer simulation programs were written using an adapted Monte Carlo method[156,157]. All simulations started by assuming that deposition occurred onto an initially perfect (0001) plane of a hexagonal close packed model. Atoms were only allowed at fixed lattice sites, thus true dislocations and screw defects could not be effectively simulated. Each site in the hexagonal close packed arrangement has 12 nearest neighbours, 3

above, 3 below and 6 in plane. The sites are represented in memory by either a 0 or 1 depending on occupancy. Hence the lattice can be handled by using binary arithmetic. This method of representation allows for the production of both vacancies and overhangs of atoms during the crystal growth. Most of the previous work on computer-simulated crystal growth [see CH 1.3.4], has used the solid on solid approximation whereby the lattice is represented as columns of atoms, given by integer numbers showing the lattice height above particular sites. Thus such models have not allowed incorporation of vacancies, defects or overhangs, whereas for this work, where a study of the morphology was required, it was necessary to provide for such representation. In particular it should be noted that without provisions for overhangs, no true dendritic growth could ever be simulated.

Atoms were assumed to have a uniform impingement rate onto the deposition surface, thus the theoretical timescale is determined in relation to this atom impingement (trial) rate. A trial is said to occur when an unoccupied site adjacent to the surface is selected. In this context adjacent sites are sites with one or more occupied neighbouring positions. Sites for impingement were selected using extensively tested random number generating routines [see CH 6.3.4]. Each site thus required selection of the X,Y and Z coordinate. The height coordinate, Z does not require random selection, since atoms can only adhere at the surface and not above (in solution) or below it (within the crystal). Thus the site is selected via random number generation of the X and Y coordinate, with the Z coordinate determined by finding the highest unoccupied position with at

least one occupied neighbouring site. If the chosen site is not filled, the next lower available site is selected. This process almost exactly corresponds to random generation of the height coordinate, but is considerably more efficient in computing time, since selection of occupied sites and sites above the surface is avoided. This height selection procedure is not used for the linear diffusion model, where selection of the height is entirely random. The question of each atom's adherence is decided by a set of probabilities, relating to the number of filled nearest neighbour sites. Initially, the probabilities were determined using a relationship whereby no equilibrium of exchange exists between atoms in the solution and the solid phase. Instead the adherence is determined by a change in the activation energy of transition as illustrated in fig 6.1. Thus transition between energy states where one bond is broken and reformed is given by;

$$k_{oo} = k_o \exp(-\Delta E^{\ddagger}/RT) \qquad \{6.1\}$$

hence transition from one state to a lower energy state is given by the rate;

$$k_{on} = k_o \exp\left[\frac{-\Delta E^{\ddagger}}{RT} + \frac{\alpha n \Psi}{RT}\right] \qquad \{6.2\}$$

where $(n\Psi/RT)$, is the energy difference between the initial and final states. The activation energy is thus lowered by some fraction α, Ψ being the energy required to break one bond, n is the number of bonds broken. Hence one can write;

$$k_{on} = k_o \exp\left[\frac{-\Delta G^{\ddagger}_{f-}}{RT} + \frac{\alpha n \Psi}{RT}\right] \qquad \{6.3\}$$

for the electrochemical equivelent transition rate. The relationship used by Gilmer et al[134,136,144], assumes a rapid exchange of atoms between solution, solid phase and adsorbed

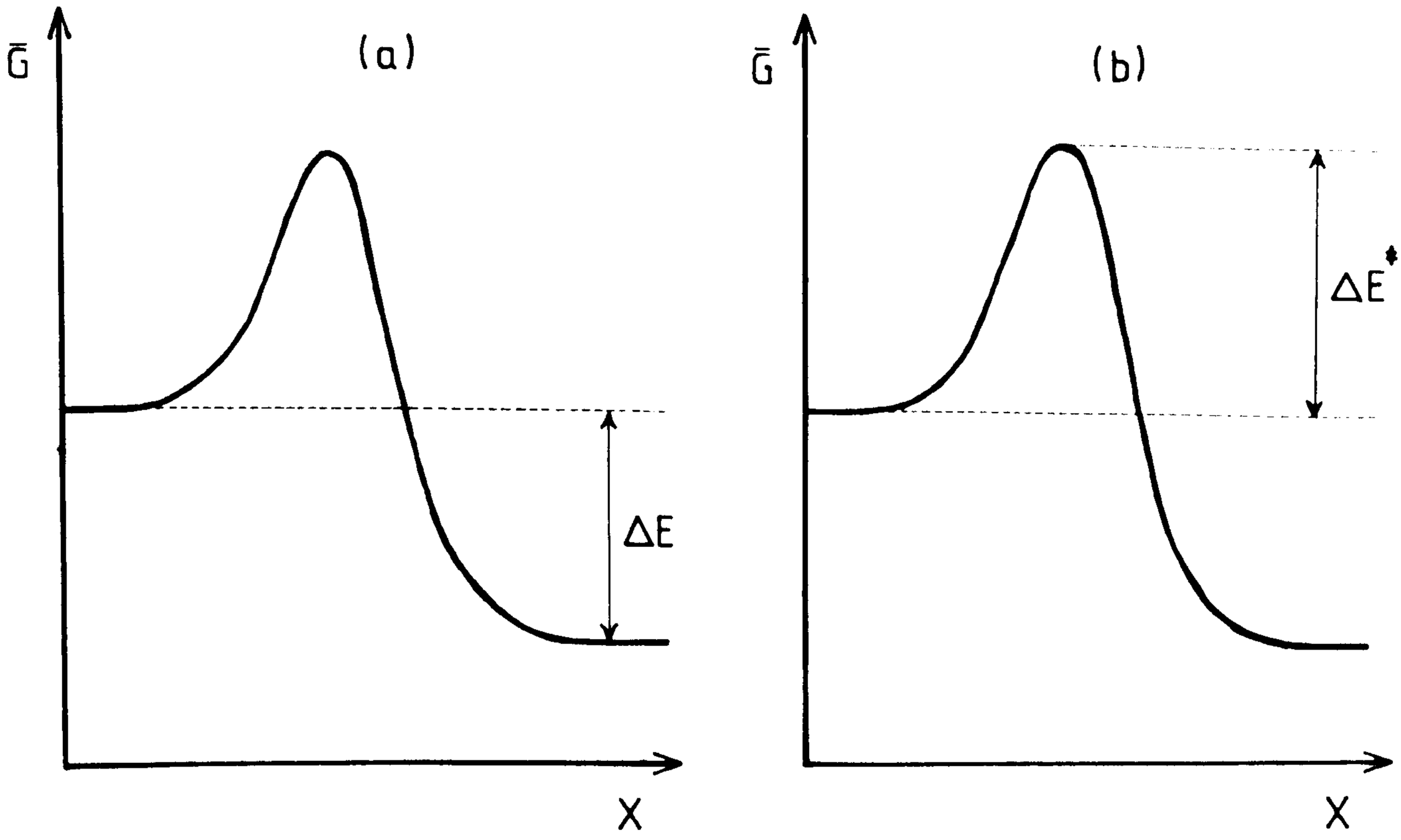

Fig 6.1 Comparison of energy barriers found for simulations using a rapid exchange (equilibrium) (a); and that where no equilibrium exists but the transition is dependent on the activation energy (b).

COMPUTER	LANGUAGE	RELATIVE TIME
Apple II (6502)	Basic (applesoft)	1
Apple II (6502)	Machine code	0.005
North Star Horizon (Z80a)	Basic (North Star)	0.3
IBM 370/timeshaired	Fortran	0.005 approx
IBM 370/c.p.u time	Fortran	0.00002

Table 6.1 Comparison of computing times for equivalent simulations.

atoms. Therefore this model requires evaporation and migration. Hence the rate of transition is dependent only on the energy change on transition, given by;

$$k = \nu \exp(-\Delta E^{\ddagger}/RT)$$

or $$k = \nu \exp(-n\Psi/RT) \qquad \{6.4\}$$

Usage of equation {6.2} is limited due to the difficulty of estimating $\Delta E^{\ddagger}$ and α, hence probabilities were finally determined empirically and kept constant for most of the simulations.

Two-dimensional nucleation was incorporated into the model by assuming that (infrequently), three atoms impinge at the same time on adjacent sites, thus forming a nucleus. This choice of three atom nucleation instead of single atom nucleation is a compromise in order to enable calculations to be carried out on a more reasonable timescale, without significantly altering the deposition model from that of a true Monte Carlo system. Once a three-coordinate site has been selected, it is treated as a nucleation site (3-coordinate sites will generally be above a filled section of lattice and will thus be nuclei). If the site is then filled, two atoms will be placed in adjacent unoccupied sites. Hence the acceptance probabilities were adjusted to incorporate this factor. Migration of surface atoms was not allowed, although four-coordinate atoms were not permitted on the assumption that they would migrate to a five-coordinate position, hence the four-coordinate probability of acceptance is set to zero. Surface evaporation of atoms was not allowed, in that it is assumed 1- and 2-coordinate sites will always evaporate and $\geqslant$ 3-coordiate sites will not. In addition to these constraints, any unoccupied site with 10-12 neighbours is

regarded as a blocked site and thus the probabilities for these sites were set to zero. The standard probability set used was as follows;

coordination	probability
3	0.001
4	0
5	0.100
6	1
7	1
8	1
9	1

To avoid edge discontinuities in a square (cubic) lattice, cyclic boundary conditions were generally imposed, whereupon the neighbours of an edge site are found at the oposite edge of the displayed lattice. Thus each site in the lattice is equivalent and no true edges exist. The cyclic or reflective system thus has the three-dimensional analogy of a torus, with lattice sites arranged upon its surface. An additional feature of the simulation method used, is that once an atom has been deposited at a particular site, the next trial is not random, in as much as the next site is selected from one of the unoccupied, in-plane neighbours of the first site (if available). Hence, it is possible for a string of atoms to be deposited in a manner analogous to kink progression, whereby an atom adhering to a kink site would be stabilised in the transition state by the presence of a nearby solvated atom. Thus continued deposition at the kink site would be expected.

Two main simulations were carried out; 1) using a diffusion independent model, whereby the atoms impinge uniformly

throughout the lattice, and 2) appliying linear diffusion conditions to the model system, such that the atom impingement rate increases linearly with distance from the surface. Case 2) is designed to model the effects of an applied Nernstian diffusion layer on deposition. In the latter case, the current was constrained to be constant with time. To this extent the simulation of case 2) will deviate from the real case, since the Nernst diffusion layer was assumed to be present from time t = 0. Figure 6.2 shows the flow diagram for the general programs of both simulations.

6.3 THE PROGRAMS

This section (together with appendices I-V), contains descriptions of not only the programs but also a somewhat detailed description of the 6502 machine code programming used. This is necessary for interpretation of the listed machine code programs [see appendix VI], since without such background, the programs are meaningless to anyone other than a 6502 microprocessor expert. It is intended by the author that the following information in CH 6.3 together with the appendices, should be sufficient to allow a basic understanding of any aspect of the programs used. A number of publications are available on machine code programming for the 6502[184-186], but most of these are deficient in particular aspects of the programming, and some contain bad errors.

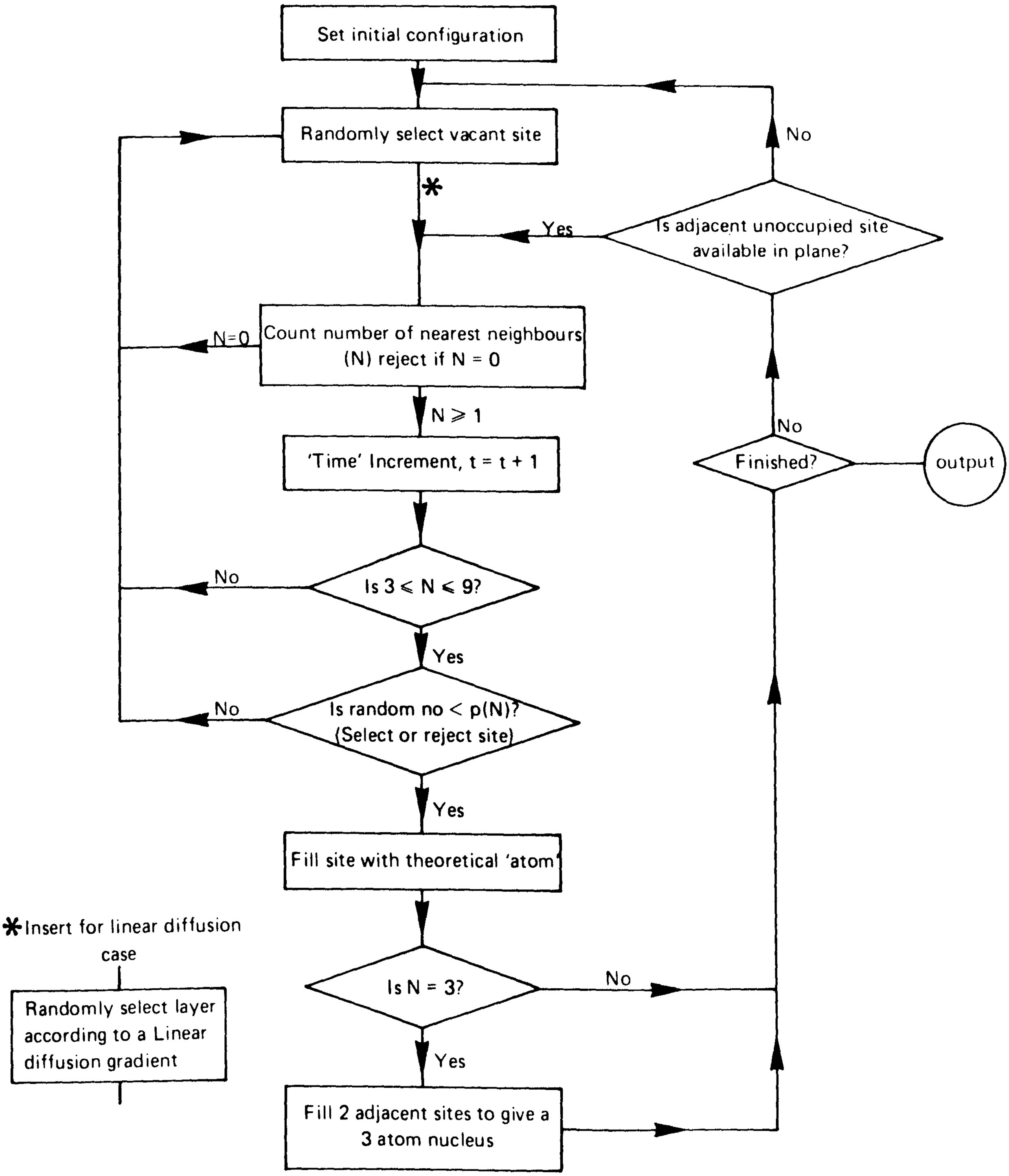

Fig 6.2 Flow diagram for the two main computer simulation programs used.

6.3.1 LANGUAGES USED AND PROGRAM SPEEDS

The bulk of the programs were written for use with the Apple microcomputer described in CH 2.5.2, with some of the early work being carried out on the North Star Horizon system, described in CH 2.5.1. Apple programs used Applesoft Basic language (Beginners All Symbolic Instruction Code), which incorporates graphics handling routines. The North Star system used North Star Basic language. However, both Basic languages were used uncompiled and required considerable running times to produce worthwhile results. Hence it was decided to write the programs directly into the machine code operating language of the 6502 microprocessor, using Applesoft for the input and output routines to the code (where the speed is unnecessary). In this way the programs were simple to use and fast in operation, whilst retaining flexibility. Referring to table 6.1, the program speeds are compared and contrasted with other systems, and with that of of estimated mainframe (IBM 370) speed. It is of interest to note that even using a compiled Basic program, there is a considerable speed difference compared with the dedicated machine code programs. This is due to the efficiency that can be achieved in programming using machine code directly. There are several disadvantages however, the main one being the considerable length of time required to produce the programs. Since machine code is a low level language, there is considerable difficulty in writing and manipulating the routines. The most significant factor in the time required to produce programs, is usually the inevitable problem of finding program errors (debugging). This cannot be underestimated since

the detection of the last 'bug' can be elusive and take longer than required to write the program in the first place. When working, the routines have given up to x 200 speed improvement. Thus an experiment that would have taken an overnight run in Applesoft Basic, could be achieved in 7 minutes. Further improvements could have been achieved with the entire program written in machine code, but the improvement would be less than a factor of x 2 in speed, and any advantage would be considerably outweighed by the time taken in programming. From table 6.1, it can be seen that program speed on the microcomputer compares favourably with that of a time-shaired mainframe, but offers easier access and usage whilst giving direct output of data, via on screen high resolution graphics. This coupled with the quick printed output on the Epson dot matrix printer, enabled the work to be carried out on a computing system costing no more than 1/2000 th of a full IBM 370 mainframe system. Typical speeds for deposition onto a 160 by 160 lattice gave ~ 200 trials per second, at a long term average of 4.2 atoms/s for the diffusion independent system. Times for the simulation with linear diffusion were considerably longer, since the speed depends on the morphology of the deposit formed, and the number of layers deposition is occurring over.

6.3.2 APPLE MICROCOMPUTER MEMORY USAGE AND OPERATION

As most of the programs used were written for this computer it is important to the understanding of program operation to give a background of the layout and usage of the Apple memory. Fig 6.3 shows a schematic of the memory layout for the Apple II

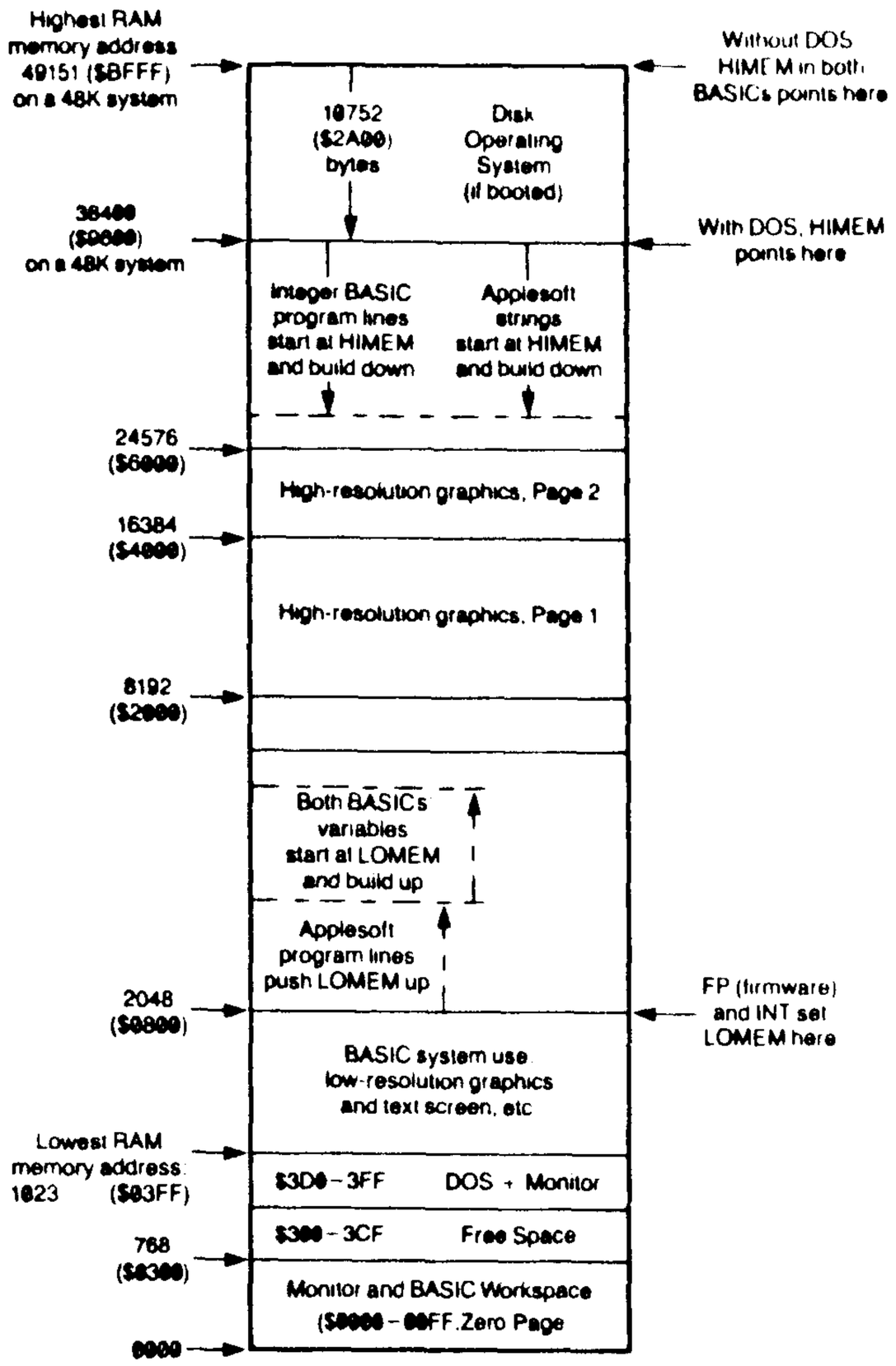

Fig 6.3 The Apple II memory map.

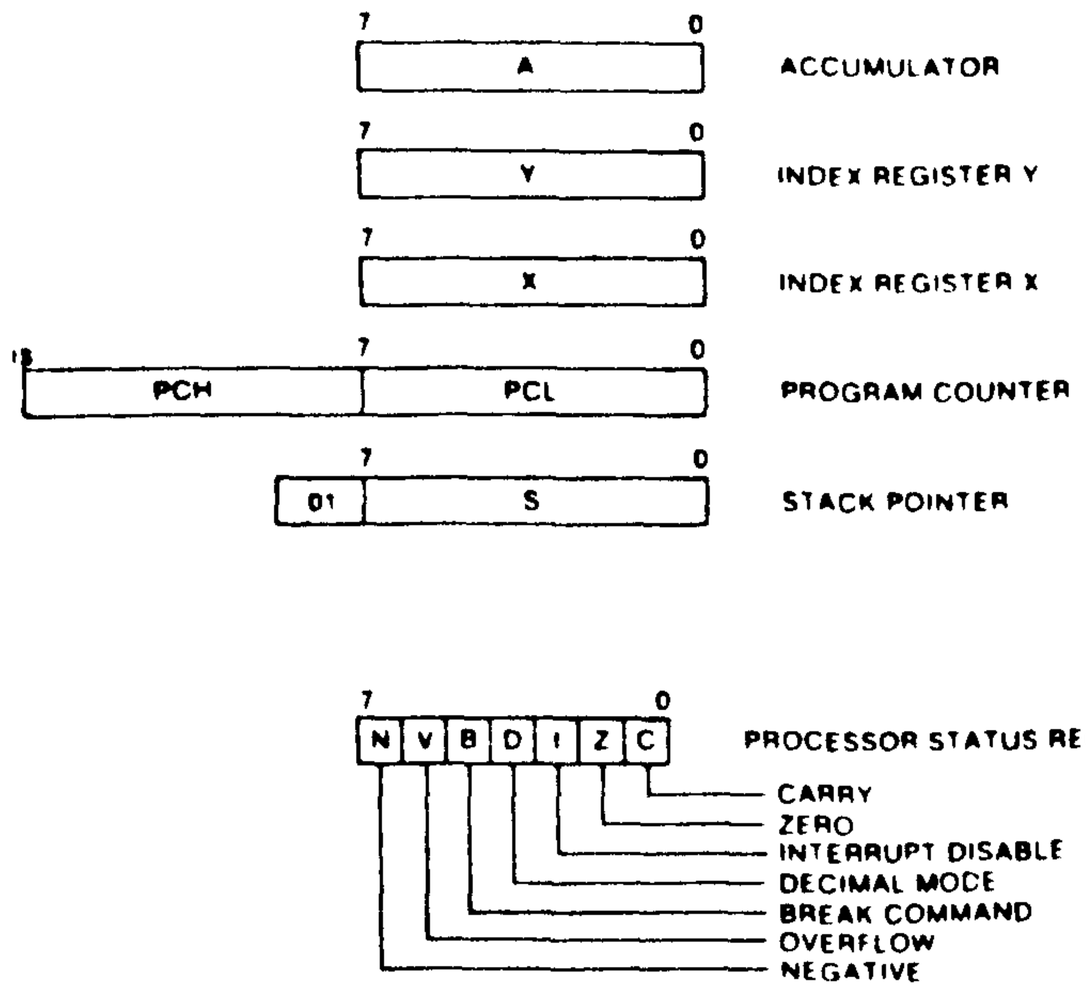

Fig 6.4 Schematic of the 6502 microprocessor.

(europlus). The lowest 256 bytes of memory (the zero page - one page being 256 bytes) are largely used for language and monitor routines. This usage is because a specific subset of the commands available in the 6502 instruction set, operate on the memory in this region [see appendix II/III]. Normal addressing of zero page memory is achieved using 2 bytes of memory, rather than the 3 bytes of memory required for other regions, thus giving rise to quicker access times. Hence this region is heavily used by Apple routines. Some 6502 operating codes can only be used via zero page, making use of 3 byte commands to allow more indirect addressing modes than achievable using other memory pages. The unused locations available to the programmer are indicated in appendix VII.

The first page of memory, comprising bytes 256-511 (or $100 - $1FF in hexadecimal notation ie base 16), is used for stack memory. This region is where the return addresses of the accessed subroutines are stored and retrieved from (via the stack pointer). The stack pointer is a memory within the 6502 that keeps track of which return address to use within the stack [see appendix III]. Page 2 of memory (locations 512 - 767 or $200 - $2FF) is used for the input routines. All typed input is taken from the keyboard, converted into a numeric code sequence and stored in this region, before being interpreted by the computers operating system. Input lines can thus be a maximum of 255 characters long, the last character must be a 'return' code to tell the computer to interpret the line. The coding system used by nearly all computer operating systems, is the ASCII code sequence (American Standard Code for Information Interchange). Page 3 is free memory for programming from $300 -

$3EF, and is conveniently used for data storage for the machine code programs (the simulation programs use this area for variable storage -see appendix V). The range of memory $400 - $7FF is used for text and low resolution graphics display, with 64 of the locations set aside for communication with peripheral devices, attached through slots 1-6 inside the Apple. The memory from $800 - $95FF is free, with Basic programs starting at $800. The locations $2000 - $3FFF and $4000 - $5FFF are used for high resolution graphics display pages, thus if programs occupy these areas, usage of the high resolution graphics is limited. For the programs presented, any display is limited to the second high resolution page (HGR2 in Applesoft). Locations $9600 - $BFFF are used for the disc operating system (DOS), but may be used by programs if the associated disc and peripheral card facilities are not required.

The standard Apple II europlus is supplied with 48k of RAM (Random Accesss Memory:- memory available for reading and writing) and 16k of ROM (Read Only Memory:- memory that cannot be written to). The RAM extends from $00 to $BFFF and ROM from $C000 - $FFFF. The ROM memory usually contains the autostart, monitor and Basic operating systems (with a few special locations of RAM within this region to allow switching of display modes and external devices; eg the games control inputs). Since the 6502 has a 16 bit addressing range, only 2^{16} = 65536 locations can be accessed directly (ie the region $00 - $FFFF). Hence additional memory (such as the 16k 'Language card' - giving a '64k' Apple) has to be double banked - that is a software switch must be incorporated to allow the computer to 'know' which of the two (or more) memory regions is

being referred to (the language card is addressed in the same region as the ROM).

6.3.3 MACHINE CODE PROGRAMMING FOR THE 6502

6.3.3.1 THE 6502 MICROPROCESSOR

At the heart of the Apple II (and many other microcomputers dated ~1976-84) is a 6502 microprocessor. This is a relatively simple 8 bit device, normally running at ~1 MHz ie 1 x 10^6 cycles/s, with each machine code instruction taking ~3-9 cycles depending on complexity.

The 6502 uses an instruction set of 56 mnemonic machine (assembly) language codes, involving 152 operating codes (most instructions have several addressing modes - see appendix III). These codes enable manipulation of data, using either binary arithmetic or binary coded decimal (BCD). In BCD, each byte can represent two decimal digits (in two four-bit nibbles) and manipulation is carried out in pseudo-decimal. Work presented in this thesis uses machine code operating in binary arithmetic only.

The 6502 comprises of an 8 bit accumulator (A), two 8 bit registers (X and Y), a 16 bit program counter (PC - high and low bytes), 8 bit stack pointer and an 8 bit processor status register (the flag register). Figure 6.4 shows a schematic of the 6502 layout. All arithmetic is carried out in the accumulator and thus data must be transferred to the accumulator before manipulation. The two registers X and Y are used for internal data storage and are most commonly used for counters.

Data can be rapidly transferred between registers and the accumulator. The stack pointer contains the position in the stack (the stack is page 1 memory), where the return address for the currently accessed routine is to be found. The address itself in page 1 memory, occupies 2 bytes (2 bytes is sufficient to describe any location in memory from $00 - $FFFF). This address is loaded to and from the program counter, the program counter contains the current operating location of the microprocessor, ie the address in memory of the next operating code instruction that the microprocessor will carry out. An 8 bit flag register (of which 7 are used) is contained, giving the operating status of the microprocessor. The 7 flags are either set, reset or left unchanged dependent on the last instruction caried out. Each of the flags is thus 0 or 1 (on or off), they indicate the following;

bit 0: c : carry status

bit 1: z : zero status

bit 2: i : interrupt status

bit 3: d : decimal mode

bit 4: b : break command

bit 5: v : overflow status

bit 6: n : negative status

The important flags as far as this work is concerned are the c,z and n flags.

6.3.3.2 6502 ASSEMBLY LANGUAGE AND OPERATION CODES

Machine language programs consist of a series of numbers, usually in successive bytes of memory, giving operating codes or

data for an operating code. Particular memory values correspond to particular operation codes or non-operating codes (NOP commands), ie in this case, there are 152 valid codes, the other 104 are ignored by the microprocessor [see appendix III]. When operating, the 6502 interprets the value at the current location in memory indicated by the program counter and if this corresponds to one of the 152 operating codes, the instruction is carried out and the program counter advanced to the next instruction (or to an address indicated by the interpreted instruction). Some codes can be followed by one or two bytes giving an address or a data value.

Listing of machine code programs is obtained (for the Apple) by the Apple monitor program (using; CALL -151 from Basic for entry into the monitor). This can be purely numeric, with a sequence of hexadecimal numbers or more usually, in both hexadecimal and mnemonic notation (the assembly language) for the operating codes indicated. Listing is effected by typing the start address, followed by L (or several LL's). Twenty instructions are then displayed on the screen at a time. Reference to appendix III gives a description of the function of all the codes available for the 6502. The following is a section of a machine language program listing;

```
$1000: 18          CLC
$1001: 3D          CLD
$1002: A5 FF       LDA $FF
$1004: 69 0A       ADC #$0A
$1006: 8D 20 10    STA $1020
$1009: 6C 20 10    JMP ($1020)
$100C: DD 20 30    CMP $1030,x
```

```
$100F: B1 20 31          LDA ($2031),y
$1012: 60                RTS
```

Each line of the listing is in the following format:- Hexadecimal address of program bytes, followed by a colon, and then the hexadecimal codes or data, with the mnemonic notation displayed to the right of the screen. It should be noted from the above example, that addresses are stored in memory with the low order byte first, followed by the high order byte. In addition the use of standard symbols for the mnemonic notation facilitates reading; "$" indicates a hexadecimal number; "#" indicates a data value rather than address; "()" indicate an indirect mode of addressing; ",y" or ",x" indicate an addressing mode where the X or Y registers are involved.

6.3.4 RANDOM NUMBER GENERATION

This is a fundamental aspect of computer simulation frequently overlooked by workers in this field. Any Monte Carlo type simulation requires the production of random numbers in some form, to enable the simulation to be carried out. Any deviation from true randomness will throw into doubt any result thus produced.

In reality, generation of true randomness is impossible, since numbers so generated must be produced by a series of logical processes. A basic axiom of science is that all observed effects are the result of logical processes and can thus be predicted, once the laws controlling them are known. Acceptable random numbers are thus numbers produced not randomly, but by logical processes that are sufficiently

complex, that their results cannot be predicted. Computer generation of random numbers is usually achieved via a series of often quite simple mathematical functions, designed to produce numbers that mimic true randomness (although some computers use an external source, eg the white noise produced in an operating electrical valve). The closeness to true randomness depends on how closely one examines the results. Many computers use generation of a cyclic loop of numbers that eventually lead back to the first number in the loop and thus repeat in the same order (the North Star Horizon has a loop of 2^{16} = 65536 numbers). With a cyclic series the statistical behaviour can be determined exactly, 'pseudo-randomness' is achieved by 'random' entry into the loop. In microcomputers this is commonly via an external connection, eg the North Star Horizon uses the orientation and status of the disc drives, the Apple uses the time taken by the user to press a key.

In the Apple computer the randomisation function was found to be inadequate in both speed and long term statistical bias[187], although the full affects of the latter upon the simulation was not established. It was decided to produce most random numbers via a machine code random number generator [listed in appendix V]. The generator produces two byte random numbers in the range 0-65535 and has been carefully tested to ensure no statistical bias. Long term tests, selecting for coordinates for atoms in a 160 by 160 array showed that all 25600 sites were eventually chosen with no apparent trends. Selection of the number of times each of the coordinates (in a range of 0-255) was chosen, showed no deviation from true with a range of selections about an average of 10000 per coordinate of 9694 - 10269, giving a

standard deviation of 103. For selection of coordinates in a range of 0-159 (for a 160 by 160 lattice), repetitive selection (producing on average 100 selections per coordinate) gave the expected Gaussian distribution of intensity about the average value of 100 (see fig 6.5). The curve in fig 6.5 represents data from the generation of 8×10^6 numbers. Other tests showed no correlations occurred between X and Y coordinates, or between successive coordinates.

In terms of speed, the machine code generator is considerably quicker than that in Applesoft Basic, typically giving a speed improvement by a factor of > 100x.

6.3.5 PROGRAM OUTPUT

With the exception of a few introductory and test programs, all simulations were carried out using the Apple computer and peripherals described in CH 2.5, hard copy output being obtained via the Epson dot matrix printer described in CH 2.5.4.

Due to the constraints of memory available for graphics and the display size (maximum of 192 by 280 pixels), visual - on screen, display of the simulation output, could only be achieved for array sizes of up to 80 by 80. Display of the lattice was given in real time as a 2D hexagonal array of filled sites and could show any layer during deposition. Printed output of the lattice on a layer by layer basis, could be obtained by a machine code loop that enabled bit programming of the Epson printer to give differing intensity characters, dependent on the height of the deposit. In addition, a conventional height map (with numbers) could be obtained. Due to the possibility

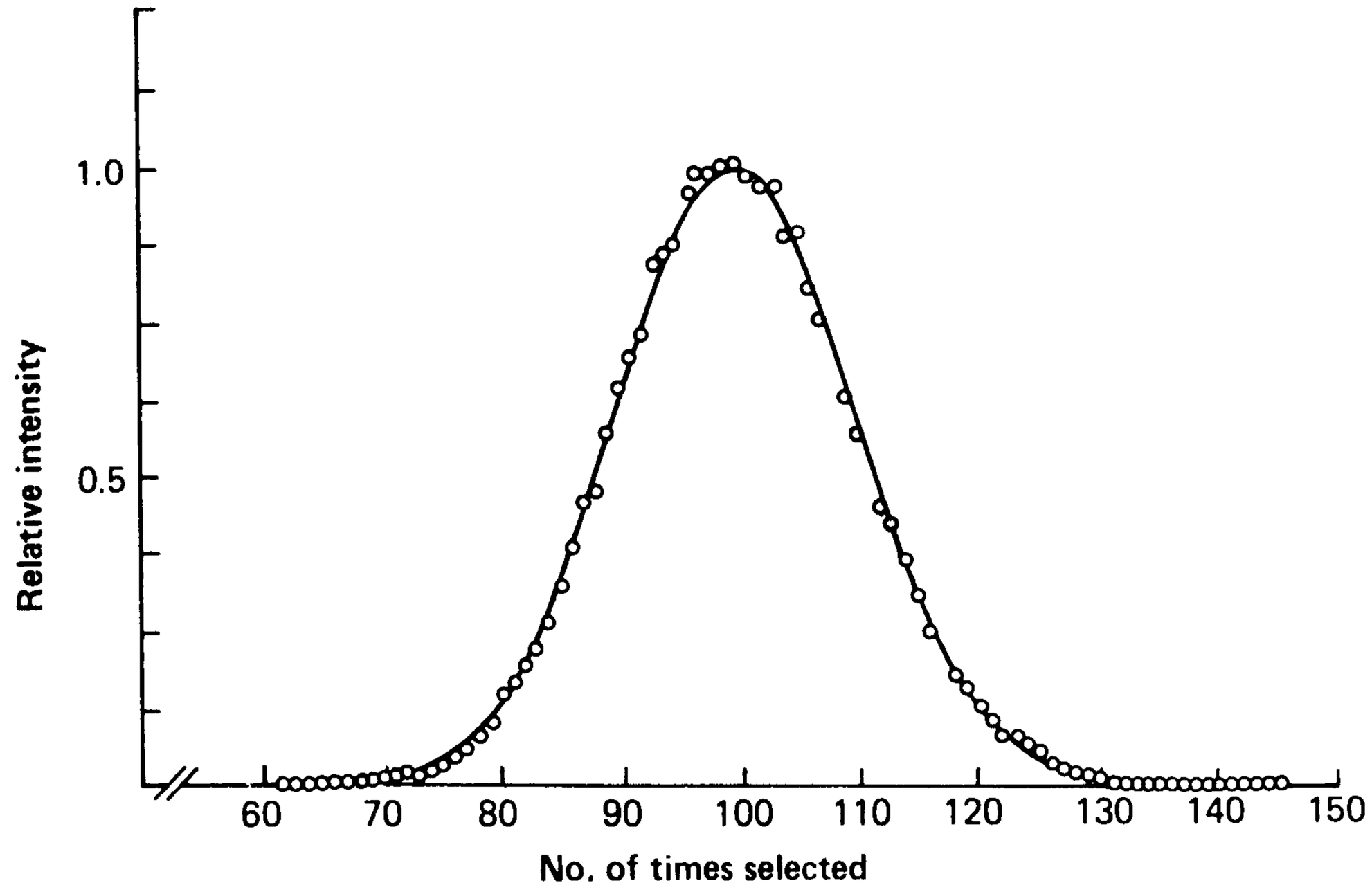

Fig 6.5 Random number distribution check, coordinates 0-159 were selected to give an average of 100 selections per coordinate. The frequency of this selection intensity about 100 has been plotted together with the theoretical Gaussian distribution expected (solid curve).

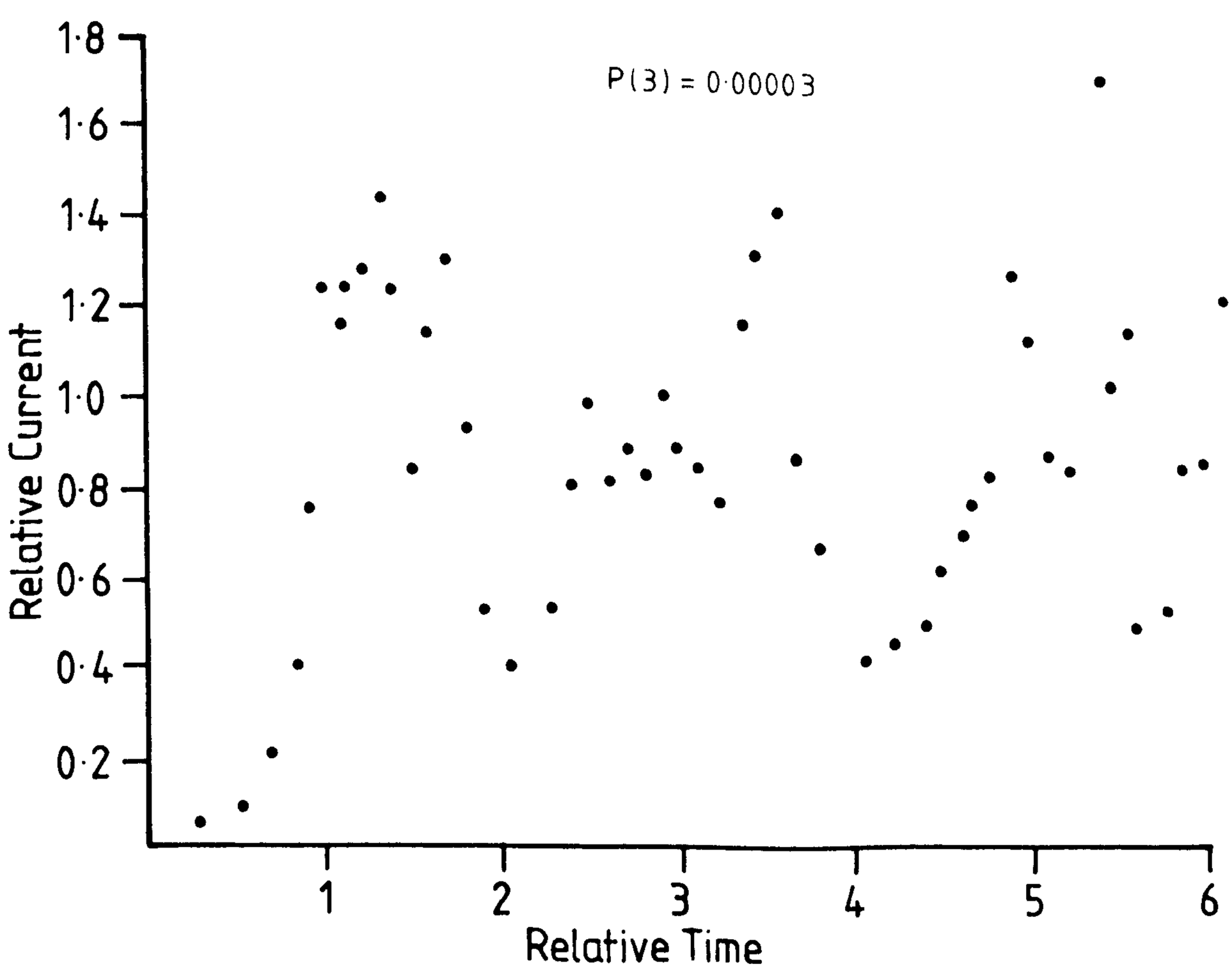

Fig 6.6 Single simulated current/time transient for an 80 by 80 lattice over the equivalent of depositing 3 layers of atoms.

allowed in the simulation, of overhangs and vacancies, some difficulty is encountered in representing what is a 3D model in 2D, unless a 3D model is actually constructed. However, the extent of overhang found from the layer by layer output, was not usually significant enough to effect the validity of the 2D intensity maps produced. Where overhangs have occurred, it is possible to indicate this by giving a cross section of the theoretical array. Graphical output of current/time transients was produced both on screen and as a direct copy on the Epson printer. The output could be further enhanced using the North Star Horizon and Hewlett Packard general plotting system described in CH 2.5 and 2.6.

6.3.6 DESCRIPTION OF SIMULATION PROGRAMS

Programs were written (as was outlined in CH 6.2), following the simplified flow diagram given in fig 6.2. To maximise efficiency in both memory space and program speed, several programs were written to carry out the simulations. The following is a catalogue of those most frequently used.

Demonstration 1: Gives display of arrays up to 40 by 40 using hexagons to represent atoms, together with on screen numeric data associated with each atom as it appears.

Sim 1: Handles a model array of 60 x 60 by 32 layers height, giving real time display.

Sim 2: Allows simulation of a 80 x 80 by 16 layers height lattice, with real time display.

Sim 3: Simulation of 120 x 120 by 16 array, without real time display, but collecting current/time transients.

Sim 4: Simulation of 170 x 170 by 8 array, without display, collecting averaged current/time transients.

Lin sim: Simulation of 80 x 80 by 16 array with real-time display, incorporating a model of Nernstian linear diffusion into layer selection routines.

Appendix V gives a listing of three of the simulation programs; 'Basic sim' is written entirely in Applesoft Basic and is presented as a further guide to the listings given of 'Sim 2' and the various subroutines contained in appendix VI. Most of the machine code programs are based on this Basic program. 'Sim 2' uses a Basic program to tranfer data to and from the machine code where necessary, this is also listed in appendix VI. The machine code subroutine that models the Nernstian linear diffusional effects, can also be found in appendix VI. All the listings are given with brief descriptions of each program section, with full lists of the variables used together with their associated memory locations.

6.4 RESULTS AND DISCUSSION

6.4.1 THE DIFFUSION INDEPENDENT MODEL

Previous workers [see CH 1.3.4] have principally been concerned with investigations into the behaviour of vapour phase deposition, none have incorporated 3D diffusional effects. The work by Franke and Lacmann[152,153], on the effect of thermal diffusion gradients on 2D deposition with the vapour deposition model, appears to be the only other work to date with an incorporated diffusion gradient. Gilmer et al[134,136,138,140,

143-148,160), has studied vapour phase deposition in some detail, but has not studied the influence of diffusion gradients. His work was however, limited to cubic lattices without overhanging configurations or vacancies. Gilmer's studies included the simulation of surface defects, such as spiral growth, impurities, and step progression. Additionally Gilmer has studied growth onto initial surfaces incorporating holes, to follow hole propagation. Using similar methods Bertocci[133] has studied systems with different crystal structures and has observed some effects of the theoretical model size upon the current/time behaviour, something not studied by other workers in any detail. In the light of this work it was decided to investigate deposit morphology and the effects of model size and boundary conditions upon current/time (i/t) transients. It was further decided to investigate the model morphology in the presence of a linear diffusion layer. Comparisons were made with the i/t behaviour of theoretical deposition obtained by Armstrong and Harrison[121], using the integral method [see CH 1.3.4].

6.4.2 CURRENT/TIME RESPONSES

Using the programs described in CH 6.3.6, with the standard nucleation rate and probabilities given in CH 6.2; i/t curves were recorded for deposition under differing boundary conditions and lattice sizes.

The simulation current is given by;

$$i = \frac{\{\text{change in the number of atoms}\}}{\{\text{change in the number of trials}\}} = \frac{\{\text{charge}\}}{\{\text{time}\}}$$

This was measured by recording the number of trials attempted for a set number of atoms deposited, the interval was arbitrarily fixed at $Ls^2/32$ atoms; where Ls is the lattice size, such that in following deposition equivalent to 5 layers of atoms, 160 data points would be obtained. Thus current values are not instantaneous values, but are averaged for the time period over which the data applies. With the limited size of the model system and the random nature of deposition, i/t curves obtained for individual transients were very erratic. Fig 6.6 shows a transient produced for a deposition of 5 layers of atoms onto an 80 by 80 lattice. Hence, to obtain satisfactory accuracy, the curves must be averaged over several simulation transients., the smoothness of the curve being dependent on the numbers of atoms deposited. Acceptable i/t curves over deposition of the first 5 layers of atoms, required 32 x integration of the simulation for an 80 by 80 lattice. This is equivalent to depositing 1024000 atoms involving $\sim 10^8$ trials. This necessitated considerable computing time, as a deposition rate of ~4.5 atoms per second was the maximum that could be achieved (compared with 0.03 atoms/s for the Applesoft Basic programs).

In fig 6.7 we can see the i/t transient produced by the equivalent of deposition over the first 10 layers for an 80 by 80 lattice. Here we see the current reaches steady-state at longer times, which can be contrasted with the curve produced by Armstrong and Metcalfe[122] using the integral method shown in fig 6.8. With the integral method, the curve is considerably more damped and models more closely the experimental transients produced by deposition obtained by Budevski[162]. Budevski's

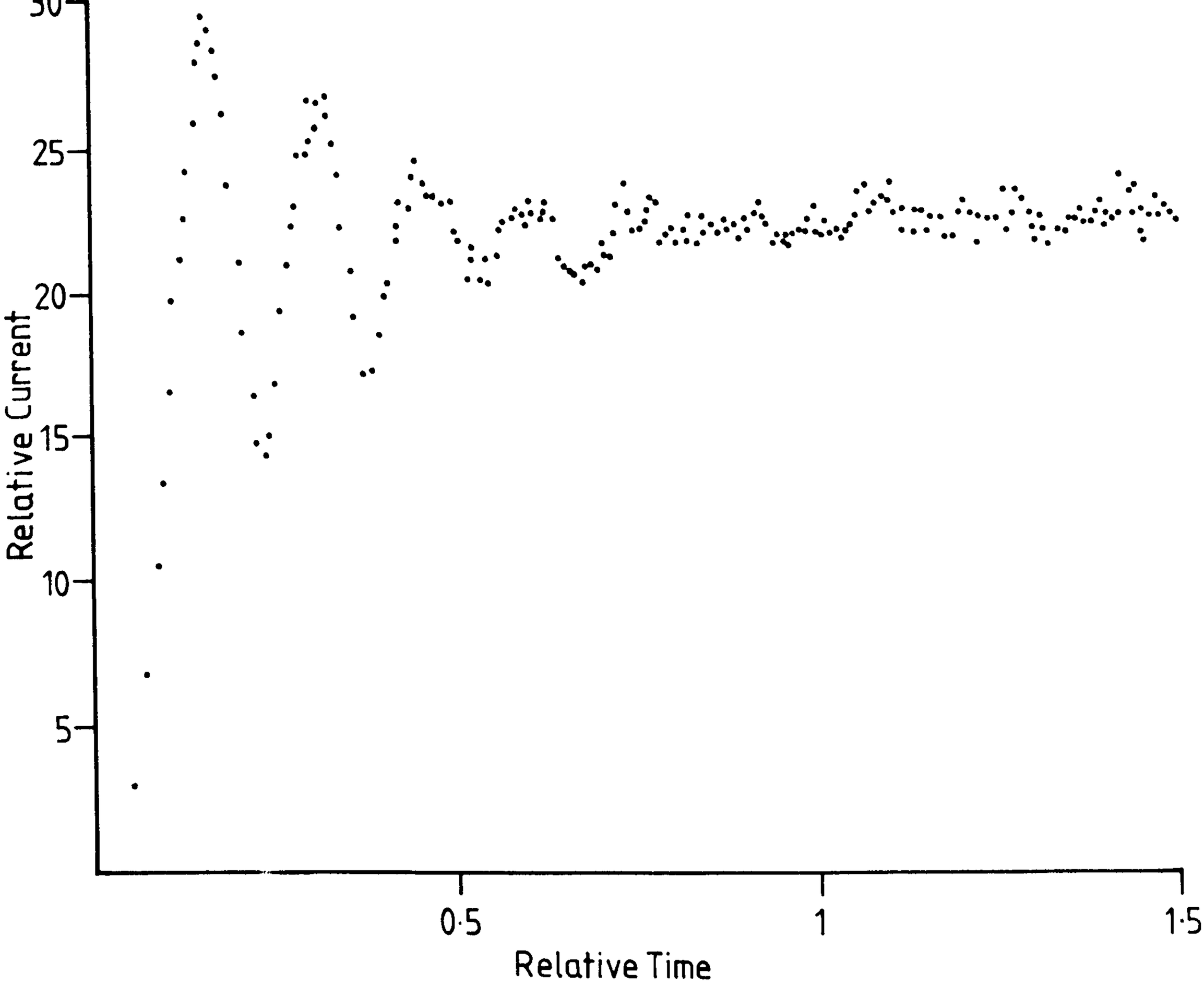

Fig 6.7 Simulated current/time transient (average of 32 curves), for an 80 by 80 lattice, over the equivalent of depositing 10 layers of atoms. The nucleation probability; p(3) = 0.005.

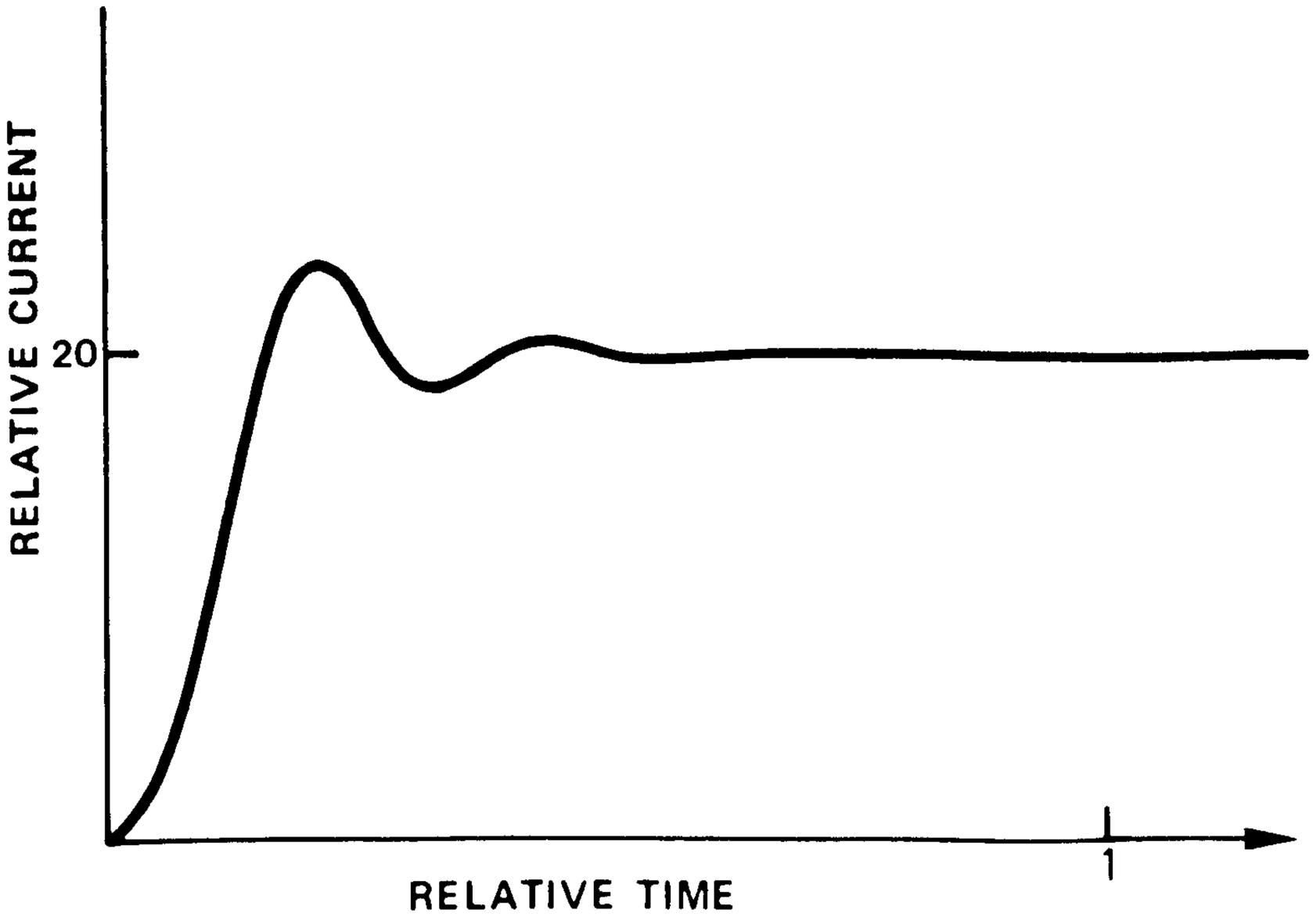

Fig 6.8 Simulated current/time transient found for the integral method, as obtained by Armstrong and Metcalfe.

work, following deposition of silver onto perfect silver single crystal faces, used overpotentials of -12 mV in 6N silver nitrate. The integral method curve corresponds to the case of deposition under activation control, without any diffusional effects; ie at the limit of η = 0 mV. Hence, since Budevski's transient is at η = -12 mV, some small diffusional component can be expected. It is possible that still lower overpotentials might produce a different response curve. Current/time curves produced by the Monte Carlo simulation method, show a marked increase in the ringing oscillations over the integral method curve. This effect is probably due to the influence of 1) lattice boundary conditions [see CH 6.4.3] and 2) the quantisation of the Monte Carlo simulations. The integral method gives a universal i/t transient, where the current observed is influenced solely by growth of the nuclei, whereas the Monte Carlo transients are quantised and thus the current observed is as sum of $i_{growth} + i_{nucleation}$; ie unlike the integral method, a nucleation current exists. Therefore in the Monte Carlo case there is an infinite number of i/t responses, dependent on the relative weighting of the nucleation rate versus the growth current. Fig 6.9 shows an i/t response found if the nucleation current is increased (conversely if the nucleation current is reduced an improved fit would be expected). This point is implicit in the work of Gilmer, where a number of responses were obtained for different model temperatures (using the vapour deposition model). In the work contained here, the ratio of the nucleation current to the growth current was kept constant.

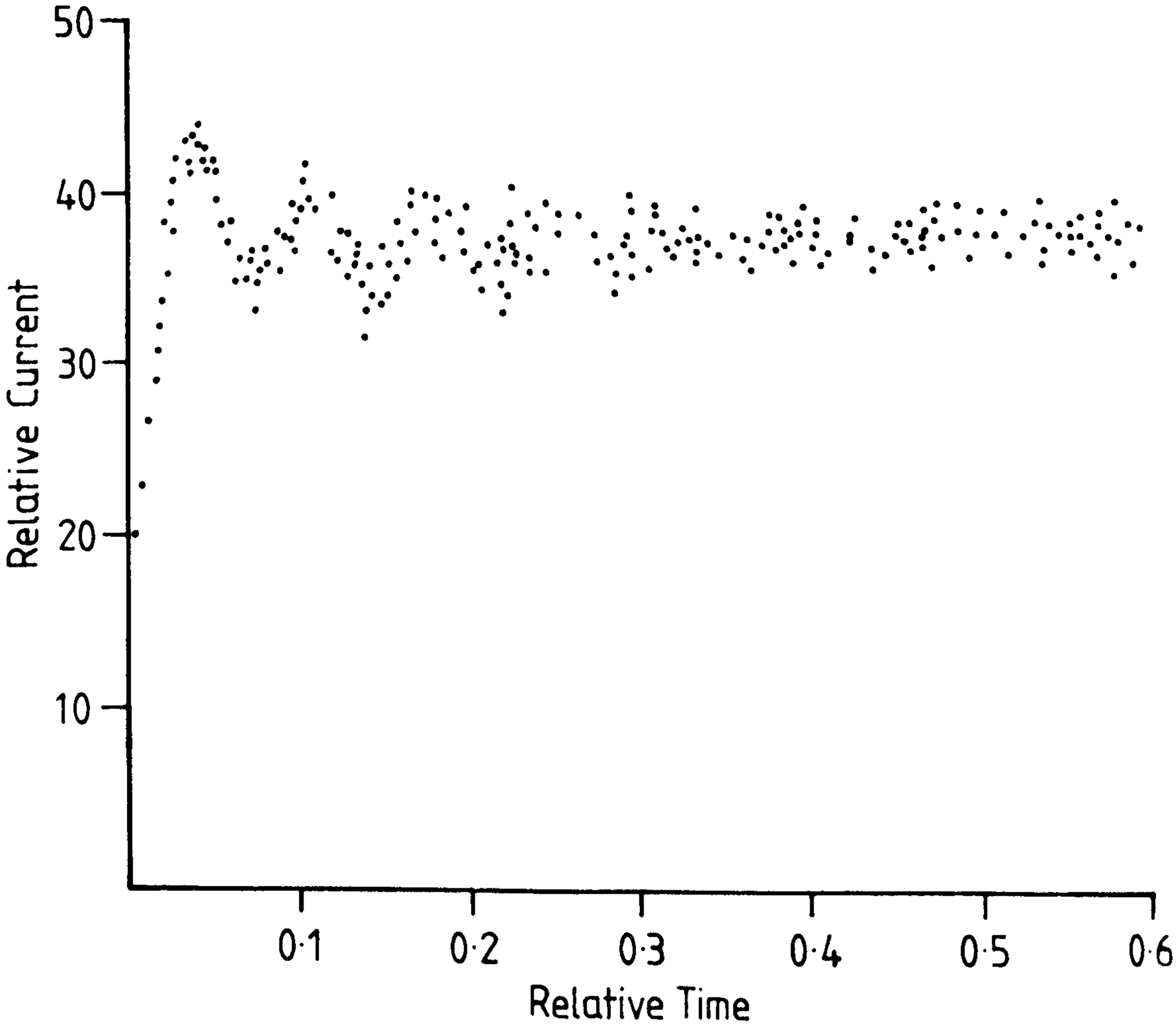

Fig 6.9 Simulated current/time transient (average of 17 curves), for an 80 by 80 lattice over the equivalent of depositing 6 layers of atoms. The nucleation probability; p(3) = 0.05.

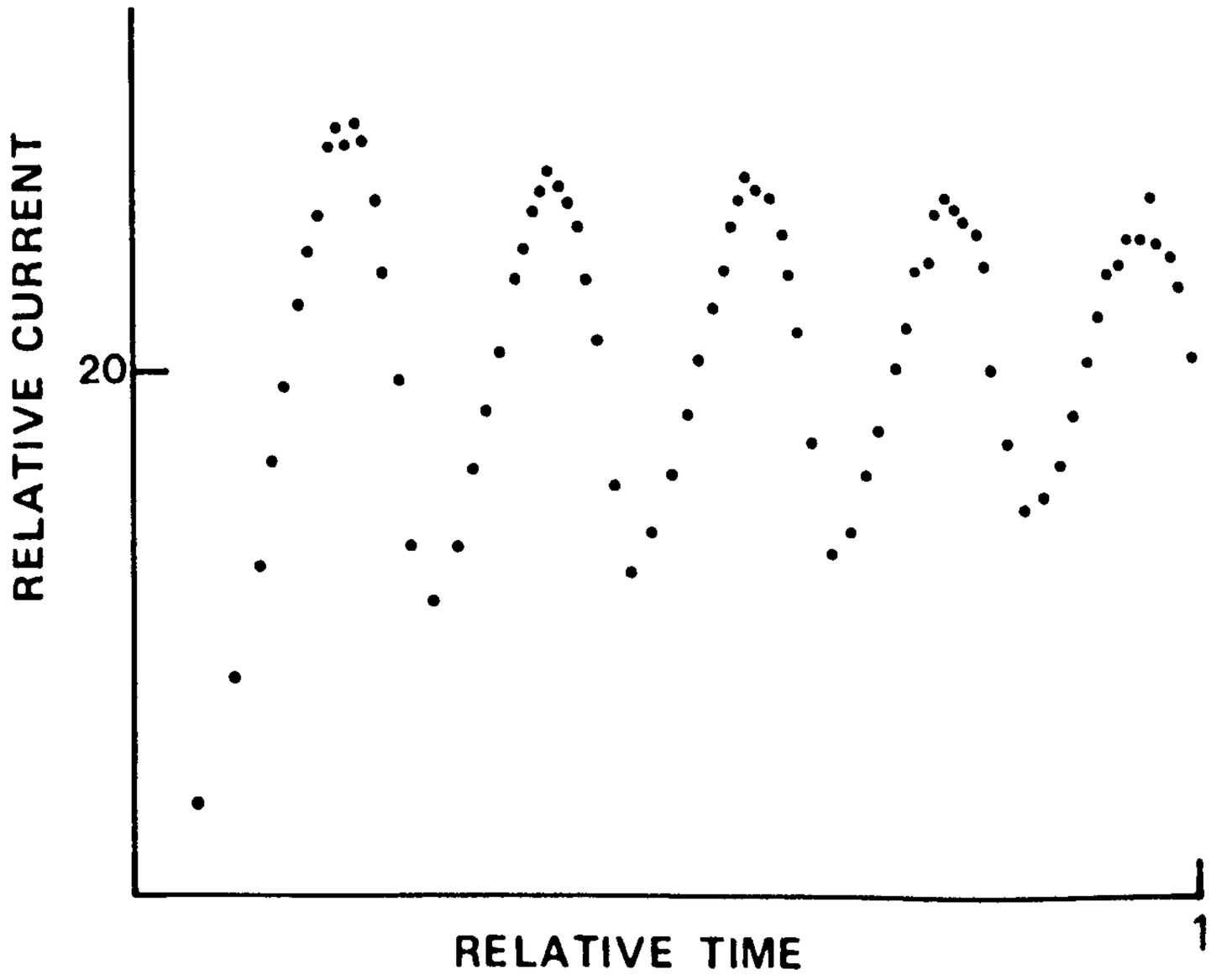

Fig 6.10 Simulated current/time transient (average of 200 curves), for a 40 by 40 lattice over the equivalent of depositing 5 layers of atoms. The nucleation probability; p(3) = 0.001.

6.4.3 DEPENDENCE OF CURRENT TIME TRANSIENTS ON LATTICE SIZE AND BOUNDARY CONDITIONS

Referring to figs 6.10 and 6.11, we can see that there is some dependence of the i/t transient response upon lattice size used for the simulation. It is seen that the smaller the lattice size the greater the current oscillation (40^2, 60^2, 80^2, 120^2 and 160^2 lattices simulated), and consequentially the system takes longer to reach steady-state. In the tordial analogy of this system, it is clear that the model is closed and of fixed size, whereas the real system is effectively infinite. Thus increasing the lattice size simply increases the surface area of the torus, at infinite size the tordial model will correspond to an infinite plane system. Examination of the tordial model makes it clear that in the smaller system, a single growth centre could extend over the entire surface, whereas under the same conditions in a larger model, the growth centre would cover a proportionately smaller area. In the former case, a growth centre could come into contact with its own growing edges (see fig 6.12) thus leading to changes in the i/t response compared with a larger system. Considering a site adjacent to the advancing edge of a single circular growth centre, where growth only occurs at the periphery (point (*) in fig 6.12), we can see that it will only have occupied in-plane neighbouring sites on one side. However, as the growth centre expands a site will continue to have occupied neighbours on one side until, in the smaller model, the site comes into contact with the opposite edge of the same growing centre. Hence at this point of self contact, the site has an increased number of occupied

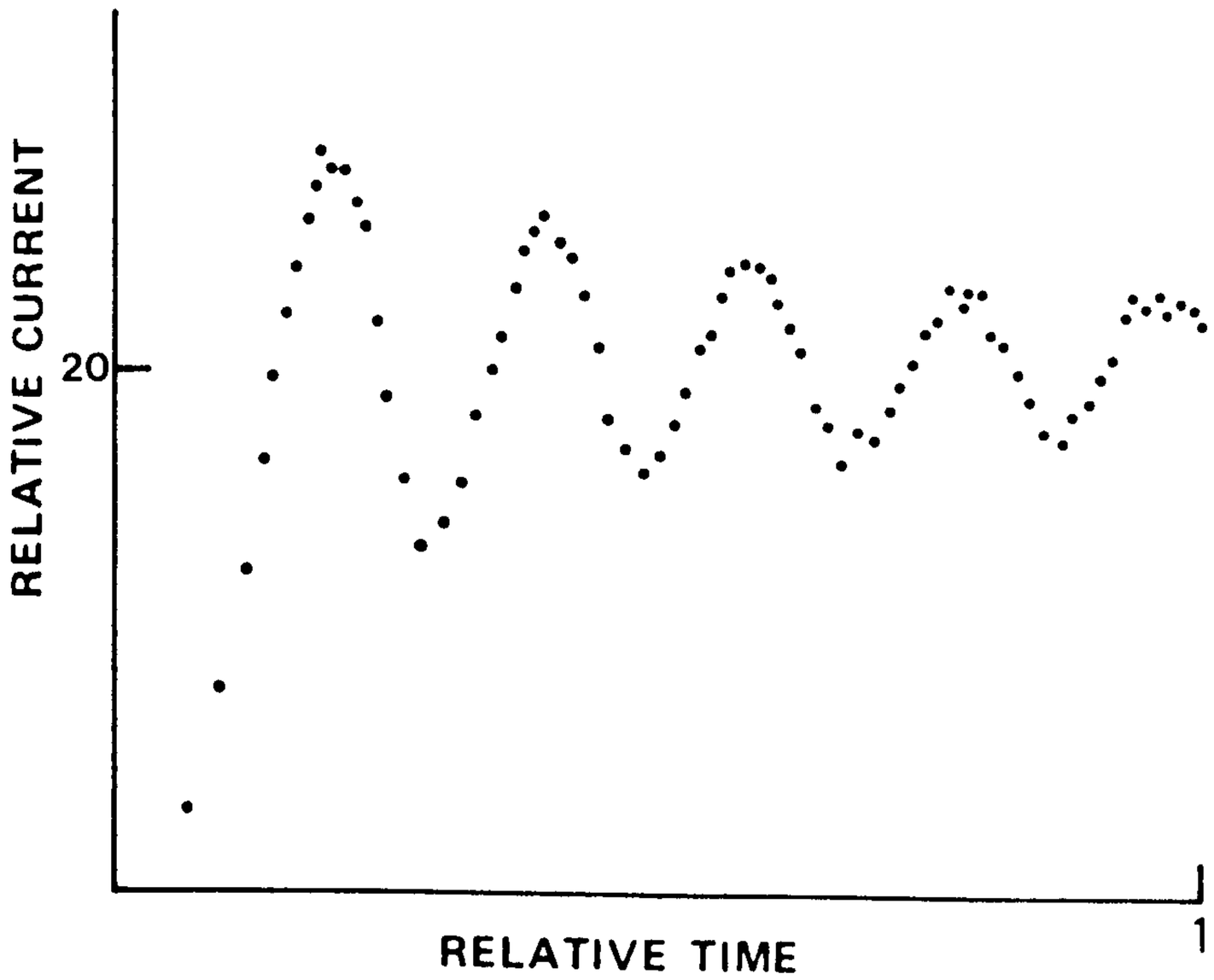

Fig 6.11 Simulated current/time transient (average of 20 curves), for a 160 by 160 lattice over the equivalent of depositing 5 layers of atoms. The nucleation probability; p(3) = 0.001.

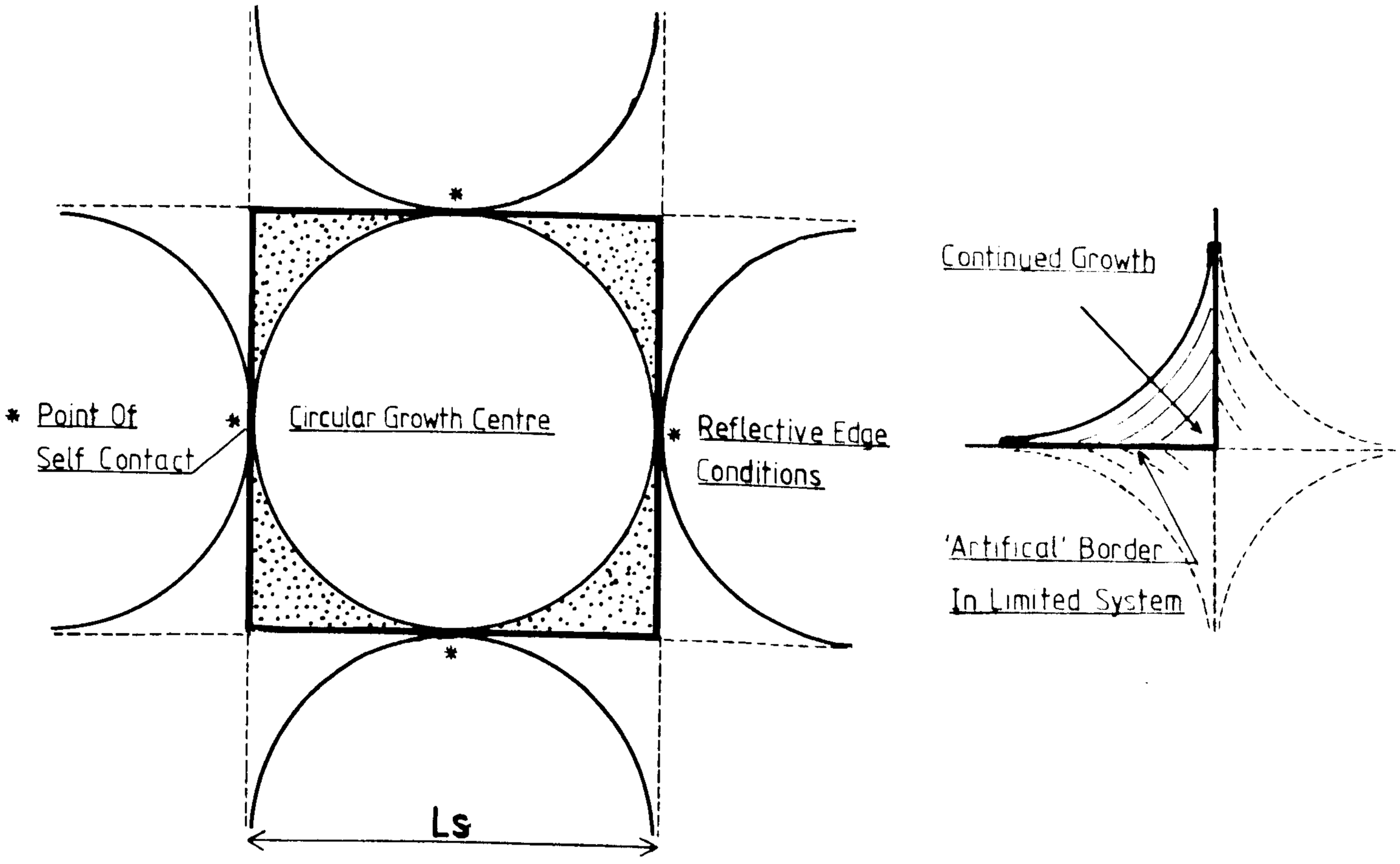

Fig 6.12 Comparison of the model for deposition of a single circular growth centre within a limited system, versus that of an infinite system where 'self contact' is impossible.

neighbours. Thus, likelihood of deposition is increased and the current will be higher than in the larger model (where the point of self contact will not have occurred). If we now consider continued growth after the point of self contact, it becomes clear that the number of sites having increased deposition (over the same surface area of a larger model) = $2Ls\rho$; ie double the lattice size x the surface density. Whereas the total number of sites available after the point of self contact is $(1 - \pi/4)Ls^2\rho^2$ (given by the shaded area in fig 6.12 - ignoring quantisation for the moment). If the time for deposition of an atom at a normal site is τ then the time for deposition at an enhanced site is τ x f where f is the ratio of the probability of deposition of the normal to the enhanced site (determined by the probabilities used in the simulation). Thus the normal current expected would be;

$$i_n = \frac{\text{No of atoms deposited}}{\text{time taken}} = \frac{(1 - \pi/4)Ls^2\rho^2}{\tau(1 - \pi/4)Ls^2\rho^2} = \frac{1}{\tau} \quad \{6.5\}$$

The enhanced current will be given by;

$$i_e = \frac{(1 - \pi/4)Ls^2\rho^2}{\tau[(1 - \pi/4)Ls^2\rho^2 - 2Ls\rho] + 2\tau f Ls\rho}$$

$$i_e = \frac{(1 - \pi/4)Ls^2\rho^2}{\tau Ls\rho[(1 - \pi/4)Ls\rho - 2 + 2f]} \quad \{6.6\}$$

where $(1 - \pi/4)Ls^2\rho^2 - 2Ls\rho$ is the number of normal sites.

Therefore;

$$i_e = \frac{(1 - \pi/4)Ls\rho}{\tau[(1 - \pi/4)Ls\rho - 2 + 2f]} \quad \{6.7\}$$

since $\Delta i = i_e - i_n$ (where i_n is the current expected for the infini system);

$$\Delta i = \frac{(1 - \pi/4)Ls\rho}{\tau[(1 - \pi/4)Ls\rho - 2 + 2f]} - \frac{1}{\tau}$$

$$\Delta i = \frac{(1 - \pi/4)Ls\rho - (1 - \pi/4)Ls\rho + 2 - 2f}{\tau[(1 - \pi/4)Ls\rho - 2 + 2f]}$$

$$\Delta i = \frac{2 - 2f}{\tau[(1 - \pi/4)Ls\rho - 2 + 2f]} \qquad \{6.8\}$$

Hence if f = 1 (no enhancement of edge sites), $\Delta i = 0$. With an estimated value of f ~ 0.5 (ie sites are twice as likely for deposition as normal sites), we get;

$$\Delta i = \frac{1}{\tau[(1 - \pi/4)Ls\rho - 1]} \doteq \frac{1}{\tau(1 - \pi/4)Ls\rho} \quad \text{if } Ls\rho >> 1$$

therefore we might expect;

$$\Delta i \propto 1/(Ls\rho) \qquad \{6.9\}$$

This is an idealistic case with non quantised deposition of a single circular growth centre, and in the example given, only shows deviation from the infinite case at the point of self contact. Current increase can however, be expected in the case where several nuclei are found, since edge sites will still have 'artificially' increased numbers of neighbours over the infinite case. In effect the reflective boundary conditions mean the growing centres will 'see' more growing neighbours than exist in the infinite system.

In the simulation two further factors are important 1) the average growing nucleus size and 2) irregularity of the growth centres. The latter factor must depend both on the deposition probabilities used (in this case kept constant), and the crystal structure modelled. As increasing the irregularity extends the total peripheral length without a similar increase in the contact between growth centres, increasing the irregularity will

decrease Δi. Considering 1), it is clear that if the growing nuclei are small in comparison to the model size, the influence of the limited model size will be less and thus the current increase will be smaller. Hence the ratio of nucleation current to growth current must be an influence. Additionally the average growing nucleus size at time t will depend upon t, mimicking the i/t transient, since both are influenced by the total peripheral length, which will only be constant when the steady-state is reached. Therefore the current enhancement ($\Delta i/t$) transient will be some form of damped oscillation in phase with the expected i/t behaviour for an infinite system. It will thus increase the amplitude and steady-state values of current observed for any limited system. Hence if the peak-peak current values for the oscillations are given by;

$$i_{pp} = \Delta i + i_n$$

if $i \propto 1/Ls$ we can write $\Delta i = k/Ls$

then;

$$i_{pp} = k/Ls + i_n \qquad \{6.10\}$$

Hence a plot of i_{pp} versus 1/Ls should be linear, intercept i_n slope k. Fig 6.13 shows a plot of peak-peak current for the first 4 oscillations versus 1/Ls for the average of several transients (see figs 6.10 and 6.11). The current values were normalised to give the same steady-state current at longer times, with all other conditions constant for the four system sizes. Although the errors are large we can indeed see linearity. From the intercepts indicated, the peak-peak current values for an infinite system should be considerably closer to the integral method curve (fig 6.8).

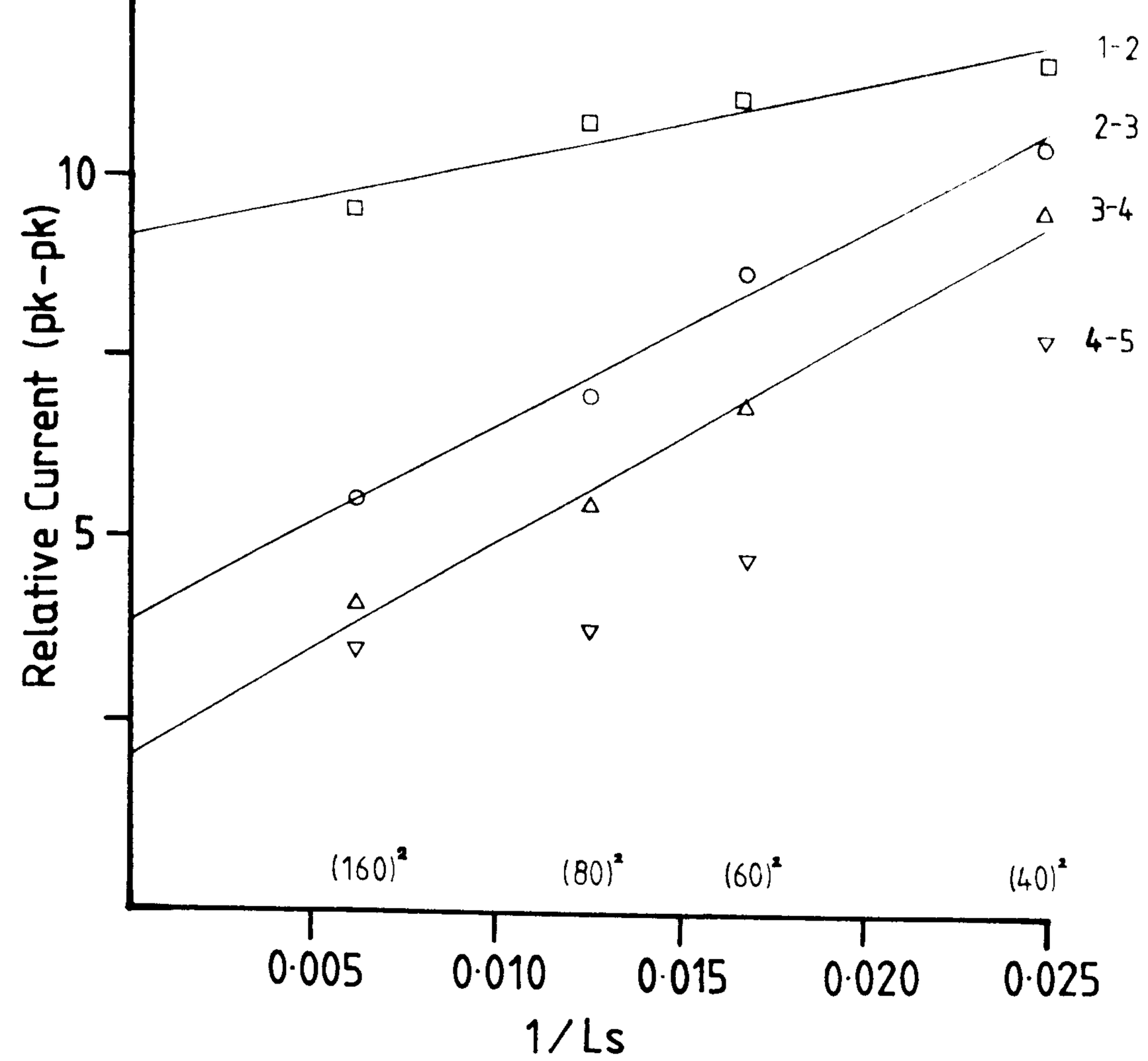

Fig 6.13 Plot of the peak simulated current oscillations (1st - 4th) versus 1/Ls (lattice edge length = Ls). Nucleation probabilities kept constant; p(3) = 0.001.

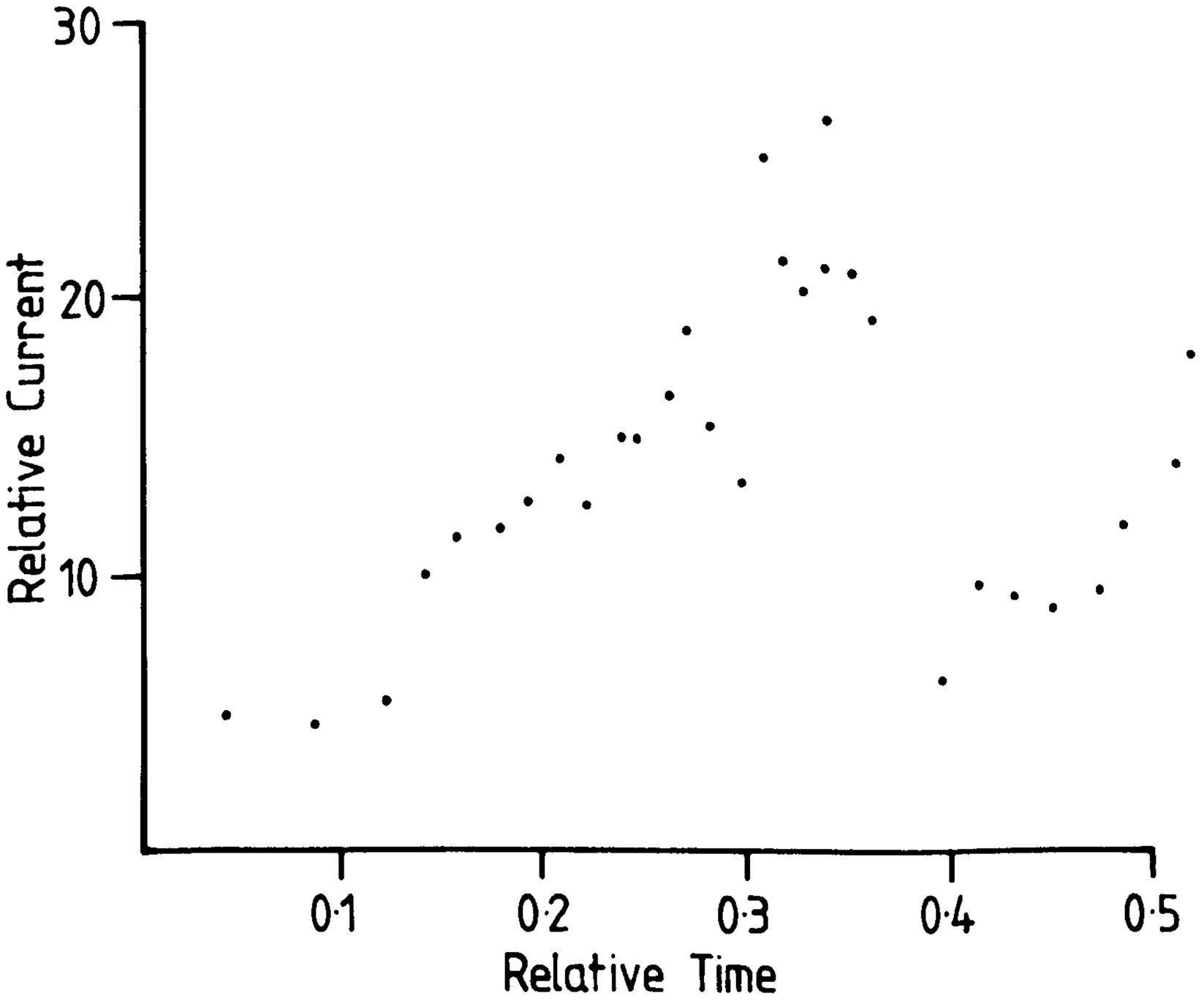

Fig 6.14 Single simulated current/time transient for an 80 by 80 lattice over the equivalent of depositing 5 layers of atoms, for the simulation incorperating a linear diffusion element. Nucleation probability; p(3) = 0.001.

In summarising this section it would be unwise to say that lattice size dependence was solely given by the 'artifical' border increase, as the results presented are not sufficient to be conclusive. Other explanations may be possible over the dependence of oscillation damping on lattice size, but it seems that artificial deposition rate increase for bordering sites must occur in a limited system, and must be a major influence in size dependence effects.

Using modified programs it was possible to observe i/t transients for systems with changed boundary conditions. Since in the tordial system all lattice sites are equivalent, the i/t behaviour should be the same for each section of the array as for the whole. As a check the i/t response for a 40 by 40 section within a 60 by 60 lattice was determined, the damped oscillations corresponded to that for a 60 by 60 system. Though in this simulation, computing time is necessarily increased by 36/16. Further changes allowed deposition onto a borderless model where reflection is avoided by 'surrounding' the perfect lattice base with empty sites. Clearly in this model, deposition at the edge sites is reduced, hence each layer up will be constrained further by the reduced deposition below, thus a pyramidal structure would be expected for the model. Hence at long times, $i \rightarrow 0$ for a limited system with infinite height, unless overhanging configurations are allowed. To overcome this effect the model size should again be as large as possible, since it is simply a ratio of the lattice surface area to volume that will determine the deviation from a true response. An alternative is to assume a limited range of edge effect and measure i/t behaviour over a smaller lattice within

the whole model.

6.4.4 CURRENT/TIME BEHAVIOUR WITH LINEAR DIFFUSION APPLIED

With the programs described in CH 6.3.6, it was possible to follow simulation deposition under the influence of a linear diffusion layer, whereby the atom impingement rate is dependent linearly on the distance out from the model surface. This models the Nernstian linear diffusion layer found over an electrode operating at steady-state in the diffusion controlled region (fig 1.8). The concentration of the active species is assumed to be zero at the surface but to rise linearly with distance out from the surface. Extrapolation of the initial linear portion to the bulk concentration, gives a distance corresponding to the Nernst diffusion layer thickness, the Nernst diffusion layer is thus an approximation to the curve found. The degree of fit to linear (and thus the accuracy of extrapolated Nernst diffusion layer thickness), is dependent on the degree of convection, high forced convection (eg rotating disc conditions), will give closest agreement. Programs using linear diffusion, have assumed that extrapolation of this region is valid down to the atomic scale simulated, and thus do not include other effects governing concentration of active species within this atomic scale region. In addition to this, the simulation differs from reality in one other respect, since the linear diffusion layer is applied from time t = 0, whereas this cannot be the case in reality. This will doubtless exaggerate to some extent, the effect of growth under these conditions, since during any time-period over which the Nernst

layer is becoming established, deposition will give a different morphology from that under steady-state conditions. A further point to be considered, is the changing position of the surface as atoms are deposited, and the associated shift in the linear diffusion layer. In this model the position of the surface was assumed to increase in height, dependent on the extent of filling of the lowest layer. In practice, simulations rarely caused an increase in surface position of more than one layer.

Fig 6.14 shows a typical i/t transient for a single run under linear diffusion conditions. This corresponds to the deposit shown in fig 6.15 and is the result of deposition of 6000 atoms (< 1 layer of atoms - see CH 6.4.6.3). The transient shows a general rising trend as would be expected, but interpretation is not possible, due to the program speed being considerably slower than that for the diffusion-independent programs [see CH 6.4.2]. This is due to a) the increased number of layers over which deposition is occurring (ie a bigger volume), and b) the favouring of higher sites, which are less likely to have sufficient coordination for deposition. Multiple averaging of i/t behaviour could thus not be obtained on a reasonable timescale, and the number atoms deposited was usually constrained by the time available for program running.

6.4.5 INFLUENCE OF RANDOM NUMBER GENERATION ON CURRENT/TIME BEHAVIOUR

It became clear during long term testing of random number generation routines, that a single flaw in the randomness, has a marked effect on the i/t behaviour (and thus presumably on

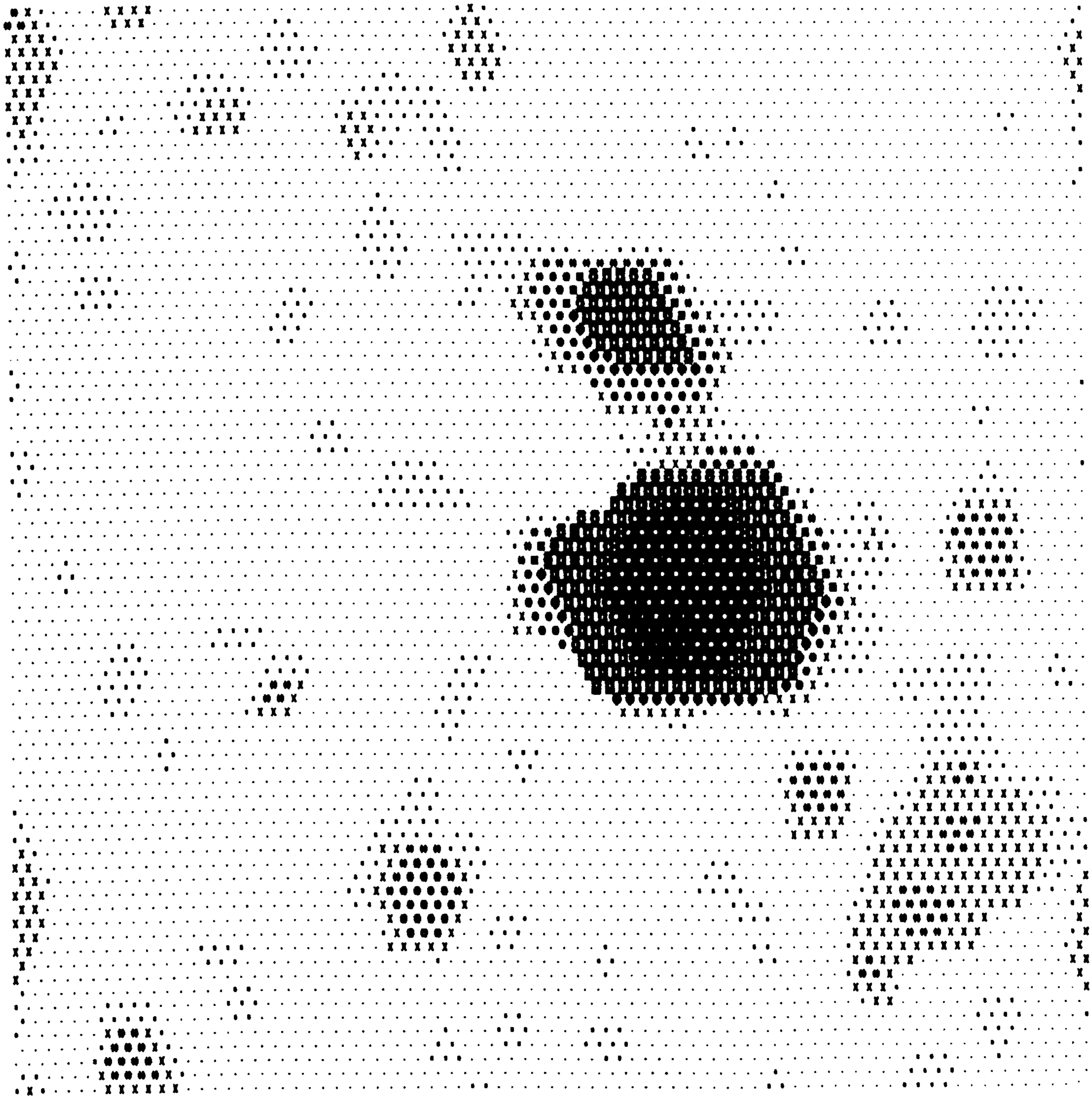

Fig 6.15 Surface morphology found for simulated deposition under linear diffusion conditions, 5300 atoms being deposited. Nucleation probability; p(3) = 0.001. Computer produced density map.

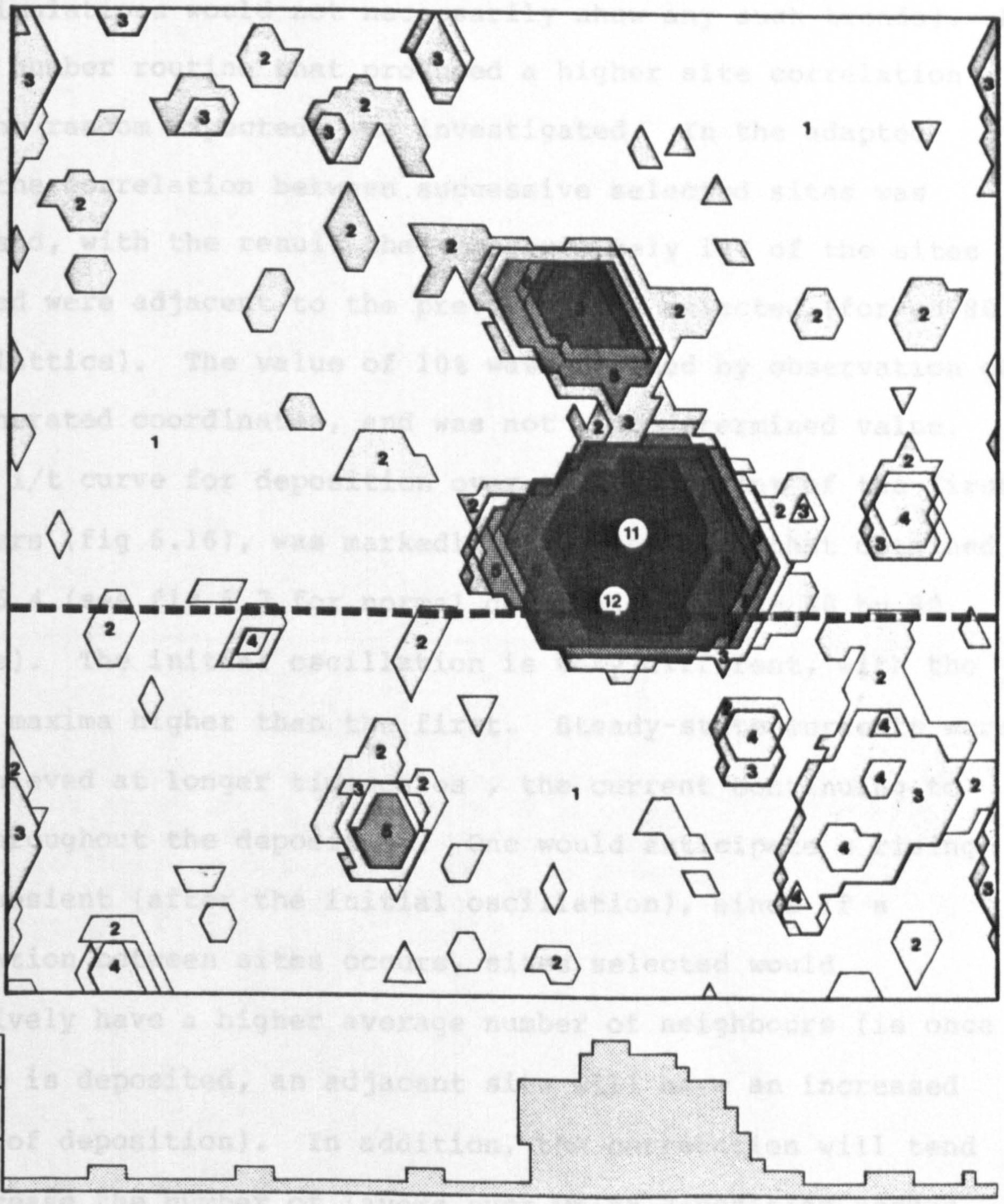

Fig 6.15 Surface morphology found for simulated deposition under linear diffusion conditions, 5300 atoms being deposited. Nucleation probability; p(3) = 0.001. Numbers indicate spot heights, cross-section shown below. Current/time transient as in fig 6.14.

morphology, although visual inspection of a limited number of such simulations would not necessarily show any such trends). A random number routine that produced a higher site correlation than the random expected, was investigated. In the adapted model the correlation between successive selected sites was increased, with the result that approximately 10% of the sites selected were adjacent to the previous site selected (for an 80 by 80 lattice). The value of 10% was obtained by observation of the generated coordinates, and was not a predetermined value.

The i/t curve for deposition over the equivalent of the first 10 layers (fig 6.16), was markedly different from that obtained in CH 6.4 (see fig 6.7 for normal deposition for an 80 by 80 lattice). The initial oscillation is very different, with the second maxima higher than the first. Steady-state currents were not achieved at longer timescales , the current continuing to rise throughout the deposition. One would anticipate a rising i/t transient (after the initial oscillation), since if a correlation between sites occurs, sites selected would effectively have a higher average number of neighbours (ie once an atom is deposited, an adjacent site will have an increased chance of deposition). In addition, the correlation will tend to increase the number of layers over which deposition occurs. It is interesting to note that some workers[126,127] have produced remarkably similar transients to that in fig 6.16, and since none present any evidence of having statistically checked the random numbers, it is possible the erroneous behaviour is in part due to correlation between the random numbers used for site coordinates. Further investigations of random number dependence were carried out using a program favouring the diagonal elements

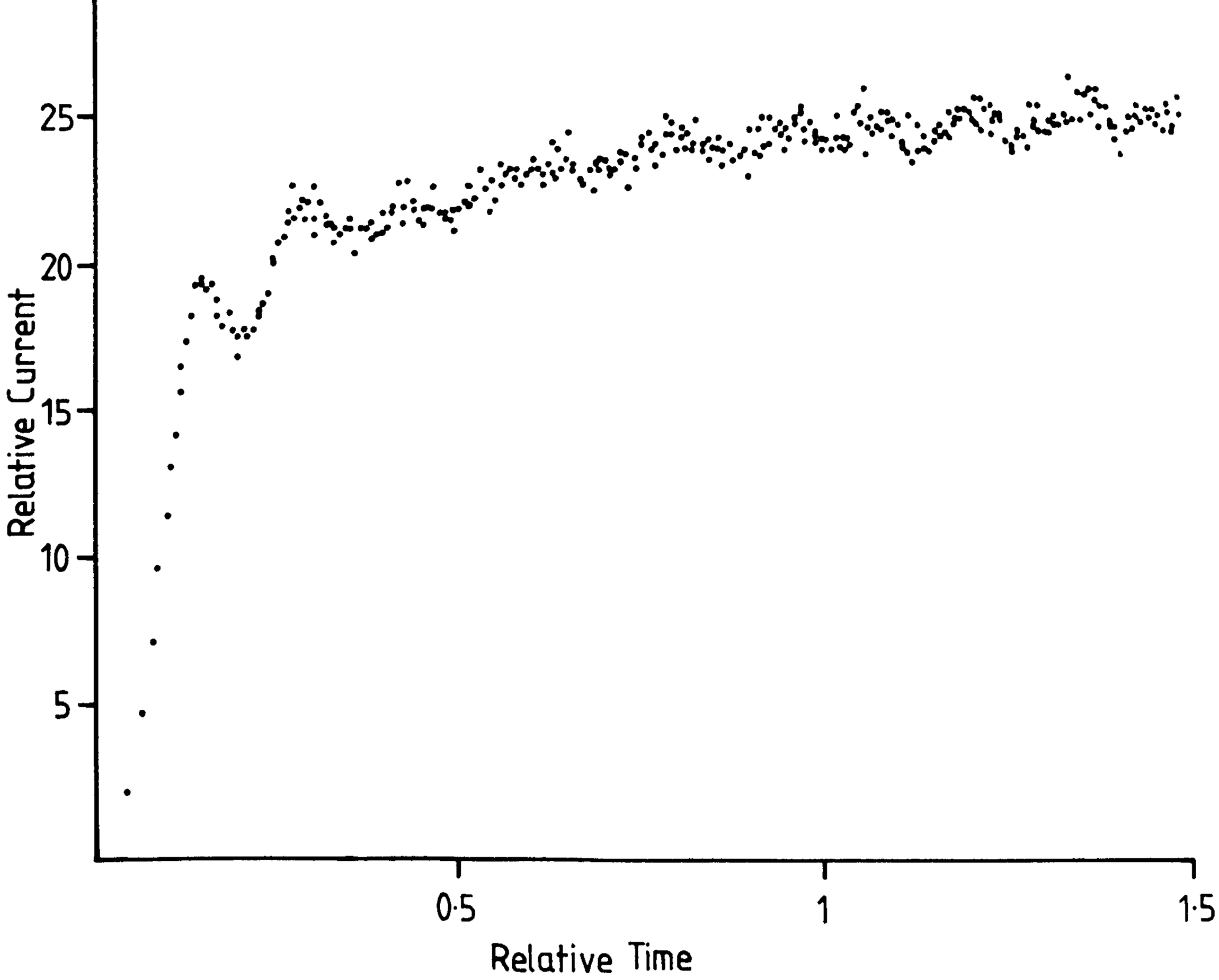

Fig 6.16 Simulated current/time transient (average of 40 curves), for an 80 by 80 lattice, with a correlation between successive selected sites, such that 10% were adjacent to the previous site. The equivalent of depositing 10 layers of atoms is shown. The nucleation probability; p(3) = 0.001.

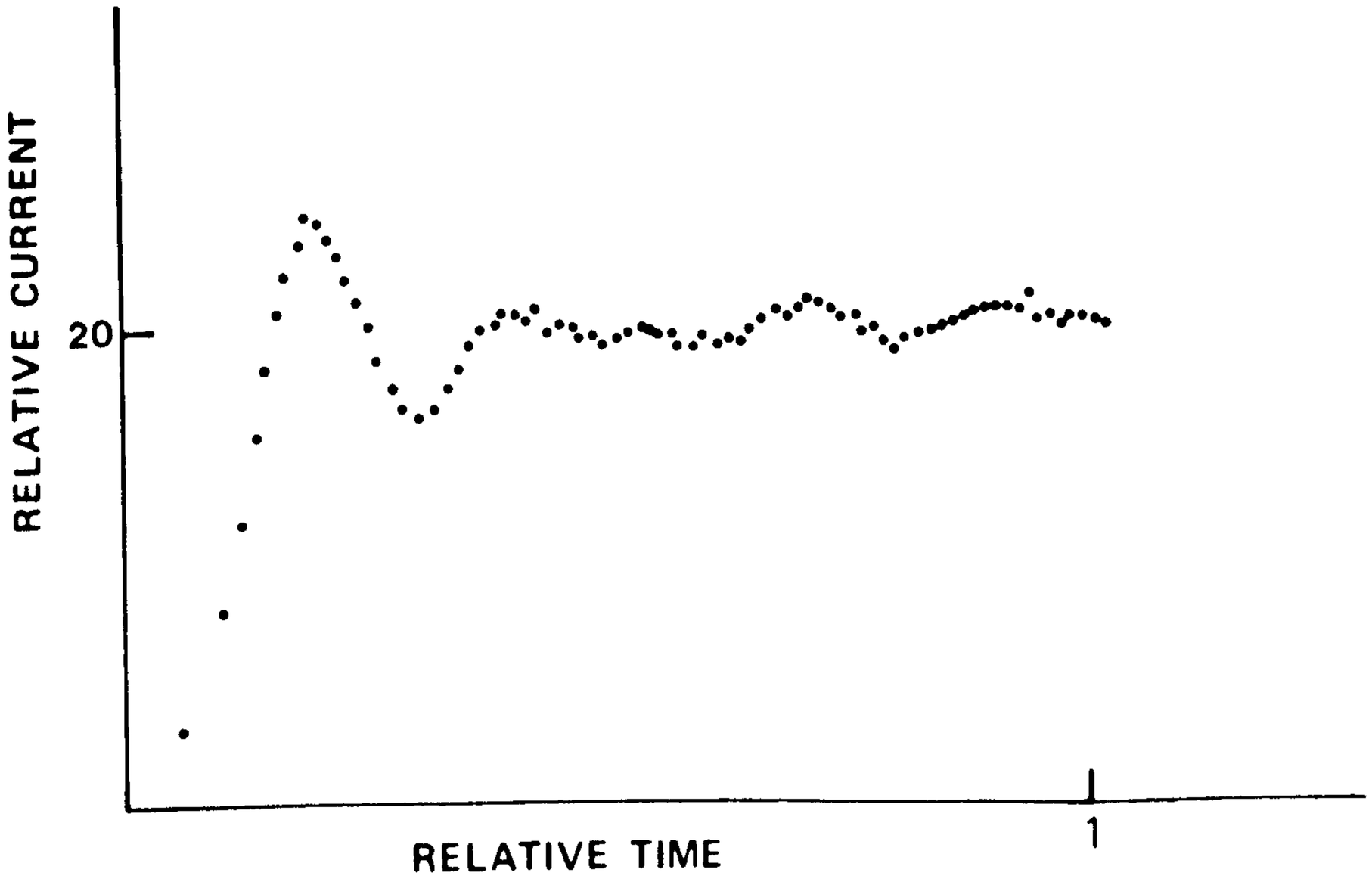

Fig 6.17 Simulated current/time transient (average of 20 curves), for a 160 by 160 lattice, favouring diagonal elements by 40% over other sites. The equivalent of depositing 5 layers of atoms is shown. The nucleation probability; p(3) = 0.001.

of the lattice by ~40% over other sites (ie each diagonal site was selected 40% more than other sites). Fig 6.17 shows the i/t transient observed for deposition on to an 80 by 80 lattice, using this program and the standard probability set [see CH 6.2]. Comparing this with the integral method curve in fig 6.8, and the correct i/t behaviour in fig 6.7 and 6.11, we can see a dramatic improvement in the agreement with the integral method curve. The small peaks produced during the latter stages of deposition appeared to be reproducible, but at this stage no simple reason for them can be put forward. The effect of increased selection of particular sites will be to cause greater localised deposition, but perhaps more significantly, it will allow deposition to occur sooner on higher layers, thus reducing the time at which the higher layers contribute to the transient. Therefore the i/t response should give rise to a more damped oscillation. This slight favouring of higher layers compared with normal transients, is analogous to a system with some limited diffusional dependence, and may be equivalent to applying a small overpotential to the model, in its effect on the i/t curve. The morphology of this deposit is inevitably going to give a false picture of the surface, although examination by inspection did not always show this up. This system also exhibited lattice size dependence, such that the smaller the lattice size, the greater the amplitude of the initial oscillations.

In summarising this section, it is clear that even a slight deviation from true randomness is likely to influence results. Indeed slight correlation between, for instance, the first and third chosen sites, may not show up in simple statistical

analysis, thus leading to possible false interpretation. The advent of cheaper, more powerful microcomputers may not necessarily be accompanied by an increase in the computer's ability to produce true random numbers. Thus, since microcomputer users are generally not statistical experts and will tend to 'trust' the machine, some false data will inevitably be produced.

6.4.6 DEPOSITION MORPHOLOGY

6.4.6.1 DETERMINATION OF SURFACE AREAS

In an atomistic model, it is not clear exactly what the surface area should be, since one cannot assess atomic surface area as the sum of the area of each atom exposed. Conversely, if we assume the surface represents a more macroscopic picture, one cannot assume the measured surface area will represent what is correct on the atomic scale. The following assessment of surface area is therefore an approximate guide, to show contrasts between systems.

Measurement of the surface area of some deposited lattices, was made by assessing the total contact area the deposit would have with a solution. This was given by evaluating the total geometric area of the deposit as a sum of the area of all the crystal faces, such that the initial area is Ls^2 and the deposited area is given by $Ls^2 + \Sigma e_l e_h$; $e_l e_h$ being the edge length x edge height. This is an approximation to reality, since faces in and perpendicular to the base (0001) plane are assessed upon a continuous edge length, whereas crystal surfaces

in planes at other angles are assessed in terms of stepped faces. This approximation will therefore give a slightly higher surface area than should be expected.

An alternative assessment of surface area on an atomic scale, would be to assume that surface area $\propto$ surface energy, where the surface energy is given by the total number of incomplete bonds of atoms at the surface. Each atom has thus (12 - coordination number) bonds available, hence summing the available bonds at the surface, will give a measure of the surface energy for the system. Measurement of the surface energy would give a much greater importance to atomic scale surface roughness, than would evaluation of geometric area, hence for this model, surface area was not assessed from surface energy. Surface areas, where given, are relative to the initial area of the perfect (0001) plane.

6.4.6.2 THE DIFFUSION INDEPENDENT CASE; DEPENDENCE ON NUCLEATION RATE AND DEPOSITION PROBABILITIES

Using the appropriate programs as described in CH 6.3.6, it was possible to observe simulation morphology under a variety of conditions, with the real-time display of deposition of individual layers, coupled with the printout of height maps [CH 6.3.5]. Real-time observation of the simulated deposition enabled a qualitative assessment of the growth mechanism, which was found to depend on the ratio of nucleation current to growth current. At high nucleation current, growth proceeded rapidly (see fig 6.9 for the i/t curve at nucleation rate p(3) = 0.05; where p(3) is the nucleation probability). Coverage of the

surface was achieved by a large number of small growth centres, that eventually overlapped, allowing a flat (low angle), but high roughness deposit to build up layer by layer. The surface area increase was x 1.26, with deposition occurring over 3 layers. Growth mainly occurs over 3 layers for all the diffusion-independent simulations. However, for this system, due to the high deposition rate and the deposit irregularity, the ´filled´ layers have a high vacancy content, at p(3) = 0.05 (80 by 80), an average of 92 vacancies per layer were found, this is to be contrasted with an average of 1 - 2 vacancies per layer at p(3) = 0.001. During subsequent growth, most of these vacancies are covered over, but since deposition above such sites is lowered (ie, the number of neighbours is decreased for sites above vacancies), some defects will be propagated through subsequent layers. At low nucleation rates, the deposition is considerably more structured, fig 6.18 shows that produced after 32000 atoms at p(3) = 0.002. Here, we see that growth is still flat in nature (surface area x 1.16) giving a low angle deposit with growth occurring over 3 layers. Vacancies are also considerably reduced in number, due to the increased probability of such high coordination sites being filled. At p(3) = 0.0001 the morphology is essentially flat (fig 6.19), it can be seen that the deposit becomes more crystalline in nature, although still of a low angle. This increasing crystallinity is reflected in the decreased surface area of x 1.08 . Deposition, as with the higher nucleaton rate systems, is observed over a maximum of 3 layers. The trend upon reduction of the nucleation rate, is summarised as follows;

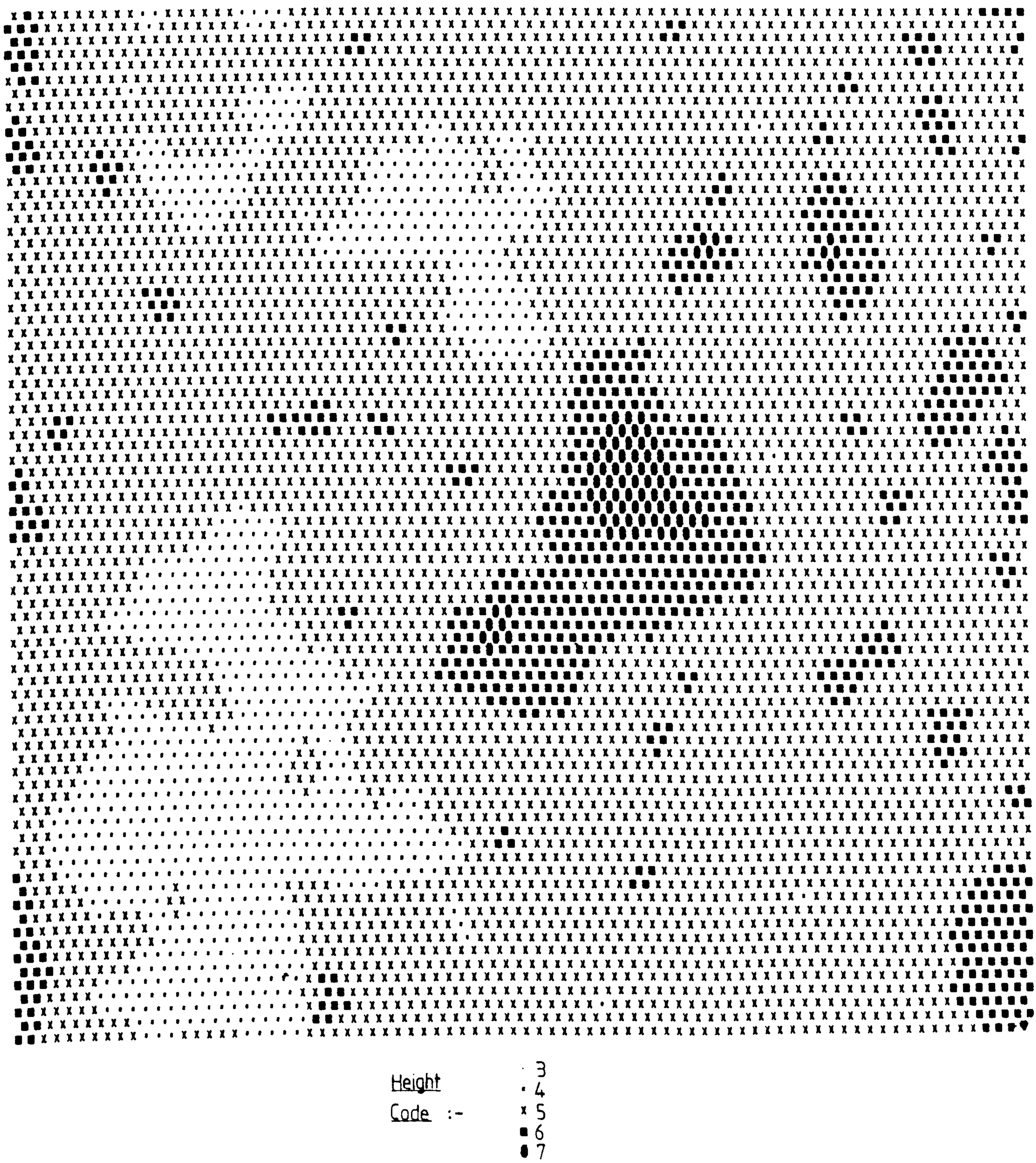

Fig 6.18 Surface morphology found for simulated deposition under diffusion-independent conditions, 32000 atoms being deposited. Nucleation probability; p(3) = 0.002. Computer produced density map.

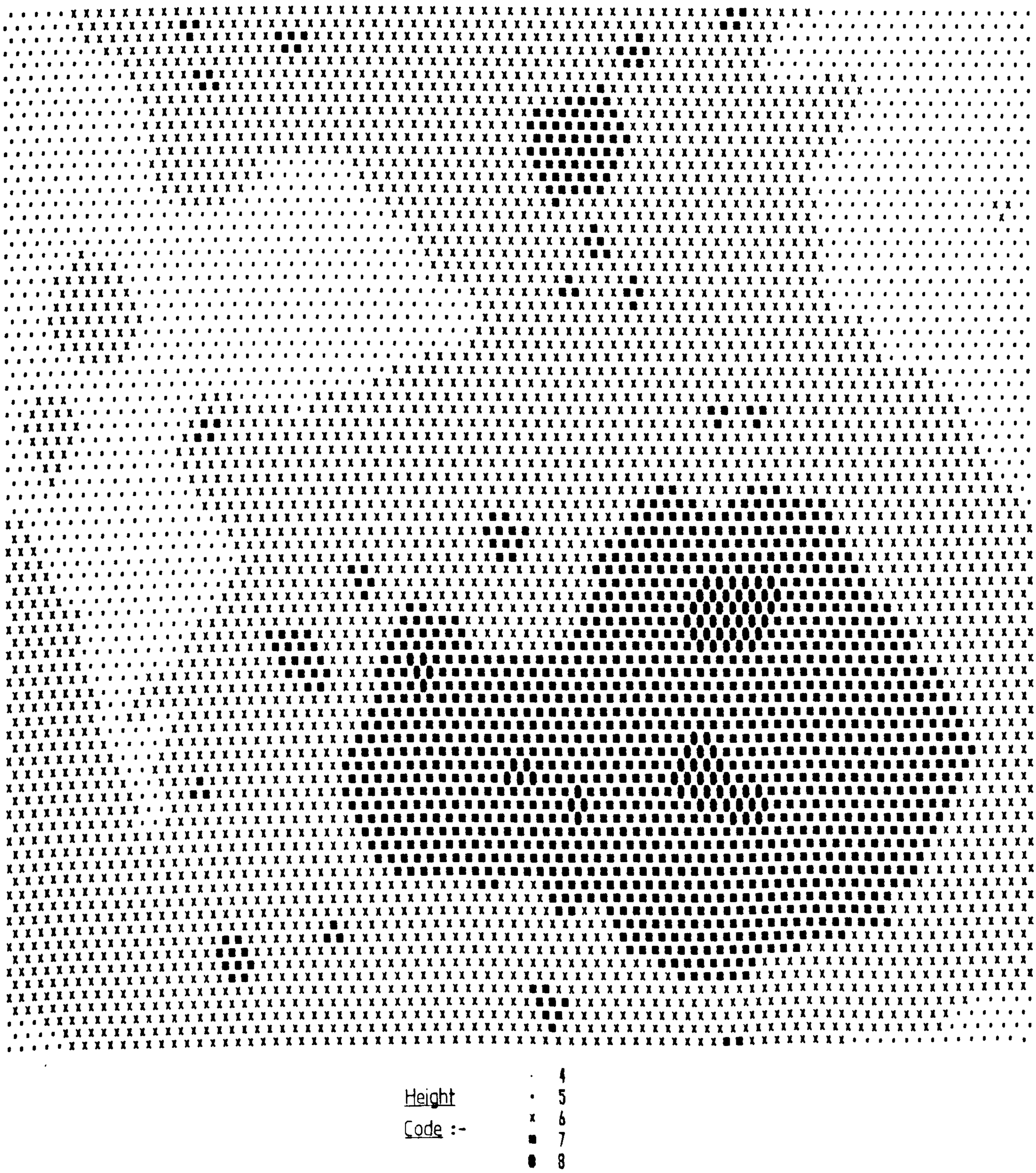

Fig 6.19 Surface morphology found for simulated deposition under diffusion-independent conditions, 32000 atoms being deposited. Nucleation probability; p(3) = 0.0001. Computer produced density map.

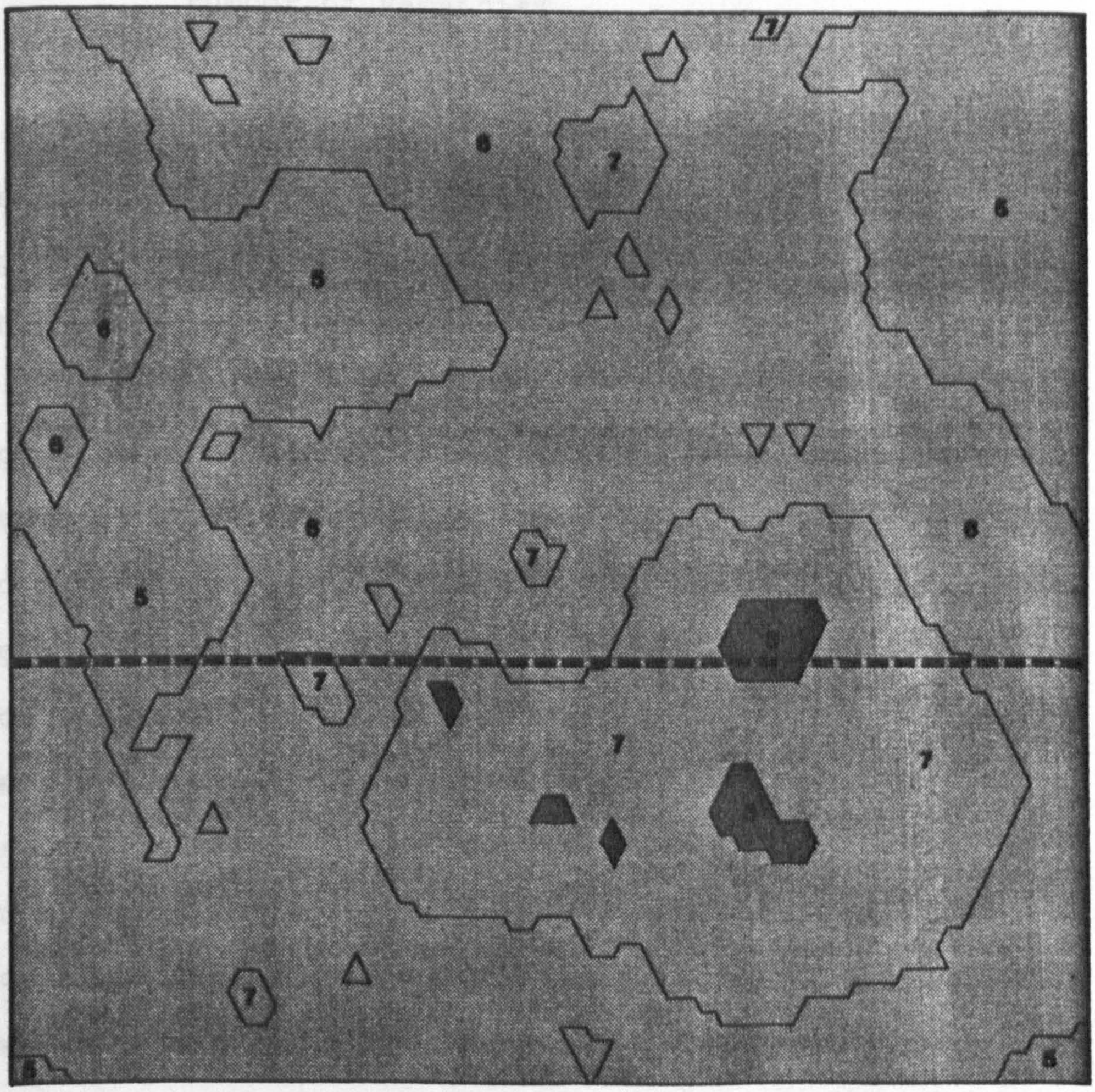

Fig 6.19 Surface morphology found for simulated deposition under diffusion-independent conditions, 32000 atoms being deposited. Nucleation probability; p(3) = 0.0001. Numbers indicate spot heights, cross-section shown below.

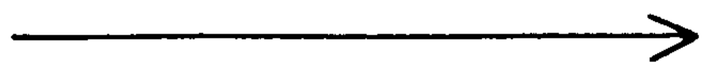

nucleation rate

number of vacancies

surface area

number of growth centres

Before establishment of the steady-state current, the morphology is dependent on the stage at which it is observed, ie, at the oscillation maxima, the number of nuclei (and growth centres) is at a maximum. Correspondingly, observation of the morphology at the oscillation minima will show a surface more uniform than at steady-state, with fewer growth centres. After continued deposition, little difference is found in surface morphology between 5 layers and 10 layers of equivalent deposition, indicating that the morphology observed is maintained, and that no surface amplification of irregularities occurs as does in some real systems [see CH 4.1.1.1]. This is indicated by the i/t transient, where a steady-state current is maintained after the initial oscillations.

At low nucleation rates the growth largely occurs by regular extension of the borders of each growth centre, giving rise to more regular (and larger) growth centres. Growth predominantly proceeds on a layer by layer basis with the majority of growth occurring on one layer, with additional deposition due to both nucleation on the layer above and filling in on the layer below. This corresponds well to observed deposition at low overpotentials[162]. Simulated layer by layer deposition of this nature has been studied by several workers[131-153], these studies also support the view that surface amplification does not occur, giving rise to essentially flat deposits. The surface appearance of the diffusion-independent system is quite

clearly dependent on the ratio of nucleation current to growth current. This is implicit in the work of Gilmer et al[143,146]. Increasing the nucleation current increases the surface roughness, but from qualitative analysis of morphology it appears that the deposit angle (flatness) is independent of nucleation current. At very high nucleation currents, one can anticipate the distinction between surface roughness and flatness becomes more indistinct, due to the propagation of defects through the lattice, and the limited simulation size.

6.4.6.3 INFLUENCE OF LINEAR DIFFUSION

Deposition simulation using the programs incorporating a linear diffusion model [as described in CH 6.2], was carried out to examine the effect application of a simulated linear diffusion layer has over deposition morphology. This models deposition under diffusion control at high overpotential where a Nernst diffusion layer has been established (see fig 1.8). Observation of figs 6.15, 6.20 and 6.21, shows the typical surface pictures found for the linear diffusion system. A striking contrast in morphology is found between the two systems (compare with fig 6.19). Discrete crystallites develop rapidly after the equivalent of less than one layer of atoms, giving rise to a high relief deposit where deposition has occurred over a large number of layers. Fig 6.21 shows deposition over 13 layers after 6000 atoms, and can be compared with 3 layers for 32000 atoms deposited under the diffusion-indpendent model (fig 6.19). The surface area of these, shows quite a marked difference, fig 6.21 has a surface area of x 1.35 after 490000

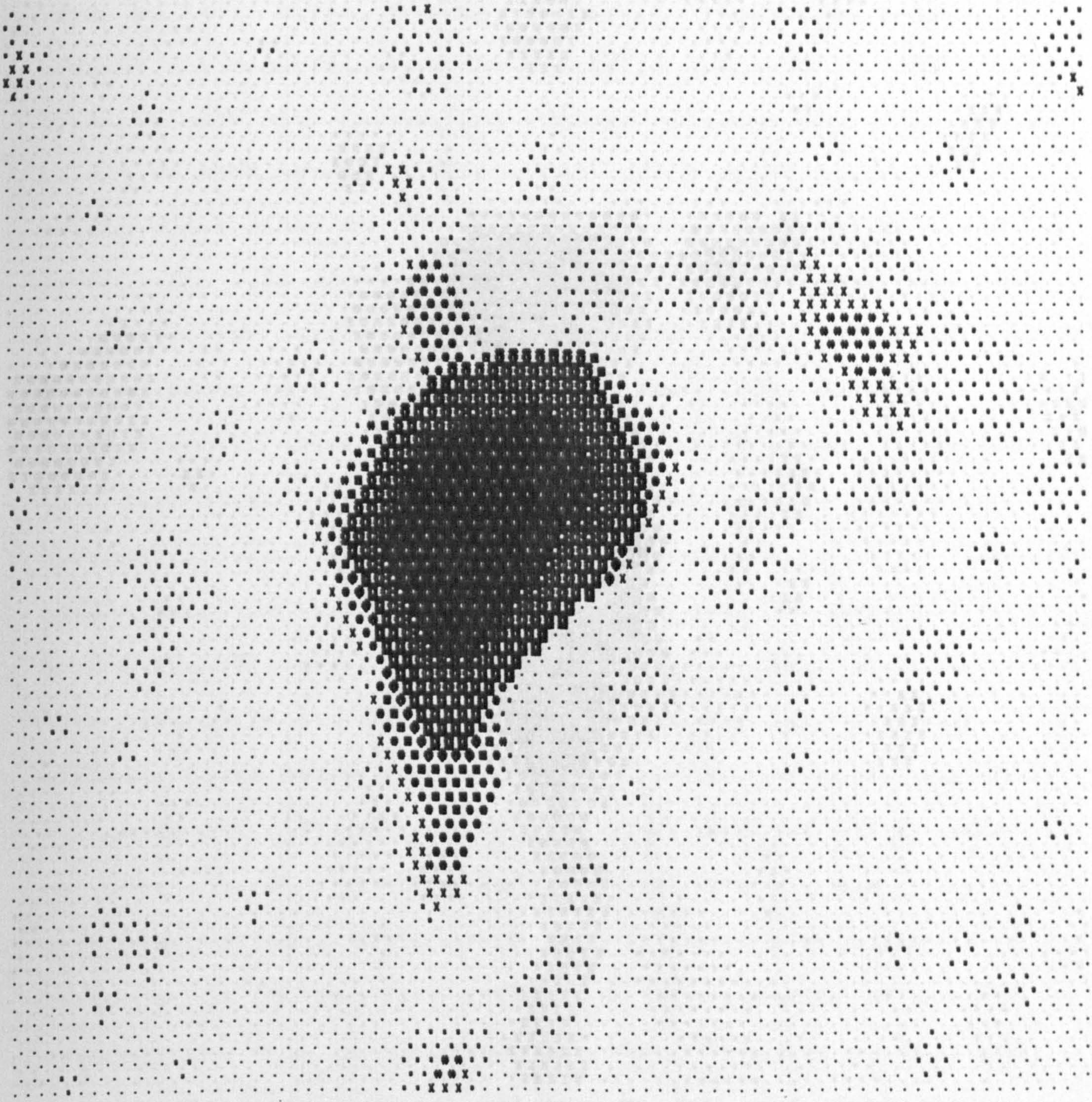

Fig 6.20 Surface morphology found for simulated deposition under linear diffusion conditions, 5800 atoms being deposited. Nucleation probability; p(3) = 0.001. Computer produced density map.

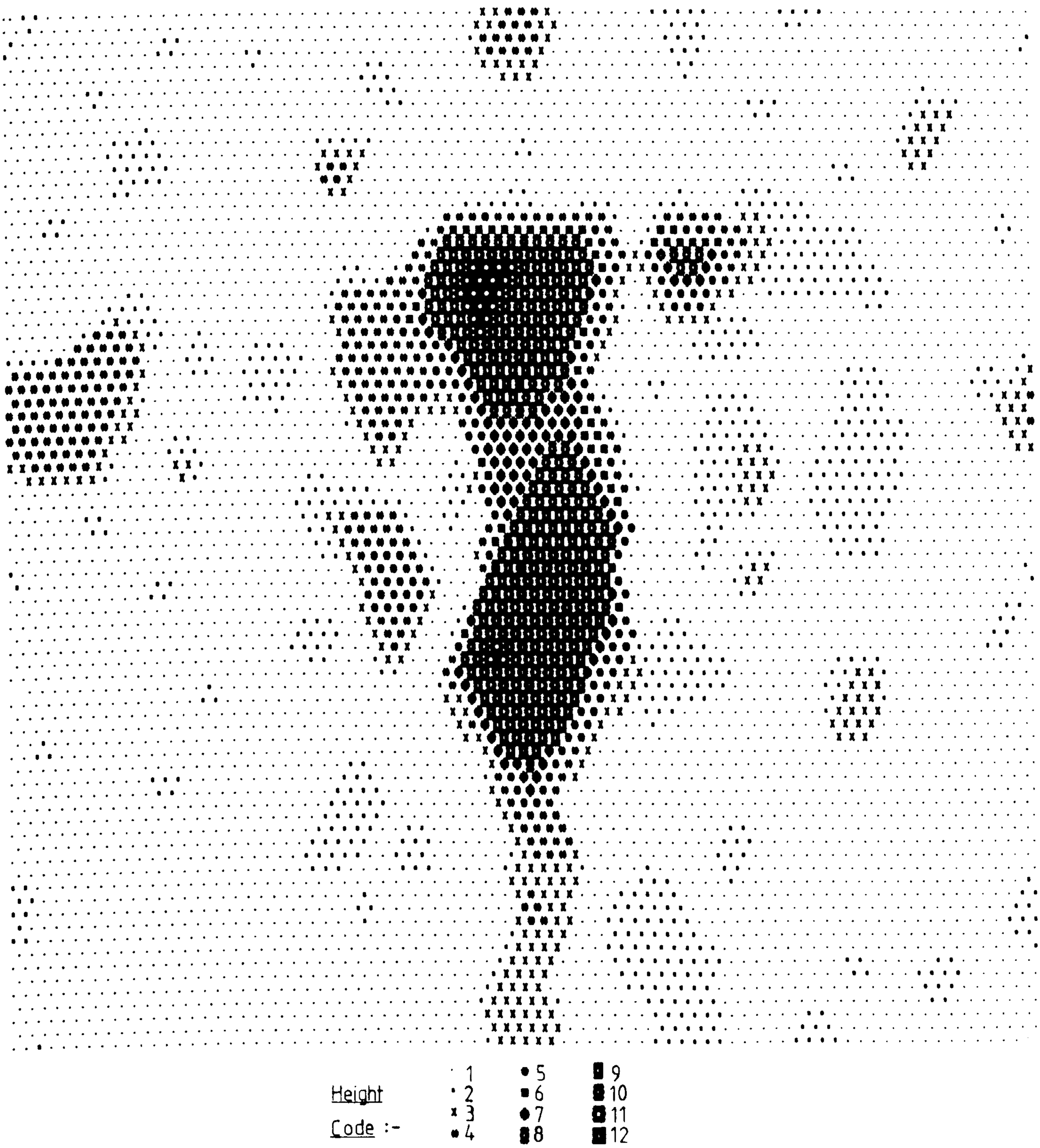

Fig 6.21 Surface morphology found for simulated deposition under linear diffusion conditions, 6000 atoms being deposited. Nucleation probability; p(3) = 0.001. Computer produced density map.

trials, compared with an area of x 1.08 for the flat deposit after 5100000 trials. Clearly deposition does not occur on a layer by layer basis, growth is largely confined to a single area of the deposit, which is generally observed to increase in crystallinity with increasing numbers of atoms deposited. This is due to each new layer deposited on the crystallite being mainly constrained to fit within the borders of the previous layer. Fig 6.20 shows a simulation after 6000 atoms have been deposited, the surface area was observed to increase from x 1.22 at 3600 atoms to x 1.32 after 6000 atoms. Upon careful examination of the layer by layer picture of these crystallites (and from 3D modelling), it is clear that both vacancies and overhanging configurations occur. The model size is too limited to estimate the vacancy density, but it would be expected to be higher than for the diffusion-independent system, since favouring of higher layers will increase the likelihood of unfilled sites being covered over. Overhanging areas and their influence are difficult to assess, most observed occurrences are not more than 2 or 3 atoms width (fig 6.15), but are sufficiently large to indicate that extended simulation using a larger model lattice size would lead to production of surface crystallites with considerable overhang. Thus using this model, it is possible for the initial stages of a dendrite to be formed, unlike most simulations employed by other workers[132,134-8, 140-151], where such overhanging configurations are not allowed. Comparison of the surface areas of the deposits formed under both linear diffusion and diffusion-independent systems (fig 6.22), indicates a rapid rising trend for the linear diffusion model, whereas the diffusion-independent system tends towards a

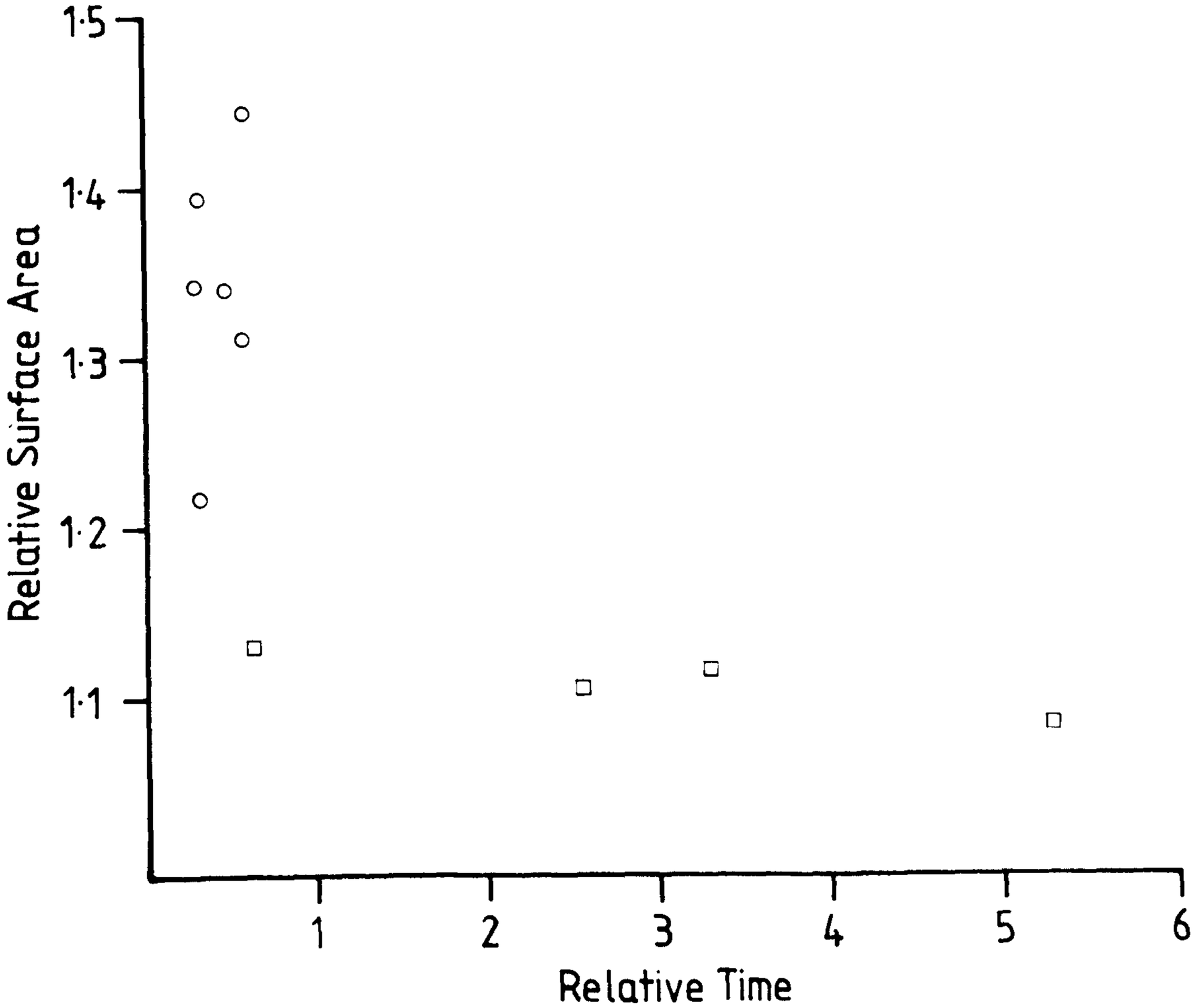

Fig 6.22 Plot of simulated surface area versus time for the diffusion-independent (□), and linear diffusion (○) systems. 80 by 80 lattices, nucleation probability; p(3) = 0.001.

limiting value, dependent on the nucleation rate used. This models the increase found for the high overpotential deposition of cadmium in both alkaline and acidic electrolytes [CH 3 and CH 5]. Examination of figs 6.15, 6.20 and 6.21, shows highly crystalline deposits, exhibiting considerable similarity in shape to real surface crystallites, obtained by cadmium deposition in acidic solutions of cadmium sulphate at η = -100 mV [see plates 5.1a and 5.3a/b in CH 5]. However, if on an atomic scale, the simulated crystallites are only 1/1000th of the scale of the real deposit. This 'micro' deposit would doubtless lead to larger crystallites if it were possible to model growth on such a scale. The crystallites observed for real cadmium deposition are quite clearly the direct precursors for dendritic growth. Favourably orientated crystallites giving rise to dendritic growth as is depicted in fig 5.2. Plates 5.3a/b show dendrites formed in this manner (after 100s deposition at η = -100 mV in 0.1M $CdSO_4$ / 0.5M H_2SO_4). The conclusion indicated from this is that the nuclei necessary for dendritic growth, can develop on an electrode surface without surface defects being present initially. For the simulated deposits observed, a density of 8 crystallites in 5 x 80 by 80 latticies was found. This would convert (on an atomic scale) to a nucleation site density of 4 x 10^{13} sites/m^2. This compares to a value of 7 x 10^{10} crystallites/m^2, for the observed deposits shown in Plates 5.3a/b. However the electron micrographs have insufficient resolution to detect crystallites below 0.1 μm, thus results are again not on a comparable scale. Comparisons with other systems give similar differences, a nucleation site density of 4.5 x $10^{10}/m^2$ for mercury on glassy

carbon at η = - 400 mV has been reported[183]. Thus one might conclude that in the absence of surface defects, a maximum of 1 in 50000 simulated microcrystallites would be likely to propagate to a sufficient size to allow dendritic growth. Of these macrocrystallites, no more than 0.1% will cause dendritic growth on the scale observed in plates 5.3a/b (from electron microsope observation of the cadmium deposits at η = - 100 mV). The role of low concentration impurities in dendritic growth thus becomes more confused. Clearly in real deposition, impurities in the electrode and the subsequent deposit have an influence, but this may not be as important as has been previously thought. Some work has been carried out on simulation of impurity incorporation, under the diffusion-independent (vapour deposition) conditions[145,146]. This showed that positive effect impurities (ie negative effect impurities reduce deposition), give an increase in simulated growth rate, accompanied by some changes in morphology. However, the mechanism of vapour deposition with impurities will be different from electrodeposition and thus its implications are open to question with respect to the electrochemical model.

In summarising the work in this chapter, it seems that physical surface defects are not required to produce nucleation sites. Rather, it seems more likely that their role is in selecting the more favourable of these sites for macroscopic deposition.

CONCLUSIONS AND SUGGESTIONS FOR FURTHER WORK

The starting point for this work was the long-standing industrial problem of the occasional sudden failure of nickel/cadmium cells. A common blame for cell failure being attributed to cadmium dendritic growth causing shorting between the positive and negative plates.

The research work carried out for this thesis has been successful, in as much as the likely cause of failure by cadmium dendritic growth has been established. Using alkaline electrolytes free from suspensions of cadmium salts, it has been seen that somewhat in excess of 150 hours of deposition at an overpotential of - 400mV, is required to produce any deposit substantial enough to pose a possibility of dendritic shorting. The presence of ~ 10^{-6}M of cadmuim salts in suspension can reduce this time to ~20 hours, with suspension concentrations in excess of 0.01M the time is further reduced to ~2 hours. Since the negative plate of the Ni/Cd cell is composed of amorphous cadmium hydroxide contained within a porous nickel matrix, it seems very probable that dendritic growth will occur in cells where this active material escapes into solution. Thus cells which suffer from ´leaky´ plate construction, vibration, excessive gas evolution or a small inter-plate distance (+ to -), are going to be the most likely to suffer dendritic failure.

This thesis has left untouched the area of confirmation of cadmuim dendrite growth in working cells (due to circumstances beyond the author´s control). It is however, an obvious area for further work. Cell failure could be studied under a variety of conditions, to establish the optimum conditions for prolonged

life. However, due to the requirement for cells, and the nature of the problem, this would require industrial cooperation of some form.

Having found the probable cause of dendritic failure, it is not so easy to recommend an industrially feasable cure, since unless a suitable dendrite inhibitor can be found, the only way of reducing the problem would be to alter the design of the cell to reduce suspension escape. This would involve substantial expense in altering production lines and considering the relatively minor extent of the problem, it would be unlikely to make economic sense, unless building a new factory. Searching for a dendrite inhibitor for the Ni/Cd cell would be an area for further work, but it would be unlikely to succeed in reducing the already slow dendrite growth of cadmium, without altering the performance. An alternative would be to find a way of removing or immobilising suspension particles before any growth could occur; eg adding a sedimentating agent to solution, or the addition of some form of 'glue' to the bottom of the cell, such that any free material, once settled, remains trapped harmlessly at the bottom of the cell.

Some progress has been made into the elucidation of dendrite growth mechanisms along conventional lines, using studies of both alkaline and acidic solutions of cadmium, but due to the very nature of the problem, the results are still qualitative in nature. The agreement between observed dendrite growth times and calculated growth times is good, provided one accepts the approximations involved. Further, more extensive, studies of dendrite growth in solution could be made, in order to improve knowledge and understanding of the factors controlling dendrite

growth. Towards this aim it would make sense to limit studies to systems having a high aqueous metal salt solubility, eg cadmium sulphate or zinc sulphate, rather than the alkaline system primarily investigated here.

Computer simulation of electrocrystallisation using a microcomputer, proved to be a successful technique, with several useful factors emerging. The establishment of a model size dependence and its influence on the simulation deposition behaviour, has not been extensively studied before, and as far as is known, no other work has simulated 3D crystal growth under the influence of a linear diffuion layer. The growth of simulated surface crystallites even in the absence of surface defects or impurities, implies that; contrary to established theory; defects are not necessary for dendritic growth (although they are likely to stimulate or speed up growth by a considerable margin). A few years ago this work could only have been achieved using a very expensive mainframe computer, but now the usage of an 'off the shelf' low cost microcomputer system can be employed equally effectively. It is doubtless going to be easier in the future, as the electronic revolution brings cheaper, more powerful computers onto the market (during the short period of this thesis, the Apple computer has been outdated by cheaper machines offering speed improvements of 20 x, and memory 10 x larger). There is considerable scope for further work on computer simulation; with the present machines, one could study different crystal lattices, boundary conditions, impurities, imperfect surface, ionic co-deposition, incorporation of evaporation, surface migration and deposition 'overpotentials', to mention but a few areas of work. The most

exciting further work would be computer simulation on the latest machines available (32 bit), to enable simulation of more macroscopic features to be carried out, such as a true dendritic growth. A new data storage system could also be developed, to use computer memory more economically. For instance, instead of storing each site in binary as a 1 or 0, one could store the positions of every solid-solution interface for each column of atoms. This would save memory, provided the number of interfaces produced was low (as was the case observed). It is thus the author's belief that the combination of new low cost machines, and an improved simulation model would now enable lattice sizes of the order 300 x 300 x 256 to be simulated.

APPENDIX I - THE 6502 INSTRUCTION SET

Name Description	Operation	Addressing Mode	Assembly Language Form	HEX OP Code	No. Bytes	Status Reg. N Z C I D V
ADC Add memory to accumulator with carry	A+M+C → A	Immediate	ADC #Oper	69	2	✓✓✓---✓
		Zero Page	ADC Oper	65	2	
		Zero Page X	ADC Oper X	75	2	
		Absolute	ADC Oper	6D	3	
		Absolute X	ADC Oper X	7D	3	
		Absolute Y	ADC Oper Y	79	3	
		(Indirect X)	ADC (Oper X)	61	2	
		(Indirect) Y	ADC (Oper) Y	71	2	
AND "AND" memory with accumulator	A AND M → A	Immediate	AND #Oper	29	2	✓✓-----
		Zero Page	AND Oper	25	2	
		Zero Page X	AND Oper X	35	2	
		Absolute	AND Oper	2D	3	
		Absolute X	AND Oper X	3D	3	
		Absolute Y	AND Oper Y	39	3	
		(Indirect X)	AND (Oper X)	21	2	
		(Indirect) Y	AND (Oper) Y	31	2	
ASL Shift left one bit (Memory or Accumulator)	(See Figure 1)	Accumulator	ASL A	0A	1	✓✓✓----
		Zero Page	ASL Oper	06	2	
		Zero Page X	ASL Oper X	16	2	
		Absolute	ASL Oper	0E	3	
		Absolute X	ASL Oper X	1E	3	
BCC Branch on carry clear	Branch on C=0	Relative	BCC Oper	90	2	------
BCS Branch on carry set	Branch on C=1	Relative	BCS Oper	B0	2	------
BEQ Branch on result zero	Branch on Z=1	Relative	BEQ Oper	F0	2	------
BIT Test bits in memory with accumulator	A AND M, M_7 → N, M_6 → V	Zero Page	BIT Oper	24	2	M_7✓---M_6
		Absolute	BIT Oper	2C	3	
BMI Branch on result minus	Branch on N=1	Relative	BMI Oper	30	2	------
BNE Branch on result not zero	Branch on Z=0	Relative	BNE Oper	D0	2	------
BPL Branch on result plus	Branch on N=0	Relative	BPL oper	10	2	------
BRK Force Break	Forced Interrupt PC+2↓P↓	Implied	BRK*	00	1	---1--
BVC Branch on overflow clear	Branch on V=0	Relative	BVC Oper	50	2	------
BVS Branch on overflow set	Branch on V=1	Relative	BVS Oper	70	2	
CLC Clear carry flag	0 → C	Implied	CLC	18	1	-----0
CLD Clear decimal mode	0 → D	Implied	CLD	D8	1	----0-
CLI	0 → I	Implied	CLI	58	1	---0--
CLV Clear overflow flag	0 → V	Implied	CLV	B8	1	-0----
CMP Compare memory and accumulator	A − M	Immediate	CMP #Oper	C9	2	✓✓✓---
		Zero Page	CMP Oper	C5	2	
		Zero Page X	CMP Oper X	D5	2	
		Absolute	CMP Oper	CD	3	
		Absolute X	CMP Oper X	DD	3	
		Absolute Y	CMP Oper Y	D9	3	
		(Indirect X)	CMP (Oper X)	C1	2	
		(Indirect) Y	CMP (Oper) Y	D1	2	
CPX Compare memory and index X	X − M	Immediate	CPX #Oper	E0	2	✓✓✓---
		Zero Page	CPX Oper	E4	2	
		Absolute	CPX Oper	EC	3	
CPY Compare memory and index Y	Y − M	Immediate	CPY #Oper	C0	2	✓✓✓---
		Zero Page	CPY Oper	C4	2	
		Absolute	CPY Oper	CC	3	
DEC Decrement memory by one	M − 1 → M	Zero Page	DEC Oper	C6	2	✓✓-----
		Zero Page X	DEC Oper X	D6	2	
		Absolute	DEC Oper	CE	3	
		Absolute X	DEC Oper X	DE	3	
DEX Decrement index X by one	X − 1 → X	Implied	DEX	CA	1	✓✓-----
DEY Decrement index Y by one	Y − 1 → Y	Implied	DEY	88	1	✓✓-----
EOR Exclusive Or memory with accumulator	A ⊻ M → A	Immediate	EOR #Oper	49	2	✓✓
		Zero Page	EOR Oper	45	2	
		Zero Page X	EOR Oper X	55	2	
		Absolute	EOR Oper	4D	3	
		Absolute X	EOR Oper X	5D	3	
		Absolute Y	EOR Oper Y	59	3	
		(Indirect X)	EOR (Oper X)	41	2	
		(Indirect) Y	EOR (Oper) Y	51	2	
INC Increment memory by one	M + 1 → M	Zero Page	INC Oper	E6	2	✓✓-----
		Zero Page X	INC Oper X	F6	2	
		Absolute	INC Oper	EE	3	
		Absolute X	INC Oper X	FE	3	
INX Increment index X by one	X + 1 → X	Implied	INX	E8	1	✓✓-----
INY Increment index Y by one	Y + 1 → Y	Implied	INY	C8	1	✓✓-----
JMP Jump to new location	(PC+1) → PCL, (PC+2) → PCH	Absolute	JMP Oper	4C	3	
		Indirect	JMP (Oper)	6C	3	
JSR Jump to new location saving return address	PC+2↓, (PC+1) → PCL, (PC+2) → PCH	Absolute	JSR Oper	20	3	

Name Description	Operation	Addressing Mode	Assembly Language Form	HEX OP Code	No. Bytes	Status Reg. N Z C I D V
LDA Load accumulator with memory	M → A	Immediate	LDA #Oper	A9	2	✓✓
		Zero Page	LDA Oper	A5	2	
		Zero Page X	LDA Oper X	B5	2	
		Absolute	LDA Oper	AD	3	
		Absolute X	LDA Oper X	BD	3	
		Absolute Y	LDA Oper Y	B9	3	
		(Indirect X)	LDA (Oper X)	A1	2	
		(Indirect) Y	LDA (Oper) Y	B1	2	
LDX Load index X with memory	M → X	Immediate	LDX #Oper	A2	2	✓✓
		Zero Page	LDX Oper	A6	2	
		Zero Page Y	LDX Oper Y	B6	2	
		Absolute	LDX Oper	AE	3	
		Absolute Y	LDX Oper Y	BE	3	
LDY Load index Y with memory	M → Y	Immediate	LDY #Oper	A0	2	✓✓
		Zero Page	LDY Oper	A4	2	
		Zero Page X	LDY Oper X	B4	2	
		Absolute	LDY Oper	AC	3	
		Absolute X	LDY Oper X	BC	3	
LSR Shift right one bit (memory or accumulator)	(See Figure 1)	Accumulator	LSR A	4A	1	0✓✓
		Zero Page	LSR Oper	46	2	
		Zero Page X	LSR Oper X	56	2	
		Absolute	LSR Oper	4E	3	
		Absolute X	LSR Oper X	5E	3	
NOP No operation	No Operation	Implied	NOP	EA	1	
ORA "OR" memory with accumulator	A ∨ M → A	Immediate	ORA #Oper	09	2	✓✓
		Zero Page	ORA Oper	05	2	
		Zero Page X	ORA Oper X	15	2	
		Absolute	ORA Oper	0D	3	
		Absolute X	ORA Oper X	1D	3	
		Absolute Y	ORA Oper Y	19	3	
		(Indirect X)	ORA (Oper X)	01	2	
		(Indirect) Y	ORA (Oper) Y	11	2	
PHA Push accumulator on stack	A↓	Implied	PHA	48	1	------
PHP Push processor status on stack	P↓	Implied	PHP	08	1	------
PLA Pull accumulator from stack	A↑	Implied	PLA	68	1	✓✓--
PLP Pull processor status from stack	P↑	Implied	PLP	28	1	From Stack
ROL Rotate one bit left (memory or accumulator)	(See Figure 2)	Accumulator	ROL A	2A	1	✓✓✓---
		Zero Page	ROL Oper	26	2	
		Zero Page X	ROL Oper X	36	2	
		Absolute	ROL Oper	2E	3	
		Absolute X	ROL Oper X	3E	3	
ROR Rotate one bit right (memory or accumulator)	(See Figure 3)	Accumulator	ROR A	6A	1	✓✓✓---
		Zero Page	ROR Oper	66	2	
		Zero Page X	ROR Oper X	76	2	
		Absolute	ROR Oper	6E	3	
		Absolute X	ROR Oper X	7E	3	
RTI Return from interrupt	P↑ PC↑	Implied	RTI	40	1	From Stack
RTS Return from subroutine	PC↑ PC+1 → PC	Implied	RTS	60	1	------
SBC Subtract memory from accumulator with borrow	A − M − C̄ → A	Immediate	SBC #Oper	E9	2	✓✓✓---✓
		Zero Page	SBC Oper	E5	2	
		Zero Page X	SBC Oper X	F5	2	
		Absolute	SBC Oper	ED	3	
		Absolute X	SBC Oper X	FD	3	
		Absolute Y	SBC Oper Y	F9	3	
		(Indirect X)	SBC (Oper X)	E1	2	
		(Indirect) Y	SBC (Oper) Y	F1	2	
SEC Set carry flag	1 → C	Implied	SEC	38	1	-----1
SED Set decimal mode	1 → D	Implied	SED	F8	1	----1-
SEI Set interrupt disable status	1 → I	Implied	SEI	78	1	---1--
STA Store accumulator in memory	A → M	Zero Page	STA Oper	85	2	------
		Zero Page X	STA Oper X	95	2	
		Absolute	STA Oper	8D	3	
		Absolute X	STA Oper X	9D	3	
		Absolute Y	STA Oper Y	99	3	
		(Indirect X)	STA (Oper X)	81	2	
		(Indirect) Y	STA (Oper) Y	91	2	
STX Store index X in memory	X → M	Zero Page	STX Oper	86	2	
		Zero Page Y	STX Oper Y	96	2	
		Absolute	STX Oper	8E	3	
STY Store index Y in memory	Y → M	Zero Page	STY Oper	84	2	
		Zero Page X	STY Oper X	94	2	
		Absolute	STY Oper	8C	3	
TAX Transfer accumulator to index X	A → X	Implied	TAX	AA	1	✓✓-----
TAY Transfer accumulator to index Y	A → Y	Implied	TAY	A8	1	✓✓-----
TSX Transfer stack pointer to index X	S → X	Implied	TSX	BA	1	✓✓-----
TXA Transfer index X to accumulator	X → A	Implied	TXA	8A	1	✓✓-----
TXS Transfer index X to stack pointer	X → S	Implied	TXS	9A	1	
TYA Transfer index Y to accumulator	Y → A	Implied	TYA	98	1	✓✓-----

APPENDIX II - ADDRESSING MODES

Data for the 6502 machine language instructions can be input when necessary, using a number of different addressing modes, each obtaining the data from a different source. A maximum of 9 addressing modes are available for the 6502, although none of the instructions can use all 9 addressing formats. Each different addressing format for the machine language instruction requires usage of a different operation code (ie a one byte hexadecimal number) to signify exactly which mode the microprocessor is to use. Taking the load accumulator (LDA) instruction as an example, the following is the full LDA instruction set, giving all 9 modes (with one that only applies to jump instructions);

addressing type	assembly language form
1) immediate	LDA £$aa (£ ≡ #)
2) zero page	LDA $aa
3) zero page,x	LDA $aa,x
4) absolute	LDA $aaaa
5) absolute,x	LDA $aaaa,x
6) absolute,y	LDA $aaaa,y
7) (indirect,x)	LDA ($aa,x)
8) (indirect),y	LDA ($aa),y
9) (indirect)	JMP ($aaaa)

1) Immediate : this mode takes the hexadecimal value following the instruction code as the actual data value, ie; in the instruction LDA £$5F, the accumulator will be loaded with the value $5F (or 95 in decimal).

2) Zero page : in this mode addressing only applies to the first page of memory (the zero page), the value following the instruction code indicates one of the 256 zero page locations. The data is thus obtained from the value in that zero page location, ie; LDA $FF will load the accumulator with the value found in memory location $FF (or 255 decimal).

3) Zero page,x : as for case 2) this applies only to the zero page of memory, the byte following the instruction is added to the value in the x register, and the resultant value (no carry used) indicates the address in zero page from which the data is to be obtained eg, for the instruction LDA $AF,x where the x register = $10 then the accumulator is loaded with the value found in location $AF + $10 = $BF

4) Absolute : similar instruction to case 2) except that it applies to all memory (thus requiring 3 bytes). The two bytes following the instruction are taken as an address (usually in the range $100 to $FFFF), of a single byte containing the data value. Hence LDA $6001, would load the accumulator with the value found at the location $6001.

5) Absolute,x : simalar to 3), the two bytes following the instruction are added to the x register value, the resultant address gives the location of the data value to which the instruction applies. For example LDA $6001,x where x contains the value $16 would load the accumulator with the data value contained in the location $6017.

6) Absolute,y : as for 5) using the y register value instead of the x. Thus LDA $4FFF,y where y contains $BD will load the accumulator with the value found in location $50BC.

7) (indirect,x) : this mode is more complex, in that the

location following the instruction is added to the x register to give an address in the zero page of memory. This new location and the subsequent byte (in zero page) contain values which indicate a further location in memory where the data value is to be found. For example, if the instruction is LDA ($1B,x), when the x register contains $10, location $2B contains $80 and the location $2C contains $64, then the location pair in zero page indicated is $1B + x reg = $2B. Since location $2B and $2C contain the address $6480, the value contained in $6480 is loaded into the accumulator.

8) (indirect),y : this is a indirect mode as for case 7), best explained by example; for the instruction LDA ($FE),y, where y reg = $20, $FF = $60 and $FE contains the value $00, the data is taken from the address $6020.

9) (indirect) : this is a variation on the other indirect modes except than it is only applicable to the jump (JMP) instruction, e.g JMP ($8000), where the addresses $8000 and $8001 contain $20 and $FE respectively, indicates a jump to the location $FE20.

The advantages of zero page and immediate modes lie in the increased speed of operation and the more economic usage of memory, since zero page and immediate addressing require one byte less than addressing to other memory regions. Some instructions can only operate in the zero page, since they would require 4 bytes elsewhere, this is beyond the 6502 microprocessors handling capability.

APPENDIX III - FUNCTION OF THE 6502 MACHINE CODE INSTRUCTIONS

A detailed description of all the more important instructions used in the programs presented is provided here, together with a few simple example machine code programs, they are listed alphabetically.

ADC : add memory to accumulator with carry. The carry should normally be zero before usage of this instruction;

```
CLC                 : clears carry flag
LDA £$20            : loads A with $20 (32 decimal)
ADC £$14            : adds $14 to accumulator (A)
```

at the end of this sequence the accumulator contains $34, the carry is zero. Usage of the following;

```
CLC
LDA £$B0
ADC £$98
```

will result in the carry being set and the value $48 being in the accumulator (the carry represents a carry over of $100 or 256 decimal, in this case). If the ADC instruction is encountered when the carry is set to 1, the ADC will add this bit into the accumulator and reset the carry to zero.

AND : and memory with accumulator. This operates on corresponding bits of the accumulator and the data, such that the resultant bit is 1 if that bit in both data and accumulator are 1. For example;

```
LDA £$53            :        0 1 0 1 0 0 1 1
AND £$10            :        0 0 0 1 0 0 0 0
 { A }              :        0 0 0 1 0 0 0 0
```

gives us a value of $10 in the accumulator after this sequence. Thus the AND instruction can be used to test specific bits of the data.

ASL : shift memory left one bit. Operates on either the accumulator or memory, setting the carry to zero, thus;

```
LDA £$32            :    c   0 0 1 1 0 0 1 0    0
ASL                 :    0   0 1 1 0 0 1 0 0    0
```

results in the accumulator containing $64 and the carry being zero. This function effectively doubles the byte value, (setting the carry = 1 if the value exceeds 255).

Branch instructions : these 2 byte instructions are conditional jumps dependent on flag status. They enable the program counter to be changed by +/- 128 bytes from the current location. The distance of the jump is specified by the second byte, if the value is < $80 (120 decimal) then it is forwards, if > $80 it is backwards, relative to the program counter, ie lower in memory relative to the current program location, with the distance given by $100 - (second byte value). For example;

```
$6000  BNE $6050
```

is stored as $D0 $4E and;

```
$6000  BNE $5FB6
```

is stored as $D0 $B4. The program counter location before operation of a branch instruction, is the location of the next byte in memory after that branch code. Thus a jump forwards can effectively go 130 bytes, whilst backwards only 126 bytes is attainable (since the branch has to jump over itself).
The following is the full branch instruction set;

BCC	: branch on carry clear	{c = 0}
BCS	: branch on carry set	{c = 1}
BEQ	: branch on result zero	{z = 1}
BMI	: branch on result minus	{n = 1}
BNE	: branch on result not zero	{z = 0}
BPL	: branch on result positive or zero	{n = 0}
BVC	: branch on overflow clear	{v = 0}
BVS	: branch on overflow set	{v = 1}

Branch instructions are particularly useful in performing program loops and unlike the jump (JMP) instructions, they are relative to the current program counter position. Therefore branch instructions can be moved from one section of memory to another without requiring adjustment for the program to work, whereas JMP instructions specify the absolute address in memory for the program, and are not so easily transferred, should the program be moved.

BIT : test bits in memory. This instruction tests bits 6 and 7 of the data by transferring them to the flag register. Bit 6 of the data is placed in the n flag and bit 7 into the v flag. This function is not used in the programs listed in appendix v.

BRK : force break. Upon encountering this instruction the program stops and if accsessed from within the monitor program all the current values of the internal registers of the microprocessor are displayed (X,Y,A,S and PC). The interrupt (i) flag is set to 1 and both the processor status and program counter registers are placed on the stack.

CLC : clear carry flag. This results in the carry bit being set to zero irrespective of its previous value.

CLD : clear decimal flag. Similar to the CLC command, in this case resulting in the decimal mode flag being set to zero. In the 6502 two types of arithmetic handling are available, normal binary and binary coded decimal. In binary coded decimal (BCD), one byte is split into two nibbles of four bits, each representing a decimal digit (a nibble could represent 16 numbers, so in the BCD mode 6 are unused). Manipulation is then carried out in the BCD notation. In the programs used here only binary notation is used, although where Basic is accessed, the BCD flag is cleared in case the BCD mode was set in Basic. BDC arithmetic is only carried out if the d flag is set to 1.

CLI : clear interrupt flag. Similar to CLC but operating on the interrupt. Not used in the programs presented.

CLV : clear overflow flag. As for CLI except for the overflow flag, also not used in programs presented.

CMP : compare memory with accumulator. This is a useful function enabling a comparison of two values whilst not altering either. It works in a similar way to the subtraction (SBC) command, in that it sets the flag register as if a subtraction had been carried out, where the chosen value is 'subtracted'

from the accumulator. This command sets the c, z and n flags enabling branch instructions to operate on the new flag status. However, if the comparison involves numbers with a difference of more than $80 (128 decimal), then the n flag status is inverted (negative answer to a comparison where a positive should result). For example;

```
LDA £$01
CMP £$82
```

results in n = 0 whereas;

```
LDA £$01
CMP £$7F
```

results in n=1 (ie the chosen value is positive in comparison to the accumulator). This is a rather limiting factor in program usage and is often a cause of program errors. Another frequently overlooked factor is that the carry flag is set on any CMP command and thus C may need to be reset after a CMP instruction.

CPX : compare memory with x register. Similar instruction to the CMP, except that the x register is substituted for the accumulator.

CPY : compare memory with y register. As for CPX using the y register.

DEC : decrement memory by one. This function results in whatever location specified in the two bytes following the DEC command being decreased by 1. The n and z flags being set, but not the c flag. Thus if a memory location contains $FF, a DEC command results in that memory location containing $FE (carry unaltered). Similarly, if the location contained $00 then DEC will result in that location containing $FF.

DEX : decrement x register by 1. Works as for DEC except using the x register as the memory location to be decreased.

DEY : decrement y register by 1. As for DEX, using the y register instead of the x.

EOR : exclusive OR memory with accumulator. This compares corresponding bits of accumulator and memory, if both are 0 then the result is 1, if either are 1 the result is 0. For example;

```
LDA £$82          :    1 0 0 0 0 0 1 0
EOR £$3A          :    0 0 1 1 1 0 1 0
 { A }            :    0 1 0 0 0 1 0 1
```

gives the value $45 (69 decimal) to the accumulator.

INC : increment the memory (or accumulator) by one. Complementary function to the DEC instruction. Whichever location specified is increased by 1, setting the n and z flags but not the c. Thus if memory containing $FF is incremented, the location will then contain $00 with c remaining unaltered.

INX : increment x register by 1. As for the INC instruction except the x index is incremented instead of memory.

INY : increment y register by 1. As for INX, but applying to the y index.

JMP : jump to a new location. In this instruction the 2 bytes following the code indicate a new address for the program to jump to. This location is loaded into the program counter to enable the program to continue from that point, the old program

location is lost. No flags are set during operation. Hence execution of;

```
location    op-codes      nemonic
$1000:      6C 03 01      JMP ($1003)
$1003:      00            DFB (data but interpreted as BRK)
$1004:      02            DFB (data but interpreted as ???)
```

would result in the program jumping indirectly to location $2000, ie the address is loaded from locations $1003 and $1004. This is a useful instruction where program options depend on a variable, ie if one changes the values in $1003 and $1004 the program will jump to a new location.

JSR : jump to a new address, saving the return location. Usage of this function allows the program to continue at a new location as with the JMP instruction except that the return address is saved at the top of the stack and the stack pointer is incremented by 2. The program counter is then loaded with the new location specified by the 2 bytes following the JSR code. Only the absolute address mode is avalable for this instruction. Subsequently when a RTS (return from subroutine) instruction is encountered, the program will return to the next code following the last JSR instruction operated. Nesting of subroutines is allowed up to a maximum of 127 accessed (opened) procedures. As with the other JMP instructions, no flags are set.

LDA : load accumulator with memory. This instruction loads the accumulator with data from memory, using the 8 different addressing modes available for loading. The n and z flags are set by this operation.

LDX : load x register with memory. As for the LDA instruction except loading the x register instead of the accumulator.

LDY : load y register with memory. As for the LDX instruction except for the y register.

LSR : shift memory right one bit. Complementary function to the ASL command, effectively dividing the value of memory or accumulator by 2 the remainder sets the carry flag. Bit 8 is set to 0. For example;

```
LDA £$32          :     0    0 0 1 1 0 0 1 0    c
LSR               :       → 0 0 0 1 1 0 0 1 → 0
```

results in the accumulator containing $19 (25 decimal) and the carry being set to zero, (c = 1 afterwards if the value was odd).

NOP : non operation code. With this instruction, nothing is altered and the program advances to the next code in memory. No flags are set. Additionally any unrecognised code although displayed as ??? in assembly language, is treated as a NOP code. This function should be used (for clarity) when any space is required within a program (for program expantion etc). NOP is a useful instruction since it is carried out in one clock cycle of the microprocessor, hence enabling accurate machine code program timing to be carried out.

ORA : or memory with accumulator. This instruction compares corresponding bits of the accumulator and memory, if both are 0 then the result is 0. If either or both are 1 then that bit in the result is set to 1 (result in accumulator), ie;

```
LDA £$82          :    1 0 0 0 0 0 1 0
ORA £$3A          :    0 0 1 1 1 0 1 0
 { A }            :    1 0 1 1 1 0 1 0
```

gives us a value of $BA in the accumulator. No flags are set.

The next four instructions concern the usage of the stack memory, by either taking or placing bytes to and from the stack (situated in page 1 of RAM). Their usage can enable faster storage and recall of data than from normal memory, since the stack page can be accessed at the same speed as the zero page (the microprocessor only needs one byte to address the stack, as the high order byte (page) of the address is always 1).

PHA : push accumulator on stack. This command takes the current accumulator value and places it on the top of the stack memory in page 1 of RAM (random accsess memory). The stack pointer is incremented by 1.

PHP : push processor status on stack. Similar instruction to PHA, except that the processor status register (ie the flag register) is placed on the top of the stack memory. The stack pointer is advanced by 1.

PLP : pull accumulator from stack. This is the complementary instruction to PHA, in that the current top byte of the stack is placed in the accumulator. The stack pointer is decreased by 1.

PLP : pull processor status from stack. Complementary instruction to PHP, the top byte of the stack is removed and placed in the flag register byte. All flags are thus reset by the new values from stack. The stack pointer is decreased by 1.

ROL : rotate one bit left. This command, operating on memory or the accumulator, is the same as the ASL instruction except that the new low order bit (bit 0), is set to the previous value of the carry flag (it is set to zero in ASL). The carry is then set by the old high order bit (bit 7) of the data value. The operation can be illustrated by;

```
CLC               :    c = 0
LDA £$82          :    0 ← 1 0 0 0 0 0 1 0 ← c
ROL               :    1   0 0 0 0 0 1 0 0
```

which results in the carry being set and tha accumulator containing $04. Hence this instruction allows any bit of the data to be rotated into the carry bit and acted upon (eg branches can be used). Like the other rotate instruction (ROR) it is used in carring out multibyte arithmetic (since a bit from one data value can be rotated via carry into another data byte). Hence they can make more complex functions such as multiplication and division somewhat easier (see examples).

ROR : rotate right one bit. Complementary function to ROL, except that in this case the new high order bit of the data value is set to the previous value of the carry bit. The carry bit is then set to the old value of the low order bit (bit 0). Thus;

```
SEC               :    1   c = 1
LDA £$82          :    1 → 1 0 0 0 0 0 1 0 → c
ROR               :    0   1 1 0 0 0 0 0 1
```

resets the carry to zero and leaves the value $C1 in the

accumulator.

RTI : return from interrupt. This return instruction enables the program to continue on after having been interrupted by a BRK. The processor status and program counter registers are retrieved from the stack.

RTS : return from subroutine. The RTS comand is the return instruction for any subroutine accessed by a JSR code, and will return the program to the next byte following the last JSR instruction encountered (unless the stack has been altered). The program counter is loaded from the two bytes at the top of the stack and the stack pointer is decreased by 2. The final RTS command in a machine code program will return the program back to the location it was accessed from (eg if accessed from a Basic call statement, it returns control to Basic and carries on the Basic program where it left off).

SBC : subtract memory from accumulator with borrow. Complementary instruction to ADC, the data value specified is subtracted from the accumulator (the carry is usually set to 1 beforehand), to give the result in the accumulator. If the carry is reset to zero, the subtraction has resulted in a borrow (ie the result is less than zero) elsewise the carry remains 1, (If a SBC instruction is carried out with C = 0 the result in accumulator will be 1 less than the correct value). For example;

```
SEC                 :    1    c = 1
LDA £$9B            :    1    1 0 0 1 1 0 1 1
SBC £$3A            :         0 0 1 1 1 0 1 0
 { A }              :    1    0 1 1 0 0 0 0 1
```

results in the accumulator containing $61. The reader may be interested to know that this function, is carried out by inverting the bits of the subtracted number, and adding the resultant inverse; hence it is a slower function than addition.

SEC : set carry flag. The carry bit is set to 1 (cf CLC).

SED : set decimal mode. The decimal mode flag is set to 1 (cf CLD).

SEI : set interrupt flag. The interrupt flag is set to 1 (cf CLI).

STA : store accumulator in memory. Complementary to LDA, this instruction stores the current value of the accumulator into the specified location within memory. No flags are set and the old value of the accumulator is retained.

STX : store x register in memory. Similar to STA, except the x register is stored instead of the accumulator. Fewer addressing modes are available for STX (and STY) than for STA.

STY : store y register in memory. As for the STX instruction except for the y register.

TAX : transfer accumulator to x register. The value of the x register is set to the current value of the accumulator. Both n and z flags are set and the value of the accumulator remains unaltered.

TAY : transfer accumulator to y register. As for TAX except using the y register.

TSX : transfer stack pointer to x register. Similar to the TAX instruction except that the stack pointer (which points to the address of the currently accessed subroutine in the stack) is transferred to the x index. Both n and z flags are set and the stack pointer value remains unaltered.

TXA : transfer x register to the accumulator. Complementary to the TAX command, the x index is copied into the accumulator with the n and z flags being set. The x register value remains unaltered.

TXS : transfer the x register to the stack pointer. Complementary function to TSX, No flags are set and the x register remains unaltered.

TYA : transfer y register to the accumulator. As for TXA except it applies to the y index.

APPENDIX IV - EXAMPLE MACHINE CODE SUBROUTINES

In this section several simple example programs are given, which perform various tasks frequently required in machine code programs. They are presented mostly without program memory locations since the routines can be put into any available space in RAM, but the operating codes are given for each instruction before the mnemonic notation, (in hexadecimal, of up to three bytes for each statement).

1] Addition of two sixteen bit numbers stored in memory as the number pairs on locations $300/1 and $305/6 (high order byte highest in memory). The result is stored in the three memory locations $309-$30B.

```
18          CLC          :  set c = 0
D8          CLD          :  set decimal mode, d = 0
AD 00 03    LDA $300     :  load first number low byte
6D 05 03    ADC $305     :  add  second number low byte
                             c = 1 if result > $FF (255)
8D 09 03    STA $309     :  store low byte of result
AD 01 03    LDA $301     :  load first number high byte
6D 06 03    ADC $306     :  add second number high byte
                             c = 1 if result + carry > $FF
8D 0A 03    STA $30A     :  store mid byte of result
A9 00       LDA £$00     :  set accumulator to zero
69 00       ADC £$00     :  add zero with carry
8D 0B 03    STA $30B     :  store high byte of result (0 or 1)
60          RTS          :  return
```

At the end of this sequence the carry will be zero and the result is contained in the memory locations $309, $30A and $30B. $30B will contain either 1 or 0 (ie the last carry value). The result is stored such that (in decimals) the result is given by;

($300/1) + ($305/6) = ($309) + 256*($30A) + 65536*($30B)

2] Subtraction of a 16 bit number (an immediate value of $4664), from a 24 bit number stored in locations $FD-$FF, the result being stored in locations $309-$30B.

```
38          SEC          :  set c = 1
A5 FD       LDA $FD      :  load low byte of number
E9 64       SBC £$64     :  subtract low byte of value, $64
8D 09 03    STA $309     :  store low byte of result
A5 FE       LDA $FE      :  load mid byte of number
E9 46       SBC £$46     :  subtract high byte of value, $46
8D 0A 03    STA $30A     :  store mid byte of result
A5 FF       LDA $FF      :  load high byte of number
E9 00       SBC £$00     :  subtract zero (for carry over)
8D 0B 03    STA $30B     :  store high byte of result
60          RTS          :  return
```

At the end of this sequence the carry is 1 if the result is positive (ie {value} - $6446 > 0). The result could have been stored in locations $FD-$FF, replacing the original number instead of locations $309-$30B.

3] Multiplication of two 8 bit numbers to give a 16 bit result stored in locations $FA and $FB, the original two numbers

being in locations $300 and $307.

```
18              CLC             :  set c = 0
A9 00           LDA £$00        :  load accumulator with zero
85 FA           STA $FA         :  clear low result byte
A2 08           LDX £$08        :  set index x (loop counter) to 8
4E              LSR $307        :  loads each bit of lst number into
                                   carry in turn, lowest first
90 04           BCC + $04       :  if c = 0, no addition
18              CLC             :  reset c = 0
6D 00 03        ADC $300        :  add if carry was 1
6A              ROR             :  rotate accumulator right
66 FA           ROR $FA         :  rotate low byte of result to take
                                   each bit of the low result (in the
                                   carry) as it is evaluated
CA              DEX             :  decrease x index (loop counter) by 1

D0 0D           BNE - $0D       :  branch back if loop counter <> 0
85 FB           STA $FB         :  store high byte of result (in
                                   accumulator) when loop finished
```

Thus the result is stored in locations $FA and $FB. The use of rotate commands to multiply (and divide) speeds the program, and compacts the total number of bytes required, when compared to the alternative of simple addition.

4] Division of a two byte number stored in locations $1D and $1E by a one byte number in $1F, the result being stored in $1B and $1C with remainder $1A. In this example the program memory locations are specified to allow the reader to follow the program through more easily. It is however possible to place the program anywhere in memory.

```
0350:  18       CLC         :  set c = 0
0351:  D8       CLD         :  set d = 0
0352:  A2 10    LDX £$10    :  load index x (counter) with $10 (16)
0354:  A9 00    LDA £$00    :  load accumulator with zero
0356:  85 1B    STA $1B     :  clear location $1B
0358:  85 1C    STA $1C     :  clear location $1C
035A:  26 1D    ROL $1D     :  rotate left low byte of number
035C:  26 1E    ROL $1E     :  rotate left high byte of number
035E:  2A       ROL         :  rotate left accumulator, thus taking
                               top bit(s) of number into accumulator
035F:  C5 1F    CMP $1F     :  compare with divisor, if smaller then;
0361:  90 02    BCC $0365   :  branch if c = 0; ie no subtraction
                               since divisor larger; hence rotate next
                               bit of number into accumulator
0363:  E5 1F    SBC $1F     :  subtract divisor (c = 1, set by CMP)
0365:  26 1B    ROL $1B     :  rotate c into low bit of the two bytes-
0367:  26 1C    ROL $1C     :  of the result (shunting bits in R to L)
0369:  06 1D    ASL $1D     :  shift left all remaining bits of number
036B:  26 1E    ROL $1E     :  - using ASL to set lowest bit to zero
036D:  2A       ROL         :  rotate accumulator to take next bit in
036E:  CA       DEX         :  decrease index x (loop counter)
036F:  D0 EE    BNE $035F   :  branch if loop not ended (ie if x <> 0)
0370:  6A       ROR         :  rotate to take last bit into remainder
0371:  85 1A    STA $1A     :  store remainder in $1A
0373:  60       RTS         :  return
```

The above four examples are clearly very simple functions to be carried out in machine code, but hopefully they serve to illustrate the usage of the various operating codes of the 6502 microprocessor. Many more complex tasks can be undertaken in machine code by usage of several quite simple routines. The best and most efficient usage of machine language is usually obtained by using the codes as a subroutine from within one of the higher level languages, such that programming is quicker, easier to understand and the in-built functions of the high level language can be accessed. In most microcomputers machine code programs will use the facilities available in the monitor (the inbuilt language controlling program), such as character generation, graphics output and peripheral usage. For the Apple computer the monitor routines lie in the ROM (read only memory) region $F800 - $FFFF, the Basic language occupies $C000 - $F800 (ROM) and the disc operating system (DOS) is to be found at $9600 - $BFFF in RAM.

For further information on Basic, DOS, memory usage and the monitor, consult the appropriate Apple reference manual.

APPENDIX V - BASIC COMPUTER SIMULATION PROGRAM

BASIC SIM

```
0  LOMEM: 24576: HIMEM: 36863
2  ONERR  GOTO 578
4  GOTO 616
6  FOR T = 1 TO H1
8  FOR S = I9 TO E8
10  IF N <  > L THEN 104
12 A =  INT ( RND (W) * G3):B =  INT ( RND (W) * G3)
14 C = B - M7 + W
16  IF C >  = H4 THEN 20
18 M7 = E: GOTO 12
20 C1 = C1 + W:M = A(A,B):Q = B(C):Q1 = B(C - W)
22  IF M -  INT (M / Q) * Q < Q1 THEN 32
24 M7 = E: GOTO 12
26  IF C <  > H4 THEN 30
28 M7 =  - W: GOTO 12
30 M7 = M7 + W: GOTO 14
32 Y = A - W:  IF A = E THEN Y = G1
34 D = B - W:  IF B = E THEN D = G1
36 F = A + W:  IF A = G1 THEN F = E
38 X = B + W:  IF B = G1 THEN X = E
40 Q2 = B(C - Z):Q3 = B(C + Z):M1 = A(A,X):P = A(A,D):O = A(F,B):M4 = A(Y
   ,B)
42  IF C * V =  INT (C * V) THEN 54
44  IF A * V =  INT (A * V) THEN 50
46 M5 = A(F,D):M6 = A(Y,D):U = M4:R = M6
48  GOTO 62
50 M5 = A(F,X):M6 = A(Y,X):U = M4:R = M6
52  GOTO 62
54  IF A * V =  INT (A * V) THEN 60
56 M5 = A(F,D):M6 = A(Y,D):U = 0:R = M5
58  GOTO 62
60 M5 = A(F,X):M6 = A(Y,X):U = 0:R = M5
62 N = 12
64  IF M1 -  INT (M1 / Q) * Q < Q1 THEN N = N - W
66  IF O -  INT (O / Q) * Q < Q1 THEN N = N - W
68  IF P -  INT (P / Q) * Q < Q1 THEN N = N - W
70  IF M4 -  INT (M4 / Q) * Q < Q1 THEN N = N - W
72  IF M5 -  INT (M5 / Q) * Q < Q1 THEN N = N - W
74  IF M6 -  INT (M6 / Q) * Q < Q1 THEN N = N - W
76  IF M -  INT (M / Q1) * Q1 < Q2 THEN N = N - W
78  IF U -  INT (U / Q1) * Q1 < Q2 THEN N = N - W
80  IF R -  INT (R / Q1) * Q1 < Q2 THEN N = N - W
82  IF M -  INT (M / Q3) * Q3 < Q THEN N = N - W
84  IF U -  INT (U / Q3) * Q3 < Q THEN N = N - W
86  IF R -  INT (R / Q3) * Q3 < Q THEN N = N - W
88  IF N < K OR N > L THEN 26
90  IF  RND (W) > P(N) THEN 26
92 A(A,B) = M + Q1
94  IF N = K THEN  GOSUB 398
96  IF C - W = G THEN G = C
98  GOSUB 344
100  NEXT
102  GOTO 144
104 R8 =  INT ( RND (W) * 6 + W)
106  IF A * V =  INT (A * V) THEN 122
108  ON R8 GOTO 110,112,114,116,118,120
110 A3 = F:B3 = B: GOTO 136
```



```
112 A3 = Y:B3 = B: GOTO 136
114 A3 = A:B3 = X: GOTO 136
116 A3 = A:B3 = D: GOTO 136
118 A3 = Y:B3 = D: GOTO 136
120 A3 = F:B3 = D: GOTO 136
122  ON R8 GOTO 124,126,128,130,132,134
124 A3 = F:B3 = B: GOTO 136
126 A3 = Y:B3 = B: GOTO 136
128 A3 = A:B3 = X: GOTO 136
130 A3 = A:B3 = D: GOTO 136
132 A3 = F:B3 = X: GOTO 136
134 A3 = Y:B3 = X
136 M = A(A3,B3)
138  IF M -  INT (M / Q) * Q < Q1 THEN 142
140  GOTO 104
142 A = A3:B = B3:C1 = C1 + W: GOTO 32
144 I9 = 1
146  FOR I = 0 TO G1
148  FOR J = 0 TO G1
150 H2 = A(I,J)
152 H3 = B(H4):H5 = B(H4 - 1)
154  IF H2 -  INT (H2 / H3) * H3 < H5 THEN H6 = H6 + 1
156  NEXT J
158  NEXT I
160  IF E9 = 0 THEN 164
162  PRINT B4$;H6
164  IF H6 = H7 THEN H4 = H4 + 1: IF H6 <  > H7 THEN 168
166 H7 = 0
168 H7 = H6:H6 = 0
170 M(T) = C1
172  NEXT T
174  TEXT : PRINT : PRINT : PRINT : PRINT : PRINT : PRINT : PRINT : PRINT
   : PRINT : PRINT : PRINT : PRINT : PRINT : PRINT
176  GET QQ$
178  PRINT "ARE YOU READY FOR THE OUTPUT -          MAKE SURE THE EPSOM P
   RINTER IS ON";: INPUT QQ$
180  IF QQ$ = "Y" THEN 188
182  GOTO 178
184  IF W$ = "N" THEN 760
186  GOTO 268
188  PRINT B5$;: INPUT Z$
190  PRINT D$;"OPEN";Z$
192  PRINT D$;"WRITE";Z$
194  PRINT P(3);D1$;P(4);D1$;P(5);D1$;P(6);D1$;P(7);D1$;P(8);D1$;P(9)
196 T = (T - 2) * E8 + S - 1
198  PRINT T;D1$;G1 + 1;D1$;G;D1$;H4
200  FOR I = 0 TO G1
202  FOR J = 0 TO G1
204  PRINT A(I,J)
206  NEXT J
208  NEXT I
210  PRINT D$;"CLOSE"
212  GOTO 240
214  PRINT B6$;: INPUT Z$
216  PRINT D$;"OPEN";Z$
218  PRINT D$;"READ";Z$
220  INPUT P(3),P(4),P(5),P(6),P(7),P(8),P(9),SUM,G3,G,H4
222 G1 = G3 - 1
224  DIM A(G1,G1)
226  FOR I = 0 TO G1
```

```
228  FOR J = 0 TO G1
230  INPUT A(I,J)
232  NEXT J
234  NEXT I
236  PRINT D$"CLOSE"
238  GOTO 400
240  REM  IF THE LATTICE>44 THEN NEED A DIFFERENT PRINTOUT
242  FOR I5 = 1 TO G - 1
244  HGR2
246  HPLOT X4 - 3,0 TO (281 - X4),0 TO (281 - X4),(8 + 4 * G1) TO X4 - 3,
     (8 + 4 * G1) TO X4 - 3,0
248 T8 = 7
250  GOTO 474
252  PR# 1: POKE 1657,80
254  PRINT "PRINTOUT OF LAYER ";I5;" FILE ";Z$
256  POKE 1913,66: PRINT  CHR$ (17); CHR$ (12)
258  POKE 53247,0
260  PR# 0
262  NEXT I5
264  TEXT
266  GOTO 272
268  PRINT B7$;: INPUT S$
270  IF S$ <  > "Y" THEN 342
272  PR# 1: POKE 1657,80
274  PRINT B8$;" FILE ";Z$
276  PRINT "((P1 ";P(1);" P2 ";P(2);" P3 ";P(3);" P4 ";P(4);" P5 ";P(5);"
     P6 ";P(6);" P7 ";P(7);" P8 ";P(8);" P9 ";P(9);"))"
278  FOR I = 0 TO G1
280  FOR J = 0 TO G1
282  FOR K = G - 1 TO 1 STEP  - 1
284 M = A(I,J) / B(K)
286  IF  INT (M / 2) =  INT (M) / 2 THEN 290
288 K2 = K: GOTO 294
290  NEXT K
292 K2 = 0
294 V$ =  STR$ (K2)
296  IF K2 > 9 THEN 300
298 T$ = T$ + " " + V$: GOTO 302
300 T$ = T$ + V$
302  NEXT J
304  IF I / 2 <  >  INT (I / 2) THEN 308
306  PRINT " ";
308  PRINT T$
310 T$ = ""
312  NEXT I
314  PRINT  CHR$ (12)
316  PR# 0
318  GOTO 322
320  PRINT B9$,E8,C1$;: INPUT F$
322  PR# 1: POKE 1657,80
324  PRINT C2$
326  FOR I = 1 TO H1
328  IF M(I) = 0 THEN 334
330 T3 = E8 / (M(I) - M(I - 1))
332  PRINT  TAB( 15);E8 * I; TAB( 16);M(I); TAB( 13);T3
334  NEXT I
336  PR# 0
338  PRINT C3$;: INPUT F$
340  IF F$ = "Y" THEN 176
342  END
```



```
344  IF E9 = 0 THEN  RETURN
346  IF I5 <  > I6 THEN  GOSUB 462
348 A5 = A(A,B) / Q6
350  IF  INT (A5 / 2) =  INT (A5) / 2 THEN 396
352 X3 = X4 + (B * 4)
354  IF A / 2 =  INT (A / 2) THEN X3 = X3 + 2
356 Y3 = A * 4 + 1
358  HPLOT X3,Y3: HPLOT X3 - 1,Y3 + 1: HPLOT X3 + 1,Y3 + 1: HPLOT X3 - 2,
     Y3 + 2: HPLOT X3 + 2,Y3 + 2
360  HPLOT X3 - 2,Y3 + 3: HPLOT X3 + 2,Y3 + 3: HPLOT X3 - 2,Y3 + 4: HPLOT
     X3 + 2,Y3 + 4
362  HPLOT X3 - 1,Y3 + 5: HPLOT X3 + 1,Y3 + 5: HPLOT X3,Y3 + 6
364  PRINT ""
366  HPLOT X3,Y3 + 3
368 Y1 = S + T * E8 - E8 + SUM
370  IF YC <  > 167 THEN 374
372 YC = 176: GOTO 380
374  IF YC <  > 176 THEN 378
376 YC = 185: GOTO 380
378 YC = 167
380 PF$ =  STR$ (C1):XC = 17: GOSUB 506
382 CS = 1
384 PF$ =  STR$ (Y1):XC = 80: GOSUB 506
386 PF$ =  STR$ (N):XC = 124: GOSUB 506
388 PF$ =  STR$ (A):XC = 164: GOSUB 506
390 PF$ =  STR$ (B):XC = 206: GOSUB 506
392 PF$ =  STR$ (C):XC = 248: GOSUB 506
394 CS = 0
396  RETURN
398 D5 =  INT ( RND (1) * 6) + 1
400  IF A / 2 =  INT (A / 2) THEN 416
402  ON D5 GOTO 404,406,408,410,412,414
404 D6 = A:D7 = X:D8 = Y:D9 = B: GOTO 430
406 D6 = A:D7 = X:D8 = F:D9 = B: GOTO 430
408 D6 = F:D7 = D:D8 = F:D9 = B: GOTO 430
410 D6 = F:D7 = D:D8 = A:D9 = D: GOTO 430
412 D6 = Y:D7 = D:D8 = A:D9 = D: GOTO 430
414 D6 = Y:D7 = D:D8 = Y:D9 = B: GOTO 430
416  ON D5 GOTO 418,420,422,424,426,428
418 D6 = Y:D7 = X:D8 = A:D9 = X: GOTO 430
420 D6 = F:D7 = X:D8 = A:D9 = X: GOTO 430
422 D6 = F:D7 = X:D8 = F:D9 = B: GOTO 430
424 D6 = A:D7 = D:D8 = F:D9 = B: GOTO 430
426 D6 = A:D7 = D:D8 = Y:D9 = B: GOTO 430
428 D6 = Y:D7 = X:D8 = Y:D9 = B
430 A(D6,D7) = A(D6,D7) + Q1:A(D8,D9) = A(D8,D9) + Q1
448 D4 = A:D5 = B
450 A = D6:B = D7: GOSUB 344
452 S = S + 1
454 A = D8:B = D9: GOSUB 344
456 S = S + 1
458 A = D4:B = D5
460  RETURN
462  HGR2 :XC = 3:YC = 159
464  HPLOT X4 - 3,0 TO (281 - X4),0 TO (281 - X4),(8 + 4 * G1) TO X4 - 3,
     (8 + 4 * G1) TO X4 - 3,0
466 PF$ = "#NO TRIALS ATOM  CO'RD  #ROW  #COL #LAYER"
468  IF T7 <  > 1 THEN  GOSUB 566
470  GOSUB 506
472 T7 = 1 + T7
```

```
474 Q6 = B(I5):I6 = I5
476  FOR I = 0 TO G1
478  FOR J = 0 TO G1
480 G6 = A(I,J) / Q6
482  IF  INT (G6 * .5) =  INT (G6) * .5 THEN 498
484 X3 = X4 + (J * 4)
486  IF I * .5 =  INT (I * .5) THEN X3 = X3 + 2
488 Y3 = I * 4 + 1
490  HPLOT X3,Y3: HPLOT X3 - 1,Y3 + 1: HPLOT X3 + 1,Y3 + 1: HPLOT X3 - 2,
    Y3 + 2: HPLOT X3 + 2,Y3 + 2
492  HPLOT X3 - 2,Y3 + 3: HPLOT X3 + 2,Y3 + 3: HPLOT X3 - 2,Y3 + 4: HPLOT
    X3 + 2,Y3 + 4
494  HPLOT X3 - 1,Y3 + 5: HPLOT X3 + 1,Y3 + 5: HPLOT X3,Y3 + 6
496  HPLOT X3,Y3 + 3
498  NEXT J
500  NEXT I
502  IF T8 = 7 THEN 252
504  RETURN
506 L1 =  LEN (PF$)
508 E = 0: IF CS = 1 THEN 514
510  HCOLOR= 0: HPLOT 3,YC TO 274,YC TO 274,YC + 1 TO 3,YC + 1 TO 3,YC +
    2 TO 274,YC + 2 TO 274,YC + 3 TO 3,YC + 3 TO 3,YC + 4 TO 274,YC + 4 TO
    274,YC + 5 TO 3,YC + 5 TO 3,YC + 6 TO 274,YC + 6
512  HCOLOR= 3
514  IF L1 < 1 THEN  RETURN
516 CH = 128 +  ASC (PF$)
518  IF CH = 160 THEN 544
520  IF CH = 163 THEN E = 1: GOTO 556
522  IF E = 1 THEN 530
524  IF CH = 222 THEN 552
526 CG = CH - 160
528  GOTO 534
530  IF CH = 222 THEN 548
532 CG = CH - 101
534  IF XC < 3 OR XC > 274 THEN AB = 1
536  IF YC < 4 OR YC > 188 THEN AB = 1
538  IF AB <  > 1 THEN 542
540  TEXT : PRINT "COORD ERROR": STOP
542  DRAW CG AT XC,YC
544 XC = XC + 7
546  GOTO 554
548 YC = YC + 3
550  GOTO 554
552 YC = YC - 3
554 E = 0
556 L1 = L1 - 1
558 PF$ =  MID$ (PF$,2)
560  GOTO 514
562  PRINT "LABEL RUNS OFF SCREEN"
564  STOP
566  IF  PEEK (37000) = 140 AND  PEEK (37001) = 3 THEN 576
568  PRINT D$"BLOAD LETTERS,A$9              000"
570  POKE 233,144: POKE 232,8
572 XC = 3:YC = 159
574  SCALE= 1: ROT= 0
576  RETURN
578 ERO =  PEEK (222): IF ERO = 8 THEN  PRINT " PUT A DISC IN THE DRIVE -
    AN I/O ERROR HAS OCCURED"
580  IF ERO = 8 THEN 604
582  IF ERO = 255 THEN 604
```



```
584  INVERSE
586  PRINT "
                                                                    "
588  NORMAL
590  PRINT "           ";
592  FLASH
594  PRINT "ERROR NO ";ERO;" HAS OCCURED "
596  NORMAL
598  INVERSE
600  PRINT "
                                                                    "
602  NORMAL
604  TEXT
606  IF ERO = 255 THEN  PRINT "TYPE CONT TO CONTINUE"
608  IF ERO = 255 THEN  STOP
610  PRINT "PRESS RETURN TO CONTINUE";: INPUT RR$
612  ONERR  GOTO 578
614  RESUME
616 A1$ = "THIS PROGRAM DOES NOT CONTAIN A DIFFUS- ION ELEMENT"
618 A2$ = "IS THE INITIAL LATTICE TO BE READ FROM   DISC "
620 A3$ = "WHAT SIZE LATTICE X BY X ,BY 31 UP "
622 A4$ = "THIS REQUIRES A SHORT THINK"
624 A5$ = "DO YOU WANT THE LATTICE PRINTED OUT (1) OR DO    YOU WISH TO C
    ONTINUE DEPOSITION (2) "
626 A6$ = "PLEASE GIVE THE PROBABILITYS FOR AN ATOM STICKING WITH 1,2,3,4
    ,5,6,7,8,9 ADJAC-ENT OCCUPIED SITES (IN THAT ORDER)"
628 A7$ = "THE VALUES PREVIOUSLY USED WERE "
630 A8$ = "THE PROBABILITYS CHOSEN ARE"
632 A9$ = "IS THIS CORRECT "
634 B1$ = "HOW MANY ATOMS DO YOU WISH TO BE DEPOSITED"
636 B2$ = "AND HOW OFTEN DO YOU WISH THE NUMBER OF   TRIALS RECORDED - NO
     MORE THAN 50 RESULTS "
638 B3$ = "DO YOU WISH TO START WITH AN INITIAL NUCL-  EUS OF THREE ATOMS
     "
640 B4$ = "NO OF FREE SITES = "
642 B5$ = "PLEASE GIVE A SUITABLE NAME FOR THE FILE"
644 B6$ = "PLEASE GIVE FILENAME "
646 B7$ = "DO YOU WISH THE HEIGHT MAP PRINTED ON THE EPSOM "
648 B8$ = "THIS A HEIGHT MAP OF  THE SIMULATED DEPOSIT"
650 B9$ = "THE NUMBER OF TRIALS PER  "
652 C1$ = " ATOMS CAN NOW BE PRINTED ON THE EPSOM - PRESS RETURN TO CONTI
    NUE "
654 C2$ = "          NO ATOMS          NO TRIALS       'ATOM RATE'"
656 C3$ = "ARE YOU SURE NO INFORMTION OR REPEAT INFORMATION IS REQUIRED,
    THE LATTICE CAN STILL BE SAVED BY ANSWERING Y "
658 W = 1:E = 0:Z = 2:V = .5:L = 9:K = 3
660  PRINT "R A N D O M I S I N G"
662  INVERSE : FLASH : PRINT "PLEASE INPUT THE RANDOM START POSITION  "
664  PRINT "INCREMENT BY ONE FOR EACH FRESH RUN ": INPUT A
666  NORMAL
668  FOR I = 1 TO A
670  PRINT  RND (1)
672  NEXT
674 D$ =  CHR$ (4):D1$ =  CHR$ (13)
676  CALL  - 936
678  PRINT A1$: PRINT : PRINT
680 M7 = 0:N = 9:E9 = 2:Y = 0:X = 0:D = 0:F = 0:M5 = 0:M6 = 0:M4 = 0:U =
    0:R = 0:M1 = 0:P = 0:O = 0:H4 = 2:G = 1:I5 = 1:I6 = 1
682  PRINT A2$: INPUT F$: PRINT : PRINT
684  IF F$ = "Y" THEN 214
```

```
686  PRINT A3$: INPUT G1: PRINT : PRINT
688  DIM T$(2 * G1 + 1)
690 X4 = 140 - G1 * 2
692  PRINT A4$: PRINT : PRINT
694 G1 = G1 - 1:G3 = G1 + 1: DIM A(G1,G1)
696  FOR I = 0 TO G1
698  FOR J = 0 TO G1
700 A(I,J) = 1
702  NEXT
704  NEXT
706  DIM B(33)
708  IF F$ <  > "Y" THEN 712
710 I5 = 1:I6 = 1:X4 = 140 - G1 * 2 - 2
712  DIM M(50):B(0) = 1
714  FOR I = 1 TO 33
716 B(I) = 2 * B(I - 1)
718  NEXT
720 P(0) = 1
722  IF F$ <  > "Y" THEN 728
724  PRINT A5$: INPUT Y6: PRINT : PRINT
726  IF Y6 = 1 THEN 2440
728  PRINT A6$: PRINT : PRINT
730  IF P(7) = 0 THEN 740
732  PRINT A7$
734  FOR I = 1 TO 9
736  PRINT "    ";I;"       ";P(I)
738  NEXT
740  INPUT P(1),P(2),P(3),P(4),P(5),P(6),P(7),P(8),P(9)
742  PRINT A8$
744  FOR K = 1 TO 9: PRINT "    ";K;"       ";P(K): NEXT
746  PRINT A9$;: INPUT W$
748  IF W$ = "N" THEN 728
750  PRINT B1$;: INPUT H: PRINT : PRINT
752  PRINT B2$;: INPUT E8:H1 =  INT (H / E8)
754  PRINT B3$;: INPUT Q$
756  IF Q$ = "Y" THEN I9 = 4
758  IF Q$ <  > "Y" THEN 768
760 K6 =  INT (G1 / 2):A(K6,K6) = 3
762 A(K6,K6 + 1) = 3
764  IF K6 / 2 <  >  INT (K6 / 2) THEN A(K6 + 1,K6) = 3
766  IF K6 / 2 =  INT (K6 / 2) THEN A(K6 + 1,K6 + 1) = 3
768  GOSUB 462
770 K = 3: GOTO 6
```

APPENDIX VI - MACHINE CODE/BASIC SIMULATION PROGRAM

Sim 2

```
2C65-  EE DD 03   INC  $03DD
2C68-  AD DD 03   LDA  $03DD
2C6B-  C9 0C      CMP  #$0C
2C6D-  30 11      BMI  $2C80
2C6F-  A9 00      LDA  #$00
2C71-  8D DD 03   STA  $03DD
2C74-  4C 9D 2E   JMP  $2E9D   ⇌
2C77-  EA         NOP
2C78-  EA         NOP
2C79-  59 59 4E   EOR  $4E59,Y
2C7C-  0D 04 BD   ORA  $BD04
2C7F-  F2         ???
2C80-  38         SEC
2C81-  AD DA 03   LDA  $03DA
2C84-  E9 01      SBC  #$01
2C86-  B0 03      BCS  $2C8B
2C88-  AD D6 03   LDA  $03D6
2C8B-  8D D6 03   STA  $03D6
2C8E-  38         SEC
2C8F-  AD DB 03   LDA  $03DB
2C92-  E9 01      SBC  #$01
2C94-  B0 03      BCS  $2C99
2C96-  AD D6 03   LDA  $03D6
2C99-  8D D7 03   STA  $03D7
2C9C-  18         CLC
2C9D-  AD DA 03   LDA  $03DA
2CA0-  69 01      ADC  #$01
2CA2-  CD E3 03   CMP  $03E3
2CA5-  D0 02      BNE  $2CA9
2CA7-  A9 00      LDA  #$00
2CA9-  8D D8 03   STA  $03D8
2CAC-  18         CLC
2CAD-  AD DB 03   LDA  $03DB
2CB0-  69 01      ADC  #$01
2CB2-  CD E3 03   CMP  $03E3
2CB5-  D0 02      BNE  $2CB9
2CB7-  A9 00      LDA  #$00
2CB9-  8D D9 03   STA  $03D9
2CBC-  18         CLC
2CBD-  AD DA 03   LDA  $03DA
2CC0-  8D 07 03   STA  $0307
2CC3-  AD DB 03   LDA  $03DB
2CC6-  8D 08 03   STA  $0308
2CC9-  20 AA 35   JSR  $35AA   ⇌
2CCC-  18         CLC
2CCD-  A0 01      LDY  #$01
2CCF-  B1 FA      LDA  ($FA),Y
2CD1-  39 3F 03   AND  $033F,Y
2CD4-  D0 09      BNE  $2CDF
2CD6-  88         DEY
2CD7-  10 F6      BPL  $2CCF
2CD9-  A9 04      LDA  #$04
2CDB-  8D 47 03   STA  $0347
2CDE-  60         RTS            **
2CDF-  18         CLC
2CE0-  AD 0C 03   LDA  $030C
2CE3-  4A         LSR
2CE4-  90 6C      BCC  $2D52
2CE6-  AD D6 03   LDA  $03D6
```

Check sites below for vacancies.

KEY

- Jump back.
- Jump forward.
- (⇌) Indirect jump.
- ⇌ Subroutine accessed.
- * Exit routine.
- ** Exit to basic.
- Branch forward.
- Branch backward.
- ▫ Basic entry point


```
2CE9-  8D 07 03   STA  $0307
2CEC-  AD DB 03   LDA  $03DB
2CEF-  8D 08 03   STA  $0308
2CF2-  20 AA 35   JSR  $35AA   ⇌
2CF5-  18         CLC
2CF6-  A0 01      LDY  #$01
2CF8-  B1 FA      LDA  ($FA),Y
2CFA-  39 3F 03   AND  $033F,Y
2CFD-  D0 09      BNE  $2D08
2CFF-  88         DEY
2D00-  10 F6      BPL  $2CFB
2D02-  A9 04      LDA  #$04
2D04-  8D 47 03   STA  $0347
2D07-  60         RTS            **
2D08-  AD DA 03   LDA  $03DA
2D0B-  4A         LSR
2D0C-  90 22      BCC  $2D30
2D0E-  AD D6 03   LDA  $03D6
2D11-  8D 07 03   STA  $0307
2D14-  AD D7 03   LDA  $03D7
2D17-  8D 08 03   STA  $0308
2D1A-  20 AA 35   JSR  $35AA   ⇌
2D1D-  18         CLC
2D1E-  A9 01      LDA  #$01
2D20-  B1 FA      LDA  ($FA),Y
2D22-  39 3F 03   AND  $033F,Y
2D25-  D0 6C      BNE  $2D93   ↓
2D27-  88         DEY
2D28-  10 F6      BPL  $2D20
2D2A-  A9 04      LDA  #$04
2D2C-  8D 47 03   STA  $0347
2D2F-  60         RTS            **
2D30-  AD D6 03   LDA  $03D6
2D33-  8D 07 03   STA  $0307
2D36-  AD D9 03   LDA  $03D9
2D39-  8D 08 03   STA  $0308
2D3C-  20 AA 35   JSR  $35AA   ⇌
2D3F-  18         CLC
2D40-  A9 01      LDA  #$01
2D42-  B1 FA      LDA  ($FA),Y
2D44-  39 3F 03   AND  $033F,Y
2D47-  D0 77      BNE  $2DC0   ↓
2D49-  88         DEY
2D4A-  10 F6      BPL  $2D42
2D4C-  A9 04      LDA  #$04
2D4E-  8D 47 03   STA  $0347
2D51-  60         RTS            **
2D52-  18         CLC
2D53-  AD D8 03   LDA  $03D8
2D56-  8D 07 03   STA  $0307
2D59-  AD DB 03   LDA  $03DB
2D5C-  8D 08 03   STA  $0308
2D5F-  20 AA 35   JSR  $35AA   ⇌
2D62-  18         CLC
2D63-  A0 01      LDY  #$01
2D65-  B1 FA      LDA  ($FA),Y
2D67-  39 3F 03   AND  $033F,Y
2D6A-  D0 09      BNE  $2D75
2D6C-  88         DEY
2D6D-  10 F6      BPL  $2D65
2D6F-  A9 04      LDA  #$04
```



```
2D71-  8D 47 03   STA  $0347
2D74-  60         RTS            **
2D75-  AD DA 03   LDA  $03DA
2D78-  4A         LSR
2D79-  90 23      BCC  $2D9E
2D7B-  18         CLC
2D7C-  AD D8 03   LDA  $03D8
2D7F-  8D 07 03   STA  $0307
2D82-  AD D7 03   LDA  $03D7
2D85-  8D 08 03   STA  $0308
2D88-  20 AA 35   JSR  $35AA   ⇌
2D8B-  18         CLC
2D8C-  A0 01      LDY  #$01
2D8E-  B1 FA      LDA  ($FA),Y
2D90-  39 3F 03   AND  $033F,Y
2D93-  D0 2B      BNE  $2DC0
2D95-  88         DEY
2D96-  10 F6      BPL  $2D8E
2D98-  A9 04      LDA  #$04
2D9A-  8D 47 03   STA  $0347
2D9D-  60         RTS            **
2D9E-  AD D8 03   LDA  $03D8
2DA1-  8D 07 03   STA  $0307
2DA4-  AD D9 03   LDA  $03D9
2DA7-  8D 08 03   STA  $0308
2DAA-  20 AA 35   JSR  $35AA   ⇌
2DAD-  18         CLC
2DAE-  A0 01      LDY  #$01
2DB0-  B1 FA      LDA  ($FA),Y
2DB2-  39 3F 03   AND  $033F,Y
2DB5-  D0 09      BNE  $2DC0
2DB7-  88         DEY
2DB8-  10 F6      BPL  $2DB0
2DBA-  A9 04      LDA  #$04
2DBC-  8D 47 03   STA  $0347
2DBF-  60         RTS            **
2DC0-  EE DC 03   INC  $03DC
2DC3-  AD DC 03   LDA  $03DC
2DC6-  C9 01      CMP  #$01
2DC8-  D0 03      BNE  $2DCD
2DCA-  4C 3B 35   JMP  $353B   ↓
2DCD-  A9 00      LDA  #$00
2DCF-  8D DD 03   STA  $03DD
2DD2-  4C 4A 35   JMP  $354A   ↓
2DD5-  EA         NOP
2DD6-  EA         NOP
2DD7-  EA         NOP
2DD8-  EA         NOP
2DD9-  EA         NOP
2DDA-  EA         NOP
2DDB-  04         ???
2DDC-  8D 47 03   STA  $0347
2DDF-  60         RTS
2DE0-  D8         CLD
2DE1-  03         ???
2DE2-  A0 18      LDY  #$18
2DE4-  D8         CLD            ▫
2DE5-  A9 09      LDA  #$09
2DE7-  CD 13 03   CMP  $0313
2DEA-  D0 03      BNE  $2DEF
2DEC-  4C 17 2E   JMP  $2E17   ↓
```

```
2DEF-   A9 03       LDA  #$03
2DF1-   8D 47 03    STA  $0347
2DF4-   60          RTS
2DF5-   00          BRK
2DF6-   00          BRK
2DF7-   00          BRK
2DF8-   00          BRK
2DF9-   00          BRK
2DFA-   00          BRK
2DFB-   00          BRK
2DFC-   00          BRK
2DFD-   00          BRK
2DFE-   00          BRK
2DFF-   00          BRK
2E00-   00          BRK
2E01-   00          BRK
2E02-   00          BRK
2E03-   00          BRK
2E04-   00          BRK
2E05-   00          BRK
2E06-   00          BRK
2E07-   00          BRK
2E08-   00          BRK
2E09-   00          BRK
2E0A-   00          BRK
2E0B-   00          BRK
2E0C-   00          BRK
2E0D-   00          BRK
2E0E-   00          BRK
2E0F-   00          BRK
2E10-   00          BRK
2E11-   00          BRK
2E12-   00          BRK
2E13-   00          BRK
2E14-   00          BRK
2E15-   00          BRK
2E16-   00          BRK
2E17-   20 1E 3C    JSR  $3C1E
2E1A-   38          SEC
2E1B-   AD 12 03    LDA  $0312
2E1E-   ED 0D 03    SBC  $030D
2E21-   69 00       ADC  #$00
2E23-   8D 0C 03    STA  $030C
2E26-   CD 09 03    CMP  $0309
2E29-   10 08       BPL  $2E33
2E2B-   A9 00       LDA  #$00
2E2D-   8D 0D 03    STA  $030D
2E30-   4C 1A 2E    JMP  $2E1A
2E33-   4C 4E 2E    JMP  $2E4E
2E36-   00          BRK
2E37-   00          BRK
2E38-   00          BRK
2E39-   00          BRK
2E3A-   00          BRK
2E3B-   00          BRK
2E3C-   00          BRK
2E3D-   00          BRK
2E3E-   00          BRK
2E3F-   00          BRK
2E40-   00          BRK
2E41-   00          BRK
```

(Generate random coordinates).


```
2E42-   00          BRK
2E43-   00          BRK
2E44-   00          BRK
2E45-   00          BRK
2E46-   00          BRK
2E47-   00          BRK
2E48-   00          BRK
2E49-   00          BRK
2E4A-   00          BRK
2E4B-   00          BRK
2E4C-   00          BRK
2E4D-   00          BRK
2E4E-   18          CLC
2E4F-   AD 0A 03    LDA  $030A
2E52-   8D 07 03    STA  $0307
2E55-   AD 0B 03    LDA  $030B
2E58-   8D 08 03    STA  $0308
2E5B-   20 AA 35    JSR  $35AA
2E5E-   A0 01       LDY  #$01
2E60-   B1 FA       LDA  ($FA),Y
2E62-   99 17 03    STA  $0317,Y
2E65-   88          DEY
2E66-   10 F8       BPL  $2E60
2E68-   AD 0C 03    LDA  $030C
2E6B-   0A          ASL
2E6C-   0A          ASL
2E6D-   69 47       ADC  #$47
2E6F-   85 FA       STA  $FA
2E71-   A9 00       LDA  #$00
2E73-   69 03       ADC  #$03
2E75-   85 FB       STA  $FB
2E77-   18          CLC
2E78-   A0 01       LDY  #$01
2E7A-   B1 FA       LDA  ($FA),Y
2E7C-   99 3B 03    STA  $033B,Y
2E7F-   88          DEY
2E80-   10 F8       BPL  $2E7A
2E82-   A0 01       LDY  #$01
2E84-   B9 17 03    LDA  $0317,Y
2E87-   39 3B 03    AND  $033B,Y
2E8A-   D0 06       BNE  $2E92
2E8C-   88          DEY
2E8D-   10 F5       BPL  $2E84
2E8F-   4C B6 2E    JMP  $2EB6
2E92-   A9 00       LDA  #$00
2E94-   8D 0D 03    STA  $030D
2E97-   4C 17 2E    JMP  $2E17
2E9A-   EA          NOP
2E9B-   EA          NOP
2E9C-   EA          NOP
2E9D-   AD 0C 03    LDA  $030C
2EA0-   CD 09 03    CMP  $0309
2EA3-   D0 0B       BNE  $2EB0
2EA5-   A9 00       LDA  #$00
2EA7-   8D 0D 03    STA  $030D
2EAA-   4C 17 2E    JMP  $2E17
2EAD-   EA          NOP
2EAE-   EA          NOP
2EAF-   EA          NOP
2EB0-   EE 0D 03    INC  $030D
2EB3-   4C 1A 2E    JMP  $2E1A
```



```
2EB6-   18          CLC
2EB7-   AE 0A 03    LDX  $030A
2EBA-   CA          DEX
2EBB-   10 03       BPL  $2EC0
2EBD-   AE 06 03    LDX  $0306
2EC0-   8E 0E 03    STX  $030E
2EC3-   AE 0B 03    LDX  $030B
2EC6-   CA          DEX
2EC7-   10 03       BPL  $2ECC
2EC9-   AE 06 03    LDX  $0306
2ECC-   8E 0F 03    STX  $030F
2ECF-   AE 0A 03    LDX  $030A
2ED2-   EC 06 03    CPX  $0306
2ED5-   D0 08       BNE  $2EDF
2ED7-   A2 00       LDX  #$00
2ED9-   8E 10 03    STX  $0310
2EDC-   4C E3 2E    JMP  $2EE3
2EDF-   F8          INX
2EE0-   8E 10 03    STX  $0310
2EE3-   AE 0B 03    LDX  $030B
2EE6-   EC 06 03    CPX  $0306
2EE9-   D0 08       BNE  $2EF3
2EEB-   A2 00       LDX  #$00
2EED-   8E 11 03    STX  $0311
2EF0-   4C F7 2E    JMP  $2EF7
2EF3-   E8          INX
2EF4-   8E 11 03    STX  $0311
2EF7-   18          CLC
2EF8-   A0 00       LDY  #$00
2EFA-   B9 3B 03    LDA  $033B,Y
2EFD-   6A          ROR
2EFE-   99 3F 03    STA  $033F,Y
2F01-   B0 05       BCS  $2F08
2F03-   C0 03       CPY  #$03
2F05-   F0 04       BEQ  $2F0B
2F07-   18          CLC
2F08-   C8          INY
2F09-   10 EF       BPL  $2EFA
2F0B-   18          CLC
2F0C-   A0 01       LDY  #$01
2F0E-   B9 3B 03    LDA  $033B,
2F11-   2A          ROL
2F12-   99 43 03    STA  $0343,
2F15-   88          DEY
2F16-   10 F6       BPL  $2F0E
2F18-   18          CLC
2F19-   AD 0A 03    LDA  $030A
2F1C-   8D 07 03    STA  $0307
2F1F-   AD 11 03    LDA  $0311
2F22-   8D 08 03    STA  $0308
2F25-   20 AA 35    JSR  $35AA
2F28-   A0 01       LDY  #$01
2F2A-   B1 FA       LDA  ($FA),Y
2F2C-   99 1B 03    STA  $031B,Y
2F2F-   88          DEY
2F30-   10 F8       BPL  $2F2A
2F32-   AD 0A 03    LDA  $030A
2F35-   8D 07 03    STA  $0307
2F38-   AD 0F 03    LDA  $030F
2F3B-   8D 08 03    STA  $0308
2F3E-   20 AA 35    JSR  $35AA
```

Start of routine to check chosen site's 12 nearest neighbours for occupancy. Stores each in memory.

Site 1 in plane.

```
:F41-  A0 01     LDY  #$01
:F43-  B1 FA     LDA  ($FA),Y
:F45-  99 1F 03  STA  $031F,Y   Site 2 in plane.
:F48-  88        DEY
:F49-  10 F8     BPL  $2F43
:F4B-  AD 10 03  LDA  $0310
:F4E-  8D 07 03  STA  $0307
:F51-  AD 0B 03  LDA  $030B
:F54-  8D 08 03  STA  $0308
:F57-  20 AA 35  JSR  $35AA   ⇌
:F5A-  A0 01     LDY  #$01
:F5C-  B1 FA     LDA  ($FA),Y
:F5E-  99 23 03  STA  $0323,Y   Site 3 in plane.
:F61-  88        DEY
:F62-  10 F8     BPL  $2F5C
:F64-  AD 0E 03  LDA  $030E
:F67-  8D 07 03  STA  $0307
:F6A-  AD 0B 03  LDA  $030B
:F6D-  8D 08 03  STA  $0308
:F70-  20 AA 35  JSR  $35AA   ⇌
:F73-  A0 01     LDY  #$01
:F75-  B1 FA     LDA  ($FA),Y
:F77-  99 27 03  STA  $0327,Y   Site 4 in plane.
:F7A-  88        DEY
:F7B-  10 F8     BPL  $2F75
:F7D-  EA        NOP
:F7E-  EA        NOP
:F7F-  EA        NOP
:F80-  EA        NOP
:F81-  EA        NOP
:F82-  EA        NOP
:F83-  EA        NOP
:F84-  EA        NOP
:F85-  EA        NOP
:F86-  EA        NOP
:F87-  EA        NOP
:F88-  18        CLC
:F89-  AD 0C 03  LDA  $030C
:F8C-  4A        LSR
:F8D-  B0 03     BCS  $2F92
:F8F-  4C 2F 30  JMP  $302F
:F92-  18        CLC
:F93-  AD 0A 03  LDA  $030A
:F96-  4A        LSR
:F97-  90 4D     BCC  $2FE6
:F99-  18        CLC
:F9A-  AD 10 03  LDA  $0310
:F9D-  8D 07 03  STA  $0307
:FA0-  AD 0F 03  LDA  $030F
:FA3-  8D 08 03  STA  $0308
:FA6-  20 AA 35  JSR  $35AA   ⇌
:FA9-  A0 01     LDY  #$01
:FAB-  B1 FA     LDA  ($FA),Y
:FAD-  99 2B 03  STA  $032B,Y   Site 5 in plane.
:FB0-  88        DEY
:FB1-  10 F8     BPL  $2FAB
:FB3-  AD 0E 03  LDA  $030E
:FB6-  8D 07 03  STA  $0307
:FB9-  AD 0F 03  LDA  $030F
:FBC-  8D 08 03  STA  $0308
:FBF-  20 AA 35  JSR  $35AA   ⇌
```



```
2FC2-  A0 01     LDY  #$01
2FC4-  B1 FA     LDA  ($FA),Y
2FC6-  99 2F 03  STA  $032F,Y   Site 6 in plane.
2FC9-  99 37 03  STA  $0337,Y
2FCC-  88        DEY
2FCD-  10 F5     BPL  $2FC4
2FCF-  A0 01     LDY  #$01
2FD1-  B9 27 03  LDA  $0327,Y
2FD4-  99 33 03  STA  $0333,Y
2FD7-  88        DEY
2FD8-  10 F7     BPL  $2FD1
2FDA-  EA        NOP
2FDB-  EA        NOP
2FDC-  EA        NOP
2FDD-  EA        NOP
2FDE-  EA        NOP
2FDF-  EA        NOP
2FE0-  EA        NOP
2FE1-  EA        NOP
2FE2-  EA        NOP
2FE3-  4C BB 30  JMP  $30BB   ↘
2FE6-  AD 10 03  LDA  $0310
2FE9-  8D 07 03  STA  $0307
2FEC-  AD 11 03  LDA  $0311
2FEF-  8D 08 03  STA  $0308
2FF2-  20 AA 35  JSR  $35AA   ⇌
2FF5-  A0 01     LDY  #$01
2FF7-  B1 FA     LDA  ($FA),Y
2FF9-  99 2B 03  STA  $032B,Y   Site 7 below.
2FFC-  88        DEY
2FFD-  10 F8     BPL  $2FF7
2FFF-  AD 0E 03  LDA  $030E
3002-  8D 07 03  STA  $0307
3005-  AD 11 03  LDA  $0311
3008-  8D 08 03  STA  $0308
300B-  20 AA 35  JSR  $35AA   ⇌
300E-  A0 01     LDY  #$01
3010-  B1 FA     LDA  ($FA),Y
3012-  99 2F 03  STA  $032F,Y   Site 8 below.
3015-  99 37 03  STA  $0337,Y
3018-  88        DEY
3019-  10 F5     BPL  $3010
301B-  A0 01     LDY  #$01
301D-  B9 27 03  LDA  $0327,Y
3020-  99 33 03  STA  $0333,Y
3023-  88        DEY
3024-  10 F7     BPL  $301D
3026-  EA        NOP
3027-  EA        NOP
3028-  EA        NOP
3029-  EA        NOP
302A-  EA        NOP
302B-  EA        NOP
302C-  4C BB 30  JMP  $30BB   ↘
302F-  18        CLC
3030-  AD 0A 03  LDA  $030A
3033-  4A        LSR
3034-  90 44     BCC  $307A   ↘
3036-  18        CLC
3037-  AD 10 03  LDA  $0310
303A-  8D 07 03  STA  $0307
```



```
303D-  AD 0F 03  LDA  $030F
3040-  8D 08 03  STA  $0308
3043-  20 AA 35  JSR  $35AA   ⇌
3046-  A0 01     LDY  #$01
3048-  B1 FA     LDA  ($FA),Y
304A-  99 2B 03  STA  $032B,Y   Site 9 below.
304D-  99 37 03  STA  $0337,Y
3050-  88        DEY
3051-  10 F5     BPL  $3048
3053-  AD 0E 03  LDA  $030E
3056-  8D 07 03  STA  $0307
3059-  AD 0F 03  LDA  $030F
305C-  8D 08 03  STA  $0308
305F-  20 AA 35  JSR  $35AA   ⇌
3062-  A0 01     LDY  #$01
3064-  B1 FA     LDA  ($FA),Y
3066-  99 2F 03  STA  $032F,Y   Site 10 above.
3069-  88        DEY
306A-  10 F8     BPL  $3064
306C-  A0 01     LDY  #$01
306E-  B9 23 03  LDA  $0323,Y
3071-  99 33 03  STA  $0333,Y
3074-  88        DEY
3075-  10 F7     BPL  $306E
3077-  4C BB 30  JMP  $30BB   ↘
307A-  18        CLC
307B-  AD 10 03  LDA  $0310
307E-  8D 07 03  STA  $0307
3081-  AD 11 03  LDA  $0311
3084-  8D 08 03  STA  $0308
3087-  20 AA 35  JSR  $35AA   ⇌
308A-  A0 01     LDY  #$01
308C-  B1 FA     LDA  ($FA),Y
308E-  99 2B 03  STA  $032B,Y   Site 11 above.
3091-  99 37 03  STA  $0337,Y
3094-  88        DEY
3095-  10 F5     BPL  $308C
3097-  AD 0E 03  LDA  $030E
309A-  8D 07 03  STA  $0307
309D-  AD 11 03  LDA  $0311
30A0-  8D 08 03  STA  $0308
30A3-  20 AA 35  JSR  $35AA   ⇌
30A6-  A0 01     LDY  #$01
30A8-  B1 FA     LDA  ($FA),Y
30AA-  99 2F 03  STA  $032F,Y   Site 12 above.
30AD-  88        DEY
30AE-  10 F8     BPL  $30A8
30B0-  A0 01     LDY  #$01
30B2-  B9 23 03  LDA  $0323,Y
30B5-  99 33 03  STA  $0333,Y
30B8-  88        DEY
30B9-  10 F7     BPL  $30B2
30BB-  18        CLC
30BC-  A9 00     LDA  #$00
30BE-  8D 13 03  STA  $0313
30C1-  EA        NOP
30C2-  EA        NOP
30C3-  EA        NOP
30C4-  EA        NOP
30C5-  EA        NOP
30C6-  EA        NOP
```

```
                                  Start or summing
30C7-  A0 01     LDY  ##01
30C9-  B9 1B 03 ►LDA  $031B,Y     number of nearest
30CC-  39 3B 03  AND  $033B,Y
30CF-  F0 06     BEQ  $30D7       neighbours routine
30D1-  EE 13 03  INC  $0313
30D4-  4C DA 30  JMP  $30DA ──┐   Site 1 in plane.
30D7-  88        DEY ◄        │
30D8-  10 EF     BPL  $30C9   │
30DA-  A0 01     LDY  ##01 ◄──┘
30DC-  B9 23 03 ►LDA  $0323,Y
30DF-  39 3B 03  AND  $033B,Y     Site 2 in plane.
30E2-  F0 06     BEQ  $30EA
30E4-  EE 13 03  INC  $0313
30E7-  4C ED 30  JMP  $30ED ──┐
30EA-  88        DEY ◄        │
30EB-  10 EF     BPL  $30DC   │
30ED-  A0 01     LDY  ##01 ◄──┘
30EF-  B9 1F 03 ►LDA  $031F,Y
30F2-  39 3B 03  AND  $033B,Y     Site 3 in plane.
30F5-  F0 06     BEQ  $30FD
30F7-  EE 13 03  INC  $0313
30FA-  4C 00 31  JMP  $3100 ──┐
30FD-  88        DEY ◄        │
30FE-  10 EF     BPL  $30EF   │
3100-  A0 01     LDY  ##01 ◄──┘
3102-  B9 27 03 ►LDA  $0327,Y
3105-  39 3B 03  AND  $033B,Y     Site 4 in plane.
3108-  F0 06     BEQ  $3110
310A-  EE 13 03  INC  $0313
310D-  4C 13 31  JMP  $3113 ──┐
3110-  88        DEY ◄        │
3111-  10 EF     BPL  $3102   │
3113-  A0 01     LDY  ##01 ◄──┘
3115-  B9 2B 03 ►LDA  $032B,Y
3118-  39 3B 03  AND  $033B,Y     Site 5 in plane.
311B-  F0 06     BEQ  $3123
311D-  EE 13 03  INC  $0313
3120-  4C 26 31  JMP  $3126 ──┐
3123-  88        DEY ◄        │
3124-  10 EF     BPL  $3115   │
3126-  A0 01     LDY  ##01 ◄──┘
3128-  B9 2F 03 ►LDA  $032F,Y
312B-  39 3B 03  AND  $033B,Y     Site 6 in plane.
312E-  F0 06     BEQ  $3136
3130-  EE 13 03  INC  $0313
3133-  4C 39 31  JMP  $3139 ──┐
3136-  88        DEY ◄        │
3137-  10 EF     BPL  $3128   │
3139-  A0 01     LDY  ##01 ◄──┘
313B-  B9 17 03 ►LDA  $0317,Y
313E-  39 3F 03  AND  $033F,Y     Site 7 below.
3141-  F0 06     BEQ  $3149
3143-  EE 13 03  INC  $0313
3146-  4C 4C 31  JMP  $314C ──┐
3149-  88        DEY ◄        │
314A-  10 EF     BPL  $313B   │
314C-  A0 01     LDY  ##01 ◄──┘
314E-  B9 33 03 ►LDA  $0333,Y
3151-  39 3F 03  AND  $033F,Y     Site 8 below.
3154-  F0 06     BEQ  $315C
3156-  EE 13 03  INC  $0313
                    10
```

```
3159-  4C 5F 31  JMP  $315F ──┐
315C-  88        DEY ◄        │
315D-  10 EF     BPL  $314E   │
315F-  A0 01     LDY  ##01 ◄──┘
3161-  B9 37 03 ►LDA  $0337,Y     Site 9 below.
3164-  39 3F 03  AND  $033F,Y
3167-  F0 06     BEQ  $316F
3169-  EE 13 03  INC  $0313
316C-  4C 72 31  JMP  $3172 ──┐
316F-  88        DEY ◄        │
3170-  10 EF     BPL  $3161   │
3172-  A0 01     LDY  ##01 ◄──┘
3174-  B9 17 03 ►LDA  $0317,Y     Site 10 above.
3177-  39 43 03  AND  $0343,Y
317A-  F0 06     BEQ  $3182
317C-  EE 13 03  INC  $0313
317F-  4C 85 31  JMP  $3185 ──┐
3182-  88        DEY ◄        │
3183-  10 EF     BPL  $3174   │
3185-  A0 01     LDY  ##01 ◄──┘
3187-  B9 33 03 ►LDA  $0333,Y     Site 11 above.
318A-  39 43 03  AND  $0343,Y
318D-  F0 06     BEQ  $3195
318F-  EE 13 03  INC  $0313
3192-  4C 98 31  JMP  $3198 ──┐
3195-  88        DEY ◄        │
3196-  10 EF     BPL  $3187   │
3198-  A0 01     LDY  ##01 ◄──┘
319A-  B9 37 03 ►LDA  $0337,Y     Site 12 above.
319D-  39 43 03  AND  $0343,Y
31A0-  F0 06     BEQ  $31A8
31A2-  EE 13 03  INC  $0313
31A5-  4C AB 31  JMP  $31AB ──┐
31A8-  88        DEY ◄        │
31A9-  10 EF     BPL  $319A   │
31AB-  AC 13 03  LDY  $0313 ◄─┘
31AE-  88        DEY
31AF-  30 03     BMI  $31B4 ──┐
31B1-  20 7B 3C  JSR  $3C7B   │
31B4-  AD 13 03  LDA  $0313 ◄─┘
31B7-  C9 03     CMP  ##03        <3 neighbours.
31B9-  10 03     BPL  $31BE ──┐
31BB-  4C 9D 2E  JMP  $2E9D ──┼──►
31BE-  C9 0A     CMP  ##0A ◄──┘   >9 neighbours.
31C0-  30 03     BMI  $31C5 ──┐
31C2-  4C 9D 2E  JMP  $2E9D ──┼──►
31C5-  4C D8 31  JMP  $31D8 ──┼──►
31C8-  EA        NOP          │
31C9-  EA        NOP          │
31CA-  EA        NOP          │
31CB-  EA        NOP          │
31CC-  EA        NOP          │
31CD-  EA        NOP          │
31CE-  EA        NOP          │
31CF-  EA        NOP          │
31D0-  EA        NOP          │
31D1-  EA        NOP          │
31D2-  EA        NOP          │
31D3-  EA        NOP          │
31D4-  EA        NOP          │
31D5-  EA        NOP          │
                    11
```

```
                                  (random number
31D6-  EA        NOP
31D7-  EA        NOP              routine).
31D8-  20 CB 3B  JSR  $3BCB ──►
31DB-  AD 13 03  LDA  $0313
31DE-  0A        ASL
31DF-  A8        TAY              Fill site or not ?
31E0-  38        SEC
31E1-  B9 DF 03  LDA  $03DF,Y     compare p(n) with
31E4-  E5 08     SBC  $08
31E6-  B9 DE 03  LDA  $03DE,Y     random number.
31E9-  E5 09     SBC  $09
31EB-  B0 0C     BCS  $31F9 ──┐
31ED-  4C 9D 2E  JMP  $2E9D ──┼──►
31F0-  EA        NOP          │
31F1-  EA        NOP          │
31F2-  EA        NOP          │
31F3-  EA        NOP          │
31F4-  EA        NOP          │
31F5-  EA        NOP          │
31F6-  EA        NOP          │
31F7-  EA        NOP          │
31F8-  EA        NOP          │
31F9-  AD 13 03  LDA  $0313 ◄─┘
31FC-  C9 03     CMP  ##03
31FE-  D0 06     BNE  $3206 ──┐
3200-  A9 04     LDA  ##04    │
3202-  8D 47 03  STA  $0347   │
3205-  60        RTS          │
3206-  D8        CLD ◄────────┘   **
3207-  18        CLC
3208-  AD 0A 03  LDA  $030A
320B-  8D 07 03  STA  $0307
320E-  AD 0B 03  LDA  $030B
3211-  8D 08 03  STA  $0308
3214-  20 AA 35  JSR  $35AA ──►
3217-  A0 01     LDY  ##01
3219-  B1 FA    ►LDA  ($FA),Y
321B-  19 3B 03  ORA  $033B,Y     Add new filled
321E-  91 FA     STA  ($FA),Y
3220-  88        DEY              site to memory.
3221-  10 F6     BPL  $3219 ◄─┘
3223-  4C 30 32  JMP  $3230 ──┐
3226-  EA        NOP          │
3227-  EA        NOP          │
3228-  EA        NOP          │
3229-  EA        NOP          │
322A-  EA        NOP          │
322B-  EA        NOP          │
322C-  EA        NOP          │
322D-  EA        NOP          │
322E-  EA        NOP          │
322F-  EA        NOP          │
3230-  AE 0C 03  LDX  $030C ◄─┘
3233-  CA        DEX
3234-  EC 12 03  CPX  $0312
3237-  D0 06     BNE  $323F ──┐
3239-  AD 0C 03  LDA  $030C   │
323C-  8D 12 03  STA  $0312   │
323F-  20 12 3F  JSR  $3F12 ◄─┘ ──►
3242-  A9 05     LDA  ##05
3244-  8D 47 03  STA  $0347
                    12
```

```
3247-   60        RTS            **
3248-   EA        NOP            Selection of adj-
3249-   18        CLC
324A-   D8        CLD            acent site for
324B-   AD 0A 03  LDA   $030A
324E-   4A        LSR            deposition routine.
324F-   90 7A     BCC   $32CB
3251-   18        CLC
3252-   AD 48 03  LDA   $0348
3255-   0A        ASL
3256-   0A        ASL
3257-   0A        ASL
3258-   0A        ASL
3259-   69 69     ADC   #$69
325B-   8D 07 03  STA   $0307
325E-   A9 32     LDA   #$32
3260-   69 00     ADC   #$00
3262-   8D 08 03  STA   $0308
3265-   6C 07 03  JMP   ($0307)
3268-   EA        NOP
3269-   AD 10 03  LDA   $0310
326C-   8D 07 03  STA   $0307
326F-   AD 0B 03  LDA   $030B
3272-   8D 08 03  STA   $0308
3275-   4C 49 33  JMP   $3349
3278-   EA        NOP
3279-   AD 0E 03  LDA   $030E
327C-   8D 07 03  STA   $0307
327F-   AD 0B 03  LDA   $030B
3282-   8D 08 03  STA   $0308
3285-   4C 49 33  JMP   $3349
3288-   EA        NOP
3289-   AD 0A 03  LDA   $030A
328C-   8D 07 03  STA   $0307
328F-   AD 0F 03  LDA   $030F
3292-   8D 08 03  STA   $0308
3295-   4C 49 33  JMP   $3349
3298-   EA        NOP
3299-   AD 0A 03  LDA   $030A
329C-   8D 07 03  STA   $0307
329F-   AD 11 03  LDA   $0311
32A2-   8D 08 03  STA   $0308
32A5-   4C 49 33  JMP   $3349
32A8-   EA        NOP
32A9-   AD 0E 03  LDA   $030E
32AC-   8D 07 03  STA   $0307
32AF-   AD 0F 03  LDA   $030F
32B2-   8D 08 03  STA   $0308
32B5-   4C 49 33  JMP   $3349
32B8-   EA        NOP
32B9-   AD 10 03  LDA   $0310
32BC-   8D 07 03  STA   $0307
32BF-   AD 0F 03  LDA   $030F
32C2-   8D 08 03  STA   $0308
32C5-   4C 49 33  JMP   $3349
32C8-   EA        NOP
32C9-   EA        NOP
32CA-   EA        NOP
32CB-   18        CLC
32CC-   AD 48 03  LDA   $0348
32CF-   0A        ASL
```

13

```
32D0-   0A        ASL
32D1-   0A        ASL
32D2-   0A        ASL
32D3-   69 E9     ADC   #$E9
32D5-   8D 07 03  STA   $0307
32D8-   A9 32     LDA   #$32
32DA-   69 00     ADC   #$00
32DC-   8D 08 03  STA   $0308
32DF-   6C 07 03  JMP   ($0307)
32E2-   EA        NOP
32E3-   EA        NOP
32E4-   EA        NOP
32E5-   EA        NOP
32E6-   EA        NOP
32E7-   EA        NOP
32E8-   EA        NOP
32E9-   AD 10 03  LDA   $0310
32EC-   8D 07 03  STA   $0307
32EF-   AD 0B 03  LDA   $030B
32F2-   8D 08 03  STA   $0308
32F5-   4C 49 33  JMP   $3349
32F8-   EA        NOP
32F9-   AD 0E 03  LDA   $030E
32FC-   8D 07 03  STA   $0307
32FF-   AD 0B 03  LDA   $030B
3302-   8D 08 03  STA   $0308
3305-   4C 49 33  JMP   $3349
3308-   EA        NOP
3309-   AD 0A 03  LDA   $030A
330C-   8D 07 03  STA   $0307
330F-   AD 11 03  LDA   $0311
3312-   8D 08 03  STA   $0308
3315-   4C 49 33  JMP   $3349
3318-   EA        NOP
3319-   AD 0A 03  LDA   $030A
331C-   8D 07 03  STA   $0307
331F-   AD 0F 03  LDA   $030F
3322-   8D 08 03  STA   $0308
3325-   4C 49 33  JMP   $3349
3328-   EA        NOP
3329-   AD 10 03  LDA   $0310
332C-   8D 07 03  STA   $0307
332F-   AD 11 03  LDA   $0311
3332-   8D 08 03  STA   $0308
3335-   4C 49 33  JMP   $3349
3338-   EA        NOP
3339-   AD 0E 03  LDA   $030E
333C-   8D 07 03  STA   $0307
333F-   AD 11 03  LDA   $0311
3342-   8D 08 03  STA   $0308
3345-   EA        NOP
3346-   EA        NOP
3347-   EA        NOP
3348-   EA        NOP
3349-   AD 07 03  LDA   $0307
334C-   8D 49 03  STA   $0349
334F-   AD 08 03  LDA   $0308
3352-   8D 4A 03  STA   $034A
3355-   EA        NOP
3356-   EA        NOP
3357-   EA        NOP
```

14

```
3358-   EA        NOP
3359-   EA        NOP
335A-   EA        NOP
335B-   20 AA 35  JSR   $35AA
335E-   A0 01     LDY   #$01
3360-   B1 FA     LDA   ($FA),Y
3362-   39 3B 03  AND   $033B,Y
3365-   D0 31     BNE   $3398
3367-   88        DEY
3368-   10 F6     BPL   $3360
336A-   AD 49 03  LDA   $0349
336D-   8D 0A 03  STA   $030A
3370-   AD 4A 03  LDA   $034A
3373-   8D 0B 03  STA   $030B
3376-   4C 91 33  JMP   $3391
3379-   00        BRK
337A-   00        BRK
337B-   00        BRK
337C-   00        BRK
337D-   00        BRK
337E-   00        BRK
337F-   00        BRK
3380-   00        BRK
3381-   00        BRK
3382-   00        BRK
3383-   00        BRK
3384-   00        BRK
3385-   00        BRK
3386-   00        BRK
3387-   00        BRK
3388-   00        BRK
3389-   00        BRK
338A-   00        BRK
338B-   00        BRK
338C-   00        BRK
338D-   00        BRK
338E-   00        BRK
338F-   00        BRK
3390-   00        BRK
3391-   A9 12     LDA   #$12
3393-   85 1E     STA   $1E
3395-   4C B6 2E  JMP   $2EB6
3398-   C6 1E     DEC   $1E
339A-   F0 06     BEQ   $33A2
339C-   A9 03     LDA   #$03
339E-   8D 47 03  STA   $0347
33A1-   60        RTS                **
33A2-   A9 12     LDA   #$12
33A4-   85 1E     STA   $1E
33A6-   4C 1A 2E  JMP   $2E1A
33A9-   EA        NOP
33AA-   EA        NOP
33AB-   EA        NOP
33AC-   18        CLC
33AD-   AD 0A 03  LDA   $030A
33B0-   4A        LSR
33B1-   B0 03     BCS   $33B6
33B3-   4C 71 34  JMP   $3471
33B6-   18        CLC
33B7-   AD 48 03  LDA   $0348
33BA-   69 C9     ADC   #$C9
```

15

```
33BC-  8D 07 03    STA  $0307
33BF-  A9 33       LDA  #$33
33C1-  69 00       ADC  #$00
33C3-  8D 08 03    STA  $0308
33C6-  6C 07 03    JMP  ($0307)
33C9-  AD 0A 03    LDA  $030A
33CC-  8D 01 03    STA  $0301
33CF-  AD 11 03    LDA  $0311
33D2-  8D 02 03    STA  $0302
33D5-  AD 0E 03    LDA  $030E
33D8-  8D 03 03    STA  $0303
33DB-  AD 0B 03    LDA  $030B
33DE-  8D 04 03    STA  $0304
33E1-  4C 2C 35    JMP  $352C
33E4-              NOP
33E7-  AD 0A 03    LDA  $030A
33EB-  8D 01 03    STA  $0301
33EE-  AD 11 03    LDA  $0311
33F1-  AD 10 03    LDA  $0310
33F4-  8D 03 03    STA  $0303
33F7-  AD 0B 03    LDA  $030B
33FA-  8D 04 03    STA  $0304
33FD-  4C 2C 35    JMP  $352C
3400-              NOP
3401-  AD 10 03    LDA  $0310
3404-  8D 01 03    STA  $0301
3407-  8D 03 03    STA  $0303
340A-  AD 0F 03    LDA  $030F
340D-  8D 02 03    STA  $0302
3410-  AD 0B 03    LDA  $030B
3413-  8D 04 03    STA  $0304
3416-  4C 2C 35    JMP  $352C
3419-              NOP
341A-              NOP
341B-              NOP
341C-              NOP
341D-  AD 10 03    LDA  $0310
3420-  8D 01 03    STA  $0301
3423-  AD 0F 03    LDA  $030F
3426-  8D 02 03    STA  $0302
3429-  8D 04 03    STA  $0304
342C-  AD 0A 03    LDA  $030A
342F-  8D 03 03    STA  $0303
3432-  4C 2C 35    JMP  $352C
3435-              NOP
3436-              NOP
3437-              NOP
3438-              NOP
3439-  AD 0E 03    LDA  $030E
343C-  8D 01 03    STA  $0301
343F-  AD 0F 03    LDA  $030F
3442-  8D 02 03    STA  $0302
3445-  8D 04 03    STA  $0304
3448-  8D 03 03    STA  $0303
344B-  AD 0A 03    LDA  $030A
344E-  4C 2C 35    JMP  $352C
3451-              NOP
3452-              NOP
3453-              NOP
3454-              NOP
```



```
34E2-  8D 02 03    STA  $0302
34E5-  AD 0E 03    LDA  $030E
34E8-              NOP
34E9-  AD 0A 03    LDA  $030A
34EC-  8D 01 03    STA  $0301
34EF-  AD 0F 03    LDA  $030F
34F2-  4C 2C 35    JMP  $352C
34F5-              NOP
34F6-              NOP
34F7-              NOP
34F8-              NOP
34F9-  AD 10 03    LDA  $0310
34FC-  8D 01 03    STA  $0301
34FF-  AD 11 03    LDA  $0311
3502-  8D 02 03    STA  $0302
3505-  AD 0A 03    LDA  $030A
3508-  8D 04 03    STA  $0304
350B-  8D 03 03    STA  $0303
350E-  AD 0B 03    LDA  $030B
3511-              NOP
3512-              NOP
3513-              NOP
3514-              NOP
3515-  AD 0E 03    LDA  $030E
3518-  8D 01 03    STA  $0301
351B-  AD 11 03    LDA  $0311
351E-  8D 02 03    STA  $0302
3521-  AD 10 03    LDA  $0310
3524-  8D 03 03    STA  $0303
3527-  AD 0F 03    LDA  $030F
352A-  8D 04 03    STA  $0304
352D-  AD 0B 03    LDA  $030B
3530-  8D 0A 03    STA  $030A
3533-  4C 2C 35    JMP  $352C
3536-              NOP
3537-              NOP
3538-              NOP
3539-              NOP
353A-  AD 0E 03    LDA  $030E
353D-  8D 01 03    STA  $0301
3540-  AD 11 03    LDA  $0311
3543-  8D 02 03    STA  $0302
3546-  AD 10 03    LDA  $0310
3549-  8D 03 03    STA  $0303
354C-  AD 0F 03    LDA  $030F
354F-  8D 04 03    STA  $0304
3552-  AD 0B 03    LDA  $030B
3555-  8D 0A 03    STA  $030A
3558-  4C 2C 35    JMP  $352C
355B-              NOP
355C-              NOP
355D-              NOP
355E-              NOP
355F-              NOP
3560-  AD 0E 03    LDA  $030E
3563-  8D 01 03    STA  $0301
3566-  AD 11 03    LDA  $0311
3569-  8D 02 03    STA  $0302
356C-  AD 10 03    LDA  $0310
356F-  8D 03 03    STA  $0303
3572-  AD 0F 03    LDA  $030F
3575-  8D 04 03    STA  $0304
3578-  AD 0B 03    LDA  $030B
357B-  8D 0A 03    STA  $030A
357E-  4C 2C 35    JMP  $352C
3581-              NOP
3582-              NOP
3583-              NOP
3584-              NOP
3585-  AD 0E 03    LDA  $030E
3588-  8D 01 03    STA  $0301
358B-  AD 11 03    LDA  $0311
358E-  8D 02 03    STA  $0302
3591-  AD 10 03    LDA  $0310
3594-  8D 03 03    STA  $0303
3597-  AD 0F 03    LDA  $030F
359A-  8D 04 03    STA  $0304
359D-  AD 0B 03    LDA  $030B
35A0-  8D 0A 03    STA  $030A
35A3-  4C 2C 35    JMP  $352C
35A6-              NOP
35A7-              NOP
35A8-              NOP
35A9-              NOP
35AA-  AD 0E 03    LDA  $030E
35AD-  8D 01 03    STA  $0301
35B0-  AD 11 03    LDA  $0311
35B3-  8D 02 03    STA  $0302
35B6-  AD 10 03    LDA  $0310
35B9-  8D 03 03    STA  $0303
35BC-  AD 0F 03    LDA  $030F
35BF-  8D 04 03    STA  $0304
35C2-  AD 0B 03    LDA  $030B
35C5-  8D 0A 03    STA  $030A
35C8-  4C 2C 35    JMP  $352C
35CB-              NOP
35CC-              NOP
35CD-              NOP
35CE-              NOP
35CF-  AD 0E 03    LDA  $030E
35D2-  8D 01 03    STA  $0301
35D5-  AD 11 03    LDA  $0311
35D8-  8D 02 03    STA  $0302
35DB-  AD 10 03    LDA  $0310
35DE-  8D 03 03    STA  $0303
35E1-  AD 0F 03    LDA  $030F
35E4-  8D 04 03    STA  $0304
35E7-  AD 0B 03    LDA  $030B
35EA-  8D 0A 03    STA  $030A
35ED-  4C 2C 35    JMP  $352C
35F0-              NOP
35F1-              NOP
35F2-              NOP
35F3-              NOP
35F4-  AD 0E 03    LDA  $030E
35F7-  8D 01 03    STA  $0301
35FA-  AD 11 03    LDA  $0311
35FD-  8D 02 03    STA  $0302
3600-  AD 10 03    LDA  $0310
3603-  8D 03 03    STA  $0303
3606-  AD 0F 03    LDA  $030F
3609-  8D 04 03    STA  $0304
360C-  AD 0B 03    LDA  $030B
360F-  8D 0A 03    STA  $030A
3612-  4C 2C 35    JMP  $352C
3615-              NOP
3616-              NOP
3617-              NOP
3618-              NOP
3619-  AD 0E 03    LDA  $030E
361C-  8D 01 03    STA  $0301
361F-  AD 11 03    LDA  $0311
3622-  8D 02 03    STA  $0302
3625-  AD 10 03    LDA  $0310
3628-  8D 03 03    STA  $0303
362B-  AD 0F 03    LDA  $030F
362E-  8D 04 03    STA  $0304
3631-  AD 0B 03    LDA  $030B
3634-  8D 0A 03    STA  $030A
3637-  4C 2C 35    JMP  $352C
363A-              NOP
363B-              NOP
363C-              NOP
363D-              NOP
363E-  AD 0E 03    LDA  $030E
3641-  8D 01 03    STA  $0301
3644-  AD 11 03    LDA  $0311
3647-  8D 02 03    STA  $0302
364A-  AD 10 03    LDA  $0310
364D-  8D 03 03    STA  $0303
3650-  AD 0F 03    LDA  $030F
3653-  8D 04 03    STA  $0304
3656-  AD 0B 03    LDA  $030B
3659-  8D 0A 03    STA  $030A
365C-  4C 2C 35    JMP  $352C
365F-              NOP
3660-              NOP
3661-              NOP
3662-              NOP
3663-  AD 0E 03    LDA  $030E
3666-  8D 01 03    STA  $0301
3669-  AD 11 03    LDA  $0311
366C-  8D 02 03    STA  $0302
366F-  AD 10 03    LDA  $0310
3672-  8D 03 03    STA  $0303
3675-  AD 0F 03    LDA  $030F
3678-  8D 04 03    STA  $0304
367B-  AD 0B 03    LDA  $030B
367E-  8D 0A 03    STA  $030A
3681-  4C 2C 35    JMP  $352C
3684-              NOP
3685-              NOP
3686-              NOP
3687-              NOP
3688-  AD 0E 03    LDA  $030E
368B-  8D 01 03    STA  $0301
368E-  AD 11 03    LDA  $0311
3691-  8D 02 03    STA  $0302
3694-  AD 10 03    LDA  $0310
3697-  8D 03 03    STA  $0303
369A-  AD 0F 03    LDA  $030F
369D-  8D 04 03    STA  $0304
36A0-  AD 0B 03    LDA  $030B
36A3-  8D 0A 03    STA  $030A
36A6-  4C 2C 35    JMP  $352C
36A9-              NOP
36AA-              NOP
36AB-              NOP
36AC-              NOP
36AD-  AD 0E 03    LDA  $030E
36B0-  8D 01 03    STA  $0301
36B3-  AD 11 03    LDA  $0311
36B6-  8D 02 03    STA  $0302
36B9-  AD 10 03    LDA  $0310
36BC-  8D 03 03    STA  $0303
36BF-  AD 0F 03    LDA  $030F
36C2-  8D 04 03    STA  $0304
36C5-  AD 0B 03    LDA  $030B
36C8-  8D 0A 03    STA  $030A
36CB-  4C 2C 35    JMP  $352C
36CE-              NOP
36CF-              NOP
36D0-              NOP
36D1-              NOP
36D2-  AD 0E 03    LDA  $030E
36D5-  8D 01 03    STA  $0301
36D8-  AD 11 03    LDA  $0311
36DB-  8D 02 03    STA  $0302
36DE-  AD 10 03    LDA  $0310
36E1-  8D 03 03    STA  $0303
36E4-  AD 0F 03    LDA  $030F
36E7-  8D 04 03    STA  $0304
36EA-  AD 0B 03    LDA  $030B
36ED-  8D 0A 03    STA  $030A
36F0-  4C 2C 35    JMP  $352C
36F3-              NOP
36F4-              NOP
36F5-              NOP
36F6-              NOP
36F7-  AD 0E 03    LDA  $030E
36FA-  8D 01 03    STA  $0301
36FD-  AD 11 03    LDA  $0311
3700-  8D 02 03    STA  $0302
3703-  AD 10 03    LDA  $0310
3706-  8D 03 03    STA  $0303
3709-  AD 0F 03    LDA  $030F
370C-  8D 04 03    STA  $0304
370F-  AD 0B 03    LDA  $030B
3712-  8D 0A 03    STA  $030A
3715-  4C 2C 35    JMP  $352C
3718-              NOP
3719-              NOP
371A-              NOP
371B-              NOP
371C-  AD 0E 03    LDA  $030E
371F-  8D 01 03    STA  $0301
3722-  AD 11 03    LDA  $0311
3725-  8D 02 03    STA  $0302
3728-  AD 10 03    LDA  $0310
372B-  8D 03 03    STA  $0303
372E-  AD 0F 03    LDA  $030F
3731-  8D 04 03    STA  $0304
3734-  AD 0B 03    LDA  $030B
3737-  8D 0A 03    STA  $030A
373A-  4C 2C 35    JMP  $352C
373D-              NOP
373E-              NOP
373F-              NOP
3740-              NOP
3741-  AD 0E 03    LDA  $030E
3744-  8D 01 03    STA  $0301
3747-  AD 11 03    LDA  $0311
374A-  8D 02 03    STA  $0302
374D-  AD 10 03    LDA  $0310
3750-  8D 03 03    STA  $0303
3753-  AD 0F 03    LDA  $030F
3756-  8D 04 03    STA  $0304
3759-  AD 0B 03    LDA  $030B
375C-  8D 0A 03    STA  $030A
375F-  4C 2C 35    JMP  $352C
3762-              NOP
3763-              NOP
3764-              NOP
3765-              NOP
3766-  A9 01       LDA  #$01
3768-  91 FA       STA  ($FA),Y
376A-  88          DEY
376B-  10 F6       BPL  $3763
376D-  AD 03 03    LDA  $0303
3770-  8D 04 03    STA  $0304
3773-  AD 02 03    LDA  $0302
3776-  8D 03 03    STA  $0303
3779-  AD 01 03    LDA  $0301
377C-  8D 02 03    STA  $0302
377F-  AD 00 03    LDA  $0300
3782-  8D 01 03    STA  $0301
3785-  A9 00       LDA  #$00
3787-  8D 00 03    STA  $0300
378A-  A9 03       LDA  #$03
378C-  8D 01 03    STA  $0301
378F-  A9 00       LDA  #$00
3791-  8D 00 03    STA  $0300
3794-  A9 03       LDA  #$03
3796-  8D 01 03    STA  $0301
3799-  A9 00       LDA  #$00
379B-  8D 00 03    STA  $0300
379E-  A9 03       LDA  #$03
37A0-  8D 01 03    STA  $0301
37A3-  A9 00       LDA  #$00
37A5-  8D 00 03    STA  $0300
37A8-  A9 03       LDA  #$03
37AA-  8D 01 03    STA  $0301
37AD-  A9 00       LDA  #$00
37AF-  8D 00 03    STA  $0300
37B2-  A9 03       LDA  #$03
37B4-  8D 01 03    STA  $0301
37B7-  A9 00       LDA  #$00
37B9-  8D 00 03    STA  $0300
37BC-  A9 03       LDA  #$03
37BE-  8D 01 03    STA  $0301
37C1-  A9 00       LDA  #$00
37C3-  8D 00 03    STA  $0300
37C6-  A9 03       LDA  #$03
37C8-  8D 01 03    STA  $0301
37CB-  A9 00       LDA  #$00
37CD-  8D 00 03    STA  $0300
37D0-  A9 03       LDA  #$03
37D2-  8D 01 03    STA  $0301
37D5-  A9 00       LDA  #$00
37D7-  8D 00 03    STA  $0300
37DA-  A9 03       LDA  #$03
37DC-  8D 01 03    STA  $0301
37DF-  A9 00       LDA  #$00
37E1-  8D 00 03    STA  $0300
37E4-  A9 03       LDA  #$03
37E6-  8D 01 03    STA  $0301
37E9-  A9 00       LDA  #$00
37EB-  8D 00 03    STA  $0300
37EE-  A9 03       LDA  #$03
37F0-  8D 01 03    STA  $0301
37F3-  A9 00       LDA  #$00
37F5-  8D 00 03    STA  $0300
37F8-  A9 03       LDA  #$03
37FA-  8D 01 03    STA  $0301
37FD-  A9 00       LDA  #$00
37FF-  8D 00 03    STA  $0300
3802-  A9 03       LDA  #$03
3804-  8D 01 03    STA  $0301
3807-  A9 00       LDA  #$00
3809-  8D 00 03    STA  $0300
380C-  A9 03       LDA  #$03
380E-  8D 01 03    STA  $0301
3811-  A9 00       LDA  #$00
3813-  8D 00 03    STA  $0300
3816-  A9 03       LDA  #$03
3818-  8D 01 03    STA  $0301
381B-  A9 00       LDA  #$00
381D-  8D 00 03    STA  $0300
3820-  A9 03       LDA  #$03
3822-  8D 01 03    STA  $0301
3825-  A9 00       LDA  #$00
3827-  8D 00 03    STA  $0300
382A-  A9 03       LDA  #$03
382C-  8D 01 03    STA  $0301
382F-  A9 00       LDA  #$00
3831-  8D 00 03    STA  $0300
3834-  A9 03       LDA  #$03
3836-  8D 01 03    STA  $0301
3839-  A9 00       LDA  #$00
383B-  8D 00 03    STA  $0300
383E-  A9 03       LDA  #$03
3840-  8D 01 03    STA  $0301
3843-  A9 00       LDA  #$00
3845-  8D 00 03    STA  $0300
3848-  A9 03       LDA  #$03
384A-  8D 01 03    STA  $0301
384D-  A9 00       LDA  #$00
384F-  8D 00 03    STA  $0300
3852-  A9 03       LDA  #$03
3854-  8D 01 03    STA  $0301
3857-  A9 00       LDA  #$00
3859-  8D 00 03    STA  $0300
385C-  A9 03       LDA  #$03
385E-  8D 01 03    STA  $0301
3861-  A9 00       LDA  #$00
3863-  8D 00 03    STA  $0300
3866-  A9 03       LDA  #$03
3868-  8D 01 03    STA  $0301
386B-  A9 00       LDA  #$00
386D-  8D 00 03    STA  $0300
3870-  A9 03       LDA  #$03
3872-  8D 01 03    STA  $0301
3875-  A9 00       LDA  #$00
3877-  8D 00 03    STA  $0300
387A-  A9 03       LDA  #$03
387C-  8D 01 03    STA  $0301
387F-  A9 00       LDA  #$00
3881-  8D 00 03    STA  $0300
3884-  A9 03       LDA  #$03
3886-  8D 01 03    STA  $0301
3889-  A9 00       LDA  #$00
388B-  8D 00 03    STA  $0300
388E-  A9 03       LDA  #$03
3890-  8D 01 03    STA  $0301
3893-  A9 00       LDA  #$00
3895-  8D 00 03    STA  $0300
3898-  A9 03       LDA  #$03
389A-  8D 01 03    STA  $0301
389D-  A9 00       LDA  #$00
389F-  8D 00 03    STA  $0300
38A2-  A9 03       LDA  #$03
38A4-  8D 01 03    STA  $0301
38A7-  A9 00       LDA  #$00
38A9-  8D 00 03    STA  $0300
38AC-  A9 03       LDA  #$03
38AE-  8D 01 03    STA  $0301
38B1-  A9 00       LDA  #$00
38B3-  8D 00 03    STA  $0300
38B6-  A9 03       LDA  #$03
38B8-  8D 01 03    STA  $0301
38BB-  A9 00       LDA  #$00
38BD-  8D 00 03    STA  $0300
38C0-  A9 03       LDA  #$03
38C2-  8D 01 03    STA  $0301
38C5-  A9 00       LDA  #$00
38C7-  8D 00 03    STA  $0300
38CA-  A9 03       LDA  #$03
38CC-  8D 01 03    STA  $0301
38CF-  A9 00       LDA  #$00
38D1-  8D 00 03    STA  $0300
38D4-  A9 03       LDA  #$03
38D6-  8D 01 03    STA  $0301
38D9-  A9 00       LDA  #$00
38DB-  8D 00 03    STA  $0300
38DE-  A9 03       LDA  #$03
38E0-  8D 01 03    STA  $0301
38E3-  A9 00       LDA  #$00
38E5-  8D 00 03    STA  $0300
38E8-  A9 03       LDA  #$03
38EA-  8D 01 03    STA  $0301
38ED-  A9 00       LDA  #$00
38EF-  8D 00 03    STA  $0300
38F2-  A9 03       LDA  #$03
38F4-  8D 01 03    STA  $0301
38F7-  A9 00       LDA  #$00
38F9-  8D 00 03    STA  $0300
38FC-  A9 03       LDA  #$03
38FE-  8D 01 03    STA  $0301
3901-  A9 00       LDA  #$00
3903-  8D 00 03    STA  $0300
3906-  A9 03       LDA  #$03
3908-  8D 01 03    STA  $0301
390B-  A9 00       LDA  #$00
390D-  8D 00 03    STA  $0300
3910-  A9 03       LDA  #$03
3912-  8D 01 03    STA  $0301
3915-  A9 00       LDA  #$00
3917-  8D 00 03    STA  $0300
391A-  A9 03       LDA  #$03
391C-  8D 01 03    STA  $0301
391F-  A9 00       LDA  #$00
3921-  8D 00 03    STA  $0300
3924-  A9 03       LDA  #$03
3926-  8D 01 03    STA  $0301
3929-  A9 00       LDA  #$00
392B-  8D 00 03    STA  $0300
392E-  A9 03       LDA  #$03
3930-  8D 01 03    STA  $0301
3933-  A9 00       LDA  #$00
3935-  8D 00 03    STA  $0300
3938-  A9 03       LDA  #$03
393A-  8D 01 03    STA  $0301
393D-  A9 00       LDA  #$00
393F-  8D 00 03    STA  $0300
3942-  A9 03       LDA  #$03
3944-  8D 01 03    STA  $0301
3947-  A9 00       LDA  #$00
3949-  8D 00 03    STA  $0300
394C-  A9 03       LDA  #$03
394E-  8D 01 03    STA  $0301
3951-  A9 00       LDA  #$00
3953-  8D 00 03    STA  $0300
3956-  A9 03       LDA  #$03
3958-  8D 01 03    STA  $0301
395B-  A9 00       LDA  #$00
395D-  8D 00 03    STA  $0300
3960-  A9 03       LDA  #$03
3962-  8D 01 03    STA  $0301
3965-  A9 00       LDA  #$00
3967-  8D 00 03    STA  $0300
396A-  A9 03       LDA  #$03
396C-  8D 01 03    STA  $0301
396F-  A9 00       LDA  #$00
3971-  8D 00 03    STA  $0300
3974-  A9 03       LDA  #$03
3976-  8D 01 03    STA  $0301
3979-  A9 00       LDA  #$00
397B-  8D 00 03    STA  $0300
397E-  A9 03       LDA  #$03
3980-  8D 01 03    STA  $0301
3983-  A9 00       LDA  #$00
3985-  8D 00 03    STA  $0300
3988-  A9 03       LDA  #$03
398A-  8D 01 03    STA  $0301
398D-  A9 00       LDA  #$00
398F-  8D 00 03    STA  $0300
3992-  A9 03       LDA  #$03
3994-  8D 01 03    STA  $0301
3997-  A9 00       LDA  #$00
3999-  8D 00 03    STA  $0300
399C-  A9 03       LDA  #$03
399E-  8D 01 03    STA  $0301
39A1-  A9 00       LDA  #$00
39A3-  8D 00 03    STA  $0300
39A6-  A9 03       LDA  #$03
39A8-  8D 01 03    STA  $0301
39AB-  A9 00       LDA  #$00
39AD-  8D 00 03    STA  $0300
39B0-  A9 03       LDA  #$03
39B2-  8D 01 03    STA  $0301
39B5-  A9 00       LDA  #$00
39B7-  8D 00 03    STA  $0300
39BA-  A9 03       LDA  #$03
39BC-  8D 01 03    STA  $0301
39BF-  A9 00       LDA  #$00
39C1-  8D 00 03    STA  $0300
39C4-  A9 03       LDA  #$03
39C6-  8D 01 03    STA  $0301
39C9-  A9 00       LDA  #$00
39CB-  8D 00 03    STA  $0300
39CE-  A9 03       LDA  #$03
39D0-  8D 01 03    STA  $0301
39D3-  A9 00       LDA  #$00
39D5-  8D 00 03    STA  $0300
39D8-  A9 03       LDA  #$03
39DA-  8D 01 03    STA  $0301
39DD-  A9 00       LDA  #$00
39DF-  8D 00 03    STA  $0300
39E2-  A9 03       LDA  #$03
39E4-  8D 01 03    STA  $0301
39E7-  A9 00       LDA  #$00
39E9-  8D 00 03    STA  $0300
39EC-  A9 03       LDA  #$03
39EE-  8D 01 03    STA  $0301
39F1-  A9 00       LDA  #$00
39F3-  8D 00 03    STA  $0300
39F6-  A9 03       LDA  #$03
39F8-  8D 01 03    STA  $0301
39FB-  A9 00       LDA  #$00
39FD-  8D 00 03    STA  $0300
3A00-  A9 03       LDA  #$03
3A02-  8D 01 03    STA  $0301
3A05-  A9 00       LDA  #$00
3A07-  8D 00 03    STA  $0300
3A0A-  A9 03       LDA  #$03
3A0C-  8D 01 03    STA  $0301
3A0F-  A9 00       LDA  #$00
3A11-  8D 00 03    STA  $0300
3A14-  A9 03       LDA  #$03
3A16-  8D 01 03    STA  $0301
3A19-  A9 00       LDA  #$00
3A1B-  8D 00 03    STA  $0300
3A1E-  A9 03       LDA  #$03
3A20-  8D 01 03    STA  $0301
3A23-  A9 00       LDA  #$00
3A25-  8D 00 03    STA  $0300
3A28-  A9 03       LDA  #$03
3A2A-  8D 01 03    STA  $0301
3A2D-  A9 00       LDA  #$00
3A2F-  8D 00 03    STA  $0300
3A32-  A9 03       LDA  #$03
3A34-  8D 01 03    STA  $0301
3A37-  A9 00       LDA  #$00
3A39-  8D 00 03    STA  $0300
3A3C-  A9 03       LDA  #$03
3A3E-  8D 01 03    STA  $0301
3A41-  A9 00       LDA  #$00
3A43-  8D 00 03    STA  $0300
3A46-  A9 03       LDA  #$03
3A48-  8D 01 03    STA  $0301
3A4B-  A9 00       LDA  #$00
3A4D-  8D 00 03    STA  $0300
3A50-  A9 03       LDA  #$03
3A52-  8D 01 03    STA  $0301
3A55-  A9 00       LDA  #$00
3A57-  8D 00 03    STA  $0300
3A5A-  A9 03       LDA  #$03
3A5C-  8D 01 03    STA  $0301
3A5F-  A9 00       LDA  #$00
3A61-  8D 00 03    STA  $0300
3A64-  A9 03       LDA  #$03
3A66-  8D 01 03    STA  $0301
3A69-  A9 00       LDA  #$00
3A6B-  8D 00 03    STA  $0300
3A6E-  A9 03       LDA  #$03
3A70-  8D 01 03    STA  $0301
3A73-  A9 00       LDA  #$00
3A75-  8D 00 03    STA  $0300
3A78-  A9 03       LDA  #$03
3A7A-  8D 01 03    STA  $0301
3A7D-  A9 00       LDA  #$00
3A7F-  8D 00 03    STA  $0300
3A82-  A9 03       LDA  #$03
3A84-  8D 01 03    STA  $0301
3A87-  A9 00       LDA  #$00
3A89-  8D 00 03    STA  $0300
3A8C-  A9 03       LDA  #$03
3A8E-  8D 01 03    STA  $0301
3A91-  A9 00       LDA  #$00
3A93-  8D 00 03    STA  $0300
3A96-  A9 03       LDA  #$03
3A98-  8D 01 03    STA  $0301
3A9B-  A9 00       LDA  #$00
3A9D-  8D 00 03    STA  $0300
3AA0-  A9 03       LDA  #$03
3AA2-  8D 01 03    STA  $0301
3AA5-  A9 00       LDA  #$00
3AA7-  8D 00 03    STA  $0300
3AAA-  A9 03       LDA  #$03
3AAC-  8D 01 03    STA  $0301
3AAF-  A9 00       LDA  #$00
3AB1-  8D 00 03    STA  $0300
3AB4-  A9 03       LDA  #$03
3AB6-  8D 01 03    STA  $0301
3AB9-  A9 00       LDA  #$00
3ABB-  8D 00 03    STA  $0300
3ABE-  A9 03       LDA  #$03
3AC0-  8D 01 03    STA  $0301
3AC3-  A9 00       LDA  #$00
3AC5-  8D 00 03    STA  $0300
3AC8-  A9 03       LDA  #$03
3ACA-  8D 01 03    STA  $0301
3ACD-  A9 00       LDA  #$00
3ACF-  8D 00 03    STA  $0300
3AD2-  A9 03       LDA  #$03
3AD4-  8D 01 03    STA  $0301
3AD7-  A9 00       LDA  #$00
3AD9-  8D 00 03    STA  $0300
3ADC-  A9 03       LDA  #$03
3ADE-  8D 01 03    STA  $0301
3AE1-  A9 00       LDA  #$00
3AE3-  8D 00 03    STA  $0300
3AE6-  A9 03       LDA  #$03
3AE8-  8D 01 03    STA  $0301
3AEB-  A9 00       LDA  #$00
3AED-  8D 00 03    STA  $0300
3AF0-  A9 03       LDA  #$03
3AF2-  8D 01 03    STA  $0301
3AF5-  A9 00       LDA  #$00
3AF7-  8D 00 03    STA  $0300
3AFA-  A9 03       LDA  #$03
3AFC-  8D 01 03    STA  $0301
3AFF-  A9 00       LDA  #$00
3B01-  8D 00 03    STA  $0300
3B04-  A9 03       LDA  #$03
3B06-  8D 01 03    STA  $0301
3B09-  A9 00       LDA  #$00
3B0B-  8D 00 03    STA  $0300
3B0E-  A9 03       LDA  #$03
3B10-  8D 01 03    STA  $0301
3B13-  A9 00       LDA  #$00
3B15-  8D 00 03    STA  $0300
3B18-  A9 03       LDA  #$03
3B1A-  8D 01 03    STA  $0301
3B1D-  A9 00       LDA  #$00
3B1F-  8D 00 03    STA  $0300
3B22-  A9 03       LDA  #$03
3B24-  8D 01 03    STA  $0301
3B27-  A9 00       LDA  #$00
3B29-  8D 00 03    STA  $0300
3B2C-  A9 03       LDA  #$03
3B2E-  8D 01 03    STA  $0301
3B31-  A9 00       LDA  #$00
3B33-  8D 00 03    STA  $0300
3B36-  A9 03       LDA  #$03
3B38-  8D 01 03    STA  $0301
3B3B-  A9 00       LDA  #$00
3B3D-  8D 00 03    STA  $0300
3B40-  A9 03       LDA  #$03
3B42-  8D 01 03    STA  $0301
3B45-  A9 00       LDA  #$00
3B47-  8D 00 03    STA  $0300
3B4A-  A9 03       LDA  #$03
3B4C-  8D 01 03    STA  $0301
3B4F-  A9 00       LDA  #$00
3B51-  8D 00 03    STA  $0300
3B54-  A9 03       LDA  #$03
3B56-  8D 01 03    STA  $0301
3B59-  A9 00       LDA  #$00
3B5B-  8D 00 03    STA  $0300
3B5E-  A9 03       LDA  #$03
3B60-  8D 01 03    STA  $0301
3B63-  A9 00       LDA  #$00
3B65-  8D 00 03    STA  $0300
3B68-  A9 03       LDA  #$03
3B6A-  8D 01 03    STA  $0301
3B6D-  A9 00       LDA  #$00
3B6F-  8D 00 03    STA  $0300
3B72-  A9 03       LDA  #$03
3B74-  8D 01 03    STA  $0301
3B77-  A9 00       LDA  #$00
3B79-  8D 00 03    STA  $0300
3B7C-  A9 03       LDA  #$03
3B7E-  8D 01 03    STA  $0301
3B81-  A9 00       LDA  #$00
3B83-  8D 00 03    STA  $0300
3B86-  A9 03       LDA  #$03
3B88-  8D 01 03    STA  $0301
3B8B-  A9 00       LDA  #$00
3B8D-  8D 00 03    STA  $0300
3B90-  A9 03       LDA  #$03
3B92-  8D 01 03    STA  $0301
3B95-  A9 00       LDA  #$00
3B97-  8D 00 03    STA  $0300
3B9A-  A9 03       LDA  #$03
3B9C-  8D 01 03    STA  $0301
3B9F-  A9 00       LDA  #$00
3BA1-  8D 00 03    STA  $0300
3BA4-  A9 03       LDA  #$03
3BA6-  8D 01 03    STA  $0301
3BA9-  A9 00       LDA  #$00
3BAB-  8D 00 03    STA  $0300
3BAE-  A9 03       LDA  #$03
3BB0-  8D 01 03    STA  $0301
3BB3-  A9 00       LDA  #$00
3BB5-  8D 00 03    STA  $0300
3BB8-  A9 03       LDA  #$03
3BBA-  8D 01 03    STA  $0301
3BBD-  A9 00       LDA  #$00
3BBF-  8D 00 03    STA  $0300
3BC2-  A9 03       LDA  #$03
3BC4-  8D 01 03    STA  $0301
3BC7-  A9 00       LDA  #$00
3BC9-  8D 00 03    STA  $0300
3BCC-  A9 03       LDA  #$03
3BCE-  8D 01 03    STA  $0301
3BD1-  A9 00       LDA  #$00
3BD3-  8D 00 03    STA  $0300
3BD6-  A9 03       LDA  #$03
3BD8-  8D 01 03    STA  $0301
3BDB-  A9 00       LDA  #$00
3BDD-  8D 00 03    STA  $0300
3BE0-  A9 03       LDA  #$03
3BE2-  8D 01 03    STA  $0301
3BE5-  A9 00       LDA  #$00
3BE7-  8D 00 03    STA  $0300
3BEA-  A9 03       LDA  #$03
3BEC-  8D 01 03    STA  $0301
3BEF-  A9 00       LDA  #$00
3BF1-  8D 00 03    STA  $0300
3BF4-  A9 03       LDA  #$03
3BF6-  8D 01 03    STA  $0301
3BF9-  A9 00       LDA  #$00
3BFB-  8D 00 03    STA  $0300
3BFE-  A9 03       LDA  #$03
3C00-  8D 01 03    STA  $0301
3C03-  A9 00       LDA  #$00
3C05-  8D 00 03    STA  $0300
3C08-  A9 03       LDA  #$03
3C0A-  8D 01 03    STA  $0301
3C0D-  A9 00       LDA  #$00
3C0F-  8D 00 03    STA  $0300
3C12-  A9 03       LDA  #$03
3C14-  8D 01 03    STA  $0301
3C17-  A9 00       LDA  #$00
3C19-  8D 00 03    STA  $0300
3C1C-  A9 03       LDA  #$03
3C1E-  8D 01 03    STA  $0301
3C21-  A9 00       LDA  #$00
3C23-  8D 00 03    STA  $0300
3C26-  A9 03       LDA  #$03
3C28-  8D 01 03    STA  $0301
3C2B-  A9 00       LDA  #$00
3C2D-  8D 00 03    STA  $0300
3C30-  A9 03       LDA  #$03
3C32-  8D 01 03    STA  $0301
3C35-  A9 00       LDA  #$00
3C37-  8D 00 03    STA  $0300
3C3A-  A9 03       LDA  #$03
3C3C-  8D 01 03    STA  $0301
3C3F-  A9 00       LDA  #$00
3C41-  8D 00 03    STA  $0300
3C44-  A9 03       LDA  #$03
3C46-  8D 01 03    STA  $0301
3C49-  A9 00       LDA  #$00
3C4B-  8D 00 03    STA  $0300
3C4E-  A9 03       LDA  #$03
3C50-  8D 01 03    STA  $0301
3C53-  A9 00       LDA  #$00
3C55-  8D 00 03    STA  $0300
3C58-  A9 03       LDA  #$03
3C5A-  8D 01 03    STA  $0301
3C5D-  A9 00       LDA  #$00
3C5F-  8D 00 03    STA  $0300
3C62-  A9 03       LDA  #$03
3C64-  8D 01 03    STA  $0301
3C67-  A9 00       LDA  #$00
3C69-  8D 00 03    STA  $0300
3C6C-  A9 03       LDA  #$03
3C6E-  8D 01 03    STA  $0301
3C71-  A9 00       LDA  #$00
3C73-  8D 00 03    STA  $0300
3C76-  A9 03       LDA  #$03
3C78-  8D 01 03    STA  $0301
3C7B-  A9 00       LDA  #$00
3C7D-  8D 00 03    STA  $0300
3C80-  A9 03       LDA  #$03
3C82-  8D 01 03    STA  $0301
3C85-  A9 00       LDA  #$00
3C87-  8D 00 03    STA  $0300
3C8A-  A9 03       LDA  #$03
3C8C-  8D 01 03    STA  $0301
3C8F-  A9 00       LDA  #$00
3C91-  8D 00 03    STA  $0300
3C94-  A9 03       LDA  #$03
3C96-  8D 01 03    STA  $0301
3C99-  A9 00       LDA  #$00
3C9B-  8D 00 03    STA  $0300
3C9E-  A9 03       LDA  #$03
3CA0-  8D 01 03    STA  $0301
3CA3-  A9 00       LDA  #$00
3CA5-  8D 00 03    STA  $0300
3CA8-  A9 03       LDA  #$03
3CAA-  8D 01 03    STA  $0301
3CAD-  A9 00       LDA  #$00
3CAF-  8D 00 03    STA  $0300
3CB2-  A9 03       LDA  #$03
3CB4-  8D 01 03    STA  $0301
3CB7-  A9 00       LDA  #$00
3CB9-  8D 00 03    STA  $0300
3CBC-  A9 03       LDA  #$03
3CBE-  8D 01 03    STA  $0301
3CC1-  A9 00       LDA  #$00
3CC3-  8D 00 03    STA  $0300
3CC6-  A9 03       LDA  #$03
3CC8-  8D 01 03    STA  $0301
3CCB-  A9 00       LDA  #$00
3CCD-  8D 00 03    STA  $0300
3CD0-  A9 03       LDA  #$03
3CD2-  8D 01 03    STA  $0301
3CD5-  A9 00       LDA  #$00
3CD7-  8D 00 03    STA  $0300
3CDA-  A9 03       LDA  #$03
3CDC-  8D 01 03    STA  $0301
3CDF-  A9 00       LDA  #$00
3CE1-  8D 00 03    STA  $0300
3CE4-  A9 03       LDA  #$03
3CE6-  8D 01 03    STA  $0301
3CE9-  A9 00       LDA  #$00
3CEB-  8D 00 03    STA  $0300
3CEE-  A9 03       LDA  #$03
3CF0-  8D 01 03    STA  $0301
3CF3-  A9 00       LDA  #$00
3CF5-  8D 00 03    STA  $0300
3CF8-  A9 03       LDA  #$03
3CFA-  8D 01 03    STA  $0301
3CFD-  A9 00       LDA  #$00
3CFF-  8D 00 03    STA  $0300
3D02-  A9 03       LDA
```

```
357F-  19 3B 03    ORA   $033B,Y
3582-  91 FA       STA   ($FA),Y
3584-  88          DEY
3585-  10 F6       BPL   $357D
3587-  20 51 3F    JSR   $3F51
358A-  A9 06       LDA   #$06
358C-  8D 47 03    STA   $0347
358F-  60          RTS
3590-  D8          CLD
3591-  A9 10       LDA   #$10
3593-  85 F9       STA   $F9
3595-  A0 00       LDY   #$00
3597-  18          CLC
3598-  A2 08       LDX   #$08
359A-  B1 FC       LDA   ($FC),Y
359C-  0A          ASL
359D-  B0 0A       BCS   $35A9
359F-  C6 F9       DEC   $F9
35A1-  CA          DEX
35A2-  D0 F8       BNE   $359C
35A4-  C8          INY
35A5-  C0 04       CPY   #$04
35A7-  D0 EE       BNE   $3597
35A9-  60          RTS
35AA-  D8          CLD
35AB-  18          CLC
35AC-  0E 08 03    ASL   $0308
35AF-  A9 00       LDA   #$00
35B1-  85 FA       STA   $FA
35B3-  A2 08       LDX   #$08
35B5-  4E 07 03    LSR   $0307
35B8-  90 04       BCC   $35BE
35BA-  18          CLC
35BB-  6D 00 03    ADC   $0300
35BE-  6A          ROR
35BF-  66 FA       ROR   $FA
35C1-  CA          DEX
35C2-  D0 F1       BNE   $35B5
35C4-  85 FB       STA   $FB
35C6-  18          CLC
35C7-  A5 FA       LDA   $FA
35C9-  6D 08 03    ADC   $0308
35CC-  85 FA       STA   $FA
35CE-  A5 FB       LDA   $FB
35D0-  69 00       ADC   #$00
35D2-  85 FB       STA   $FB
35D4-  18          CLC
35D5-  A5 FA       LDA   $FA
35D7-  69 01       ADC   #$01
35D9-  85 FA       STA   $FA
35DB-  A5 FB       LDA   $FB
35DD-  69 60       ADC   #$60
35DF-  85 FB       STA   $FB
35E1-  60          RTS
35E2-  EA          NOP
35E3-  EA          NOP
35E4-  EA          NOP
35E5-  EA          NOP
35E6-  EA          NOP
35E7-  EA          NOP
35E8-  EA          NOP
```

Find site location in memory routine.


```
 18 D8 A2 08 A9
*3BCBLLLLLLLLLLLLLLLLLLLLL
3BCB-  18          CLC
3BCC-  D8          CLD
3BCD-  A2 08       LDX   #$08
3BCF-  A9 62       LDA   #$62
3BD1-  4A          LSR
3BD2-  90 04       BCC   $3BD8
3BD4-  18          CLC
3BD5-  65 09       ADC   $09
3BD7-  6A          ROR
3BD8-  66 06       ROR   $06
3BDA-  CA          DEX
3BDB-  D0 F4       BNE   $3BD1
3BDD-  85 07       STA   $07
3BDF-  18          CLC
3BE0-  A2 08       LDX   #$08
3BE2-  A9 2D       LDA   #$2D
3BE4-  4A          LSR
3BE5-  90 04       BCC   $3BEB
3BE7-  18          CLC
3BE8-  65 08       ADC   $08
3BEA-  6A          ROR
3BEB-  66 1B       ROR   $1B
3BED-  CA          DEX
3BEE-  D0 F4       BNE   $3BE4
3BF0-  85 1C       STA   $1C
3BF2-  18          CLC
3BF3-  A5 06       LDA   $06
3BF5-  65 ED       ADC   $ED
3BF7-  85 06       STA   $06
3BF9-  A5 07       LDA   $07
3BFB-  65 EE       ADC   $EE
3BFD-  85 07       STA   $07
3BFF-  A5 EB       LDA   $EB
3C01-  85 ED       STA   $ED
3C03-  A5 EC       LDA   $EC
3C05-  85 EE       STA   $EE
3C07-  A5 08       LDA   $08
3C09-  85 EB       STA   $EB
3C0B-  A5 09       LDA   $09
3C0D-  85 EC       STA   $EC
3C0F-  A5 06       LDA   $06
3C11-  65 1B       ADC   $1B
3C13-  85 08       STA   $08
3C15-  A5 07       LDA   $07
3C17-  65 1C       ADC   $1C
3C19-  85 09       STA   $09
3C1B-  60          RTS
3C1C-  00          BRK
3C1D-  00          BRK
3C1E-  20 CB 3B    JSR   $3BCB
3C21-  A5 08       LDA   $08
3C23-  4A          LSR
3C24-  38          SEC
3C25-  ED 05 03    SBC   $0305
3C28-  90 12       BCC   $3C3C
3C2A-  A5 EE       LDA   $EE
3C2C-  4A          LSR
```

Random coordinate generating routine.

Random number generating routine.


```
3C2D-  38          SEC
3C2E-  ED 05 03    SBC   $0305
3C31-  90 09       BCC   $3C3C
3C33-  4C 1E 3C    JMP   $3C1E
3C36-  EA          NOP
3C37-  EA          NOP
3C38-  EA          NOP
3C39-  EA          NOP
3C3A-  EA          NOP
3C3B-  EA          NOP
3C3C-  6D 05 03    ADC   $0305
3C3F-  8D 0A 03    STA   $030A
3C42-  A5 09       LDA   $09
3C44-  4A          LSR
3C45-  38          SEC
3C46-  ED 05 03    SBC   $0305
3C49-  90 15       BCC   $3C60
3C4B-  A5 ED       LDA   $ED
3C4D-  4A          LSR
3C4E-  38          SEC
3C4F-  ED 05 03    SBC   $0305
3C52-  90 0C       BCC   $3C60
3C54-  20 CB 3B    JSR   $3BCB
3C57-  4C 42 3C    JMP   $3C42
3C5A-  EA          NOP
3C5B-  EA          NOP
3C5C-  EA          NOP
3C5D-  EA          NOP
3C5E-  EA          NOP
3C5F-  EA          NOP
3C60-  6D 05 03    ADC   $0305
3C63-  8D 0B 03    STA   $030B
3C66-  60          RTS
3C67-  EA          NOP
3C68-  EA          NOP
3C69-  EA          NOP
3C6A-  EA          NOP
3C6B-  EA          NOP
3C6C-  EA          NOP
3C6D-  EA          NOP
3C6E-  EA          NOP
3C6F-  EA          NOP
3C70-  EA          NOP
3C71-  EA          NOP
3C72-  EA          NOP
3C73-  EA          NOP
3C74-  EA          NOP
3C75-  EA          NOP
3C76-  EA          NOP
3C77-  EA          NOP
3C78-  EA          NOP
3C79-  EA          NOP
3C7A-  EA          NOP
3C7B-  AD 14 03    LDA   $0314
3C7E-  69 01       ADC   #$01
3C80-  8D 14 03    STA   $0314
3C83-  90 10       BCC   $3C95
3C85-  AD 15 03    LDA   $0315
3C88-  69 00       ADC   #$00
3C8A-  8D 15 03    STA   $0315
```

```
3C8D-  AD 16 03   LDA  $0316
3C90-  69 00      ADC  #$00
3C92-  8D 16 03   STA  $0316
3C95-  60         RTS
3C96-  18         CLC
3C97-  D8         CLD
3C98-  A0 01      LDY  #$01
3C9A-  A9 01      LDA  #$01
3C9C-  91 FE      STA  ($FE),Y
3C9E-  A9 00      LDA  #$00
3CA0-  88         DEY
3CA1-  91 FE      STA  ($FE),Y
3CA3-  EA         NOP
3CA4-  EA         NOP
3CA5-  EA         NOP
3CA6-  38         SEC
3CA7-  A5 FE      LDA  $FE
3CA9-  E9 02      SBC  #$02
3CAB-  85 FE      STA  $FE
3CAD-  A5 FF      LDA  $FF
3CAF-  E9 00      SBC  #$00
3CB1-  85 FF      STA  $FF
3CB3-  A5 FC      LDA  $FC
3CB5-  E9 02      SBC  #$02
3CB7-  85 FC      STA  $FC
3CB9-  A5 FD      LDA  $FD
3CBB-  E9 00      SBC  #$00
3CBD-  85 FD      STA  $FD
3CBF-  B0 D7      BCS  $3C98
3CC1-  60         RTS
3CC2-  D8         CLD
3CC3-  18         CLC
3CC4-  A9 00      LDA  #$00
3CC6-  85 E3      STA  $E3
3CC8-  A0 02      LDY  #$02
3CCA-  A5 EF      LDA  $EF
3CCC-  6A         ROR
3CCD-  66 E3      ROR  $E3
3CCF-  88         DEY
3CD0-  10 FA      BPL  $3CCC
3CD2-  46 E3      LSR  $E3
3CD4-  46 E3      LSR  $E3
3CD6-  46 E3      LSR  $E3
3CD8-  18         CLC
3CD9-  A9 00      LDA  #$00
3CDB-  85 FE      STA  $FE
3CDD-  85 FF      STA  $FF
3CDF-  A5 EF      LDA  $EF
3CE1-  0A         ASL
3CE2-  0A         ASL
3CE3-  4A         LSR
3CE4-  4A         LSR
3CE5-  4A         LSR
3CE6-  4A         LSR
3CE7-  4A         LSR
3CE8-  18         CLC
3CE9-  6A         ROR
3CEA-  66 FE      ROR  $FE
3CEC-  85 FF      STA  $FF
3CEE-  A5 EF      LDA  $EF
```

Reset array to initial condition routine.

Graphics plotting routine (find screen memory location).


```
3CF0-  4A         LSR
3CF1-  4A         LSR
3CF2-  4A         LSR
3CF3-  4A         LSR
3CF4-  4A         LSR
3CF5-  4A         LSR
3CF6-  18         CLC
3CF7-  6A         ROR
3CF8-  90 0B      BCC  $3D05
3CFA-  6A         ROR
3CFB-  90 04      BCC  $3D01
3CFD-  A9 78      LDA  #$78
3CFF-  10 0D      BPL  $3D0E
3D01-  A9 28      LDA  #$28
3D03-  10 09      BPL  $3D0E
3D05-  6A         ROR
3D06-  90 04      BCC  $3D0C
3D08-  A9 50      LDA  #$50
3D0A-  10 02      BPL  $3D0E
3D0C-  A9 00      LDA  #$00
3D0E-  18         CLC
3D0F-  65 FE      ADC  $FE
3D11-  85 FE      STA  $FE
3D13-  A5 FF      LDA  $FF
3D15-  65 E3      ADC  $E3
3D17-  69 40      ADC  #$40
3D19-  85 FF      STA  $FF
3D1B-  18         CLC
3D1C-  A2 08      LDX  #$08
3D1E-  A5 CF      LDA  $CF
3D20-  06 CE      ASL  $CE
3D22-  2A         ROL
3D23-  C9 07      CMP  #$07
3D25-  90 04      BCC  $3D2B
3D27-  E9 07      SBC  #$07
3D29-  E6 CE      INC  $CE
3D2B-  CA         DEX
3D2C-  D0 F2      BNE  $3D20
3D2E-  A8         TAY
3D2F-  A9 00      LDA  #$00
3D31-  38         SEC
3D32-  2A         ROL
3D33-  88         DEY
3D34-  30 03      BMI  $3D39
3D36-  0A         ASL
3D37-  10 FA      BPL  $3D33
3D39-  85 EF      STA  $EF
3D3B-  A5 CE      LDA  $CE
3D3D-  18         CLC
3D3E-  65 FE      ADC  $FE
3D40-  85 FE      STA  $FE
3D42-  A5 FF      LDA  $FF
3D44-  69 00      ADC  #$00
3D46-  85 FF      STA  $FF
3D48-  A0 00      LDY  #$00
3D4A-  B1 FE      LDA  ($FE),Y
3D4C-  05 EF      ORA  $EF
3D4E-  91 FE      STA  ($FE),Y
3D50-  60         RTS
3D51-  EA         NOP
```



```
3D52-  EA         NOP
3D53-  EA         NOP
3D54-  EA         NOP
3D55-  EA         NOP
3D56-  EA         NOP
3D57-  EA         NOP
3D58-  EA         NOP
3D59-  EA         NOP
3D5A-  EA         NOP
3D5B-  EA         NOP
3D5C-  EA         NOP
3D5D-  EA         NOP
3D5E-  EA         NOP
3D5F-  EA         NOP
3D60-  18         CLC
3D61-  D8         CLD
3D62-  38         SEC
3D63-  A5 1E      LDA  $1E
3D65-  E9 01      SBC  #$01
3D67-  85 1E      STA  $1E
3D69-  B0 0F      BCS  $3D7A
3D6B-  AD 06 03   LDA  $0306
3D6E-  85 1E      STA  $1E
3D70-  38         SEC
3D71-  A5 1F      LDA  $1F
3D73-  E9 01      SBC  #$01
3D75-  B0 01      BCS  $3D78
3D77-  60         RTS
3D78-  85 1F      STA  $1F
3D7A-  A5 1F      LDA  $1F
3D7C-  0A         ASL
3D7D-  EA         NOP
3D7E-  18         CLC
3D7F-  69 02      ADC  #$02
3D81-  85 EF      STA  $EF
3D83-  18         CLC
3D84-  A5 1E      LDA  $1E
3D86-  0A         ASL
3D87-  EA         NOP
3D88-  6D E2 03   ADC  $03E2
3D8B-  85 CE      STA  $CE
3D8D-  A9 00      LDA  #$00
3D8F-  69 00      ADC  #$00
3D91-  85 CF      STA  $CF
3D93-  A5 1F      LDA  $1F
3D95-  6A         ROR
3D96-  B0 0C      BCS  $3DA4
3D98-  A5 CE      LDA  $CE
3D9A-  69 01      ADC  #$01
3D9C-  85 CE      STA  $CE
3D9E-  A5 CF      LDA  $CF
3DA0-  69 00      ADC  #$00
3DA2-  85 CF      STA  $CF
3DA4-  38         SEC
3DA5-  A5 FC      LDA  $FC
3DA7-  E9 02      SBC  #$02
3DA9-  85 FC      STA  $FC
3DAB-  A5 FD      LDA  $FD
3DAD-  E9 00      SBC  #$00
3DAF-  85 FD      STA  $FD
```

Graphics plotting routine.

```
3DB1-  18        CLC
3DB2-  A0 01     LDY   #$01
3DB4-  B1 FC     LDA   ($FC),Y
3DB6-  31 FA     AND   ($FA),Y
3DB8-  D0 06     BNE   $3DC0
3DBA-  88        DEY
3DBB-  10 F7     BPL   $3DB4
3DBD-  4C 62 3D  JMP   $3D62
3DC0-  20 C6 3D  JSR   $3DC6
3DC3-  4C 62 3D  JMP   $3D62
3DC6-  A5 CE     LDA   $CE
3DC8-  85 19     STA   $19
3DCA-  A5 CF     LDA   $CF
3DCC-  85 1A     STA   $1A     Plot point.
3DCE-  A5 EF     LDA   $EF
3DD0-  85 1D     STA   $1D
3DD2-  20 C2 3C  JSR   $3CC2
3DD5-  60        RTS
3DD6-  A5 19     LDA   $19
3DD8-  E9 01     SBC   #$01
3DDA-  85 CE     STA   $CE
3DDC-  A5 1A     LDA   $1A
3DDE-  E9 00     SBC   #$00
3DE0-  85 CF     STA   $CF     Plot point.
3DE2-  E6 1D     INC   $1D
3DE4-  A5 1D     LDA   $1D
3DE6-  85 EF     STA   $EF
3DE8-  20 C2 3C  JSR   $3CC2
3DEB-  18        CLC
3DEC-  A5 19     LDA   $19
3DEE-  69 01     ADC   #$01
3DF0-  85 CE     STA   $CE
3DF2-  A5 1A     LDA   $1A
3DF4-  69 00     ADC   #$00    Plot point.
3DF6-  85 CF     STA   $CF
3DF8-  A5 1D     LDA   $1D
3DFA-  85 EF     STA   $EF
3DFC-  20 C2 3C  JSR   $3CC2
3DFF-  38        SEC
3E00-  A5 19     LDA   $19
3E02-  E9 02     SBC   #$02
3E04-  85 CE     STA   $CE
3E06-  A5 1A     LDA   $1A
3E08-  E9 00     SBC   #$00    Plot point.
3E0A-  85 CF     STA   $CF
3E0C-  E6 1D     INC   $1D
3E0E-  A5 1D     LDA   $1D
3E10-  85 EF     STA   $EF
3E12-  20 C2 3C  JSR   $3CC2
3E15-  18        CLC
3E16-  A5 19     LDA   $19
3E18-  69 02     ADC   #$02
3E1A-  85 CE     STA   $CE
3E1C-  A5 1A     LDA   $1A
3E1E-  69 00     ADC   #$00    Plot point.
3E20-  85 CF     STA   $CF
3E22-  A5 1D     LDA   $1D
3E24-  85 EF     STA   $EF
3E26-  20 C2 3C  JSR   $3CC2
3E29-  38        SEC
```

Plot point.

* or CLC in plotting mode.


```
3E2A-  A5 19     LDA   $19
3E2C-  E9 02     SBC   #$02
3E2E-  85 CE     STA   $CE
3E30-  A5 1A     LDA   $1A
3E32-  E9 00     SBC   #$00
3E34-  85 CF     STA   $CF
3E36-  E6 1D     INC   $1D
3E38-  A5 1D     LDA   $1D
3E3A-  85 EF     STA   $EF
3E3C-  20 C2 3C  JSR   $3CC2
3E3F-  18        CLC
3E40-  A5 19     LDA   $19
3E42-  69 02     ADC   #$02
3E44-  85 CE     STA   $CE
3E46-  A5 1A     LDA   $1A
3E48-  69 00     ADC   #$00
3E4A-  85 CF     STA   $CF
3E4C-  A5 1D     LDA   $1D
3E4E-  85 EF     STA   $EF
3E50-  20 C2 3C  JSR   $3CC2
3E53-  A5 19     LDA   $19
3E55-  85 CE     STA   $CE
3E57-  A5 1A     LDA   $1A
3E59-  85 CF     STA   $CF
3E5B-  A5 1D     LDA   $1D
3E5D-  85 EF     STA   $EF
3E5F-  20 C2 3C  JSR   $3CC2
3E62-  38        SEC
3E63-  A5 19     LDA   $19
3E65-  E9 02     SBC   #$02
3E67-  85 CE     STA   $CE
3E69-  A5 1A     LDA   $1A
3E6B-  E9 00     SBC   #$00
3E6D-  85 CF     STA   $CF
3E6F-  E6 1D     INC   $1D
3E71-  A5 1D     LDA   $1D
3E73-  85 EF     STA   $EF
3E75-  20 C2 3C  JSR   $3CC2
3E78-  18        CLC
3E79-  A5 19     LDA   $19
3E7B-  69 02     ADC   #$02
3E7D-  85 CE     STA   $CE
3E7F-  A5 1A     LDA   $1A
3E81-  69 00     ADC   #$00
3E83-  85 CF     STA   $CF
3E85-  A5 1D     LDA   $1D
3E87-  85 EF     STA   $EF
3E89-  20 C2 3C  JSR   $3CC2
3E8C-  38        SEC
3E8D-  A5 19     LDA   $19
3E8F-  E9 01     SBC   #$01
3E91-  85 CE     STA   $CE
3E93-  A5 1A     LDA   $1A
3E95-  E9 00     SBC   #$00
3E97-  85 CF     STA   $CF
3E99-  E6 1D     INC   $1D
3E9B-  A5 1D     LDA   $1D
```



```
3E9D-  85 EF     STA   $EF
3E9F-  20 C2 3C  JSR   $3CC2
3EA2-  18        CLC
3EA3-  A5 19     LDA   $19
3EA5-  69 01     ADC   #$01
3EA7-  85 CE     STA   $CE
3EA9-  A5 1A     LDA   $1A
3EAB-  69 00     ADC   #$00
3EAD-  85 CF     STA   $CF
3EAF-  A5 1D     LDA   $1D
3EB1-  85 EF     STA   $EF
3EB3-  20 C2 3C  JSR   $3CC2
3EB6-  A5 19     LDA   $19
3EB8-  85 CE     STA   $CE
3EBA-  A5 1A     LDA   $1A
3EBC-  85 CF     STA   $CF
3EBE-  E6 1D     INC   $1D
3EC0-  A5 1D     LDA   $1D
3EC2-  85 EF     STA   $EF
3EC4-  20 C2 3C  JSR   $3CC2
3EC7-  60        RTS
3EC8-  EA        NOP
3EC9-  EA        NOP
3ECA-  EA        NOP
3ECB-  EA        NOP
3ECC-  EA        NOP
3ECD-  EA        NOP
3ECE-  EA        NOP
3ECF-  EA        NOP
3ED0-  EA        NOP
3ED1-  18        CLC
3ED2-  A9 00     LDA   #$00
3ED4-  8D E0 03  STA   $03E0
3ED7-  8D E1 03  STA   $03E1
3EDA-  A0 01     LDY   #$01
3EDC-  B1 FE     LDA   ($FE),Y
3EDE-  31 FA     AND   ($FA),Y
3EE0-  D0 14     BNE   $3EF6
3EE2-  88        DEY
3EE3-  10 F7     BPL   $3EDC
3EE5-  18        CLC
3EE6-  AD E0 03  LDA   $03E0
3EE9-  69 01     ADC   #$01
3EEB-  8D E0 03  STA   $03E0
3EEE-  AD E1 03  LDA   $03E1
3EF1-  69 00     ADC   #$00
3EF3-  8D E1 03  STA   $03E1
3EF6-  38        SEC
3EF7-  A5 FE     LDA   $FE
3EF9-  E9 02     SBC   #$02
3EFB-  85 FE     STA   $FE
3EFD-  A5 FF     LDA   $FF
3EFF-  E9 00     SBC   #$00
3F01-  85 FF     STA   $FF
3F03-  A5 FC     LDA   $FC
3F05-  E9 02     SBC   #$02
3F07-  85 FC     STA   $FC
3F09-  A5 FD     LDA   $FD
3F0B-  E9 00     SBC   #$00
3F0D-  85 FD     STA   $FD
```

Sheets 28-33 Replacment sections for linear difusion program.

```
2E17-  20 1E 3C   JSR  $3C1E
2E1A-  A0 02      LDY  #$02
2E1C-  38         SEC
2E1D-  B9 00 3A   LDA  $3A00,Y
2E20-  E5 EC      SBC  $EC
2E22-  90 17      BCC  $2E3B
2E24-  B9 FF 39   LDA  $39FF,Y
2E27-  E5 EB      SBC  $EB
2E29-  90 10      BCC  $2E3B
2E2B-  18         CLC
2E2C-  98         TYA
2E2D-  4A         LSR
2E2E-  18         CLC
2E2F-  6D 09 03   ADC  $0309
2E32-  38         SEC
2E33-  E9 01      SBC  #$01
2E35-  8D 0C 03   STA  $030C
2E38-  4C 4E 2E   JMP  $2E4E
2E3B-  C8         INY
2E3C-  C8         INY
2E3D-  C4 E3      CPY  $E3
2E3F-  D0 DB      BNE  $2E1C
2E41-  4C 4E 2E   JMP  $2E4E
2E44-  00         BRK
2E45-  00         BRK
2E46-  00         BRK
2E47-  00         BRK
2E48-  00         BRK
2E49-  00         BRK
2E4A-  00         BRK
2E4B-  00         BRK
2E4C-  00         BRK
2E4D-  00         BRK
2E4E-  18         CLC
2E4F-  AD 0A 03   LDA  $030A
2E52-  8D 07 03   STA  $0307
2E55-  AD 0B 03   LDA  $030B
2E58-  8D 08 03   STA  $0308
2E5B-  20 AA 35   JSR  $35AA
2E5E-  A0 01      LDY  #$01
2E60-  B1 FA      LDA  ($FA),Y
2E62-  99 17 03   STA  $0317,Y
2E65-  88         DEY
2E66-  10 FB      BPL  $2E60
2E68-  AD 0C 03   LDA  $030C
2E6B-  0A         ASL
2E6C-  0A         ASL
2E6D-  69 47      ADC  #$47
2E6F-  85 FA      STA  $FA
2E71-  A9 00      LDA  #$00
2E73-  69 03      ADC  #$03
2E75-  85 FB      STA  $FB
2E77-  18         CLC
2E78-  A0 01      LDY  #$01
2E7A-  B1 FA      LDA  ($FA),Y
2E7C-  99 3B 03   STA  $033B,Y
2E7F-  88         DEY
```



```
2E80-  10 F8      BPL  $2E7A
2E82-  A0 01      LDY  #$01
2E84-  B9 17 03   LDA  $0317,Y

2E17-  20 1E 3C   JSR  $3C1E
2E1A-  A0 02      LDY  #$02
2E1C-  38         SEC
2E1D-  B9 00 3A   LDA  $3A00,Y
2E20-  E5 EC      SBC  $EC
2E22-  90 17      BCC  $2E3B
2E24-  B9 FF 39   LDA  $39FF,Y
2E27-  E5 EB      SBC  $EB
2E29-  90 10      BCC  $2E3B
2E2B-  18         CLC
2E2C-  98         TYA
2E2D-  4A         LSR
2E2E-  18         CLC
2E2F-  6D 09 03   ADC  $0309
2E32-  38         SEC
2E33-  E9 01      SBC  #$01
2E35-  8D 0C 03   STA  $030C
2E38-  4C 4E 2E   JMP  $2E4E
2E3B-  C8         INY
2E3C-  C8         INY
```



```
3C1E-  20 CB 3B   JSR  $3BCB
3C21-  A5 08      LDA  $08
3C23-  18         CLC
3C24-  6A         ROR
3C25-  CD 05 03   CMP  $0305
3C28-  30 12      BMI  $3C3C
3C2A-  A5 ED      LDA  $ED
3C2C-  18         CLC
3C2D-  6A         ROR
3C2E-  CD 05 03   CMP  $0305
3C31-  30 0C      BMI  $3C3F
3C33-  A5 EB      LDA  $EB
3C35-  18         CLC
3C36-  6A         ROR
3C37-  CD 05 03   CMP  $0305
3C3A-  30 03      BMI  $3C3F
3C3C-  4C 1E 3C   JMP  $3C1E
3C3F-  CD E3 03   CMP  $03E3
3C42-  30 05      BMI  $3C49
3C44-  ED E3 03   SBC  $03E3
3C47-  10 F6      BPL  $3C3F
3C49-  8D 0A 03   STA  $030A
3C4C-  A5 09      LDA  $09
3C4E-  18         CLC
3C4F-  6A         ROR
3C50-  CD 05 03   CMP  $0305
3C53-  30 18      BMI  $3C6D
3C55-  A5 EC      LDA  $EC
3C57-  18         CLC
3C58-  6A         ROR
3C59-  CD 05 03   CMP  $0305
3C5C-  30 0F      BMI  $3C6D
3C5E-  A5 EE      LDA  $EE
3C60-  18         CLC
3C61-  6A         ROR
3C62-  CD 05 03   CMP  $0305
3C65-  30 06      BMI  $3C6D
3C67-  20 CB 3B   JSR  $3BCB
3C6A-  4C 4C 3C   JMP  $3C4C
3C6D-  CD E3 03   CMP  $03E3
3C70-  30 05      BMI  $3C77
3C72-  ED E3 03   SBC  $03E3
3C75-  10 F6      BPL  $3C6D
3C77-  8D 0B 03   STA  $030B
3C7A-  60         RTS
3C7B-  AD 14 03   LDA  $0314
3C7E-  69 01      ADC  #$01
3C80-  8D 14 03   STA  $0314
3C83-  90 10      BCC  $3C95
3C85-  AD 15 03   LDA  $0315
3C88-  69 00      ADC  #$00
3C8A-  8D 15 03   STA  $0315
3C8D-  AD 16 03   LDA  $0316
3C90-  69 00      ADC  #$00
3C92-  8D 16 03   STA  $0316
3C95-  60         RTS
3C96-  18         CLC
3C97-  D8         CLD
```

```
3CF5- 4A      LSR
3CF4- 4A      LSR
3CF3- 4A      LSR
3CF2- 4A      LSR
3CF1- 4A      LSR
3CF0- 4A      LSR
3CEE- A5 EF   LDA  $EF
3CEC- 85 FF   STA  $FF
3CEA- 66 FE   ROR  $FE
3CE9- 6A      ROR
3CE8- 18      CLC
3CE7- 4A      LSR
3CE6- 4A      LSR
3CE5- 4A      LSR
3CE4- 4A      LSR
3CE3- 4A      LSR
3CE2- 0A      ASL
3CE1- 0A      ASL
3CDF- A5 EF   LDA  $EF
3CDD- 85 FF   STA  $FF
3CDB- 85 FE   STA  $FE
3CD9- A9 00   LDA  #$00
3CD8- 18      CLC
3CD6- 46 1D   LSR  $1D
3CD4- 46 1D   LSR  $1D
3CD2- 46 1D   LSR  $1D
3CD0- 10 FA   BPL  $3CCC
3CCF- 88      DEY
3CCD- 66 1D   ROR  $1D
3CCC- 6A      ROR
3CCA- A5 EF   LDA  $EF
3CC8- A0 02   LDY  #$02
3CC6- 85 1D   STA  $1D
3CC4- A9 00   LDA  #$00
3CC3- 18      CLC
3CC2- D8      CLD
3CC1- 60      RTS
3CBF- B0 D7   BCS  $3C98
3CBD- 85 FD   STA  #FD
3CBB- E9 00   SBC  #$00
3CB9- A5 FD   LDA  $FD
3CB7- 85 FC   STA  $FC
3CB5- E9 02   SBC  #$02
3CB3- A5 FC   LDA  $FC
3CB1- 85 FF   STA  $FF
3CAF- E9 00   SBC  #$00
3CAD- A5 FF   LDA  $FF
3CAB- 85 FE   STA  $FE
3CA9- E9 02   SBC  #$02
3CA7- A5 FE   LDA  $FE
3CA6- 38      SEC
3CA5- EA      NOP
3CA4- EA      NOP
3CA3- EA      NOP
3CA1- 91 FE   STA  ($FE),Y
3CA0- 88      DEY
3C9E- A9 00   LDA  #$00
3C9C- 91 FE   STA  ($FE),Y
3C9A- A9 01   LDA  #$01
3C98- A0 01   LDY  #$01
```

31

```
3CF6- 18      CLC
3CF7- 6A      ROR
3CF8- 90 0B   BCC  $3D05
3CFA- 6A      ROR
3CFB- 90 04   BCC  $3D01
3CFD- A9 78   LDA  #$78
3CFF- 10 0D   BPL  $3D0E
3D01- A9 28   LDA  #$28
3D03- 10 09   BPL  $3D0E
3D05- 6A      ROR
3D06- 90 04   BCC  $3D0C
3D08- A9 50   LDA  #$50
3D0A- 10 02   BPL  $3D0E
3D0C- A9 00   LDA  #$00
3D0E- 18      CLC
3D0F- 65 FE   ADC  $FE
3D11- 85 FE   STA  $FE
3D13- A5 FF   LDA  $FF
3D15- 65 1D   ADC  $1D
3D17- 69 40   ADC  #$40
3D19- 85 FF   STA  $FF
3D1B- 18      CLC
3D1C- A2 08   LDX  #$08
3D1E- A5 CF   LDA  $CF
3D20- 06 CE   ASL  $CE
3D22- 2A      ROL
3D23- C9 07   CMP  #$07
3D25- 90 04   BCC  $3D2B
3D27- E9 07   SBC  #$07
3D29- E6 CE   INC  $CE
3D2B- CA      DEX
3D2C- D0 F2   BNE  $3D20
3D2E- A8      TAY
3D2F- A9 00   LDA  #$00
3D31- 38      SEC
3D32- 2A      ROL
3D33- 88      DEY
3D34- 30 03   BMI  $3D39
3D36- 0A      ASL
3D37- 10 FA   BPL  $3D33
3D39- 85 EF   STA  $EF
3D3B- A5 CE   LDA  $CE
3D3D- 18      CLC
3D3E- 65 FE   ADC  $FE
3D40- 85 FE   STA  $FE
3D42- A5 FF   LDA  $FF
3D44- 69 00   ADC  #$00
3D46- 85 FF   STA  $FF
3D48- A0 00   LDY  #$00
3D4A- B1 FE   LDA  ($FE),Y
3D4C- 05 EF   ORA  $EF
3D4E- 91 FE   STA  ($FE),Y
3D50- 60      RTS
3D51- EA      NOP
3D52- EA      NOP
3D53- EA      NOP
3D54- EA      NOP
3D55- EA      NOP
3D56- EA      NOP
3D57- EA      NOP
```

32

```
3D58- EA      NOP
3D59- EA      NOP
3D5A- EA      NOP
3D5B- EA      NOP
3D5C- EA      NOP
3D5D- EA      NOP
3D5E- EA      NOP
3D5F- EA      NOP
3D60- 18      CLC
3D61- D8      CLD
3D62- 38      SEC
3D63- A5 1E   LDA  $1E
3D65- E9 01   SBC  #$01
3D67- 85 1E   STA  $1E
3D69- B0 0F   BCS  $3D7A
3D6B- AD 06 03 LDA  $0306
3D6E- 85 1E   STA  $1E
3D70- 38      SEC
3D71- A5 1F   LDA  $1F
3D73- E9 01   SBC  #$01
3D75- B0 01   BCS  $3D78
3D77- 60      RTS
3D78- 85 1F   STA  $1F
3D7A- A5 1F   LDA  $1F
3D7C- 0A      ASL
3D7D- EA      NOP
3D7E- 18      CLC
3D7F- 69 02   ADC  #$02
3D81- 85 EF   STA  $EF
3D83- 18      CLC
3D84- A5 1E   LDA  $1E
3D86- 0A      ASL
3D87- EA      NOP
3D88- 6D E2 03 ADC  $03E2
3D8B- 85 CE   STA  $CE
3D8D- A9 00   LDA  #$00
3D8F- 69 00   ADC  #$00
3D91- 85 CF   STA  $CF
3D93- A5 1F   LDA  $1F
3D95- 6A      ROR
3D96- B0 0C   BCS  $3DA4
3D98- A5 CE   LDA  $CE
3D9A- 69 01   ADC  #$01
3D9C- 85 CE   STA  $CE
3D9E- A5 CF   LDA  $CF
3DA0- 69 00   ADC  #$00
3DA2- 85 CF   STA  $CF
3DA4- 38      SEC
3DA5- A5 FC   LDA  $FC
3DA7- E9 02   SBC  #$02
3DA9- 85 FC   STA  $FC
3DAB- A5 FD   LDA  $FD
3DAD- E9 00   SBC  #$00
3DAF- 85 FD   STA  $FD
3DB1- 18      CLC
3DB2- A0 01   LDY  #$01
3DB4- B1 FC   LDA  ($FC),Y
3DB6- 31 FA   AND  ($FA),Y
3DB8- D0 06   BNE  $3DC0
3DBA- 88      DEY
```

33

BASIC Section

```
]LIST

0  HIMEM: 11365
2  ONERR  GOTO 578
4  GOTO 616
5  FOR Z = 1 TO EE
6  FOR T = 1 TO H1
7  POKE 839,1
8  FOR S = I9 TO E8
9  CALL 11747
10  ON  PEEK (839) GOTO 15,20,25,30,35,40
15  PRINT
20  PRINT
25  POKE 840, RND (W) * 6: CALL 12873
27  GOTO 10
30  POKE 840, INT ( RND (W) * 6) * 28: CALL 13228
33  GOTO 10
35  IF I5 <  > I6 THEN  GOSUB 462
36  GOTO 100
40 S = S + 2: CALL 12806
45  GOTO 10
100  NEXT
102  GOTO 144
144 I9 = 1
146 H4 =  PEEK (777):M7 = 839 + 4 * H4
147  POKE 250,M7 -  INT (M7 / 256) * 256: POKE 251, INT (M7 / 256)
148 I = 2 * G3 * G3: POKE 252,I -  INT (I / 256) * 256: POKE 253, INT (I /
    256)
150 I = I + 24577: POKE 254,I -  INT (I / 256) * 256: POKE 255, INT (I /
    256)
152  CALL 16081
154 H6 =  PEEK (992) +  PEEK (993) * 256
160  IF E9 = 0 THEN 164
162  PRINT B4$;H6
164  IF H6 = H7 THEN  POKE 777,H4 + 1
165  IF H6 <  > H7 THEN 168
166 H7 = 0
168 H7 = H6:H6 = 0
170 M(T) =  PEEK (788) + 256 *  PEEK (789) + 65536 *  PEEK (790) + M(T)
172  NEXT T
173  IF Z <  > EE THEN  GOSUB 1000
174  NEXT Z
175  TEXT
176  GET QQ$
178  PRINT "ARE YOU READY FOR THE OUTPUT -          MAKE SURE THE EPSOM P
    RINTER IS ON";: INPUT QQ$
180  IF QQ$ = "Y" THEN 188
182  GOTO 178
184  IF W$ = "N" THEN 760
186  GOTO 268
188  PRINT B5$;: INPUT Z$
190  PRINT D$;"OPEN";Z$
192  PRINT D$;"WRITE";Z$
194  PRINT P(3);D1$;P(4);D1$;P(5);D1$;P(6);D1$;P(7);D1$;P(8);D1$;P(9)
196 T = (T - 2) * E8 + S - 1 + SUM
197  PRINT T;D1$;G1 + 1;D1$;G;D1$;H4
198  FOR I = 1 TO H1
199  PRINT D1$,E8 / (M(I) - M(I - 1))
200  NEXT
```



```
201  PRINT D$;"CLOSE"
202 Z$ = "B" + Z$
204 M7 = G3 * G3 * 2
206  PRINT D$;"BSAVE";Z$;",A$6001,L";M7
207 Z$ = "B" + Z$
208  PRINT D$;"BSAVE";Z$;",A$300,                L256"
212  GOTO 240
214  PRINT B6$;: INPUT Z$
216  PRINT D$;"OPEN";Z$
218  PRINT D$;"READ";Z$
220  INPUT P(3),P(4),P(5),P(6),P(7),P(8),P(9),SUM,G3,G,H4
222 G1 = G3 - 1
224  PRINT D$;"CLOSE"
226 Z$ = "B" + Z$
228  PRINT D$;"BLOAD";Z$;",A$6001"
229 Z$ = "B" + Z$
230  PRINT D$;"BLOAD";Z$;",A300"
238  GOTO 708
242  FOR I5 = 1 TO  PEEK (786) - 1
244  HGR2
246  HPLOT X4 - 2,0 TO (281 - X4),0 TO (281 - X4),(4 + 2 * G1) TO X4 - 2,
    (4 + 2 * G1) TO X4 - 2,0
248 T8 = 7
250  GOTO 473
252  PR# 1: POKE 1657,80
254  PRINT "PRINTOUT OF LAYER ";I5;" FILE ";Z$
256  POKE 1913,66: PRINT  CHR$ (17); CHR$ (12)
258  POKE 53247,0
260  PR# 0
262  NEXT I5
264  TEXT
266  GOTO 272
268  PRINT B7$;: INPUT S$
270  IF S$ <  > "Y" THEN 342
272  PR# 1: POKE 1657,72: PRINT  CHR$ (15): PRINT  CHR$ (27); CHR$ (65); CH
    (6): POKE 255,57
274  PRINT B8$;" FILE ";Z$
275 ZZ = 0:C3 = 0
276  PRINT "((P1 ";P(1);" P2 ";P(2);" P3 ";P(3);" P4 ";P(4);" P5 ";P(5);"
    P6 ";P(6);" P7 ";P(7);" P8 ";P(8);" P9 ";P(9);"))"
277  PRINT : PRINT  CHR$ (27); CHR$ (76); CHR$ (06); CHR$ (0);: POKE 254,
    00: CALL 14688
278  FOR I = 24577 TO 24573 + G3 * G3 * 2 STEP 2
280  POKE 252,I -  INT (I / 256) * 256: POKE 253, INT (I / 256)
282  CALL 13712
284 K2 =  PEEK (249) - H4 + 1
286 C2 = C2 + 1: POKE 254,K2 * 12:C3 = C3 + 1
287  IF ZZ = 0 THEN 291
288  PRINT  CHR$ (27); CHR$ (76); CHR$ (12); CHR$ (0);
289  GOTO 299
291  IF (C3 - 1) / 8 <  >  INT ((C3 - 1) / 8) THEN 299
292  IF C3 + 7 > G3 THEN 296
293  PRINT  CHR$ (27); CHR$ (76); CHR$ (96); CHR$ (0);
294  GOTO 299
296 ZZ = 1: PRINT  CHR$ (27); CHR$ (76); CHR$ (12); CHR$ (0);
299  CALL 14688
301  IF C2 / G3 =  INT (C2 / G3) THEN 306
302  NEXT I
303  PRINT : PRINT : PRINT  CHR$ (18): POKE 1657,80: PRINT : PRINT "HEIGH
    T CODE :- ": PRINT  CHR$ (27); CHR$ (65); CHR$ (10)
```

```
304  FOR J = 0 TO 7: PRINT "  ";H4 + J;"  ";: POKE 254,12 * J: PRINT  CHR$
     (27); CHR$ (76); CHR$ (12); CHR$ (0);: CALL 14688
305 :50
306  IF C2 = 2 * G3 THEN 308
307  PRINT : GOTO 311
308  PRINT : PRINT  CHR$ (27); CHR$ (76); CHR$ (06); CHR$ (0);: POKE 254,
     12: CALL 14688
311 ZZ = 0:C3 = 0: IF C2 = 2 * G3 THEN C2 = 0
312  GOTO 302
314  PRINT  CHR$ (12)
316  PR# 0
318  GOTO 322
320  PRINT B9$,E8,C1$;: INPUT F$
322  PR# 1: POKE 1657,80
324  PRINT C2$
326  FOR I = 1 TO H1
328  IF M(I) = 0 THEN 334
330 T3 = E8 * (Z - 1) / (M(I) - M(I - 1))
332  PRINT  TAB( 15);E8 * I; TAB( 16);M(I) / (Z - 1); TAB( 13);T3
334  NEXT I
335  PRINT "AVERAGE OF ";Z - 1;" RUNS"
436  PR# 0
438  PRINT C3$;: INPUT F$
440  IF F$ = "Y" THEN 176
442  END
462  HGR2
464  HPLOT X4 - 2,0 TO (281 - X4),0 TO (281 - X4),(4 + 2 * G1) TO X4 - 2,
     (4 + 2 * G1) TO X4 - 2,0
468  IF T7 <  > 1 THEN  GOSUB 566
472 T7 = 1 + T7
473 M7 = 843 + 4 * I5: POKE 250,M7 -  INT (M7 / 256) * 256: POKE 251, INT
    (M7 / 256)
476  POKE 30,G3: POKE 994,X4
478 M7 = 24579 + G3 * G1 * 2 + 2 * G1
479  POKE 252,M7 -  INT (M7 / 256) * 256: POKE 253, INT (M7 / 256)
480  POKE 31,G1
484  CALL 15712
502  IF T8 = 7 THEN 252
503  POKE 976,I5 + 1:I6 = I5
504  RETURN
566  IF  PEEK (13960) = 140 AND  PEEK (13961) = 3 THEN 575
568  PRINT D$"BLOADSEPT21,A$2C65"
570  POKE 233,54: POKE 232,8
572 XC = 3:YC = 159
574  SCALE= 1: ROT= 0
575  POKE 233,54: POKE 232,8
576  RETURN
578 ERO =  PEEK (222)
582  IF ERO = 255 THEN 604
584  INVERSE
586  PRINT "                                                              "

588  NORMAL
590  PRINT "          ";
592  FLASH
594  PRINT "ERROR NO ";ERO;" HAS OCCURED "
596  NORMAL
598  INVERSE
600  PRINT "                                                              "
```



```
602  NORMAL
604  TEXT
605  PRINT "NO ATOMS; ";S + T * E8 - E8 + SUM;"   NO TRIALS; "; PEEK (788
     ) +  PEEK (789) * 256 +  PEEK (790) * 256 * 256
606  IF ERO = 255 THEN  PRINT "TYPE CONT TO CONTINUE": STOP : RESUME
608  IF ERO > 15 THEN  STOP : RESUME
610  PRINT "PRESS RETURN TO CONTINUE";: INPUT RR$
614  GOTO 188
616 A1$ = "THIS PROGRAM DOES NOT CONTAIN A DIFFUS- ION ELEMENT"
618 A2$ = "IS THE INITIAL LATTICE TO BE READ FROM   DISC "
620 A3$ = "WHAT SIZE LATTICE X BY X ,BY 16 UP "
622 A4$ = "THIS REQUIRES A SHORT THINK"
624 A5$ = "DO YOU WANT THE LATTICE PRINTED OUT (1) OR DO    YOU WISH TO C
    ONTINUE DEPOSITION (2) "
626 A6$ = "PLEASE GIVE THE PROBABILITYS FOR AN ATOM STICKING WITH 1,2,3,4
    ,5,6,7,8,9 ADJAC-ENT OCCUPIED SITES (IN THAT ORDER)"
628 A7$ = "THE VALUES PREVIOUSLY USED WERE "
630 A8$ = "THE PROBABILITYS CHOSEN ARE"
632 A9$ = "IS THIS CORRECT "
634 B1$ = "HOW MANY ATOMS DO YOU WISH TO BE DEPOSITED"
636 B2$ = "AND HOW OFTEN DO YOU WISH THE NUMBER OF   TRIALS RECORDED - NO
     MORE THAN 50 RESULTS "
638 B3$ = "DO YOU WISH TO START WITH AN INITIAL NUCL-  EUS OF THREE ATOMS
    "
640 B4$ = "NO OF FREE SITES = "
642 B5$ = "PLEASE GIVE A SUITABLE NAME FOR THE FILE"
644 B6$ = "PLEASE GIVE FILENAME "
646 B7$ = "DO YOU WISH THE HEIGHT MAP PRINTED ON THE EPSOM "
648 B8$ = "THIS A HEIGHT MAP OF THE SIMULATED DEPOSIT"
650 B9$ = "THE NUMBER OF TRIALS PER  "
652 C1$ = " ATOMS CAN NOW BE PRINTED ON THE EPSOM - PRESS RETURN TO CONTI
    NUE "
654 C2$ = "            NO ATOMS          NO TRIALS       'ATOM RATE'"
656 C3$ = "ARE YOU SURE NO INFORMTION OR REPEAT INFORMATION IS REQUIRED,
    THE LATTICE CAN STILL BE SAVED BY ANSWERING Y "
658 W = 1:E = 0:Z = 2:V = .5:L = 9:K = 3
660  PRINT "R A N D O M I S I N G"
662  INVERSE : PRINT "PLEASE INPUT THE RANDOM START POSITION  "
664  PRINT "INCREMENT BY ONE FOR EACH FRESH RUN ": INPUT A
665  NORMAL
668  FOR I = 1 TO A
671  PRINT  RND (1)
672  NEXT
673  POKE 8,256 *  RND (1): POKE 9,256 *  RND (1): POKE 235, RND (1) * 25
    6: POKE 236,256 *  RND (1): POKE 237,256 *  RND (1): POKE 238,256 *  RND
    (1)
674 D$ =  CHR$ (4):D1$ =  CHR$ (13)
676  CALL  - 936
678  PRINT A1$: PRINT : PRINT
680  POKE 781,0: POKE 787,9: POKE 777,2: POKE 786,1:E9 = 2:I5 = 1:I6 = 1:
     POKE 255,18: POKE 976,I5 + 1
682  PRINT A2$: INPUT F$: PRINT : PRINT
684  IF F$ = "Y" THEN 214
686  PRINT A3$: INPUT G1: PRINT : PRINT
687  POKE 773,G1
690 X4 = 140 - G1
692  PRINT A4$: PRINT : PRINT
693 G1 = G1 - 1:G3 = G1 + 1: POKE 768,2 * G3: POKE 774,G1: POKE 995,G3
694  IF  PEEK (233) = 54 AND  PEEK (232) = 8 THEN 698
695  PRINT D$"BLOADSEPT21,A$2C65"
```

```
696  POKE 233,54: POKE 232,8
698 I = 2 * G3 * G3: POKE 252,I -  INT (I / 256) * 256: POKE 253, INT (I /
    256)
702 I = I + 24577: POKE 254,I - INT (I / 256) * 256: POKE 255, INT (I /
    256)
704  CALL 15510
706  POKE 788,0: POKE 789,0: POKE 790,0
708  IF F$ < > "Y" THEN 712
710 I5 = 1:I6 = 1:X4 = 140 - G1 - 1
712  DIM M(170)
713 FOR I = 0 TO 127: POKE 843 + I,0: NEXT
714  FOR I = 0 TO 3
715  FOR J = 0 TO 7
716  POKE 841 + (J + I * 8) * 4 - I + 3,2 ^ J
717  NEXT
718  NEXT
720 P(0) = 1
722  IF F$ < > "Y" THEN 728
724  PRINT A5$: INPUT Y6: PRINT : PRINT
726  IF Y6 = 1 THEN 242
728  PRINT A6$: PRINT : PRINT
730  IF P(7) = 0 THEN 739
732  PRINT A7$
734  FOR I = 1 TO 9
736  PRINT "    ";I;"       ";P(I)
738  NEXT
739  INPUT P(1),P(2),P(3),P(4),P(5),P(6),P(7),P(8),P(9)
740  FOR I = 3 TO 9: IF P(I) = 1 THEN P(I) = P(I) - .0000001
741  NEXT
742  FOR I = 3 TO 9: POKE 990 + I * 2,P(I) * 256: POKE 991 + 2 * I,P(I) *
    65536 - 256 *  INT (P(I) * 256): NEXT
743  PRINT A8$
744  FOR K = 1 TO 9: PRINT "    ";K;"       ";P(K): NEXT
746  PRINT A9$;: INPUT W$
748  IF W$ = "N" THEN 728
750  PRINT B1$;: INPUT H: PRINT : PRINT
752  PRINT B2$;: INPUT E8:H1 =  INT (H / E8)
753  INPUT "HOW MANY REPITITIONS ";EE
754  PRINT " I.E ";EE * E8 * H1;" ATOMS "
755  PRINT B3$;: INPUT Q$
756  IF Q$ = "Y" THEN I9 = 4
758  IF Q$ < > "Y" THEN 768
760 K6 =  INT (G1 / 2): POKE 24577 + G3 * 2 * K6 + 2 * K6 + 1,3
762  POKE 24577 + G3 * 2 * K6 + 2 * K6 + 3,3
764  IF K6 / 2 < > INT (K6 / 2) THEN  POKE 24577 + G3 * 2 * K6 + 2 * K6
    + 1 + 2 * G3,3
766  IF K6 / 2 =  INT (K6 / 2) THEN  POKE 24577 + G3 * 2 * K6 + 2 * K6 +
    3 + 2 * G3,3
768  GOSUB 462
769  POKE 778,K6: POKE 779,K6
770 K = 3: GOTO 5
1000  POKE 781,0: POKE 787,9: POKE 777,2: POKE 786,1: POKE 255,18: POKE 9
    76,2: POKE 788,0: POKE 789,0: POKE 790,0
1010 I5 = 1:I6 = 1
1020 I = 2 * G3 * G3: POKE 252,I -  INT (I / 256) * 256: POKE 253, INT (I
    / 256)
1030 I = I + 24577: POKE 254,I -  INT (I / 256) * 256: POKE 255, INT (I /
    256)
1050  CALL 15510
1060  HGR2
```



```
1100  IF Q$ = "Y" THEN I9 = 4
1101  IF Q$ < > "Y" THEN 1111
1103 K6 =  INT (G1 / 2): POKE 24577 + G3 * 2 * K6 + 2 * K6 + 1,3
1105  POKE 24577 + G3 * 2 * K6 + 2 * K6 + 3,3
1107  IF K6 / 2 < > INT (K6 / 2) THEN  POKE 24577 + G3 * 2 * K6 + 2 * K
    6 + 1 + 2 * G3,3
1109  IF K6 / 2 =  INT (K6 / 2) THEN  POKE 24577 + G3 * 2 * K6 + 2 * K6 +
    3 + 2 * G3,3
1111  GOSUB 462
1120  POKE 778,K6: POKE 779,K6
1150  POKE 8,256 *  RND (1): POKE 9,256 *  RND (1): POKE 235, RND (1) * 2
    56: POKE 236,256 *  RND (1): POKE 237,256 *  RND (1): POKE 238,256 *
     RND (1)
1200  RETURN

J
```

APPENDIX VII - VARIABLES

Zero page usage

DECIMAL	$ HEX	VARIABLE
6	* 6	re used internal Var for RND NO Sub routs
7	* 7	
8	8	two byte RND NO (Latest)
9	9	
25	* 19	Copy of X pixel address
26	* 1A	
27	~ 1B	re usable internal Var for RND NO
28	~ 1C	
29	* 1D	Copy of Y pixel addr
30	* 1E	addres of site loc given by A=1E, B=1F
31	* 1F	
206	*CE	X Coord for addres of pixel to be plotted in mem H&R2 usually
207	*CF	
227	* E3	re usable Var in Pixel loc routine
235	EB	RND No pair (latest-1)
236	EC	
237	ED	Rnd no pair (latest-2)
238	EE	
239	* EF	Y coord of pixel to be plotted
249	F9	Counter for :.:.: loop
250	~ FA	Site location
251	~ FB	
252	~ FC	addres of site loc obtained from 1E, 1F Used by 2 routines
253	~ FD	
254	~ FE	addres of loc of site for Subroutines re usable
255	~ FF	
768	300	4*G3 (2*G3)
769	301	D6
770	302	D7
771	303	D8
772	304	D9
773	305	INT(128/G3)*G3
774	306	G1 = G3-1
775	307	[A1]
776	308	[B1]
777	309	H4
778	30A	A
779	30B	B
780	30C	C
781	30D	M7

DEC	$ HEX	VAR
782	30E	Y
783	30F	D
784	310	F
785	311	X
786	312	G
787	313	N
788	314	C1 Lo
789	315	C1 mid
790	316	C1 Hi
791	† 317-31A	M
	† 31B-31E	M1
	† 31F-322	P
	† 323-326	O
	† 327-32A	M4
	† 32B-32E	M5
	† 32F-332	M6
	† 333-336	U
	† 337-33A	R
	† 33B-33E	Q
	† 33F-342	Q1
	† 343-346	Q2
839	347	Return Status
840	348	R8/D5 #28
841	349	A3
842	34A	B3
	† 34B-3CA	B Array
971	3CB	
972	3CC	
973	3CD	
974	3CE	
975	3CF	
976	3D0	I5-1
977	3D1	
978	3D2	
979	3D3	
980	3D4	
981	3D5	
982	3D6	'A'-1
983	3D7	'B'-1
984	3D8	'A'+1
985	3D9	'B'+1
986	3DA	'A' chosen for ∴
987	3DB	'B' chosen for ∴

DEC	$ HEX	VAR
988	3DC	Counter 1 or 2
989	3DD	Counter ∴ plot <12
990	3DE	
991	3DF	
992	3E0	No of free sites in lowest layer
993	3E1	
994	3E2	edge position for displayed letter
995	3E3	G3
996	3E4/5	P(3)
998	3E6/7	P(4)
1000	3E8/9	P(5)
1002	3EA/B	P(6)
1004	3EC/D	P(7)
1006	3EE/F	P(8)
1008	ϕ 3F0/1	P(9)

x used by integer basic
ǂ 4 byte version 132 atoms height
ϕ used by monitor Subroutines
R Re-usable outside of subroutine
M Maybe reusable on some occasions

APPENDIX VIII - SYMBOLS

Symbol	Meaning	Units
A	area	cm^2
A_n	nucleation rate	sites/cm^2
a	reaction coordiate of species R	
a_j	activity of species j in phase α	mol/dm^3
C/val	charge or discharge rate of a cell, the value being the number of hours taken	
C	capacitance	μF
C_t	charge passed in time t	C
C_{dl}	double layer capacity	$\mu F/cm^2$
C_b	bulk concentration	mol/dm^3
C_o	concentration of species O (oxidised)	mol/dm^3
$C_o(x,t)$	concentration of species O at time t, distance x	mol/dm^3
C_o^s	concentration of species O at the surface	mol/dm^3
C_x	concentration at height x	mol/dm^3
D	diffusion coefficient	cm^2/s
D_o	diffusion coefficient of species O	cm^2/s
D_r	diffusion coefficient of species R	cm^2/s
E_{cell}	emf produced by an electrochemical cell	V
$E^{\ominus}$	standard potential of an electrode	V
E^o	standard potential of a half-reaction	V
E_o	amplitude of an a.c. voltage	V
E_p	peak potential	V
ΔE^*	activation energy for transition of an atom between sites	

F	Faraday	96487 C/mol
f	ratio of deposition at a normal site to an enhanced site	
$f_a(\eta)$	$= \exp([1-\alpha]F\eta/RT)$	none
$f_c(\eta)$	$= \exp(-\alpha F\eta/RT)$	none
$\bar{G}$	electrochemical free energy	J/mol
G	chemical free energy (Gibbs free energy)	J/mol
$\bar{G}_o(x)$	free energy of O at reaction coordiate x	J/mol
$\bar{G}_r(x)$	free energy of R at reaction coordiate x	J/mol
$\bar{G}_{o,(min)}$	minimum free energy of species O	J/mol
$\bar{G}_{r,(min)}$	minimum free energy of species R	J/mol
$\Delta\bar{G}$	change in electrochemical free energy	J/mol
ΔG	change in chemical free energy	J/mol
$\Delta G^{\ddagger}$	change in activation energy	J/mol
$^{\ominus}\Delta G^{\ddagger}$	change in standard free activation energy	J/mol
$\Delta G_b^{\ddagger}$	change in backward activation energy	J/mol
$\Delta G_f^{\ddagger}$	change in forward activation energy	J/mol
h	Planck constant	6.63×10^{-34} Js
h	final dendrite height	μm
h_i	critical dendrite height	μm
h_o	initial dendrite height	μm
h_t	height of a dendrite at time t	μm
I_o	amplitude of an a.c. current	A
i	current density	A/cm^2
i_c	cathodic current component	A
i_e	enhanced simulation current	
i_f	flat surface current density	A/cm^2
i_i	current component due to species i	A
i_L	limiting tip current density	A/cm^2

i_n	current density due to the n-th layer		A/cm^2
i_n	normal simulated current		
i_o	exchange current		A
i_p	peak current		A
i_{pp}	peak - peak simulated current		
i_t	tip current density		A/cm^2
Δi	artificial increase in simulated current		
$J_o(x,t)$	flux of a species O at time t, location x		$molcm^2/s$
j	root -1		
k	proportionality constant		
k^+	atom impingement rate		atoms/s
k_n^-	atom evaporation rate		atoms/s
k_B	Boltmann constant	1.38×10^{-23}	J/K
k_b	backward rate constant		cm/s
k_f	forward rate constant		cm/s
k^{Θ}	standard rate constant		cm/s
K_o	rate constant for deposition onto a flat surface		cm/s
k_r	rate constant for deposition onto a dendrite tip		cm/s
k_h^{Θ}	standard heterogenous rate constant		variable
k_b^h	heterogenous backward rate constant		variable
k_f^h	heterogenous forward rate constant		variable
k_{oo}	transition rate constant between equal energy level sites		
k_{on}	transition rate constant to lower energy sites		
Ls	lattice size (sites per lattice edge)		
M	molecular weight		g/mol

n	Faradays per mole electrolysed	none
n	number of nearest neighbours	none
n_i	number of moles of a species i	mol
O	oxidised species	
P	pressure	Pa
q	bond force constant	
q	number of dendrite cones on a surface	sites/cm^2
q_{mon}	charge involved in the formation of a monolayer	C/cm^2
R	gas constant	8.314 $Jmol^{-1}K^{-1}$
R	reduced species	
R	resistance	Ω
R_{ct}	charge transfer resistance	Ω
R_s	solution resistance	Ω
r	dendrite tip radius	cm
r_{opt}	optimum tip radius	cm
S	fraction of area with account taken of overlap	
S_{ex}	fraction of area with no account taken of overlap	
T	absolute temperature	K
T_d	growth time for dendritic growth	s
t	time	s
Δt	dendrite growth time	s
t_i	initiation time for dendrite growth	s
u	time	s
V	molar volume	cm^3/mol
V_c	volume of a dendrite cone	cm^3
V_t	total volume of dendrite cones on a surface	cm^3

v_d	rate of dendrite growth beyond the Nernst diffusion layer	cm/s
w	half a dendrite cone width	cm
x	distance	cm
x	reaction coordinate	
$x^{\neq}$	reaction coordiate of activated complex	
Z	total complex plane impedance	Ω
Z′	real (in phase) component of the complex plane impedance	Ω
Z′′	imaginary (out of phase) component of the complex plane impedance	Ω
z	= n; Faradays per mole electrolysed	none
z	coordination number	none
α	phase	
α	transfer coefficient	none
β	= 1 - α	none
β	= $k_B T/h$	
β	= $\pi v^2 A_n/3$	
γ	surface tension	dyne/cm
$\bar{\Delta}$	rate of diffusion layer growth	cm/s
$\Delta\Phi$	Galvani (absolute) potential difference	V
$\Delta\chi$	Dipole potential difference	V
$\Delta\Psi$	Volta potential difference	V
δ	Nernst diffusion layer thickness	cm
δ_o	diffusion layer thickness for species o	cm
η_r	curvature overpotential (Kelvin surface tension effect)	V
η	overpotential	V
η_c	critical overpotential for dendrite growth	V

η_o	= RT/nF slope of the Tafel line	V
η_p	critical overpotential for powdery deposition	V
θ	angle of a dendrite cone	radians
θ	phase angle of an a.c. signal	radians
μ_i^α	chemical potential of a species i in phase α	kJ/mol
$\bar{\mu}_i^\alpha$	electrochemical potential of a species i in phase α	kJ/mol
$\mu_i^\ominus$	standard chemical potential of a species i	kJ/mol
π	pi = 3.1416	
ρ	density	g/cm^3
ρ	lattice site surface density	$sites/cm^2$
σ	Warburg coefficient	$\Omega/s^{1/2}$
τ	time for deposition at a normal site	
υ	sweep rate	V/s
ν	kinematic viscocity	cm^2/s
ν	rate of advance of an edge	cm/s
ν	frequency factor	
Φ_α	potential difference accross a phase α	V
φ	energy required to break one bond	J
Ψ	energy required to break one bond	J/mol
ω	rotation rate	rad/s
ω	a.c. frequency	rad/s

ABBREVIATIONS

d.l.c.	double layer capacity
EDAX	Energy Dispersive Analysis of X-rays
IHP	Inner Helmholtz Plane
OHP	Outer Helmholtz Plane
RMS	Root Mean Square
SHE	Standard (or normal) Hydrogen Electrode
SEM	Scanning Electron Microscopy

REFERENCES

1. F. L. Tye, private communication.

2. F. L. Tye and R. Barnard, private communication.

3. P. C. Milner and U. B. Thomas, in 'Advances in Electrochemistry and Electrochemical Engineering', Vol 5, Eds, P. Delahay and C. W. Tobias, Interscience, New York (1967) pl.

4. R. Barnard, J. Appl. Electrochem., 11 (1981) 217.

5. D. Dryssen and P. Lumme, Acta Chem. Scand., 16 (1962) 1785.

6. R. D. Armstrong, K. Edmondson and G. D. West, Chem. Soc. Specialist Report, Electrochemistry, 4 (1974) 18.

7. D. E. Ryan, J. R. Dean and R. M. Cassidy, Canad. J. Chem., 43 (1965) 999.

8. R. D. Armstrong, J. D. Milewski, W. P. Race and H. R. Thirsk, J. Electroanal. Chem., 21 (1969) 517.

9. R. D. Armstrong and K. Edmondson, J. Electroanal. Chem., 53 (1974) 371.

10. R. D. Armstrong and G. D. West, J. Electroanal. Chem., 30 (1971) 385.

11. P. E. Lake and J. M. Goodings, Canad. J. Chem., 36 (1958) 1089.

12. R. D. Armstrong, A. Sperrin, F. L. Tye and G. D. West, J. Appl. Electrochem., 2 (1972) 265.

13. E. J. Casey and C. L. Gardner, J. Electrochem. Soc., 122 (1975) 851.

14. J. A. Karvtsova and Ya. D. Zytner, Z. Prikl. Khim., 50 (1977) 918.

15. I. A. Kazarinov, L. A. L'vova, D. K. Grachev and Yu. I. Obedkov, Elektrokhim., 10 (1974) 964.

16. R. Barnard and F. L. Tye, private communication.

17. commercial literature, Alcad. Pocket Plate Cells (1980).

18. commercial literature, Varta. (1974)

19. J. Sandera, M. Cenek, A. Touskova, M. Calabek, J. Mrha and J. Jindra, 'Power Sources 7', Proc 11th Int. Power Sources Symp. Ed J. Thompson. Academic Press, London, (1979) 239.

20. G. W. Briggs, Electrochemistry Vol 4, Specialist periodical report, 4 (1974) 33.

21. E. Deltombe and M. Pourbaix, CITCE (6th), 6 (1954) 133.

22. B. N. Afansev, V. J. Bukarinov and N. N. Milyutin, Elektrokhim., 10 (1974) 134.

23. M. W. Breiter, Electrochim. Acta, 22 (1977) 1219.

24. R. E. Visco and R. H. Sonner, Ext. Abs. Batt. Div. fall meeting, (1969) 18.

25. K. H. Gayer and L. Wootner, J. Phys. Chem., 61 (1957) 364.

26. Y. Okinaka, J. Electrochem. Soc., 117 (1970) 289.

27. G. T. Croft, J. Electrochem. Soc., 106 (1959) 278.

28. E. J. Rubin, J. Electrochem. Soc., 114 (1967) 1980.

29. P. V. Popapat and E. J. Rubin, J. Electrochem. Soc., 113 (1966) 201C.

30 S. Yoshizawa and Z. Takehara, Electrochim. Acta, 5 (1961) 240.

31. M. H. Gottlieb, Electrochem. Tech., 5 (1967) 12.

32. Y. Okinaka and C. M. Whitehurst, J. Electrochem. Soc., 117 (1970) 583.

33. M. W. Breiter and W. Vedder, Trans. Farad. Soc., 63 (1967) 1042.

34. F. G. Will and H. J. Hess, J. Electrochem. Soc., 120 (1973) 1.

35. M. W. Breiter and J. L. Weininger, J. Electrochem. Soc., 113 (1969) 651.

36. L. A. Kazarinov, R. E. Tugushev, L. A. L´vova, I. K. Kucheava and N. V. Kadnikova, Z. Prikl. Khim., 50 (1977) 2359.

37. R. Barnard, G. S. Edwards, J. A. Lee and F. L. Tye, J. Appl. Electrochem., 6 (1976) 107.

38. Yu. I. Obedkov and L. A. L´vova, Elektrokhim., 10 (1974) 341.

39. Yu. I. Obedkov and L. A. L´vova, Elektrokhim., 9 (1973) 1649.

40. Yu. I. Obedkov and L. A. L´vova, Elektrokhim., 11 (1975) 130.

41. I. A. Kazarinov, N. V. Kadnikova and L. A. L´vova, Z. Prikl. Khim., 51 (1978) 1950.

42. O. R. Pyrakhin, V. P. Galushko and E. F. Zavgorodnyaya, Elektrokhim., 9 (1973) 60.

43. I. Sanghi, S. Visvanathan and S. Anantharayanan, Electrochim. Acta, 3 (1960) 65.

44. Ya. D. Zytner, E. A. Maksimyuk, V. A. Nikolskii, N. I. Alekseeva and E. A. Berkman, Elektrokhim. 7 (1971) 1581.

45. V. P. Galushko, E. F. Zavgorodnayaya, N. V. Podolskaya and Yu. P. Rodak, Elektrokhim., 8 (1972) 1216.

46. A. A. Abdul Azim, K. M. El-Sobki, Electrochim. Acta, 17 (1972) 601.

47. I. A. Kazarinova, Ya. D. Zytner, A. N. Sashinin and E. M. Baranovskaya, Elektrokhim., 10 (1974) 959.

48. S. Gilman and L. D. Sangermano, J. Electrochem. Soc., 118 (1971) 1953.

49. W. M. Latimer, 'Oxidation potentials', 2nd Ed'n, Prentice Hall New York, 1953.

50. K. Edmondson, PhD thesis (1975), University of Newcastle Upon Tyne.

51. J. Piater, Z. Anorg. Allgem. Chem.,174 (1938) 321.

52. R. Scholder and E. Staufenbiel, Z. Anorg. Allgem. Chem., 274 (1941) 259.

53. V. P. Galushko, O. R. Pryakhin and I. A. Oshe, Ukr. Khim. Z. 39 (1973) 1115.

54. V. P. Galushko, O. R. Pryakhin and I. A. Oshe, Ukr. Khim. Z. 39 (1973) 1212.

55. H. Bode and W. Dennstedt, Electrochim. Acta,17 (1972) 609.

56. O. Glemser, U. Hauschild and H. Richert, Z. Anorg. Allgem. Chem., 290 (1957) 58.

57. K. Appelt, Electrochim. Acta, 13 (1968) 1727.

58. P. M. de Wolff, Acta crystallogr., 21 (1966) 432.

59. J. S. Choi, Y. H. Kang and K. H. Kim, J. Phys. Chem. 81 (1977) 2208.

60. I. A. Kazarinov, N. V. Kadnikova and L. A. L'vova, Z. Prikl. Khim., 51 (1978) 1950.

61. K. Dick, PhD thesis (1978), University of Newcastle Upon Tyne.

62. J. Kukk, I. Kruse and V. Past, Tartu Ulikooli Toimet. Uch. Zap. Tartus Un-ta, 378 (1976) 24.

63. R. W. Bramham, R. J. Doran, S. E. A. Pomroy and J. Thompson, 'Power Sources 6', Proc. 10th Int. Power Sources Symp., Ed, D. H. Collins, Academic Press, London (1977) 129.

64. B. S. Hobbs, T. Kelly and A. G. Palmer, J. Appl. Electrochem., 9 (1978) 305.

65. E. I. Papazova, V. A. Nikolski and N. G. Krivoplyas, Sb. Rab. Khim. 1st. Toka., 9 (1974) 145.

66. E. I. Papazova, V. A. Nikolski and N. G. Kirvoplyas, Sb. Rab. Khim. 1st. Toka., 11 (1976) 123.

67. NASA Report, N73-21957, Battery Workshop meeting (1972).

68. S. F. Pensabene and J. W. Gould, IEEE Spectrum (1976) 33.

69. R. Barnard, J. A. Lee, A. Rafinski and F. L. Tye, in 'Power sources 5', Proc. 9th Int. Power Sources Symp., Ed, D. H. Collins, Academic Press, London (1975) 183.

70. R. Barnard, G. S. Edwards, J. A. Lee and F. L. Tye, J. Appl. Electrochem., 6 (1976) 431.

71. R. Barnard, K. Edmondson, J. A. Lee and F. L. Tye, J. Appl. Electrochem., 6 (1976) 107.

72. A. H. Reed, P. W. Cover and J. McCallum, Tech. Report AFAPL-TR-72-20, AD74017, Battelle (1969).

73. A. Fleisher, US Patent no. 2802043 (1957).

74. P. V. Vasudeva-Rao, T. Vasanthi and H. V. K. Udapa, J. Power Sources, 1 (1976/77) 81.

75. K. M. Soloeva and E. M. Ryzhok, Sb. Rab. Khim. 1st. Toka. 9 (1974) 121.

76. B. S. Hobbs, T. Keily and A. G. Palmer, J. Appl. Electrochem. 10 (1980) 721.

77. N. Ea and J. C. Niepce, Thermochim. Acta, 23 (1978) 345.

78. N. K. Terentev and Yu. M. Pozin, Sb. Rab. Khim. 1st. Toka. Vzez. Nacho Issled Akkt, 8 (1973) 856.

79. Yu. M. Pozin, N. K. Terentev and N. A. Makalov, Elektrokhim., 12 (1976) 79.

80. R. Barnard, G. T. Crickmore, J. A. Lee and F. L. Tye, 'Power Sources 6', Proc. 10th Int. Power Sources Symp., Ed, D. H. Collins, Academic Press, London (1977), 161.

81. Yu. M. Pozin and N. K. Terentev, Z. Prikl. Khim., 46 (1973) 187

82. J. S. Langer, R. F. Sekerka and T. Fujioka, J. Cryst. Growth, 44 (1978) 414.

83. J. S. Langer, Supp. Prog. Theor. Phys., 64 (1978) 463.

84. F. Ogburn, C. Bechtoldt, J. B. Morris and A. de Korangi, J. Electrochem. Soc., 112 (1965) 574.

85. G. Wranglen, Trans. Royal Inst. Tech., 94 (1959).

86. J. W. Faust Jr and H. E. Johns, J. Electrochem. Soc., 108 (1961) 109.

87. J. W. Faust Jr and H. E. Johns, J. Electrochem. Soc., 110 (1963) 463.

88. K. I. Popov, M. D. Maksimovic, M. G. Pavlovic and J. D. Trnjancev, J. Appl. Electrochem., 11 (1981) 239.

89. K. I. Popov, L. J. M. Djukic, M. G. Pavlovic and M. D. Maksimovic, J. Appl. Electrochem., 9 (1979) 527.

90. J. Barton and J. O'M. Bockris, Proc Roy. Soc., A268 (1962) 485.

91. J. Smith, F. Ogburn and C. J. Bechtoldt, J. Electrochem. Soc., 115 (1968) 371.

92. T. B. Reddy, J. Electrochem. Soc., 113 (1966) 117.

93. P. B. Price, Phil. Mag., 4 (1959) 1229.

94. R. D. Armstrong and S. J. Churchouse, Electrochim. Acta, 28 (1983) 185.

95. R. Barnard, F. L. Tye, J. Holloway and C. F. Randell, J. Appl. Electrochem., 13 (1983) 751.

96. R. Barnard, F. L. Tye, J. Holloway and C. F. Randell, J. Appl. Electrochem., 13 (1983) 765.

97. R. Barnard, F. L. Tye, J. Holloway and C. F. Randell, J. Appl. Electrochem., 14 (1984) 187 & 560 (correction).

98. R. D. Naybour, J. Electrochem. Soc., 116 (1969) 320.

99. J. O'M. Bockris, Z. Nagy, D. Drazic, J. Electrochem. Soc., 120 (1973) 31.

100. A. R. Despic, J. Diggle and J. O'M. Bockris, J. Electrochem. Soc., 115 (1968) 507.

101. R. V. Moshtev and P. Zlatilova, J. Appl. Electrochem., 8 (1978) 213.

102. J. W. Diggle, A. R. Despic and J. O'M. Bockris, J. Electrochem. Soc., 116 (1969) 1503.

103. F. Mansfield and S. Gilman, J. Electrochem. Soc., 117 (1970) 588.

104. F. Mansfield and S. Gilman, J. Electrochem. Soc., 117 (1970) 1154.

105. J. W. Diggle and A. Damjanovic, J. Electrochem. Soc., 119 (1972) 1649.

106. S. Szpak, C. J. Gabriel and T. Katan, J. Electrochem. Soc., 127 (1980) 1063.

107. J. W. Diggle and A. Damjanovic, J. Electrochem. Soc., 117 (1970) 65.

108. J. Bressan and R. Wiart, J. Appl. Electrochem., 9 (1979) 43.

109. J. Bressan and R. Wiart, J. Appl. Electrochem., 7 (1977) 505.

110. Y. Oren and U. Landau, Electrochim. Acta, 27 (1982) 739.

111. K. I. Popov, M. G. Pavlovic, M. D. Spasojevic and V. M. Nakic, J. Appl. Electrochem., 9 (1979) 533.

112. D. Kralik and J. Jorne, J. Electrochem. Soc., 127 (1980) 2335.

113. J. T. Kim and J. Jorne, J. Electrochem. Soc., 127 (1980) 8.

114. A. R. Despic and M. M. Purenovic, J. Electrochem. Soc., 121 (1974) 329.

115. A. R. Despic, D. M. Drazic and M. D. Mirjanic, Farad. Symp. Chem. Soc. (southampton), 12 (1977) 126.

116. A. R. Despic and K. I. Popov, Mod. Aspects Electrochem., 7 (1972) 199.

117. D. R. Hamilton, Electrochim. Acta, 8 (1963) 731.

118. K. I. Popov and A. R. Despic, Bull. Soc. Chim. Beograd, 36 (1971) 173.

119. Modern Electroplating [Electrochem. Soc. Publication]. Ed, F. A. Lowenheim, John Wiley and Sons, New York, 3rd edition, (1974).

120. A. Damjanovic, M. Paunovic and J. O´M. Bockris, J. Electroanal. Chem., 9 (1965) 93.

121. R. D. Armstrong and J. A. Harrison, J. Electrochem. Soc., 116 (1969) 328.

122. R. D. Armstrong and A. A. Metcalfe, J. Electroanal. Chem., 65 (1975) 19.

123. M. M. Clark, J. A. Harrison and H. R. Thirsk, Z. Phys. Chem. N. F., 98 (1975) 153.

124. A. Smith and S. Fletcher, Cand. J. Chem., 57 (1979) 1304.

125. A. Bewick, M. Fleischmann and H. R. Thirsk, Trans. Farad, Soc., 58 (1962) 2200.

126. J. Oldfield, Electrodeposition and surface treatment, 2 (1973/4) 395.

127. J. A. Harrison and W. J. Lorenz, J. Electroanal. Chem., 76 (1977) 375.

128. J. A. Harrison and S. Rangarajan, Proc. Farad. Symp. Chem. Soc. (Southampton), 12 (1977) 70.

129. R. G. Barradas and T. J. Vandernoot, J. Electroanal. Chem., 142 (1982) 107.

130. M. S. Viola, K. A. Vanwormer and G. D. Botsaris. J. Cryst. Growth, 47 (1979) 127.

131. U. Bertocci, Surface Science, 15 (1969) 286.

132. F. F. Abraham and G. M. White, J. Appl. Phys., 41 (1970) 1841.

133. U. Bertocci, J. Electrochem. Soc., 119 (1972) 822.

134. G. H. Gilmer and P. Bennema, J. Appl. Phys., 43 (1972) 1346.

135. A. C. Adams and K. A. Jackson, J. Cryst. Growth, 13/14 (1972) 144.

136. G. H. Gilmer and P. Bennema, J. Cryst. Growth, 13/14 (1972) 148.

137. A. I. Michaels, G. M. Pound and F. F. Abraham, J. Appl. Phys., 45 (1974) 9.

138. S. W. H. de Haan, V. J. A. Meeussen, B/ P. Veltman, P. Bennema, C. van Leeuwen and G. H. Gilmer, J. Cryst. Growth, 24/25 (1974) 491.

139. U. Bertocci, J. Cryst. Growth, 26 (1974) 219.

140. G. H. Gilmer and H. J. Leamy, J. Cryst. Growth, 24/25 (1974) 499.

141. A. Bonissent and B. Mutaftschiev, J. Cryst. Growth, 24/25 (1974) 503.

142. J. P. van der Eerdem, C. van Leeuwen, P. Bennema, W. L. van der Kruk and B. P. Veltman, J. Appl. Phys., 48 (1977) 2124.

143. J. D. Weeks, G. H. Gilmer and K. A. Jackson, J. Chem Phys., 65 (1976) 712.

144. G. H. Gilmer, Proc. Farad. Symp. Chem. Soc. (Southampton) 12 (1977) 59.

145. G. H. Gilmer, Science, 208 (1980) 355.

146. G. H. Gilmer, J. Cryst. Growth, 42 (1977) 3.

147. G. H. Gilmer, J. Cryst. Growth, 35 (1976) 15.

148. G. H. Gilmer, J. Cryst. Growth, 49 (1980) 465.

149. P. Bennema and J. P. van der Eerden, J. Cryst. Growth, 42 (1977) 201.

150. T. A. Cherepanova, J. P. van der Eerden and P. Bennema, J. Cryst. Growth, 44 (1978) 537.

151. T. A. Cherepanova, J. Cryst. Growth, 52 (1981) 319.

152. H, Franke and R. Lacmann, Phys. Stat. Sol., (a) 55 (1979) 415.

153. H, Franke and R. Lacmann, Phys. Stat. Sol., (a) 60 (1980) 475.

154. R. D. Armstrong and S. J. Churchouse, J. Electroanal. Chem., 167 (1984) 265.

155. A. N. Kolmogoroff, Bul. Acad. Sci. URSS/Sci. Math. Nat., 9 (1937) 355.

156. M. Avrami, J. Chem. Phys., 7 (1939) 1103; 8 (1940) 212; 9 (1941) 177.

157. M. Fleischmann and H. R. Thirsk in P. Delahay (Ed.), Advances in Electrochemistry and Electrochemical Engineering, Vol. 3, Interscience, New York, 1963, p123.

158. E. D. Cashwell and C. J. Everett, Monte Carlo Method, Pergamon, New York, 1959.

159. J. M. Hammersley and D. C. Handscomb, Monte Carlo Methods, Methuen and Company Ltd., London, 1964.

160. G. H. Gilmer, H. J. Leamy, K. A. Jackson and H. Reiss, J. Cryst. Growth, 24/25 (1974) 495.

161. D. E. Temkin, Soviet Phys.-Cryst., 14 (1969) 344.

162. E. B. Budevski, 'Progress in Surface and membrane Science', vol 11, Eds D. A. Cadenhead and J. F. Daielli, Academic press (1976) p71

163. K. Huang, Statistical Mechanics, Wiley, New York 1963.

164. A. I. Michaels, M. B. Ives, React. Solids, Proc. 8th Int. Symp. 1976 p593.

165. A. J. Bard and L. R. Faulkner, 'Electrochemical methods, Fundamentals and applications', Wiley, New York.

166. J. O'M. Bockris and A. K. N. Reddy, 'Modern Electrochemistry' Vols 1 and 2, Plenum, New York.

167. J. A. V. Butler, Proc. Roy. Soc. 157a (1936) 423.

168. J. Tafel, Z. Physik. Chem., 50 (1905) 641.

169. A. Sevcik, Collect. Czech. Chem. Commun., 13 (1948) 349.

170. W. H. Reinmuth, J. Am. Chem. Soc., 79 (1957) 6358.

171. H. Matsuda and Y. Ayabe, Z. Electrochim., 59 (1955) 494.

172. R. S. Nicholson and I. Shain, Anal. Chem., 36 (1964) 706.

173. V. G. Levich, 'Physiochemical Hydrodynamics', (Eng trans), Prentice Hall, New Jersey (1962).

174. W. J. Albery and M. L. Hitchman, Ring Disc Electrodes, Oxford University Press, London (1971).

175. R. D. Armstrong, M. Bell and A. A. Metcalfe, J. Electroanal. Chem., 77 (1977) 287.

176. F. D. Rossini, D. D. Wagman, W. H. Evans, S. Levine and I. Jaffe, 'Selected Values of Chemical Thermodynamic Properties', Natl. Bur. Std. Circ. 500, US. Govt. printing office, Washington (1952).

177. K. S. Kim and N. Winograd, Surface Science 43 (1974) 625.

178. K. S. Kim and R. E. Davis, J. Electron Spectr. and Rel. Phen., 1 (1972/73) 251.

179. P. Lukowzew, S. Lewina and A. Frumkin, Acta Physicochhi (URSS) 11 (1939) 29.

180. V. I. Levina and S. A. Rozentsvig, Issled. Obl. Khim. 1st Toka. (1965) 53.

181. Yu. M. Pozin and N. K. Terentev, Z. Prikl. Khim. 46 (1973) 187.

182. 'Handbook of Chemistry and Physics', Chemical Rubber Company Press (1973).

183. G. A. Gunawardena, G. J. Hills and I. Montenegro, Electrochimica. Acta, 23 (1978) 693.

184. '6502 Assembly Language Programming', L. A. Leventhal, Berkeley Calif., Osbourne - McGraw Hill 1979.

185. 'Programming the 6502 - 6502 Series v.1', R. Zaks, Berkeley Calif., Sybex 1980.

186. 'Apple Machine Language', D. Inman, K. Inman, Reston, Va., Reston Pub. Co. 1981.

187. O. R. Brown, private communication.

ACKNOWLEDGEMENTS

I am deeply indebted to my supervisor Dr Ron Armstrong, without whose guidance, this thesis would not have been possible. I would also like to thank Dr Frank Tye and Dr Robert Barnard of Ever Ready, for the many helpful discussions and advice during the earlier part of this work. Additional thanks must go to the staff of the departmental workshops, and the glassblowers for making much of the experimental apparatus used in this thesis. Finally I would like to thank Gary Evans who co-wrote the general plotting and computerised a.c. impedance programs.